Qualitative Methods for Inverse Scattering in Solid Mechanics

Cédric Bellis

Qualitative Methods for Inverse Scattering

in Solid Mechanics

Thèse présentée pour l'obtention des titres de

DOCTEUR DE L'ÉCOLE POLYTECHNIQUE

Spécialité : Mécanique

&

DOCTOR OF PHILOSOPHY OF THE UNIVERSITY OF MINNESOTA

Major : Civil Engineering

par

Cédric Bellis

Soutenue le 3 décembre 2010 devant le jury composé de

Président :	**Houssem Haddar**	Directeur de recherche, INRIA, France
Rapporteurs :	**Didier Auroux**	Professeur, Université de Nice Sophia Antipolis, France
	Dominique Leguillon	Directeur de recherche, CNRS, France
Examinateur :	**Vaughan Voller**	Professeur, University of Minnesota, USA
Directeurs :	**Marc Bonnet**	Directeur de recherche, CNRS, France
	Bojan B. Guzina	Professeur, University of Minnesota, USA

BITS & **PIECES** PUT TOGETHER TO PRESENT A SEMBLANCE OF A WHOLE
Lawrence Weiner

Courtesy of Scott Kim

To Cécile

Acknowledgments

I would like to express my deep and sincere gratitude to my academic advisors Marc Bonnet and Bojan Guzina for their great scientific and intellectual guidance during my research as well as for the stimulating liberty they offered me during this project. I would like to thank them for their intellectual rigor, presence and enthusiasm that helped me bring this thesis to completion. I have learnt tremendously from them, and I sincerely hope our future collaborations will remain friendly and fruitful as they have always been.

I also had the chance to meet and work with Fioralba Cakoni, and I want to acknowledge her gratefully for our rewarding interactions and her inspiring energy.

I would like to thank Houssem Haddar for accepting of being the Chairman of my committee as well as for the insightful comments he made on this work. I am also grateful to Dominique Leguillon and Didier Auroux for their time and effort in reviewing this dissertation, and to Vaughan Voller for his participation in my committee.

I owe my gratitude to Bernard Halphen and Patrick Le Tallec, the successive directors of the Laboratoire de Mécanique des Solides at the École Polytechnique, as well as to Roberto Ballarini and Raymond Hozalski, respectively Head and Director of graduate studies of the Department of Civil Engineering of the University of Minnesota. They welcomed me in these two institutions of highest scientific level and intellectual flowering.

I sincerely thank Andrei Constantinescu, Antoine Chaigne and Ziad Moumni who trusted in me and thanks to whom I had the opportunity to teach at the École Polytechnique and the École Nationale Supérieure des Techniques Avancées. Teaching was a delightful experience for three years and I would like to thank the students I met for the fulfilling interactions I had with them.

Very special thanks must go to the office staffs on either side of the Atlantic who made this joint Ph.D. program and more generally this work successful. I am grateful to Alexandra Joly, Christiane Periam, Flora Marguerite, Lisa Sherman, Tiffany Ralston and Teresa Rosen who helped me a lot along the way. I would also like to thank Pascale Hennion and Christian Roy warmly for their computer and technical assistance during these years.

This Ph.D. thesis was not a lonely quest and I owe part of the following work to many of the faculties, students and friends in the Laboratoire de Mécanique des Solides of the École Polytechnique and the Department of Civil Engineering of the University of Minnesota. I doubt that I will ever be able to appreciate each of their contributions fairly but I gratefully thank them for their continuous help, support and friendship which go far beyond the context of this thesis.

Warmest thanks must go to my friends and to my family for their love and encouragement. But above all, I would like to express my deepest gratitude to Cécile whose constant love, patience and support made this thesis possible. I can never thank her enough for all she gave during these years.

i

Abstract

Nowadays, inverse scattering problems in solid mechanics bear relevance to a wide range of applications such as seismic tomography and imaging, non-destructive material testing, and medical diagnosis. To help advance the state of the art on the subject, this research deals with detecting and identifying unknown scatterers i.e. obstacles (e.g. material defects, cracks, or lesions in soft tissues) in an elastic background solid through the use of acoustic or elastic illuminating waves. To circumvent the limitations underpinning the conventional imaging algorithms based on e.g. weak scatterer approximations or non-linear optimization techniques, a variety of the so-called sampling methods have been proposed over the past decade or so. Jointly, these methods constitute a paradigm shift in the approach of inverse scattering in that they seek only a qualitative information on the scatterer geometry and material characteristics within a computationally efficient and robust framework based on full-waveform (or partial) measurements of the scattered field.

The recent emergence of these non-iterative probing methods allows to consider the study of two or three-dimensional elastic waves propagation inverse problems in a new light. Earlier works have shown in particular, within the framework of the hypothesis adopted in this subject, the interest of methods such as i) the Topological Sensitivity Method that relies on a heuristic interpretation of the asymptotic perturbation of a featured cost functional generated by introducing an infinitesimal flaw at a prescribed location (the so-called sampling point), and ii) the Linear Sampling Method based on the resolution of a linear integral equation of the first kind featuring a fundamental singular solution to the wave equation.

The present study comes within the scope of the development of the two methods mentioned with application within the framework of the mechanics of deformable solids, i.e. inverse scattering problems in acoustic and elastic media. The proposed developments aim to i) provide key results underpinning the validity of these two techniques, ii) demonstrate their usefulness as implemented in conventional computational platforms for approximate but fast defect/lesion detection, and iii) extend their range of application in terms of the geometry and nature of hidden scatterers.

This research described in this dissertation has been performed within the framework of a joint Ph.D. program between the Laboratoire de Mécanique des Solides at the École Polytechnique (France) and the Department of Civil Engineering at the University of Minnesota (USA).

Contents

List of Figures

Conventions and Notations

This section summarizes the conventions and notations used in the sequel. Possible alternate uses of the ensuing definitions are explicitly stated where applicable.

Scalar quantities: Typeface latin or greek letters (d, t, ω, λ, ...)

Vectors, second-order tensors: Boldface lower case letters ($\boldsymbol{u}$, $\boldsymbol{\xi}$, ...)

Higher-order tensors: Boldface capital letters ($\boldsymbol{\mathcal{A}}$, $\boldsymbol{C}$, $\boldsymbol{I}$, ...)

Summation convention: Einstein convention is used on repeated indexes

$\boldsymbol{a} \cdot \boldsymbol{b}$	Contraction of tensors
$\boldsymbol{A} : \boldsymbol{B}$	Double contraction of tensors
$\otimes$	Tensor product
$\star$	Time convolution
δ_{ij}	Kronecker symbol
$\mathbb{R}^d$	Euclidian d-space
$(\boldsymbol{e}_i)_i$	Orthonormal basis of euclidian space
t	Time variable
ω	Frequency
k	Wave number
$\boldsymbol{\delta}$	Plane wave incident direction
$\boldsymbol{x}$, $\boldsymbol{\xi}$, $\boldsymbol{\zeta}$	Field points
$\bar{\boldsymbol{x}}$, $\bar{\boldsymbol{\xi}}$	Scaled coordinates
$\hat{\boldsymbol{\xi}}$, $\hat{\boldsymbol{\zeta}}$	Unit tensors
$\boldsymbol{I}$	Second-order identity tensor $\boldsymbol{I} = \delta_{ij} \boldsymbol{e}_i \otimes \boldsymbol{e}_j$
$\boldsymbol{\mathcal{I}}$	Fourth-order identity tensor $\boldsymbol{\mathcal{I}} = \delta_{il} \delta_{jk} \boldsymbol{e}_i \otimes \boldsymbol{e}_j \otimes \boldsymbol{e}_k \otimes \boldsymbol{e}_l$
$\boldsymbol{\mathcal{I}}^{\mathrm{sym}}$	Symmetric fourth-order identity tensor $\boldsymbol{\mathcal{I}}^{\mathrm{sym}} = \frac{1}{2}(\delta_{il}\delta_{jk} + \delta_{ik}\delta_{jl}) \boldsymbol{e}_i \otimes \boldsymbol{e}_j \otimes \boldsymbol{e}_k \otimes \boldsymbol{e}_l$
$\mathrm{d}S$	Surface differential element, possibly indexed by integration variable
$\mathrm{d}V$	Volume differential element, possibly indexed by integration variable
$\fint$	Singular integral in Cauchy principal value sense
Ω	Background elastic or viscoelastic solid
B, D	Unknown scattering objects
Σ	Set of unit directions
S_{D}, S_{N}	Surfaces with imposed Dirichlet and Neumann conditions

S_s	Source surface
S^{obs}, S_r	Observation and receiver surface
$\boldsymbol{\mathcal{C}}$	Fourth-order (visco-)elasticity tensor
c, C	Lower and upper bounds of (real part of) elasticity tensor
μ	Shear modulus
λ	Lamé's parameter
ν	Poisson's ratio
κ	Bulk modulus
E	Young's modulus
ρ	Mass density
p, P	Lower and upper bounds of mass density
c	Sound speed
$\boldsymbol{u}$, u	Incident (or free) fields, resp. elastic and acoustic
$\boldsymbol{v}$, v	Scattered fields, resp. elastic and acoustic
$\boldsymbol{w}$, w	Interior fields, resp. elastic and acoustic
$\hat{\boldsymbol{u}}$, $\hat{u}$	Adjoints fields, resp. elastic and acoustic
φ, ψ, $\boldsymbol{\varphi}$, $\boldsymbol{\psi}$, $\boldsymbol{\Phi}$, $\boldsymbol{\Psi}$	Test functions
$\bar{\varphi}$, $\bar{\boldsymbol{u}}$, $\bar{\boldsymbol{\Psi}}$	Complex-conjugated tensor fields
$\boldsymbol{\sigma}$	Cauchy stress tensor
$\boldsymbol{t}$	Cauchy stress vector
$\boldsymbol{n}$	Unit outward normal on surface
$\boldsymbol{z}$	Sampling point
$\mathbb{J}$	Misfit cost functional
$\mathbb{T}$	Topological derivative
$\boldsymbol{\mathcal{A}}$	Polarization tensor
$g_{\boldsymbol{z}}$	Indicator function of Linear Sampling Method
j_n, y_n	nth-order spherical Bessel functions of first and second kind
h_n	nth-order spherical Hankel functions of the first kind
P_n	nth-order Legendre polynomial
Y_n^m	(n,m)th-order spherical harmonics
$G(\boldsymbol{\xi},\boldsymbol{\zeta})$	Radiating fundamental solution to Helmholtz equation $G(\boldsymbol{\xi},\boldsymbol{\zeta}) = \frac{e^{ik|\boldsymbol{\xi}-\boldsymbol{\zeta}|}}{4\pi|\boldsymbol{\xi}-\boldsymbol{\zeta}|}$

$L^2(\mathcal{O})$ Hilbert space of functions $f : \mathcal{O} \to \mathbb{R}^d$ verifying
$$\|f\|_{L^2(\mathcal{O})}^2 = \int_{\mathcal{O}} |f|^2 \,\mathrm{d}V < \infty$$

$H^1(\mathcal{O})$ Sobolev space of functions $f \in L^2(\mathcal{O})$ with $\boldsymbol{\nabla}f \in L^2(\mathcal{O})$ as a distribution
$$\|f\|_{H^1(\mathcal{O})}^2 = \|f\|_{L^2(\mathcal{O})}^2 + \|\boldsymbol{\nabla}f\|_{L^2(\mathcal{O})}^2$$

$H_0^1(\mathcal{O})$ Space of functions $f \in H^1(\mathcal{O})$ such that $f = 0$ on $\partial\mathcal{O}$

$H^{\frac{1}{2}}(\partial\mathcal{O})$ Image of $H^1(\mathcal{O})$ by the trace operator $f \mapsto f_{|\partial\mathcal{O}}$

$H^{-\frac{1}{2}}(\partial\mathcal{O})$ Dual space of $H^{\frac{1}{2}}(\partial\mathcal{O})$ and associated with trace operator $f \mapsto \boldsymbol{\nabla}f\cdot\boldsymbol{n}$ on $\partial\mathcal{O}$

Introduction

Contents

Context

The investigation of inverse problems that arise in the context of the mechanics of deformable solids (Bonnet and Constantinescu, 2005), as well as in other areas of physics involving continuous media such as acoustics, electrostatics and electromagnetism, are motivated by the necessity to overcome a lack of information concerning the properties of the system (in this study a deformable solid body or structure). Inverse scattering problems (Pike and Sabatier, 2002; Ramm, 2005), that focus on the reconstruction of objects or inhomogeneities hidden in a solid using illuminating waves, have been the subject of numerous investigations and have lead to the development of a variety of mathematical and numerical tools (Colton and Kress, 1992; Kress, 1999; Aki and Richards, 1980; Bonnet, 1995; Dorn and Lesselier, 2006; Ramm, 1992) with a broad spectrum of applications such as nondestructive material testing, underground object detection, seismology and medical imaging. Such inverse problems generally require the knowledge of boundary data (provided by the measurements) that are "overdetermined" relative to what is normally necessary for solving a well-posed forward (i.e. direct) problem. Notwithstanding the significant progress made on the subject over the last decades, however, the development of practical and robust algorithms that are also computationally effective remains a challenge in the context of inverse scattering problems in solids owing in part to the fact that the latter are mathematically ill-posed, i.e. that they entail non-uniqueness, ill-conditioning or lack of stability towards the input data (see Hadamard, 1923; Kirsch, 1996). In such situations, linearization techniques (Bleistein, 1984) are often too restrictive, either in the context of physical configurations they can accommodate or the information they can provide. Moreover, the minimization-based approaches that exploit the data through a misfit cost function and have a potential of overcoming the latter restrictions unfortunately bear considerable computational cost associated with repeated solutions to the forward problem (Plessix et al., 1999; Rekanos et al., 1999; Nintcheu Fata et al., 2003; Guzina et al., 2003; Bonnet and Guzina, 2009). Such high computational cost associated with the solution of an inverse problem is even more prominent in the context of global optimization methods, which are, at present, impractical in the context of realistic three-dimensional configurations. More traditional gradient-based optimization is a computationally reasonable alternative for solving the featured class of inverse problems, especially when enhanced by adjoint-based shape sensitivity estimates (Bonnet, 1995; Bonnet and Guzina, 2009). However, their performance depends on

choosing adequately the initial guess (location, topology and geometry) of a hidden object or scatterer.

Over the past two decades, the above considerations led to the paradigm shift in mathematical theories of inverse scattering that have, to a large degree, focused on the development of the so-called *qualitative* methods (Cakoni and Colton, 2006) for non-iterative obstacle reconstruction from remote measurements of the scattered field. These techniques, which provide a powerful alternative to the customary minimization approaches and weak-scatterer approximations, are commonly centered around the development of an indicator function, that varies with coordinates of the interior sampling point, and projects remote observations of the scattered field onto a suitable functional space synthesizing the "baseline" wave motion inside the background (i.e. obstacle-free) domain. Such indicator function is normally designed to reach extreme values when the sampling point belongs to the support of the hidden scatterer, thereby providing a computationally-effective platform for geometric obstacle reconstruction. Among the diverse field of methods using approaches that can be classified as *probe* or *sampling* techniques (Colton and Kress, 2006; Potthast, 2006), one may mention the so-called *factorization method* (Kirsch, 1998, 2002; Kirsch and Grinberg, 2008; Charalambopoulos et al., 2007), the *probe method* (Erhard and Potthast, 2006; Ikehata, 1998a,b) and the point source method (Potthast, 1996, 2001) among the most prominent examples, as well as the **Topological Sensitivity Method** and the **Linear Sampling Method** which are the focus of this dissertation.

The concept of *Topological Sensitivity* (TS) – in the literature also referred to as the Topological Gradient, revolves around the quantification of the perturbation of a given cost function due to the creation of an object (e.g. a cavity) of vanishingly small characteristic size at a prescribed location z inside the reference (i.e. defect-free) solid. This concept first appeared in Eschenauer et al. (1994) and Schumacher (1995) in the context of topological optimization of mechanical structures, and has since been investigated in various contexts as a method for defining a defect indicator function, see e.g. Gallego and Rus (2004); Jackowska-Strumillo et al. (2002) for 2D elastostatics, Feijóo (2004) for 2D linear acoustics, Guzina and Bonnet (2006) for frequency-domain 3D acoustics, Bonnet and Guzina (2004); Guzina and Bonnet (2004) for frequency-domain 3D elastodynamics and Masmoudi et al. (2005) for 3D Maxwell equations. The particular appeal of this approach to solving inverse scattering problems resides in the fact that the computational cost required to evaluate a TS field is, in general, *of the order of one forward solution*, and therefore minimal compared to that of standard minimization-based iterative techniques. Here it is also noted that the concept of topological sensitivity is closely related to the broader class of asymptotic methods, where unknown defects, whose geometry involves a small parameter, are sought by means of an expansion of the forward solution (rather than the misfit function) with respect to that parameter, see Ammari and Kang (2004, 2006).

The *Linear Sampling Method* (LSM) likewise represents a minimization-free, grid-based approach to the reconstruction of internal scatterers (e.g. material defects). This technique makes use of a linear integral equation of the first kind, written with reference to the defect-free solid and features a kernel constructed form the measurements of the scattered field. A particular property of the latter equation, that makes it suitable for solving scattering problems, resides in the fact that the norm of its solution, used as an obstacle indicator, remains bounded for sampling points lying inside the support of the scatterers and "blows up" otherwise. This method, that does not require any prior information on the geometries or physical properties of a hidden obstacles (or a set thereof), was initially introduced in far-field acoustic inverse scattering (Colton and Kirsch, 1996; Kirsch, 1998; Colton et al., 2000) involving impenetrable or penetrable obstacles, and then extended to electromagnetic (Colton and Monk, 1998; Colton et al., 2003; Haddar and Monk, 2002; Cakoni and Colton, 2004) and elastodynamic problems (Arens, 2001; Charalambopoulos et al., 2002; Nintcheu Fata and Guzina, 2004; Guzina and Madyarov, 2007) in various configurations.

Overview of the thesis

The present study focuses on the advancement of the TS and LSM approaches to inverse scattering within the framework of the mechanics of deformable solids, i.e. inverse scattering problems in elastic (and acoustic) media. The main lines for this research work are:

- Examination of the methods' capabilities and performance especially when deployed in the context of classical forward solvers such as finite element models.

- Application of the TS and LSM techniques toward *combined* (geometric and material) qualitative characterization of a variety of material defects (e.g. cracks, inclusions, cavities) "hidden" in a given reference solid.

- Extension of these methods toward time-domain or multi-frequency treatment of inverse scattering problems.

- Investigation of the fundamental theoretical questions (e.g. those of uniqueness and existence) raised by the development of the Linear Sampling Method.

- Investigation of the theoretical link between the Topological Sensitivity and Linear Sampling Methods.

In light of the above topics and issues, the present work resides at the interface of theoretical solid mechanics and applied mathematics, while including a number of relevant numerical applications.

The research described in this dissertation has been performed within the framework of a joint Ph.D. program between the *Solid Mechanics Laboratory* at *Ecole Polytechnique (France)* and the *Department of Civil Engineering* of the *University of Minnesota (USA)*. The work has roughly been distributed as follows: the study of the *Topological Sensitivity Method* at *Ecole Polytechnique* under the supervision of Marc Bonnet, and that of the *Linear Sampling Method* with Bojan Guzina at the *University of Minnesota*. Both studies have progressed, to a large extent, independently of one another. They, however, constitute two approaches towards a common goal, namely that of advancing non-iterative, qualitative methods for inverse scattering. Moreover, a preliminary comparative study is conducted in the last chapter.

This dissertation is divided into three parts. Parts I and II address the two featured qualitative methods (TS and LSM), while Part III discusses and compares some of their common features via selected analytical solutions. Each part includes chapters that are *self-contained* in the sense that each chapter is either a published article or a journal paper in preparation. Where applicable, appendices appearing in the referenced ("mother") papers are also included in this thesis for clarity and ease of reading.

Part I. The first part of this dissertation is dedicated to the Topological Sensitivity Method for solving inverse scattering problems in solid bodies formulated in the time-domain. Chapter 1, which essentially reproduces article [3], presents a comprehensive numerical investigation of the method designed to evaluate its performance within the framework of a conventional finite-element (FEM) computational platform, and employed to deal with three-dimensional identification and reconstruction of internal cavities. Chapter 2 presents a novel topological sensitivity analysis for the identification of three-dimensional cracks in homogeneous or bimaterial elastic bodies. The theoretical developments presented are an extension of the method to this problem and the study includes a set of numerical results. An early version

of the work presented in this chapter appeared in the short article [4], a full-length journal paper [6] being in the final stages of preparation.

Part II.   The second part deals with the Linear Sampling Method. Chapter 3, corresponding to the article [1], investigates a multi-frequency formulation of the method for the reconstruction of obstacles illuminated by acoustic waves and conveniently provides a comprehensive presentation of how inverse scattering problems can be addressed by the linear sampling method. In the context of penetrable scatterers, this method (as well as the *factorization method*) has exposed the need to study and understand a non-traditional boundary value problem, termed the *interior transmission problem*. Chapter 4, that corresponds to article [2], is dedicated to the study of existence and uniqueness of a solution to this problem in elasticity, and highlights some of its particular features when dealing with viscoelastic and piecewise-homogeneous materials. Chapter 5, ending Part II, represents a generalization of the study of this problem – interpreted as an eigenvalue problem, and is currently in its final stages of preparation as a journal article [5].

Part III.   The third part of this dissertation is composed of a single chapter, Chapter 6, which represents an attempt to deepen the understanding of the TS and LSM techniques, and to establish a fundamental link between the two. This last investigation is based on an analytical example of scattering by a spherical obstacle which permits both (TS and LSM) indicator functions to be derived in an explicit form.

Summary of contributions.   The main contributions of this work are:

- A comprehensive simulation campaign that aims at validating and highlighting the effectiveness of the use of the Topological Sensitivity Method toward the elastodynamic reconstruction of material defects (cavities) from transient scattered waveforms within the framework of finite element methods. To our best knowledge, it constitutes the first comprehensive numerical study of TS-based defect identification methodology in time-dependent 3D settings and implemented within general-purpose computational environments.

- Extension of the Topological Sensitivity Method to deal with 3D inverse scattering by cracks, including the formulation of the required previously unavailable, *polarization tensor* and the proposition of an original methodology for a qualitative reconstruction of cracks.

- Study of the *interior transmission problem*, a non-conventional boundary value problem underpinning the Linear Sampling Method. The existence and uniqueness results, which are fundamental for establishing the validity of the LSM, have been established and certain particular features of this problem in viscoelastic bodies have been emphasized. This study also provides a theoretical framework that enables, for the first time, a qualitative identification of the material properties of the elastic scatterers via the LSM.

- Formulation of a multi-frequency approach of the Linear Sampling Method. The personal contribution is concerned with validation, via analytical and numerical examples, of the proposed methodology.

- Development of a platform that aims at exposing possible theoretical links between the TS and LSM approaches to inverse scattering. The proposed study relies on a canonic example allowing

i) the analytical implementation of both indicator functions, and ii) the generation of quantitative reconstruction results which, in of themselves, permit one-to-one comparison between the two methods. The issue of comprehensive (geometric and material) characterization of internal scatterers, i.e. defects, is also addressed there. This attempt to provide better understanding of the methods led to interesting preliminary results, but an in-depth analysis is still needed for significant advances on the subject.

Published referred papers.

[1]   Guzina, B. B., Cakoni, F. and Bellis, C (2010). On the multi-frequency reconstruction of Dirichlet and penetrable obstacles by the linear sampling method. *Inverse Problems*, 26: 125005.

[2]   Bellis, C. and Guzina, B. B. (2010). On the existence and uniqueness of a solution to the interior transmission problem for piecewise-homogeneous solids. *Journal of Elasticity*, 101:29–57.

[3]   Bellis, C. and Bonnet, M. (2010). A FEM-based topological sensitivity approach for fast qualitative identification of buried cavities from elastodynamic overdetermined boundary data. *Int. J. Solids and Struct.*, 47:1221–1242.

[4]   Bellis, C. and Bonnet, M. (2009). Crack identification by 3D time-domain elastic or acoustic topological sensitivity. *Comptes Rendus Mécanique*, 337:124–130.

Papers in preparation.

[5]   Bellis, C., Cakoni, F. and Guzina, B. B. Nature of the transmission eigenvalue spectrum for elastic bodies. *Submitted*.

[6]   Bellis, C. and Bonnet, M. Qualitative identification of cracks using 3D elastodynamic topological sensitivity.

[7]   Bellis, C., Bonnet, M. and Guzina, B. B. Analytical and numerical studies of topological sensitivity and linear sampling methods in acoustic inverse scattering.

Part I

Topological Sensitivity Method

Introduction and Overview

Identification of flaws embedded in three-dimensional elastic solids, in situations where overdetermined boundary data are available, is a challenging problem arising in a number of applications. Qualitative and non-iterative methods centered around the development of indicator functions of hidden defects are of particular relevance in 3D configurations with dynamical measurements since conventional identification methodologies, based on the minimization of a cost functional $\mathbb{J}(D)$ which quantifies the misfit between a measured quantity and its counterpart for a trial defect configuration D, entail high computational costs due to the need for repeated elastodynamic forward solutions.

In this part, defect indicator functions are defined on the basis of the *topological sensitivity* (TS) of the featured misfit function. Initially introduced for topology optimization (Jackowska-Strumillo et al., 2002), the TS concept stems from the quantification of the perturbation induced to the misfit functional by the creation of a flaw $D_{\varepsilon,\boldsymbol{z}}$ of infinitesimal linear size ε at a prescribed sampling location $\boldsymbol{z}$ inside the reference solid. The TS concept then naturally arises from the asymptotic analysis (in terms of the vanishingly small size of the trial defect) of the misfit functional, which takes the general form

$$\mathbb{J}(D_{\varepsilon,\boldsymbol{z}}) = \mathbb{J}(\emptyset) + \eta(\varepsilon)\mathbb{T}(\boldsymbol{z}) + o(\eta(\varepsilon))$$

where $\eta(\varepsilon)$ quantifies the asymptotic behavior of $\mathbb{J}(D_{\varepsilon,\boldsymbol{z}})$ as $\varepsilon \to 0$ and is such that $\lim_{\varepsilon \to 0} \eta(\varepsilon) = 0$, and the function $\mathbb{T}(\boldsymbol{z})$ is the TS (or topological gradient) of $\mathbb{J}$. The asymptotic behavior $\eta(\varepsilon)$ and the precise form of the TS function $\mathbb{T}(\boldsymbol{z})$ depend on the assumed nature and shape of the vanishing trial defect, with $\eta(\varepsilon) = \varepsilon^3$ for traction-free cavities or cracks and for perfectly-bonded penetrable inclusions. The most pronounced negative values of $\mathbb{T}(\boldsymbol{z})$ correspond to locations where the nucleation of a small flaw would induce the most pronounced decrease of $\mathbb{J}$, i.e. improve the fit with the measurements. For this reason, the TS function $\mathbb{T}(\boldsymbol{z})$ is used as a defect indicator function. Over the last few years the topological sensitivity method has been investigated in elasticity in problems involving different types of defects (Garreau et al., 2001; Bonnet and Guzina, 2004; Guzina and Bonnet, 2004; Chikichev and Guzina, 2008).

In Chapter 1, a time-domain topological sensitivity (TS) approach is developed for elastic-wave imaging of media of arbitrary geometry. The TS, which quantifies the sensitivity of the misfit cost functional to the creation at a specified location of an infinitesimal hole, is expressed in terms of the time convolution of the free field and a supplementary adjoint field as a function of that specified location. Following previous studies performed under (mostly) static or time-harmonic conditions, the TS field is here considered as a natural and computationally efficient approach for defining a defect indicator function. This study emphasizes the implementation and exploitation of TS fields using standard displacement-based FEM approaches, a straightforward task once the correct sensitivity formulation is available. A comprehensive set of numerical experiments on 3D and 2D elastodynamic and acoustic configurations is reported, allowing to assess and highlight many features of the proposed TS-based fast

qualitative identification such as its ability to identify multiple defects and its robustness against data noise.

In Chapter 2, the topological sensitivity is derived for three-dimensional crack identification exploiting over-determined transient elastodynamic boundary data. Simple and efficient adjoint-state based formulations are proposed in elasticity and acoustics, enhanced by the recourse to closed-form expressions of a polarization tensor arising in the featured asymptotic analysis when the trial small crack is circular or elliptic. This approach, which allows a qualitative reconstruction of cracks in terms of their location and orientation, is implemented within a conventional FEM platform. Extensive 3D time-domain numerical experiments highlight its usefulness and performance.

Chapter 1

FEM-based topological sensitivity method for cavity identification

Contents

1.1   Introduction

Defect identification using TS under transient dynamical conditions have so far been the subject of only a few investigations, notably Dominguez et al. (2005) where the connection with time-reversal is explored, Bonnet (2006) in which an adjoint-based form of the TS is derived for 3D elastodynamics and acoustics, Malcolm and Guzina (2008) and Chikichev and Guzina (2008) where the case of penetrable inclusions in acoustic and elastic media (respectively) is considered, and Bellis and Bonnet (2009) which is devoted to a specialized formulation for crack identification problems. This chapter addresses defect identification in elastic solids by means of the TS function defined for small-cavity nucleation in the context of 3D time-domain elastodynamics. In a previous publication (Bonnet, 2006), the TS function was obtained as a bilinear expression featuring the (time-forward) free field and the (time-backward) adjoint solution by considering the asymptotic behavior of a system of governing integral equations based on the transient full-space elastodynamic Green's tensor, the corresponding (analogous and simpler) formulation for scalar waves was derived as a by-product, and a semi-analytical example based on transient 3D acoustic data was presented. As in many other derivations of TS formulations published thus far, the integral-equation setting is convenient for performing the mathematical asymptotic analysis but is then just one of several possible approaches for doing numerical computations once the necessary formulae are established.

The intended contributions of this chapter are twofold. Firstly, on the theoretical side, the derivation of the TS field proposed in Bonnet (2006) is clarified and extended as follows: (a) the validity of the previously-established asymptotic behavior of the time-domain governing integral equation (and hence of the resulting TS formulation) is shown to depend on smoothness assumptions on the free field, an issue not touched upon in Bonnet (2006); (b) a simpler and more compact version of the derivation, using Green's tensors rather than full-space fundamental solutions, is presented; (c) proofs are also given for two-dimensional problems. Secondly, a comprehensive set of numerical experiments, including 3D elastodynamic examples, is reported and discussed. Unlike previous publications where the time-domain TS is computed by means of specialized techniques based on Green's tensors, this study emphasizes the implementation and exploitation of TS fields using the standard displacement-based FEM, and indeed the ease of doing so once the correct sensitivity formulation is available. To the authors' best knowledge, this chapter presents the first comprehensive numerical study of TS-based defect identification methodology in time-dependent 3D settings and implemented within general-purpose computational environments.

This chapter is organized as follows. The forward and inverse problems of interest are reviewed in Section 1.2. Topological sensitivity is defined and established, in both direct and adjoint-based forms, in Section 1.3, the more technical parts of the derivations being deferred to 1.A for ease of reading. Section 1.4 then discusses some important features of the methodology and introduces additional concepts and notations pertaining to the FEM-based implementation and its exploitation in subsequently presented numerical results. Then, the results of FEM-based numerical experiments are presented and discussed in Sections 1.5 (2D scalar wave equation) and 1.6 (3D and 2D elastodynamics).

1.2   Cavity identification model problem

Let Ω denote a finite elastic body in $\mathbb{R}^d$ ($d = 3$ or $d = 2$), bounded by the external surface S and characterized by the shear modulus μ, Poisson's ratio ν and mass density ρ, and referred in the following as the *reference body*. A cavity (or a set thereof) B bounded by the closed traction-free surface(s) Γ is

embedded in Ω. The external surface S, which is identical for the reference domain Ω and the cavitated domain $\Omega(B) = \Omega \setminus B$, is split into a Neumann part S_{N} and a Dirichlet part S_{D}, respectively associated with prescribed time-varying tractions $\boldsymbol{t}_{\mathrm{N}}$ and displacements $\boldsymbol{u}_{\mathrm{D}}$. Under this dynamical loading, an elastodynamic state $\boldsymbol{u}_B$ arises in $\Omega(B)$, which satisfies the following set of field equations, boundary and initial conditions (hereinafter referred to for generic B as $\mathcal{P}(B)$):

$$\mathcal{P}(B) : \begin{aligned} \left[\mathcal{L}\boldsymbol{u}_B\right](\boldsymbol{\xi},t) &= \boldsymbol{0} & (\boldsymbol{\xi} \in \Omega(B), t \geqslant 0) \\ \boldsymbol{t}[\boldsymbol{u}_B](\boldsymbol{\xi},t) &= \boldsymbol{0} & (\boldsymbol{\xi} \in \Gamma, t \geqslant 0) \\ \boldsymbol{t}[\boldsymbol{u}_B](\boldsymbol{\xi},t) &= \boldsymbol{t}_{\mathrm{N}}(\boldsymbol{\xi},t) & (\boldsymbol{\xi} \in S_{\mathrm{N}}, t \geqslant 0) \\ \boldsymbol{u}_B(\boldsymbol{\xi},t) &= \boldsymbol{u}_{\mathrm{D}}(\boldsymbol{\xi},t) & (\boldsymbol{\xi} \in S_{\mathrm{D}}, t \geqslant 0) \\ \boldsymbol{u}_B(\boldsymbol{\xi},0) = \dot{\boldsymbol{u}}_B(\boldsymbol{\xi},0) &= \boldsymbol{0} & (\boldsymbol{\xi} \in \Omega(B)) \end{aligned} \tag{1.2.1}$$

where $\boldsymbol{\xi}$ and t denotes the position vector and the time; $\mathcal{L}$ denotes the governing Navier space-time partial differential operator defined by

$$\mathcal{L}\boldsymbol{w}(\boldsymbol{\xi},t) = \boldsymbol{\nabla} \cdot \boldsymbol{\sigma}[\boldsymbol{w}](\boldsymbol{\xi},t) - \rho\ddot{\boldsymbol{w}}(\boldsymbol{\xi},t) \tag{1.2.2}$$

where $\boldsymbol{\sigma}[\boldsymbol{w}] = \boldsymbol{\mathcal{C}} : \boldsymbol{\nabla}\boldsymbol{w}$ denotes the elastic stress tensor associated with a displacement $\boldsymbol{w}$, the fourth-order elasticity tensor $\boldsymbol{\mathcal{C}}$ being given (for isotropic materials) by

$$\boldsymbol{\mathcal{C}} = 2\mu\left[\boldsymbol{\mathcal{I}}^{\mathrm{sym}} + \frac{\nu}{1-2\nu}\boldsymbol{I} \otimes \boldsymbol{I}\right] \tag{1.2.3}$$

(with $\boldsymbol{\mathcal{I}}^{\mathrm{sym}}$ and $\boldsymbol{I}$ respectively denoting the symmetric fourth-order and the second-order identity tensors), $\boldsymbol{t}[\boldsymbol{w}] = \boldsymbol{\sigma}[\boldsymbol{w}] \cdot \boldsymbol{n}$ is the traction vector associated with $\boldsymbol{w}$ ($\boldsymbol{n}$ being the unit normal on $S \cup \Gamma$ oriented outward from $\Omega(B)$), and $\dot{(\ )}$ and $\ddot{(\ )}$ indicate first- and second-order time derivatives.

Cavity identification problem. The location, topology and geometry of an unknown cavity system B^{true} (or equivalently Γ^{true}) is sought by exploiting measured values of the response of the flawed solid $\Omega^{\mathrm{true}} = \Omega(B^{\mathrm{true}})$ arising due to the probing excitation. Specifically, the displacement $\boldsymbol{u}^{\mathrm{obs}}$ induced in Ω^{true} by $(\boldsymbol{u}_{\mathrm{D}}, \boldsymbol{t}_{\mathrm{N}})$ is monitored over the measurement surface $S^{\mathrm{obs}} \subset S_{\mathrm{N}}$ and time interval $t \in [0,T]$ (other possibilities, e.g. finite sets of measurement locations and/or times, being also allowed by the ensuing treatment). Ideally, a defect configuration B^{true} such that

$$\boldsymbol{u}^{\mathrm{true}}(\boldsymbol{\xi},t) = \boldsymbol{u}^{\mathrm{obs}}(\boldsymbol{\xi},t) \qquad (\boldsymbol{\xi} \in S^{\mathrm{obs}}, \ 0 \leqslant t \leqslant T) \tag{1.2.4}$$

is sought, where $\boldsymbol{u}^{\mathrm{true}}$ solves problem $\mathcal{P}(B^{\mathrm{true}})$ defined by (1.2.1). In practice, due to many factors (e.g. incomplete and/or inexact measurements, modelling uncertainties), the cavity is sought so as to minimize a misfit cost functional which is naturally (in the present context) expressed as a double integral over the measurement surface and the experiment duration:

$$\mathbb{J}(\Omega(B),T) = \int_0^T \int_{S^{\mathrm{obs}}} \varphi[\boldsymbol{u}_B(\boldsymbol{\xi},t),\boldsymbol{\xi},t] \, \mathrm{d}S_{\boldsymbol{\xi}} \, \mathrm{d}t \tag{1.2.5}$$

where $\Omega(B)$ is a trial cavitated solid defined by the trial cavity B, $\boldsymbol{u}_B$ solves problem $\mathcal{P}(B)$ defined by (1.2.1), and the misfit function φ is chosen so as to define a distance between $\boldsymbol{u}_B$ and $\boldsymbol{u}^{\mathrm{obs}}$. Numerical experiments presented herein are based on the commonly-used least squares misfit function:

$$\varphi[\boldsymbol{w},\boldsymbol{\xi},t] = \frac{1}{2}|\boldsymbol{w} - \boldsymbol{u}^{\mathrm{obs}}(\boldsymbol{\xi},t)|^2 \tag{1.2.6}$$

1.3 Topological sensitivity

1.3.1 Small-cavity asymptotics

The topological sensitivity of the cost functional (1.2.5) is defined as its sensitivity with respect to the creation of an infinitesimal object of characteristic size ε at a given location $\boldsymbol{z}$ in Ω. Here, such infinitesimal object is taken to be a trial cavity $B_\varepsilon(\boldsymbol{z})$, defined by $B_\varepsilon(\boldsymbol{z}) = \boldsymbol{z} + \varepsilon\mathcal{B}$ in terms of its center $\boldsymbol{z}$, its shape specified by the unit bounded set $\mathcal{B} \subset \mathbb{R}^{\mathrm{d}}$ (with boundary $\mathcal{S}$ and volume $|\mathcal{B}|$) containing the origin, and its radius $\varepsilon > 0$. The corresponding trial cavitated solid is denoted $\Omega_\varepsilon(\boldsymbol{z})$. Following Sokolowski and Zochowski (1999) or Garreau et al. (2001), one seeks the asymptotic behavior of $\mathbb{J}(\Omega_\varepsilon(\boldsymbol{z}), T)$ as $\varepsilon \to 0$ through the expansion:

$$\mathbb{J}(\Omega_\varepsilon(\boldsymbol{z}), T) = \mathbb{J}(\Omega, T) + \eta(\varepsilon)|\mathcal{B}|\mathbb{T}(\boldsymbol{z}, T) + o(\eta(\varepsilon)) \qquad (\varepsilon \to 0) \tag{1.3.1}$$

where the function $\eta(\varepsilon)$, to be determined, vanishes in the limit $\varepsilon \to 0$ and the *topological sensitivity* $\mathbb{T}(\boldsymbol{z}, T)$ is a function of the sampling point $\boldsymbol{z}$ and duration T.

To evaluate the expansion (1.3.1) and find the value of $\mathbb{T}(\boldsymbol{z}, T)$, it is necessary to consider the asymptotic behavior of the displacement $\boldsymbol{u}_\varepsilon$ governed by problem $\mathcal{P}(B_\varepsilon(\boldsymbol{z}))$. Towards that aim, it is convenient to decompose $\boldsymbol{u}_\varepsilon$ as

$$\boldsymbol{u}_\varepsilon(\boldsymbol{\xi}, t) = \boldsymbol{u}(\boldsymbol{\xi}, t) + \boldsymbol{v}_\varepsilon(\boldsymbol{\xi}, t) \tag{1.3.2}$$

where the free field $\boldsymbol{u}$ is the response of the cavity-free domain Ω to the prescribed excitation, i.e.

$$\mathcal{P}(\emptyset) : \begin{array}{ll} \big[\mathcal{L}\boldsymbol{u}\big](\boldsymbol{\xi}, t) = \boldsymbol{0} & (\boldsymbol{\xi} \in \Omega, t \geqslant 0) \\ \boldsymbol{t}[\boldsymbol{u}](\boldsymbol{\xi}, t) = \boldsymbol{t}_{\mathrm{N}}(\boldsymbol{\xi}, t) & (\boldsymbol{\xi} \in S_{\mathrm{N}}, t \geqslant 0) \\ \boldsymbol{u}(\boldsymbol{\xi}, t) = \boldsymbol{u}_{\mathrm{D}}(\boldsymbol{\xi}, t) & (\boldsymbol{\xi} \in S_{\mathrm{D}}, t \geqslant 0) \\ \boldsymbol{u}(\boldsymbol{\xi}, 0) = \dot{\boldsymbol{u}}(\boldsymbol{\xi}, 0) = \boldsymbol{0} & (\boldsymbol{\xi} \in \Omega) \end{array} \tag{1.3.3}$$

while the scattered field $\boldsymbol{v}_\varepsilon$ solves

$$\begin{array}{ll} \big[\mathcal{L}\boldsymbol{v}_\varepsilon\big](\boldsymbol{\xi}, t) = \boldsymbol{0} & (\boldsymbol{\xi} \in \Omega, t \geqslant 0) \\ \boldsymbol{t}[\boldsymbol{v}_\varepsilon](\boldsymbol{\xi}, t) = -\boldsymbol{t}[\boldsymbol{u}](\boldsymbol{\xi}, t) & (\boldsymbol{\xi} \in \Gamma_\varepsilon(\boldsymbol{z}), t \geqslant 0) \\ \boldsymbol{t}[\boldsymbol{v}_\varepsilon](\boldsymbol{\xi}, t) = \boldsymbol{0} & (\boldsymbol{\xi} \in S_{\mathrm{N}}, t \geqslant 0) \\ \boldsymbol{v}_\varepsilon(\boldsymbol{\xi}, t) = \boldsymbol{0} & (\boldsymbol{\xi} \in S_{\mathrm{D}}, t \geqslant 0) \\ \boldsymbol{v}_\varepsilon(\boldsymbol{\xi}, 0) = \dot{\boldsymbol{v}}_\varepsilon(\boldsymbol{\xi}, 0) = \boldsymbol{0} & (\boldsymbol{\xi} \in \Omega), \end{array} \tag{1.3.4}$$

with $\Gamma_\varepsilon(\boldsymbol{z})$ denoting the boundary of $B_\varepsilon(\boldsymbol{z})$. Since the scattered field is expected to vanish for infinitesimal cavities, i.e. $\|\boldsymbol{v}_\varepsilon(\boldsymbol{\xi}, t)\| = o(\varepsilon)$, expansion (1.3.1) is sought by invoking the first-order Taylor expansion of φ with respect to its first argument. The topological sensitivity $\mathbb{T}(\boldsymbol{z}, T)$ and the leading asymptotic behavior $\eta(\varepsilon)$ are thus to be identified on the basis of:

$$\int_0^T \int_{S^{\mathrm{obs}}} \frac{\partial\varphi}{\partial\boldsymbol{u}}[\boldsymbol{u}(\boldsymbol{\xi}, t), \boldsymbol{\xi}, t]\boldsymbol{v}_\varepsilon(\boldsymbol{\xi}, t) \, \mathrm{d}S_\xi \, \mathrm{d}t = \eta(\varepsilon)|\mathcal{B}|\mathbb{T}(\boldsymbol{z}, T) + o\big(\eta(\varepsilon)\big) \tag{1.3.5}$$

In what follows, emphasis will be given to the 3D case.

1.3.2 Leading contribution of v_ε as $\varepsilon \to 0$

To address this issue, it is convenient to reformulate the governing boundary-initial problem (1.3.4) in terms of an integral equation. Let $U(x, t, \xi)$ and $T(x, t, \xi; n)$ denote the time-impulsive elastodynamic Green's tensors, defined such that $e_k \cdot U(x, t, \xi)$ and $e_k \cdot T(x, t, \xi)$ are the displacement and traction vectors at $\xi \in \Omega$ resulting from a unit time-impulsive point force acting at x in the k-th direction at time $t = 0$ and satisfying the boundary conditions

$$U(x, t, \xi) = 0 \ \ (\xi \in S_D, t \geqslant 0), \qquad T(x, t, \xi; n) = 0 \ \ (\xi \in S_N, t \geqslant 0), \tag{1.3.6}$$

One also defines the elastodynamic *full-space* fundamental tensors $U_\infty(x, t, \xi)$ and $T_\infty(x, t, \xi; n)$ in a similar way, replacing boundary conditions (1.3.6) with decay and radiation conditions at infinity (Eringen and Suhubi, 1975, see Section 1.A.2). The governing integral equation for the scattered field v_ε then reads (see Section 1.A.1)

$$\frac{1}{2} v_\varepsilon(x, t) + \fint_{\Gamma_\varepsilon(z)} T(x, t, \xi; n) \star v_\varepsilon(\xi, t) \, \mathrm{d}S_\xi = - \int_{\Gamma_\varepsilon(z)} U(x, t, \xi) \star t(\xi, t) \, \mathrm{d}S_\xi$$
$$(x \in \Gamma_\varepsilon(z), \ t \geqslant 0), \quad (1.3.7)$$

in which $\fint$ indicates a (strongly singular) integral defined in the Cauchy principal value (CPV) sense and $\star$ denotes the time convolution at instant $t \geqslant 0$ defined by

$$[a \star b](\xi, t) = \int_0^t a(\xi, \tau) \cdot b(\xi, t - \tau) \, \mathrm{d}\tau. \tag{1.3.8}$$

where the inner product appearing in the integral is such that $a \cdot b$ is a tensor of the lowest possible order (e.g. $U \star t$ has order 1, $\nabla u \star \sigma[v]$ is a scalar), and generic tensor fields a and b respectively verify initial and final conditions

$$a(\cdot, \tau) = \dot{a}(\cdot, \tau) = 0 \ \ (\tau \leqslant 0), \qquad b(\cdot, \tau) = \dot{b}(\cdot, \tau) = 0 \ \ (\tau \geqslant t) \tag{1.3.9}$$

Equations governing the leading contribution of v_ε on $\Gamma_\varepsilon(z)$ as $\varepsilon \to 0$ are sought as the asymptotic form of integral equation (1.3.7). For this purpose, scaled coordinates $\bar{x}$ or $\bar{\xi}$, defined by

$$\bar{x} = (x - z)/\varepsilon, \quad \bar{\xi} = (\xi - z)/\varepsilon \qquad (x, \xi \in \Gamma_\varepsilon(z), \ \bar{x}, \bar{\xi} \in \mathcal{S}) \tag{1.3.10}$$

are introduced. Consequently, the volume and surface differential elements in ξ-space are rescaled according to

$$\text{(a)} \ \ \mathrm{d}V_\xi = \varepsilon^3 \, \mathrm{d}V_{\bar{\xi}}, \qquad \text{(b)} \ \ \mathrm{d}S_\xi = \varepsilon^2 \, \mathrm{d}S_{\bar{\xi}} \qquad (\xi \in \Gamma_\varepsilon(z), \bar{\xi} \in \mathcal{S}) \tag{1.3.11}$$

where $\mathrm{d}V_{\bar{\xi}}$, $\mathrm{d}S_{\bar{\xi}}$ denote corresponding volume and surface differential elements on $\mathcal{B}$ and $\mathcal{S}$, respectively. The leading behavior as $\varepsilon \to 0$ of the right- and left-hand sides of integral equation (1.3.7) are then given by the following Lemmas 1 and 2, whose proof is given in Section 1.A.2.

Lemma 1. *Assume that $\tau \mapsto \nabla u(\xi, \tau)$ is Lipschitz-continuous (uniformly for ξ in a neighbourhood of z) and differentiable in a neighbourhood of $\tau = t$. Then, one has*

$$\int_{\Gamma_\varepsilon(z)} U(x, t, \xi) \star t(\xi, t) \, dS_\xi = \varepsilon \left\{ \int_\mathcal{S} U_\infty(\bar{x}, \bar{\xi}) \otimes n(\bar{\xi}) \, dV_{\bar{\xi}} \right\} : \sigma[u](z, t) + o(\varepsilon) \quad (x \in \Gamma_\varepsilon(z))$$
$$(1.3.12)$$

where $U_\infty(\bar{x}, \bar{\xi})$ is the elastostatic *full-space (Kelvin) fundamental displacement, given by (1.A.12).*

Lemma 2. *Let the vector function $\bar{\boldsymbol{v}}_\varepsilon(\bar{\boldsymbol{\xi}},t)$ be defined by $\bar{\boldsymbol{v}}_\varepsilon(\bar{\boldsymbol{\xi}},t) = \boldsymbol{v}_\varepsilon(\boldsymbol{\xi},t)$, with $\bar{\boldsymbol{\xi}}$ and $\boldsymbol{\xi}$ related through (1.3.10). Then, one has*

$$\fint_{\Gamma_\varepsilon(z)} \boldsymbol{T}(\boldsymbol{x},t,\boldsymbol{\xi};\boldsymbol{n}) \star \boldsymbol{v}_\varepsilon(\boldsymbol{\xi},t)\, dS_\xi = \fint_{\mathcal{S}} \boldsymbol{T}_{\infty,\varepsilon}(\bar{\boldsymbol{x}},t,\bar{\boldsymbol{\xi}};\boldsymbol{n}) \star \bar{\boldsymbol{v}}_\varepsilon(\bar{\boldsymbol{\xi}},t)\, dS_{\bar{\xi}} + o(\|\bar{\boldsymbol{v}}_\varepsilon(\cdot,t)\|) \quad (\boldsymbol{x} \in \Gamma_\varepsilon(z))$$

(1.3.13)

where $\boldsymbol{T}_{\infty,\varepsilon}$ is the full-space *elastodynamic fundamental traction tensor defined in terms of rescaled wave velocities c_L/ε, c_T/ε and $\|\bar{\boldsymbol{v}}_\varepsilon(\cdot,t)\|$ is a norm of $\bar{\boldsymbol{\xi}} \mapsto \bar{\boldsymbol{v}}_\varepsilon(\bar{\boldsymbol{\xi}},t)$, e.g. its L^2-norm on $\mathcal{S}$.*

Lemma 1 means that the leading contribution to the right-hand side of integral equation (1.3.7) as $\varepsilon \to 0$ has a special structure wherein the time variable t and the (normalized) space variable $\bar{\boldsymbol{x}}$ are separated. Lemma 2 indicates that the left-hand side of integral equation (1.3.7) is of order $O(\|\boldsymbol{v}_\varepsilon\|)$ as $\varepsilon \to 0$. Lemmas 1 and 2 together thus suggest to seek the leading contribution to $\bar{\boldsymbol{v}}_\varepsilon(\bar{\boldsymbol{\xi}},\tau) = \boldsymbol{v}_\varepsilon(\boldsymbol{\xi},\tau)$ as $\varepsilon \to 0$ in the following form, in which the third-order tensor function $\bar{\boldsymbol{\xi}} \in \mathcal{S} \mapsto \boldsymbol{\mathcal{V}}(\bar{\boldsymbol{\xi}})$ is to be determined:

$$\bar{\boldsymbol{v}}_\varepsilon(\bar{\boldsymbol{\xi}},t) = \varepsilon \boldsymbol{\mathcal{V}}(\bar{\boldsymbol{\xi}}) : \boldsymbol{\sigma}[\boldsymbol{u}](\boldsymbol{z},t) + o(\varepsilon) \quad (\boldsymbol{\xi} \in \Gamma_\varepsilon(z), \bar{\boldsymbol{\xi}} \in \mathcal{S}). \tag{1.3.14}$$

Lemma 3. *Let $\bar{\boldsymbol{v}}_\varepsilon(\bar{\boldsymbol{\xi}},t)$ be of form (1.3.14) for some $\boldsymbol{\mathcal{V}}(\bar{\boldsymbol{\xi}})$. Under the assumptions of Lemma 1, one has*

$$\fint_{\Gamma_\varepsilon(z)} \boldsymbol{T}(\boldsymbol{x},t,\boldsymbol{\xi};\boldsymbol{n}) \star \boldsymbol{v}_\varepsilon(\boldsymbol{\xi},t)\, dS_\xi = \varepsilon \left\{ \fint_{\mathcal{S}} \boldsymbol{T}_\infty(\bar{\boldsymbol{x}},\bar{\boldsymbol{\xi}};\boldsymbol{n}) \cdot \boldsymbol{\mathcal{V}}(\bar{\boldsymbol{\xi}})\, dS_{\bar{\xi}} \right\} : \boldsymbol{\sigma}[\boldsymbol{u}](\boldsymbol{z},t) + o(\varepsilon) \quad (\boldsymbol{x} \in \Gamma_\varepsilon(z))$$

(1.3.15)

where $\boldsymbol{T}_\infty(\bar{\boldsymbol{x}},\bar{\boldsymbol{\xi}};\boldsymbol{n})$ is the traction associated with the elastostatic Kelvin solution, given by (1.A.22).

Proof. See Section 1.A.2. □

Combining lemmas 1 and 3, one finds that representation (1.3.14) indeed holds provided that $\boldsymbol{\mathcal{V}}$ solves the integral equation

$$\frac{1}{2}\boldsymbol{\mathcal{V}}(\bar{\boldsymbol{x}}) + \fint_{\mathcal{S}} \boldsymbol{T}_\infty(\bar{\boldsymbol{x}},\bar{\boldsymbol{\xi}};\boldsymbol{n}) \cdot \boldsymbol{\mathcal{V}}(\bar{\boldsymbol{\xi}})\, \mathrm{d}S_{\bar{\xi}} = -\int_{\mathcal{S}} \boldsymbol{U}_\infty(\bar{\boldsymbol{x}},\bar{\boldsymbol{\xi}}) \otimes \boldsymbol{n}(\bar{\boldsymbol{\xi}})\, \mathrm{d}S_{\bar{\xi}} \qquad (\bar{\boldsymbol{x}} \in \mathcal{S}) \tag{1.3.16}$$

Upon inspection, (1.3.16) can in fact be interpreted as an integral equation formulation governing the solutions $\boldsymbol{\mathcal{V}}_{k\ell} = \boldsymbol{\mathcal{V}}_{\ell k} = (\boldsymbol{e}_k \otimes \boldsymbol{e}_\ell) : \boldsymbol{\mathcal{V}}$ to a set of six canonical *elastostatic* exterior problems

$$\begin{aligned}
\nabla_{\bar{\xi}} \cdot (\boldsymbol{\mathcal{C}} : \nabla_{\bar{\xi}} \boldsymbol{\mathcal{V}}_{k\ell})(\bar{\boldsymbol{\xi}}) &= \boldsymbol{0} & (\bar{\boldsymbol{\xi}} \in \mathbb{R}^3 \setminus \mathcal{B}), \\
(\boldsymbol{\mathcal{C}} : \nabla_{\bar{\xi}} \boldsymbol{\mathcal{V}}_{k\ell})(\bar{\boldsymbol{\xi}}) \cdot \boldsymbol{n}(\bar{\boldsymbol{\xi}}) &= -\frac{1}{2}(n_k(\bar{\boldsymbol{\xi}})\boldsymbol{e}_\ell + n_\ell(\bar{\boldsymbol{\xi}})\boldsymbol{e}_k) & (\bar{\boldsymbol{\xi}} \in \mathcal{S})
\end{aligned} \qquad 1 \leqslant k \leqslant \ell \leqslant 3 \tag{1.3.17}$$

which are independent of $\boldsymbol{z}$, ε and time. The tensor function $\boldsymbol{\mathcal{V}}(\bar{\boldsymbol{\xi}})$ is in fact completely defined, through problems (1.3.17), by $\mathcal{B}$.

The scattered field $\boldsymbol{v}_\varepsilon$ at any point of S^{obs} (and more generally at any point away from the trial cavity $B_\varepsilon(z)$) is given by the integral representation formula (see Section 1.A.1):

$$\begin{aligned}
\boldsymbol{v}_\varepsilon(\boldsymbol{x},t) = \int_{B_\varepsilon(z)} &\left\{ \rho \boldsymbol{U}(\boldsymbol{x},t,\boldsymbol{\xi}) \star \ddot{\boldsymbol{u}}(\boldsymbol{\xi},t) + \boldsymbol{E}(\boldsymbol{x},t,\boldsymbol{\xi}) \star \boldsymbol{\sigma}(\boldsymbol{\xi},t) \right\} \mathrm{d}V_\xi \\
&- \int_{\Gamma_\varepsilon(z)} \boldsymbol{T}^k(\boldsymbol{x},t,\boldsymbol{\xi};\boldsymbol{n}) \star \boldsymbol{v}_\varepsilon(\boldsymbol{\xi},t)\, \mathrm{d}S_\xi \qquad (\boldsymbol{x} \in S^{\text{obs}},\ t \geqslant 0), \quad (1.3.18)
\end{aligned}$$

where $\boldsymbol{E}(\boldsymbol{x}, t, \boldsymbol{\xi})$ denotes the strain associated with $\boldsymbol{U}(\boldsymbol{x}, t, \boldsymbol{\xi})$. Expanding the first integral by means of (1.3.11a) and a Taylor expansion of the densities about $\boldsymbol{\xi} = \boldsymbol{z}$, substituting (1.3.14) and introducing scaled coordinates $\bar{\boldsymbol{\xi}}$ into the second integral, one obtains the leading contribution of $\boldsymbol{v}_\varepsilon$ as $\varepsilon \to 0$ as:

$$\boldsymbol{v}_\varepsilon(\boldsymbol{x}, t) = \varepsilon^3 \boldsymbol{W}(\boldsymbol{x}, t; \boldsymbol{z}) + o(\varepsilon^3) \tag{1.3.19}$$

with

$$\boldsymbol{W}(\boldsymbol{x}, t; \boldsymbol{z}) = |\mathcal{B}| \big\{ [\boldsymbol{\mathcal{C}} \!:\! \boldsymbol{E}(\boldsymbol{x}, t, \boldsymbol{z})] \star [\boldsymbol{\mathcal{A}} \!:\! \boldsymbol{\sigma}](\boldsymbol{z}, t) + \rho \dot{\boldsymbol{U}}(\boldsymbol{x}, t, \boldsymbol{z}) \star \dot{\boldsymbol{u}}(\boldsymbol{z}, t) \big\} \tag{1.3.20}$$

and where the constant *polarization tensor* $\boldsymbol{\mathcal{A}}$ depends only on $\mathcal{B}$ (through $\boldsymbol{\mathcal{V}}$) and is defined by

$$\boldsymbol{\mathcal{A}} = \boldsymbol{\mathcal{C}}^{-1} - \frac{1}{|\mathcal{B}|} \left\{ \int_{\mathcal{S}} \boldsymbol{n}(\bar{\boldsymbol{\xi}}) \otimes \boldsymbol{\mathcal{V}}(\bar{\boldsymbol{\xi}}) \, \mathrm{d}S_{\bar{\xi}} \right\} \tag{1.3.21}$$

Inserting (1.3.19) into (1.3.5), the TS $\mathbb{T}(\boldsymbol{z}, t)$ and leading behavior $\eta(\varepsilon)$ are then found to be given by

$$\mathbb{T}(\boldsymbol{z}, T) = \int_0^T \int_{S^{\mathrm{obs}}} \frac{\partial \varphi}{\partial \boldsymbol{u}} [\boldsymbol{u}(\boldsymbol{\xi}, t), \boldsymbol{\xi}, t] \cdot \boldsymbol{W}(\boldsymbol{\xi}, t; \boldsymbol{z}) \, \mathrm{d}S_\xi \, \mathrm{d}t, \qquad \eta(\varepsilon) = \varepsilon^3 \tag{1.3.22}$$

Expression (1.3.22) provides a useful basis for discussing some of the features of the time-domain TS, see Section 1.4.1. It can also conceivably be used for the purpose of computing the field $\mathbb{T}(\boldsymbol{z}, T)$, and is indeed so used in Chikichev and Guzina (2008) wherein Ω is an elastic half-space with a traction-free surface, a configuration for which the Green's tensor is known. For arbitrary reference bodies Ω, an implementation of (1.3.22) would require a numerical evaluation of the Green's tensor for source points located on S^{obs} (typically taken as Gauss quadrature points associated with the evaluation of the integral over S^{obs}) and field points taken as sampling points $\boldsymbol{z}$.

However, a computationally more efficient approach for evaluating the field $\mathbb{T}(\boldsymbol{z}, T)$, based on an adjoint solution, is usually preferable and was used for all numerical examples presented thereafter.

1.3.3 Adjoint field formulation

The adjoint formulation, previously presented in Bonnet (2006) and now summarized for completeness, stems from treating the integral in (1.3.5) as one of the terms arising in the elastodynamic reciprocity identity. For any generic domain $\mathcal{O}$ and pair of elastodynamic states $\boldsymbol{u}_1, \boldsymbol{u}_2$ satisfying the homogeneous elastodynamic field equations in $\mathcal{O}$ as well as homogenous initial conditions

$$\boldsymbol{u}_1(\boldsymbol{\xi}, 0) = \dot{\boldsymbol{u}}_1(\boldsymbol{\xi}, 0) = \boldsymbol{0} \quad \text{and} \quad \boldsymbol{u}_2(\boldsymbol{\xi}, 0) = \dot{\boldsymbol{u}}_2(\boldsymbol{\xi}, 0) = \boldsymbol{0} \quad (\boldsymbol{\xi} \in \mathcal{O}),$$

the following reciprocity identity holds (see e.g. Eringen and Suhubi, 1975; Achenbach, 2003):

$$\int_{\partial \mathcal{O}} \{ \boldsymbol{t}[\boldsymbol{u}_1] \star \boldsymbol{u}_2 - \boldsymbol{t}[\boldsymbol{u}_2] \star \boldsymbol{u}_1 \}(\boldsymbol{\xi}, t) \, \mathrm{d}S_\xi = 0 \tag{1.3.23}$$

Defining the adjoint state $\hat{\boldsymbol{u}}$ as the solution of:

$$\begin{aligned}
[\mathcal{L}\hat{\boldsymbol{u}}](\boldsymbol{\xi}, t) &= \boldsymbol{0} & (\boldsymbol{\xi} \in \Omega, 0 \leqslant t \leqslant T) \\
\boldsymbol{t}[\hat{\boldsymbol{u}}](\boldsymbol{\xi}, t) &= \frac{\partial \varphi}{\partial \boldsymbol{u}} [\boldsymbol{u}(\boldsymbol{\xi}, T-t), \boldsymbol{\xi}, T-t] & (\boldsymbol{\xi} \in S^{\mathrm{obs}}, 0 \leqslant t \leqslant T) \\
\boldsymbol{t}[\hat{\boldsymbol{u}}](\boldsymbol{\xi}, t) &= \boldsymbol{0} & (\boldsymbol{\xi} \in S_{\mathrm{N}} \backslash S^{\mathrm{obs}}, 0 \leqslant t \leqslant T) \\
\hat{\boldsymbol{u}}(\boldsymbol{\xi}, t) &= \boldsymbol{0} & (\boldsymbol{\xi} \in S_{\mathrm{D}}, 0 \leqslant t \leqslant T) \\
\hat{\boldsymbol{u}}(\boldsymbol{\xi}, 0) &= \dot{\hat{\boldsymbol{u}}}(\boldsymbol{\xi}, 0) = \boldsymbol{0} & (\boldsymbol{\xi} \in \Omega)
\end{aligned} \tag{1.3.24}$$

using relation (1.3.23) with $\mathcal{O} = \Omega_\varepsilon(\boldsymbol{z})$, $\boldsymbol{u}_1 = \hat{\boldsymbol{u}}$ and $\boldsymbol{u}_2 = \boldsymbol{v}_\varepsilon$ and exploiting the relevant boundary conditions in (1.3.4) and (1.3.24), equation (1.3.5) becomes:

$$\eta(\varepsilon)|\mathcal{B}|\mathbb{T}(\boldsymbol{z},T) + o\big(\eta(\varepsilon)\big) = -\int_{\Gamma_\varepsilon(z)} \{\boldsymbol{t}[\hat{\boldsymbol{u}}] \star \boldsymbol{v}_\varepsilon\}(\boldsymbol{\xi},t)\,\mathrm{d}S_\xi - \int_{\Gamma_\varepsilon(z)} \{\boldsymbol{t}[\boldsymbol{u}] \star \hat{\boldsymbol{u}}\}(\boldsymbol{\xi},t)\,\mathrm{d}S_\xi \quad (1.3.25)$$

On inserting the asymptotic behavior (1.3.14) in the first integral, recasting the second integral as a volume integral over $B_\varepsilon(\boldsymbol{z})$ using the divergence identity, and working out the leading contribution as $\varepsilon \to 0$ in the resulting equality, one arrives at

$$\mathbb{T}(\boldsymbol{z},T) = \{\boldsymbol{\sigma}[\hat{\boldsymbol{u}}] \star (\boldsymbol{\mathcal{A}} : \boldsymbol{\sigma}[\boldsymbol{u}]) + \rho\dot{\hat{\boldsymbol{u}}} \star \dot{\boldsymbol{u}}\}(\boldsymbol{z},T), \qquad \eta(\varepsilon) = \varepsilon^3 \qquad (1.3.26)$$

where the polarization tensor $\boldsymbol{\mathcal{A}}$ is again defined by (1.3.21).

Remark 1. *The $O(\varepsilon^d)$ asymptotic behavior (1.3.26) of $\mathbb{J}(\Omega_\varepsilon(\boldsymbol{z}),T)$ relies on $\boldsymbol{v}_\varepsilon$ approaching (up to a scaling factor) a* static *solution as $\varepsilon \to 0$. This requires the free-field to be sufficiently regular at $(\boldsymbol{z},t)$, e.g. according to the sufficient condition given in Lemmas 1 and 2. To put this another way, the TS (1.3.26) may (invoking the Fourier convolution theorem) be formulated as the inverse Fourier transform of the (previously established in* Bonnet and Guzina, 2004*) frequency-domain expression*

$$\mathbb{T}(\boldsymbol{z},\omega) = \{\boldsymbol{\sigma}[\hat{\boldsymbol{u}}]\!:\!(\boldsymbol{\mathcal{A}} : \boldsymbol{\sigma}[\boldsymbol{u}]) - \rho\omega^2\hat{\boldsymbol{u}}\!\cdot\!\boldsymbol{u}\}(\boldsymbol{z},\omega)$$

The Fourier integral then converges if $\omega \mapsto \mathbb{T}(\boldsymbol{z},\omega) \in L^1(\mathbb{R})$, i.e. provided the high-frequency content of the excitation is limited. Related considerations are developed in Ammari et al. (2009)*, where the order in ε of the leading perturbation by a small inclusion of the fundamental solution of the transient wave equation is shown to depend on the high-frequency content of the time-modulated point source.*

Remark 2. *In a previous article (*Bonnet, 2006*), the small-cavity asymptotics was conducted by relying on estimates*

$$\boldsymbol{U}(\boldsymbol{x},t,\boldsymbol{\xi}) \star \boldsymbol{a}(\boldsymbol{\xi},t) = \frac{1}{\varepsilon}\boldsymbol{U}_\infty(\bar{\boldsymbol{x}},\bar{\boldsymbol{\xi}})\!\cdot\!\boldsymbol{a}(\boldsymbol{z},t) + O(1) \qquad (a)$$
$$\boldsymbol{T}(\boldsymbol{x},t,\boldsymbol{\xi};\boldsymbol{n}) \star \boldsymbol{b}(\boldsymbol{\xi},t) = \frac{1}{\varepsilon^2}\boldsymbol{T}_\infty(\bar{\boldsymbol{x}},\bar{\boldsymbol{\xi}};\boldsymbol{n})\!\cdot\!\boldsymbol{b}(\boldsymbol{z},t) + O(1) \quad (b)$$
$$(\boldsymbol{x},\boldsymbol{\xi} \in \Gamma_\varepsilon(\boldsymbol{z}))$$

(i.e. identities (27) therein) instead of Lemmas 1 and 2, yielding the same result (1.3.26) but in a not entirely correct way: (i) these estimates hold under smoothness conditions on $\boldsymbol{a},\boldsymbol{b}$, similar to the sufficient conditions given in Lemmas 1 and 2, that were not mentioned, and (ii) estimate (b) above is in fact not directly applicable here as it is needed for $\boldsymbol{b}(\boldsymbol{\xi},t) = \boldsymbol{v}_\varepsilon(\boldsymbol{\xi},t)$, which is not defined at $\boldsymbol{\xi} = \boldsymbol{z}$. Lemmas 1 and 2 were therefore needed to fix this flaw in the asymptotic analysis.

Remark 3. *The cavity-identification setting of the model inverse problem formulated in Section 1.2 is consistent with, but does not constitute a mathematical prerequisite for, the small-cavity asymptotics developed in this section. In fact, the latter procedure may in principle be applied to any cost function of format (1.2.5) whatsoever, regardless of its physical meaning or engineering motivation.*

Remark 4. *The same canonical problems (1.3.17) and subsequent polarization tensor (1.3.21) also occur in* Bonnet (2006) *and in a previous frequency-domain formulation of the TS (*Guzina and Bonnet, 2004*).*

Remark 5. *The foregoing analysis has been performed for the 3D case, deemed the most important, but can be reproduced with the necessary adjustments for the 2D case (see 1.A.4), leading to similar results where $\eta(\varepsilon) = \varepsilon^2$ instead of $\eta(\varepsilon) = \varepsilon^3$.*

1.4 Discussion and implementation

1.4.1 Discussion

Topological sensitivity as a defect indicator function. $\mathbb{T}(z, T)$ quantifies the sensitivity of the featured cost functional $\mathbb{J}$ to a perturbation of the reference medium in the form of an infinitesimal cavity at z. It is then natural to consider $\mathbb{T}(z, T)$ as a possible defect indicator function, as was previously done on several occasions (see Section 1.1), whereby actual defects are expected to be located at sampling points z at which $\mathbb{T}(z, T)$ attains its most pronounced negative values, i.e. at which a sufficiently small defect would induce the most pronounced decrease of $\mathbb{J}$. In other words, *infinitesimal* trial cavities placed at such sampling points improve the fit between simulated and actual measurements, and intuition then suggests that *finite* defects having the same location also induce a decrease of the cost function. It is important to emphasize that such exploitation of the information provided by the field $\mathbb{T}(\cdot, T)$ is natural but not backed by a rigorous mathematical proof, despite the fact that the analysis of the cost function leading to the definition and evaluation of $\mathbb{T}(z, T)$ is itself mathematically rigorous. It is however substantiated by various numerical experiments performed for several classes of physical settings (see references given in Section 1.1). The present study aims at contributing to this substantiation within the present context of time-domain elastodynamics, seldom considered in this context, through the examples of Sections 1.5 and 1.6.

Topological sensitivity allows non-iterative approximate global search. Defect identification based on the TS field $\mathbb{T}(\cdot, T)$ of a misfit function has the following important characteristics:

(a) The numerical procedure is non-iterative, as it just requires two solutions evaluated on the reference (defect-free) configuration, namely the free field (1.3.3) and the adjoint field (1.3.24). It is thus computationally much faster than usual iterative optimization-based inversion methods. This non-iterative nature is also one of the main features of the linear sampling method (Arens, 2001; Nintcheu Fata and Guzina, 2007).

(b) The approach is of a qualitative nature, as the underlying approximation (1.3.1) of $\mathbb{J}$ does not lend itself to optimization with respect to ε.

(c) It is global in nature, as (i) it does not require an initial guess, and (ii) it allows simultaneous identification of multiple defects without prior knowledge of their number (see last example of Section 1.5 and the dual-cavity example in Section 1.6.2).

(d) The experimental information about sought defects entering $\mathbb{T}(\cdot, T)$ is entirely contained in the adjoint solution (through the definition of the adjoint forces in terms of the density φ).

(e) A TS field may be defined and computed using the present approach for cost functions associated to any overdetermined data, no matter how scarce, which makes TS-based identification a very flexible approach.

Transient versus time-harmonic data; time reversal. Compared to previous works based on wave-based imaging under time-harmonic conditions (e.g. Bonnet and Guzina, 2004; Feijóo, 2004; Guzina and Bonnet, 2006; Masmoudi et al., 2005), the time-domain approach to TS benefits from richer data as it exploits measurements taken over a duration T (the mathematical framework allowing to exploit other ways to collect data over time). Dominguez et al. (2005) have compared this approach to imaging processes based on time reversal (Cassereau et al., 1990), since the adjoint field $\hat{\boldsymbol{u}}$ defined by (1.3.24) constitutes a time-reversed state related to the field $\boldsymbol{v}^{\text{true}}$ scattered by the actual defect B^{true}.

Influence of measurement noise.   When observed values $\boldsymbol{u}^{\mathrm{obs}}$ differ from their true counterpart $\boldsymbol{u}^{\mathrm{true}}$ because of measurement noise or modelling uncertainties, the sensitivity of $\mathbb{T}(\cdot, T)$ to such uncertainties is directly related to the sensitivity of the adjoint solution to the same uncertainties. In the frequently-used case of least-squares cost functionals, based on (possibly weighted) L^2 norms of measurement residuals $\boldsymbol{\delta} = \boldsymbol{u} - \boldsymbol{u}^{\mathrm{obs}}$, the adjoint forces featured in (1.3.24) depend linearly on $\boldsymbol{\delta}$. More generally, misfit functionals based on a L^{α} norm (with $1 < \alpha < \infty$) lead to $O(\|\boldsymbol{\delta}\|^{\alpha-1})$ adjoint forces (the cases $\alpha = 1, \infty$ do not satisfy the required differentiability of misfit density φ). As $\mathbb{T}(\cdot, T)$ also depends linearly on the adjoint solution (irrespective of the nature of the cost functional), the perturbation undergone by the topological sensitivity of least-squares cost functions is, when using L^2 norms, *linear* in the measurement uncertainties. This suggests that identification procedures based on the TS field are better-behaved with respect to measurement noise than usual inversion procedures, known to be highly sensitive to the latter unless properly regularized. Indeed, numerical results of Section 1.6.5, based on misfit functionals without regularization term, corroborate this expectation.

Dynamical versus static measurements.   Expression (1.3.22) shows the value of $\mathbb{T}(\boldsymbol{z}, T)$ to be influenced by that of $\boldsymbol{W}(\cdot, \cdot; \boldsymbol{z})$. The latter, defined by (1.3.20) in terms of the elastodynamic Green's displacement and strain tensors, is a decreasing function of the distance $d(\boldsymbol{z}, S^{\mathrm{obs}})$ of $\boldsymbol{z}$ to S^{obs}. Hence, sampling points located close to S^{obs} are more apt to lead to high (negative) values of $\mathbb{T}$, increasing the risk of false identifications there when seeking a buried defect. Moreover, it is instructive to compare the behavior of $\mathbb{T}$ for sampling points remote from the observation surface according to whether $\mathbb{T}$ is evaluated under dynamic (i.e. time-dependent) or static (i.e. time-independent) loading conditions. Indeed, $\boldsymbol{W}(\cdot, \cdot; \boldsymbol{z})$ behaves like $[d(\boldsymbol{z}, S^{\mathrm{obs}})]^{-1}$ in the former case, but like $[d(\boldsymbol{z}, S^{\mathrm{obs}})]^{-2}$ in the latter case: (i) this behavior is directly observed for $\boldsymbol{E}(\cdot, \cdot; \boldsymbol{z})$ on the full-space Green's tensor, see equations (1.A.4ab) and remark 6, and is also explicit for scalar half-space Green's functions, constructed from their full-space counterpart using the method of images; (ii) the second term in (1.3.19) vanishes in the time-independent case. The static TS is thus a priori less sensitive than its dynamic counterpart to defects that are remote from the measurement surface.

Computational issues.   Anticipating on the finite element implementation discussed next, all numerical results of Secs. 1.5 and 1.6 are based on solving *linear* dynamical problems in the time domain, using an unconditionally-stable version of the Newmark time-marching algorithm. Such linear evolution problems have well-established convergence properties with respect to decreasing mesh size and time step, and hence do not raise mesh dependency issues. Note however that discretization error affecting displacement solutions affect quadratically the TS due to the bilinear structure of formula (1.3.26). The meshes and time steps used thereafter are chosen solely so as to adequately model geometry and represent expected spatial and time variations in the computed "true", free and adjoint solutions. Also, no attempt to improve the accuracy of computed stresses through refined postprocessing of displacement solutions has been made (although such procedures might conceivably improve TS evaluation), so as to show the usefulness of the TS concept within a standard FEM framework.

1.4.2   Implementation and numerical experiments

In spite of the previously-mentioned current lack of a mathematical proof to validate rigorously the heuristic idea of a TS-based defect indicator function, it is nevertheless useful to evaluate its practical efficiency through numerical experiments. This study aims at establishing the ability of the time-domain

TS to identify defects (here mostly taken as impenetrable objects such as cavities in elastic solids), emphasizing the computational efficiency of the approach and its ease of implementation within a standard finite element framework, and discussing the main features of such wave-based imaging approach. In the sections to follow, results from numerical experiments will be presented for the 2D scalar wave equation (Section 1.5), then for 2D and 3D elastodynamics (Section 1.6).

Discretization. Aiming at a FEM-based implementation of the time-domain topological sensitivity of $\mathbb{J}$, let Ω_h and $\Omega_h(B)$ denote FEM discretizations of the reference domain Ω and any cavitated trial domain $\Omega(B)$, whose meshes are assumed to coincide over the (discretized) observation surface S_h^{obs}. Then, a discretized least-squares cost function is be set up in the form

$$\mathbb{J}_h(\Omega_h(B), T) = \sum_{i=1}^{n^{\text{obs}}} \sum_{j=0}^{n_T} \frac{1}{2} \| \boldsymbol{u}_{B,h}(\boldsymbol{\xi}_i, t_j) - \boldsymbol{u}_h^{\text{obs}}(\boldsymbol{\xi}_i, t_j) \|^2 \tag{1.4.1}$$

where n^{obs} denote the number of nodes located on S_h^{obs}, $\{t_0 = 0, \ldots, t_{n_T} = T\}$ is a sequence of discrete time instants (a constant time step Δt being assumed for simplicity), and $\boldsymbol{u}_{B,h}$, $\boldsymbol{u}_h^{\text{obs}}$ denote the FE-computed trial displacement and the observed displacement sampled at the nodes of S_h^{obs}, respectively. For the purposes of computing the TS field, it is necessary to set up the discretized reference domain Ω_h, whereas the discretized trial domain $\Omega_h(B)$ is introduced for the purpose of a consistent definition of $\mathbb{J}_h$ but is not actually needed.

In the numerical results to follow, the data $\boldsymbol{u}_h^{\text{obs}}$ is generated synthetically, using a discretized version Ω_h^{true} of the "true" domain with the defects (or set thereof) to be identified. In that case, the meshes of Ω_h^{true} and S_h^{obs} are not required to coincide over S_h^{obs}.

All forward and adjoint solutions are performed using an unconditionally-stable Newmark time-marching scheme with parameters $\beta = 1/4, \gamma = 1/2$ (Hughes, 1987).

Discretized time convolution. A discrete version of the time convolution (1.3.8) is also adopted as

$$[\boldsymbol{v}_h \star \boldsymbol{w}_h](\boldsymbol{\xi}_i, t_k) \approx \Delta t \sum_{j=0}^{k} \boldsymbol{v}_h(\boldsymbol{\xi}_i, t_j) \boldsymbol{w}_h(\boldsymbol{\xi}_i, t_k - t_j) \quad (0 \leqslant k \leqslant n_T). \tag{1.4.2}$$

Then the adjoint state $\hat{\boldsymbol{u}}_h$ corresponding to the discretized cost function (1.4.1) is defined on Ω_h and results from time-dependent *nodal* forces $\hat{\boldsymbol{F}}_h$ over S_h^{obs} defined by

$$\hat{\boldsymbol{F}}_h(\boldsymbol{\xi}_i, t_j) = \boldsymbol{u}_h(\boldsymbol{\xi}_i, t_T - t_j) - \boldsymbol{u}_h^{\text{obs}}(\boldsymbol{\xi}_i, t_T - t_j) \quad (1 \leqslant i \leqslant n^{\text{obs}}, \ 0 \leqslant k \leqslant n_T) \tag{1.4.3}$$

Truncated topological sensitivity. To focus on areas of Ω where $\mathbb{T}$ attains sufficiently low (negative) values, a thresholded version $\mathbb{T}_\alpha$ of $\mathbb{T}$ depending on a cut-off parameter α is used in some of the following examples. It is defined by

$$\mathbb{T}_\alpha(\boldsymbol{z}, T) = \begin{cases} \mathbb{T}(\boldsymbol{z}, T) & (\mathbb{T} \leqslant \alpha \mathbb{T}^{\text{min}}), \\ 0 & (\mathbb{T} > \alpha \mathbb{T}^{\text{min}}) \end{cases} \quad \text{with} \ \mathbb{T}^{\text{min}} = \min_{\boldsymbol{z}} \mathbb{T}(\boldsymbol{z}, T), \ \alpha < 1, \tag{1.4.4}$$

with the implicit assumption that $\mathbb{T}^{\text{min}} < 0$. Moreover, let $B_{\text{eq}}(\alpha)$ denote the geometrical support of $\mathbb{T}_\alpha(\boldsymbol{z}, T)$, i.e. the region of Ω defined by

$$B_{\text{eq}}(\alpha) = \left\{ \boldsymbol{z} \in \Omega \ \big| \ \mathbb{T}_\alpha(\boldsymbol{z}, T) < 0 \right\}. \tag{1.4.5}$$

Thus an estimation of the unknown cavity (or set thereof) suggested by the thresholded TS may be defined in terms of $B_{\mathrm{eq}}(\alpha)$. The following additional definitions will also be useful: the characteristic radius $R_{\mathrm{eq}}(\alpha)$ of $B_{\mathrm{eq}}(\alpha)$, given by

$$R_{\mathrm{eq}} = \left(\frac{1}{\pi} |B_{\mathrm{eq}}| \right)^{1/2} \text{(2D)}, \qquad R_{\mathrm{eq}} = \left(\frac{3}{4\pi} |B_{\mathrm{eq}}| \right)^{1/3} \text{(3D)}, \qquad (1.4.6)$$

where $|B_{\mathrm{eq}}|$ stands for the volume of B_{eq}, and the distance $d(\alpha)$ between the centroid $\boldsymbol{x}_{\mathrm{eq}}$ of $B_{\mathrm{eq}}(\alpha)$ and the true cavity centroid $\boldsymbol{x}^{\mathrm{true}} \in \Omega$, i.e.

$$d = |\boldsymbol{x}^{\mathrm{true}} - \boldsymbol{x}_{\mathrm{eq}}| \quad \text{with } \boldsymbol{x}_{\mathrm{eq}} = \frac{1}{|B_{\mathrm{eq}}|} \int_{B_{\mathrm{eq}}} \boldsymbol{\xi} \, \mathrm{d}V_\xi \qquad (1.4.7)$$

1.5 Defect imaging using acoustic time-domain data

In this set of examples, the reference domain Ω is the unit square, i.e. $\Omega = \{0 \leqslant \xi_1, \xi_2 \leqslant 1\}$ (Fig. 1.1). The primary field is governed by the two-dimensional scalar wave equation of e.g. linear acoustics. The identification of a set B^{true} of impenetrable obstacles, such that a homogeneous Neumann boundary condition describing a zero normal velocity is prescribed on the obstacle boundary Γ^{true}, is considered, based on four (simulated) experiments of duration T. The free pressure field $u^{(k)}$ associated to experiment number k is defined through the boundary-initial value problem

$$
\begin{aligned}
\Delta u^{(k)}(\boldsymbol{\xi}, t) - \ddot{u}^{(k)}(\boldsymbol{\xi}, t) &= 0 & (\boldsymbol{\xi} \in \Omega, \ 0 \leqslant t \leqslant T) \\
\boldsymbol{\nabla} u^{(k)}(\boldsymbol{\xi}, t) \cdot \boldsymbol{n}(\boldsymbol{\xi}) &= 1 & (\boldsymbol{\xi} \in S_k, \ 0 \leqslant t \leqslant T) \\
\boldsymbol{\nabla} u^{(k)}(\boldsymbol{\xi}, t) \cdot \boldsymbol{n}(\boldsymbol{\xi}) &= 0 & (\boldsymbol{\xi} \in S_\ell \ (\ell \neq k), \ 0 \leqslant t \leqslant T) \\
u^{(k)}(\boldsymbol{\xi}, 0) = \dot{u}^{(k)}(\boldsymbol{\xi}, 0) &= 0 & (\boldsymbol{\xi} \in \Omega)
\end{aligned}
\qquad (1.5.1)
$$

where each S_ℓ is one of the sides of the square boundary of Ω, numbered according to Fig. 1.1, and Δ denotes the two-dimensional Laplacian operator. Note that the wave velocity is set to $c = 1$, so that the travel time of waves propagating vertically from S_1 to S_3 or horizontally from S_2 to S_4 is one unit of time. All simulations presented in this section were performed using a finite element method based on a piecewise-linear interpolation, i.e. three-noded triangular elements. The cost function

$$J^{(k)}(B, T) = \frac{1}{2} \int_0^T \int_{S_1+S_2+S_3+S_4} |u_B^{(k)}(\boldsymbol{\xi}, t) - u_{\mathrm{obs}}^{(k)}(\boldsymbol{\xi}, t)|^2 \, \mathrm{d}s_\xi \, \mathrm{d}t$$

is then introduced (in a discretized form similar to (1.4.1)), where $u_{\mathrm{true}}^{(k)}$ denotes the pressure field arising in $\Omega^{\mathrm{true}} = \Omega \setminus B^{\mathrm{true}}$ from the external excitation defined in (1.5.1), $u_{\mathrm{obs}}^{(k)}$ is the corresponding (possibly polluted) observation, and $u_\Gamma^{(k)}$ is the predicted measurement for an assumed configuration B of the obstacle. The topological sensitivity $\mathbb{T}(\boldsymbol{z}, T)$ of $J^{(k)}$, such that

$$J^{(k)}(\Omega_\varepsilon(\boldsymbol{z}), T) = J^{(k)}(\Omega, T) + \varepsilon^2 |\mathcal{B}| \mathbb{T}(\boldsymbol{z}, T) + o(\varepsilon^2)$$

is given (following an analysis similar to that of Section 1.3) by

$$\mathbb{T}(\boldsymbol{z}, T) = \left\{ 2\pi \boldsymbol{\nabla} \hat{u}^{(k)} \star \boldsymbol{\nabla} u^{(k)} + \frac{4\pi}{3} \hat{u}^{(k)} \star u^{(k)} \right\}(\boldsymbol{z}, t)$$
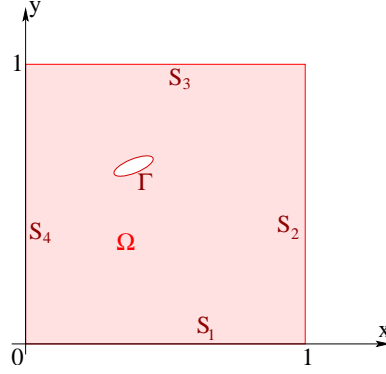
Figure 1.1: *Defect imaging using acoustic time-domain data: geometry and notations.*
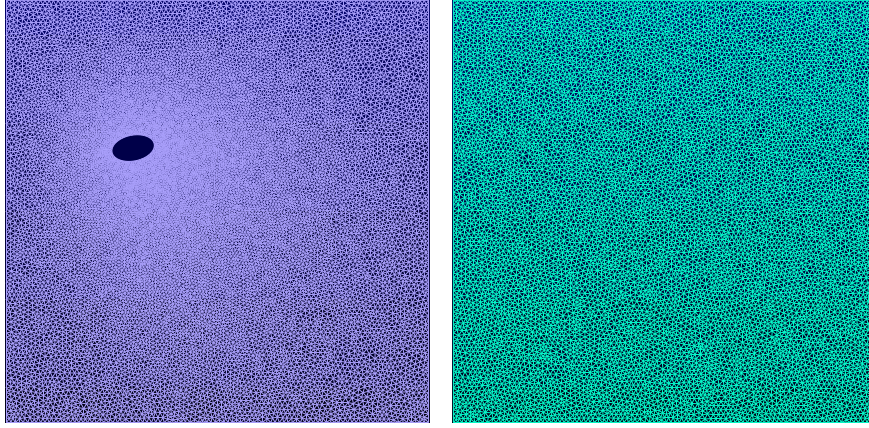
Figure 1.2: *Identification of a single scatterer: meshes used for generating the synthetic data (left) and computing the topological sensitivity (right).*

Identification of a single scatterer. Let B^{true} denote the ellipse with parameters as given for scatterer 1 in Table 1.1 (where "inclination" refers to the angle between the ξ_1-direction and the major principal axis). The meshes used for generating the synthetic data $u_{\text{true}}^{(k)}$ and for computing $u, \hat{u}$ and $\mathbb{T}(\cdot, T)$ (Fig. 1.2) feature $16,268$ and $9,841$ DOFs, respectively.

Figure 1.3 shows the distribution of $\mathbb{T}_\alpha(\cdot, T)$ obtained for the above-defined single-scatterer identification problem (having used $T = 2$, $\alpha = 0.5$ and $\Delta t = 2.5\,10^{-2}$). The region $B_{\text{eq}}(\alpha)$ clearly pinpoints correctly the location of the defect, while its size gives a reasonable estimation of the actual defect size. Figure 1.4 moreover shows, by means of a sequence of blow-ups of the region surrounding the actual defects for α ranging from 0.1 to 0.9, that $B_{\text{eq}}(\alpha)$ is relatively insensitive to the choice of α within a fairly wide range of values (approximately $0.2 \leqslant \alpha \leqslant 0.6$ for this example).

Figure 1.5 then illustrates how the choice of experiment configuration and duration affects the results. Figure 1.5(a), which repeats Fig. 1.3, is based on the single experiment $k = 1$ and a duration $T = 2$ large enough for a wave emanating from S_1 to hit the defect and send scattered signals back to various parts of the boundary. Hence, the cost function contains enough data about the object to make an identification possible. In contrast, under the same conditions but with data collected only until $T = 1$, the scattering
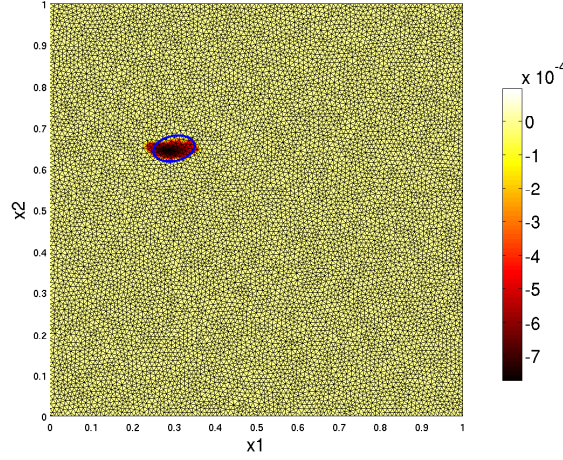
Figure 1.3: *Identification of a single scatterer: distribution of thresholded topological sensitivity $\mathbb{T}_\alpha$, with $T = 2$ and $\alpha = 0.5$.*

of a wave emanating from S_1 seldom has sufficient time to send information to the boundary, and the defect is not identified (Fig. 1.5(b)). Using the same reduced experiment duration $T = 1$ but with an incident wave emanating from surface S_4, located closer to the defect, some of the scattered signals reach the boundary before $t = 1$ resulting in an identification (Fig. 1.5(c)) that is not as good as in Fig. 1.5(a) but still acceptable. Finally, maintaining $T = 1$ and using a multiple experiment $k = 1, 2, 3, 4$ (with experiments $k = 3, 4$ contributing most of the usable data due to the chosen duration) yields again a satisfactory identification (Fig. 1.5(d)). These observations entirely conform with what one would expect based on physical intuition.

Scatterer #	Semiaxes	Centroid	Inclination
1	$\sqrt{26}/100,\ 3\sqrt{26}/500$	$(0.30, 0.65)$	$\tan^{-1}(1/5)$
2	$\sqrt{29}/100,\ 3\sqrt{26}/400$	$(0.60, 0.35)$	$\tan^{-1}(5/2)$
3	$\sqrt{17}/100,\ 3\sqrt{17}/200$	$(0.25, 0.30)$	$\tan^{-1}(1/5)$
4	$\sqrt{13}/100,\ 3\sqrt{13}/200$	$(0.55, 0.75)$	$\tan^{-1}(5/2)$

Table 1.1: *Identification of a multiple scatterer: geometrical parameters.*

Simultaneous identification of a multiple scatterer. The simultaneous identification of a set of four elliptical scatterers, whose characteristics are gathered in Table 1.1, is now considered. The mesh used for generating the synthetic data $u_{\text{true}}^{(k)}$ now features $24,098$ DOFs. The resulting distribution of $\mathbb{T}_\alpha(\cdot, T)$ obtained for a multiple simulated experiment $k = 1, 2, 3, 4$ with duration $T = 2$ and a cut-off $\alpha = 0.5$ is shown in Fig. 1.6. The corresponding region $B_{\text{eq}}(\alpha)$ is split into four connected components, each one correctly located at one of the defects. The identification is simultaneous in that the topological sensitivity is computed at once on the basis of the free and adjoint solutions, with no prior information about the number of defects fed into the computation.

(a) $\alpha = 0.1$ (b) $\alpha = 0.2$ (c) $\alpha = 0.3$

(d) $\alpha = 0.4$ (e) $\alpha = 0.5$ (f) $\alpha = 0.6$

(g) $\alpha = 0.7$ (h) $\alpha = 0.8$ (i) $\alpha = 0.9$
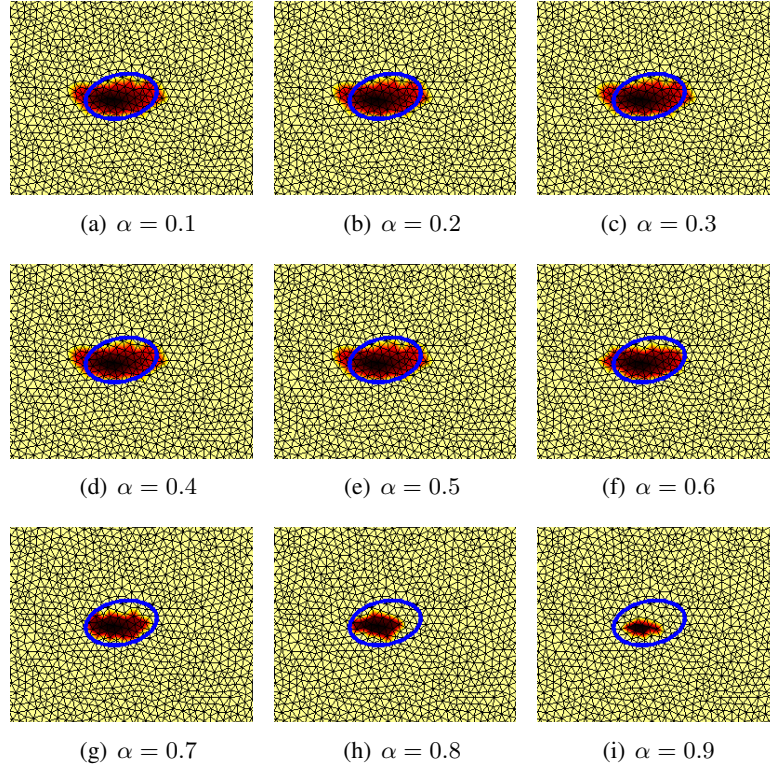
Figure 1.4: *Identification of a single scatterer: influence of cut-off parameter α.*

1.6 Defect imaging using elastodynamic time-domain data

1.6.1 Methodology

Synthetic experiment configuration.   The reference elastic domains considered are the unit cube $\Omega = \{0 \leqslant \xi_1, \xi_2, \xi_3 \leqslant 1\}$ or the unit square $\Omega = \{0 \leqslant \xi_1, \xi_2 \leqslant 1\}$. The material parameters μ, ν, ρ are set so that the longitudinal wave velocity (which is fastest) is unity:

$$c_{\mathrm{L}} = \sqrt{\mu/\rho\kappa^2} = 1 \tag{1.6.1}$$

(with κ defined by (1.A.5)), so that $T = 1$ corresponds to the travel time of longitudinal waves propagating between any two opposite faces of $\partial\Omega$ in a direction normal to them. For both 3D and 2D cases, a single synthetic experiment is considered throughout this section, whereby a compressional loading $\boldsymbol{t}_{\mathrm{N}} = -H(t)\boldsymbol{e}_2$ (where $H(t)$ denotes the Heaviside step function) is applied on the face $\xi_2 = 1$ of $\partial\Omega$ while a homogenous Dirichlet condition is prescribed on the face $S_{\mathrm{D}} = \{\xi_2 = 0\}$. The observation surface is taken as the whole Neumann surface: $S_h^{\mathrm{obs}} = S_{\mathrm{N}} = \partial\Omega_h \setminus S_{\mathrm{D}}$.

The reference mesh Ω_h is based on an isoparametric piecewise-linear interpolation employing three-noded triangular elements and $1,988$ nodes (2D case) or four-noded tetrahedral elements and $19,683$ nodes (3D case). Moreover, to guard against the "inverse crime" (Colton and Kress, 1992), the synthetic data $\boldsymbol{u}^{\mathrm{obs}}$ is computed by means of a finer discretization, with Ω_h^{true} discretized into isoparametric piecewise-quadratic elements, i.e. six-noded triangular elements (2D case) or ten-noded tetrahedral ele-

(a) $k = 1,\ T = 2$

(b) $k = 1,\ T = 1$

(c) $k = 4,\ T = 1$

(d) $k = 1, 2, 3, 4,\ T = 1$
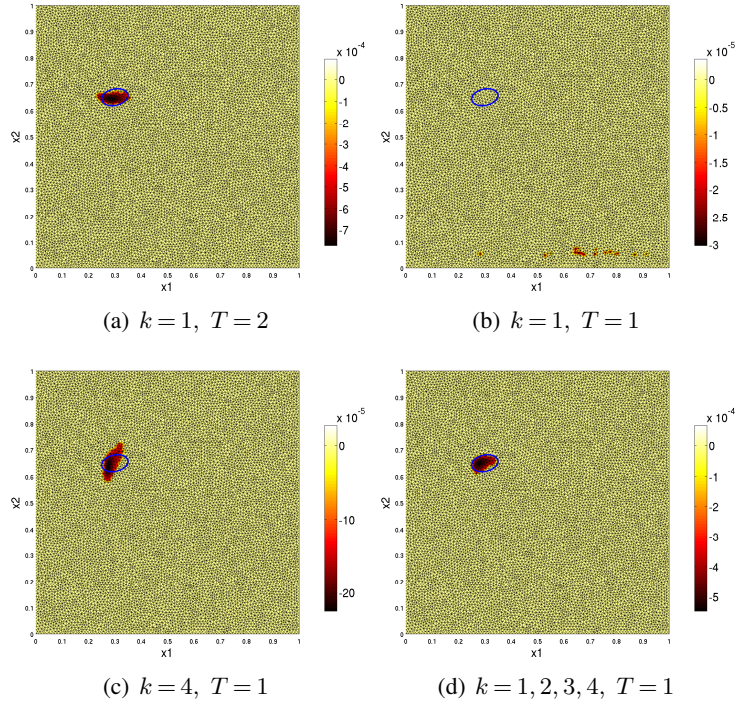
Figure 1.5: *Identification of a single scatterer: influence of experiment configuration and duration.*
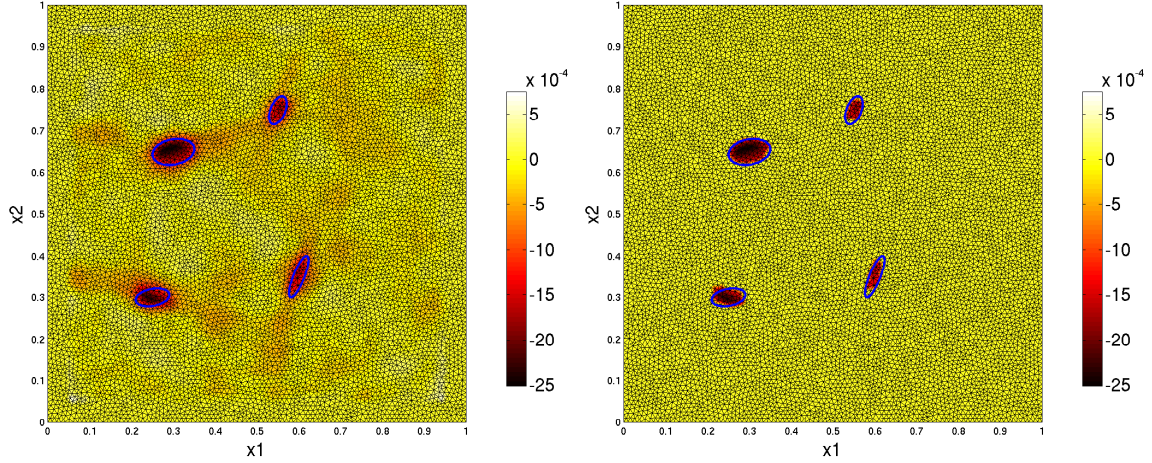
Figure 1.6: *Identification of a multiple scatterer, with $k = 1, 2, 3, 4$ and $T = 2$: TS field $\mathbb{T}$ (left) and its thresholded version $\mathbb{T}_\alpha$ with $\alpha = 0.5$ (right).*

ments (3D case), arranged for convenience so that the elements of Ω_h and Ω_h^{true} coincide on S^{obs}. The simulated displacements at the vertex nodes of Ω_h^{true} on S^{obs} are then retained (and the values at the midside nodes discarded), which provide the nodal values of $\boldsymbol{u}^{\text{obs}}$ on S_h^{obs} used in the discrete cost function (1.4.1).

1.6.2 Single or dual cavity identification

(a) $R_1 = 0.05$, $\boldsymbol{x}^{\text{true}} = (0.75,\ 0.75)$ (b) $R_1 = 0.1$, $\boldsymbol{x}^{\text{true}} = (0.4,\ 0.5)$
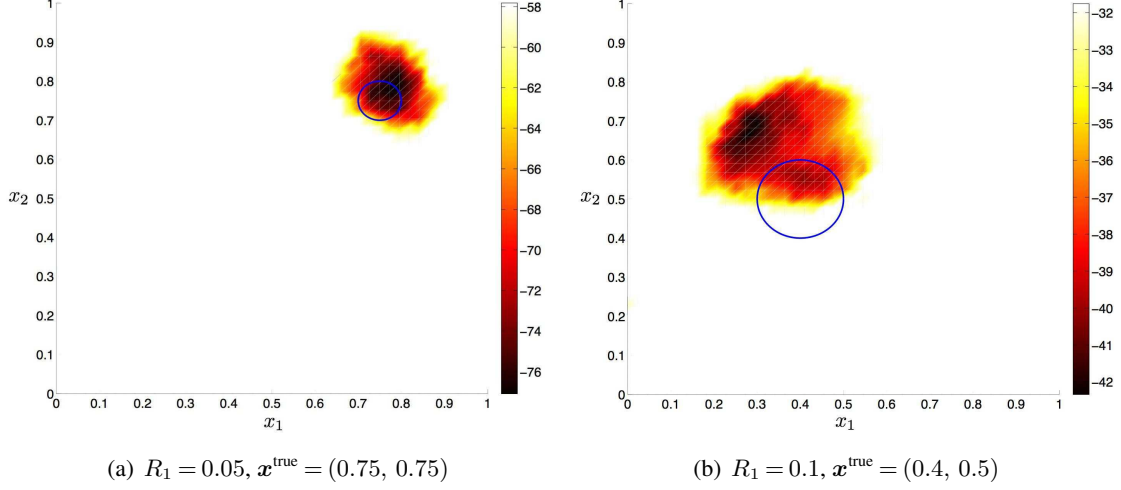
Figure 1.7: *Single cavity identification, 2D: thresholded TS field* $\mathbb{T}_\alpha$ *with* $\alpha = 0.75$.

(a) Same mesh as Fig. 1.7 (1988 nodes)   (b) Refined mesh 1 (3027 nodes)   (c) Refined mesh 2 (4416 nodes)
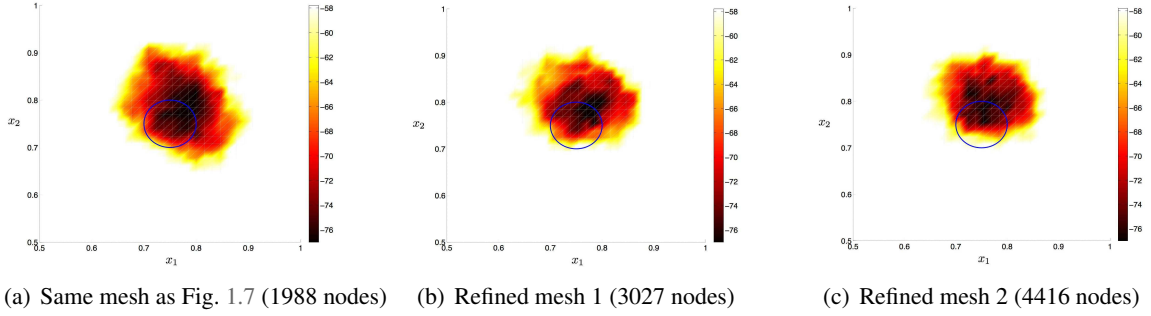
Figure 1.8: *Single cavity identification, 2D (* $R_1 = 0.05$, $\boldsymbol{x}^{true} = (0.75,\ 0.75)$ *): thresholded TS field* $\mathbb{T}_\alpha$ *with* $\alpha = 0.75$ *for three different meshes.*

In this section, the effectiveness of the topological sensitivity indicator is assessed on 2D or 3D single- or dual-cavity configurations, with the simulated experiment duration set to $T = 1$.

The thresholded TS $\mathbb{T}_\alpha(\cdot, T)$ for a single unknown circular cavity and a set of two unknown circular cavities are presented, for two configurations in each case, in Figs. 1.7 and 1.9, respectively (with details on cavity geometry provided therein). In each figure, case (a) corresponds to unknown cavities close enough to the excitation surface, so that the experiment duration $T = 1$ lets sufficient amount of information reach the observation surface, leading to satisfactory identification for both the single- or dual-cavity cases. In contrast, case (b) for each figure features a cavity located in such a way that little information about its presence can reach the observation surface within the time frame $T = 1$, and these cavities are poorly located by the $\mathbb{T}_\alpha(\cdot, T)$ distribution. In addition, a computation on two finer meshes of the thresholded TS of Fig. 1.7(a), keeping the same measurement grid and definition (1.4.3) of adjoint nodal forces, indicates that $\mathbb{T}_\alpha(\cdot, T)$ is only moderately sensitive to mesh size (Fig. 1.8).

Then, similar numerical experiments are conducted for the 3D case, with results for single- or dual-cavity configurations shown in Figs. 1.10 and 1.11 (where details on cavity geometry are again provided

(a) $\alpha = 0.75$, $R_1 = R_2 = 0.05$,
   $\boldsymbol{x}_1^{\text{true}} = (0.25,\, 0.75)$, $\boldsymbol{x}_2^{\text{true}} = (0.75,\, 0.75)$

(b) $\alpha = 0.65$, $R_1 = 0.05$, $R_2 = 0.1$,
   $\boldsymbol{x}_1^{\text{true}} = (0.2,\, 0.75)$, $\boldsymbol{x}_2^{\text{true}} = (0.75,\, 0.55)$
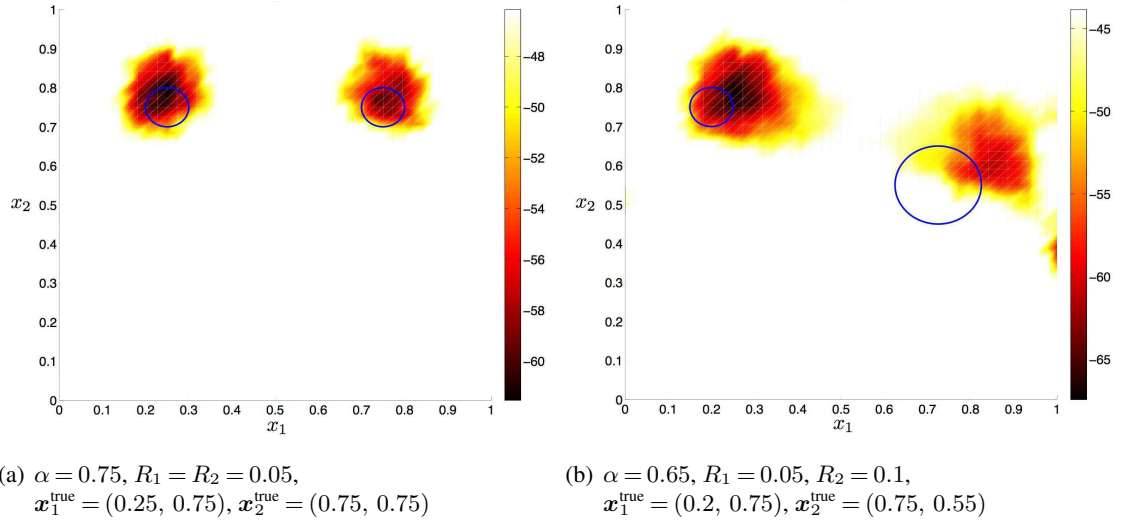
Figure 1.9: *Dual cavity identification, 2D: thresholded TS field $\mathbb{T}_\alpha$.*

(a) $R = 0.05$, $\boldsymbol{x}^{\text{true}} = (0.75,\, 0.75,\, 0.75)$

(b) $R = 0.1$, $\boldsymbol{x}^{\text{true}} = (0.4,\, 0.4,\, 0.5)$
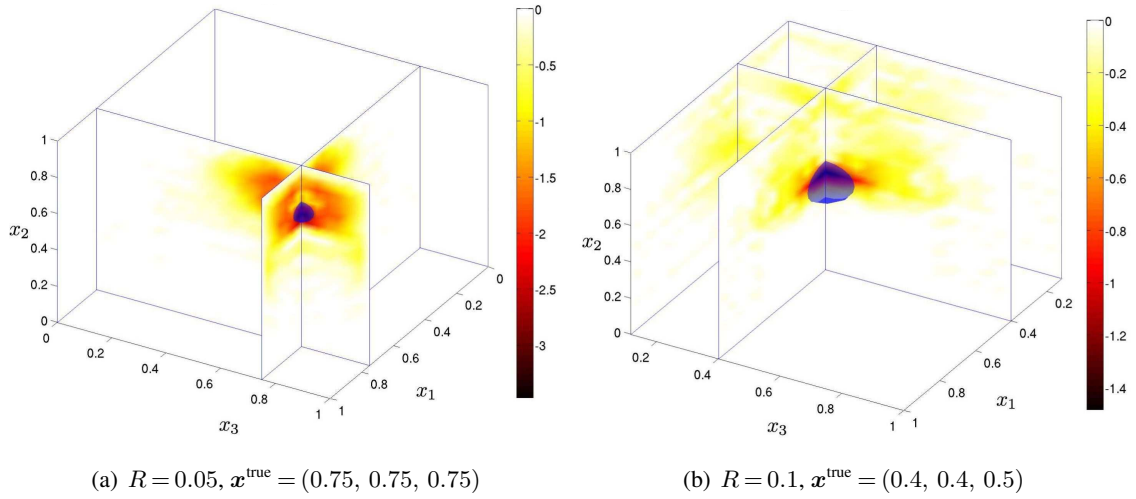
Figure 1.10: *Single cavity identification, 3D: thresholded TS field $\mathbb{T}_\alpha$ with $\alpha = 0$.*

therein, and the correct cavity boundaries are depicted as blue spheres). Moreover, the regions $B_{\text{eq}}(\alpha)$ defined by (1.4.5), plotted respectively in Figs. 1.12 and 1.13 for the single- and dual-cavity cases, are seen to indicate the correct location and number of sought cavities based on the sole information $\boldsymbol{u}^{\text{obs}}$ and do not predict other, spurious, defects.

1.6.3 Influence of experiment duration

The duration T over which data is collected will obviously have a major effect on the results, an effect which is now investigated. For this purpose, in addition to the previously-defined unit cube or square Ω, an elongated variant Ω' of Ω such that $-1 \leqslant \xi_2 \leqslant 1$ is also considered, with $S'_{\text{D}} = \{\xi_2 = -1\}$ and all other dimensions and boundary conditions defined as before, and the corresponding observation surface

(a) $R_1 = R_2 = 0.05$, $\boldsymbol{x}_1^{\text{true}} = (0.25,\ 0.25,\ 0.75)$, $\boldsymbol{x}_2^{\text{true}} = (0.75,\ 0.75,\ 0.75)$

(b) $R_1 = 0.05 \quad R_2 = 0.1$, $\boldsymbol{x}_1^{\text{true}} = (0.25,\ 0.25,\ 0.75)$, $\boldsymbol{x}_2^{\text{true}} = (0.75,\ 0.75,\ 0.5)$
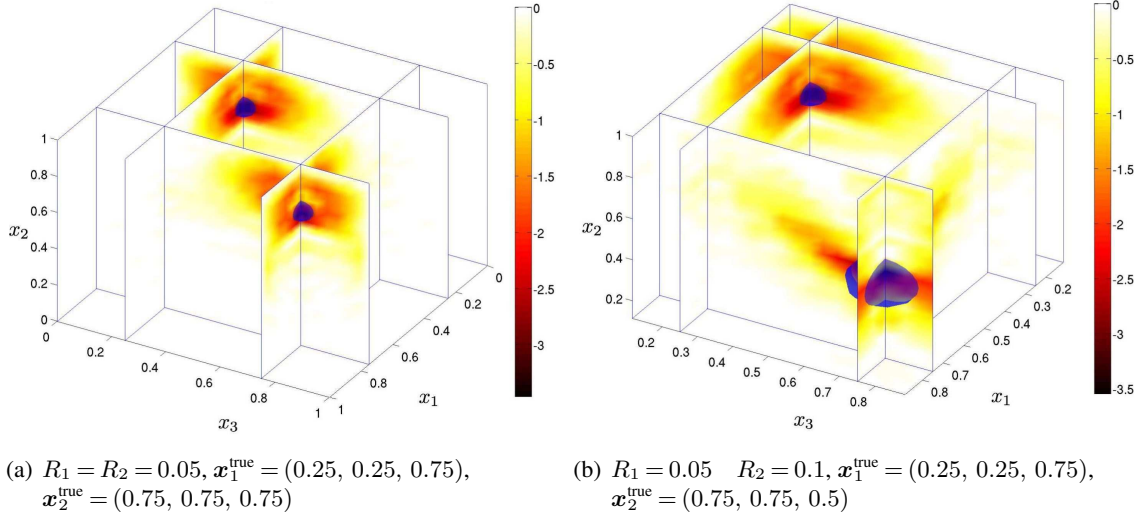
Figure 1.11: *Dual cavity identification, 3D: thresholded TS field $\mathbb{T}_\alpha$ with $\alpha = 0$.*

(a) $R = 0.05$, $\alpha = 0.6$

(b) $R = 0.1$, $\alpha = 0.6$
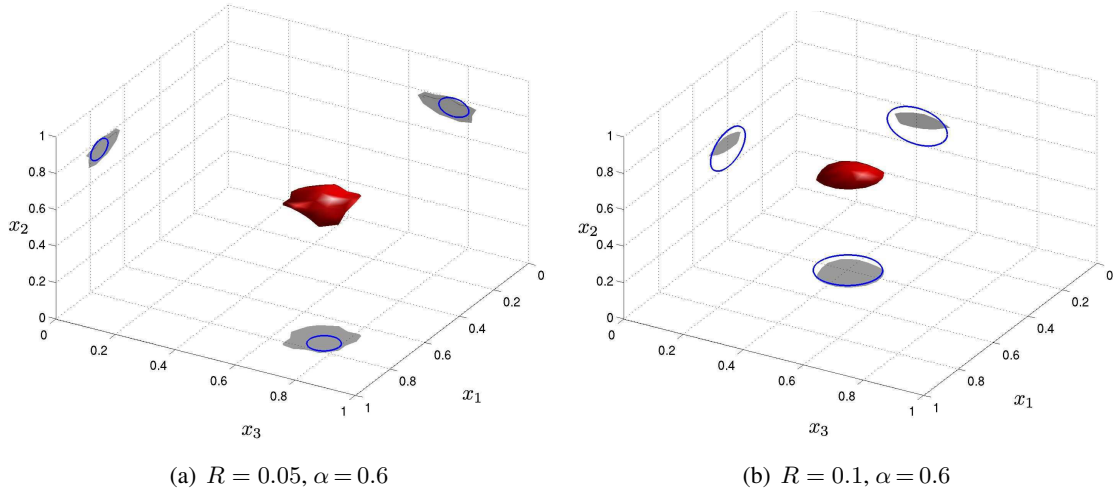
Figure 1.12: *Single cavity identification, 3D: $B_{eq}(\alpha)$.*

S'^{obs} set as $S'^{\text{obs}} = S'_{\text{N}} = \partial\Omega' \setminus S'_{\text{D}}$.

Figures 1.14 and 1.15 plot $d(0.75)$ and $R_{\text{eq}}(0.75)$ as functions of the simulated experiment duration T for the identification of a single cavity of radius $R = 0.1$ embedded in domain Ω or Ω'. Both the 2D case (with $\boldsymbol{x}_1^{\text{true}} = (0.5,\ 0.5)$ in Ω or $\boldsymbol{x}_2^{\text{true}} = (-0.5,\ 0.5)$ in Ω') and the 3D case (with $\boldsymbol{x}_1^{\text{true}} = (0.5,\ 0.5,\ 0.5)$ in Ω or $\boldsymbol{x}_2^{\text{true}} = (0.5,\ -0.5,\ 0.5)$ in Ω') are considered. These results can be divided into three cases (indicated on Figs. 1.14 and 1.15 using circled '1', '2' and '3' symbols) according to the value taken by T. For $0 < T \leqslant T_1$ (where T_1 is typically the time for the wave to reach the cavity), the identification is not satisfactory, as was to be expected since the scattered waves do not have time to reach S^{obs} and be recorded in the cost function. Next, the case $T_1 \leqslant T \leqslant T_2$ (relatively narrow in terms of the range of T) corresponds to d decreasing, and R_{eq} increasing, with T i.e. estimations of defect location and size that are sensitive to the experiment duration (figures 1.14(b), 1.15(a), 1.15(b)) and hence also not reliable.

(a) $R_1 = R_2 = 0.05$, $\alpha = 0.6$

(b) $R_1 = 0.05$ $R_2 = 0.1$, $\alpha = 0.7$
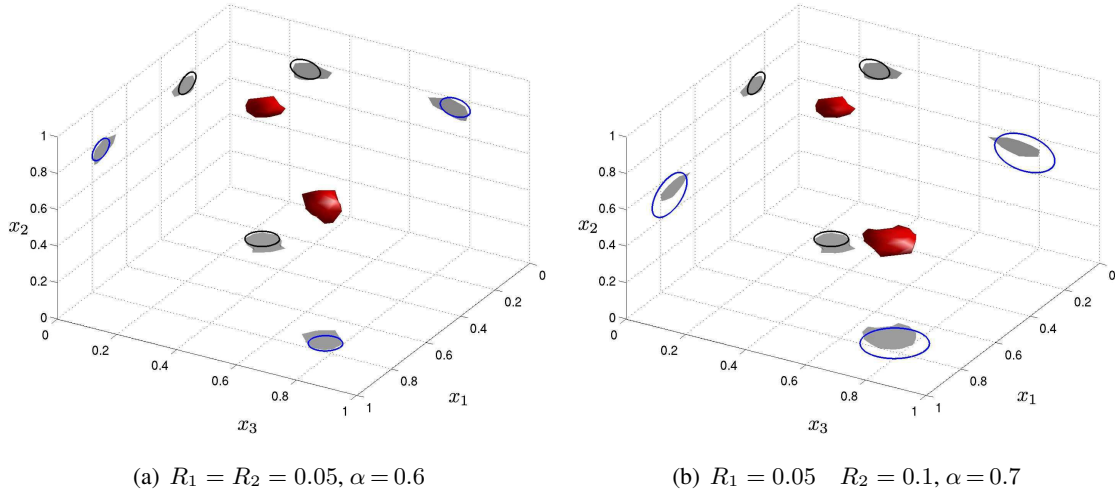
Figure 1.13: *Dual cavity identification, 3D: $B_{eq}(\alpha)$.*

(a) $R = 0.1$, $\boldsymbol{x}_1^{\text{true}} = (0.5, \, 0.5)$

(b) $R = 0.1$, $\boldsymbol{x}_2^{\text{true}} = (0.5, \, -0.5)$
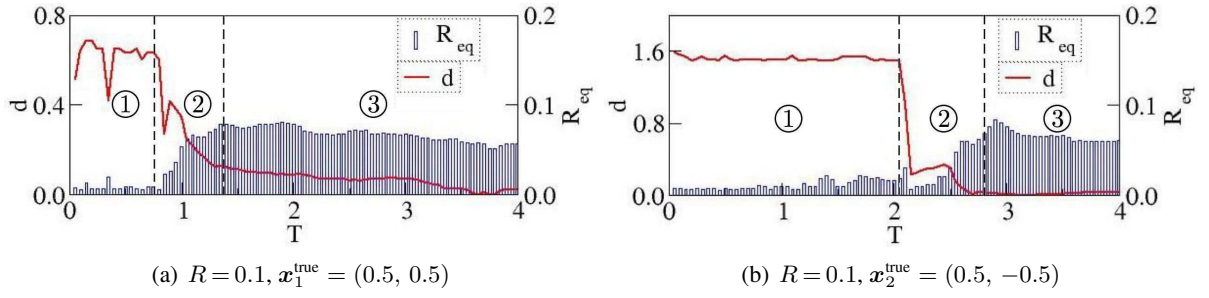
Figure 1.14: *Influence of experiment duration: identification under 2D conditions.*

Finally, in the case $T \geqslant T_2$ (with T_2 large enough for a substantial amount of information to reach S^{obs}), d reaches small values (indicating a correct identification of the cavity location) while R_{eq}, the estimated cavity size, attains stable values.

(a) $R = 0.1$, $\boldsymbol{x}_1^{\text{true}} = (0.5, \, 0.5, \, 0.5)$

(b) $R = 0.1$, $\boldsymbol{x}_2^{\text{true}} = (0.5, \, -0.5, \, 0.5)$
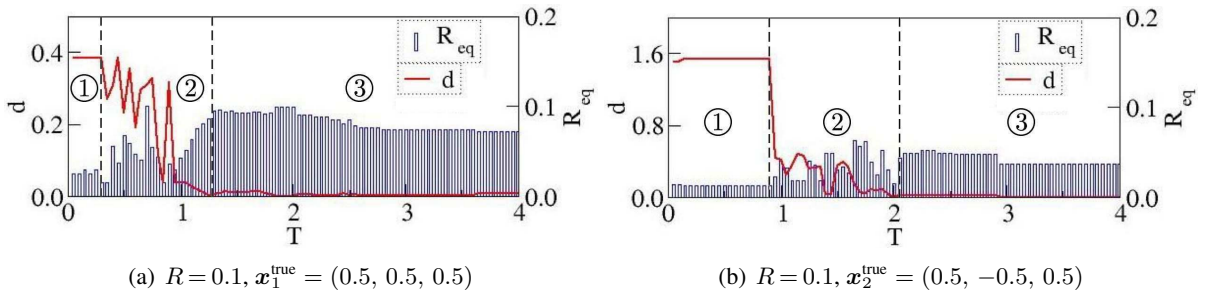
Figure 1.15: *Influence of experiment duration: identification under 3D conditions.*

1.6.4 Influence of observation surface configuration

All results so far were based on dense and full-aperture measurements (for a single experiment). The effect of relaxing either the measurement grid density or the measurement aperture is now considered.

Influence of measurement grid density. The influence of using coarser measurement grids featuring $N \times N$ points on each face of S_N is now considered. Figure 1.16 illustrates the effect of a decreasing measurement density (i.e. decreasing N) on the computed field $\mathbb{T}_\alpha(\cdot, T)$. The numerical value of $\mathbb{T}_\alpha(\cdot, T)$ is seen to decrease, reflecting the fact that the definition (1.4.1) of $\mathbb{J}$ and that of the adjoint forces (1.4.3) is strongly influenced by the number of measurement points. This in itself is of secondary importance, as (i) the support of $\mathbb{T}_\alpha(\cdot, T)$, not its numerical value, is of primary importance, and (ii) one could easily renormalize the definition of $\mathbb{J}$. However, one also notices that a decreasing measurement density induces a qualitative deterioration of the identification provided by $\mathbb{T}_\alpha(\cdot, T)$. This observation is confirmed by Fig. 1.17, where the reconstructed cavity is taken to be the support $B_{\mathrm{eq}}(\alpha)$ of $\mathbb{T}_\alpha(\cdot, T)$ and

(a) $N = 27$

(b) $N = 14$

(c) $N = 9$

(d) $N = 7$
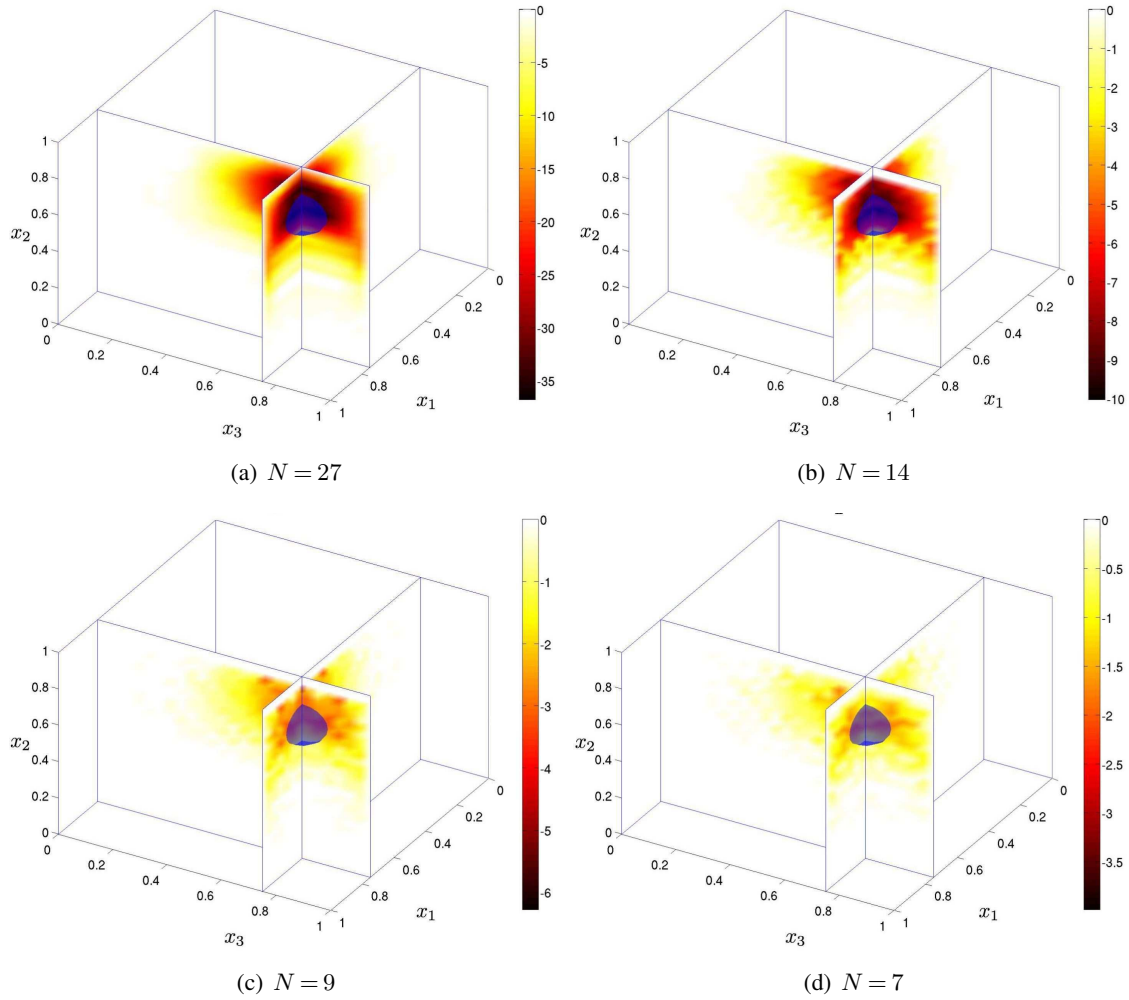
Figure 1.16: *Influence of measurement grid density on thresholded TS field $\mathbb{T}_\alpha$ ($\alpha = 0$, $R = 0.1$)*

(a) $N = 27$ $\alpha = 0.75$

(b) $N = 14$ $\alpha = 0.75$

(c) $N = 9$ $\alpha = 0.4$

(d) $N = 7$ $\alpha = 0.35$
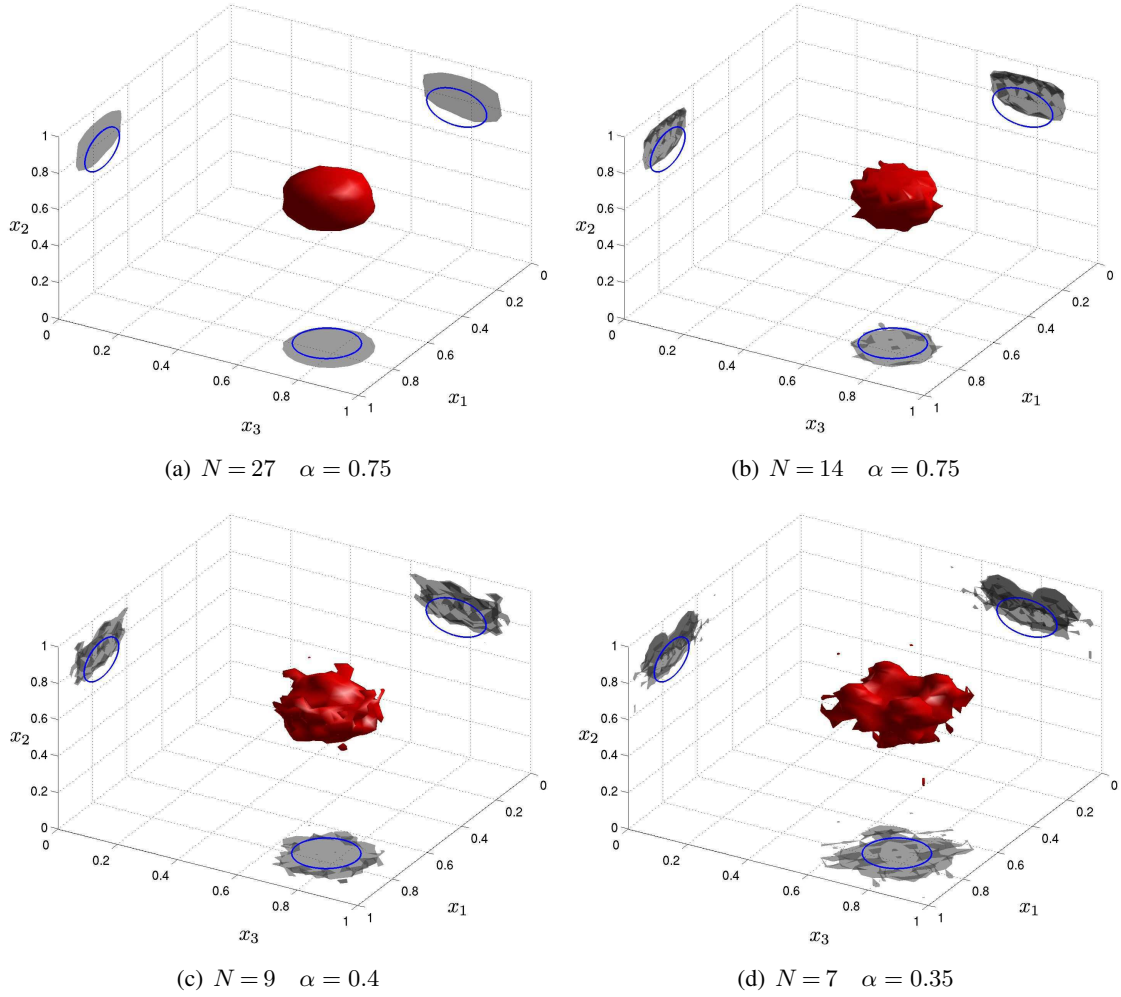
Figure 1.17: *Influence of measurement grid density: blurring effect on $B_{eq}(\alpha)$.*

which shows that α must decrease with N to have $B_{\mathrm{eq}}(\alpha)$ reasonably estimating B^{true} for all grid densities. Remarkably, the cavity location remains correctly estimated even as the shape of $B_{\mathrm{eq}}(\alpha)$ becomes irregular due to the decreasing number of observation points.

Influence of limited aperture.   Here, the effect of restricting the observation surface to a portion $S^{\mathrm{obs}} \subsetneq S_{\mathrm{N}}$ of the boundary is examined. Figure 1.18 shows the identification result in terms of $B_{\mathrm{eq}}(\alpha)$ for two cases with limited aperture. For data collected on the top face $\xi_2 = 1$ (Fig. 1.18(a)), the observation surface is orthogonal to the propagation direction of the compressional wave in the reference solid, and the horizontal location of the sought cavity is correctly found while its vertical estimated position is offset compared to the correct one. For data collected on the lateral face $\xi_3 = 0$ (Fig. 1.18(b)), the TS field does not resolve correctly the unknown cavity. Moreover, plots of $B_{\mathrm{eq}}(\alpha)$ corresponding to observations surfaces $S^{\mathrm{obs}} = \{\xi_2 = 1\}$ and $S^{\mathrm{obs}} = \{\xi_3 = 1\}$ (chosen closest to B^{true} to yield sufficient usable data) indicate satisfactory reconstruction of B^{true} (Fig. 1.19). For the two cases shown, B_{true} is better estimated along the direction orthogonal to S^{obs}, with the best identification obtained in Fig. 1.19(a) corresponding

to S^{obs} orthogonal to the propagation direction of the incident wave.

(a) $S^{\text{obs}} = \{\xi_2 = 1\}$ (b) $S^{\text{obs}} = \{\xi_3 = 0\}$
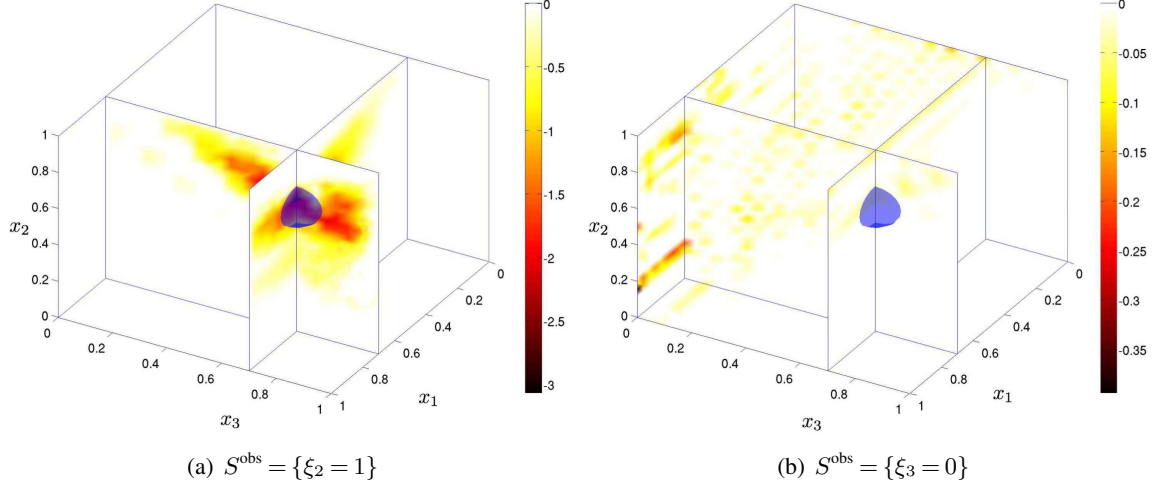
Figure 1.18: *Influence of limited aperture: distribution of $\mathbb{T}_\alpha$ for two choices of S^{obs}.*

(a) $S^{\text{obs}} = \{\xi_2 = 1\}$ (b) $S^{\text{obs}} = \{\xi_3 = 1\}$
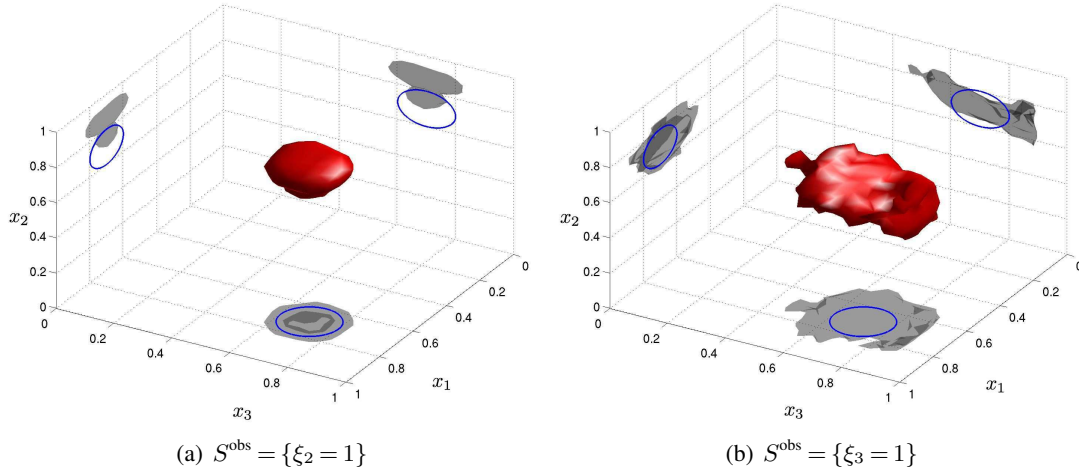
Figure 1.19: *Influence of limited aperture: $B_{eq}(\alpha)$ for two choices of partial observation surface S^{obs}.*

1.6.5 Influence of data noise

In this section the influence of data noise is studied by considering noisy simulated data of the form

$$\boldsymbol{u}_h^{\text{obs}}(\cdot, t_j) = \boldsymbol{u}_h^{\text{true}}(\cdot, t_j) + \sigma \chi \boldsymbol{u}_j^{\text{max}}, \quad \boldsymbol{u}_j^{\text{max}} = \left\{ \max_{1 \le i \le n^{\text{obs}}} \left(\left[\boldsymbol{u}_h^{\text{true}}(\boldsymbol{\xi}_i, t_j) - \boldsymbol{u}_h(\boldsymbol{\xi}_i, t_j) \right] \cdot e_k \right) \right\} e_k \quad (1.6.2)$$

where χ is a Gaussian random variable with zero mean and unit standard deviation. Figure 1.20 depicts the behavior of the imaging method for increasing noise level σ. Remarkably, the cavity location is correctly estimated even for high noise levels (Figs. 1.20(c) and 1.20(d)). TS-based identification thus still

(a) $\sigma = 0.1$, $\boldsymbol{x}^{\text{true}} = (0.75,\ 0.75,\ 0.75)$, $\alpha = 0.75$ (b) $\sigma = 0.2$, $\boldsymbol{x}^{\text{true}} = (0.75,\ 0.75,\ 0.75)$, $\alpha = 0.75$

(c) $\sigma = 0.5$, $\boldsymbol{x}^{\text{true}} = (0.75,\ 0.75,\ 0.75)$, $\alpha = 0.75$ (d) $\sigma = 1$, $\boldsymbol{x}^{\text{true}} = (0.75,\ 0.75,\ 0.75)$, $\alpha = 0.6$
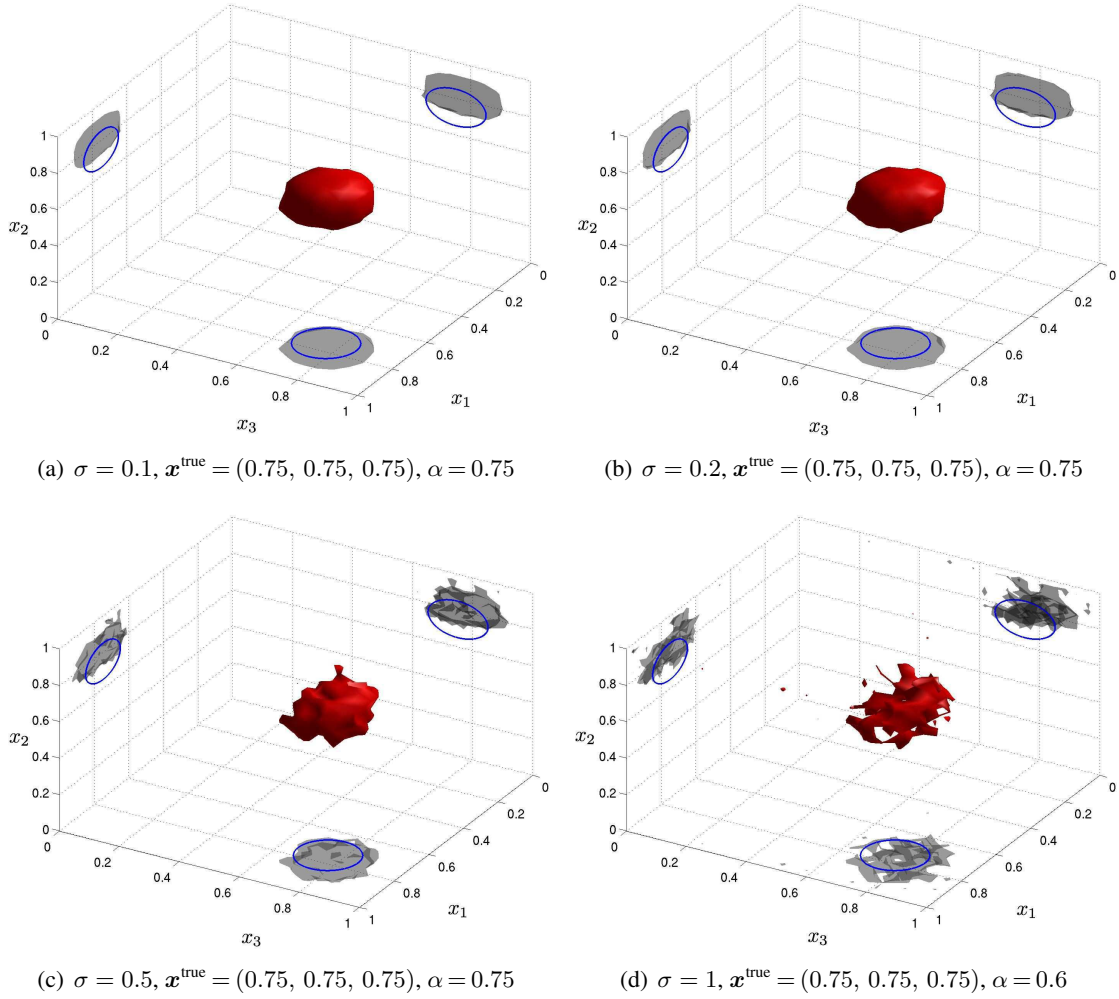
Figure 1.20: *Influence of data noise on $\mathbb{T}$: $B_{eq}(\alpha)$ for various levels of noise.*

yields usable results if applied to noisy data, as anticipated in Section 1.4.1 based on the mathematical structure of the TS formula, even though no regularization is used in the cost functional. This feature is very promising for applications. Note that the reference $\boldsymbol{u}_h^{\text{true}}$ used in (1.6.2) is itself "noisy", being a FEM-based approximation of $\boldsymbol{u}^{\text{true}}$. The discretization error level thus superimposed to the simulated data noise is expected not to exceed a few percent in the examples presented here (and thus to be much lower than the noise levels of Figs. 1.20(c) and 1.20(d)). For instance, synthetic data evaluations for the 2D elastodynamic examples presented a $2.1\,10^{-2}$ relative discrepancy (in L^2-norm) when performed on meshes featuring 2420 and 5453 nodes.

1.6.6   Identification of non-cavity defects

To conclude this series of numerical experiments, the identification of a crack and an inclusion is now considered, whose geometrical or material characteristics do not conform to those assumed in deriving the topological sensitivity.

Crack identification. The identification of a penny-shaped crack (radius $R = 0.1$, unit normal $\boldsymbol{n} = -\sin\theta\boldsymbol{e}_1 + \cos\theta\boldsymbol{e}_2$) leads to results that are satisfactory in terms of crack location and size, as shown in Fig. 1.21 for two choices $\theta = 0$ and $\theta = \pi/4$ of the crack inclination, while lacking sensitivity to the crack inclination. A recently-proposed specific formulation for crack problems (Bellis and Bonnet, 2009) features a polarization tensor that depends explicitly on an assumed crack orientation, thus offering (not yet investigated) possibilities for finding the crack orientation on that basis.
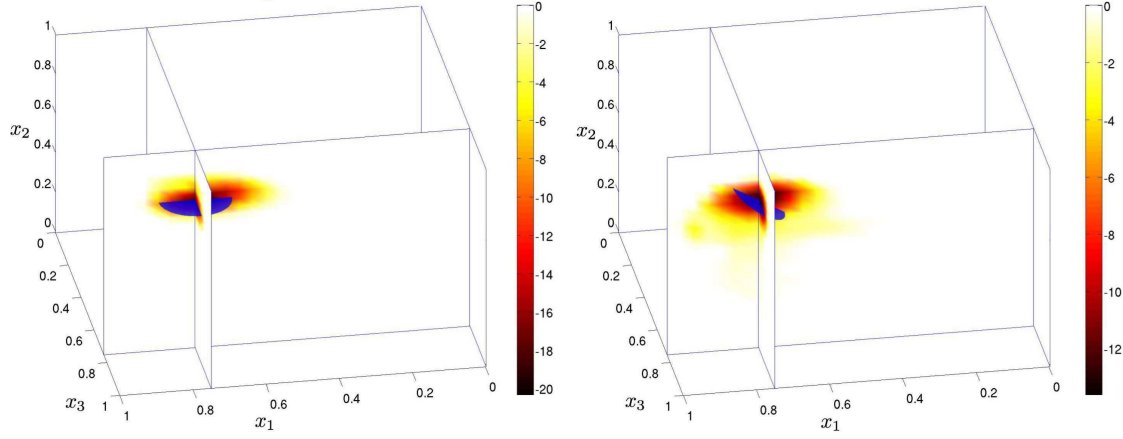
(a) $\theta = 0$ (horizontal), $\alpha = 0$, $\boldsymbol{x}^{\text{true}} = (0.75,\,0.75,\,0.75)$ (b) $\theta = \pi/4$ (inclined), $\alpha = 0$, $\boldsymbol{x}^{\text{true}} = (0.75,\,0.75,\,0.75)$

Figure 1.21: *Penny-shaped crack identification: thresholded TS field* $\mathbb{T}_\alpha$.

Inclusion identification. The identification of a penetrable spherical inclusion characterized by the radius $R = 0.1$ and material parameters $\mu^\star$, $\nu^\star = \nu$, $\rho^\star = \rho$ is now considered. The TS defined for cavities is found to identify satisfactorily *soft* spherical inclusions (such that $\mu^\star \leqslant \mu$), see Fig. 1.22.
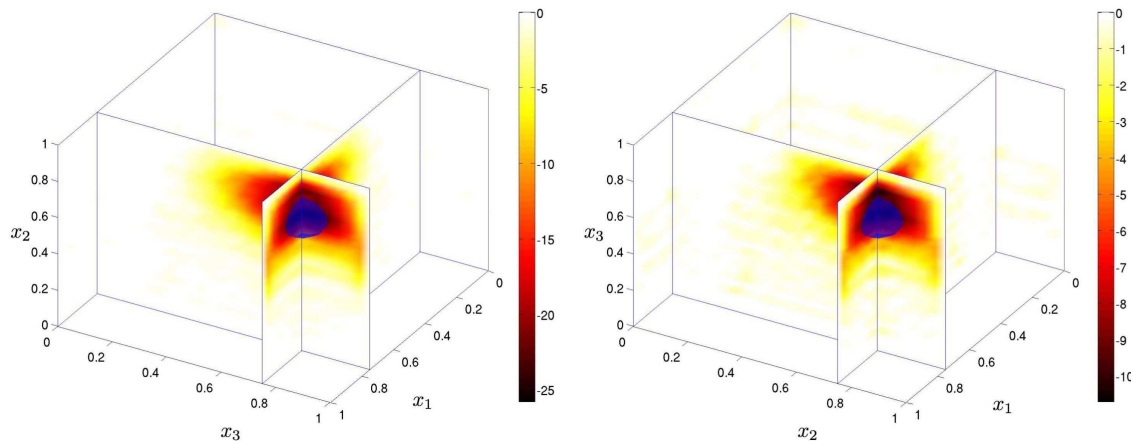
(a) $\mu^\star = 0.1\mu$, $\alpha = 0$, $\boldsymbol{x}^{\text{true}} = (0.75,\,0.75,\,0.75)$ (b) $\mu^\star = 0.5\mu$, $\alpha = 0$, $\boldsymbol{x}^{\text{true}} = (0.75,\,0.75,\,0.75)$

Figure 1.22: *Identification of a soft spherical inclusion using cavity-related thresholded TS field* $\mathbb{T}_\alpha$.
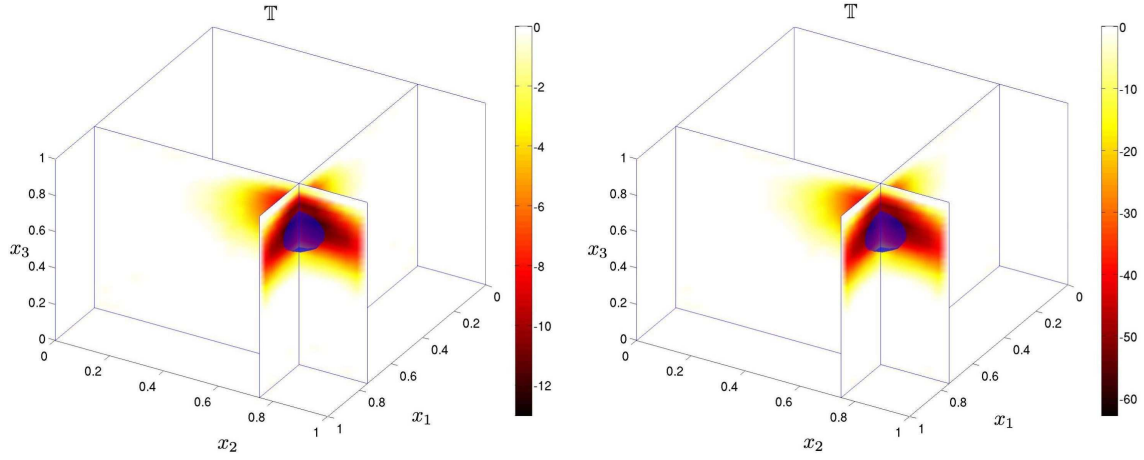
(a) $\mu^\star = 5\mu,\ \alpha = 0,\ \boldsymbol{x}^{\text{true}} = (0.75,\ 0.75,\ 0.75)$ (b) $\mu^\star = 10\mu,\ \alpha = 0,\ \boldsymbol{x}^{\text{true}} = (0.75,\ 0.75,\ 0.75)$

Figure 1.23: *Identification of a stiff spherical inclusion using inclusion-related thresholded TS field $\mathbb{T}_\alpha^\star$.*

However, employing this method for *stiff* inclusions (such that $\mu^\star > \mu$) leads to an contrast inversion in the TS field, the defect location now corresponding to a *maximum* of $\mathbb{T}(\cdot, T)$. Moreover, the TS defined for spherical elastic inclusions with assumed material parameters $\mu^\star, \nu^\star, \rho^\star$, given by

$$\mathbb{T}^\star(\boldsymbol{z}, T) = \{\boldsymbol{\sigma}[\hat{\boldsymbol{u}}] \star (\boldsymbol{\mathcal{A}}^\star : \boldsymbol{\sigma}[\boldsymbol{u}]) + (\rho - \rho^\star)\dot{\hat{\boldsymbol{u}}} \star \dot{\boldsymbol{u}}\}(\boldsymbol{z}, T) \tag{1.6.3}$$

with the polarization tensor $\boldsymbol{\mathcal{A}}^\star$ given by (1.B.2) and established in Chikichev and Guzina (2008), has also been implemented within the present FEM approach. Then, the TS field $\mathbb{T}^\star$ computed for the correct values of $\mu^\star, \nu^\star, \rho^\star$ is seen in Fig. 1.23 to allow a correct identification of a stiff inclusion.

1.7 Conclusion

In this study, the concept of topological sensitivity (TS) is developed for elastic and acoustic-wave imaging of media of arbitrary geometry using data in the time domain. On seeking the limiting form of the boundary integral equation governing the scattered field caused by a cavity with vanishing size ε, the TS field is found to be expressed in terms of the time convolution of the free field and an adjoint field. The ε^{d} asymptotic behavior of the cost function revealed by the analysis, identical to that established earlier for identification in static of frequency-domain settings, requires a degree of smoothness of the free field with respect to the time variable. The main analysis is devoted to 3D configurations, but 2D time-domain formulations are addressed as well.

While its derivation and formulation results from a mathematically rigorous asymptotic analysis, subsequent applications of the TS concept to the identification of finite-sized defects remains heuristic. Here, a comprehensive set of numerical examples is presented so as to substantiate the usefulness of the TS in applications and assess its performances. In contrast with the relatively involved analysis required to arrive at the correct formulation of the TS field, subsequent numerical implementations are quite simple. To emphasize the ease of application of the TS concept, all examples presented in this chapter rely on straightforward FEM formulations of the free and adjoint field, rather than more-specialized

integral-equation techniques previously used by the same group of authors. Several important features of the method are discussed through these examples, including its ability to identify multiple defects or to withstand significant data noise, and the effect of restrictions on the data through insufficient experiment duration or partial aperture. It is important to note that most examples consider identification based on a *single* (simulated) time-domain experiment.

From this study, it can be concluded that computing and exploiting the TS field constitutes a powerful and efficient tool for defect identification, as it is very simple to implement, computationally much faster than minimization-based inversion methods, and allows multiple defect identification without prior information. The present "one-shot" TS-based identification is qualitative rather than quantitative in nature. In addition to the stand-alone one-shot TS-based procedure emphasized in this chapter (of a qualitative rather than quantitative nature, and hence useful if speed or ease of implementation is more important than accurate defect sizing), the TS may also be implemented using an iterative matter removal strategy of the kind used in topology optimization (Allaire et al., 2005; Garreau et al., 2001), or be used in computing good initial guesses for subsequent refined inversion (perhaps based on exploiting $B_{eq}(\alpha)$ and $R_{eq}(\alpha)$ defined by (1.4.5) and (1.4.6)). Quantitative defect identification may also be achieved on the basis of time-domain versions (to be developed) of higher-order topological expansions along the lines of Bonnet (2008, 2009).

1.A   Asymptotic behavior of elastodynamic integral operators

1.A.1   Elastodynamic governing BIE

The integral representation formula for the scattered field $\boldsymbol{v}_\varepsilon$ reads (Eringen and Suhubi, 1975)

$$\boldsymbol{v}_\varepsilon(\boldsymbol{x}, t) = - \int_{\Gamma_\varepsilon(z)} \big\{ \boldsymbol{T}(\boldsymbol{x}, t, \boldsymbol{\xi}; \boldsymbol{n}) \star \boldsymbol{v}_\varepsilon(\boldsymbol{\xi}, t) + \boldsymbol{U}(\boldsymbol{x}, t, \boldsymbol{\xi}) \star \boldsymbol{t}[\boldsymbol{u}](\boldsymbol{\xi}, t) \big\} \, \mathrm{d}S_\xi \qquad (1.A.1)$$

In the present situation, where the free field featured in the right-hand side of (1.A.1) is also defined *inside* the cavity region $B_\varepsilon(\boldsymbol{z})$, one has

$$- \int_{\Gamma_\varepsilon(z)} \boldsymbol{U}(\boldsymbol{x}, t, \boldsymbol{\xi}) \star \boldsymbol{t}[\boldsymbol{u}](\boldsymbol{\xi}, t) \, \mathrm{d}S_\xi = \int_{B_\varepsilon(z)} \big[\rho \boldsymbol{U}(\boldsymbol{x}, t, \boldsymbol{\xi}) \star \ddot{\boldsymbol{u}}(\boldsymbol{\xi}, t) + \boldsymbol{E}(\boldsymbol{x}, t, \boldsymbol{\xi}) \star \boldsymbol{\sigma}[\boldsymbol{u}](\boldsymbol{\xi}, t) \big] \, \mathrm{d}V_\xi$$

by virtue of the divergence formula (note that $-\boldsymbol{n}$ in (1.A.1) is the *outward* unit normal to $B_\varepsilon(\boldsymbol{z})$) and the field equation (1.3.3a) verified by $\boldsymbol{u}$. Integral equation (1.3.7) then follows by invoking the following property of time convolution (1.3.8), easily established using integration by parts and conditions (1.3.9):

$$[\boldsymbol{a} \star \ddot{\boldsymbol{b}}](\boldsymbol{\xi}, t) = [\dot{\boldsymbol{a}} \star \dot{\boldsymbol{b}}](\boldsymbol{\xi}, t) = [\ddot{\boldsymbol{a}} \star \boldsymbol{b}](\boldsymbol{\xi}, t)$$

1.A.2   Elastodynamic fundamental solutions and proof of Lemmas 1 to 3

The time convolutions featured in integral equation (1.3.7) can be expressed as

$$\boldsymbol{U}(\boldsymbol{x}, t, \boldsymbol{\xi}) \star \boldsymbol{t}(\boldsymbol{\xi}, t) = \boldsymbol{U}[\boldsymbol{x}, t, \boldsymbol{\xi} | \boldsymbol{e}_i \cdot \boldsymbol{t}(\boldsymbol{\xi}, \cdot)] \cdot \boldsymbol{e}_i \qquad (1.A.2a)$$

$$\boldsymbol{T}(\boldsymbol{x}, t, \boldsymbol{\xi}; \boldsymbol{n}) \star \boldsymbol{v}_\varepsilon(\boldsymbol{\xi}, t) = \boldsymbol{T}[\boldsymbol{x}, t, \boldsymbol{\xi}; \boldsymbol{n} | \boldsymbol{e}_i \cdot \boldsymbol{v}_\varepsilon(\boldsymbol{\xi}, \cdot)] \cdot \boldsymbol{e}_i \qquad (1.A.2b)$$

where $\boldsymbol{U}[\boldsymbol{x}, t, \boldsymbol{\xi} | f]$ and $\boldsymbol{T}[\boldsymbol{x}, t, \boldsymbol{\xi}; \boldsymbol{n} | f]$ are the time-modulated elastodynamic Green's tensors, defined such that $\boldsymbol{e}_k \cdot \boldsymbol{U}$ and $\boldsymbol{e}_k \cdot \boldsymbol{T}$ are the displacement and traction vectors at $\boldsymbol{\xi} \in \Omega$ resulting from a point force acting at $\boldsymbol{x}$ in the k-direction with prescribed time-varying magnitude $f(t)$. The latter solve the boundary-initial value problem

$$\mathcal{L}_\xi \boldsymbol{U}[\boldsymbol{x}, t, \boldsymbol{\xi} | f] + \delta(\boldsymbol{\xi} - \boldsymbol{x}) f(t) \boldsymbol{I} = \boldsymbol{0} \qquad\qquad (\boldsymbol{\xi} \in \Omega, t \geqslant 0) \qquad (1.A.3a)$$

$$\boldsymbol{T}[\boldsymbol{x}, t, \boldsymbol{\xi}; \boldsymbol{n} | f] = \boldsymbol{0} \qquad\qquad\qquad\qquad (\boldsymbol{\xi} \in S_{\mathrm{N}}, t \geqslant 0) \qquad (1.A.3b)$$

$$\boldsymbol{U}[\boldsymbol{x}, t, \boldsymbol{\xi} | f] = \boldsymbol{0} \qquad\qquad\qquad\qquad (\boldsymbol{\xi} \in S_{\mathrm{D}}, t \geqslant 0) \qquad (1.A.3c)$$

$$\boldsymbol{U}[\boldsymbol{x}, 0, \boldsymbol{\xi} | f] = \dot{\boldsymbol{U}}[\boldsymbol{x}, 0, \boldsymbol{\xi} | f] = \boldsymbol{0} \qquad\qquad\quad (\boldsymbol{\xi} \in \Omega) \qquad\qquad (1.A.3d)$$

Similarly, let $\boldsymbol{U}_\infty[\boldsymbol{x}, t, \boldsymbol{\xi} | f]$ and $\boldsymbol{T}_\infty[\boldsymbol{x}, t, \boldsymbol{\xi}; \boldsymbol{n} | f]$ denote the time-modulated infinite-space fundamental solution, which satisfy equations (1.A.3a) and (1.A.3d) with $\Omega = \mathbb{R}^3$ and radiation conditions instead of boundary conditions (1.A.3b) and (1.A.3c), and is given by (Eringen and Suhubi, 1975)

$$\boldsymbol{U}_\infty[\boldsymbol{x}, t, \boldsymbol{\xi} | f] = \frac{1}{4\pi\mu r} \Big[A[\boldsymbol{x}, t, \boldsymbol{\xi} | f] \, \boldsymbol{I} + B[\boldsymbol{x}, t, \boldsymbol{\xi} | f] \, (\hat{\boldsymbol{r}} \otimes \hat{\boldsymbol{r}}) \Big] \qquad (1.A.4a)$$

$$\boldsymbol{E}[\boldsymbol{x}, t, \boldsymbol{\xi} | f] = \frac{1}{8\pi\mu r^2} \Big[B[\boldsymbol{x}, t, \boldsymbol{\xi} | f](\hat{\boldsymbol{r}} \otimes \boldsymbol{I}) + D[\boldsymbol{x}, t, \boldsymbol{\xi} | f](\mathcal{I}^{\mathrm{sym}} \cdot \hat{\boldsymbol{r}}) + 2E[\boldsymbol{x}, t, \boldsymbol{\xi} | f](\hat{\boldsymbol{r}} \otimes \hat{\boldsymbol{r}} \otimes \hat{\boldsymbol{r}}) \Big]$$
$$(1.A.4b)$$

$$\boldsymbol{T}_\infty[\boldsymbol{x}, t, \boldsymbol{\xi}; \boldsymbol{n} | f] = \frac{1}{4\pi r^2} \Big[C[\boldsymbol{x}, t, \boldsymbol{\xi} | f] \, (\hat{\boldsymbol{r}} \otimes \boldsymbol{n}) + D[\boldsymbol{x}, t, \boldsymbol{\xi} | f] \, (\hat{\boldsymbol{r}} \otimes \boldsymbol{n} + (\hat{\boldsymbol{r}} \cdot \boldsymbol{n}) \boldsymbol{I})$$
$$+ 2E[\boldsymbol{x}, t, \boldsymbol{\xi} | f] \, (\boldsymbol{n} \cdot \hat{\boldsymbol{r}}) \hat{\boldsymbol{r}} \otimes \hat{\boldsymbol{r}} \Big] \qquad (1.A.4c)$$

where $\boldsymbol{r} = (\boldsymbol{\xi} - \boldsymbol{x})$, $r = \|\boldsymbol{r}\|$, $\hat{\boldsymbol{r}} = \boldsymbol{r}/r$, κ is the ratio of bulk wave velocities as defined by

$$\kappa^2 = \frac{c_T^2}{c_L^2} = \frac{1 - 2\nu}{2(1-\nu)} = \frac{\mu}{\lambda + 2\mu} \tag{1.A.5}$$

and with $A = A[\boldsymbol{x}, t, \boldsymbol{\xi}|f], \ldots$ defined by

$$
\begin{aligned}
A[\boldsymbol{x}, t, \boldsymbol{\xi}|f] &= f\left(t - \frac{r}{c_T}\right) + \int_1^\kappa \eta f\left(t - \frac{\eta r}{c_T}\right) \mathrm{d}\eta \\
B[\boldsymbol{x}, t, \boldsymbol{\xi}|f] &= -3A[\boldsymbol{x}, t, \boldsymbol{\xi}|f] + 2f\left(t - \frac{r}{c_T}\right) + \kappa^2 f\left(t - \frac{r}{c_L}\right) \\
C[\boldsymbol{x}, t, \boldsymbol{\xi}|f] &= 2B[\boldsymbol{x}, t, \boldsymbol{\xi}|f] - (1 - 2\kappa^2)\left\{f\left(t - \frac{r}{c_L}\right) + \frac{r}{c_L}\dot{f}\left(t - \frac{r}{c_L}\right)\right\} \\
D[\boldsymbol{x}, t, \boldsymbol{\xi}|f] &= 2B[\boldsymbol{x}, t, \boldsymbol{\xi}|f] - f\left(t - \frac{r}{c_T}\right) - \frac{r}{c_T}\dot{f}\left(t - \frac{r}{c_T}\right) \\
E[\boldsymbol{x}, t, \boldsymbol{\xi}|f] &= -3B[\boldsymbol{x}, t, \boldsymbol{\xi}|f] - D[\boldsymbol{x}, t, \boldsymbol{\xi}|f] - \kappa^2\left\{f\left(t - \frac{r}{c_L}\right) + \frac{r}{c_L}\dot{f}\left(t - \frac{r}{c_L}\right)\right\}.
\end{aligned}
\tag{1.A.6}
$$

Define now the time-modulated complementary elastodynamic Green's tensor $\boldsymbol{U}_{\mathrm{C}}$ by

$$\boldsymbol{U}[\boldsymbol{x}, t, \boldsymbol{\xi}|f] = \boldsymbol{U}_\infty[\boldsymbol{x}, t, \boldsymbol{\xi}|f] + \boldsymbol{U}_{\mathrm{C}}[\boldsymbol{x}, t, \boldsymbol{\xi}|f] \tag{1.A.7}$$

By virtue of superposition arguments, $\boldsymbol{U}_{\mathrm{C}}$ is governed by the boundary-initial value problem

$$
\begin{aligned}
\mathcal{L}_\xi \boldsymbol{U}_{\mathrm{C}}[\boldsymbol{x}, t, \boldsymbol{\xi}|f] &= \boldsymbol{0} & (\boldsymbol{\xi} \in \Omega, t \geqslant 0) \\
\boldsymbol{T}_{\mathrm{C}}[\boldsymbol{x}, t, \boldsymbol{\xi}; \boldsymbol{n}|f] &= -\boldsymbol{T}_\infty[\boldsymbol{x}, t, \boldsymbol{\xi}; \boldsymbol{n}|f] & (\boldsymbol{\xi} \in S_{\mathrm{N}}, t \geqslant 0) \\
\boldsymbol{U}_{\mathrm{C}}[\boldsymbol{x}, t, \boldsymbol{\xi}|f] &= -\boldsymbol{U}_\infty[\boldsymbol{x}, t, \boldsymbol{\xi}|f] & (\boldsymbol{\xi} \in S_{\mathrm{D}}, t \geqslant 0) \\
\boldsymbol{U}_{\mathrm{C}}[\boldsymbol{x}, 0, \boldsymbol{\xi}|f] &= \dot{\boldsymbol{U}}_{\mathrm{C}}[\boldsymbol{x}, 0, \boldsymbol{\xi}|f] = \boldsymbol{0} & (\boldsymbol{\xi} \in \Omega)
\end{aligned}
\tag{1.A.8}
$$

One can then show (using e.g. an integral representation formula) that $\boldsymbol{U}_{\mathrm{C}}[\boldsymbol{x}, t, \boldsymbol{\xi}|f]$ is bounded in the limit $\boldsymbol{\xi} \to \boldsymbol{x}$, i.e. that the singular behavior of $\boldsymbol{U}[\boldsymbol{x}, t, \boldsymbol{\xi}|f]$ at $\boldsymbol{\xi} = \boldsymbol{x}$ is identical to that of its full-space counterpart $\boldsymbol{U}_\infty[\boldsymbol{x}, t, \boldsymbol{\xi}|f]$. Hence, one has

$$\boldsymbol{U}_{\mathrm{C}}[\boldsymbol{z} + \varepsilon\bar{\boldsymbol{x}}, t, \boldsymbol{z} + \varepsilon\bar{\boldsymbol{\xi}}|f] = O(1) \qquad (\varepsilon \to 0) \tag{1.A.9}$$

Proof of Lemma 1. With decomposition (1.A.7) of $\boldsymbol{U}[\boldsymbol{x}, t, \boldsymbol{\xi}|f]$ in mind, consider first the evaluation of the leading contribution to

$$\int_{\Gamma_\varepsilon(z)} \boldsymbol{U}_\infty(\boldsymbol{x}, t, \boldsymbol{\xi}) \star \boldsymbol{t}(\boldsymbol{\xi}, t) \, \mathrm{d}S_\xi \tag{1.A.10}$$

as $\varepsilon \to 0$, where $\boldsymbol{U}_\infty(\boldsymbol{x}, t, \boldsymbol{\xi}) \star \boldsymbol{t}(\boldsymbol{\xi}, t)$ is, by virtue of (1.A.2a), given by (1.A.4a) with $f(t) = \boldsymbol{e}_i \cdot \boldsymbol{t}(\boldsymbol{\xi}, t)$. Setting $f(\tau) = f(t) + (f(\tau) - f(t)) = f(t) + \Delta f(\tau)$ in (1.A.6), one obtains

$$A[\boldsymbol{x}, t, \boldsymbol{\xi}|f] = \frac{1 + \kappa^2}{2}f(t) + A[\boldsymbol{x}, t, \boldsymbol{\xi}|\Delta f], \quad B[\boldsymbol{x}, t, \boldsymbol{\xi}|f] = \frac{1 - \kappa^2}{2}f(t) + B[\boldsymbol{x}, t, \boldsymbol{\xi}|\Delta f]. \tag{1.A.11}$$

The cofactors of $f(t)$ in (1.A.11) correspond to a *constant* point force of unit magnitude, and hence yield, through (1.A.4a), the *elastostatic* full-space Green's tensor (i.e. Kelvin's solution) $\boldsymbol{U}_\infty(\bar{\boldsymbol{x}}, \bar{\boldsymbol{\xi}})$:

$$\boldsymbol{U}_\infty(\bar{\boldsymbol{x}}, \bar{\boldsymbol{\xi}}) = \frac{1}{8\pi\mu\bar{r}}\left[(1 + \kappa^2)\boldsymbol{I} + (1 - \kappa^2)\hat{\bar{\boldsymbol{r}}} \otimes \hat{\bar{\boldsymbol{r}}}\right] \tag{1.A.12}$$

Moreover, the Lipschitz-continuity assumption made on $t \mapsto \boldsymbol{\sigma}[\boldsymbol{u}](\boldsymbol{\xi}, t)$ implies that

$$|f(t) - f(\tau)| \leqslant K|t - \tau|, \quad |\dot{f}(\tau)| \leqslant K \qquad 0 \leqslant \tau \leqslant t$$

(with K the Lipschitz continuity modulus of f) and hence that

$$A[\boldsymbol{x}, t, \boldsymbol{\xi}|\Delta f] \leqslant KC_{\mathrm{A}}r/c_{\mathrm{T}}, \qquad B[\boldsymbol{x}, t, \boldsymbol{\xi}|\Delta f] \leqslant KC_{\mathrm{B}}r/c_{\mathrm{T}} \qquad (1.\mathrm{A}.13)$$

with appropriate constants $C_{\mathrm{A}}, C_{\mathrm{B}}$. Combining (1.A.4a), (1.A.11) and (1.A.13), one thus obtains

$$\boldsymbol{U}_\infty(\boldsymbol{x}, t, \boldsymbol{\xi}) \star \boldsymbol{t}(\boldsymbol{\xi}, t) = \boldsymbol{U}_\infty(\boldsymbol{x}, \boldsymbol{\xi}) \cdot \boldsymbol{t}(\boldsymbol{\xi}, t) + \boldsymbol{U}_\infty(\boldsymbol{x}, t, \boldsymbol{\xi}) \star \Delta\boldsymbol{t}(\boldsymbol{\xi}, t),$$
$$\big\| \boldsymbol{U}_\infty(\boldsymbol{x}, t, \boldsymbol{\xi}) \star \Delta\boldsymbol{t}(\boldsymbol{\xi}, t) \big\| \leqslant C_{\mathrm{U}}K, \qquad (1.\mathrm{A}.14)$$

where C_{U} is a constant. Hence, upon introducing scaling (1.3.10), (1.3.11) into (1.A.10), noting that $\boldsymbol{U}_\infty(\boldsymbol{\xi}, \boldsymbol{x})$ is homogeneous of degree -1 in $\bar{\boldsymbol{\xi}} - \bar{\boldsymbol{x}}$, making use of the expansion $\boldsymbol{\sigma}[\boldsymbol{u}](\boldsymbol{\xi}, t) = \boldsymbol{\sigma}[\boldsymbol{u}](\boldsymbol{z}, t) + o(1)$, and invoking (1.A.14), one obtains

$$\int_{\Gamma_\varepsilon(z)} \boldsymbol{U}_\infty(\boldsymbol{x}, t, \boldsymbol{\xi}) \star \boldsymbol{t}(\boldsymbol{\xi}, t) \, \mathrm{d}S_\xi = \varepsilon \left\{ \int_{\mathcal{S}} \boldsymbol{U}_\infty(\bar{\boldsymbol{x}}, \bar{\boldsymbol{\xi}}) \otimes \boldsymbol{n}(\bar{\boldsymbol{\xi}}) \, \mathrm{d}S_{\bar\xi} \right\} : \boldsymbol{\sigma}[\boldsymbol{u}](\boldsymbol{z}, t) + o(\varepsilon) \qquad (1.\mathrm{A}.15)$$

Finally, Lemma 1 follows from (1.A.7) and (1.A.15) together with the following estimate stemming from (1.A.9):

$$\int_{\Gamma_\varepsilon(z)} \boldsymbol{U}_{\mathrm{C}}(\boldsymbol{x}, t, \boldsymbol{\xi}) \star \boldsymbol{t}(\boldsymbol{\xi}, t) \, \mathrm{d}S_\xi = O(\varepsilon^2). \qquad (1.\mathrm{A}.16)$$

Remark 6. *The presence of $r\dot{f}(t - r/c_{L,T})$ in expressions (1.A.6) of C, D, E implies that the fundamental strains $\boldsymbol{E}[\boldsymbol{x}, t, \boldsymbol{\xi}|f]$ and stresses behave as $O(r^{-1})$ in the time-modulated case ($\dot{f} \neq 0$) but as as $O(r^{-2})$ in the static case ($\dot{f} = 0$).*

Proof of Lemma 2. The proof again exploits decomposition (1.A.7). First, upon introducing scaled coordinates (1.3.10) into expression (1.A.4c) of $\boldsymbol{T}_\infty$ and definitions (1.A.6) of $C[\boldsymbol{x}, t, \boldsymbol{\xi}|f], D[\boldsymbol{x}, t, \boldsymbol{\xi}|f]$ and $E[\boldsymbol{x}, t, \boldsymbol{\xi}|f]$ (wherein $f(t) = \boldsymbol{e}_i \cdot \boldsymbol{v}_\varepsilon(\boldsymbol{\xi}, t)$ according to 1.A.2b), it is a simple matter to show that

$$\boldsymbol{T}_\infty(\boldsymbol{x}, t, \boldsymbol{\xi}; \boldsymbol{n}) \star \boldsymbol{v}_\varepsilon(\boldsymbol{\xi}, t) = \frac{1}{\varepsilon^2} \boldsymbol{T}_{\infty,\varepsilon}(\bar{\boldsymbol{x}}, t, \bar{\boldsymbol{\xi}}; \boldsymbol{n}) \star \bar{\boldsymbol{v}}_\varepsilon(\bar{\boldsymbol{\xi}}, t) \qquad (1.\mathrm{A}.17)$$

where $\boldsymbol{T}_{\infty,\varepsilon}$ is defined by (1.A.4c) and (1.A.6) with wave velocities $c_{\mathrm{L}}, c_{\mathrm{T}}$ replaced by rescaled values $c_{\mathrm{L}}/\varepsilon$ and $c_{\mathrm{T}}/\varepsilon$. Equation (1.A.17) and scaling (1.3.11) then imply

$$\fint_{\Gamma_\varepsilon(z)} \boldsymbol{T}_\infty(\boldsymbol{x}, t, \boldsymbol{\xi}; \boldsymbol{n}) \star \boldsymbol{v}_\varepsilon(\boldsymbol{\xi}, t) \, \mathrm{d}S_\xi = \fint_{\mathcal{S}} \boldsymbol{T}_{\infty,\varepsilon}(\bar{\boldsymbol{x}}, t, \bar{\boldsymbol{\xi}}; \boldsymbol{n}) \star \bar{\boldsymbol{v}}_\varepsilon(\bar{\boldsymbol{\xi}}, t) \, \mathrm{d}S_{\bar\xi} \qquad (1.\mathrm{A}.18)$$

Moreover, owing to the boundedness (1.A.9) of the complementary Green'a tensor $\boldsymbol{U}_{\mathrm{C}}$, one has, upon using again coordinate scaling (1.3.10):

$$\fint_{\Gamma_\varepsilon(z)} \boldsymbol{T}_{\mathrm{C}}(\boldsymbol{x}, t, \boldsymbol{\xi}; \boldsymbol{n}) \star \boldsymbol{v}_\varepsilon(\boldsymbol{\xi}, t) \, \mathrm{d}S_\xi = O(\varepsilon^2) \|\bar{\boldsymbol{v}}_\varepsilon(\cdot, t)\| \qquad (1.\mathrm{A}.19)$$

where $\|\bar{\boldsymbol{v}}_\varepsilon(\cdot, t)\|$ is a norm of $\bar{\boldsymbol{\xi}} \mapsto \bar{\boldsymbol{v}}_\varepsilon(\bar{\boldsymbol{\xi}}, t)$, e.g. its L^2-norm over $\mathcal{S}$. Lemma 2 then follows from combining (1.A.18) and (1.A.19).

Proof of Lemma 3. The proposed ansatz (1.3.14) is, by assumption in Lemma 1, Lipschitz-continuous with respect to t. It is therefore appropriate to investigate the behavior of $\boldsymbol{T}_\infty$ as defined by (1.A.4c) and (1.A.6) for a Lipschitz-continuous time-modulation f. Proceeding along the lines of Lemma 1, and in particular invoking again the decomposition $f(\tau) = f(t) + (f(\tau) - f(t)) = f(t) + \Delta f(\tau)$, one has

$$
\begin{aligned}
C[\bar{\boldsymbol{x}}, t, \bar{\boldsymbol{\xi}}|f] &= \kappa^2 f(t) + C[\bar{\boldsymbol{x}}, t, \bar{\boldsymbol{\xi}}|\Delta f] \\
D[\bar{\boldsymbol{x}}, t, \bar{\boldsymbol{\xi}}|f] &= -\kappa^2 f(t) + D[\bar{\boldsymbol{x}}, t, \bar{\boldsymbol{\xi}}|\Delta f] \\
E[\bar{\boldsymbol{x}}, t, \bar{\boldsymbol{\xi}}|f] &= -\frac{3}{2}(1-\kappa^2)f(t) + E[\bar{\boldsymbol{x}}, t, \bar{\boldsymbol{\xi}}|\Delta f]
\end{aligned}
\tag{1.A.20}
$$

Substituting the above values into (1.A.4c) and (1.A.6), one obtains the decomposition

$$
\boldsymbol{T}_\infty[\bar{\boldsymbol{x}}, t, \bar{\boldsymbol{\xi}}|f] = \boldsymbol{T}_\infty(\bar{\boldsymbol{x}}, \bar{\boldsymbol{\xi}}; \boldsymbol{n})f(t) + \boldsymbol{T}_\infty[\bar{\boldsymbol{x}}, t, \bar{\boldsymbol{\xi}}|\Delta f]
\tag{1.A.21}
$$

with $\boldsymbol{T}_\infty(\bar{\boldsymbol{x}}, \bar{\boldsymbol{\xi}}; \boldsymbol{n})$, the traction associated with the elastostatic Kelvin solution $\boldsymbol{U}_\infty(\bar{\boldsymbol{x}}, \bar{\boldsymbol{\xi}})$, given by

$$
\boldsymbol{T}_\infty(\bar{\boldsymbol{x}}, \bar{\boldsymbol{\xi}}; \boldsymbol{n}) = \frac{1}{4\pi\bar{r}^2}\Big[\kappa^2\big(\hat{\bar{\boldsymbol{r}}} \otimes \boldsymbol{n} - \boldsymbol{n} \otimes \hat{\bar{\boldsymbol{r}}} - (\hat{\bar{\boldsymbol{r}}}\cdot\boldsymbol{n})\boldsymbol{I}\big) + 3(\kappa^2-1)(\hat{\bar{\boldsymbol{r}}}\cdot\boldsymbol{n})\hat{\bar{\boldsymbol{r}}} \otimes \boldsymbol{n}\Big].
\tag{1.A.22}
$$

Decomposition (1.A.21) is in particular applicable to $\boldsymbol{T}_{\infty,\varepsilon}[\ldots|f]$ defined by replacing velocities c_L, c_T by the rescaled values c_L/ε, c_T/ε in $\boldsymbol{T}_\infty[\ldots|f]$. Owing to the assumed Lipschitz continuity of f, one easily shows that

$$
\big\|\boldsymbol{T}_{\infty,\varepsilon}[\bar{\boldsymbol{x}}, t, \bar{\boldsymbol{\xi}}|\Delta f]\big\| \leqslant C_T K\varepsilon \qquad (\varepsilon \to 0)
$$

where K is the Lipschitz constant of f and C_T is a constant. Consequently, using the fact that $\boldsymbol{T}_\infty(\bar{\boldsymbol{x}}, \bar{\boldsymbol{\xi}}; \boldsymbol{n})f(t)$ is unaffected by the wave velocity rescaling, decomposition (1.A.21) implies

$$
\boldsymbol{T}_{\infty,\varepsilon}[\bar{\boldsymbol{x}}, t, \bar{\boldsymbol{\xi}}|f] = \boldsymbol{T}_\infty(\bar{\boldsymbol{x}}, \bar{\boldsymbol{\xi}}; \boldsymbol{n})f(t) + o(1) \qquad (\varepsilon \to 0)
$$

Lemma 3 then follows from equating $f(t)$ to the components of $\varepsilon\boldsymbol{\mathcal{V}}(\bar{\boldsymbol{\xi}}):\boldsymbol{\sigma}[\boldsymbol{u}](\boldsymbol{z}, t)$, according to (1.A.2b), in the above estimate.

1.A.3 3D Scalar wave equation

The reference domain $\Omega \subset \mathbb{R}^3$ is now filled by an acoustic fluid characterized by the wave velocity c. The acoustic pressure field u_B generated by given excitations $\bar{p}(\boldsymbol{\xi}, t)$ (proportional to normal wall acceleration) and $\bar{u}(\boldsymbol{\xi}, t)$ (applied pressure) in the presence of a (possibly multiply-connected) sound-hard obstacle occupying a region B bounded by Γ is governed by the following set of equations:

$$
\mathcal{P}(B): \quad
\begin{aligned}
[\mathcal{L}_c u_B](\boldsymbol{\xi}, t) &= 0 & (\boldsymbol{\xi} \in \Omega, t \geqslant 0) \\
q[u_B](\boldsymbol{\xi}, t) &= 0 & (\boldsymbol{\xi} \in \Gamma, t \geqslant 0) \\
q[u_B](\boldsymbol{\xi}, t) &= \bar{p}(\boldsymbol{\xi}, t) & (\boldsymbol{\xi} \in S_N, t \geqslant 0) \\
u_B(\boldsymbol{\xi}, t) &= \bar{u}(\boldsymbol{\xi}, t) & (\boldsymbol{\xi} \in S_D, t \geqslant 0) \\
u_B(\boldsymbol{\xi}, 0) = \dot{u}_B(\boldsymbol{\xi}, 0) &= 0 & (\boldsymbol{\xi} \in \Omega)
\end{aligned}
\tag{1.A.23}
$$

where $w \mapsto q[w] = \boldsymbol{\nabla} w \cdot \boldsymbol{n}$ is the normal derivative operator and $\mathcal{L}_c$, defined by

$$
[\mathcal{L}_c w](\boldsymbol{\xi}, t) = \Delta w(\boldsymbol{\xi}, t) - \frac{1}{c^2}\ddot{w}(\boldsymbol{\xi}, t)
\tag{1.A.24}
$$

is the governing partial differential operator of linear acoustics. Objective functions of format (1.2.5), with densities now having the form $\varphi\big[u_B(\boldsymbol{\xi}, t), \boldsymbol{\xi}, t\big]$, are again considered. Define a small scatterer $B_\varepsilon(\boldsymbol{z})$ of size ε as in Section 1.3, and let u denote the free field (which solves $\mathcal{P}(\emptyset)$) and v_ε the scattered field (such that the total field $u_\varepsilon = u + v_\varepsilon$ solves problem $\mathcal{P}(B_\varepsilon(\boldsymbol{z}))$). The governing integral equation for the scattered field v_ε reads

$$\frac{1}{2}v_\varepsilon(\boldsymbol{x}, t) + \fint_{\Gamma_\varepsilon(z)} H[\boldsymbol{x}, t, \boldsymbol{\xi}; \boldsymbol{n} | v_\varepsilon(\boldsymbol{\xi}, t)] \, \mathrm{d}S_\xi = - \int_{\Gamma_\varepsilon(z)} G[\boldsymbol{x}, t, \boldsymbol{\xi}; \boldsymbol{n} | q[u]](\boldsymbol{\xi}, t)] \, \mathrm{d}S_\xi$$
$$(\boldsymbol{x} \in \Gamma_\varepsilon(\boldsymbol{z}), \ t \geqslant 0), \quad (1.A.25)$$

where the time-modulated Green's function $G[\boldsymbol{x}, t, \boldsymbol{\xi}|f]$ solves the boundary-initial value problem

$$\begin{aligned}
\mathcal{L}_{c,\xi} G[\boldsymbol{x}, t, \boldsymbol{\xi}|f] &= 0 & (\boldsymbol{\xi} \in \Omega, t \geqslant 0) \\
G[\boldsymbol{x}, t, \boldsymbol{\xi}|f] &= 0 & (\boldsymbol{\xi} \in S_\mathrm{D}, t \geqslant 0), \\
H[\boldsymbol{x}, t, \boldsymbol{\xi}|f] &= 0 & (\boldsymbol{\xi} \in S_\mathrm{N}, t \geqslant 0), \\
G[\boldsymbol{x}, 0, \boldsymbol{\xi}|f] &= \dot{G}[\boldsymbol{x}, 0, \boldsymbol{\xi}|f] = 0 & (\boldsymbol{\xi} \in \Omega)
\end{aligned} \qquad (1.A.26)$$

and with $H[\boldsymbol{x}, t, \boldsymbol{\xi}; \boldsymbol{n}|f] = \boldsymbol{\nabla}_\xi G[\boldsymbol{x}, t, \boldsymbol{\xi}|f] \cdot \boldsymbol{n}(\boldsymbol{\xi})$. Moreover, let $G_\infty[\boldsymbol{x}, t, \boldsymbol{\xi}|f]$ denote the time-modulated *full-space* fundamental solution, given by (Eringen and Suhubi, 1975)

$$G_\infty[\boldsymbol{x}, t, \boldsymbol{\xi}|f] = \frac{1}{4\pi r} f\left(t - \frac{r}{c}\right) \qquad (1.A.27)$$

$$\boldsymbol{\nabla}_\xi G_\infty[\boldsymbol{x}, t, \boldsymbol{\xi}|f] = -\frac{1}{4\pi r^2}\left[f\left(\boldsymbol{\xi}, t - \frac{r}{c}\right) + \frac{r}{c}\dot{f}\left(t - \frac{r}{c}\right)\right]\hat{\boldsymbol{r}} \qquad (1.A.28)$$

and define the complementary Green's function G_C, bounded in the limit $\boldsymbol{\xi} \to \boldsymbol{x}$, by $G_\mathrm{C}[\boldsymbol{x}, t, \boldsymbol{\xi}|f] = G[\boldsymbol{x}, t, \boldsymbol{\xi}|f] - G_\infty[\boldsymbol{x}, t, \boldsymbol{\xi}|f]$. The counterparts of Lemmas 1 and 2 then correspond to estimate

$$\int_{\Gamma_\varepsilon(z)} G(\boldsymbol{x}, t, \boldsymbol{\xi}) \star q[u] \, \mathrm{d}S_\xi = \varepsilon\left\{\int_{\mathcal{S}} G_\infty(\bar{\boldsymbol{x}}, \bar{\boldsymbol{\xi}}) \otimes \boldsymbol{n}(\bar{\boldsymbol{\xi}}) \, \mathrm{d}S_{\bar{\xi}}\right\} \cdot \boldsymbol{\nabla} u(\boldsymbol{z}, t) + o(\varepsilon), \qquad (1.A.29)$$

assuming $\tau \mapsto \boldsymbol{\nabla} u(\boldsymbol{x}, \tau)$ is Lipschitz-continuous and differentiable in a neighbourhood of $\tau = t$, and

$$\fint_{\Gamma_\varepsilon(z)} H[\boldsymbol{x}, t, \boldsymbol{\xi}; \boldsymbol{n}|v_\varepsilon(\boldsymbol{\xi}, t)] \, \mathrm{d}S_\xi = \int_{\mathcal{S}} H_{\infty, \varepsilon}(\bar{\boldsymbol{x}}, \bar{\boldsymbol{\xi}}; \boldsymbol{n})\bar{v}_\varepsilon(\bar{\boldsymbol{\xi}}, t) \, \mathrm{d}S_{\bar{\xi}} + o(\|\bar{v}_\varepsilon\|) \quad (\varepsilon \to 0) \qquad (1.A.30)$$

(with $H_\infty(\bar{\boldsymbol{x}}, \bar{\boldsymbol{\xi}}; \boldsymbol{n}) = \boldsymbol{\nabla}_{\bar{\xi}} G_\infty(\bar{\boldsymbol{x}}, \bar{\boldsymbol{\xi}})\boldsymbol{n}(\boldsymbol{\xi})$, $H_{\infty, \varepsilon}$ defined by (1.A.28) with c replaced with c/ε, and $\bar{v}_\varepsilon(\bar{\boldsymbol{\xi}}, t)$ defined by $\bar{v}_\varepsilon(\bar{\boldsymbol{\xi}}, t) = v_\varepsilon(\boldsymbol{\xi}, t)$ with $\bar{\boldsymbol{\xi}}$ and $\boldsymbol{\xi}$ related through (1.3.10)). Estimates (1.A.29) and (1.A.30), established following the steps used for Lemmas 1 and 2, suggest the following asymptotic behavior for $v_\varepsilon(\boldsymbol{\xi}, t)$:

$$\bar{v}_\varepsilon(\bar{\boldsymbol{\xi}}, t) = \varepsilon\boldsymbol{\mathcal{V}}(\bar{\boldsymbol{\xi}}, t) \cdot \boldsymbol{\nabla} u(\boldsymbol{z}, t) + o(\varepsilon) \quad (\boldsymbol{\xi} \in \Gamma_\varepsilon(\boldsymbol{z}), \bar{\boldsymbol{\xi}} \in \mathcal{S}) \qquad (1.A.31)$$

Upon substituting (1.A.31) into the right-hand side of (1.A.30), making use of the assumed Lipschitz continuity of $\tau \mapsto \boldsymbol{\nabla} u(\boldsymbol{x}, \tau)$, and retaining only the leading $O(\varepsilon)$ contributions as $\varepsilon \to 0$ according to (1.A.29) and (1.A.30), $\boldsymbol{\mathcal{V}}$ is readily found to verify an integral equation that corresponds to the following canonical exterior problem for the vector Laplace equation:

$$\Delta_{\bar{\xi}}\boldsymbol{\mathcal{V}}(\bar{\boldsymbol{\xi}}) = \boldsymbol{0} \quad (\bar{\boldsymbol{\xi}} \in \mathbb{R}^3 \setminus \mathcal{B}), \qquad \boldsymbol{\nabla}_{\bar{\xi}}\boldsymbol{\mathcal{V}}(\bar{\boldsymbol{\xi}}) \cdot \boldsymbol{n}(\bar{\boldsymbol{\xi}}) = -\boldsymbol{n}(\bar{\boldsymbol{\xi}}) \quad (\bar{\boldsymbol{\xi}} \in \mathcal{S}) \qquad (1.A.32)$$

The scattered field v_ε at any point of S^{obs} is then found (inserting (1.A.31) into the integral representation formula associated with integral equation (1.A.25)) to have the expansion

$$v_\varepsilon(\boldsymbol{x}, t) = \varepsilon^3 |\mathcal{B}| \{ \boldsymbol{\nabla}_\xi G(\boldsymbol{x}, t, \boldsymbol{z}) \star [\boldsymbol{A} \cdot \boldsymbol{\nabla} u](\boldsymbol{z}, t) + \rho \dot{\boldsymbol{U}}(\boldsymbol{x}, t, \boldsymbol{z}) \star \dot{\boldsymbol{u}}(\boldsymbol{z}, t) \} + o(\varepsilon^3) \qquad (1.A.33)$$

where the constant second-order polarization tensor $\boldsymbol{A} = \boldsymbol{A}(\mathcal{B})$ depends only on $\mathcal{B}$ and is defined by

$$\boldsymbol{A} = \boldsymbol{I} - \frac{1}{|\mathcal{B}|} \left\{ \int_{\mathcal{S}} \boldsymbol{n}(\bar{\boldsymbol{\xi}}) \otimes \boldsymbol{\mathcal{V}}(\bar{\boldsymbol{\xi}}) \, \mathrm{d} S_{\bar{\xi}} \right\} \qquad (1.A.34)$$

Finally, upon defining the adjoint solution $\hat{u}$ as the solution of the initial-boundary value problem

$$\begin{aligned}
\left[\mathcal{L}_c \hat{u} \right](\boldsymbol{\xi}, t) &= 0 & (\boldsymbol{\xi} \in \Omega, 0 \leqslant t \leqslant T), \\
q[\hat{u}](\boldsymbol{\xi}, t) &= \frac{\partial \varphi}{\partial u} [u(\boldsymbol{\xi}, T - t), \boldsymbol{\xi}, T - t] & (\boldsymbol{\xi} \in S^{\text{obs}}, 0 \leqslant t \leqslant T), \\
q[\hat{u}](\boldsymbol{\xi}, t) &= 0 & (\boldsymbol{\xi} \in S_{\text{N}} \backslash S^{\text{obs}}, 0 \leqslant t \leqslant T), \\
\hat{u}(\boldsymbol{\xi}, t) &= 0 & (\boldsymbol{\xi} \in S_{\text{D}}, 0 \leqslant t \leqslant T), \\
\hat{u}(\boldsymbol{\xi}, 0) = \dot{\hat{u}}(\boldsymbol{\xi}, 0) &= 0 & (\boldsymbol{\xi} \in \Omega),
\end{aligned} \qquad (1.A.35)$$

using reciprocity identity (1.3.23) suitably modified for linear acoustics, and exploiting the relevant boundary conditions, expansion (1.3.5) with $\boldsymbol{u}$ and $\boldsymbol{v}_\varepsilon$ respectively replaced with u and v_ε yields

$$\begin{aligned}
\eta(\varepsilon) |\mathcal{B}| \mathbb{T}(\boldsymbol{z}, T) + o\big(\eta(\varepsilon)\big) &= \int_0^T \int_{S^{\text{obs}}} \frac{\partial \varphi}{\partial u} [u(\boldsymbol{\xi}, t), \boldsymbol{\xi}, t] v_\varepsilon(\boldsymbol{\xi}, t) \, \mathrm{d} S_\xi \, \mathrm{d} t \\
&= - \int_{\Gamma_\varepsilon(z)} \{ q[\hat{u}] \star v_\varepsilon + q[u] \star \hat{u} \}(\boldsymbol{\xi}, t) \, \mathrm{d} S_\xi \\
&= \varepsilon^3 |\mathcal{B}| \{ \boldsymbol{\nabla} \hat{u} \star (\boldsymbol{A} \cdot \boldsymbol{\nabla} u) + \frac{1}{c^2} \dot{\hat{u}} \star \dot{u} \}(\boldsymbol{z}, t) + o(\varepsilon^3) \qquad (1.A.36)
\end{aligned}$$

with the polarization tensor $\boldsymbol{A}$ still defined by (1.A.34). Hence, the TS $\mathbb{T}(\boldsymbol{z}, t)$ and leading behavior $\eta(\varepsilon)$ are found to be given by

$$\mathbb{T}(\boldsymbol{z}, t) = \{ \boldsymbol{\nabla} \hat{u} \star (\boldsymbol{A} \cdot \boldsymbol{\nabla} u) + \frac{1}{c^2} \dot{\hat{u}} \star \dot{u} \}(\boldsymbol{z}, t), \qquad \eta(\varepsilon) = \varepsilon^3 \qquad (1.A.37)$$

1.A.4 Two-dimensional case

The time-modulated full-space fundamental solution is given by (Eringen and Suhubi, 1975)

$$G_\infty[\boldsymbol{x}, t, \boldsymbol{\xi} | f] = \frac{1}{2\pi} \int_0^{\eta^\star(r,t)} \frac{1}{[\eta^2 + r^2]^{1/2}} f\left(t - \frac{[\eta^2 + r^2]^{1/2}}{c}\right) \mathrm{d}\eta \qquad (1.A.38)$$

$$\begin{aligned}
\boldsymbol{\nabla}_\xi G_\infty[\boldsymbol{x}, t, \boldsymbol{\xi} | f] = -\frac{1}{2\pi} \boldsymbol{r} \int_0^{\eta^\star(r,t)} & \left\{ \frac{1}{[\eta^2 + r^2]^{3/2}} f\left(t - \frac{[\eta^2 + r^2]^{1/2}}{c}\right) \right. \\
& \left. + \frac{1}{c[\eta^2 + r^2]} \dot{f}\left(t - \frac{[\eta^2 + r^2]^{1/2}}{c}\right) \right\} \mathrm{d}\eta \qquad (1.A.39)
\end{aligned}$$

where $\boldsymbol{\xi}$, $\boldsymbol{x}$ now denote points in the two-dimensional space spanned by $(\boldsymbol{e}_1, \boldsymbol{e}_2)$, and the upper bound $\eta^\star(r, t)$ of the above integrals stems from the causality condition $f(\tau) = 0$, $\tau < 0$ and is given by

$$\eta^\star(r, t) = [(ct)^2 - r^2]^{1/2} \qquad (1.A.40)$$

Proof of lemma 1.   Assume that $\tau \mapsto \boldsymbol{\nabla} \dot{u}(\boldsymbol{\xi}, \tau)$ is bounded for $0 \leqslant \tau \leqslant t$ uniformly in a neighbourhood $V(\boldsymbol{z})$ of $\boldsymbol{z}$, which implies that $\tau \mapsto \boldsymbol{\nabla} u(\boldsymbol{\xi}, \tau)$ is Lipschitz-continuous for $0 \leqslant \tau \leqslant t$ uniformly in $V(\boldsymbol{z})$. Hence, for some positive constant K, one has

$$\|\boldsymbol{\nabla} \dot{u}(\boldsymbol{\xi}, \tau)\| \leqslant K, \quad \|\boldsymbol{\nabla} u(\boldsymbol{\xi}, \tau) - \boldsymbol{\nabla} u(\boldsymbol{\xi}, \tau')\| \leqslant K|\tau - \tau'| \qquad 0 \leqslant \tau, \tau' \leqslant t, \ \boldsymbol{\xi} \in V(\boldsymbol{z}) \qquad (1.A.41)$$

Here, the tail effect, i.e. the fact (reflected in the integration bounds of (1.A.38) and (1.A.39), and typical of 2D time-domain fundamental solutions) that a time-impulsive source generates at $(\boldsymbol{\xi}, t)$ a nonzero response over a continuous time interval, entails a proof method that is slightly more involved than for the previously-addressed 3D cases. First, the main quantity of interest is recast into a domain integral along the lines of Section 1.A.1:

$$-\int_{\Gamma_\varepsilon(z)} G_\infty(\boldsymbol{x}, t, \boldsymbol{\xi}) \star q[u](\boldsymbol{\xi}, t) \, \mathrm{d}S_\xi$$
$$= \int_{B_\varepsilon(z)} \left\{ \boldsymbol{\nabla}_\xi G_\infty(\boldsymbol{x}, t, \boldsymbol{\xi}) \star \boldsymbol{\nabla} u(\boldsymbol{\xi}, t) + \frac{1}{c^2} G_\infty(\boldsymbol{x}, t, \boldsymbol{\xi}) \star \ddot{u}(\boldsymbol{\xi}, t) \right\} \mathrm{d}V_\xi \qquad (1.A.42)$$

Now, setting $f(\tau) = f(t) + \Delta f(\tau)$ in (1.A.39) and equating $f(\tau)$ to the components of $\boldsymbol{\nabla} u(\boldsymbol{\xi}, \tau)$ in the resulting equality, one obtains

$$\boldsymbol{\nabla}_\xi G_\infty(\boldsymbol{x}, t, \boldsymbol{\xi}) \star \boldsymbol{\nabla} u(\boldsymbol{\xi}, t) = G_\infty(\boldsymbol{x}, \boldsymbol{\xi}) \cdot \boldsymbol{\nabla} u(\boldsymbol{\xi}, t) + \boldsymbol{\nabla}_\xi G_\infty(\boldsymbol{x}, t, \boldsymbol{\xi}) \star \boldsymbol{\nabla} \Delta u(\boldsymbol{\xi}, t), \qquad (1.A.43)$$

where $G_\infty(\boldsymbol{x}, \boldsymbol{\xi})$ is the static 2D full-space Laplace fundamental solution, given by

$$G_\infty(\boldsymbol{x}, \boldsymbol{\xi}) = -\frac{1}{2\pi} r \int_0^{\eta^\star(r,t)} \frac{1}{[\eta^2 + r^2]^{3/2}} \, \mathrm{d}\eta = -\frac{1}{2\pi} \ln r, \qquad \boldsymbol{\nabla}_\xi G_\infty(\boldsymbol{x}, \boldsymbol{\xi}) = -\frac{1}{2\pi r^2} \boldsymbol{r} \qquad (1.A.44)$$

(with the second equality established via analytical integration). Moreover, utilizing the assumed Lipschitz continuity of $t \mapsto \boldsymbol{\nabla} u(\boldsymbol{\xi}, t)$ for bounding the last term in (1.A.43) yields (noting that $\eta^\star(r, t) \leqslant ct$)

$$\big| \boldsymbol{\nabla}_\xi G_\infty(\boldsymbol{x}, t, \boldsymbol{\xi}) \star \boldsymbol{\nabla} \Delta u(\boldsymbol{\xi}, t) \big| \leqslant \frac{r}{2\pi} \frac{2K}{c} \int_0^{\eta^\star(r,t)} \frac{\mathrm{d}\eta}{\eta^2 + r^2} = \frac{K}{\pi c} \tan^{-1} \left[\frac{(ct)^2}{r^2} - 1 \right]^{1/2} \leqslant \frac{K}{2c} \qquad (1.A.45)$$

with the last inequality stemming from the fact that $-\pi/2 \leqslant \tan^{-1} x \leqslant \pi/2$ for any x. Next, introducing the scaled coordinates (1.3.10), one obtains (by virtue of $\boldsymbol{\nabla}_\xi G_\infty(\boldsymbol{x}, \boldsymbol{\xi})$ being homogeneous of degree -1 in $\boldsymbol{x} - \boldsymbol{\xi}$)

$$G_\infty(\boldsymbol{x}, \boldsymbol{\xi}) \cdot \boldsymbol{\nabla} u(\boldsymbol{\xi}, t) = \frac{1}{\varepsilon} G_\infty(\bar{\boldsymbol{x}}, \bar{\boldsymbol{\xi}}) \cdot [\boldsymbol{\nabla} u(\boldsymbol{z}, t) + o(1)] \qquad (1.A.46)$$

Finally, upon integrating decomposition (1.A.43) over B_ε, applying estimates (1.A.45) and (1.A.46), and noting that $\mathrm{d}V_\xi = \varepsilon^2 \, \mathrm{d}V_{\bar{\xi}}$ for the present 2D case, one obtains (with the last equality stemming from applying the divergence formula):

$$\int_{B_\varepsilon(z)} \boldsymbol{\nabla}_\xi G_\infty(\boldsymbol{x}, t, \boldsymbol{\xi}) \star \boldsymbol{\nabla} u(\boldsymbol{\xi}, t) \, \mathrm{d}V_\xi = \varepsilon \left\{ \int_{\mathcal{B}} \boldsymbol{\nabla}_{\bar{\xi}} G_\infty(\bar{\boldsymbol{x}}, \bar{\boldsymbol{\xi}}) \, \mathrm{d}V_{\bar{\xi}} \right\} \cdot \boldsymbol{\nabla} u(\boldsymbol{\xi}, t) + o(\varepsilon)$$
$$= \varepsilon \left\{ \int_{\mathcal{S}} G_\infty(\bar{\boldsymbol{x}}, \bar{\boldsymbol{\xi}}) \otimes \boldsymbol{n}(\bar{\boldsymbol{\xi}}) \, \mathrm{d}S_{\bar{\xi}} \right\} \cdot \boldsymbol{\nabla} u(\boldsymbol{\xi}, t) + o(\varepsilon) \qquad (1.A.47)$$

Finally, assuming in addition that $\ddot{u}(\boldsymbol{\xi}, \tau)$ is uniformly bounded, i.e. $|\ddot{u}(\boldsymbol{\xi}, \tau)| \leqslant M$ for some positive constant M, for $\boldsymbol{\xi} \in V(\boldsymbol{z})$, $0 \leqslant \tau \leqslant t$, one has

$$\left| G_{\infty}(\boldsymbol{x}, t, \boldsymbol{\xi}) \star \ddot{u}(\boldsymbol{\xi}, t) \right| = \left| G_{\infty}[\boldsymbol{x}, t, \boldsymbol{\xi} | \ddot{u}(\boldsymbol{\xi}, t)] \right| \leqslant \frac{M}{2\pi c^2} \int_0^{\eta^\star(r,t)} \frac{1}{[\eta^2 + r^2]^{1/2}} \, \mathrm{d}\eta$$

$$= \frac{M}{2\pi c^2} \ln\left[ct + \eta^\star(r, t)\right] - \ln r \quad (1.A.48)$$

which implies, for ε small enough to have $B_\varepsilon(\boldsymbol{z}) \subset V(\boldsymbol{z})$ and after effecting scaling (1.3.10):

$$\left| \int_{B_\varepsilon(z)} G_{\infty}(\boldsymbol{x}, t, \boldsymbol{\xi}) \star \ddot{u}(\boldsymbol{\xi}, t) \, \mathrm{d}V_\xi \right| \leqslant \frac{M}{2\pi c^2} \varepsilon O(\varepsilon \ln \varepsilon) = o(\varepsilon) \quad (1.A.49)$$

Hence, combining (1.A.47) and (1.A.49), one arrives at an estimate formally identical to (1.A.29) where of course $\mathcal{B}$ is now the unit disk and G_{∞} the 2D static fundamental solution.

Proof of lemma 2. Introducing the scaled coordinates (1.3.10) into (1.A.39), performing the change of variable $\eta = \varepsilon \bar{\eta}$ in the resulting integral and noting that its upper bound $\bar{\eta}^\star(\bar{r}, t)$ is given by (1.A.40) with r and c respectively replaced by $\bar{r}$ and c/ε. The 2D analog of Lemma 2 is then readily obtained by invoking again the decomposition $G[\boldsymbol{x}, t, \boldsymbol{\xi}|f] = G_{\infty}[\boldsymbol{x}, t, \boldsymbol{\xi}|f] + G_{\mathrm{C}}[\boldsymbol{x}, t, \boldsymbol{\xi}|f]$ and noting that

$$\int_{\Gamma_\varepsilon(z)} H_{\mathrm{C}}[\boldsymbol{x}, t, \boldsymbol{\xi} | v_\varepsilon(\boldsymbol{\xi}, t)] \, \mathrm{d}S_\xi = \varepsilon \int_{\mathcal{S}} H_{\mathrm{C}}[\bar{\boldsymbol{x}}, t, \bar{\boldsymbol{\xi}} | \bar{v}_\varepsilon(\boldsymbol{\xi}, t)] \, \mathrm{d}S_{\bar{\xi}} = O(\varepsilon \| \bar{v}_\varepsilon(\cdot, t) \|).$$

Proof of lemma 3. The proposed ansatz (1.A.31) is, by assumption in Lemma 1, Lipschitz-continuous with respect to t, which leads to investigating the behavior of H_{∞} as defined through (1.A.39) for a Lipschitz-continuous time-modulation f. Proceeding along the lines of Lemma 1, and in particular invoking yet again the decomposition $f(\tau) = f(t) + \Delta f(\tau)$, one finds

$$H_{\infty}[\bar{\boldsymbol{x}}, t, \bar{\boldsymbol{\xi}} | f] = H_{\infty}(\bar{\boldsymbol{x}}, \bar{\boldsymbol{\xi}}) f(t) + H_{\infty}[\bar{\boldsymbol{x}}, t, \bar{\boldsymbol{\xi}} | \Delta f]$$

where the cofactor $H_{\infty}(\bar{\boldsymbol{x}}, \bar{\boldsymbol{\xi}})$ of $f(t)$, established via analytical integration, is the normal derivative of the static fundamental solution (1.A.44). Moreover, exploiting the Lipschitz-continuity of f in the now-familiar way leads to

$$\left| H_{\infty}[\bar{\boldsymbol{x}}, t, \bar{\boldsymbol{\xi}} | \Delta f] \right| \leqslant \frac{\bar{r}}{2\pi c^2} \frac{2K}{c} \int_0^{\eta_\varepsilon^\star(\bar{r}, t)} \frac{\mathrm{d}\bar{\eta}}{\bar{\eta}^2 + \bar{r}^2} = \frac{K}{\pi c} \tan^{-1}\left[1 - \frac{(ct)^2}{\bar{r}^2} \right]^{1/2}$$

Two-dimensional elastodynamics. The infinite-plane time-modulated fundamental solution for two-dimensional elastodynamics is given by (Eringen and Suhubi, 1975):

$$\boldsymbol{U}_{\infty}[\boldsymbol{x}, t, \boldsymbol{\xi}|f] = \frac{1}{\rho c_{\mathrm{T}}^2} G_{\mathrm{T}\infty}[\boldsymbol{x}, t, \boldsymbol{\xi}|f] \boldsymbol{I}$$

$$+ \frac{1}{4\pi\rho} \boldsymbol{\nabla}_\xi \boldsymbol{\nabla}_\xi \left\{ \int_0^{t-r/c_{\mathrm{L}}} \tau G_{\mathrm{L}\infty}[\boldsymbol{x}, t-\tau, \boldsymbol{\xi}|f] \, \mathrm{d}\tau - \int_0^{t-r/c_{\mathrm{T}}} \tau G_{\mathrm{T}\infty}[\boldsymbol{x}, t-\tau, \boldsymbol{\xi}|f] \, \mathrm{d}\tau \right\} r \quad (1.A.50)$$

where $G_{\mathrm{L}\infty}$, $G_{\mathrm{T}\infty}$ are defined by (1.A.38) with $c = c_{\mathrm{L}}$ and $c = c_{\mathrm{T}}$, respectively. Lemmas 1 to 3 can then be established by adapting the proof for the scalar case, a task left to the reader.

1.B   Summary of explicit formulae for polarization tensors

Explicit formulae for polarization tensors $\boldsymbol{\mathcal{A}}$ have been established in earlier works (e.g. Sokolowski and Zochowski, 1999; Garreau et al., 2001; Guzina and Bonnet, 2004) for many situations. Moreover, the recent book by Ammari and Kang (2007) presents a comprehensive study of the concept of polarization tensor in connection with small-defect asymptotics and homogenization. For the case of spherical or (resp. circular) cavities nucleating in 3D (resp. 2D) isotropic elastic bodies, one has $|\mathcal{B}| = 4\pi/3$ (3D) or $|\mathcal{B}| = \pi$ (2D)

$$\boldsymbol{\mathcal{A}} = \frac{3(1-\nu)}{2\mu(7-\nu)}\left[5\boldsymbol{\mathcal{I}}^{\text{sym}} - \frac{1+5\nu}{2(1+\nu)}\boldsymbol{I}\otimes\boldsymbol{I}\right] \qquad \text{(3D)} \qquad (1.B.1a)$$

$$\boldsymbol{\mathcal{A}} = \frac{1}{\mu(1+\nu)}\left[2\boldsymbol{\mathcal{I}}^{\text{sym}} - \frac{2\nu^2-\nu+1}{2(1+\nu)(1-\nu)}\boldsymbol{I}\otimes\boldsymbol{I}\right] \qquad \text{(2D plane stress)} \qquad (1.B.1b)$$

$$\boldsymbol{\mathcal{A}} = \frac{1-\nu}{\mu}\left[2\boldsymbol{\mathcal{I}}^{\text{sym}} - \frac{1}{2(1+\nu)}\boldsymbol{I}\otimes\boldsymbol{I}\right] \qquad \text{(2D plane strain)} \qquad (1.B.1c)$$

The polarization tensor associated with the nucleation of a small spherical elastic inclusion with assumed elastic constants $\mu^\star, \nu^\star$ is given (see Chikichev and Guzina, 2008) by

$$\boldsymbol{\mathcal{A}}^\star = \mathcal{A}_{\text{dev}}\boldsymbol{\mathcal{I}}^{\text{sym}} + \frac{1}{3}(\mathcal{A}_{\text{sph}} - \mathcal{A}_{\text{dev}})\boldsymbol{I}\otimes\boldsymbol{I} \qquad (1.B.2)$$

having set

$$\begin{cases} \mathcal{A}_{\text{sph}} = -\dfrac{3(1-2\nu)}{2\mu(1+\nu)}\dfrac{(1-\nu)(\bar{\chi}-1)}{(1+\nu)(\bar{\chi}-1)+3(1-\nu)} \\[2ex] \mathcal{A}_{\text{dev}} = -\dfrac{1}{2\mu}\dfrac{15(1-\nu)(\bar{\mu}-1)}{(8-10\nu)(\bar{\mu}-1)+15(1-\nu)} \end{cases} \qquad \text{with} \quad \bar{\chi} = \frac{\mu^\star(1+\nu^\star)(1-2\nu)}{\mu(1+\nu)(1-2\nu^\star)}, \ \ \bar{\mu} = \frac{\mu^\star}{\mu}$$

The second-order polarization tensor associated with the nucleation of a small spherical sound-hard obstacle in an acoustic medium is given by

$$\text{(a) } \boldsymbol{A} = \frac{3}{2}\boldsymbol{I} \quad \text{(3D)}, \qquad\qquad \text{(b) } \boldsymbol{A} = 2\boldsymbol{I} \quad \text{(2D)} \qquad (1.B.3)$$

Chapter 2

Topological sensitivity method for qualitative identification of cracks

Contents

2.1   Introduction

The reconstruction of cracks embedded in a solid using transient elastic waves is a classical inverse problem that arises in a number of applications such as nondestructive material testing or seismic imaging (Bui, 2006; Stavroulakis, 2001). Among the most prominent qualitative and non-iterative approaches, relevant for the problem of crack identification in elastodynamics, stand the probe method (Ikehata, 2006), the linear sampling method (Colton and Kress, 1992; Cakoni and Colton, 2003b; Nintcheu Fata and Guzina, 2004), the reciprocity gap principle (Ben Abda et al., 1999; Andrieux et al., 1999; Bui et al., 2004), and the concept of topological sensitivity considered herein.

The topological sensitivity analysis has been broaden to identification problems under transient dynamical conditions within time-domain formulations (Bonnet, 2006; Ammari and Kang, 2006; Amstutz et al., 2008) showing analogies with time reversal methods (Dominguez et al., 2005; Wang and Huang, 2004). A growing variety of inhomogeneities has been the subject of investigations, see Garreau et al. (2001); Guzina and Chikichev (2007); Ammari and Kang (2007) in elasticity, but in the context of crack identification only a few studies have been done, notably Amstutz et al. (2005) for 2D Laplace equation, Ammari et al. (2010) and Amstutz and Dominguez (2008) for 2D and 3D Helmholtz equation respectively, and Gallego and Rus (2004) in 2D elastostatics. This chapter is devoted to crack identification in three dimensional elastic solids using time-domain topological sensitivity. The asymptotic behaviors of functionals, characterizing their topological sensitivities, relatively to the nucleation of a crack of infinitesimal size are addressed in elasticity and acoustics, using adjoint-based approach (Bonnet, 1995) to provide simple and efficient formulations. To the authors' best knowledge, this study constitutes the first analysis of the topological sensitivity method applied to the identification of cracks within a 3D elastodynamic context.

The chapter is organized as follows. The analysis of the topological sensitivity is presented for the elasticity case in Section 2.2, and in acoustics in Section 2.3 in adjoint-based formulations. In each case, the asymptotic analysis is detailed, and closed-form is addressed featuring the nucleation of infinitesimal circular plane crack while alternative proof or technical considerations are deferred in 2.A.2. Finally, a set of FEM-based numerical examples are included Section 2.5 for illustration and discussion.

Consider a crack identification problem where the reference homogeneous, linearly elastic, solid Ω with boundary S, containing a crack Γ^{true} (or a set thereof), is interrogated by means of a dynamic excitation. The reference medium is characterized by its mass density ρ and elasticity tensor $\mathcal{C}$ which, for isotropic materials, is given in terms of the shear modulus μ and Poisson's ratio ν by

$$\mathcal{C} = 2\mu\Big[\mathcal{I}^{\text{sym}} + \frac{\nu}{1-2\nu}\boldsymbol{I}\otimes\boldsymbol{I}\Big], \tag{2.1.1}$$

$\boldsymbol{I}$ being the second-order identity tensor and $\mathcal{I}^{\text{sym}}$ the symmetric fourth-order identity tensor. To identify the hidden crack Γ^{true}, transient excitations are applied in the form of tractions applied over $S_{\text{N}} \subset S$ and displacements prescribed on the complementary external surface $S_{\text{D}} = S \setminus S_{\text{N}}$, with initial rest conditions assumed at time $t = 0$. Letting Γ denote a trial crack, the prescribed excitation gives rise to elastodynamic displacement fields $\boldsymbol{u}$ (the free field) in the reference (uncracked) domain Ω and $\boldsymbol{u}_\Gamma$ in the cracked domain $\Omega_\Gamma = \Omega \setminus \Gamma$.

The identification of the crack Γ^{true} is here based on the assumed availability of over-determined data on the external boundary, in the form of the measured value $\boldsymbol{u}^{\text{obs}}$ on the measurement surface $S^{\text{obs}} \subset S_{\text{N}}$ and during the time interval $[0, T]$ of the displacement induced in the flawed solid by the

prescribed excitation (other possibilities can be considered with minimal changes to the formulation). The discrepancy between a trial configuration Ω_Γ and the correct configuration $\Omega_{\Gamma^{\text{true}}}$ is evaluated by means of a cost functional $\mathbb{J}$ defined in terms of a misfist density function φ:

$$\mathbb{J}(\Omega_\Gamma, T) = \int_0^T \int_{S^{\text{obs}}} \varphi[\boldsymbol{u}_\Gamma(\boldsymbol{\xi}, t), \boldsymbol{\xi}, t] \, \mathrm{d}S_\xi \, \mathrm{d}t. \tag{2.1.2}$$

The misfit function φ is chosen so as to measure the gap between measurements $\boldsymbol{u}^{\text{obs}}$ and the displacement $\boldsymbol{u}_\Gamma$ arising in a trial cracked solid Ω_Γ. Numerical experiments presented in this work are based on the commonly-used least squares misfit function:

$$\varphi[\boldsymbol{w}, \boldsymbol{\xi}, t] = \frac{1}{2} \|\boldsymbol{w} - \boldsymbol{u}^{\text{obs}}(\boldsymbol{\xi}, t)\|^2. \tag{2.1.3}$$

2.2 Elastic topological sensitivity

2.2.1 Preliminaries

The topological sensitivity of the cost functional (2.1.2) is here defined as its sensitivity with respect to the creation of an infinitesimal crack of characteristic size ε at a given location $\boldsymbol{z} \in \Omega$, defined by $\Gamma_\varepsilon(\boldsymbol{z}) = \boldsymbol{z} + \varepsilon \bar{\Gamma}$ in terms of of a normalized open surface $\bar{\Gamma}$ containing the origin and specifying a chosen crack shape (e.g. $\bar{\Gamma}$ is a unit disk for a nucleating penny-shaped crack) and its characteristic radius $\varepsilon > 0$. The corresponding trial cracked solid is denoted $\Omega_{\varepsilon, \boldsymbol{z}}$. Following earlier works on topological sensitivity, e.g. Sokolowski and Zochowski (1999); Garreau et al. (2001); Bonnet and Guzina (2004), one seeks the asymptotic behavior of $\mathbb{J}(\Omega_{\varepsilon, \boldsymbol{z}}, T)$ as $\varepsilon \to 0$ through the expansion:

$$\mathbb{J}(\Omega_{\varepsilon, \boldsymbol{z}}, T) = \mathbb{J}(\Omega, T) + \eta(\varepsilon) \mathbb{T}(\boldsymbol{z}, \bar{\Gamma}, T) + o(\eta(\varepsilon)) \qquad (\varepsilon \to 0) \tag{2.2.1}$$

where the function $\eta(\varepsilon)$, to be determined, vanishes in the limit $\varepsilon \to 0$ and the *topological sensitivity* $\mathbb{T}(\boldsymbol{z}, \bar{\Gamma}, T)$ is a function of the sampling point $\boldsymbol{z}$ and experiment duration T.

The prescribed dynamical loading applied on $\Omega_{\varepsilon, \boldsymbol{z}}$ gives rise to an elastodynamic state $\boldsymbol{u}_{\varepsilon, \boldsymbol{z}}$ that can be conveniently decomposed into $\boldsymbol{u}_{\varepsilon, \boldsymbol{z}} = \boldsymbol{u} + \boldsymbol{v}_{\varepsilon, \boldsymbol{z}}$, where the free-field $\boldsymbol{u}$ is the response of the reference domain Ω while the scattered field $\boldsymbol{v}_{\varepsilon, \boldsymbol{z}}$ is governed by the initial-boundary value problem (IBVP)

$$\begin{aligned}
\boldsymbol{\nabla} \cdot [\boldsymbol{\mathcal{C}} : \boldsymbol{\nabla} \boldsymbol{v}_{\varepsilon, \boldsymbol{z}}](\boldsymbol{\xi}, t) &= \rho \ddot{\boldsymbol{v}}_{\varepsilon, \boldsymbol{z}}(\boldsymbol{\xi}, t) & (\boldsymbol{\xi} \in \Omega_{\varepsilon, \boldsymbol{z}}, t \geqslant 0) \\
\boldsymbol{t}^\pm[\boldsymbol{v}_{\varepsilon, \boldsymbol{z}}^\pm](\boldsymbol{\xi}, t) &= -\boldsymbol{t}^\pm[\boldsymbol{u}](\boldsymbol{\xi}, t) & (\boldsymbol{\xi} \in \Gamma_{\varepsilon, \boldsymbol{z}}^\pm, t \geqslant 0) \\
\boldsymbol{t}[\boldsymbol{v}_{\varepsilon, \boldsymbol{z}}](\boldsymbol{\xi}, t) &= \boldsymbol{0} & (\boldsymbol{\xi} \in S_{\text{N}}, t \geqslant 0) \\
\boldsymbol{v}_{\varepsilon, \boldsymbol{z}}(\boldsymbol{\xi}, t) &= \boldsymbol{0} & (\boldsymbol{\xi} \in S_{\text{D}}, t \geqslant 0) \\
\boldsymbol{v}_{\varepsilon, \boldsymbol{z}}(\boldsymbol{\xi}, 0) = \dot{\boldsymbol{v}}_{\varepsilon, \boldsymbol{z}}(\boldsymbol{\xi}, 0) &= \boldsymbol{0} & (\boldsymbol{\xi} \in \Omega_{\varepsilon, \boldsymbol{z}}),
\end{aligned} \tag{2.2.2}$$

where the two crack faces $\Gamma_{\varepsilon, \boldsymbol{z}}^\pm$ support scattered displacements $\boldsymbol{v}_{\varepsilon, \boldsymbol{z}}^\pm$, and the traction vector $\boldsymbol{t}[\boldsymbol{w}] = (\boldsymbol{\mathcal{C}} : \boldsymbol{\nabla} \boldsymbol{w}) \cdot \boldsymbol{n} = \boldsymbol{\sigma}[\boldsymbol{w}] \cdot \boldsymbol{n}$ (resp. $\boldsymbol{t}^\pm[\boldsymbol{w}^\pm] = \boldsymbol{\sigma}[\boldsymbol{w}^\pm] \cdot \boldsymbol{n}^\pm$) is associated with a displacement $\boldsymbol{w}$ and the outward normal $\boldsymbol{n}$ on S (resp. $\boldsymbol{n}^\pm$ on $\Gamma_{\varepsilon, \boldsymbol{z}}^\pm$). In (2.2.2) and hereinafter, the symbols '$\cdot$' and '$:$' denote single and double tensor contractions, with the convention $\boldsymbol{a} : \boldsymbol{b} = a_{ij} b_{ij}$ used in the latter case.

Expanding the cost functional (2.1.2) about $\boldsymbol{u}_{\varepsilon, \boldsymbol{z}} = \boldsymbol{u}$ to first order w.r.t. $\boldsymbol{v}_{\varepsilon, \boldsymbol{z}} = \boldsymbol{u}_{\varepsilon, \boldsymbol{z}} - \boldsymbol{u}$, one obtains

$$\mathbb{J}(\Omega_{\varepsilon, \boldsymbol{z}}, T) = \mathbb{J}(\Omega, T) + \int_0^T \int_{S^{\text{obs}}} \frac{\partial \varphi}{\partial \boldsymbol{u}} [\boldsymbol{u}(\boldsymbol{\xi}, t), \boldsymbol{\xi}, t] \cdot \boldsymbol{v}_{\varepsilon, \boldsymbol{z}}(\boldsymbol{\xi}, t) \, \mathrm{d}S_\xi \, \mathrm{d}t + o(\|\boldsymbol{v}_{\varepsilon, \boldsymbol{z}}\|_{L^2(S^{\text{obs}})}). \tag{2.2.3}$$

Then, since the scattered field is expected to vanish for infinitesimal cracks, i.e. $\lim_{\varepsilon \to 0} \|\boldsymbol{v}_{\varepsilon,\boldsymbol{z}}\| = 0$, the topological sensitivity $\mathbb{T}(\boldsymbol{z}, \bar{\Gamma}, T)$ and the leading asymptotic behavior $\eta(\varepsilon) = o(\|\boldsymbol{v}_{\varepsilon,\boldsymbol{z}}\|_{L^2(S^{\mathrm{obs}})})$ featured in (2.2.1) are to be found by identification from

$$\int_0^T \int_{S^{\mathrm{obs}}} \frac{\partial \varphi}{\partial \boldsymbol{u}} [\boldsymbol{u}(\boldsymbol{\xi}, t), \boldsymbol{\xi}, t] \cdot \boldsymbol{v}_{\varepsilon,\boldsymbol{z}}(\boldsymbol{\xi}, t) \, \mathrm{d}S_\xi \, \mathrm{d}t = \eta(\varepsilon)\mathbb{T}(\boldsymbol{z}, \bar{\Gamma}, T) + o(\eta(\varepsilon)). \qquad (2.2.4)$$

This requires finding the leading asymptotic behavior as $\varepsilon \to 0$ of the left-hand side of (2.2.4). One possible way, along the lines of the so-called direct differentiation approach of parameter or shape sensitivity analysis (Haug et al., 1986), consists in seeking the asymptotic behavior of $\boldsymbol{v}_{\varepsilon,\boldsymbol{z}}$ on S^{obs} and plugging the result into (2.2.4). As previously discussed on several occasions (Bonnet, 2006; Bellis and Bonnet, 2010), however, a more compact formulation for the actual evaluation of $\mathbb{T}(\boldsymbol{z}, \bar{\Gamma}, T)$ can be set up using an adjoint solution and is adopted here.

The adjoint formulation stems from treating the integral in the left-hand side of (2.2.4) as one of the terms arising in the reciprocity identity linking two elastodynamic states (Wheeler and Sternberg, 1968; Achenbach, 2003), in which one state is the scattered field $\boldsymbol{v}_{\varepsilon,\boldsymbol{z}}$ while the other is, like in Bonnet (2006); Bellis and Bonnet (2010), chosen as the *adjoint state* $\hat{\boldsymbol{u}}$ governed by the following IBVP

$$\begin{aligned}
\boldsymbol{\nabla} \cdot [\boldsymbol{\mathcal{C}} : \boldsymbol{\nabla}\hat{\boldsymbol{u}}](\boldsymbol{\xi}, t) &= \rho \ddot{\hat{\boldsymbol{u}}}(\boldsymbol{\xi}, t) && (\boldsymbol{\xi} \in \Omega, 0 \leqslant t \leqslant T) \\
\boldsymbol{t}[\hat{\boldsymbol{u}}](\boldsymbol{\xi}, t) &= \frac{\partial \varphi}{\partial \boldsymbol{u}}[\boldsymbol{u}(\boldsymbol{\xi}, T - t), \boldsymbol{\xi}, T - t] && (\boldsymbol{\xi} \in S^{\mathrm{obs}}, 0 \leqslant t \leqslant T) \\
\boldsymbol{t}[\hat{\boldsymbol{u}}](\boldsymbol{\xi}, t) &= \boldsymbol{0} && (\boldsymbol{\xi} \in S_{\mathrm{N}} \backslash S^{\mathrm{obs}}, 0 \leqslant t \leqslant T) \\
\hat{\boldsymbol{u}}(\boldsymbol{\xi}, t) &= \boldsymbol{0} && (\boldsymbol{\xi} \in S_{\mathrm{D}}, 0 \leqslant t \leqslant T) \\
\hat{\boldsymbol{u}}(\boldsymbol{\xi}, 0) &= \dot{\hat{\boldsymbol{u}}}(\boldsymbol{\xi}, 0) = \boldsymbol{0} && (\boldsymbol{\xi} \in \Omega).
\end{aligned} \qquad (2.2.5)$$

Now, for any generic domain $\mathcal{O}$ and pair of elastodynamic states $\boldsymbol{u}_1, \boldsymbol{u}_2$ satisfying the homogeneous elastodynamic field equations in $\mathcal{O}$ as well as initial-rest conditions

$$\boldsymbol{u}_1(\boldsymbol{\xi}, 0) = \dot{\boldsymbol{u}}_1(\boldsymbol{\xi}, 0) = \boldsymbol{0} \quad \text{and} \quad \boldsymbol{u}_2(\boldsymbol{\xi}, 0) = \dot{\boldsymbol{u}}_2(\boldsymbol{\xi}, 0) = \boldsymbol{0} \quad (\boldsymbol{\xi} \in \mathcal{O}),$$

the following reciprocity identity holds (Wheeler and Sternberg, 1968; Achenbach, 2003):

$$\int_{\partial \mathcal{O}} \{ \boldsymbol{t}[\boldsymbol{u}_1] \star \boldsymbol{u}_2 - \boldsymbol{t}[\boldsymbol{u}_2] \star \boldsymbol{u}_1 \}(\boldsymbol{\xi}, t) \, \mathrm{d}S_\xi = 0 \qquad (2.2.6)$$

in which $\star$ denotes the time convolution at instant $t \geqslant 0$ defined, for generic tensor fields $\boldsymbol{a}$ and $\boldsymbol{b}$ assumed to be at rest at all negative times, by

$$[\boldsymbol{a} \star \boldsymbol{b}](\boldsymbol{\xi}, t) = \int_0^t \boldsymbol{a}(\boldsymbol{\xi}, \tau) \cdot \boldsymbol{b}(\boldsymbol{\xi}, t - \tau) \, \mathrm{d}\tau, \qquad (2.2.7)$$

the inner product appearing in the integral being such that $\boldsymbol{a} \cdot \boldsymbol{b}$ is a tensor of the lowest possible order (e.g. $\boldsymbol{u} \star \boldsymbol{\sigma}[\boldsymbol{v}]$ has order 1, $\boldsymbol{\nabla}\boldsymbol{u} \star \boldsymbol{\sigma}[\boldsymbol{v}]$ is a scalar). On writing the reciprocity identity (2.2.6) for the domain $\mathcal{O} = \Omega_{\varepsilon,\boldsymbol{z}}$ (with boundary $\partial \Omega_{\varepsilon,\boldsymbol{z}} = S \cup \Gamma_{\varepsilon,\boldsymbol{z}}$) and elastodynamic states $\boldsymbol{u}_1 = \hat{\boldsymbol{u}}$ and $\boldsymbol{u}_2 = \boldsymbol{v}_{\varepsilon,\boldsymbol{z}}$, (2.2.4) is recast as

$$\int_0^T \int_{\Gamma_{\varepsilon,\boldsymbol{z}}} \boldsymbol{t}[\hat{\boldsymbol{u}}](\boldsymbol{\xi}, T - t) \cdot [\![\boldsymbol{v}_{\varepsilon,\boldsymbol{z}}]\!](\boldsymbol{\xi}, t) \, \mathrm{d}S_\xi \, \mathrm{d}t = \eta(\varepsilon)\mathbb{T}(\boldsymbol{z}, \bar{\Gamma}, T) + o(\eta(\varepsilon)), \qquad (2.2.8)$$

where $[\![\boldsymbol{v}_{\varepsilon,\boldsymbol{z}}]\!] = \boldsymbol{v}_{\varepsilon,\boldsymbol{z}}^+ - \boldsymbol{v}_{\varepsilon,\boldsymbol{z}}^-$ denotes the crack opening displacement (COD), the traction vector $\boldsymbol{t}[\hat{u}]$ is defined on $\Gamma_{\varepsilon,\boldsymbol{z}}$ in terms of the unit normal $\boldsymbol{n} = \boldsymbol{n}^-$, and having used the boundary conditions in problems (2.2.2) and (2.2.5) and the continuity of the adjoint displacement $\hat{\boldsymbol{u}}$ across $\Gamma_{\varepsilon,\boldsymbol{z}}$. Finding $\mathbb{T}(\boldsymbol{z}, \bar{\Gamma}, T)$ and $\eta(\varepsilon)$ from (2.2.8) now requires determining the leading behavior of the COD $[\![\boldsymbol{v}_{\varepsilon,\boldsymbol{z}}]\!]$ as $\varepsilon \to 0$.

2.2.2 Asymptotic analysis

Small-crack asymptotics of the COD

This issue is conveniently addressed by reformulating the governing IBVP (2.2.2) in terms of an integral equation, as the geometrical support of the latter is the vanishing crack surface. Let $\boldsymbol{U}(\boldsymbol{x}, t, \boldsymbol{\xi})$ and $\boldsymbol{\Sigma}(\boldsymbol{x}, t, \boldsymbol{\xi})$ denote the time-impulsive elastodynamic Green's tensors, defined such that $\boldsymbol{e}_k \cdot \boldsymbol{U}(\boldsymbol{x}, t, \boldsymbol{\xi})$ and $\boldsymbol{e}_k \cdot \boldsymbol{\Sigma}(\boldsymbol{x}, t, \boldsymbol{\xi})$ are the displacement and stress at $\boldsymbol{\xi} \in \Omega$ and time t resulting from a unit time-impulsive point force applied at $\boldsymbol{x} \in \Omega$ in the k-th direction at time $t = 0$ and satisfying the boundary conditions

$$\boldsymbol{U}(\boldsymbol{x}, t, \boldsymbol{\xi}) = \boldsymbol{0} \ (\boldsymbol{\xi} \in S_{\mathrm{D}}, t \geqslant 0), \qquad \boldsymbol{\Sigma}(\boldsymbol{x}, t, \boldsymbol{\xi}) \cdot \boldsymbol{n} = \boldsymbol{0} \ (\boldsymbol{\xi} \in S_{\mathrm{N}}, t \geqslant 0), \qquad (2.2.9)$$

One also defines the elastodynamic *full-space* fundamental tensors $\boldsymbol{U}_\infty(\boldsymbol{x}, t, \boldsymbol{\xi})$ and $\boldsymbol{\Sigma}_\infty(\boldsymbol{x}, t, \boldsymbol{\xi})$ by replacing boundary conditions (2.2.9) with radiation conditions at infinity (Eringen and Suhubi, 1975), see 1.A.2. Taking into account the homogeneous boundary conditions in (2.2.2), the COD verifies the singular integral equation (Bonnet, 1999)

$$\boldsymbol{t}[\boldsymbol{u}](\boldsymbol{x}, t) = \fint_{\Gamma_{\varepsilon,\boldsymbol{z}}} \left[\boldsymbol{n}(\boldsymbol{x}) \cdot \boldsymbol{\mathcal{C}} \cdot \boldsymbol{\Sigma}(\boldsymbol{x}, t, \boldsymbol{\xi}) \right] \star \boldsymbol{\mathcal{D}}[\![\boldsymbol{v}_{\varepsilon,\boldsymbol{z}}]\!](\boldsymbol{\xi}, t) \, \mathrm{d}S_\xi$$

$$+ \rho \boldsymbol{n}(\boldsymbol{x}) \cdot \boldsymbol{\mathcal{C}} : \left\{ \int_{\Gamma_{\varepsilon,\boldsymbol{z}}} \left[\boldsymbol{U}(\boldsymbol{x}, t, \boldsymbol{\xi}) \star [\![\ddot{\boldsymbol{v}}_{\varepsilon,\boldsymbol{z}}]\!](\boldsymbol{\xi}, t) \right] \otimes \boldsymbol{n}(\boldsymbol{\xi}) \, \mathrm{d}S_\xi \right\} \qquad (\boldsymbol{x} \in \Gamma_{\varepsilon,\boldsymbol{z}}, \, 0 \leqslant t \leqslant T) \quad (2.2.10)$$

where $\boldsymbol{w} \mapsto \boldsymbol{\mathcal{D}}\boldsymbol{w} = \nabla \boldsymbol{w} \otimes \boldsymbol{n} - \boldsymbol{n} \otimes \nabla \boldsymbol{w}$ defines a (tensorial) tangential differential operator (upon splitting the gradients into sums of tangential and normal parts, all normal derivatives cancel out), whose value hence depends only on the surface trace of $\boldsymbol{w}$, and $\fint$ indicates a strongly singular integral defined in the Cauchy principal value sense.

The asymptotic form of integral equation (2.2.10) as $\varepsilon \to 0$ is now sought. For this purpose, and following customary practice for such asymptotic analyses, scaled coordinates $\bar{\boldsymbol{\xi}}$ are introduced so that

$$\text{(a) } \boldsymbol{\xi} = \boldsymbol{z} + \varepsilon \bar{\boldsymbol{\xi}}, \qquad \text{(b) } \mathrm{d}S_\xi = \varepsilon^2 \, \mathrm{d}S_{\bar{\xi}} \qquad (\boldsymbol{\xi} \in \Gamma_{\varepsilon,\boldsymbol{z}}, \bar{\boldsymbol{\xi}} \in \bar{\Gamma}). \qquad (2.2.11)$$

Assuming that the free field is such that $\boldsymbol{x} \mapsto \boldsymbol{\sigma}[\boldsymbol{u}](\boldsymbol{x}, t)$ is continuous at $\boldsymbol{x} = \boldsymbol{z}$, one has

$$\boldsymbol{t}[\boldsymbol{u}](\boldsymbol{\xi}, t) = \boldsymbol{\sigma}[\boldsymbol{u}](\boldsymbol{z}, t) \cdot \boldsymbol{n}(\boldsymbol{\xi}) + o(1) \qquad (\boldsymbol{\xi} \in \Gamma_{\varepsilon,\boldsymbol{z}}) \qquad (2.2.12)$$

Investigating the small-crack asymptotic behavior of the right-hand side of (2.2.10) is more involved, and is helped by the following lemma, whose proof is given in 1.A.2:

Lemma 4. *Let the vector function* $\bar{\boldsymbol{v}}_{\varepsilon,\boldsymbol{z}}(\bar{\boldsymbol{\xi}},t)$ *be defined by* $\bar{\boldsymbol{v}}_{\varepsilon,\boldsymbol{z}}(\bar{\boldsymbol{\xi}},t) = \boldsymbol{v}_{\varepsilon,\boldsymbol{z}}(\boldsymbol{\xi},t)$, *with* $\bar{\boldsymbol{\xi}}$ *and* $\boldsymbol{\xi}$ *related through (2.2.11a). Then, one has*

$$
\fint_{\Gamma_{\varepsilon,\boldsymbol{z}}} \big[\boldsymbol{n}(\boldsymbol{x}){\cdot}\boldsymbol{\mathcal{C}}{\cdot}\boldsymbol{\Sigma}(\boldsymbol{x},t,\boldsymbol{\xi}) \big] \star \boldsymbol{\mathcal{D}}[\![\boldsymbol{v}_{\varepsilon,\boldsymbol{z}}]\!](\boldsymbol{\xi},t) \, dS_{\xi}
$$
$$
= \frac{1}{\varepsilon}\left\{ \fint_{\bar{\Gamma}} \big[\boldsymbol{n}(\bar{\boldsymbol{x}}){\cdot}\boldsymbol{\mathcal{C}}{\cdot}\boldsymbol{\Sigma}_{\infty,\varepsilon}(\bar{\boldsymbol{x}},t,\bar{\boldsymbol{\xi}}) \big] \star \boldsymbol{\mathcal{D}}[\![\bar{\boldsymbol{v}}_{\varepsilon,\boldsymbol{z}}]\!](\bar{\boldsymbol{\xi}},t) \, dS_{\bar{\xi}} \; + o(\|[\![\bar{\boldsymbol{v}}_{\varepsilon,\boldsymbol{z}}]\!](\cdot,t)\|_{L^2(\bar{\Gamma})}) \right\}
$$
$$(2.2.13)$$

$$
\int_{\Gamma_{\varepsilon,\boldsymbol{z}}} \big[\boldsymbol{U}(\boldsymbol{x},t,\boldsymbol{\xi}) \star [\![\ddot{\boldsymbol{v}}_{\varepsilon,\boldsymbol{z}}]\!](\boldsymbol{\xi},t) \big] \otimes \boldsymbol{n}(\boldsymbol{\xi}) \, dS_{\xi}
$$
$$
= \varepsilon\left\{ \int_{\bar{\Gamma}} \big[\boldsymbol{U}_{\infty,\varepsilon}(\bar{\boldsymbol{x}},t,\bar{\boldsymbol{\xi}}) \star [\![\ddot{\bar{\boldsymbol{v}}}_{\varepsilon,\boldsymbol{z}}]\!](\bar{\boldsymbol{\xi}},t) \big] \otimes \boldsymbol{n}(\bar{\boldsymbol{\xi}}) \, dS_{\bar{\xi}} \; + o(\|[\![\ddot{\bar{\boldsymbol{v}}}_{\varepsilon,\boldsymbol{z}}]\!](\cdot,t)\|_{L^2(\bar{\Gamma})}) \right\}
$$
$$(2.2.14)$$

where $\boldsymbol{U}_{\infty,\varepsilon}, \boldsymbol{\Sigma}_{\infty,\varepsilon}$ *is the* full-space *elastodynamic fundamental solution defined in terms of rescaled wave velocities* c_L/ε, c_T/ε.

The left-hand side of equation (2.2.10) is $O(1)$ as $\varepsilon \to 0$, with its leading contribution linear in $\boldsymbol{\sigma}[\boldsymbol{u}](\boldsymbol{z},t)$ as seen in (2.2.12). The combination of this remark and Lemma 4 suggest to consider the following ansatz for $[\![\bar{\boldsymbol{v}}_{\varepsilon,\boldsymbol{z}}]\!](\bar{\boldsymbol{\xi}},\tau)$, in terms of unknown vector fields $\boldsymbol{V}^{ij}(\bar{\boldsymbol{\xi}})$ $(1 \leqslant i,j \leqslant 3)$ defined on $\bar{\Gamma}$:

$$
\bar{\boldsymbol{v}}_{\varepsilon,\boldsymbol{z}}(\bar{\boldsymbol{\xi}},t) = \varepsilon \sigma_{ij}[\boldsymbol{u}](\boldsymbol{z},t)\boldsymbol{V}^{ij}(\bar{\boldsymbol{\xi}}) + o(\varepsilon) \qquad (\boldsymbol{\xi} \in \Gamma_{\varepsilon,\boldsymbol{z}}, \bar{\boldsymbol{\xi}} \in \bar{\Gamma}). \tag{2.2.15}
$$

This ansatz indeed causes the first and second integrals in the right-hand side of (2.2.10) to be $O(1)$ and $o(1)$ as $\varepsilon \to 0$, respectively:

Lemma 5. *Assume that* $\tau \mapsto \boldsymbol{\nabla}\boldsymbol{u}(\boldsymbol{\xi},\tau)$ *is twice differentiable in a neighbourhood of* $\tau = t$, *and let* $\bar{\boldsymbol{v}}_{\varepsilon,\boldsymbol{z}}(\bar{\boldsymbol{\xi}},t)$ *be of form (2.2.15) for some* $\boldsymbol{V}^{ij}$. *Then:*

$$
\fint_{\Gamma_{\varepsilon,\boldsymbol{z}}} \big[\boldsymbol{n}(\boldsymbol{x}){\cdot}\boldsymbol{\mathcal{C}}{\cdot}\boldsymbol{\Sigma}(\boldsymbol{x},t,\boldsymbol{\xi}) \big] \star \boldsymbol{\mathcal{D}}[\![\boldsymbol{v}_{\varepsilon,\boldsymbol{z}}]\!](\boldsymbol{\xi},t) \, dS_{\xi}
$$
$$
= \sigma_{ij}[\boldsymbol{u}](\boldsymbol{z},t) \fint_{\bar{\Gamma}} \big[\boldsymbol{n}(\bar{\boldsymbol{x}}){\cdot}\boldsymbol{\mathcal{C}}{\cdot}\boldsymbol{\Sigma}_{\infty}(\bar{\boldsymbol{\xi}}-\bar{\boldsymbol{x}}) \big] \mathbin{\vdots} \boldsymbol{\mathcal{D}}[\![\boldsymbol{V}]\!]^{ij}(\bar{\boldsymbol{\xi}}) \, dS_{\bar{\xi}} + o(1), \quad (2.2.16a)
$$

where $\boldsymbol{\Sigma}_{\infty}(\bar{\boldsymbol{r}})$ *is the stress associated with the elastostatic Kelvin solution, given by (2.B.13), and*

$$
\int_{\Gamma_{\varepsilon,\boldsymbol{z}}} \big[\boldsymbol{U}(\boldsymbol{x},t,\boldsymbol{\xi}) \star [\![\ddot{\boldsymbol{v}}_{\varepsilon,\boldsymbol{z}}]\!](\boldsymbol{\xi},t) \big] \otimes \boldsymbol{n}(\boldsymbol{\xi}) \, dS_{\xi} = O(\varepsilon^2) \tag{2.2.16b}
$$

Proof. See 1.A.2. $\qquad\qquad\square$

Combining (2.2.12) with lemma 5 allows to set up the asymptotic form of integral equation (2.2.10) in the small-crack limit (it is in particular noted that the second integral of (2.2.10) does not contribute to the limiting integral equation as its order in ε is higher than that of the first integral). On enforcing the limiting integral equation for any choice of $\sigma_{ij}[\boldsymbol{u}](\boldsymbol{z},t)$, the asymptotic behavior of the COD is found to follow the representation (2.2.15), with the $\boldsymbol{V}^{ij}$ solving the integral equation

$$
\frac{1}{2}\big(\boldsymbol{e}_i \otimes \boldsymbol{e}_j + \boldsymbol{e}_j \otimes \boldsymbol{e}_i\big){\cdot}\boldsymbol{n}(\bar{\boldsymbol{x}}) = \fint_{\bar{\Gamma}} \big[\boldsymbol{n}(\bar{\boldsymbol{x}}){\cdot}\boldsymbol{\mathcal{C}}{\cdot}\boldsymbol{\Sigma}_{\infty}(\bar{\boldsymbol{\xi}}-\bar{\boldsymbol{x}}) \big] \mathbin{\vdots} \boldsymbol{\mathcal{D}}[\![\boldsymbol{V}]\!]^{ij}(\bar{\boldsymbol{\xi}}) \, dS_{\bar{\xi}} \qquad (\bar{\boldsymbol{x}} \in \bar{\Gamma}) \tag{2.2.17}
$$

which is readily recognised (Bonnet, 1999) as governing the exterior elastostatic problem for the crack $\bar{\Gamma}$ embedded in an infinite elastic medium and subjected on its faces to tractions $\boldsymbol{t}^{\pm} = -\frac{1}{2}(\boldsymbol{e}_j \otimes \boldsymbol{e}_k + \boldsymbol{e}_k \otimes \boldsymbol{e}_j) \cdot \boldsymbol{n}^{\pm}(\bar{\boldsymbol{x}})$. The left-hand side of (2.2.17) being symmetric in i, j, there are six distinct such equations, governing six canonical solutions $\boldsymbol{V}^{ij}(\bar{\boldsymbol{\xi}})$ ($1 \leqslant i \leqslant j \leqslant 3$) which are time-independent. Like for the previously-considered small-cavity asymptotics in the time domain (Bonnet, 2006; Bellis and Bonnet, 2010), the functions $\boldsymbol{V}^{ij}$ depend only on the chosen (crack) shape $\bar{\Gamma}$; in particular, they depend neither on the shape of the solid Ω being probed, nor on the location of the sampling point $\boldsymbol{z}$. Finding the $\boldsymbol{V}^{ij}(\bar{\boldsymbol{\xi}})$ entails in the worst case the numerical solution of the elastostatic integral equation (2.2.17), using e.g. boundary elements, for six different sets of prescribed tractions, with analytical solutions known for simple crack shapes (see Sec. 2.2.2).

Once the $\boldsymbol{V}^{ij}(\bar{\boldsymbol{\xi}})$ are known, and arranging for notational convenience the vector fields $\boldsymbol{V}^{ij}(\bar{\boldsymbol{\xi}})$ into a third-order tensor field $\boldsymbol{\mathcal{V}}(\bar{\boldsymbol{\xi}})$ such that $\boldsymbol{V}^{ij} = \mathcal{V}_{ijk}\boldsymbol{e}_k$, the asymptotic behavior of the COD can be readily evaluated, using (2.2.15), at any sampling point $\boldsymbol{z}$ and for any given stress history $\boldsymbol{\sigma}[\boldsymbol{u}](\boldsymbol{z}, t)$, to obtain

$$[\![\bar{\boldsymbol{v}}_{\varepsilon,\boldsymbol{z}}]\!](\bar{\boldsymbol{\xi}}, t) = \varepsilon \boldsymbol{\sigma}[\boldsymbol{u}](\boldsymbol{z}, t) : [\![\boldsymbol{\mathcal{V}}]\!](\bar{\boldsymbol{\xi}}) + o(\varepsilon) \tag{2.2.18}$$

Topological sensitivity

Now, inserting expansion (2.2.18) into the left-hand side of (2.2.8) and invoking (2.2.11b), one obtains

$$\int_0^T \int_{\Gamma_{\varepsilon,\boldsymbol{z}}} \boldsymbol{t}[\hat{\boldsymbol{u}}](\boldsymbol{\xi}, T - t) \cdot [\![\boldsymbol{v}_{\varepsilon,\boldsymbol{z}}]\!](\boldsymbol{\xi}, t) \, \mathrm{d}S_\xi \, \mathrm{d}t$$

$$= \varepsilon^3 \int_0^T \int_{\bar{\Gamma}} \boldsymbol{\sigma}[\boldsymbol{u}](\bar{\boldsymbol{\xi}}, t) : \left([\![\boldsymbol{\mathcal{V}}]\!](\bar{\boldsymbol{\xi}}) \otimes \boldsymbol{n}(\bar{\boldsymbol{\xi}})\right) : \boldsymbol{\sigma}[\hat{\boldsymbol{u}}](\bar{\boldsymbol{\xi}}, T - t) \, \mathrm{d}S_{\bar{\xi}} \, \mathrm{d}t + o(\varepsilon^3). \tag{2.2.19}$$

A comparison of (2.2.19) with (2.2.8) then readily allows to identify $\mathbb{T}(\boldsymbol{z}, \bar{\Gamma}, T)$ and $\eta(\varepsilon)$, leading to the main result of this section:

Proposition 1. *The topological sensitivity $\mathbb{T}(\boldsymbol{z}, \bar{\Gamma}, T)$ of $\mathbb{J}$ and its small-crack asymptotic behavior $\eta(\varepsilon)$ are given by*

$$(a) \; \mathbb{T}(\boldsymbol{z}, \bar{\Gamma}, T) = \boldsymbol{\sigma}[\boldsymbol{u}] \star \left(\boldsymbol{\mathcal{A}}^{\sigma} : \boldsymbol{\sigma}[\hat{\boldsymbol{u}}]\right)(\boldsymbol{z}, T) \qquad (b) \; \eta(\varepsilon) = \varepsilon^3, \tag{2.2.20}$$
$$= \nabla \boldsymbol{u} \star \left(\boldsymbol{\mathcal{A}} : \nabla \hat{\boldsymbol{u}}\right)(\boldsymbol{z}, T),$$

in terms of the free and adjoint solutions $\boldsymbol{u}$ and $\hat{\boldsymbol{u}}$. Moreover, the fourth-order polarization tensors $\boldsymbol{\mathcal{A}}^{\sigma}$ and $\boldsymbol{\mathcal{A}}$ are given, in terms of the third-order tensor function $\boldsymbol{\mathcal{V}}(\bar{\boldsymbol{\xi}})$ defined in Sec. 2.2.2, by

$$\boldsymbol{\mathcal{A}}^{\sigma}(\bar{\Gamma}) = \int_{\bar{\Gamma}} [\![\boldsymbol{\mathcal{V}}]\!](\bar{\boldsymbol{\xi}}) \otimes \boldsymbol{n}(\bar{\boldsymbol{\xi}}) \, dS_{\bar{\xi}}, \qquad \boldsymbol{\mathcal{A}} = \boldsymbol{\mathcal{C}} : \boldsymbol{\mathcal{A}}^{\sigma} : \boldsymbol{\mathcal{C}}. \tag{2.2.21}$$

$\boldsymbol{\mathcal{A}}^{\sigma}$ and $\boldsymbol{\mathcal{A}}$ are shown in 2.A.2 to have major symmetry, which implies

$$\boldsymbol{\sigma}[\boldsymbol{u}] \star \left(\boldsymbol{\mathcal{A}}^{\sigma} : \boldsymbol{\sigma}[\hat{\boldsymbol{u}}]\right) = \boldsymbol{\sigma}[\hat{\boldsymbol{u}}] \star \left(\boldsymbol{\mathcal{A}}^{\sigma} : \boldsymbol{\sigma}[\boldsymbol{u}]\right), \qquad \nabla \boldsymbol{u} \star \left(\boldsymbol{\mathcal{A}} : \nabla \hat{\boldsymbol{u}}\right) = \nabla \hat{\boldsymbol{u}} \star \left(\boldsymbol{\mathcal{A}} : \nabla \boldsymbol{u}\right).$$

The topological sensitivity (2.2.20a) depends on the canonical solutions $\boldsymbol{\mathcal{V}}$ through $\boldsymbol{\mathcal{A}}$ or $\boldsymbol{\mathcal{A}}^{\sigma}$, and is therefore intrinsically related to the assumed crack shape $\bar{\Gamma}$. As previously mentioned, the tensor field $\boldsymbol{\mathcal{V}}(\bar{\boldsymbol{\xi}})$ can be computed (at least numerically) for any assumed shape $\bar{\Gamma}$, with analytical solutions available for simple shapes of $\bar{\Gamma}$ as discussed next.

Polarization tensor for a penny-shaped crack

Closed form solutions for $\mathcal{V}$ are available in the case of a penny-shaped crack (Kassir and Sih, 1975; Chen et al., 2003), i.e. a circular plane crack for which $\bar{\Gamma}$ is the unit disk with normal $\boldsymbol{n}$. Selecting the orthonormal basis $(\boldsymbol{e}_1, \boldsymbol{e}_2, \boldsymbol{e}_3)$ such that $\boldsymbol{e}_3 \equiv \boldsymbol{n}$, the $[\![\boldsymbol{V}]\!]^{ij}$ are given by

$$[\![\boldsymbol{V}]\!]^{ij}(\bar{\boldsymbol{\xi}}) = \frac{2(1-\nu)}{\pi\mu(2-\nu)}\sqrt{1-|\bar{\boldsymbol{\xi}}|^2}\,\boldsymbol{n}\cdot(\boldsymbol{e}_i\otimes\boldsymbol{e}_j + \boldsymbol{e}_j\otimes\boldsymbol{e}_i)\cdot[2\boldsymbol{I} - \nu\boldsymbol{n}\otimes\boldsymbol{n}] \qquad (\bar{\boldsymbol{\xi}} \in \bar{\Gamma}), \qquad (2.2.22)$$

Using that

$$\int_{\bar{\Gamma}}\sqrt{1-|\bar{\boldsymbol{\xi}}|^2}\,\mathrm{d}S_{\bar{\xi}} = \frac{2\pi}{3}, \qquad\qquad (2.2.23)$$

the tensor $\mathcal{A}^\sigma$ defined by (2.2.21) reduces to

$$\mathcal{A}^\sigma = \frac{8(1-\nu)}{3\mu(2-\nu)}\boldsymbol{n}\otimes\big(2\boldsymbol{I} - \nu\boldsymbol{n}\otimes\boldsymbol{n}\big)\otimes\boldsymbol{n} \qquad\qquad (2.2.24)$$

In view of the relationship (2.2.21) between $\mathcal{A}$ and $\mathcal{A}^\sigma$, one may equivalently use the following version of $\mathcal{A}^\sigma$ which, unlike (2.2.24), has the minor symmetries:

$$\mathcal{A}^\sigma = \frac{4(1-\nu)}{3\mu(2-\nu)}\big([\boldsymbol{n}\otimes\boldsymbol{e}_\alpha + \boldsymbol{e}_\alpha\otimes\boldsymbol{n}]\otimes[\boldsymbol{n}\otimes\boldsymbol{e}_\alpha + \boldsymbol{e}_\alpha\otimes\boldsymbol{n}] + 2(2-\nu)\boldsymbol{n}\otimes\boldsymbol{n}\otimes\boldsymbol{n}\otimes\boldsymbol{n}\big), \qquad (2.2.25)$$

where $\alpha \in \{1, 2\}$. This form corresponds to the result given in Proposition 2 of 2.A.2. Then, using (2.1.1), (2.2.21) and (2.2.25), one finds

$$\mathcal{A} = \frac{8\mu(1-\nu)}{3}\Big[\Big(\frac{2\nu}{1-2\nu}\Big)^2\boldsymbol{I}\otimes\boldsymbol{I} + \frac{4\nu}{1-2\nu}[\boldsymbol{n}\otimes\boldsymbol{n}\otimes\boldsymbol{I} + \boldsymbol{I}\otimes\boldsymbol{n}\otimes\boldsymbol{n}] + 4\boldsymbol{n}\otimes\boldsymbol{n}\otimes\boldsymbol{n}\otimes\boldsymbol{n}$$

$$+ \frac{2}{(2-\nu)}[\boldsymbol{n}\otimes\boldsymbol{e}_\alpha + \boldsymbol{e}_\alpha\otimes\boldsymbol{n}]\otimes[\boldsymbol{n}\otimes\boldsymbol{e}_\alpha + \boldsymbol{e}_\alpha\otimes\boldsymbol{n}]\Big].$$

Polarization tensor for an elliptic crack

The case of an elliptic crack is also amenable to analytical treatment, based on using the exact solution for an ellipsoidal cavity (which is itself a special case of Eshelby solution for an ellipsoidal inclusion Mura (1982)) and considering the limiting case where the cavity becomes infinitely thin. The details of this approach, being somewhat lengthy, are deferred to 2.A.3 and lead to the following result:

Proposition 2. *The polarization tensor for a normalized elliptical crack whose major semiaxis ℓ_1 and minor semiaxis $\ell_2 = (1 - m^2)^{1/2}\ell_1$ (with $0 \leqslant m < 1$) are respectively aligned with the $\boldsymbol{e}_1$ and $\boldsymbol{e}_2$ directions of a Cartesian frame is given (see Eq. (2.2.21)) by $\mathcal{A} = \mathcal{C} : \mathcal{A}^\sigma : \mathcal{C}$, where the only nonzero entries of $\mathcal{A}^\sigma$ are given (using the functions $\alpha(m), \beta(m)$ defined by (2.A.12)) by*

$$\mathcal{A}^\sigma_{1313} = \mathcal{A}^\sigma_{3113} = \mathcal{A}^\sigma_{1331} = \mathcal{A}^\sigma_{3131} = \ell_1^3(1-m^2)^{1/2}\frac{\pi(1-\nu)}{3\mu(\nu\alpha(m) + (1-\nu)\beta(m))} \qquad (2.2.26a)$$

$$\mathcal{A}^\sigma_{2323} = \mathcal{A}^\sigma_{3223} = \mathcal{A}^\sigma_{2332} = \mathcal{A}^\sigma_{3232} = \ell_1^3(1-m^2)^{1/2}\frac{\pi(1-\nu)}{3\mu(\beta(m) - \nu\alpha(m))} \qquad (2.2.26b)$$

$$\mathcal{A}^\sigma_{3333} = \ell_1^3(1-m^2)^{1/2}\frac{4\pi(1-\nu)}{3\mu\beta(m)}. \qquad (2.2.26c)$$

As explained in 2.A.3, this result reduces as expected to (2.2.25) for the special case of a circular crack of unit radius, corresponding to $m = 0$ and $\ell_1 = 1$.

2.3 Acoustic topological sensitivity

For completeness, the case where the reference medium is an acoustic fluid characterized by the wave velocity c is now treated. In this context, a "crack" supporting homogeneous Neumann conditions models a thin rigid screen across which the acoustic pressure may be discontinuous. The scattered acoustic pressure field $v_{\varepsilon,\boldsymbol{z}}$ arising in $\Omega_{\varepsilon,\boldsymbol{z}}$ due to the presence of a screen of small size ε and shape $\bar{\Gamma}$ located at $\boldsymbol{z}$ is governed by the following IBVP:

$$
\begin{aligned}
\Delta v_{\varepsilon,\boldsymbol{z}}(\boldsymbol{\xi},t) &= c^{-2}\ddot{v}_{\varepsilon,\boldsymbol{z}}(\boldsymbol{\xi},t) & (\boldsymbol{\xi} \in \Omega_{\varepsilon,\boldsymbol{z}}, t \geqslant 0) \\
q^{\pm}[v_{\varepsilon,\boldsymbol{z}}^{\pm}] &= -q^{\pm}[u](\boldsymbol{\xi},t) & (\boldsymbol{\xi} \in \Gamma_{\varepsilon,\boldsymbol{z}}^{\pm}, t \geqslant 0) \\
q[v_{\varepsilon,\boldsymbol{z}}] &= 0 & (\boldsymbol{\xi} \in S_{\mathrm{N}}, t \geqslant 0) \\
v_{\varepsilon,\boldsymbol{z}}(\boldsymbol{\xi},t) &= 0 & (\boldsymbol{\xi} \in S_{\mathrm{D}}, t \geqslant 0) \\
v_{\varepsilon,\boldsymbol{z}}(\boldsymbol{\xi},0) &= \dot{v}_{\varepsilon,\boldsymbol{z}}(\boldsymbol{\xi},0) = 0 & (\boldsymbol{\xi} \in \Omega_{\varepsilon,\boldsymbol{z}}),
\end{aligned}
\tag{2.3.1}
$$

where u is the free field, $w \mapsto q[w] = \boldsymbol{\nabla} w \cdot \boldsymbol{n}$ is the normal derivative operator (with the superscript $\pm$ referring where necessary to the relevant crack face and its unit normal). Then in the same fashion as in equation (2.2.3) the topological sensitivity is defined for scalar wave through

$$
\int_0^T \int_{S^{\mathrm{obs}}} \frac{\partial \varphi}{\partial u}[u(\boldsymbol{\xi},t),\boldsymbol{\xi},t] v_{\varepsilon,\boldsymbol{z}}(\boldsymbol{\xi},t)\,\mathrm{d}S_\xi\,\mathrm{d}t = \eta(\varepsilon)\mathbb{T}(\boldsymbol{z},\bar{\Gamma},T) + o(\eta(\varepsilon)).
\tag{2.3.2}
$$

Introducing the adjoint field $\hat{u}$ solution of the IBVP

$$
\begin{aligned}
\Delta \hat{u}(\boldsymbol{\xi},t) &= c^{-2}\ddot{\hat{u}}(\boldsymbol{\xi},t) & (\boldsymbol{\xi} \in \Omega, 0 \leqslant t \leqslant T) \\
q[\hat{u}] &= \frac{\partial \varphi}{\partial u}[u(\boldsymbol{\xi},T-t),\boldsymbol{\xi},T-t] & (\boldsymbol{\xi} \in S^{\mathrm{obs}}, 0 \leqslant t \leqslant T) \\
q[\hat{u}] &= 0 & (\boldsymbol{\xi} \in S_{\mathrm{N}}\backslash S^{\mathrm{obs}}, 0 \leqslant t \leqslant T) \\
\hat{u}(\boldsymbol{\xi},t) &= 0 & (\boldsymbol{\xi} \in S_{\mathrm{D}}, 0 \leqslant t \leqslant T) \\
\hat{u}(\boldsymbol{\xi},0) &= \dot{\hat{u}}(\boldsymbol{\xi},0) = 0 & (\boldsymbol{\xi} \in \Omega),
\end{aligned}
\tag{2.3.3}
$$

and invoking the scalar dynamical reciprocity identity, equation (2.3.2) reduces to

$$
\eta(\varepsilon)\mathbb{T}(\boldsymbol{z},\bar{\Gamma},T) + o(\eta(\varepsilon)) = \int_0^T \int_{\Gamma_{\varepsilon,\boldsymbol{z}}} q[\hat{u}](\boldsymbol{\xi},T-t)[\![v_{\varepsilon,\boldsymbol{z}}]\!](\boldsymbol{\xi},t)\,\mathrm{d}S_\xi\,\mathrm{d}t,
\tag{2.3.4}
$$

where $[\![v_{\varepsilon,\boldsymbol{z}}]\!] = v_{\varepsilon,\boldsymbol{z}}^+ - v_{\varepsilon,\boldsymbol{z}}^-$ denotes the acoustic pressure jump through the screen and the flux $q[\hat{u}]$ is defined on $\Gamma_{\varepsilon,\boldsymbol{z}}$ in terms of the unit normal $\boldsymbol{n} = \boldsymbol{n}^-$

Leading contributions as $\varepsilon \to 0$. To determine the leading contributions of $v_{\varepsilon,\boldsymbol{z}}$ in the limit $\varepsilon \to 0$, it is convenient to reformulate the scattering IBVP (2.3.1) as a singular boundary integral equation (Bonnet, 1999):

$$
\begin{aligned}
q[u](\boldsymbol{x},t) = \boldsymbol{n}(\boldsymbol{x}) \cdot \Bigg\{ & \fint_{\Gamma_{\varepsilon,\boldsymbol{z}}} \boldsymbol{\nabla} G(\boldsymbol{x},t,\boldsymbol{\xi}) \star \boldsymbol{\mathcal{D}}[\![v_{\varepsilon,\boldsymbol{z}}]\!](\boldsymbol{\xi},t)\,\mathrm{d}S_\xi \\
& + \frac{1}{c^2}\int_{\Gamma_{\varepsilon,\boldsymbol{z}}} \boldsymbol{n}(\boldsymbol{\xi}) G(\boldsymbol{x},t,\boldsymbol{\xi}) \star [\![\ddot{v}_{\varepsilon,\boldsymbol{z}}]\!](\boldsymbol{\xi},t)\,\mathrm{d}S_\xi \Bigg\} & (\boldsymbol{x} \in \Gamma_{\varepsilon,\boldsymbol{z}},\ 0 \leqslant t \leqslant T) \quad (2.3.5)
\end{aligned}
$$

with the tangential differential operator $\boldsymbol{\mathcal{D}}$ defined by $w \mapsto \boldsymbol{\mathcal{D}}w = \boldsymbol{\nabla}w \otimes \boldsymbol{n} - \boldsymbol{n} \otimes \boldsymbol{\nabla}w$ and where $G(\boldsymbol{x}, t, \boldsymbol{\xi})$ is the acoustic Green's function, i.e. the pressure at $\boldsymbol{\xi}$ and time t created in Ω by a time-impulsive point source acting at $\boldsymbol{x} \in \Omega$ and $t = 0$ and satisfying the boundary conditions

$$G(\boldsymbol{x}, t, \boldsymbol{\xi}) = 0 \quad (\boldsymbol{\xi} = S_{\mathrm{D}}, t \geqslant 0), \qquad q[G](\boldsymbol{x}, t, \boldsymbol{\xi}) = 0 \quad (\boldsymbol{\xi} = S_{\mathrm{N}}, t \geqslant 0) \tag{2.3.6}$$

Proceeding along the same lines as in Sec. 2.2.2, one arrives at a representation of $v_{\varepsilon, \boldsymbol{z}}$ of the form

$$[\![v_{\varepsilon, \boldsymbol{z}}]\!](\boldsymbol{\xi}, t) = \varepsilon \, \frac{\partial u}{\partial z_i}(\boldsymbol{z}, t) \cdot [\![V]\!]^i(\bar{\boldsymbol{\xi}}) + o(\varepsilon) \tag{2.3.7}$$

and at the following expansions, which are the acoustic counterparts of (2.2.16a,b):

$$\oint_{\Gamma_{\varepsilon, \boldsymbol{z}}} \boldsymbol{\nabla}G(\boldsymbol{x}, t, \boldsymbol{\xi}) \star \boldsymbol{\mathcal{D}}[\![v_{\varepsilon, \boldsymbol{z}}]\!](\boldsymbol{\xi}, t) \, \mathrm{d}S_\xi = \frac{\partial u}{\partial z_i}(\boldsymbol{z}, t) \left\{ \oint_{\bar{\Gamma}} \boldsymbol{\nabla}G_\infty(\bar{\boldsymbol{\xi}} - \bar{\boldsymbol{x}}) \cdot \boldsymbol{\mathcal{D}}[\![V]\!]^i(\bar{\boldsymbol{\xi}}) \, \mathrm{d}S_{\bar{\xi}} + o(1) \right\} \tag{2.3.8a}$$

$$\int_{\Gamma_{\varepsilon, \boldsymbol{z}}} \boldsymbol{n}(\boldsymbol{\xi}) G(\boldsymbol{x}, t, \boldsymbol{\xi}) \star [\![\ddot{v}_{\varepsilon, \boldsymbol{z}}]\!](\boldsymbol{\xi}, t) \, \mathrm{d}S_\xi = O(\varepsilon^2) \tag{2.3.8b}$$

(with $G_\infty(\boldsymbol{r}) = 1/4\pi \|\boldsymbol{r}\|$ denoting the full-space Laplace fundamental solution). Thus, deriving the limiting form of integral equation (2.3.5) as $\varepsilon \to 0$ and enforcing the result for any value of $\partial u / \partial z_i(\boldsymbol{z}, t)$ yields governing integral equations for the $[\![V]\!]^i$:

$$\boldsymbol{n}(\bar{\boldsymbol{x}}) \cdot \boldsymbol{e}_i = \boldsymbol{n}(\bar{\boldsymbol{x}}) \cdot \oint_{\bar{\Gamma}} \boldsymbol{\nabla}G_\infty(\bar{\boldsymbol{\xi}} - \bar{\boldsymbol{x}}) \cdot \boldsymbol{\mathcal{D}}[\![V]\!]^i(\bar{\boldsymbol{\xi}}) \, \mathrm{d}S_{\bar{\xi}} \qquad (\bar{\boldsymbol{x}} \in \bar{\Gamma}) \tag{2.3.9}$$

which correspond to exterior Laplace problems for the normalized screen $\bar{\Gamma}$ whose faces are subjected to fluxes $q^\pm(\bar{\boldsymbol{x}}) = -\boldsymbol{n}^\pm(\bar{\boldsymbol{x}}) \cdot \boldsymbol{e}_i$.

Topological sensitivity.   Inserting (2.2.18) into the right-hand side of (2.3.4), one finally obtains

$$\text{(a) } \mathbb{T}(\boldsymbol{z}, \bar{\Gamma}, T) = \int_0^T \boldsymbol{\nabla}\hat{u}(\boldsymbol{z}, T - t) \cdot \boldsymbol{\mathcal{B}} \cdot \boldsymbol{\nabla}u(\boldsymbol{z}, t) \, \mathrm{d}t, \qquad \text{(b) } \eta(\varepsilon) = \varepsilon^3, \tag{2.3.10}$$

with the second-order polarization tensor $\boldsymbol{\mathcal{B}}$ defined, upon arranging the V^i into a vector field $\boldsymbol{\mathcal{V}} = V^i \boldsymbol{e}_i$, by

$$\boldsymbol{\mathcal{B}} = \int_{\bar{\Gamma}} [\![\boldsymbol{\mathcal{V}}]\!](\bar{\boldsymbol{\xi}}) \otimes \boldsymbol{n}(\bar{\boldsymbol{\xi}}) \, \mathrm{d}S_{\bar{\xi}}. \tag{2.3.11}$$

An argument similar to that of 2.A.2 shows that the tensor $\boldsymbol{\mathcal{B}}$ is symmetric.

Polarization tensor for the elliptic screen.   The polarization tensor for an elliptic sound-hard plane screen has the following closed-form expression (see 2.A.4 for details):

$$\boldsymbol{\mathcal{B}} = \frac{4\pi}{3} \frac{(1 - m^2)}{E(m)} \ell_1^3 \boldsymbol{n} \otimes \boldsymbol{n}, \tag{2.3.12}$$

with ℓ_1, m as defined in Proposition 2 and $E(m)$ defined by (2.A.13). The case of the circular plane screen of unit radius then corresponds to $m = 0$, $\ell_1 = 1$ and $E(m) = \pi/2$, i.e.:

$$\boldsymbol{\mathcal{B}} = \frac{8}{3} \boldsymbol{n} \otimes \boldsymbol{n}. \tag{2.3.13}$$

2.4 TS-based crack identification: heuristics and implementation

Topological sensitivity as a crack indicator function. Since $\mathbb{T}(\boldsymbol{z}, \bar{\Gamma}, T)$ quantifies the sensitivity of the featured cost functional $\mathbb{J}$ to the appearance at $\boldsymbol{z}$ of an infinitesimal crack in the reference medium, it is natural to consider $\boldsymbol{z} \mapsto \mathbb{T}(\boldsymbol{z}, \bar{\Gamma}, T)$ as a possible crack indicator function. This heuristic approach consists in seeking actual crack(s) at locations $\boldsymbol{z}$ at which $\mathbb{T}(\boldsymbol{z}, \bar{\Gamma}, T)$ attains its most pronounced negative values (i.e. such that *infinitesimal* trial cracks placed there improve the fit between predicted and actual measurements). A simple shape (usually circular) will be assumed for $\bar{\Gamma}$, with its orientation chosen so as to minimize $\mathbb{T}(\boldsymbol{z}, \bar{\Gamma}, T)$ as explained later in this section. While intuition (and previous studies on the same approach carried out for other types of defects) suggests that *finite* defects having the same location also induce a decrease of the cost function, this proposed exploitation of the TS field $\mathbb{T}(\cdot, \bar{\Gamma}, T)$ is not backed by a rigorous mathematical proof (whereas the analysis of the cost function leading to the definition and evaluation of $\mathbb{T}(\boldsymbol{z}, \bar{\Gamma}, T)$ is itself mathematically rigorous). This proposed heuristic identification approach, whose main features are discussed in the remainder of this section, will be tested against numerical experiments in Sec. 2.5.

Evaluation of the topological sensitivity field. Computing the field $\mathbb{T}(\cdot, \bar{\Gamma}, T)$ using (2.2.20) entails the evaluation of a time-convolution integral. Performing the latter operation requires storage of the entire histories for the free and adjoint fields (which may be discarded once the convolution is computed). To hold this memory space over the shortest possible time in the course of the computation, it is useful to recast $\mathbb{T}(\boldsymbol{z}, \bar{\Gamma}, T)$ into the equivalent form

$$\mathbb{T}(\boldsymbol{z}, \bar{\Gamma}, T) = \boldsymbol{\Pi}(\boldsymbol{z}, T) :: \boldsymbol{\mathcal{A}}^{\sigma}(\bar{\Gamma}) \tag{2.4.1}$$

where the fourth-order tensor field $\boldsymbol{\Pi}(\boldsymbol{z}, T)$ is defined by

$$\boldsymbol{\Pi}(\boldsymbol{z}, T) = \int_0^T \frac{1}{2} \left\{ \boldsymbol{\sigma}[\hat{\boldsymbol{u}}](\boldsymbol{z}, T - t) \otimes \boldsymbol{\sigma}[\boldsymbol{u}](\boldsymbol{z}, t) + \boldsymbol{\sigma}[\boldsymbol{u}](\boldsymbol{z}, t) \otimes \boldsymbol{\sigma}[\hat{\boldsymbol{u}}](\boldsymbol{z}, T - t) \right\} \mathrm{d}t. \tag{2.4.2}$$

The computational advantage of (2.4.1) over (2.2.20a) is materialized by evaluating $\boldsymbol{\Pi}(\boldsymbol{z}, T)$ immediately after solving the free and adjoint IBVPs, after which the discretized free and adjoint solutions are no longer needed and may be discarded from the memory. This treatment has at least two advantages. First, when the featured cost function additively aggregates several experiments, in which case the $\boldsymbol{\Pi}_m(\boldsymbol{z}, T)$ associated with the m-th experiment can be computed sequentially and the topological sensitivity for the whole set of experiments is given by

$$\mathbb{T}(\boldsymbol{z}, \bar{\Gamma}, T) = \left\{ \sum_m \boldsymbol{\Pi}_m(\boldsymbol{z}, T) \right\} :: \boldsymbol{\mathcal{A}}^{\sigma}(\bar{\Gamma}). \tag{2.4.3}$$

Second, $\boldsymbol{\Pi}(\boldsymbol{z}, T)$ does not depend on the shape or orientation of $\bar{\Gamma}$, which affect only the constant polarization tensor $\boldsymbol{\mathcal{A}}^{\sigma}(\bar{\Gamma})$. This makes it easier, and computationally inexpensive, to evaluate the influence of the choice of $\bar{\Gamma}$ on the value of $\mathbb{T}$ at a given sampling location $\boldsymbol{z}$.

In the scalar (acoustic) case, similar remarks apply, with $\mathbb{T}(\boldsymbol{z}, \bar{\Gamma}, T)$ recast in the form

$$\mathbb{T}(\boldsymbol{z}, \bar{\Gamma}, T) = \boldsymbol{\Pi}(\boldsymbol{z}, T) : \boldsymbol{\mathcal{B}}(\bar{\Gamma}) \tag{2.4.4}$$

in terms of the second-order tensor $\boldsymbol{\Pi}(\boldsymbol{z}, T)$ defined by

$$\boldsymbol{\Pi}(\boldsymbol{z}, T) = \frac{1}{2} \int_0^T \left[\boldsymbol{\nabla} \hat{u}(\boldsymbol{z}, T - t) \otimes \boldsymbol{\nabla} u(\boldsymbol{z}, t) + \boldsymbol{\nabla} u(\boldsymbol{z}, t) \otimes \boldsymbol{\nabla} \hat{u}(\boldsymbol{z}, T - t) \right] \mathrm{d}t. \tag{2.4.5}$$

In practice, a local orientation n^{true} corresponding to the crack Γ^{true} can be known beforehand, so that the methodology suggested is to seek the crack at point z where $\mathbb{T}(z, n^{\text{true}}, T)$ attains its most pronounced negative values.

Crack orientation. An important feature of the sought crack is its orientation, which is normally not known *a priori*. Let $\mathcal{R}$ denote an affine rotation that leaves the origin in $\bar{\xi}$-space (i.e. z in the physical space) invariant and is otherwise characterized by the orthogonal matrix $R \in \text{SO}(3)$. Then, for a fixed shape of the trial infinitesimal crack $\bar{\Gamma}$, $\mathbb{T}(z, \bar{\Gamma}, T)$ depends on the chosen orientation of $\bar{\Gamma}$ via $\mathcal{A}$ (or $\mathcal{A}^\sigma$) through

$$\mathcal{A}_{ijk\ell}(\mathcal{R}(\bar{\Gamma})) = R_{iI}R_{jJ}R_{kK}R_{\ell L}\mathcal{A}_{IJKL}(\bar{\Gamma}), \qquad (2.4.6)$$

by virtue of the fact that evaluating (say) $\nabla u : \mathcal{A}(\mathcal{R}(\bar{\Gamma})) : \nabla \hat{u}$ can be achieved by expressing $\nabla u, \nabla \hat{u}$ in the rotated frame (E_1, E_2, E_3) such that $E_i = R^{-1}e_i$ and employing the original polarization tensor $\mathcal{A}(\bar{\Gamma})$. Then, in keeping with the previously-presented heuristic, it is natural to seek the orientation such that, for a given sampling point z and crack shape, $\mathbb{T}(z, \bar{\Gamma}, T)$ is lowest. Acordingly, define

$$\begin{aligned}
\mathbb{T}^{\text{opt}}(z, T) &= \min_{R \in \text{SO}(3)} \mathbb{T}(z, \mathcal{R}(\bar{\Gamma}), T) \\
n^{\text{opt}}(z, T) &= \arg\min_{R \in \text{SO}(3)} \mathbb{T}(z, \mathcal{R}(\bar{\Gamma}), T)
\end{aligned} \qquad (z \in \Omega). \qquad (2.4.7)$$

If the trial crack $\bar{\Gamma}$ is penny-shaped, the minimization (2.4.7) reduces to a minimization w.r.t. the unit normal $n \in \mathcal{S}$ (where $\mathcal{S}$ is the unit sphere); the topological sensitivity will in this case be denoted $\mathbb{T}(z, n, T)$ for emphasis. Furthermore, since $\mathcal{A}$ (or $\mathcal{A}^\sigma$) is in this case an even function of n, the search space for n may be limited to one-half of $\mathcal{S}$. In the acoustic case, where the polarization tensor is of second-order, the minimization problem w.r.t. n is solvable exactly using an algebraic argument similar to that of Amstutz et al. (2005). On noting $\pi^{\min}(z, T)$ the eigenvector corresponding to the smallest (real) eigenvalue of the symmetric tensor $\Pi(z, T)$, the solution to (2.4.7) is

$$\mathbb{T}^{\text{opt}}(z, T) = \mathbb{T}(z, \pi^{\min}(z, T), T), \qquad n^{\text{opt}}(z, T) = \pi^{\min}(z, T) \qquad (z \in \Omega). \qquad (2.4.8)$$

Thus, using indicators $\mathbb{T}_\lambda$ (2.4.9) and Γ_λ (2.4.10) that focus on the spatial reconstruction of the crack Γ^{true}, the identification of the *optimal* normals in the sense of the local minimization of the topological sensitivity (2.3.10) are obtain by diagonalization of (2.4.5) varying $z \in \Omega$.

The argument leading to (2.4.8) cannot be easily carried over to the elastic case, involving fourth-order polarization tensors, so that the minimization w.r.t. n is at the moment carried out numerically. As a side remark, the similar (but not identical) problem of finding directions of anisotropy that yield a pointwise optimal strain energy density is addressed in Rovati and Taliercio (2003).

Thresholded topological sensitivity. To focus on *sampling* points $z \in \Omega$ where the topological sensitivity $\mathbb{T}^{\text{opt}}(z, T)$ reaches sufficiently low (negative) values, a thresholded version $\mathbb{T}_\lambda$ of $\mathbb{T}^{\text{opt}}$ is defined as

$$\mathbb{T}_\lambda(z, T) = \begin{cases} \mathbb{T}^{\text{opt}}(z, T) & \text{if } \mathbb{T}^{\text{opt}}(z, T) \leqslant \lambda\mathbb{T}^{\min} \\ 0 & \text{if } \mathbb{T}^{\text{opt}}(z, T) > \lambda\mathbb{T}^{\min} \end{cases} \qquad \text{with } \mathbb{T}^{\min} = \min_{z \in \Omega} \mathbb{T}^{\text{opt}}(z, T), \qquad (2.4.9)$$

(where $\lambda > 0$ is a cut-off parameter and with the implicit assumption that $\mathbb{T}^{\mathrm{min}} < 0$). Moreover, let $\Gamma_\lambda \in \Omega$ denote the support of $\mathbb{T}_\lambda(\cdot, T)$, i.e.

$$\Gamma_\lambda = \{ z \in \Omega \mid \mathbb{T}_\lambda(z, T) < 0 \}. \tag{2.4.10}$$

Thus an estimation of the unknown crack (or set of cracks) suggested by the thresholded topological sensitivity may be defined in terms of Γ_λ.

Moreover, assuming that $\bar{\Gamma}$ is the unit circular crack, let $\mathcal{S}^{\mathrm{opt}}(z, T) \subset \mathcal{S}$ denote the half-sphere *oriented* by $n^{\mathrm{opt}}(z, T)$, i.e.

$$\mathcal{S}^{\mathrm{opt}}(z, T) = \left\{ n \in \mathcal{S}, \; n^{\mathrm{opt}}(z, T) \cdot n \geqslant 0 \right\} \qquad (z \in \Omega). \tag{2.4.11}$$

and, with reference to the thresholded topological sensitivity (2.4.9), let the subset $\mathcal{S}^{\mathrm{opt}}_\lambda(z, T)$ of $\mathcal{S}^{\mathrm{opt}}(z, T)$ be defined by

$$\mathcal{S}^{\mathrm{opt}}_\lambda(z, T) = \left\{ n \in \mathcal{S}^{\mathrm{opt}}(z, T) \mid \mathbb{T}(z, n, T) < \lambda \mathbb{T}^{\mathrm{min}} \right\}, \tag{2.4.12}$$

Then, the average optimal normal n^{opt}_λ is defined at sampling points $z \in \Gamma_\lambda$ by

$$n^{\mathrm{opt}}_\lambda(z, T) = \int_{\mathcal{S}^{\mathrm{opt}}_\lambda(z, T)} n \, \mathrm{d}S_{\bar{\xi}} \qquad (z \in \Gamma_\lambda), \tag{2.4.13}$$

with the condition $z \in \Gamma_\lambda$ ensuring that $\mathcal{S}^{\mathrm{opt}}_\lambda(z, T)$ is not empty. Although this is not *a priori* required, the cut-off parameter λ entering the definitions of Γ_λ and n^{opt}_λ will for simplicity be assumed to coincide.

2.5 Numerical examples

In this section, numerical experiments are presented to evaluate the topological sensitivity method efficiency. Using a generic FEM code, synthetic data will be produced for different meshes containing a crack and topological sensitivities corresponding to cost functionals (2.1.2) with least-square misfit function of format

$$\varphi[u(\xi, t), \xi, t] = \frac{1}{2} \| u(\xi, t) - u^{\mathrm{obs}}(\xi, t) \|^2 \tag{2.5.1}$$

will be computed.

The evaluation of the field $\mathbb{T}$ requires the knowledge of the tensor field $\mathbf{\Pi}$ resulting from the computation of just two solutions, namely free and adjoint fields, that are both defined on crack-free configuration. Elastodynamic solutions are computed using isoparametric piecewise-linear interpolation in four-noded tetrahedral elements and unconditionally-stable Newmark algorithm with parameters $\beta = 1/4$, $\gamma = 1/2$ (Hughes, 1987). Related space and time discretized version of (2.1.2), (2.2.20) and (2.3.10) are implemented using analytical formulations of the polarization tensors corresponding to the nucleation of infinitesimal penny-shaped crack, i.e. (2.2.24) and (2.3.13) respectively. Finally, the computations are time-adimensionalized by a parameter $\bar{c}$, to be adjusted in each example, implying that, in a unit time, the length traveled by waves propagating at velocity $\bar{c}$ is unity.

2.5.1   Cubic domain

The reference domain Ω considered in this section is a unit cubic mesh containing 27840 nodes. A penny-shaped crack Γ^{true} of radius $R = 0.1$, centered at $\boldsymbol{x}^{\text{true}} = (0.65, 0.65, 0.7)$ in a cartesian coordinate system (x_1, x_2, x_3) and oriented by the normal $\boldsymbol{n}^{\text{true}} = -\sin\theta\boldsymbol{e}_1 + \cos\theta\boldsymbol{e}_3$ (see Fig. 2.1) constitutes the crack to be identified. The surface S_{N} with imposed Neumann conditions is given by $S_{\text{N}} = \{x_3 = 1\}$, and no Dirichlet condition is imposed during the simulations so that $S_{\text{D}} = \emptyset$. The observation surface S^{obs} considered coincides with the whole discretized external boundary of the domain Ω and the duration of the experiment is set to $T = 2$.
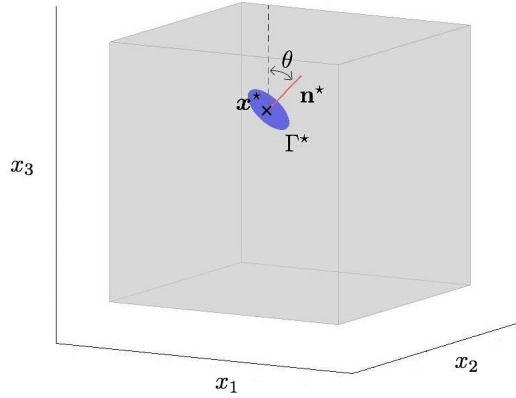
Figure 2.1: *Cracked cubic domain*

Acoustics.   In the numerical experiment considered, a uniform normal gradient $\boldsymbol{\nabla} u_{\Gamma^\star}(\boldsymbol{\xi}, t) \cdot \boldsymbol{n} = -H(t)$ (where $H(t)$ denotes the Heaviside step function) is applied on S_{N} and the computation time adimensionalization parameter correspond to the sound speed c, i.e. the velocity of isotropic compressibility elastic waves

(a) $\theta = 0$ (b) $\theta = \frac{\pi}{10}$ (c) $\theta = \frac{\pi}{4}$
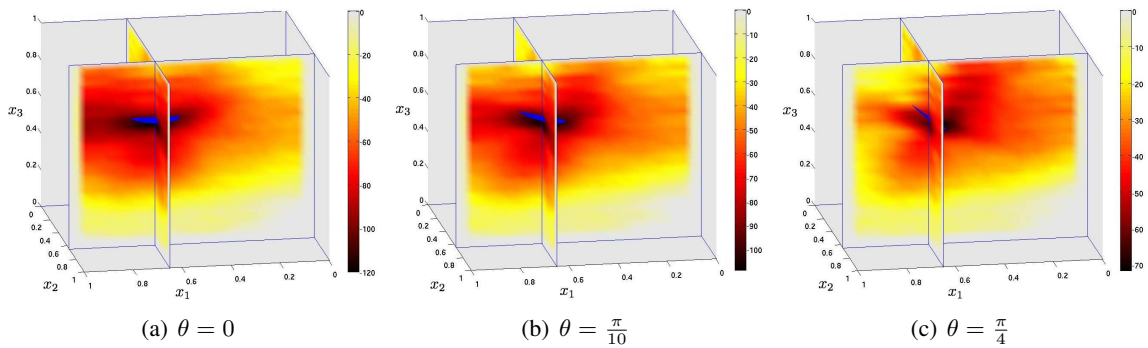
Figure 2.2: Acoustic *field* $\mathbb{T}_0$

(a) $\theta = 0$, $\lambda = 0.9$ (b) $\theta = \frac{\pi}{10}$, $\lambda = 0.85$ (c) $\theta = \frac{\pi}{4}$, $\lambda = 0.8$
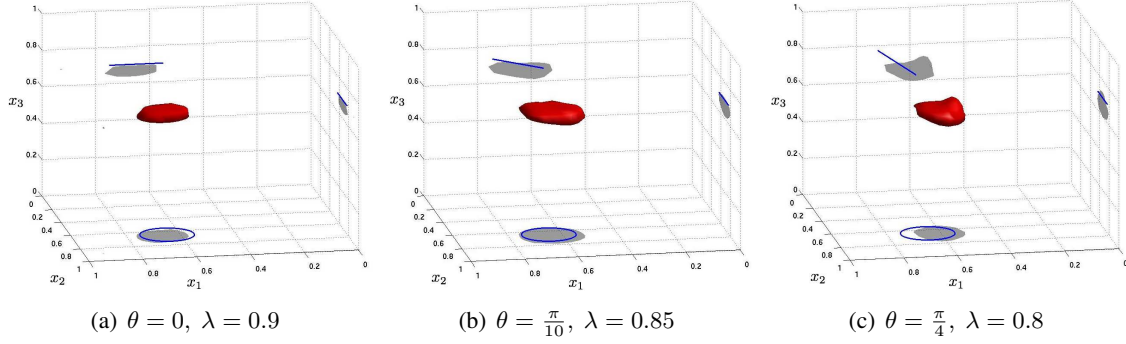
Figure 2.3: Acoustic *domain* Γ_λ

(a) $\theta = 0$, $\lambda = 0.9$ (b) $\theta = \frac{\pi}{10}$, $\lambda = 0.85$ (c) $\theta = \frac{\pi}{4}$, $\lambda = 0.8$
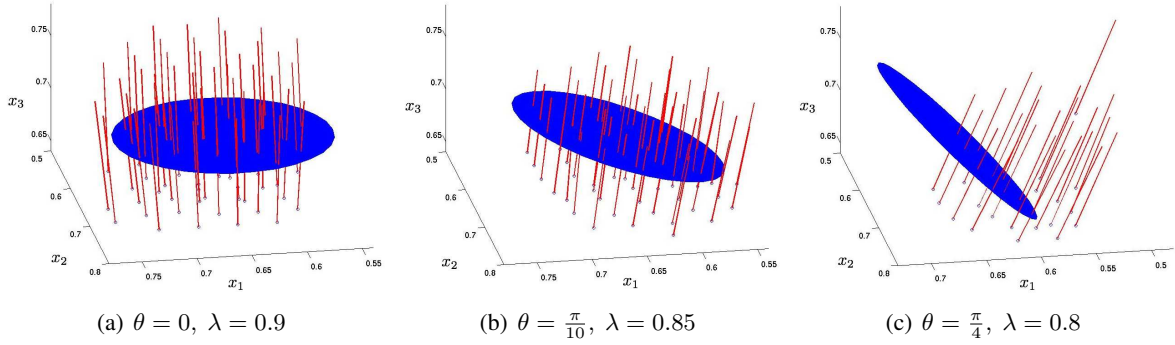
Figure 2.4: Acoustic *normals* $\mathbf{n}_\lambda^{\min}$

$$\bar{c} = c = \sqrt{\frac{2\mu(1-\nu)}{3\rho(1-2\nu)}}. \tag{2.5.2}$$

The numerical results are presented on Figures 2.2, 2.3 and 2.4.

Elasticity. A uniform constant compressional loading $\boldsymbol{t}[\boldsymbol{u}_{\Gamma^\star}](\boldsymbol{\xi}, t) = -H(t)\boldsymbol{e}_3$ is imposed on S_{N} and the computation is adimensionalized by the longitudinal wave velocity

$$\bar{c} = c_{\mathrm{L}} = \sqrt{\frac{2\mu(1-\nu)}{\rho(1-2\nu)}}. \tag{2.5.3}$$

See Figs. 2.5, 2.6 and 2.7.

2.5.2 Cylindrical shell

The reference domain Ω considered is an elongated thin cylindrical shell with radii interior $R_i = 0.9$, exterior $R_e = 1$ and length $H = 4$ which mesh involves 40650 nodes. A cracked configuration contains a helicoidal crack centered at $\boldsymbol{x}^{\mathrm{true}}$ in a cylindrical coordinate system (r, θ, z) and parametrized by fixed

(a) $\theta = 0$ (b) $\theta = \frac{\pi}{10}$ (c) $\theta = \frac{\pi}{4}$
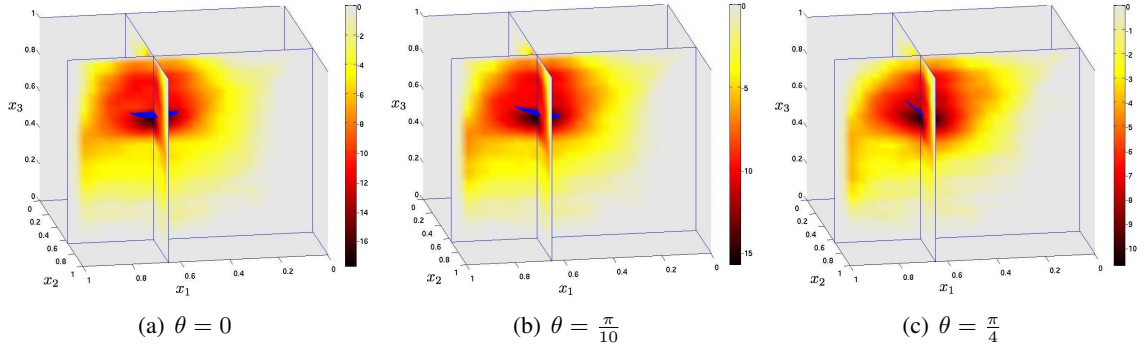
Figure 2.5: Elastic *field* $\mathbb{T}_0$

(a) $\theta = 0$, $\lambda = 0.7$ (b) $\theta = \frac{\pi}{10}$, $\lambda = 0.75$ (c) $\theta = \frac{\pi}{4}$, $\lambda = 0.75$
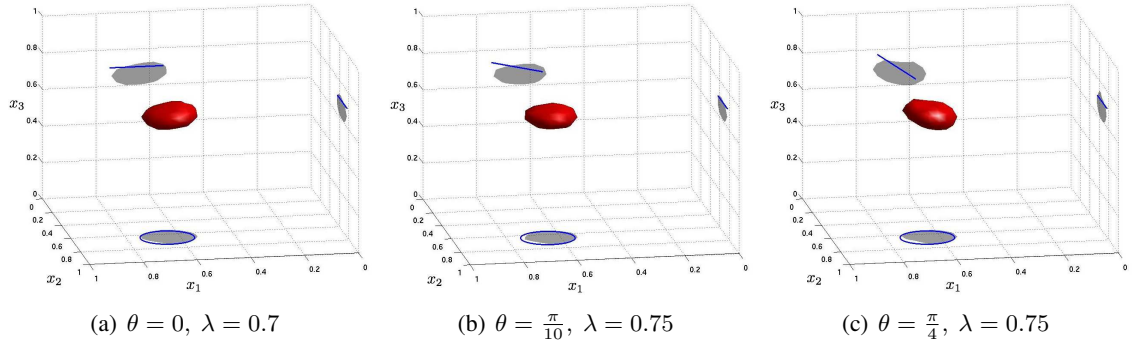
Figure 2.6: Elastic *domain* Γ_λ

(a) $\theta = 0$ (b) $\theta = \frac{\pi}{10}$, $\lambda = 0.$ (c) $\theta = \frac{\pi}{4}$, $\lambda = 0.$
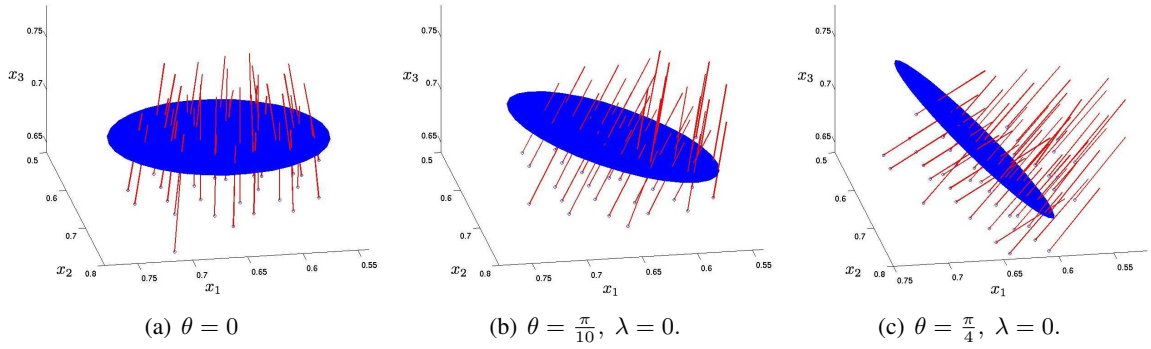
Figure 2.7: Elastic *normals* $\mathbf{n}_\lambda^{\min}$

lengths h and l, and a varying *oriented* angle α as indicated on Fig. 2.8. Geometrical parameters are such that possible crack breaks through the interior surface of the shell but not its exterior. Finally, the observation surface is given by $S^{\text{obs}} = \{r = 1,\ 0 < z < 4\}$.
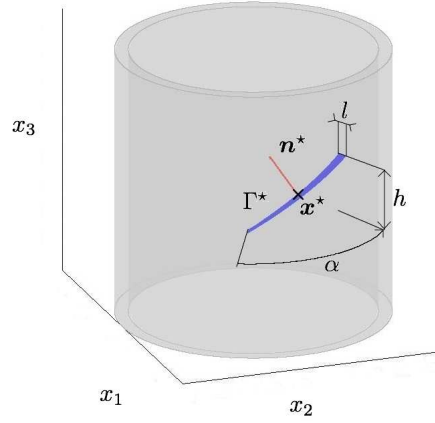
Figure 2.8: *Cracked cylindrical shell*

Single experiment

A first set of results is presented in this section for a configuration involving a single crack centered at $x^{\text{true}} = (0.945, 0, 1.75)$ and characterized by $h = 0.5$ and $l = 0.09$. Synthetic data are produced using a unique experiment during which Neumann conditions have been imposed on $S_{\text{N}} = \{r = 1, (\theta, z) \in [0, 2\pi] \times [3.9, 4]\}$ while $S_{\text{D}} = \emptyset$, and using an experiment duration set to $T = 8$.

For further references, let $g(t, m, d)$ denote the Gaussian function of parameter t with mean m and standard deviation d such that

$$g(t, m, d) = e^{-\frac{(t-m)^2}{2d^2}}, \tag{2.5.4}$$

and verifying $g(0, m, d) = 0$.

(a) $\alpha = \frac{\pi}{20}$ (b) $\alpha = \frac{\pi}{4}$ (c) $\alpha = \frac{\pi}{2}$
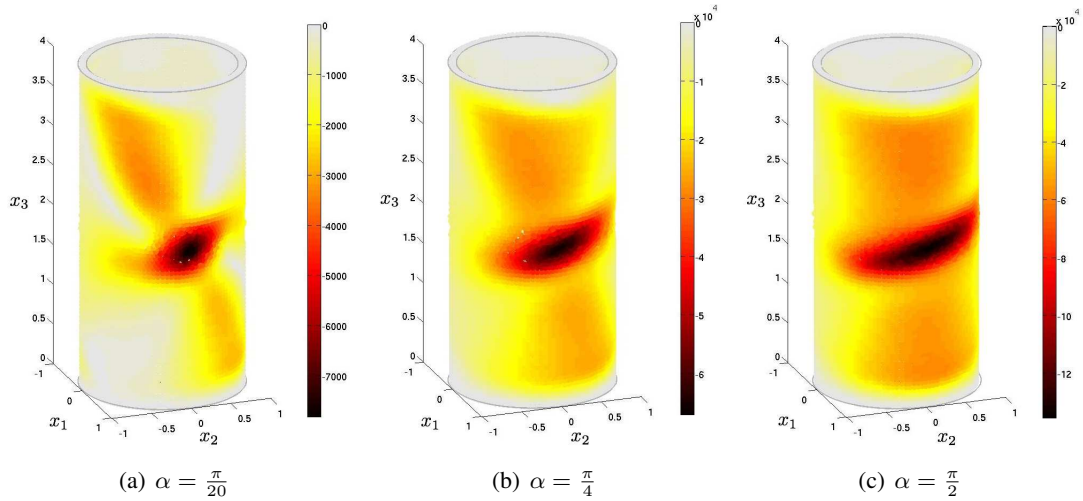
Figure 2.9: *Single experiment:* Acoustic *field* $\mathbb{T}_0$

(a) $\alpha = \frac{\pi}{20}, \lambda = 0.85$ (b) $\alpha = \frac{\pi}{4}, \lambda = 0.8$ (c) $\alpha = \frac{\pi}{2}, \lambda = 0.75$
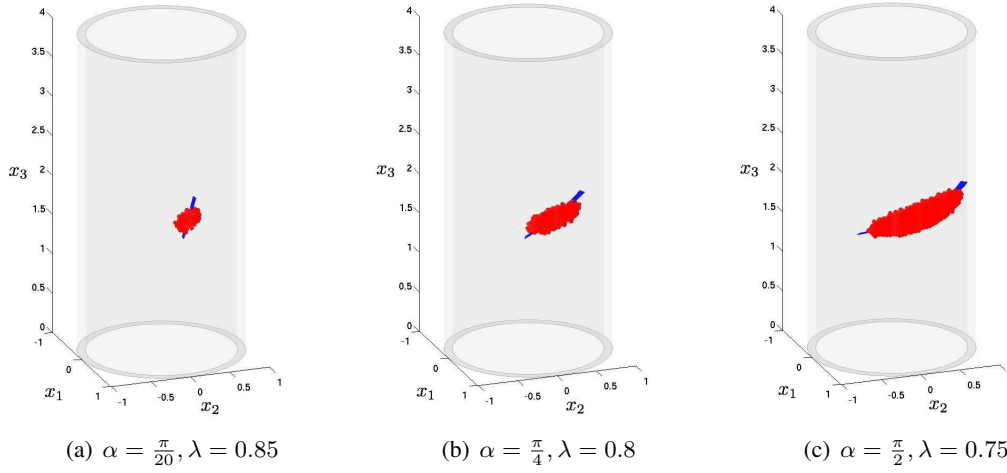
Figure 2.10: *Single experiment:* Acoustic *domain* Γ_λ

Acoustics. In the acoustic case, synthetic measurements are produced by applying a normal gradient $\nabla u_{\Gamma^\star}(\boldsymbol{\xi}, t) \cdot \boldsymbol{n} = -g(t, 1, 0.3)$ at points of S_N, and again it is chosen that $\bar{c} = c$. Results are presented on Figures 2.9, 2.10 and 2.11.

Elasticity. A loading corresponding to a combined traction and torsion is applied on S_N as $\boldsymbol{t}[\boldsymbol{u}_{\Gamma^\star}](\boldsymbol{\xi}, t) = (-\sin\theta \boldsymbol{e}_1 + \cos\theta \boldsymbol{e}_2 + \boldsymbol{e}_3) g(t, 1, 0.3)$. In the elastic case, the choice of a relevant adimensionalization velocity $\bar{c}$ for the present geometry of a thin cylindrical shell impose to take into consideration geometrical effects on the wave propagation. It is known from Graff (1991) that if transverse shear forces and bending and twisting moments can be assumed to be negligibly small then longitudinal and flexural (i.e. radial) elastic waves at frequency ω propagate at a velocity c verifying the dispersion relation

$$c = c_P \sqrt{\frac{R^2\omega^2 - c_B^2}{R^2\omega^2 - c_P^2}} \tag{2.5.5}$$

where R is the mean radius of the cylindrical membrane, $c_B = \sqrt{2\mu(1+\nu)/\rho}$ the longitudinal bar velocity and $c_P = \sqrt{2\mu/\rho(1-\nu)}$ the thin-plate longitudinal wave velocity. Moreover, torsional (i.e. tangential) waves propagate at the shear wave velocity

$$c_S = \sqrt{\frac{\mu}{\rho}}. \tag{2.5.6}$$

Thus, owing to assumption of the positiveness of the Poisson's ratio ν, one has $c_P > c_B > c_S$ which leads to the choice of an adimensionalization using $\bar{c} = c_S$ the lowest *reference* wave velocity. Figures 2.12, 2.13 and 2.14 present the numerical results obtained.

Cumulated experiments

In this section, four different experiments are considered and combined to image a single crack characterized by $\boldsymbol{x}^{\text{true}} = (0.945, 0, 1.75)$, $h = 0.5$, $l = 0.09$ and a fixed angle $\alpha = \pi/4$. During the experiment

(a) $\alpha = \frac{\pi}{20}, \lambda = 0.85$

(b) $\alpha = \frac{\pi}{4}, \lambda = 0.8$

(c) $\alpha = \frac{\pi}{2}, \lambda = 0.75$
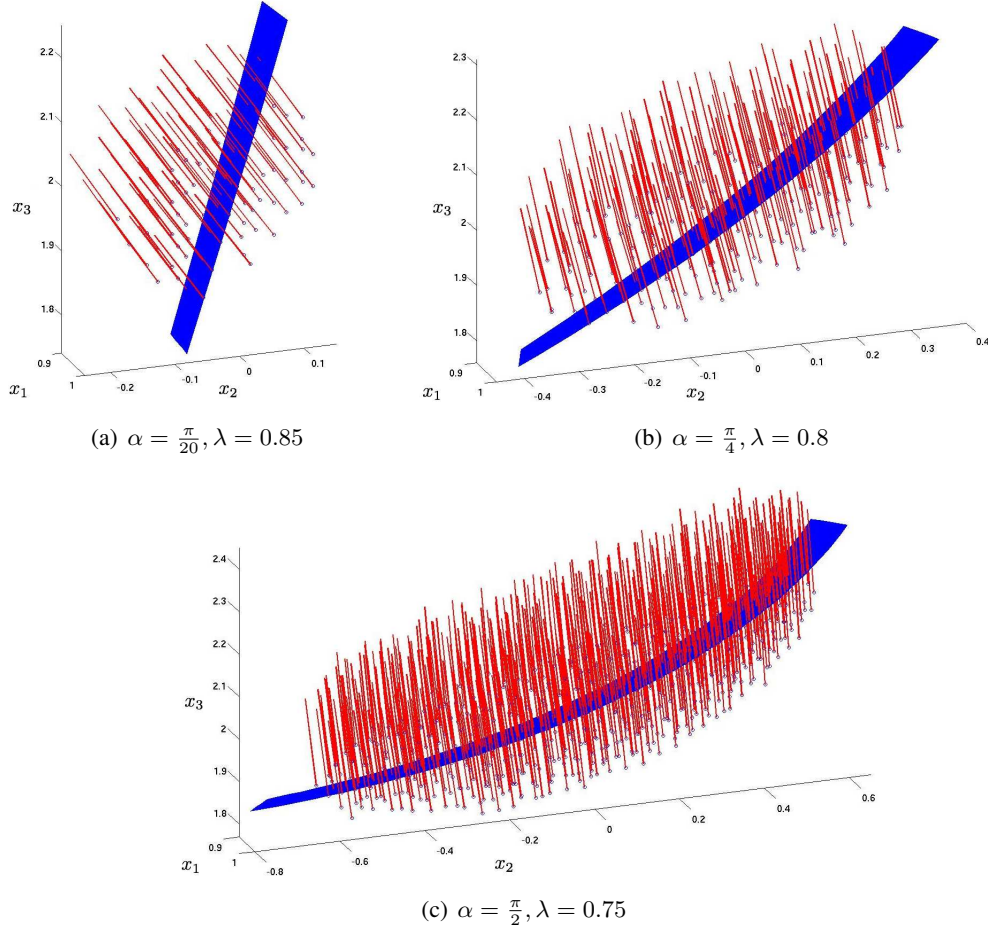
Figure 2.11: *Single experiment:* Acoustic *normals* $\mathbf{n}_\lambda^{\min}$

number k, the excitation is applied on a *squared* patch $S_{\mathrm{N,k}}$ of area equals to $1.6 \cdot 10^{-3}|S^{\mathrm{obs}}|$ (where $|S^{\mathrm{obs}}|$ denotes the area of the observation surface) and containing 25 nodes *centered* at a point P_k with parameters given in Table 2.1. The duration experiment is set to $T = 4$.

Moreover, if K denotes the number of experiments combined in the identification procedure, then the corresponding acoustic (2.4.5) and elastic (2.4.2) tensors $\mathbf{\Pi}(\boldsymbol{x}, T)$ are computed as

$$\mathbf{\Pi}(\boldsymbol{x}, T) = \sum_{k=1}^{K} \mathbf{\Pi}_k(\boldsymbol{x}, T), \tag{2.5.7}$$

where each $\mathbf{\Pi}_k$ is synthesized using quantities relative to the experiment number k. Thus the computational cost of the topological sensitivity itself is independent of the number of experiments.

Acoustics. Synthetic measurements are produced by a prescribed $\boldsymbol{\nabla} u_{\Gamma^\star}(\boldsymbol{\xi}, t) \cdot \boldsymbol{n} = -g(t, 1, 0.3)$ on $S_{\mathrm{N,k}}$, with $\bar{c} = c$. See Figs. 2.15, 2.16 and 2.17.
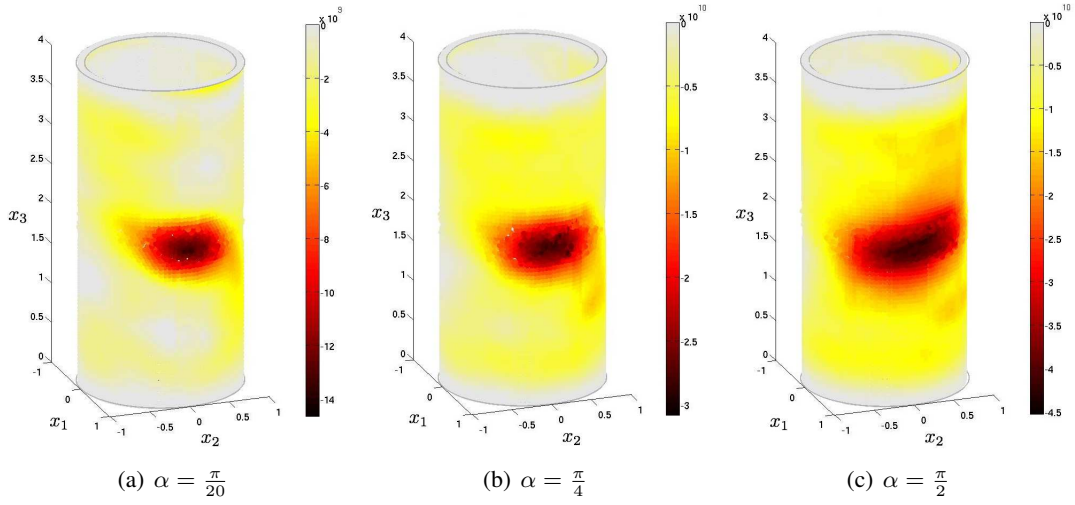
Figure 2.12: *Single experiment:* Elastic *field* $\mathbb{T}_0$

Elasticity.   In elasticity, the applied boundary condition on the patch $S_{\mathrm{N,k}}$ is again given by $\boldsymbol{\nabla} \boldsymbol{u}_{\Gamma^\star}(\boldsymbol{\xi}, t) \cdot \boldsymbol{n} = (-\sin\theta \boldsymbol{e}_1 + \cos\theta \boldsymbol{e}_2 + \boldsymbol{e}_3)g(t, 1, 0.3)$ and the adimensionalization parameter is $\bar{c} = c_S$. See results on Figures 2.18, 2.19 and 2.20.

Dual crack identification

In this section, a unique experiment is used to image a configuration containing two cracks centered at $\boldsymbol{x}_1^{\mathrm{true}} = (0.945, 0, 1.25)$ and $\boldsymbol{x}_2^{\mathrm{true}} = (0.945, 7\pi/9, 3)$, respectively characterized by the angles $\alpha_1 = \pi/2$ and $\alpha_1 = -\pi/4$, and lengths $h = 0.5$, $l = 0.09$. The loading and time parameters are then identical to those described in Section 2.5.2.
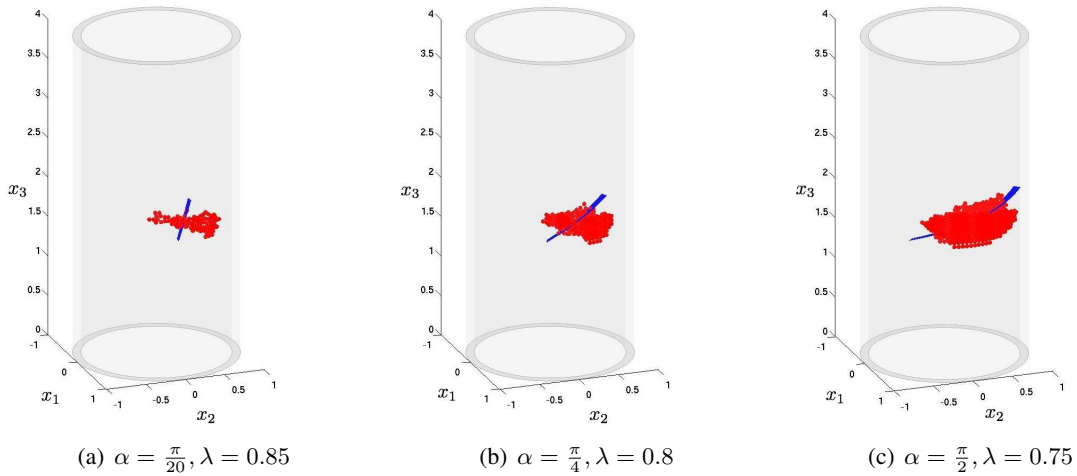
Figure 2.13: *Single experiment:* Elastic *domain* Γ_λ
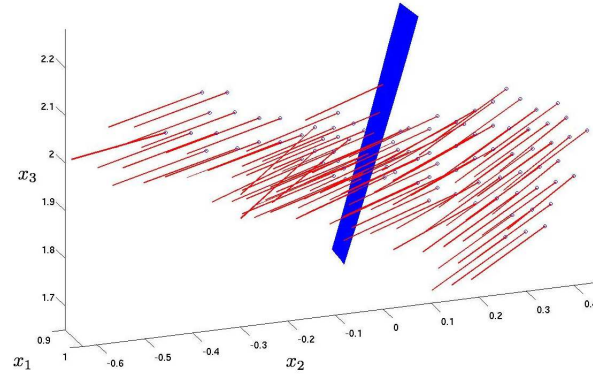
(a) $\alpha = \frac{\pi}{20}, \lambda = 0.85$
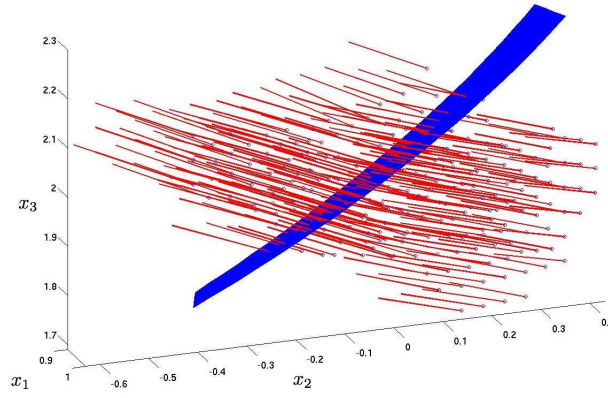
(b) $\alpha = \frac{\pi}{4}, \lambda = 0.8$
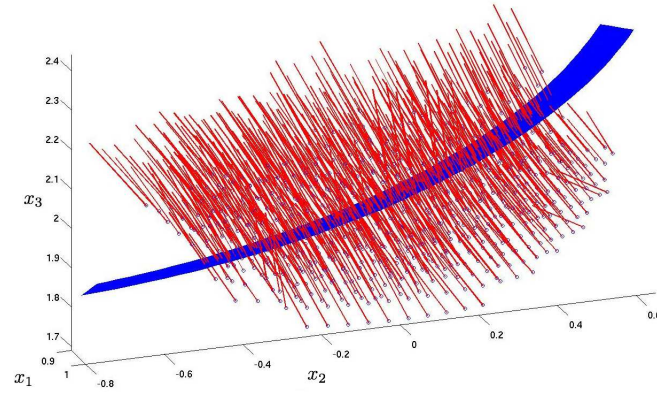
(c) $\alpha = \frac{\pi}{2}, \lambda = 0.75$

Figure 2.14: *Single experiment:* Elastic *normals* $\mathbf{n}_\lambda^{\min}$

Acoustic. The numerical results in the acoustic case are represented by the Figures 2.21 and 2.22.

Table 2.1: *Multiple excitation: Geometrical parameters*

Excitation point	P_1	P_2	P_3	P_4
r	1	1	1	1
θ	$\pi/3$	$-\pi/3$	$2\pi/3$	$-2\pi/3$
z	3.5	0.5	1.25	2.75

(a) Experiment $\{1\}$ (b) Experiments $\{1, 2\}$ (c) Experiments $\{1, 2, 3, 4\}$
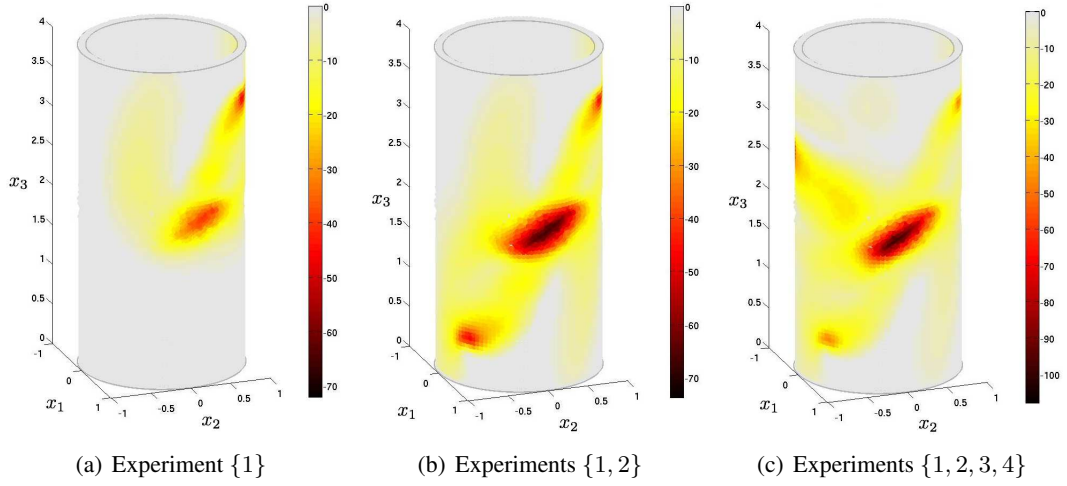
Figure 2.15: *Cumulated experiments:* Acoustic *field* $\mathbb{T}_0$

(a) Experiment $\{1\}$, $\lambda = 0.5$ (b) Experiments $\{1, 2\}$, $\lambda = 0.6$ (c) Experiments $\{1, 2, 3, 4\}$, $\lambda = 0.5$
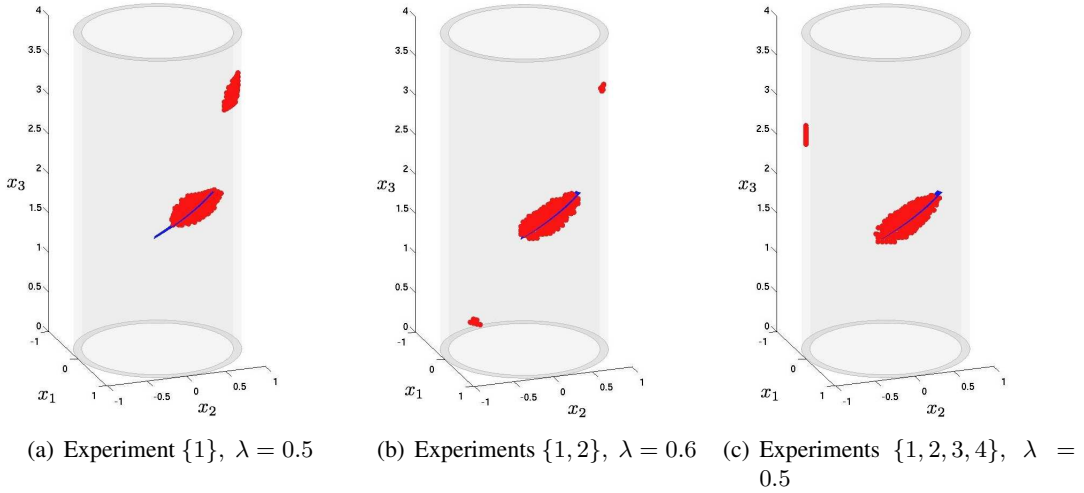
Figure 2.16: *Cumulated experiments:* Acoustic *domain* Γ_λ

Elasticity. In the elastic case, Figs 2.23 and 2.24 show the obtained results, and comments are deferred to Section 2.5.3.

(a) Experiment $\{1\}$, $\lambda = 0.5$

(b) Experiments $\{1, 2\}$, $\lambda = 0.6$

(c) Experiments $\{1, 2, 3, 4\}$, $\lambda = 0.5$
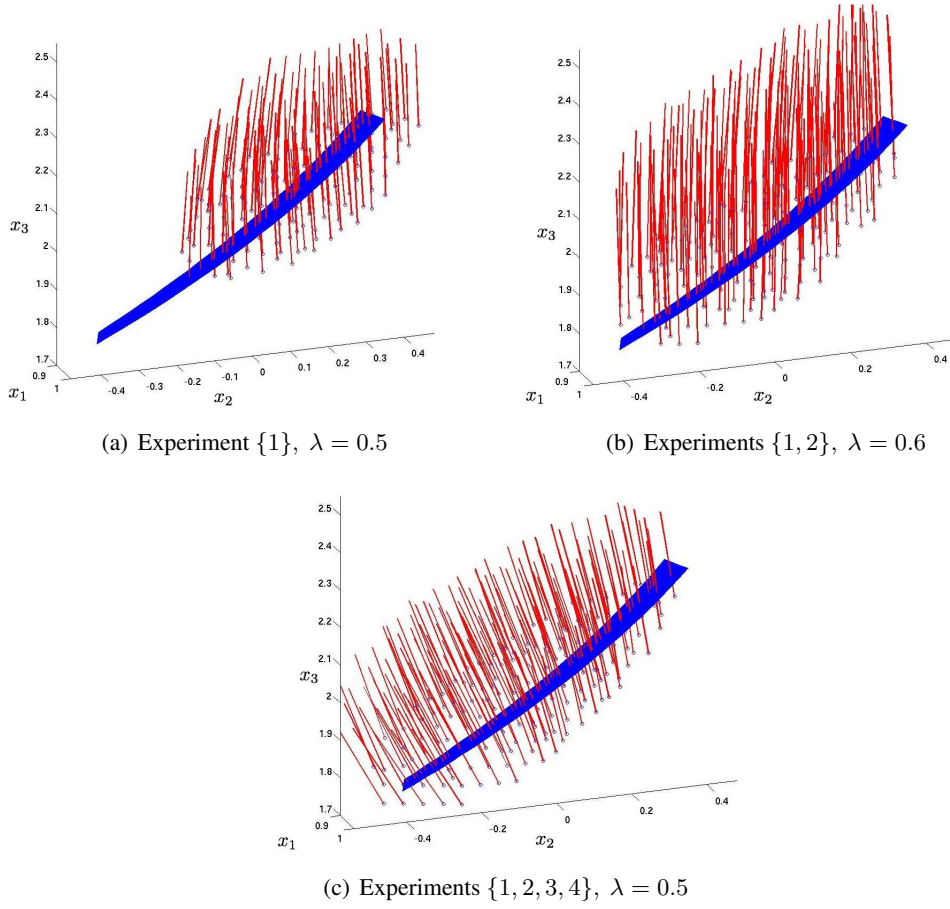
Figure 2.17: *Cumulated experiments:* Acoustic *normals* $\mathbf{n}_\lambda^{\min}$

Elliptical crack in the elastic case

In previous elastic examples, the crack identification analysis has exploited the topological sensitivity employing a polarization tensor corresponding to the nucleation of a circular planar (or penny-shaped) crack. In order to highlight the influence of the choice of the shape $\bar{\Gamma}$, the elastic polarization tensor for an elliptical crack (see Sec. 2.2.2) has been used in the single experiment described in Section 2.5.2 in a configuration where the crack is characterized by an angle $\alpha = \pi/4$.

In the results presented Figure 2.25, the topological sensitivity (2.4.1) is computed employing the *correct* normal $\boldsymbol{n}^{\text{true}} = (0, -h/L, \alpha R/L)$, and tangential vectors $\boldsymbol{\tau}_1^{\text{true}} = (1, 0, 0)$ and $\boldsymbol{\tau}_2^{\text{true}} = (0, \alpha R/L, h/L)$ in cartesian coordinates and where $R = (R_i + R_e)/2$ and $L = \sqrt{h^2 + \alpha^2 R^2}$. The polarization tensor (2.2.26) associated with an elliptical crack with its principal axes lying in a plane $(\boldsymbol{\tau}_1^{\text{true}}, \boldsymbol{\tau}_2^{\text{true}})$ and a varying ratio of major and minor semiaxes is then employed.

(a) Experiment $\{1\}$ (b) Experiments $\{1, 2\}$ (c) Experiments $\{1, 2, 3, 4\}$
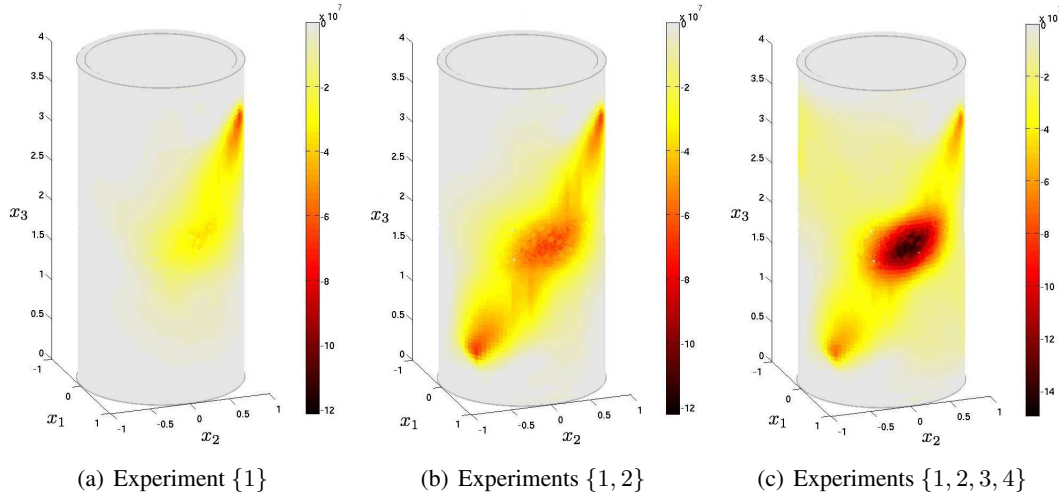
Figure 2.18: *Cumulated experiments:* Elastic *field* $\mathbb{T}_0$

(a) Experiment $\{1\}$, $\lambda = 0.5$ (b) Experiments $\{1, 2\}$, $\lambda = 0.75$ (c) Experiments $\{1, 2, 3, 4\}$, $\lambda = 0.6$
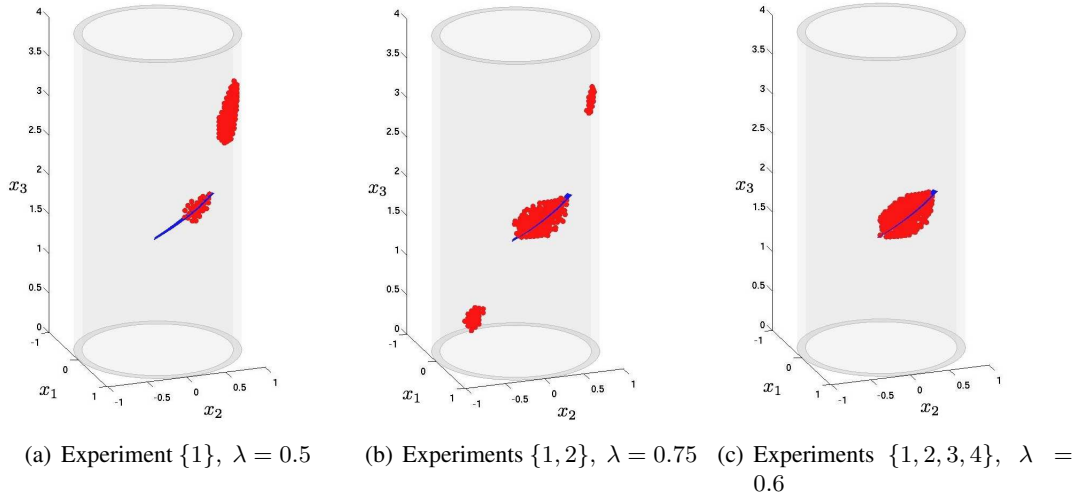
Figure 2.19: *Cumulated experiments:* Elastic *domain* Γ_λ

2.5.3 Discussion

The results that are presented in this section are in accordance with the heuristic of the topological sensitivity method. The maps of topological sensitivity in acoustics (Figs. 2.2, 2.9, 2.15, 2.21(a)) and in elasticity (Figs. 2.5, 2.12, 2.18, 2.23(a)) reveal global negative minima in the areas of the cracks sought. The use of a truncation parameter λ to reveal possible cracks geometries gives satisfactorily results in that the domains Γ_λ are correctly located (Figs. 2.3, 2.6, 2.10, 2.13, 2.16, 2.19, 2.21(b), 2.23(b)), and the field $\mathbf{n}_\lambda^{\min}$ of normal vectors coincides reasonably well with the orientation of the cracks (Figs. 2.4, 2.7, 2.11, 2.14, 2.17, 2.20, 2.22, 2.24). Also, as illustrated by Figures 2.21-2.24, the topological sensitivity method is of global nature since it enables a simultaneous identification of multiple cracks without prior

(a) Experiment $\{1\}$, $\lambda = 0.5$

(b) Experiments $\{1, 2\}$, $\lambda = 0.75$

(c) Experiments $\{1, 2, 3, 4\}$, $\lambda = 0.6$
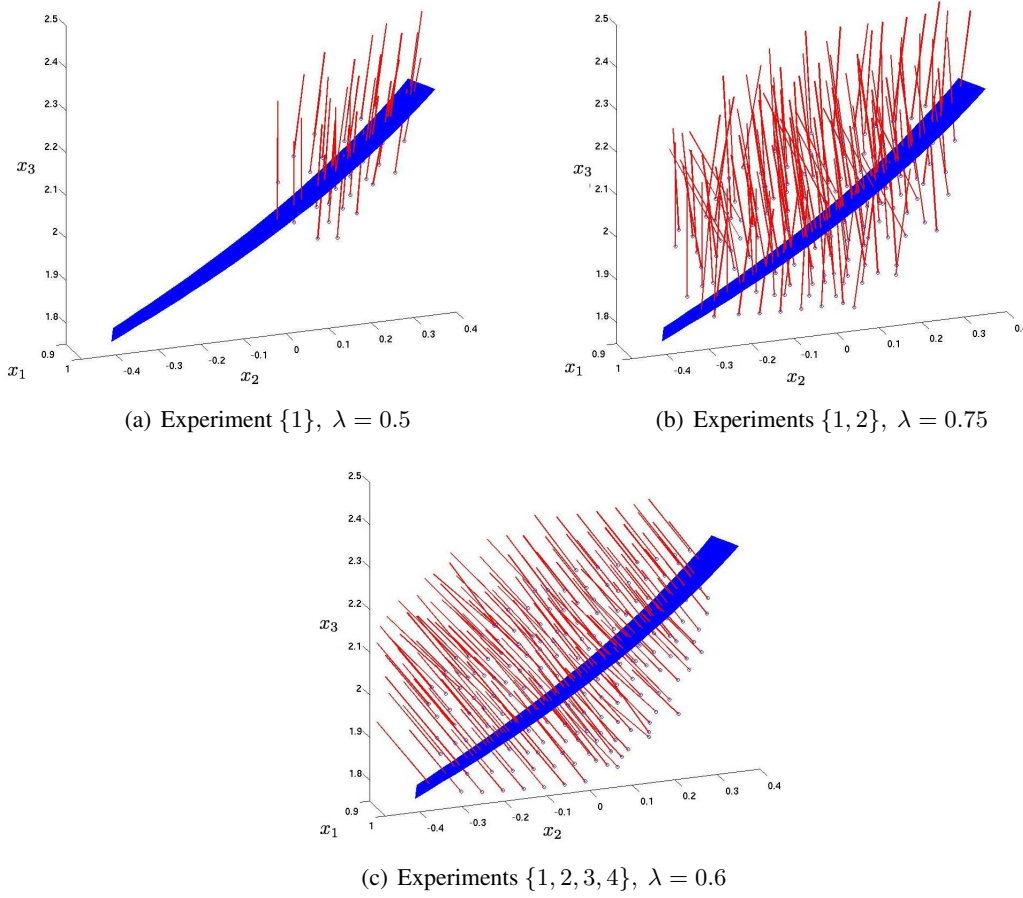
Figure 2.20: *Cumulated experiments:* Elastic *normals* $\mathbf{n}_\lambda^{\min}$

knowledge of their number.

Analysing the cracked cylindrical shell configuration, the examples shown suggest that the pronounced negative values of the *acoustic* topological sensitivity describe the geometry of the crack more accurately than its *elastic* counterpart: Compare couple of Figures 2.10-2.13, 2.16-2.19 and 2.21(b)-2.23(b). Nevertheless, it appears also that the reconstruction of the normal vector field is more sensitive in elasticity than in acoustics: Compare couple of Figures 2.11-2.14, 2.17-2.20 and 2.22-2.24.

It is noticeable that the computation of the topological sensitivity field may lead to significant negative values spread out around a direction nearly orthogonal to the cracks' planes (See Figs. 2.2(c), 2.9, 2.12(a), 2.12(b)) possibly due to waves reflecting on these planes. If these values can possibly lead to an inaccurate identification of the cracks geometries (see e.g. Figs. 2.13(a), 2.13(b)), the reconstruction of their local orientations through the computation of the field $\mathbf{n}_\lambda^{\min}$ allows to resolve the ambiguity (see corresponding Figures 2.14(a), 2.14(b)). It appears also in practice that the indicator function $\mathbb{T}$ computed in the elastic case is relatively sensitive to the nature of the illuminating waves and thus to the loading applied to generate the measurements.

The method proposed leads to a qualitatively correct identification of cracks even in situations where a single experiment is used (Figs. 2.2-2.14). The exploitation of a growing number of experiments, that

(a) $\mathbb{T}_0$ field   (b) Domain $\Gamma_{0.6}$
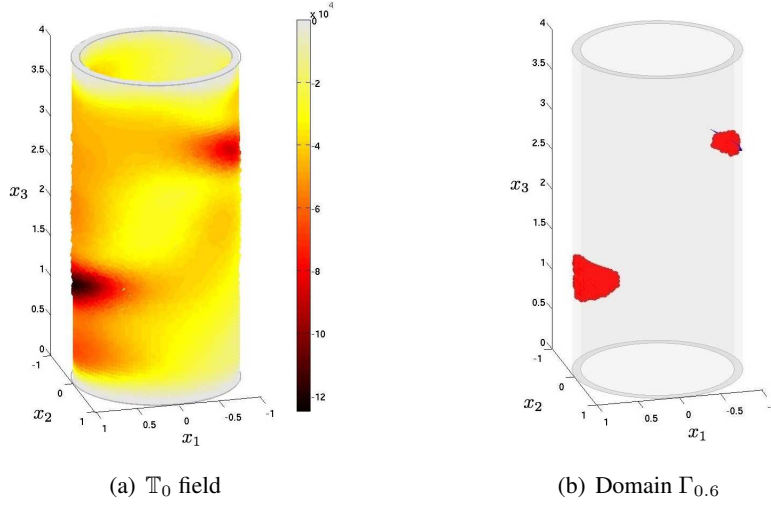
Figure 2.21: *Dual crack* acoustic *identification*

(a) Crack 1   (b) Crack 2
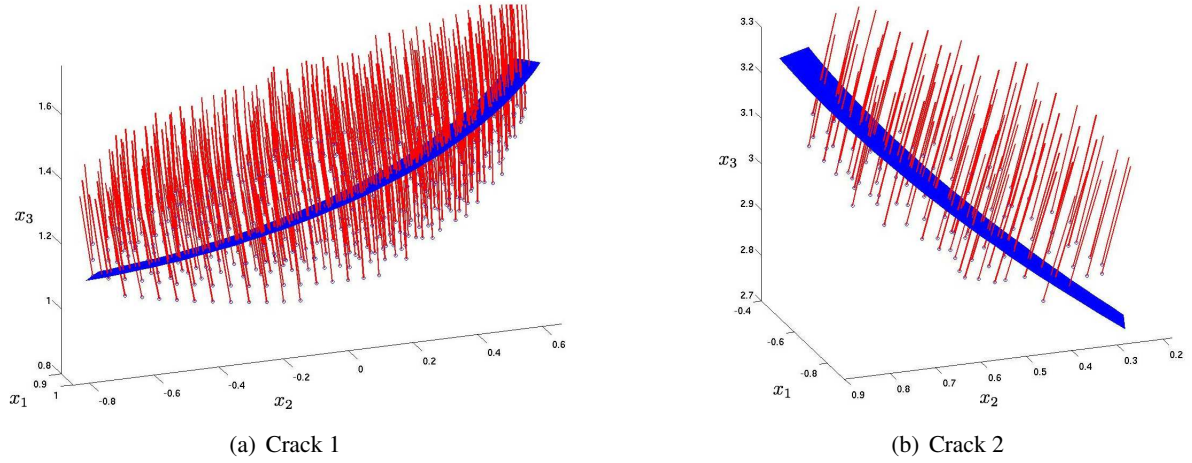
Figure 2.22: *Dual crack identification:* Acoustic *normals* $\mathbf{n}_{0.6}^{\min}$

are combined linearly to compute the topological sensitivity as in equation (2.5.7), significantly improves the quality of the reconstruction (Figs. 2.15-2.20). In this later examples, the pronounced negative values of the topological sensitivity that can appear away from the crack are in reality located around the loading application points, and can thus be clearly set aside in the identification procedure.

Finally, owing to the examples in elasticity illustrated by Figures 2.25, the use of a polarization tensor associated with an infinitesimal elliptical plane crack to compute the topological sensitivity does not lead to significant difference if the featured major semiaxis of the infinitesimal crack coincides with the direction of *privileged* elongation of the crack Γ^{true} (Fig. 2.25(b)) or orthogonal to it (Fig. 2.25(c)) compare with the reference circular case (Fig. 2.25(a)).

(a) $\mathbb{T}_0$ field

(b) Domain $\Gamma_{0.65}$
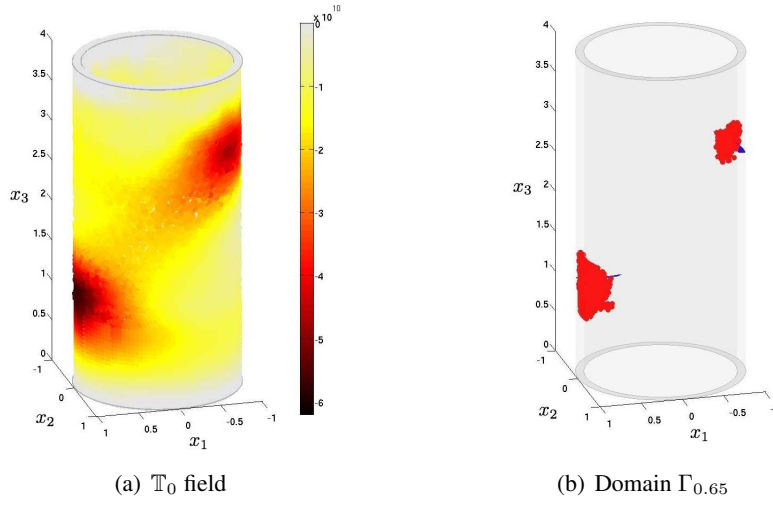
Figure 2.23: *Dual crack* elastic *identification*

(a) Crack 1

(b) Crack 2
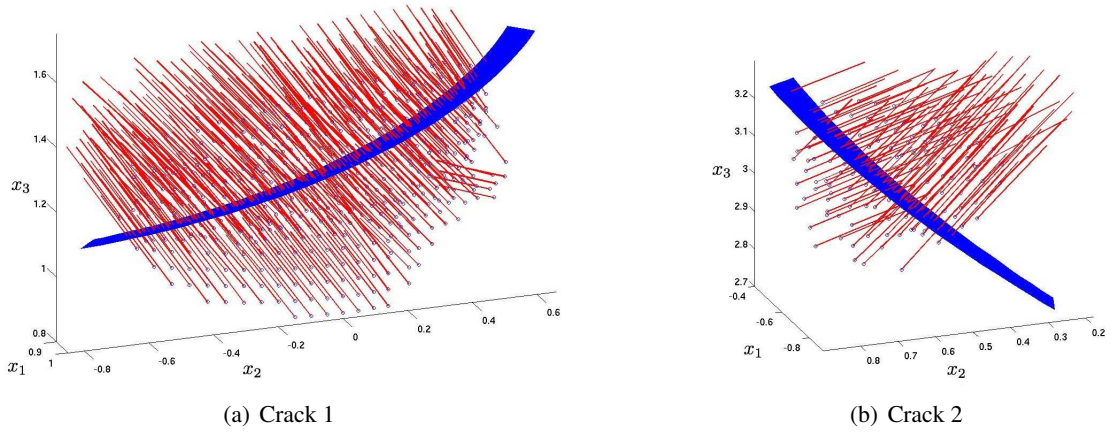
Figure 2.24: *Dual crack identification:* Elastic *normals* $\mathbf{n}_{0.65}^{\min}$

2.6 Extension to interface cracks

In this section, the previous analysis is extended to the identification of interface cracks in a bimaterial domain. Interface cracks appear in a number of applications and can be seen as delamination cracks in composite materials, due for example to fatigue behaviors of laminates, but also as matrix-matrix and fibre-matrix interface debonding zones. In this context, the reference domain Ω considered is constituted by two homogeneous linear elastic subdomains $\Omega^{\pm}$ such that $\Omega = \Omega^+ \cup \Omega^-$ and characterized by the corresponding mass densities $\rho^{\pm}$, shear moduli $\mu^{\pm}$ and Poisson's ratios $\nu^{\pm}$. Moreover, let $S^{\text{int}} = \partial\Omega^+ \cap \partial\Omega^-$ denote the interface of the two subdomains, which location and orientation is generally known beforehand in applications, and which contains a crack (or a set) Γ^{true} to be sought.

The topological sensitivity analysis can be reproduced in this situation and previous reasoning and developments of Section 2.2 still hold by employing the elastodynamic Green's and fundamental tensors of

(a) $\frac{a_1}{a_2} = 1$

(b) Major axis: $\boldsymbol{\tau}_2$, $\frac{a_1}{a_2} = 4$

(c) Major axis: $\boldsymbol{\tau}_1$, $\frac{a_1}{a_2} = 4$
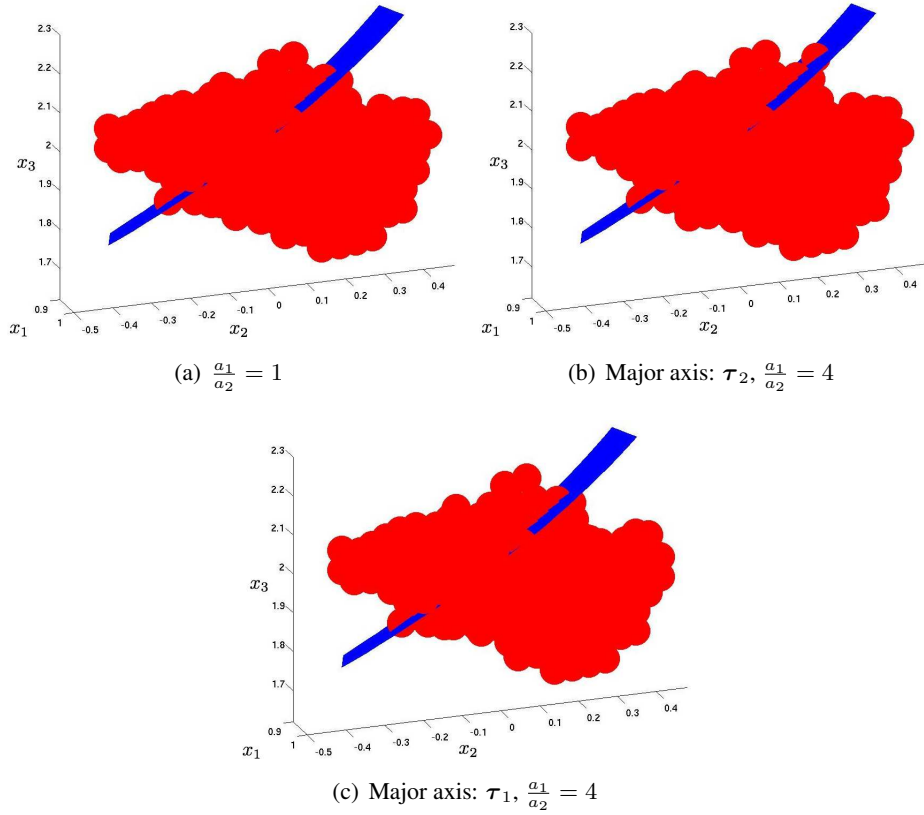
Figure 2.25: *Infinitesimal* elliptical *crack:* Elastic *domain* $\Gamma_{0.8}$

the relevant *composite full-space*. Thus, the topological sensitivity is given by the relation (2.2.20) and the corresponding polarization tensor $\mathcal{A}_{\pm}^{\sigma}$ is defined by the counterpart for the bimaterial domain of the integral (2.2.21).

2.6.1   Polarization tensor for a penny-shaped crack

As it has been shown previously, the polarization tensor $\mathcal{A}_{\pm}^{\sigma}$ can be found analytically for the simple case where $\bar{\Gamma}$ is a circular plane crack. This can be achieved by employing the analytical form of the canonical crack opening displacement $[\![\mathcal{V}]\!]$ corresponding to a penny-shaped crack on the interface of two linear elastic half-space as given in Willis (1972) and which developments, employing the Radon transform, are partially reproduced hereafter for the ease of reading.

For a given $(i, j) \in \{1, 2, 3\}$ the COD related to the corresponding canonical solution is noted $\boldsymbol{\Phi} \equiv [\![\boldsymbol{V}]\!]^{ij}$ for brevity, and from definition (2.C.1) and notation of the unit circle as $\hat{\mathcal{C}} = \{\boldsymbol{\eta} \in \mathbb{R}^2 \text{ and } |\boldsymbol{\eta}| = 1\}$, its Radon transform is given by

$$\check{\boldsymbol{\Phi}}(r, \boldsymbol{\eta}) = \int_{\bar{\Gamma}} \boldsymbol{\Phi}(\bar{\boldsymbol{\xi}}) \delta(r - \boldsymbol{\eta} \cdot \bar{\boldsymbol{\xi}}) \, \mathrm{d}S_{\bar{\xi}} \qquad (r \in [-1, 1], \boldsymbol{\eta} \in \hat{\mathcal{C}}) \qquad (2.6.1)$$

since $\boldsymbol{\Phi}(\bar{\boldsymbol{\xi}}) = \boldsymbol{0}$ if $\bar{\boldsymbol{\xi}} \notin \bar{\Gamma}$.

Then the integral (2.2.21), can be advantageously recast in terms of the Radon transform $\check{\boldsymbol{\Phi}}$ using property (2.C.2), i.e. that

$$\int_{\bar{\Gamma}} \boldsymbol{\Phi}(\bar{\boldsymbol{\xi}}) \, dS_{\bar{\xi}} = \int_{-1}^{1} \check{\boldsymbol{\Phi}}(r, \boldsymbol{\eta}) \, dr \tag{2.6.2}$$

where the right-hand side term turns out to be independent of $\boldsymbol{\eta}$.

The Radon transform of the COD corresponding to a penny-shaped crack at the interface between the two elastic half-spaces $\mathbb{R}^3_+$ and $\mathbb{R}^3_-$ with respective shear moduli μ^+ and μ^-, and Poisson's ratios ν^+ and ν^- can be found in Willis (1972) in the form of the expansion

$$\check{\boldsymbol{\Phi}}(r, \boldsymbol{\eta}) = (1 - r^2) \sum_{n=1}^{3} \check{\boldsymbol{\Phi}}_n \boldsymbol{\Psi}_n(r, \boldsymbol{\eta}) \qquad (r \in [-1, 1], \boldsymbol{\eta} \in \hat{\mathcal{C}}) \tag{2.6.3}$$

where for all $r \in [-1, 1]$ and $\boldsymbol{\eta} = (\eta_1, \eta_2) \in \mathbb{R}^2$ such that $|\boldsymbol{\eta}| = 1$

$$\boldsymbol{\Psi}_1(r, \boldsymbol{\eta}) = \begin{pmatrix} -\eta_2 \\ \eta_1 \\ 0 \end{pmatrix} \qquad \boldsymbol{\Psi}_2(r, \boldsymbol{\eta}) = \begin{pmatrix} -\eta_1 c(r) \\ -\eta_2 c(r) \\ s(r) \end{pmatrix} \qquad \boldsymbol{\Psi}_3(r, \boldsymbol{\eta}) = \begin{pmatrix} \eta_1 s(r) \\ \eta_2 s(r) \\ c(r) \end{pmatrix} \tag{2.6.4}$$

with the real-valued function c and s defined by

$$c(r) + i s(r) = \left(e^{\pi \kappa} - e^{-\pi \kappa} \right) \left(\frac{1-r}{1+r} \right)^{i\kappa} \tag{2.6.5}$$

which depend on the following material parameters

$$\alpha = \frac{1 - \nu^+}{2\pi\mu^+} + \frac{1 - \nu^-}{2\pi\mu^-} \qquad \beta = \frac{1 - 2\nu^+}{4\pi\mu^+} - \frac{1 - 2\nu^-}{4\pi\mu^-} \qquad \kappa = \frac{1}{2\pi} \log\left(\frac{\alpha + \beta}{\alpha - \beta} \right) \tag{2.6.6}$$

Thus with reference to integral (2.6.2), expansion (2.6.3), and equation (2.6.5) one has

$$\int_{-1}^{1} (1 - r^2) c(r) \, dr = \frac{8}{3} \pi \kappa (1 + \kappa^2)$$

$$\int_{-1}^{1} (1 - r^2) s(r) \, dr = 0 \tag{2.6.7}$$

Moreover, in the case of a uniform loading applied on the crack $\bar{\Gamma}$, which corresponds to the definition (2.2.17) of the canonical problems, the coefficients in the series (2.6.3) are given analytically by

$$\check{\boldsymbol{\Phi}}_1 = \frac{4\pi^2 \kappa (1 + \kappa^2)(\alpha^2 - \beta^2)}{(\alpha - \delta)\pi\kappa(1 + \kappa^2) + \beta} (\eta_2 t_1^{ij} - \eta_1 t_2^{ij})$$

$$\check{\boldsymbol{\Phi}}_2 = \frac{2\pi(\alpha^2 - \beta^2)}{(\alpha - \delta)\pi\kappa(1 + \kappa^2) + \beta} (\eta_1 t_1^{ij} + \eta_2 t_2^{ij}) \tag{2.6.8}$$

$$\check{\boldsymbol{\Phi}}_3 = -\frac{\pi}{\beta} (\alpha^2 - \beta^2) t_3^{ij}$$

using notation

$$\boldsymbol{t}^{ij} = -\frac{1}{2}\big(\boldsymbol{e}_i \otimes \boldsymbol{e}_j + \boldsymbol{e}_j \otimes \boldsymbol{e}_i\big)\cdot\boldsymbol{n} \tag{2.6.9}$$

and material parameters

$$\gamma = \frac{\nu_+}{2\pi\mu_+} + \frac{\nu_-}{2\pi\mu_-} \qquad \delta = \frac{\alpha\gamma + \beta^2}{\alpha + \gamma} \tag{2.6.10}$$

Then using property (2.6.7), parameters (2.6.8) and the fact that $|\boldsymbol{\eta}| = 1$, the integral (2.6.2) reduces to

$$\int_{\bar{\Gamma}} \boldsymbol{\Phi}(\bar{\boldsymbol{\xi}})\,\mathrm{d}S_{\bar{\xi}} = -\frac{8}{3}\pi^2\kappa(1+\kappa^2)(\alpha^2-\beta^2)\left\{ \frac{2}{(\alpha-\delta)\pi\kappa(1+\kappa^2)+\beta}\begin{pmatrix} t_1^{ij} \\ t_2^{ij} \\ 0 \end{pmatrix} + \frac{1}{\beta}\begin{pmatrix} 0 \\ 0 \\ t_3^{ij} \end{pmatrix}\right\} \tag{2.6.11}$$

With reference to the applied loading (2.2.17) defining canonical solutions, the polarization tensor $\mathcal{A}_{\pm}^{\sigma}$ can finally be deduced from (2.2.21) and (2.6.11) in the form

$$\mathcal{A}_{\pm}^{\sigma} = \frac{8}{3}\frac{\pi^2\kappa(1+\kappa^2)(\alpha^2-\beta^2)}{(\alpha-\delta)\pi\kappa(1+\kappa^2)+\beta}\boldsymbol{n}\otimes\left\{2\boldsymbol{I} + \frac{(\alpha-\delta)\pi\kappa(1+\kappa^2)-\beta}{\beta}\boldsymbol{n}\otimes\boldsymbol{n}\right\}\otimes\boldsymbol{n} \tag{2.6.12}$$

Again, the following version of $\mathcal{A}_{\pm}^{\sigma}$ which has the minor symmetries can equivalently be used:

$$\mathcal{A}_{\pm}^{\sigma} = \frac{4}{3}\pi^2\kappa(1+\kappa^2)(\alpha^2-\beta^2)\left\{\frac{[\boldsymbol{n}\otimes\boldsymbol{e}_\alpha + \boldsymbol{e}_\alpha\otimes\boldsymbol{n}]\otimes[\boldsymbol{n}\otimes\boldsymbol{e}_\alpha + \boldsymbol{e}_\alpha\otimes\boldsymbol{n}]}{(\alpha-\delta)\pi\kappa(1+\kappa^2)+\beta} + \frac{2}{\beta}\boldsymbol{n}\otimes\boldsymbol{n}\otimes\boldsymbol{n}\otimes\boldsymbol{n}\right\}, \tag{2.6.13}$$

where $\alpha \in \{1, 2\}$.

Remark 7. *Polarization tensors (2.2.24) and (2.2.25) corresponding to the case of a homogenous domain containing a penny-shaped crack, can be respectively recovered from previous expressions (2.6.12) and (2.6.13) with $\mu^+ = \mu^- = \mu$ and $\nu^+ = \nu^- = \nu$, i.e. in the limit $\beta \to 0$.*

2.6.2   Numerical examples

This section provides the illustration of the ability of the topological sensitivity to identify interface cracks. Within the framework described in Section 2.5 of FEM-based simulations, dynamical measurements corresponding to one or two circular cracks in a parallelepipedic bimaterial domain $\Omega = \{\boldsymbol{\xi} \in [0,1]\times[0,2]\times[0,0.4]\}$ with the interface lying in the plane $\xi_3 = 0.2$ as described on Figure 2.26 and characterized by material parameters $\nu^+ = \nu^- = \nu = 0.3$, $\mu^+ = 2\mu^- = 7.7$ and $\rho^+ = 2\rho^- = 10$ are synthesized. The domain is loaded by a uniform compressional traction $\boldsymbol{t}[\boldsymbol{u}_{\Gamma^\star}](\boldsymbol{\xi},t) = -g(t,0.5,0.3)\boldsymbol{e}_3$ imposed on its top face and the computation is adimensionalized by the longitudinal wave velocity.

In this application, it is considered that the geometry of the interface is known, in particular in this example, the topological sensitivity field defined by (2.4.8) is employed with $\boldsymbol{n}^{\mathrm{opt}}(\boldsymbol{z},T) = \boldsymbol{e}_3$, then its thresholded version (2.4.9) at the interface, where the crack is a-priori supposed to be located, is plotted on Figure 2.27.
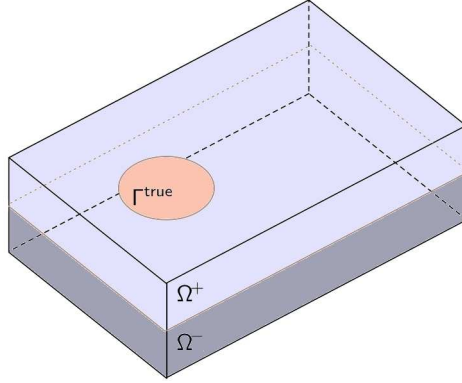
Figure 2.26: *Cracked bimaterial domain*

(a) $R = 0.1$, $\boldsymbol{x}^{\text{true}} = (0.5, \, 0.5, \, 0.2)$

(b) $R_1 = 0.1$, $\boldsymbol{x}_1^{\text{true}} = (0.3, \, 0.5, \, 0.2)$, $R_2 = 0.125$, $\boldsymbol{x}_2^{\text{true}} = (0.7, \, 1.7, \, 0.2)$
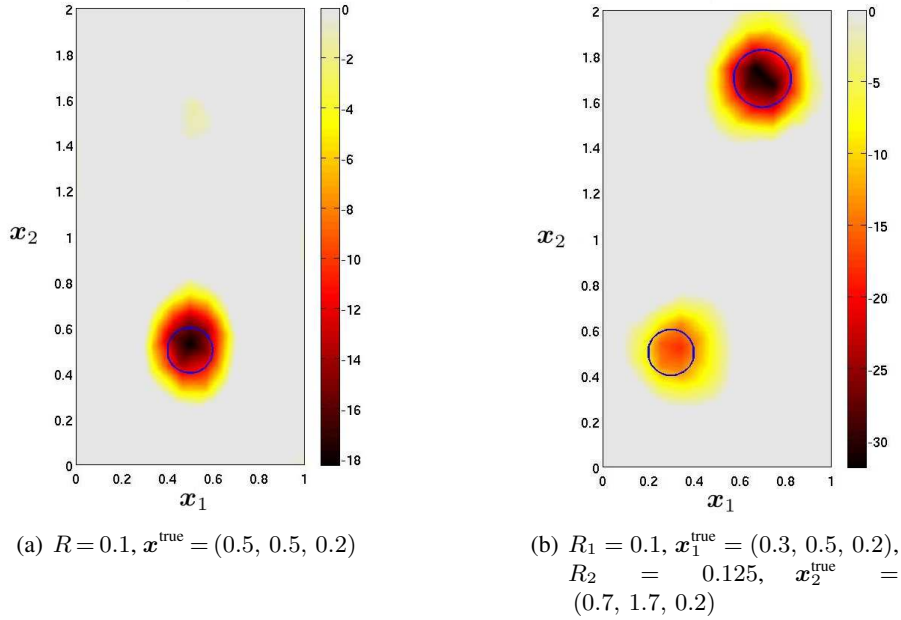
Figure 2.27: *Thresholded TS field $\mathbb{T}_\lambda$ at the interface with $\lambda = 0$.*

2.7 Conclusion

The topological sensitivity method proposed constitutes a non-iterative global qualitative approach to the problem of elastodynamic crack identification. The adjoint-based formulation employed, which entails the cost of only two direct problems with the computation of free and adjoint fields defined on crack-free configuration, are computationally efficient compared to minimization-based inversion methods. The indicator function proposed is of global nature that is it evaluates possible location of crack at every point independently without requiring any initial guess. On the basis of the heuristic that motivates the method, the use of closed-form solutions corresponding to circular-plane cracks featured in the asymptotic analysis, allow qualitative evaluations of cracks in terms of locations and orientations. Finally, implementation within a classical FEM platform, assesses for the simplicity and efficiency of the method.

2.A   Polarization tensors

2.A.1   Matrix representation of fourth-order tensors

Consider a tensor relationship of the form

$$\boldsymbol{B} = \boldsymbol{\mathcal{Q}} : \boldsymbol{A}, \tag{2.A.1}$$

where $\boldsymbol{A}$, $\boldsymbol{B}$ are second-order *symmetric* tensors and $\boldsymbol{\mathcal{Q}}$ is a fourth-order tensor having minor symmetry but not necessarily major symmetry, e.g. $\boldsymbol{\mathcal{Q}} = \boldsymbol{\mathcal{S}}$ (Eshelby tensor, which does *not* have major symmetry) or $\boldsymbol{\mathcal{Q}} = \boldsymbol{\mathcal{C}}$ (elasticity tensor, which has major symmetry). Tensor $\boldsymbol{A}$ (and also $\boldsymbol{B}$, of course) has six independent components, which can be arranged into a 6-vector $\hat{\boldsymbol{A}}$ according to the convention:

$$\hat{\boldsymbol{A}} = \begin{bmatrix} \hat{\boldsymbol{A}}^1 \\ \hat{\boldsymbol{A}}^2 \end{bmatrix}, \qquad \hat{\boldsymbol{A}}^1 = [A_{11} \; A_{22} \; A_{33}]^{\mathrm{T}}, \quad \hat{\boldsymbol{A}}^2 = \sqrt{2}[A_{12} \; A_{13} \; A_{23}]^{\mathrm{T}}.$$

Then, relation (2.A.1) can be recast into the following equivalent matrix relation between $\hat{\boldsymbol{A}}$ and $\hat{\boldsymbol{B}}$

$$\hat{\boldsymbol{B}} = \hat{\boldsymbol{Q}} \hat{\boldsymbol{A}}, \tag{2.A.2}$$

where the (6×6)-matrix $\hat{\boldsymbol{Q}}$ representing the tensor $\boldsymbol{\mathcal{Q}}$ is given in block-matrix form by

$$\hat{\boldsymbol{Q}} = \begin{bmatrix} \hat{\boldsymbol{Q}}^{11} & \hat{\boldsymbol{Q}}^{12} \\ \hat{\boldsymbol{Q}}^{21} & \hat{\boldsymbol{Q}}^{22} \end{bmatrix} \qquad \text{with} \quad \begin{cases} \hat{Q}^{11}_{ij} = \mathcal{Q}_{iijj}, & \hat{Q}^{12}_{i(k\ell)} = \sqrt{2}\mathcal{Q}_{iik\ell}, \\ \hat{Q}^{21}_{(ij)k} = \sqrt{2}\mathcal{Q}_{ijkk}, & \hat{Q}^{22}_{(ij)(k\ell)} = 2\mathcal{Q}_{ijkl} \end{cases} \quad (1 \leqslant i \leqslant j \leqslant 3, \; 1 \leqslant k \leqslant \ell \leqslant 3),$$

having used the indexing convention $(12) = 1$, $(13) = 2$, $(23) = 3$. Note in particular that this convention (and particularly the $\sqrt{2}$ and 2 factors that enter the definition of $\hat{\boldsymbol{A}}$ and $\hat{\boldsymbol{Q}}$) ensure consistency between quadratic forms written in tensor and matrix forms, i.e.

$$\boldsymbol{A} : \boldsymbol{\mathcal{Q}} : \boldsymbol{A} = \hat{\boldsymbol{A}}^{\mathrm{T}} \hat{\boldsymbol{Q}} \hat{\boldsymbol{A}},$$

Using this convention, the matrix representation of the symmetric fourth-order identity $\boldsymbol{\mathcal{I}}^{\mathrm{sym}}$ is simply the 6-dimensional identity matrix, i.e.

$$\left(\hat{\boldsymbol{I}}^{\mathrm{sym}}\right)^{11} = \left(\hat{\boldsymbol{I}}^{\mathrm{sym}}\right)^{22} = \boldsymbol{I}, \quad \left(\hat{\boldsymbol{I}}^{\mathrm{sym}}\right)^{12} = \left(\hat{\boldsymbol{I}}^{\mathrm{sym}}\right)^{21} = \boldsymbol{0},$$

while the elastic compliance tensor $\boldsymbol{\mathcal{D}} = \boldsymbol{\mathcal{C}}^{-1}$ for an isotropic material is such that

$$\hat{\boldsymbol{D}}^{11} = \frac{1}{2\mu(1+\nu)} \begin{bmatrix} 1 & -\nu & -\nu \\ -\nu & 1 & -\nu \\ -\nu & -\nu & 1 \end{bmatrix}, \qquad \hat{\boldsymbol{D}}^{22} = \frac{1}{2\mu} \boldsymbol{I}, \qquad \hat{\boldsymbol{D}}^{12} = \hat{\boldsymbol{D}}^{21} = \boldsymbol{0}. \tag{2.A.3}$$

Finally, for the Eshelby tensor associated with an ellipsoidal cavity whose principal axes coincide with those of the Cartesian frame, one has (Mura, 1982)

$$\hat{\boldsymbol{S}}^{11} = \begin{bmatrix} S_{1111} & S_{1122} & S_{1133} \\ S_{2211} & S_{2222} & S_{2233} \\ S_{3311} & S_{3322} & S_{3333} \end{bmatrix}, \qquad \hat{\boldsymbol{S}}^{22} = \begin{bmatrix} 2S_{1212} & 0 & 0 \\ 0 & 2S_{1313} & 0 \\ 0 & 0 & 2S_{2233} \end{bmatrix}, \qquad \hat{\boldsymbol{S}}^{12} = \hat{\boldsymbol{S}}^{21} = \boldsymbol{0},$$

$$\tag{2.A.4}$$

in terms of the nonzero entries of $\boldsymbol{\mathcal{S}}$.

2.A.2 Major symmetry of polarization tensor

Lemma 6. *The polarization tensor $\boldsymbol{\mathcal{A}}$ has major symmetry: for any second-order symmetric tensors $\boldsymbol{B}, \boldsymbol{B}'$, one has*

$$\boldsymbol{B} : \boldsymbol{\mathcal{A}} : \boldsymbol{B}' = \boldsymbol{B}' : \boldsymbol{\mathcal{A}} : \boldsymbol{B}. \tag{2.A.5}$$

Proof. The proof rests upon exploiting a governing weak formulation for the third-order tensor function $\boldsymbol{\mathcal{V}}(\bar{\boldsymbol{\xi}})$, which is such that for any given second-order symmetric tensor $\boldsymbol{\sigma}$ the vector field $\boldsymbol{\sigma} : \boldsymbol{\mathcal{V}}(\bar{\boldsymbol{\xi}})$ solves the *elastostatic* exterior problem for the normalized crack $\bar{\Gamma}$ whose faces are subjected to applied tractions $\boldsymbol{t}^{\pm} = -\boldsymbol{\sigma} \cdot \boldsymbol{n}^{\pm}$. As a result, $\boldsymbol{\sigma} : \boldsymbol{\mathcal{V}}(\bar{\boldsymbol{\xi}})$ obeys for any $\boldsymbol{\sigma}$ the weak formulation

$$\int_{\mathbb{R}^3 \setminus \bar{\Gamma}} [\boldsymbol{\sigma} : \boldsymbol{\nabla}\boldsymbol{\mathcal{V}}(\bar{\boldsymbol{\xi}})] : \boldsymbol{\mathcal{C}} : \boldsymbol{\nabla}\boldsymbol{w}(\bar{\boldsymbol{\xi}}) \, \mathrm{d}V_{\bar{\xi}} = \int_{\bar{\Gamma}} \boldsymbol{\sigma} : ([\![\boldsymbol{w}]\!](\bar{\boldsymbol{\xi}}) \otimes \boldsymbol{n}(\bar{\boldsymbol{\xi}})) \, \mathrm{d}S_{\bar{\xi}} \quad \forall \boldsymbol{w} \in H^1(\mathbb{R}^3 \setminus \bar{\Gamma}), \tag{2.A.6}$$

where $[\![\boldsymbol{w}]\!]$ denotes the jump of the trial function $\boldsymbol{w}$ through $\bar{\Gamma}$.

Now, recalling expression (2.2.21) of $\boldsymbol{\mathcal{A}}^{\sigma}$ and taking the inner product of Eq. (2.2.21) by $\boldsymbol{\sigma}$ (on the left) and $\boldsymbol{\sigma}'$ (on the right), one obtains

$$\boldsymbol{\sigma} : \left\{ \int_{\bar{\Gamma}} [\![\boldsymbol{\mathcal{V}}]\!](\bar{\boldsymbol{\xi}}) \otimes \boldsymbol{n} \, \mathrm{d}S_{\bar{\xi}} \right\} : \boldsymbol{\sigma}' = \boldsymbol{\sigma} : \boldsymbol{\mathcal{A}}^{\sigma} : \boldsymbol{\sigma}'. \tag{2.A.7}$$

Then, using variational formulation (2.A.6) with $\boldsymbol{w} = \boldsymbol{\sigma}' : \boldsymbol{\mathcal{V}}$, noting that

$$\boldsymbol{\sigma} : \boldsymbol{\mathcal{C}} : (\boldsymbol{\sigma}' : \boldsymbol{\nabla}\boldsymbol{\mathcal{V}}) = (\boldsymbol{\sigma}' : \boldsymbol{\nabla}\boldsymbol{\mathcal{V}}) : \boldsymbol{\mathcal{C}} : \boldsymbol{\sigma},$$

by virtue of the major symmetry of $\boldsymbol{\mathcal{C}}$, and exploiting the known symmetry of the bilinear form in the left-hand side of (2.A.6), one obtains

$$\boldsymbol{\sigma}' : \left\{ \int_{\bar{\Gamma}} [\![\boldsymbol{\mathcal{V}}]\!](\bar{\boldsymbol{\xi}}) \otimes \boldsymbol{n} \, \mathrm{d}S_{\bar{\xi}} \right\} : \boldsymbol{\sigma} = \int_{\mathbb{R}^3 \setminus \bar{\Gamma}} [\boldsymbol{\sigma} : \boldsymbol{\nabla}\boldsymbol{\mathcal{V}}(\bar{\boldsymbol{\xi}})] : \boldsymbol{\mathcal{C}} : [\boldsymbol{\sigma}' : \boldsymbol{\nabla}\boldsymbol{\mathcal{V}}(\bar{\boldsymbol{\xi}})] \, \mathrm{d}V_{\bar{\xi}}$$

$$= \int_{\mathbb{R}^3 \setminus \bar{\Gamma}} [\boldsymbol{\sigma}' : \boldsymbol{\nabla}\boldsymbol{\mathcal{V}}(\bar{\boldsymbol{\xi}})] : \boldsymbol{\mathcal{C}} : [\boldsymbol{\sigma} : \boldsymbol{\nabla}\boldsymbol{\mathcal{V}}(\bar{\boldsymbol{\xi}})] \, \mathrm{d}V_{\bar{\xi}} = \boldsymbol{\sigma} : \left\{ \int_{\bar{\Gamma}} [\![\boldsymbol{\mathcal{V}}]\!](\bar{\boldsymbol{\xi}}) \otimes \boldsymbol{n} \, \mathrm{d}S_{\bar{\xi}} \right\} : \boldsymbol{\sigma}'. \tag{2.A.8}$$

The major symmetry of $\boldsymbol{\mathcal{A}}^{\sigma}$ then follows from (2.A.7) and (2.A.8). Finally, the major symmetry of $\boldsymbol{\mathcal{A}}$ stems directly from that of $\boldsymbol{\mathcal{A}}^{\sigma}$ through $\boldsymbol{\mathcal{A}} = \boldsymbol{\mathcal{C}} : \boldsymbol{\mathcal{A}}^{\sigma} : \boldsymbol{\mathcal{C}}$. $\qquad\square$

Remark 8. *The symmetry property (2.A.5) is also established in Ammari et al. (2002), following a more involved proof which assumes isotropic elastic properties for both reference and inclusion materials.*

Remark 9. *The major symmetry of $\boldsymbol{\mathcal{A}}$ or $\boldsymbol{\mathcal{A}}^{\sigma}$ defined for cracks instead of cavities follows from Lemma 6 by considering a crack as the limiting case of an infinitely thin cavity.*

2.A.3 Elliptical crack

Polarization tensor of an ellipsoidal cavity. For an ellipsoidal cavity, an equivalent-inclusion argument allows to express $\boldsymbol{\mathcal{A}}^{\sigma}(\mathcal{B})$ in terms of the Eshelby tensor $\boldsymbol{\mathcal{S}}$ of $\mathcal{B}$ (Mura, 1982), resulting in Bonnet and Guzina (2004)

$$\boldsymbol{\mathcal{A}}^{\sigma}(\mathcal{B}) = |\mathcal{B}| \boldsymbol{\mathcal{C}}^{-1} : [\boldsymbol{\mathcal{I}}^{\mathrm{sym}} - \boldsymbol{\mathcal{S}}^{\mathrm{T}}]^{-1} \tag{2.A.9}$$

where, for any fourth-order tensor $\boldsymbol{\mathcal{Q}}$ having minor symmetry, the transposed tensor $\boldsymbol{\mathcal{Q}}^{\mathrm{T}}$ is defined so that $\boldsymbol{\mathcal{Q}} : \boldsymbol{B} = \boldsymbol{B} : \boldsymbol{\mathcal{Q}}^{\mathrm{T}}$ for any second-order tensor $\boldsymbol{B}$, and is represented by the matrix $\hat{Q}^{\mathrm{T}}$.

Elliptic crack as limiting case of ellipsoidal cavity. Consider an elliptic crack embedded in an infinite isotropic elastic body. By defining appropriately the Cartesian frame, the crack can be assumed to lie in the $x_{1,2}$-plane, with its principal axes aligned with e_1, e_2 and its semiaxes such that $\ell_1 \geqslant \ell_2$, and hence to have its unit normal given by $n = e_3$. The polarization tensor for such crack may be derived by considering the limiting case as $\eta \to 0$ of a thin ellipsoidal cavity with $\ell_3 = \eta\ell_1$, $\eta \ll 1$. The Eshelby tensor for such thin ellipsoid is given by Mura (1982)

$$\boldsymbol{S}(\eta) = \boldsymbol{S}_0 + \boldsymbol{S}_1\eta + o(\eta), \tag{2.A.10}$$

with $\boldsymbol{S}_0$ and $\boldsymbol{S}_1$ given in block-matrix form, following the conventions of 2.A.1 for the matrix representation of fourth-order tensors, by

$$\hat{\boldsymbol{S}}_0^{11} = \begin{bmatrix} 0 & 0 & 0 \\ 0 & 0 & 0 \\ \dfrac{\nu}{1-\nu} & \dfrac{\nu}{1-\nu} & 1 \end{bmatrix}, \quad \hat{\boldsymbol{S}}_1^{11} = \frac{1}{2(1-\nu)}\begin{bmatrix} \gamma+2(1-\nu)\alpha+\beta & -\gamma+(1+2\nu)\alpha-\beta & (2\nu-1)\alpha \\ -\gamma+(1-2\nu)(\alpha-\beta) & \gamma+2(2-\nu)(\beta-\alpha) & (1-2\nu)(\alpha-\beta) \\ -\alpha-2\nu\beta & \alpha-(1+2\nu)\beta & (2\nu-1)\beta \end{bmatrix},$$

$$\hat{\boldsymbol{S}}_0^{22} = \mathrm{Diag}[0,\, 1,\, 1]\,, \qquad \hat{\boldsymbol{S}}_1^{22} = \frac{1}{1-\nu}\mathrm{Diag}\big[-\gamma+\alpha-\nu\beta,\ -\nu\alpha-(1-\nu)\beta,\ \nu\alpha-\beta\big]\,,$$

$$\hat{\boldsymbol{S}}_0^{12} = \hat{\boldsymbol{S}}_0^{21} = \hat{\boldsymbol{S}}_1^{12} = \hat{\boldsymbol{S}}_1^{21} = \boldsymbol{0}, \tag{2.A.11}$$

with $\mathrm{Diag}[a,b,c]$ denoting the (3×3) diagonal matrix whose diagonal entries are a,b,c. Moreover, the constants α, β, γ appearing in (2.A.11) are given by

$$\alpha = \frac{(1-m^2)^{1/2}}{m^2}\big(F(m) - E(m)\big), \qquad \beta = \frac{E(m)}{(1-m^2)^{1/2}}, \qquad \gamma = \frac{2\alpha-\beta}{m^2}, \tag{2.A.12}$$

where $F(m)$ and $E(m)$ are the complete elliptic integrals of the first and second kind, respectively (Abramowitz and Stegun, 1965):

$$F(m) = \int_0^{\pi/2}\big(1 - m^2\sin^2\phi\big)^{-1/2}\,\mathrm{d}\phi, \qquad E(m) = \int_0^{\pi/2}\big(1 - m^2\sin^2\phi\big)^{1/2}\,\mathrm{d}\phi, \tag{2.A.13}$$

and the modulus m is given by

$$m = \big(1 - a_2^2/a_1^2\big)^{1/2}, \qquad (0 < m \leqslant 1).$$

Noting that the volume of the thin ellipsoid is $|\mathcal{B}| = (4\pi/3)\ell_1^3(1-m^2)^{1/2}\eta$, formula (2.A.9) becomes

$$\boldsymbol{A}^\sigma(\eta) = \frac{4\pi}{3}\ell_1^3(1-m^2)^{1/2}\eta\,\boldsymbol{C}^{-1} : \big[\boldsymbol{\mathcal{I}}^{\mathrm{sym}} - \boldsymbol{S}^{\mathrm{T}}(\eta)\big]^{-1}. \tag{2.A.14}$$

The task at hand is to find the limit as $\eta \to 0$ of the polarization tensor $\boldsymbol{A}(\eta) = \boldsymbol{C} : \boldsymbol{A}^\sigma(\eta) : \boldsymbol{C}$ by exploiting (2.A.14). A natural approach consists in expanding $\eta\big[\boldsymbol{\mathcal{I}}^{\mathrm{sym}} - \boldsymbol{S}^{\mathrm{T}}(\eta)\big]^{-1}$ in powers of η about $\eta = 0$. However, care must be exercised as $\boldsymbol{\mathcal{I}}^{\mathrm{sym}} - \boldsymbol{S}_0^{\mathrm{T}}$ is not invertible. Owing to the block-diagonal structure of $\hat{\boldsymbol{S}}$ and the major symmetry of $\boldsymbol{\mathcal{I}}^{\mathrm{sym}}$, inverting $\big[\boldsymbol{\mathcal{I}}^{\mathrm{sym}} - \boldsymbol{S}^{\mathrm{T}}(\eta)\big]^{-1}$ is reduced to separately inverting $\boldsymbol{I} - \hat{\boldsymbol{S}}^{11}(\eta)$ and $\boldsymbol{I} - \hat{\boldsymbol{S}}^{22}(\eta)$ (where $\boldsymbol{I}$ is the (3×3) identity matrix). As neither $\boldsymbol{I} - \hat{\boldsymbol{S}}_0^{11}$ nor $\boldsymbol{I} - \hat{\boldsymbol{S}}_0^{22}$ are invertible, some care must be exercised. First, using formulae (2.A.11), one obtains

$$\boldsymbol{I} - \hat{\boldsymbol{S}}^{22}(\eta) = \mathrm{Diag}\Big[1 + \Big(\frac{\gamma-\alpha+\nu\beta}{1-\nu}\Big)\eta,\ 1,\ 1\Big]\,\mathrm{Diag}\Big[1,\ \Big(\frac{\nu\alpha+(1-\nu)\beta}{1-\nu}\Big)\eta,\ \Big(\frac{\beta-\nu\alpha}{1-\nu}\Big)\eta\Big]\,(\boldsymbol{I}+o(1)).$$

Each diagonal matrix in the above formula is invertible for nonzero η, which ensures invertibility of the expansion for sufficiently small $\eta > 0$. Upon performing this inversion, one obtains

$$\eta\big[\boldsymbol{I} - \hat{\boldsymbol{S}}^{22}(\eta)\big]^{-1} = \mathrm{Diag}\Big[\, 0,\ \frac{1-\nu}{\nu\alpha + (1-\nu)\beta},\ \frac{1-\nu}{\beta - \nu\alpha}\Big] + o(1).$$

Similarly, using again formulae (2.A.11), one finds

$$\boldsymbol{I} - \hat{\boldsymbol{S}}^{11}(\eta) = [\boldsymbol{R}_0 - \boldsymbol{R}_1\eta]\mathrm{Diag}\Big[\, 1,\ 1,\ \frac{1-2\nu}{2(1-\nu)}\eta\Big],$$

where the matrices $\boldsymbol{R}_0$ and $\boldsymbol{R}_1$ are given by

$$\boldsymbol{R}_0 = \begin{bmatrix} 1 & 0 & \alpha \\ 0 & 1 & \beta - \alpha \\ \dfrac{-\nu}{1-\nu} & \dfrac{-\nu}{1-\nu} & \beta \end{bmatrix}, \qquad \boldsymbol{R}_1 = \frac{1}{2(1-\nu)}\begin{bmatrix} \gamma + 2(1-\nu)\alpha + \beta & -\gamma + (1+2\nu)\alpha - \beta & 0 \\ -\gamma + (1-2\nu)(\alpha - \beta) & \gamma + 2(2-\nu)(\beta - \alpha) & 0 \\ -\alpha - 2\nu\beta & \alpha - (1+2\nu)\beta & 0 \end{bmatrix}.$$

The matrix $\boldsymbol{R}_0$ is invertible (one readily finds $\mathrm{Det}(\boldsymbol{R}_0) = \beta/(1-\nu)$; then, as β is given by (2.A.12) and $E(m) \neq 0$ for any $0 \leqslant m < 1$, $\mathrm{Det}(\boldsymbol{R}_0) \neq 0$), which implies that $\boldsymbol{R}_0 - \boldsymbol{R}_1\eta$ is invertible for sufficient small η. One therefore finds

$$\eta\big[\boldsymbol{I} - \hat{\boldsymbol{S}}^{11}(\eta)\big]^{-1} = \mathrm{Diag}\Big[\, \eta,\ \eta,\ \frac{2(1-\nu)}{1-2\nu}\Big]\big[\boldsymbol{R}_0^{-1} + o(1)\big] + o(1) = \frac{2(1-\nu)}{1-2\nu}\mathrm{Diag}\big[\, 0,\ 0,\ 1\big]\boldsymbol{R}_0^{-1} + o(1)$$

$$= \frac{2(1-\nu)}{(1-2\nu)\beta}\begin{bmatrix} 0 & 0 & 0 \\ 0 & 0 & 0 \\ \nu & \nu & 1-\nu \end{bmatrix} + o(1).$$

Finally, using matrix representation (2.A.2) for the inverse elasticity tensor $\boldsymbol{\mathcal{C}}^{-1}$, one obtains

$$\eta\big[\boldsymbol{I} - \hat{\boldsymbol{S}}^{22}(\eta)\big]^{-1}\hat{\boldsymbol{D}}^{22} = \frac{1}{2\mu}\mathrm{Diag}\Big[\, 0,\ \frac{1-\nu}{\nu\alpha + (1-\nu)\beta},\ \frac{1-\nu}{\beta - \nu\alpha}\Big] + o(1),$$

$$\eta\big[\boldsymbol{I} - \hat{\boldsymbol{S}}^{11}(\eta)\big]^{-1}\hat{\boldsymbol{D}}^{11} = \frac{(1-\nu)}{\mu\beta}\begin{bmatrix} 0 & 0 & 0 \\ 0 & 0 & 0 \\ 0 & 0 & 1 \end{bmatrix} + o(1),$$

and expressions (2.2.26a-c) follow by taking the transpose of the above result, applying the matrix-tensor equivalence of 2.A.1, inserting the obtained value of $\eta\big[\boldsymbol{\mathcal{I}}^{\mathrm{sym}} - \boldsymbol{\mathcal{S}}^{\mathrm{T}}(\eta)\big]^{-1}$ into (2.A.14) and taking the limit $\eta \to 0$ (i.e. removing the $o(1)$ remainder).

Penny-shaped crack as a special case of elliptic crack. To find the value of (2.2.26a-c) for the special case of a penny-shaped crack (for which $\ell_1 = \ell_2$, i.e. $m = 0$), one invokes the following expansions (Abramowitz and Stegun, 1965)

$$F(m) = \frac{\pi}{2}\Big[1 + \frac{m^2}{4} + \frac{9m^4}{64}\Big] + o(m^4), \quad E(m) = \frac{\pi}{2}\Big[1 - \frac{m^2}{4} - \frac{3m^4}{64}\Big] + o(m^4),$$

which, inserted into (2.A.12), readily yield

$$\alpha(m) = \frac{\pi}{4} + o(1), \quad \beta(m) = \frac{\pi}{2} + o(1), \quad \gamma(m) = -\frac{\pi}{4} + o(1).$$

On inserting these values into (2.2.26a-c), one easily verifies that expression (2.2.25) for the penny-shaped crack is recovered.

2.A.4 Elliptical sound-hard screen

The polarization tensor $\boldsymbol{\mathcal{B}}$ for the elliptic sound-hard thin screen can also be derived as a limiting case of that for the ellipsoidal sound-hard scatterer. The latter is given, using the present notations, by Guzina and Bonnet (2006)

$$\boldsymbol{\mathcal{B}}_{\text{ellipsoid}} = |\mathcal{B}| \sum_{q=1}^{3} \frac{1}{1 - I_q/4\pi} \boldsymbol{e}_q \otimes \boldsymbol{e}_q \tag{2.A.15}$$

with the I_q defined as in Mura (1982), Eq. (11.14). In the flat-scatterer limit $\eta = \ell_3/\ell_1 \to 0$, the I_q are given (Mura, 1982) by

$$I_1 = 4\pi\eta\alpha(m) + o(\eta), \quad I_2 = 4\pi\eta(\beta(m) - \alpha(m)) + o(\eta), \quad I_3 = 4\pi(1 - \eta\beta(m)) + o(\eta)$$

with the functions $\alpha(m), \beta(m)$ again defined by (2.A.12). Hence, the sought polarization tensor $\boldsymbol{\mathcal{B}}$ is obtained (recalling that $|\mathcal{B}| = (4\pi/3)\ell_1^3(1 - m^2)^{1/2}\eta$) as

$$\boldsymbol{\mathcal{B}} = \lim_{\eta \to 0} \boldsymbol{\mathcal{B}}_{\text{ellipsoid}}(\eta) = \frac{4\pi}{3} \frac{(1 - m^2)^{1/2}}{\beta(m)} \ell_1^3 \boldsymbol{e}_3 \otimes \boldsymbol{e}_3, \tag{2.A.16}$$

Expression (2.3.12) finally follows from substituting the definition (2.A.12) of $\beta(m)$ into the above formula.

2.B Elastodynamic fundamental solutions and proof of Lemmas 4,5

The time convolutions featured in integral equation (2.2.10) can be expressed as

$$\boldsymbol{U}(\boldsymbol{x}, t, \boldsymbol{\xi}) \star [\![\ddot{\boldsymbol{v}}_{\varepsilon, \boldsymbol{z}}]\!](\boldsymbol{\xi}, t) = \boldsymbol{U}[\boldsymbol{x}, t, \boldsymbol{\xi}|\boldsymbol{e}_i \cdot [\![\ddot{\boldsymbol{v}}_{\varepsilon, \boldsymbol{z}}]\!](\boldsymbol{\xi}, \cdot)] \cdot \boldsymbol{e}_i \tag{2.B.1a}$$

$$\big(\boldsymbol{n}(\boldsymbol{x}) \cdot \boldsymbol{\mathcal{C}} \cdot \boldsymbol{\Sigma}(\boldsymbol{x}, t, \boldsymbol{\xi})\big) \star \boldsymbol{\mathcal{D}}[\![\boldsymbol{v}_{\varepsilon, \boldsymbol{z}}]\!](\boldsymbol{\xi}, t) = \big(\boldsymbol{n}(\boldsymbol{x}) \cdot \boldsymbol{\mathcal{C}} \cdot \boldsymbol{\Sigma}[\boldsymbol{x}, t, \boldsymbol{\xi}|(\boldsymbol{e}_q \otimes \boldsymbol{e}_i \otimes \boldsymbol{e}_j) \vdots \boldsymbol{\mathcal{D}}[\![\boldsymbol{v}_{\varepsilon, \boldsymbol{z}}]\!](\boldsymbol{\xi}, \cdot)]\big) \vdots (\boldsymbol{e}_q \otimes \boldsymbol{e}_i \otimes \boldsymbol{e}_j) \tag{2.B.1b}$$

where $\boldsymbol{U}[\boldsymbol{x}, t, \boldsymbol{\xi}|f]$ and $\boldsymbol{\Sigma}[\boldsymbol{x}, t, \boldsymbol{\xi}|f]$ are the time-modulated elastodynamic Green's tensors, defined such that $\boldsymbol{e}_k \cdot \boldsymbol{U}$ and $\boldsymbol{e}_k \cdot \boldsymbol{\Sigma}$ are the displacement vector and stress tensor at $\boldsymbol{\xi} \in \Omega$ resulting from a point force applied at $\boldsymbol{x}$ in the k-direction with prescribed time-varying magnitude $f(t)$ and satisfying boundary conditions (2.2.9). Homogeneous initial conditions at $t = 0$ and vanishing time modulation $f(t)$ for $t < 0$ are assumed, so that $\boldsymbol{U}[\boldsymbol{x}, t, \boldsymbol{\xi}|f]$ and $\boldsymbol{\Sigma}[\boldsymbol{x}, t, \boldsymbol{\xi}|f]$ have quiescent past. Similarly, let $\boldsymbol{U}_\infty[\boldsymbol{x}, t, \boldsymbol{\xi}|f]$ and $\boldsymbol{\Sigma}_\infty[\boldsymbol{x}, t, \boldsymbol{\xi}; \boldsymbol{n}|f]$ denote the time-modulated full-space fundamental solution, which satisfy radiation conditions instead of boundary conditions (2.2.9), and is given by (Eringen and Suhubi, 1975)

$$\boldsymbol{U}_\infty[\boldsymbol{x}, t, \boldsymbol{\xi}|f] = \frac{1}{4\pi\mu r} \Big[A[\boldsymbol{x}, t, \boldsymbol{\xi}|f] \, \boldsymbol{I} + B[\boldsymbol{x}, t, \boldsymbol{\xi}|f] \, (\hat{\boldsymbol{r}} \otimes \hat{\boldsymbol{r}}) \Big] \tag{2.B.2a}$$

$$\boldsymbol{\Sigma}_\infty[\boldsymbol{x}, t, \boldsymbol{\xi}|f] = \frac{1}{4\pi r^2} \Big[C[\boldsymbol{x}, t, \boldsymbol{\xi}|f](\hat{\boldsymbol{r}} \otimes \boldsymbol{I}) + 2D[\boldsymbol{x}, t, \boldsymbol{\xi}|f](\hat{\boldsymbol{r}} \cdot \boldsymbol{\mathcal{I}}^{\text{sym}}) + 2E[\boldsymbol{x}, t, \boldsymbol{\xi}|f](\hat{\boldsymbol{r}} \otimes \hat{\boldsymbol{r}} \otimes \hat{\boldsymbol{r}}) \Big] \tag{2.B.2b}$$

where $\boldsymbol{r} = (\boldsymbol{\xi} - \boldsymbol{x})$, $r = \|\boldsymbol{r}\|$, $\hat{\boldsymbol{r}} = \boldsymbol{r}/r$, κ is the ratio of bulk wave velocities as defined by

$$\kappa^2 = \frac{c_T^2}{c_L^2} = \frac{1 - 2\nu}{2(1 - \nu)} = \frac{\mu}{\lambda + 2\mu} \tag{2.B.3}$$

and with $A = A[\boldsymbol{x}, t, \boldsymbol{\xi}|f], \ldots$ defined by

$$A[\boldsymbol{x}, t, \boldsymbol{\xi}|f] = f\left(t - \frac{r}{c_T}\right) + \int_1^\kappa \eta f\left(t - \frac{\eta r}{c_T}\right) \mathrm{d}\eta$$

$$B[\boldsymbol{x}, t, \boldsymbol{\xi}|f] = -3A[\boldsymbol{x}, t, \boldsymbol{\xi}|f] + 2f\left(t - \frac{r}{c_T}\right) + \kappa^2 f\left(t - \frac{r}{c_L}\right)$$

$$C[\boldsymbol{x}, t, \boldsymbol{\xi}|f] = 2B[\boldsymbol{x}, t, \boldsymbol{\xi}|f] - (1 - 2\kappa^2)\left\{f\left(t - \frac{r}{c_L}\right) + \frac{r}{c_L}\dot{f}\left(t - \frac{r}{c_L}\right)\right\} \qquad (2.\mathrm{B}.4)$$

$$D[\boldsymbol{x}, t, \boldsymbol{\xi}|f] = 2B[\boldsymbol{x}, t, \boldsymbol{\xi}|f] - f\left(t - \frac{r}{c_T}\right) - \frac{r}{c_T}\dot{f}\left(t - \frac{r}{c_T}\right)$$

$$E[\boldsymbol{x}, t, \boldsymbol{\xi}|f] = -3B[\boldsymbol{x}, t, \boldsymbol{\xi}|f] - D[\boldsymbol{x}, t, \boldsymbol{\xi}|f] - \kappa^2\left\{f\left(t - \frac{r}{c_L}\right) + \frac{r}{c_L}\dot{f}\left(t - \frac{r}{c_L}\right)\right\}.$$

Next, define the time-modulated complementary elastodynamic Green's tensor $\boldsymbol{U}_\mathrm{C}$ by

$$\boldsymbol{U}[\boldsymbol{x}, t, \boldsymbol{\xi}|f] = \boldsymbol{U}_\infty[\boldsymbol{x}, t, \boldsymbol{\xi}|f] + \boldsymbol{U}_\mathrm{C}[\boldsymbol{x}, t, \boldsymbol{\xi}|f] \qquad (2.\mathrm{B}.5)$$

By virtue of superposition arguments, $\boldsymbol{U}_\mathrm{C}$ is governed by an IBVP with vanishing body forces and initial conditions, and (when $\boldsymbol{x} \notin S$) smooth boundary data involving boundary traces $\boldsymbol{U}_\infty[\boldsymbol{x}, t, \boldsymbol{\xi}|f]$ ($\bar{\boldsymbol{\xi}} \in S_\mathrm{D}$) and $\boldsymbol{\Sigma}_\infty[\boldsymbol{x}, t, \boldsymbol{\xi}|f] \cdot \boldsymbol{n}(\bar{\boldsymbol{\xi}})$ ($\bar{\boldsymbol{\xi}} \in S_\mathrm{N}$). Thus, $\boldsymbol{U}_\mathrm{C}[\boldsymbol{x}, t, \boldsymbol{\xi}|f]$ is bounded in the limit $\boldsymbol{\xi} \to \boldsymbol{x}$, i.e. the singular behavior of $\boldsymbol{U}[\boldsymbol{x}, t, \boldsymbol{\xi}|f]$ at $\boldsymbol{\xi} = \boldsymbol{x}$ is identical to that of its full-space counterpart $\boldsymbol{U}_\infty[\boldsymbol{x}, t, \boldsymbol{\xi}|f]$, and one has

$$\boldsymbol{U}_\mathrm{C}[\boldsymbol{z} + \varepsilon\bar{\boldsymbol{x}}, t, \boldsymbol{z} + \varepsilon\bar{\boldsymbol{\xi}}|f] = O(1), \quad \boldsymbol{\Sigma}_\mathrm{C}[\boldsymbol{z} + \varepsilon\bar{\boldsymbol{x}}, t, \boldsymbol{z} + \varepsilon\bar{\boldsymbol{\xi}}|f] = O(1) \qquad (\varepsilon \to 0) \qquad (2.\mathrm{B}.6)$$

Proof of Lemma 4. The proof exploits decomposition (2.B.5). First, upon introducing scaled coordinates (2.2.11a) into expression (2.B.2a) of $\boldsymbol{\Sigma}_\infty$ and definitions (2.B.4) of $A[\boldsymbol{x}, t, \boldsymbol{\xi}|f]$ and $B[\boldsymbol{x}, t, \boldsymbol{\xi}|f]$ (wherein $f(t) = [\![\ddot{\boldsymbol{v}}_{\varepsilon,\boldsymbol{z}}]\!](\boldsymbol{\xi}, t)$ according to 2.B.1b), it is a simple matter to show that

$$\boldsymbol{U}_\infty(\boldsymbol{x}, t, \boldsymbol{\xi}) \star [\![\ddot{\boldsymbol{v}}_{\varepsilon,\boldsymbol{z}}]\!](\boldsymbol{\xi}, t) = \frac{1}{\varepsilon}\boldsymbol{U}_{\infty,\varepsilon}(\bar{\boldsymbol{x}}, t, \bar{\boldsymbol{\xi}}) \star [\![\ddot{\boldsymbol{v}}_{\varepsilon,\boldsymbol{z}}]\!](\bar{\boldsymbol{\xi}}, t) \qquad (2.\mathrm{B}.7)$$

where $\boldsymbol{U}_{\infty,\varepsilon}$ is defined by (2.B.2a) and (2.B.4) with wave velocities $c_\mathrm{L}, c_\mathrm{T}$ replaced by rescaled values c_L/ε and c_T/ε. Equation (2.B.7) and scaling (2.2.11b) then imply

$$\int_{\Gamma_{\varepsilon,\boldsymbol{z}}} \boldsymbol{U}_\infty(\boldsymbol{x}, t, \boldsymbol{\xi}) \star [\![\ddot{\boldsymbol{v}}_{\varepsilon,\boldsymbol{z}}]\!](\boldsymbol{\xi}, t) \, \mathrm{d}S_\xi = \varepsilon \int_{\bar{\Gamma}} \boldsymbol{U}_{\infty,\varepsilon}(\bar{\boldsymbol{x}}, t, \bar{\boldsymbol{\xi}}) \star [\![\ddot{\boldsymbol{v}}_{\varepsilon,\boldsymbol{z}}]\!](\bar{\boldsymbol{\xi}}, t) \, \mathrm{d}S_{\bar{\xi}} \qquad (2.\mathrm{B}.8)$$

Moreover, owing to the boundedness (2.B.6) of the complementary Green's tensor $\boldsymbol{U}_\mathrm{C}$, one has, upon using again coordinate scaling (2.2.11b):

$$\int_{\Gamma_{\varepsilon,\boldsymbol{z}}} \boldsymbol{U}_\mathrm{C}(\boldsymbol{x}, t, \boldsymbol{\xi}) \star [\![\ddot{\boldsymbol{v}}_{\varepsilon,\boldsymbol{z}}]\!](\boldsymbol{\xi}, t) \, \mathrm{d}S_\xi = O(\varepsilon^2)\|[\![\ddot{\boldsymbol{v}}_{\varepsilon,\boldsymbol{z}}]\!](\cdot, t)\|_{L^2(\bar{\Gamma})} \qquad (2.\mathrm{B}.9)$$

The desired identity (2.2.14) then follows from combining (2.B.8) and (2.B.9). Identity (2.2.14) is establish in a similar way, noting that

$$\left[\boldsymbol{n}(\boldsymbol{x}) \cdot \mathcal{C} \cdot \boldsymbol{\Sigma}_\infty(\boldsymbol{x}, t, \boldsymbol{\xi})\right] \star \mathcal{D}[\![\boldsymbol{v}_{\varepsilon,\boldsymbol{z}}]\!](\boldsymbol{\xi}, t) = \frac{1}{\varepsilon^3}\left[\boldsymbol{n}(\boldsymbol{x}) \cdot \mathcal{C} \cdot \boldsymbol{\Sigma}_{\infty,\varepsilon}(\bar{\boldsymbol{x}}, t, \bar{\boldsymbol{\xi}})\right] \star \mathcal{D}[\![\bar{\boldsymbol{v}}_{\varepsilon,\boldsymbol{z}}]\!](\bar{\boldsymbol{\xi}}, t)$$

with the ε^{-3} behavior resulting from the combined effect of the $\|\boldsymbol{\xi} - \boldsymbol{x}\|^{-2}$ singularity of $\boldsymbol{\Sigma}_\infty$ and the following behavior of the operator $\mathcal{D}$ under the scaling (2.2.11a):

$$\mathcal{D}\boldsymbol{w}(\boldsymbol{\xi}, t) = \frac{1}{\varepsilon}\mathcal{D}\bar{\boldsymbol{w}}(\bar{\boldsymbol{\xi}}, t) \qquad (2.\mathrm{B}.10)$$

Proof of Lemma 5.   Since the proposed ansatz (2.2.15) is, by assumption, differentiable w.r.t. t, it is appropriate to investigate the behavior of $\boldsymbol{U}_\infty$ defined by (2.B.2a) and (2.B.4) for a differentiable time modulation f. Introducing the decomposition $f(\tau) = f(t) + (f(\tau) - f(t)) = f(t) + \Delta f(\tau)$, one has

$$\begin{aligned}
C[\bar{\boldsymbol{x}}, t, \bar{\boldsymbol{\xi}}|f] &= \kappa^2 f(t) + C[\bar{\boldsymbol{x}}, t, \bar{\boldsymbol{\xi}}|\Delta f] \\
D[\bar{\boldsymbol{x}}, t, \bar{\boldsymbol{\xi}}|f] &= -\kappa^2 f(t) + D[\bar{\boldsymbol{x}}, t, \bar{\boldsymbol{\xi}}|\Delta f] \\
E[\bar{\boldsymbol{x}}, t, \bar{\boldsymbol{\xi}}|f] &= -\frac{3}{2}(1 - \kappa^2) f(t) + E[\bar{\boldsymbol{x}}, t, \bar{\boldsymbol{\xi}}|\Delta f]
\end{aligned} \tag{2.B.11}$$

Substituting the above values into (2.B.2b) yields the decomposition

$$\boldsymbol{\Sigma}_\infty[\bar{\boldsymbol{x}}, t, \bar{\boldsymbol{\xi}}|f] = \boldsymbol{\Sigma}_\infty(\bar{\boldsymbol{\xi}} - \bar{\boldsymbol{x}}) f(t) + \boldsymbol{\Sigma}_\infty[\bar{\boldsymbol{x}}, t, \bar{\boldsymbol{\xi}}|\Delta f] \tag{2.B.12}$$

where $\boldsymbol{\Sigma}_\infty(\bar{\boldsymbol{r}})$ is the elastostatic Kelvin fundamental stress, given by

$$\boldsymbol{\Sigma}_\infty(\bar{\boldsymbol{r}}) = \frac{1}{4\pi\bar{r}^2}\left[\kappa^2\left(\hat{\bar{\boldsymbol{r}}} \otimes \boldsymbol{I} - 2\hat{\bar{\boldsymbol{r}}} \cdot \boldsymbol{\mathcal{I}}^{\text{sym}}\right) + 3(\kappa^2 - 1)\hat{\bar{\boldsymbol{r}}} \otimes \hat{\bar{\boldsymbol{r}}} \otimes \hat{\bar{\boldsymbol{r}}}\right] \tag{2.B.13}$$

Decomposition (2.B.12) in particular holds for $\boldsymbol{\Sigma}_{\infty,\varepsilon}[\ldots|f]$ defined by replacing velocities c_{L}, c_{T} with the rescaled values $\varepsilon^{-1}c_{\text{L}}$, $\varepsilon^{-1}c_{\text{T}}$ in $\boldsymbol{\Sigma}_\infty[\ldots|f]$. Owing to the assumed differentiability of f, one easily shows that

$$\left\| \boldsymbol{\Sigma}_{\infty,\varepsilon}[\bar{\boldsymbol{x}}, t, \bar{\boldsymbol{\xi}}|\Delta f] \right\| = O(\varepsilon) \qquad (\varepsilon \to 0)$$

Since $\boldsymbol{\Sigma}_\infty(\bar{\boldsymbol{r}})f(t)$ is unaffected by the wave velocity rescaling, decomposition (2.B.12) implies

$$\boldsymbol{\Sigma}_{\infty,\varepsilon}[\bar{\boldsymbol{x}}, t, \bar{\boldsymbol{\xi}}|f] = \boldsymbol{\Sigma}_\infty(\bar{\boldsymbol{x}}, \bar{\boldsymbol{\xi}}) f(t) + o(1) \qquad (\varepsilon \to 0) \tag{2.B.14}$$

Consequently, noting that combining ansatz (2.2.15) with (2.B.10) implies

$$\boldsymbol{\mathcal{D}}[\![\bar{\boldsymbol{v}}_{\varepsilon,\boldsymbol{z}}]\!](\bar{\boldsymbol{\xi}}, t) = \boldsymbol{\sigma}[\boldsymbol{u}](\boldsymbol{z}, t) : \boldsymbol{\mathcal{D}}[\![\boldsymbol{\mathcal{V}}]\!](\bar{\boldsymbol{\xi}}) + o(1), \qquad (\varepsilon \to 0)$$

equating $f(t)$ to the components of the above expansion of $\boldsymbol{\mathcal{D}}[\![\bar{\boldsymbol{v}}_{\varepsilon,\boldsymbol{z}}]\!](\bar{\boldsymbol{\xi}}, t)$ according to (2.B.1b), and using (2.B.14) one finds that

$$\fint_{\bar{\Gamma}} \left[\boldsymbol{n}(\bar{\boldsymbol{x}}) \cdot \boldsymbol{\mathcal{C}} \cdot \boldsymbol{\Sigma}_{\infty,\varepsilon}(\bar{\boldsymbol{x}}, t, \bar{\boldsymbol{\xi}})\right] \star \boldsymbol{\mathcal{D}}[\![\bar{\boldsymbol{v}}_{\varepsilon,\boldsymbol{z}}]\!](\bar{\boldsymbol{\xi}}, t) \, \mathrm{d}S_{\bar{\xi}}$$

$$= \sigma_{ij}[\boldsymbol{u}](\boldsymbol{z}, t) \fint_{\bar{\Gamma}} \left[\boldsymbol{n}(\bar{\boldsymbol{x}}) \cdot \boldsymbol{\mathcal{C}} \cdot \boldsymbol{\Sigma}_\infty(\bar{\boldsymbol{\xi}} - \bar{\boldsymbol{x}})\right] \vdots \boldsymbol{\mathcal{D}}[\![\boldsymbol{V}]\!]^{ij}(\bar{\boldsymbol{\xi}}) \, \mathrm{d}S_{\bar{\xi}} + o(1)$$

The desired expansion (2.2.16a) finally follows from combining the above estimate with identity (2.2.14).

The estimate (2.2.16b) stems directly from plugging ansatz (2.2.15) into (2.2.14) and the assumed twice-differentiability of f.

2.C   Radon transform

On introducing the unit circle as $\hat{\mathcal{C}} = \{\boldsymbol{\eta} \in \mathbb{R}^2 \text{ and } |\boldsymbol{\eta}| = 1\}$, the Radon transform $(r, \boldsymbol{\eta}) \in \mathbb{R} \times \hat{\mathcal{C}} \mapsto \check{\boldsymbol{f}}(r, \boldsymbol{\eta})$ of the tensorial function $\boldsymbol{\xi} \in \mathbb{R}^2 \mapsto \boldsymbol{f}(\boldsymbol{\xi})$ is given by

$$\check{\boldsymbol{\Phi}}(r, \boldsymbol{\eta}) = \int_{\mathbb{R}^2} \boldsymbol{f}(\boldsymbol{\xi}) \delta(r - \boldsymbol{\eta} \cdot \boldsymbol{\xi}) \, \mathrm{d}S_\xi \qquad (r \in \mathbb{R}, \boldsymbol{\eta} \in \hat{\mathcal{C}}) \tag{2.C.1}$$

where δ is Dirac delta function.

For any $m \in \mathbb{N}$, the following property holds

$$\int_{\mathbb{R}^2} (\boldsymbol{\eta} \cdot \boldsymbol{\xi})^m \boldsymbol{f}(\boldsymbol{\xi}) \, \mathrm{d}S_\xi = \int_{\mathbb{R}} r^m \check{\boldsymbol{f}}(r, \boldsymbol{\eta}) \, \mathrm{d}r \tag{2.C.2}$$

which has as a consequence that $\int_{\mathbb{R}} r^m \check{\boldsymbol{f}}(r, \boldsymbol{\eta}) \, \mathrm{d}r$ is a polynomial of degree m in $\boldsymbol{\eta}$.

Part II

Linear Sampling Method

Introduction and Overview

In the context of inverse scattering theories that have, over the past two decades, witnessed the inception and growth of a range of non-iterative techniques for obstacle reconstruction, Part II of this dissertation is concerned with the study of the Linear Sampling Method (LSM) whose principles and fundamental results are (in the context of the Helmholtz equation) summarized in Chapter 3.

On introducing the basic notions and theorems, this chapter investigates, for the first time, the possibility of multi-frequency reconstruction of sound-soft and penetrable obstacles via this method involving either far-field or near-field observations of the scattered field. On establishing a suitable approximate solution to the linear sampling equation and making an assumption of continuous frequency sweep (in terms of experimental measurements of the scattered field), two possible choices for a cumulative multi-frequency indicator function of the scatterer's support are proposed. The first alternative, termed the "serial" indicator, is taken as a natural extension of its monochromatic companion in the sense that its computation entails *space-frequency* (as opposed to space) L^2-norm of a solution to the linear sampling equation. Under a set of assumptions that include experimental observations down to zero frequency and compact frequency support of the wavelet used to illuminate the obstacle, this indicator function is further related to its time-domain counterpart. As a second possibility, the so-called "parallel" indicator is alternatively proposed as an L^2-norm, in the frequency domain, of the monochromatic indicator function. On the basis of a perturbation analysis which demonstrates that the monochromatic solution of the linear sampling equation behaves as $O(|k^2 - k_*^2|^{-m})$, $m \geqslant 1$ in the neighborhood of an isolated eigenvalue, k_*^2, of the associated interior (Dirichlet or transmission) problem, it is found that the "serial" indicator is unable to distinguish the interior from the exterior of a scatterer in situations when the prescribed frequency band traverses at least one such eigenvalue. In contrast the "parallel" indicator is, due to its particular structure, shown to be insensitive to the presence of pertinent interior eigenvalues (unknown beforehand and typically belonging to a countable set), and thus to be robust in a generic scattering configuration. A set of numerical results, including both "fine" and "coarse" frequency sampling, is included to illustrate the performance of the competing (multi-frequency) indicator functions, demonstrating behavior that is consistent with the theoretical results.

The interior transmission problem (ITP), which plays a fundamental role in the LSM and related studies involving penetrable defects, is investigated in Chapter 4 within the framework of mechanical waves scattered by piecewise-homogeneous, elastic or viscoelastic obstacles in a likewise heterogeneous background solid. For generality, the obstacle is allowed to be multiply connected, having both penetrable components (inclusions) and impenetrable parts (cavities). A variational formulation is employed to establish *sufficient* conditions for the existence and uniqueness of a solution to the ITP, provided that the excitation frequency does not belong to (at most) countable spectrum of transmission eigenvalues characterizing the "obstacle-background" pair. The featured sufficient conditions, expressed in terms of the mass density and elasticity parameters of the problem, represent an advancement over earlier works

on the subject in that i) they pose a precise, previously unavailable provision for the well-posedness of the ITP in situations when both the obstacle and the background solid are heterogeneous, and ii) they are dimensionally consistent i.e. invariant under the choice of physical units. For the case of a viscoelastic scatterer in an elastic solid it is further shown, consistent with earlier studies in acoustics, electromagnetism, and elasticity that the uniqueness of a solution to the ITP is maintained irrespective of the vibration frequency. When applied to the situation where *both* the scatterer and the background medium are viscoelastic i.e. dissipative, on the other hand, the same type of analysis shows that the analogous claim of uniqueness does not hold. Physically, such anomalous behavior of the "viscoelastic-viscoelastic" case (that has eluded previous studies) has its origins in a lesser known fact that the homogeneous ITP is not mechanically insulated from its surroundings – a feature that is particularly cloaked in situations when either the background medium or the scatterer are dissipative. A set of numerical results, computed for ITP configurations that meet the sufficient conditions for the existence of a solution, is included to illustrate the problem. Consistent with the preceding analysis, the results indicate that the set of transmission values is indeed empty in the "elastic-viscoelastic" case, and countable for "elastic-elastic" and "viscoelastic-viscoelastic" configurations. The analysis of the conditions of existence and uniqueness of a solution to the ITP is then generalized in Chapter 5 to account for a wider class of elastic material configurations. In the latter study, interior transmission problem is seen as an eigenvalue problem and an extensive study of the material (and excitation frequency) conditions, under which the ITP maintains its well-posedness, is exposed. Further, the existence of transmission eigenvalues and their corresponding lower bounds are established for the first time in elasticity.

Chapter 3

Linear sampling method for multi-frequency obstacle reconstruction

Contents

3.1   Introduction

Among the range of non-iterative point-probing algorithms for obstacle reconstruction, techniques such as linear sampling, factorization or point source methods, commonly operate within the framework of monochromatic i.e. single-frequency obstacle illumination which postulates that the squared wave number, computed with reference to the background medium, is not an eigenvalue of the associated interior (e.g. Dirichlet or transmission) problem. For common scattering configurations such eigenvalues form an at most countable set, with no accumulation points other than infinity (Pockels, 1892; Rynne and Slee- man, 1991; Cakoni et al., 2002; Päivärinta and Sylvester, 2008; Kirsch, 2009; Cakoni and Kirsch, 2010; Cakoni et al., 2010d), which makes the featured restriction manageable if not desirable in the context of practical applications.

Besides (and before) the choice of an appropriate reconstruction technique, the critical issue for most inverse scattering problems is the richness of the observed data set. In general the latter can be extended either spatially, in terms of the aperture of experimental observations, or temporally, by considering multi-frequency or time-domain scattered waveforms. Notwithstanding the fact that the latter alternative is often far more tractable in terms of experimental implementation, the literature dealing with point-probing algorithms that transcend the customary monochromatic framework is relatively scarce. In particular, one may mention the multi-frequency and time-domain treatments of the point source method in Luke (2004); Lines and Chandler-Wilde (2005); Luke and Potthast (2006) as well as the time-domain formulation of the linear sampling method (Chen et al., 2010) which, by making reference to the space-time Sobolev spaces of order four, voids the need to use the Fourier transform and thus to deal with associated causality issues. What largely remains unclear, however, is the role of the eigenvalues of the germane interior problem (defined over the support of a hidden scatterer) toward the performance of point-probing methods in situations where the former are traversed by a given frequency sweep or the Fourier spectrum of a prescribed transient signal. So far, the only light in this direction was shed in Luke and Potthast (2006) who demonstrated that the regularized solution density, affiliated with the point source method, is uniformly bounded with respect to the wavenumber over compact subsets of the real axis.

To help bridge the gap, this study focuses on the multi-frequency reconstruction of Dirichlet and pen- etrable obstacles via the linear sampling method entailing either far-field or near-field observations of the scattered field. On assuming that the (monochromatic) sampling equation is solved over a compact con- nected set of real-valued excitation frequencies ω, two possible choices for a cumulative, multi-frequency indicator function of the scatterer's support are considered. In the first proposition, the indicator func- tion is taken as a reciprocal space-frequency L^2-norm of the featured solution density. Upon subtle modification this "serial" construct is shown, via the use of Plancherel identity and hypothesis that the observations of the scattered field extend toward zero frequency, to be identifiable with the corresponding time-domain indicator function. To furnish an alternative, a "parallel" indicator function is also proposed as an L^2-norm, in the frequency domain, of its monochromatic counterpart. For a close examination of the utility of the proposed indicators in a generic multi-frequency environment, the developments are complemented by a perturbation analysis of the relevant interior problem, which demonstrates that the featured (linear sampling) solution density behaves as $O(|\omega - \omega_*|^{-m})$, $m \geqslant 1$ in the neighborhood of a characteristic frequency ω_* which corresponds to an isolated eigenvalue of the interior problem. This result in turn exposes the robustness of the "parallel" indicator, and futility of its "serial" compan- ion in situations when the prescribed frequency sweep traverses at least one such ω_* – a finding that is highlighted by the fact that the support of an obstacle, and thus its (Dirichlet or transmission) eigenval-

ues, are unknown beforehand. A set of numerical results, assuming far-field scattering by Dirichlet and penetrable obstacles, is included to illustrate the analytical findings.

3.2 Preliminaries

Scattering by Dirichlet obstacle. Consider the time-harmonic scattering of scalar waves by a sound-soft obstacle D in an otherwise homogeneous unbounded medium $\mathbb{R}^3$, endowed with sound speed c_o (not necessarily real-valued), due to *either* set of incident fields

$$u = \begin{cases} e^{\mathrm{i}k\boldsymbol{\xi}\cdot\boldsymbol{\delta}}, & \boldsymbol{\delta} \in \Sigma \quad \text{(plane waves)}, \\ G(\boldsymbol{\xi}, \boldsymbol{\zeta}, k), & \boldsymbol{\zeta} \in S_s \quad \text{(point sources)}. \end{cases} \tag{3.2.1}$$

Here $k = \omega/c_\mathrm{o}$ is the wavenumber; ω denotes the frequency of excitation;

$$G(\boldsymbol{\xi}, \boldsymbol{\zeta}, k) = \frac{1}{4\pi} \frac{e^{\mathrm{i}k|\boldsymbol{\xi}-\boldsymbol{\zeta}|}}{|\boldsymbol{\xi} - \boldsymbol{\zeta}|}, \qquad \boldsymbol{\xi} \neq \boldsymbol{\zeta}$$

is the radiating fundamental solution of the Helmholtz equation; Σ is the unit sphere centered at the origin; S_s is a suitable surface containing the point sources used to illuminate the obstacle, and c_o is such that its real and imaginary parts are respectively $\mathcal{R}(c_\mathrm{o}) > 0$ and $\mathcal{I}(c_\mathrm{o}) \leqslant 0$. The support of D is assumed to be such that $\mathbb{R}^3 \setminus \overline{D}$ is connected, and that ∂D is of Lipschitz type. With such premises the direct scattering problem can be written as

$$\begin{aligned} \Delta v + k^2 v = 0 & \quad \text{in} \quad \mathbb{R}^3 \setminus \overline{D}, \\ v = -u & \quad \text{on} \quad \partial D, \\ \lim_{|\boldsymbol{\xi}|\to\infty} |\boldsymbol{\xi}| \left(\frac{\partial v}{\partial |\boldsymbol{\xi}|} - \mathrm{i}kv \right) = 0, & \end{aligned} \tag{3.2.2}$$

where the Sommerfeld radiation condition holds uniformly with respect to $\hat{\boldsymbol{\xi}} = \boldsymbol{\xi}/|\boldsymbol{\xi}|$. It is well known (Colton and Kress, 1992) that (3.2.2) permits a unique solution $v \in H^1_{\mathrm{loc}}(\mathbb{R}^3 \setminus \overline{D})$, see McLean (2000) for Lipschitz domains, where the field equation and the boundary condition are interpreted respectively in the sense of distributions and the sense of the trace.

Scattering by penetrable obstacle. As a canonical example of the scattering by a penetrable obstacle, consider next the case where D is characterized by a spatially-varying sound speed $c(\boldsymbol{\xi})$ and associated index of refraction, $n(\boldsymbol{\xi}) = (c_\mathrm{o}/c)^2$, such that i) $\mathcal{R}(c) > c_D > 0$ and $\mathcal{I}(c) \leqslant 0$ where c_D is a constant; ii) $n \in L_\infty(D)$, and iii) $\boldsymbol{\nabla}n$ is sufficiently small so that it can be omitted from the field equation. For simplicity of exposition, an additional hypothesis is made that the mass density of the system, ρ, is constant throughout (this restriction can however be relaxed, see Remark 12). On retaining the hypotheses on the geometry of D as in the sound-soft case, the relevant scattering problem can be written as

$$\begin{aligned} \Delta v + k^2 v = 0 & \quad \text{in} \quad \mathbb{R}^3 \setminus \overline{D}, \\ \Delta w + k^2 n\, w = 0 & \quad \text{in} \quad D, \\ w - v = u, \quad w,_{\boldsymbol{n}} - v,_{\boldsymbol{n}} = u,_{\boldsymbol{n}} & \quad \text{on} \quad \partial D, \\ \lim_{|\boldsymbol{\xi}|\to\infty} |\boldsymbol{\xi}| \left(\frac{\partial v}{\partial |\boldsymbol{\xi}|} - \mathrm{i}kv \right) = 0, & \end{aligned} \tag{3.2.3}$$

where $v_{,\boldsymbol{n}} = \boldsymbol{\nabla} v \cdot \boldsymbol{n}$, and $\boldsymbol{n}$ is the normal on ∂D (defined almost everywhere) oriented toward the exterior of D. Similar to the case of scattering by a Dirichlet obstacle, it is known (Colton and Kress, 1992) that (3.2.3) permits a unique solution $(v, w) \in H^1_{\text{loc}}(\mathbb{R}^3 \setminus \overline{D}) \times H^1(D)$.

By way of Green's theorem, it can be shown (Colton and Kress, 1992; McLean, 2000) that the scattered field v solving either (3.2.2) or (3.2.3) permits integral representation

$$v(\boldsymbol{x}, \bullet) = \int_{\partial D} \Big(v(\boldsymbol{\xi}, \bullet) G_{,\boldsymbol{n}}(\boldsymbol{x}, \boldsymbol{\xi}, k) - v_{,\boldsymbol{n}}(\boldsymbol{\xi}, \bullet) G(\boldsymbol{x}, \boldsymbol{\xi}, k) \Big) \, \mathrm{d}S_{\xi}, \quad \begin{cases} \bullet = \boldsymbol{\delta} \in \Sigma & \text{(plane waves)}, \\ \bullet = \boldsymbol{\zeta} \in S_s & \text{(point sources)} \end{cases}$$
(3.2.4)

which, assuming illumination by plane waves, exposes its asymptotic behavior

$$v(\boldsymbol{\xi}, \boldsymbol{\delta}) = \frac{e^{ik|\boldsymbol{\xi}|}}{|\boldsymbol{\xi}|} v_\infty(\hat{\boldsymbol{\xi}}, \boldsymbol{\delta}) + O\left(|\boldsymbol{\xi}|^{-2}\right) \qquad \text{as} \quad |\boldsymbol{\xi}| \to \infty,$$
(3.2.5)

where

$$v_\infty(\hat{\boldsymbol{x}}, \boldsymbol{\delta}) = \int_{\partial D} \Big(v(\boldsymbol{\xi}, \boldsymbol{\delta})(e^{-ik\hat{\boldsymbol{x}}\cdot\boldsymbol{\xi}})_{,\boldsymbol{n}} - v_{,\boldsymbol{n}}(\boldsymbol{\xi}, \boldsymbol{\delta}) e^{-ik\hat{\boldsymbol{x}}\cdot\boldsymbol{\xi}} \Big) \, \mathrm{d}S_{\xi}$$
(3.2.6)

is the so-called far-field pattern of the scattered field (Colton and Kress, 1992).

3.3 Inverse scattering via the linear sampling method

With reference to the direct scattering framework established earlier, the goal is to reconstruct the support D of a hidden obstacle on the basis of available information on the scattered field, synthesized via v_∞ or v, for multiple incident fields. Depending on the character and nature of such data, however, it is useful to distinguish between the "far-field" and "near-field" inverse scattering problems as described in the sequel. For the remainder of this section it is assumed, following the usual treatment (Colton and Kress, 1992; Colton et al., 2000), that the data are available at a single excitation frequency, ω, such that k^2 is not a *Dirichlet eigenvalue* (Colton and Kress, 1992) for the bounded domain D when dealing with sound-soft obstacles, nor a *transmission eigenvalue* (Rynne and Sleeman, 1991; Colton et al., 2007) for D when dealing with penetrable scatterers.

Far-field observations. For this configuration, it is for simplicity assumed that the far-field pattern v_∞ is known for every direction of observation and every direction of plane-wave incidence, i.e. that the data are given by $v_\infty(\hat{\boldsymbol{\xi}}, \boldsymbol{\delta})$ for $\hat{\boldsymbol{\xi}}, \boldsymbol{\delta} \in \Sigma$ (the reader is referred to Cakoni and Colton (2003a) for an account of the limited-aperture case). In this setting, the linear sampling method revolves around the equation of the first kind

$$(Fg_{\boldsymbol{z}})(\hat{\boldsymbol{\xi}}) = G_\infty(\hat{\boldsymbol{\xi}}, \boldsymbol{z}, k), \qquad \hat{\boldsymbol{\xi}} \in \Sigma,$$
(3.3.1)

where $F : L^2(\Sigma) \to L^2(\Sigma)$ is the so-called far-field operator given by

$$(Fg)(\hat{\boldsymbol{\xi}}) := \int_\Sigma v_\infty(\hat{\boldsymbol{\xi}}, \boldsymbol{\delta}) \, g(\boldsymbol{\delta}) \, \mathrm{d}S_\delta;$$
(3.3.2)

$g_{\boldsymbol{z}}$ is the solution density used to construct an indicator function; $\boldsymbol{z}$ denotes the sampling point, and G_∞ is the far-field pattern of G, namely

$$G_\infty(\hat{\boldsymbol{\xi}}, \boldsymbol{z}, k) = \frac{1}{4\pi} e^{-ik\hat{\boldsymbol{\xi}}\cdot\boldsymbol{z}}, \qquad G(\boldsymbol{\xi}, \boldsymbol{z}, k) = \frac{e^{ik|\boldsymbol{\xi}|}}{|\boldsymbol{\xi}|} G_\infty(\hat{\boldsymbol{\xi}}, \boldsymbol{z}, k) + O\left(|\boldsymbol{\xi}|^{-2}\right) \quad \text{as} \quad |\boldsymbol{\xi}| \to \infty. \text{ (3.3.3)}$$

With such premises, it can be shown (Cakoni and Colton, 2003c; Kirsch and Grinberg, 2008) that

- If $z \in D$ then for every $\varepsilon > 0$, there exists a solution $g_z^\varepsilon \in L^2(\Sigma)$ of (3.3.1) such that

$$\| F g_z^\varepsilon(\cdot) - G_\infty(\cdot, z, k) \|_{L^2(\Sigma)} < \varepsilon; \tag{3.3.4}$$

- When $z \in D$, one further has

$$\lim_{z \to \partial D} \| g_z^\varepsilon \|_{L^2(\Sigma)} \to \infty, \qquad \lim_{z \to \partial D} \| u_{g_z^\varepsilon} \|_X \to \infty,$$

where

$$u_g(\boldsymbol{\xi}) := \int_\Sigma e^{ik\boldsymbol{\xi}\cdot\boldsymbol{\delta}} \, g(\boldsymbol{\delta}) \, \mathrm{d}S_\delta \tag{3.3.5}$$

is the Herglotz wave function with kernel g, and

- When $z \in \mathbb{R}^3 \setminus \overline{D}$, then for every $\varepsilon > 0$ there exists a solution $g_z^\varepsilon \in L^2(\Sigma)$ such that

$$\| F g_z^\varepsilon(\cdot) - G_\infty(\cdot, z, k) \|_{L^2(\Sigma)} < \varepsilon$$

and

$$\lim_{\varepsilon \to 0} \| g_z^\varepsilon \|_{L^2(\Sigma)} \to \infty, \qquad \lim_{\varepsilon \to 0} \| u_{g_z^\varepsilon} \|_X \to \infty$$

where $X := H^1(D)$ when considering (3.2.2), and $X := L^2(D)$ when considering (3.2.3).
With the above result in place, D can be reconstructed by employing a suitable regularization technique to solve the far-field equation $F g_z = G_\infty(\cdot, z, k)$ over an appropriate grid of sampling points, and using $\Pi(z) := 1 / \| g_z \|_{L^2(\Sigma)}$ as a characteristic function of the support of the scatterer.
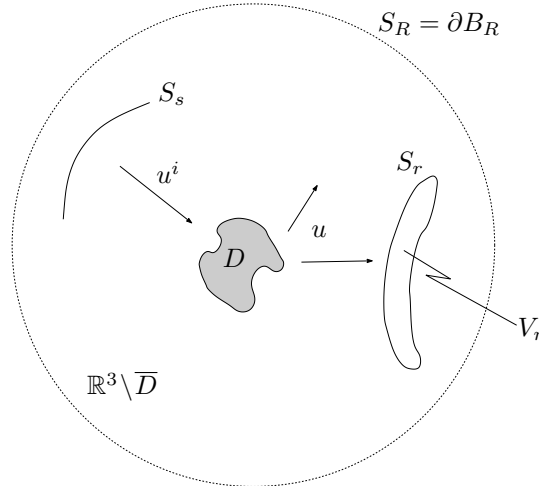
Figure 3.1: *Near-field scattering configuration.*

Near-field observations. In this case it is assumed that the obstacle is illuminated using point sources located on the source surface S_s, while the scattered field is monitored over a (union of) *closed* C^1 surface(s) S_r, see Fig. 3.1. Accordingly the data is given by $v(\boldsymbol{\xi}, \boldsymbol{\zeta})$ for $\boldsymbol{\xi} \in S_r$ and $\boldsymbol{\zeta} \in S_s$. Hereon it is assumed that $S_s \cap D = \emptyset$ and $S_r \cap D = \emptyset$, with no restrictions imposed on the intersection between S_s and S_r. For further reference, let V_r denote the finite domain bounded by S_r whereby $\partial V_r = S_r$. Assuming further that k^2 is not a Dirichlet eigenvalue for V_r (see Remark 10), the near-field counterpart of (3.3.1), see e.g. Colton et al. (2000), can be written as

$$(Ng_{\boldsymbol{z}})(\boldsymbol{\xi}) \;=\; G(\boldsymbol{\xi}, \boldsymbol{z}, k), \qquad \boldsymbol{\xi} \in S_r, \tag{3.3.6}$$

where $N : L^2(S_s) \to L^2(S_r)$ is the so-called near-field operator given by

$$(Ng)(\boldsymbol{\xi}) := \int_{S_s} v(\boldsymbol{\xi}, \boldsymbol{\zeta})\, g(\boldsymbol{\zeta})\, \mathrm{d}S_\zeta. \tag{3.3.7}$$

With the aforementioned restriction on k, the existence of a unique solution to the interior Dirichlet problem over V_r guarantees that, when (3.3.6) is met, sound fields $Ng_{\boldsymbol{z}}(\cdot)$ and $G(\cdot, \boldsymbol{z}, k)$ share the Cauchy data on S_r. By way of Holmgren's uniqueness theorem (Petrovskii, 1967), this result in turn helps ensure that the solution of the near-field equation (3.3.6) possesses approximation and unboundedness properties that mirror those of its far-field counterpart (see e.g. Guzina and Madyarov (2007) in the context of elastodynamics), namely

- If $\boldsymbol{z} \in D$ then for every $\varepsilon > 0$, there exists a solution $g_{\boldsymbol{z}}^\varepsilon \in L^2(S_s)$ of (3.3.6) such that

$$\| Ng_{\boldsymbol{z}}^\varepsilon(\cdot) - G(\cdot, \boldsymbol{z}, k) \|_{L^2(S_r)} < \varepsilon; \tag{3.3.8}$$

- When $\boldsymbol{z} \in D$, one additionally has

$$\lim_{\boldsymbol{z} \to \partial D} \| g_{\boldsymbol{z}}^\varepsilon \|_{L^2(S_s)} \to \infty, \qquad \lim_{\boldsymbol{z} \to \partial D} \| \mathcal{U}_{g_{\boldsymbol{z}}^\varepsilon} \|_X \to \infty,$$

  where

$$\mathcal{U}_g(\boldsymbol{\xi}) := \int_{S_s} G(\boldsymbol{\xi}, \boldsymbol{\zeta}, k)\, g(\boldsymbol{\zeta})\, \mathrm{d}S_\zeta \tag{3.3.9}$$

  is a single-layer potential with density g, and

- When $\boldsymbol{z} \in \mathbb{R}^3 \setminus (\overline{D} \cup S_s \cup S_r)$, then for every $\varepsilon > 0$ there exists a solution $g_{\boldsymbol{z}}^\varepsilon \in L^2(S_s)$ such that

$$\| Ng_{\boldsymbol{z}}^\varepsilon(\cdot) - G(\cdot, \boldsymbol{z}, k) \|_{L^2(S_r)} < \varepsilon$$

  and

$$\lim_{\varepsilon \to 0} \| g_{\boldsymbol{z}}^\varepsilon \|_{L^2(S_s)} \to \infty, \qquad \lim_{\varepsilon \to 0} \| \mathcal{U}_{g_{\boldsymbol{z}}^\varepsilon} \|_X \to \infty,$$

where $X := H^1(D)$ when considering (3.2.2), and $X := L^2(D)$ when considering (3.2.3).

Similar to the case of far-field observations, the support of D can in this case be exposed by computing a regularized solution of the near-field equation $Ng_{\boldsymbol{z}} = G(\cdot, \boldsymbol{z}, k)$ over an appropriate grid of sampling points, and deploying $\Pi(\boldsymbol{z}) := 1/\| g_{\boldsymbol{z}} \|_{L^2(S_s)}$ as a characteristic function of the support of the scatterer.

3.3.1 Relationship with the solution to the interior problem

To shed light on the denseness claims (3.3.4) and (3.3.8), let $\overline{\overline{\mathbb{H}}} = \{u \in H^1(D) : \Delta u + k^2 u = 0\}$ and $\overline{\mathbb{L}} = \{u \in L^2(D) : \Delta u + k^2 u = 0\}$ denote respectively the closures of the space of $C^2(D)$ solutions to the Helmholtz equation in D with respect to the $H^1(D)$-norm and the $L^2(D)$-norm. In what follows, the sought relationship between an approximate solution to the linear sampling equation and that of the companion interior problem will be exposed for situations featuring either Dirichlet or penetrable scatterers, and testing configurations involving either far-field or near-field observations. Owing to the fact that this relationship has so far been investigated solely on a case-specific basis (see e.g. Cakoni and Colton (2006) and references therein), the study proceeds with a unifying treatment of the problem, starting with inverse scattering by a Dirichlet obstacle in a near-field setting. Here it is particularly important to note that the ensuing estimates, while established in a time-harmonic setting, hold *uniformly* with respect to k over any closed region in the complex plane (hereon denoted by $\mathbb{C}$) – a result that provides a linchpin for the extension of the linear sampling to multi-frequency scattering configurations.

Dirichlet obstacle. First, consider the scattering by a sound-soft obstacle (3.2.2) and associated (interior) Dirichlet problem

$$
\begin{aligned}
\Delta u_{\boldsymbol{z}} + k^2 u_{\boldsymbol{z}} &= 0 && \text{in} \quad D, \\
u_{\boldsymbol{z}} + G(\cdot, \boldsymbol{z}, k) &= 0 && \text{on} \quad \partial D
\end{aligned}
\tag{3.3.10}
$$

at vibration frequency ω such that k^2 is not a Dirichlet eigenvalue for D. Under the latter assumption, it is known that (3.3.10) admits a unique solution $u_{\boldsymbol{z}} \in H^1(D)$.

As shown in Colton and Sleeman (2001), the set $\mathbb{F}_F = \{u_g|_D : g \in L^2(\Sigma)\}$ of Herglotz wave functions (3.3.5) with square-integrable kernel g is dense in $\overline{\overline{\mathbb{H}}}$ with respect to the $H^1(D)$ norm. In the context of near-field observations, the same approximation property in $\overline{\overline{\mathbb{H}}}$ can be established for the set of single-layer potentials (3.3.9) with square-integrable kernel $\mathbb{F}_N = \{\mathcal{U}_g|_D : g \in L^2(S_s)\}$. Indeed, the proof of this claim follows along the lines of Section 2.3 in Cakoni and Colton (2003a) where, for the purpose of this study, quantity "V_g" should be superseded by single-layer potential (3.3.9).

Lemma 7. *Assume that $\boldsymbol{z} \in D$, and let k be such that $|k - k_0| \leqslant r$ for some $r > 0$ and $k_0 \in \mathbb{C}$. Under such hypotheses there is a constant c_0 independent of k (but dependent on k_0 and r), such that any density $g_{\boldsymbol{z}}^\varepsilon \in L^2(S_s)$ for which the associated single-layer potential (3.3.9) approximates the unique solution of (3.3.10) as $\|\mathcal{U}_{g_{\boldsymbol{z}}^\varepsilon} - u_{\boldsymbol{z}}\|_{H^1(D)} < c_0 \varepsilon$, also satisfies the near-field inequality (3.3.8). In addition, for any $\varepsilon > 0$ there exists density $g_{\boldsymbol{z}}^\varepsilon \in L^2(S_s)$ such that $\mathcal{U}_{g_{\boldsymbol{z}}^\varepsilon}$ satisfies the prescribed $H^1(D)$ inequality.*

Proof. Let $\mathcal{B} \colon H^{1/2}(\partial D) \to L^2(S_r)$ denote the linear operator that maps functions $f \in H^{1/2}(\partial D)$ to $v|_{S_r}$, where $v \in H^1_{loc}(\mathbb{R}^3 \backslash \overline{D})$ is the unique radiating solution to the exterior Dirichlet problem with boundary data f, i.e. v satisfies (3.2.2) with $-u$ replaced by f. By virtue of the embedding of $H^{1/2}(S_r)$ in $L^2(S_r)$, the well-posedness of the exterior Dirichlet problem, Green's representation formula (3.2.4) for v, and the boundedness of the Dirichlet-to-Neumann mapping whereby $\|v_{,\boldsymbol{n}}\|_{H^{-1/2}(\partial D)} \leqslant C \|v\|_{H^{1/2}(\partial D)}$ for some $C > 0$, one finds that

$$
\|\mathcal{B}f\|_{L^2(S_r)} = \|v\|_{L^2(S_r)} \leqslant \|v\|_{H^{1/2}(S_r)} \leqslant c_1 \|f\|_{H^{1/2}(\partial D)}
\tag{3.3.11}
$$

for some $c_1 > 0$. Owing to the fact that the solution to the exterior Dirichlet problem depends continuously on k, constant c_1 can be further chosen independent of k such that (3.3.11) holds everywhere

within the ball $|k - k_0| \leqslant r$, whereby $\mathcal{B}$ is *uniformly* bounded from $H^{1/2}(\partial D)$ to $L^2(S_r)$ with respect to k in $|k - k_0| \leqslant r$. Since $(\Delta + k^2)G(\cdot, \boldsymbol{z}, k) = 0$ in $\mathbb{R}^3 \setminus \overline{D}$ for $\boldsymbol{z} \in D$, one obviously has $\mathcal{B}G(\cdot, \boldsymbol{z}, k) = G(\cdot, \boldsymbol{z}, k)|_{S_r}$. With reference to (3.3.7), on the other hand, it follows by the linearity of the problem that the near-field operator can be decomposed as $N = \mathcal{B}\mathcal{P}$, where $\mathcal{P}g := -\mathcal{U}_g|_{\partial D}$. Next, let $g_{\boldsymbol{z}}^\varepsilon \in L^2(S_s)$ be such that $\| \mathcal{U}_{g_{\boldsymbol{z}}^\varepsilon} - u_{\boldsymbol{z}} \|_{H^1(D)} < c_0 \varepsilon$. By virtue of the trace theorem and the fact that $u_{\boldsymbol{z}}$ solves (3.3.10), one has

$$\|\mathcal{P}g_{\boldsymbol{z}}^\varepsilon - G(\cdot, \boldsymbol{z}, k)\|_{H^{1/2}(\partial D)} \leqslant c_2 \|\mathcal{U}_{g_{\boldsymbol{z}}^\varepsilon} - u_{\boldsymbol{z}}\|_{H^1(D)},$$

where c_2 is independent of k. Thus

$$
\begin{aligned}
\| N g_{\boldsymbol{z}}^\varepsilon(\cdot) - G(\cdot, \boldsymbol{z}, k) \|_{L^2(S_r)} &= \| \mathcal{B}\mathcal{P}g_{\boldsymbol{z}}^\varepsilon - \mathcal{B}G(\cdot, \boldsymbol{z}, k) \|_{L^2(S_r)} \\
&= \| \mathcal{B}(\mathcal{P}g_{\boldsymbol{z}}^\varepsilon - G(\cdot, \boldsymbol{z}, k)) \|_{L^2(S_r)} \leqslant c_1 \|\mathcal{P}g_{\boldsymbol{z}}^\varepsilon - G(\cdot, \boldsymbol{z}, k)\|_{H^{1/2}(\partial D)} \leqslant c_1 c_2 c_0\, \varepsilon \quad (3.3.12)
\end{aligned}
$$

and, by taking $0 < c_0 < (c_1 c_2)^{-1}$,

$$\| N g_{\boldsymbol{z}}^\varepsilon(\cdot) - G(\cdot, \boldsymbol{z}, k) \|_{L^2(S_r)} < \ \varepsilon.$$

By the denseness property of $\mathbb{F}_N$ in $\overline{\mathbb{H}}$ stipulated earlier, for any $c_0 \varepsilon > 0$ and $u_{\boldsymbol{z}} \in \overline{\mathbb{H}}$ there is a single-layer potential (3.3.9) with density $g_{\boldsymbol{z}}^\varepsilon \in L^2(S_s)$ such that

$$\|\mathcal{U}_{g_{\boldsymbol{z}}^\varepsilon} - u_{\boldsymbol{z}}\|_{H^1(D)} < c_0 \varepsilon,$$

which establishes the claim of the lemma. $\qquad\qquad\square$

Lemma 8. *Let $\boldsymbol{z} \in D$, and let k be such that $|k - k_0| \leqslant r$ for some $r > 0$ and $k_0 \in \mathbb{C}$. With such premises there exists constant c_0 independent of k (but dependent on k_0 and r), such that any density $g_{\boldsymbol{z}}^\varepsilon \in L^2(\Sigma)$ for which the affiliated Herglotz wave function (3.3.5) approximates the unique solution of (3.3.10) as $\| u_{g_{\boldsymbol{z}}^\varepsilon} - u_{\boldsymbol{z}} \|_{H^1(D)} < c_0 \varepsilon$, also satisfies the <u>far-field</u> inequality (3.3.4). Further, for any $c_0 \varepsilon > 0$ there is density $g_{\boldsymbol{z}}^\varepsilon \in L^2(\Sigma)$ such that $u_{g_{\boldsymbol{z}}^\varepsilon}$ satisfies the postulated $H^1(D)$ inequality.*

Proof. Here the proof mirrors that of Lemma 7, provided that i) $\mathcal{B} : H^{1/2}(\partial D) \rightarrow L^2(\Sigma)$ maps any $f \in H^{1/2}(\partial D)$ to the far-field pattern (v_∞) of the radiating solution v to the exterior Dirichlet problem with boundary data f, ii) the near-field operator N is superseded by its far-field counterpart $F : L^2(\Sigma) \rightarrow L^2(\Sigma)$, and iii) linear operator $\mathcal{P}g := -\mathcal{U}_g|_{\partial D}$ is replaced by $\mathcal{H}g := -u_g|_{\partial D}$ where u_g is given by (3.3.5). $\qquad\square$

Penetrable obstacle. In the case of scattering by a penetrable obstacle, the relevant interior problem is the so-called *interior transmission problem* (Colton et al., 2007)

$$
\begin{aligned}
\Delta u_{\boldsymbol{z}} + k^2 u_{\boldsymbol{z}} &= 0 && \text{in} \quad D, \\
\Delta w_{\boldsymbol{z}} + k^2 n\, w_{\boldsymbol{z}} &= 0 && \text{in} \quad D, \\
w_{\boldsymbol{z}} - u_{\boldsymbol{z}} &= G(\cdot, \boldsymbol{z}, k) && \text{on} \quad \partial D, \\
(w_{\boldsymbol{z}})_{,\boldsymbol{n}} - (u_{\boldsymbol{z}})_{,\boldsymbol{n}} &= G_{,\boldsymbol{n}}(\cdot, \boldsymbol{z}, k) && \text{on} \quad \partial D
\end{aligned}
\qquad (3.3.13)
$$

which is, following earlier hypothesis, considered under the restriction that k^2 is not a transmission eigenvalue for D (Cakoni et al., 2010d) – defined as the value of k^2 for which the homogeneous counterpart of (3.3.13) permits non-trivial solution. Under such limitation, (3.3.13) permits a unique solution (u_z, w_z) understood in the sense of distributions, such that $u_z \in L^2(D)$, $w_z \in L^2(D)$, and $w_z - u_z \in H^2(D)$, see Rynne and Sleeman (1991).

Owing to the $L^2(D)$-regularity of the solution to (3.3.13), it is next useful to make an appeal to the denseness of the set of Herglotz wave functions (3.3.5) with square-integrable kernel, namely $\mathbb{F}_F = \{u_g|_D : g \in L^2(\Sigma)\}$, in $\overline{\mathbb{L}}$ with respect to the $L^2(D)$ norm (Colton and Kress, 1992). In the context of near-field observations, the same approximation property in $\overline{\mathbb{L}}$ holds true for the set $\mathbb{F}_N = \{\mathcal{U}_g|_D : g \in L^2(S_s)\}$ of single-layer potentials (3.3.9) with square-integrable kernel.

To facilitate the ensuing discussion, one may recall that $(\Delta + k^2)G(\cdot, z, k) = 0$ in $\mathbb{R}^3 \setminus \overline{D}$ for $z \in D$ which, assuming that (u_z, w_z) solves (3.3.13), demonstrates that the "difference" field defined as $v_z := w_z - u_z$ in D and $v_z := G(\cdot, z, k)$ in $\mathbb{R}^3 \setminus \overline{D}$ solves the source problem

$$\Delta v_z + k^2 n \, v_z = k^2(1-n)u_z \quad \text{in} \quad \mathbb{R}^3,$$
$$\lim_{|\boldsymbol{\xi}| \to \infty} |\boldsymbol{\xi}| \left(\frac{\partial v_z}{\partial |\boldsymbol{\xi}|} - \mathrm{i}kv_z \right) = 0 \tag{3.3.14}$$

assuming the continuity of v_z and $(v_z)_{,n}$ across ∂D (note that $n = 1$ outside D). By writing (3.3.14) in the form of a Lippmann-Schwinger equation and slightly modifying the argument in Colton and Kress (1992), p. 215, to accommodate for the $L^\infty(D)$ index of refraction $n(\boldsymbol{\xi})$, one easily sees that the unique solution v_z of (3.3.14) satisfies the a priori estimate $\|v_z\|_{H^2(B_R)} \leqslant c\|u_z\|_{L^2(D)}$, where B_R is a ball of radius R containing D.

Lemma 9. *Assume that $z \in D$, and let k be such that $|k - k_0| \leqslant r$ for some $r > 0$ and $k_0 \in \mathbb{C}$. Under such restrictions there is a constant c_0 independent of k (but dependent on k_0 and r), such that any density $g_z^\varepsilon \in L^2(\Sigma)$ for which the affiliated Herglotz wave function (3.3.5) approximates component u_z of the unique solution (u_z, w_z) to (3.3.13) as $\|u_{g_z^\varepsilon} - u_z\|_{L^2(D)} < c_0\varepsilon$, also satisfies the <u>far-field</u> inequality (3.3.4). Further, for any $c_0\varepsilon > 0$ there exists density $g_z^\varepsilon \in L^2(\Sigma)$ such that $u_{g_z^\varepsilon}$ meets the postulated $L^2(D)$ inequality.*

Proof. Consider the space of solutions to the Helmholtz equation $\overline{\mathbb{L}} = \{u \in L^2(D) : \Delta u + k^2 u = 0\}$ equipped with the $L^2(D)$ norm, and define the linear operator $\mathcal{B} : \overline{\mathbb{L}} \to L^2(\Sigma)$ which maps $u_z \in \overline{\mathbb{L}}$ to the far-field pattern of the radiating field v_z solving (3.3.14). From the well-posedness of the source problem (3.3.14), one concludes that $\mathcal{B}$ is uniformly bounded with respect to k in $|k - k_0| \leqslant r$, i.e. that there exists constant c_1 such that $\|\mathcal{B}u_z\|_{L^2(\Sigma)} \leqslant c_1\|u_z\|_{L^2(D)}$. By the linearity of the problem it further follows that $\mathcal{B}u_g = Fg$, where F is the far-field operator given by (3.3.2) and u_g is the Herglotz wave function with kernel g. On the basis of this result, (3.3.1) and (3.3.14), it can be shown that $\mathcal{B}u_z = G_\infty(\cdot, z, k)$ whenever u_z is such that the pair (u_z, w_z) uniquely solves (3.3.13). Now let $g_z^\varepsilon \in L^2(\Sigma)$ for which the affiliated Herglotz wave function (3.3.5) satisfies $\|u_{g_z^\varepsilon} - u_z\|_{L^2(D)} < c_0\varepsilon$. As a result, one finds by taking $0 < c_0 < 1/c_1$ (independent of k in $|k - k_0| \leqslant r$) that

$$\|Fg_z^\varepsilon - G_\infty(\cdot, z, k)\|_{L^2(\Sigma)} = \|\mathcal{B}(u_{g_z^\varepsilon} - u_z)\|_{L^2(\Sigma)} \leqslant c_1\|u_{g_z^\varepsilon} - u_z\|_{L^2(D)} \leqslant c_1 c_0 \, \varepsilon < \varepsilon. \tag{3.3.15}$$

With this result in place, the claim of the lemma is established by recalling the denseness in $\overline{\mathbb{L}}$ of the set of Herglotz wave functions (3.3.5) with density $g_z^\varepsilon \in L^2(\Sigma)$. $\qquad \square$

Lemma 10. *Let $z \in D$, and let k be such that $|k - k_0| \leqslant r$ for some $r > 0$ and $k_0 \in \mathbb{C}$. With such hypotheses there exists constant c_0 independent of k (but dependent on k_0 and r), such that any density $g_z^\varepsilon \in L^2(S_s)$ for which the affiliated single-layer potential (3.3.9) approximates component u_z of the unique solution (u_z, w_z) to (3.3.13) as $\|\mathcal{U}_{g_z^\varepsilon} - u_z\|_{L^2(D)} < c_0\varepsilon$, also satisfies the near-field inequality (3.3.8). Further, for any $c_0\varepsilon > 0$ there exists density $g_z^\varepsilon \in L^2(S_s)$ such that $\mathcal{U}_{g_z^\varepsilon}$ meets the featured $L^2(D)$ inequality.*

Proof. Let $\mathcal{B} : \overline{\mathbb{L}} \to L^2(S_r)$ denote the linear operator which maps $u_z \in \overline{\mathbb{L}}$ to $v_z|_{S_r}$, where v_z solves (3.3.14). By virtue of the trace theorem and the well-posedness of (3.3.14), it is easy to see that

$$\|\mathcal{B}u_z\|_{L^2(S_r)} \ \leqslant \ c_1\|v_z\|_{H^{3/2}(S_r)} \ \leqslant \ c_1c_2\|v_z\|_{H^2(B_R)} \ \leqslant \ c_1c_2c_3\|u_z\|_{L^2(D)}$$

where c_1, c_2 and c_3 can be chosen to be independent of k in $|k - k_0| \leqslant r$ due to the fact that the solution of (3.3.14) depends continuously on k. The rest of the proof follows that accompanying Lemma 9, and is omitted for brevity.

$\square$

3.3.2   Regularized solution

It is well known that both the far-field equation (3.3.1) and its near-field companion (3.3.6) are ill-posed, a feature that is attributed to the compactness of the respective linear operators $F : L^2(\Sigma) \to L^2(\Sigma)$ and $N : L^2(S_s) \to L^2(S_r)$. Moreover, these linear sampling equations generally do not have a solution for any sampling point z. As a result, the characteristic function of the support of a scatterer is constructed on the basis of the behavior of the Herglotz wave function (3.3.5) or single-layer potential (3.3.9), affiliated with a suitable approximate solution to these equations. In realistic situations, the kernel of F or N is further polluted by noise in the measurements which necessitates the use of regularization techniques. In the context of the linear sampling method, the key question associated with the use of any regularization scheme (e.g. Tikhonov regularization), is whether such computed solution exhibits the desired properties that make the affiliated Herglotz wave function (3.3.5) or single-layer potential (3.3.9) useful toward constructing a characteristic function of the support of a scatterer. This question was affirmatively answered in Arens (2001); Arens and Lechleiter (2009) for the situations involving far-field scattering by both Dirichlet and penetrable obstacles. To date, however, the question remains open in the context of near-field scattering.

To affix specificity to the discussion, consider next the far-field equation (3.3.1) corresponding to either direct scattering problem (3.2.2) or (3.2.3). Denoting by F^δ the far-field operator corresponding to noise-polluted measurements of the scattered field where $\delta > 0$ is a measure of the noise level, one seeks a Tikhonov-regularized solution $g_{z,\delta}^\varepsilon$ of (3.3.1), defined as a unique minimizer of the Tikhonov functional

$$\|F^\delta g_{z,\delta}^\varepsilon - G_\infty(\cdot, z, k)\|_{L^2(S^2)}^2 \ + \ \varepsilon \, \|g_{z,\delta}^\varepsilon\|_{L^2(S^2)}^2, \tag{3.3.16}$$

where $\varepsilon > 0$ is known as the Tikhonov regularization parameter (Colton and Kress, 1992). In the context of (3.3.16), it is important to know whether such regularized solution adheres to the claim of Lemma 8 or Lemma 9, depending on the nature of the scatterer. To this end, let $\varepsilon(\delta)$ be a sequence of regularization parameters such that $\varepsilon(\delta) \to 0$ as $\delta \to 0$, and let $g_{z,\delta}^\varepsilon$ be the minimizer of (3.3.16) with $\varepsilon = \varepsilon(\delta)$. In Arens (2001), it was shown assuming scattering by sound-soft obstacle (3.2.2) at wavenumber k such that k^2 is not a Dirichlet eigenvalue for D, that $u_{g_{z,\delta}^\varepsilon}$, $z \in D$ converges in the $H^1(D)$-norm to the unique solution u_z of (3.3.10) as $\delta \to 0$. This argument can be carried over, verbatim, to obstacle reconstruction

involving scattering by penetrable obstacles (3.2.3) provided that $n(\boldsymbol{\xi})$ and k are both real-valued. If the latter condition is met and k^2 is not a transmission eigenvalue for D, then $u_{g_{\boldsymbol{z},\delta}^\varepsilon}$, $\boldsymbol{z} \in D$ converges in the $L^2(D)$-norm to $u_{\boldsymbol{z}}$ as $\delta \to 0$, where $u_{\boldsymbol{z}}$ is such that pair $(u_{\boldsymbol{z}}, w_{\boldsymbol{z}})$ uniquely solves (3.3.13).

In concluding this section it is noted that, even though no commensurate analysis is available for a Tikhonov-regularized solution to the near-field equation (3.3.6), all numerical experiments indicate that such computed solution, $g_{\boldsymbol{z},\delta}^\varepsilon$, exhibits the same properties as the "mother" approximate solution $g_{\boldsymbol{z}}^\varepsilon$ examined in Lemma 7 and Lemma 10.

3.4 Multi-frequency reconstruction

As examined earlier, the linear sampling method considers inverse scattering at a single excitation frequency, ω, such that $k^2 = \omega^2/c_o^2$ is not an eigenvalue of the germane interior (Dirichlet or transmission) problem for D. In the case of near-field observations, an additional restriction is made that k^2 is not a Dirichlet eigenvalue of region V_r bounded by the closed observation surface(s) S_r; however, this restriction can be removed through a suitable adjustment of the experimental setup, see Remark 10. Assuming that ∂D is of Lipschitz type, it can be shown (Pockels, 1892; Rynne and Sleeman, 1991; Cakoni et al., 2002; Päivärinta and Sylvester, 2008; Kirsch, 2009; Cakoni and Kirsch, 2010; Cakoni et al., 2010d) that the eigenspectrum of either Dirichlet or interior transmission problem over D is at most countable with no finite accumulation points. In particular, the results show that

- The Dirichlet eigenvalues form a countable set located on the positive real axis, $\Lambda \subset \mathbb{R}^+$ with $+\infty$ as the only accumulation point. From this fact and relationship $k^2 = \omega^2/c_o^2$, it further follows that if the background medium is sound-absorbing, i.e. $\mathcal{I}(c_o) < 0$, there are no (real-valued) excitation frequencies ω that give rise to the Dirichlet eigenvalues.

- The investigation of transmission eigenvalues is at present incomplete. To date, it is known that the transmission eigenvalues $k^2 > 0$ form a real-valued, countable set with $+\infty$ as the only accumulation point, provided that both $\mathcal{I}(c_o) = 0$ and $\mathcal{I}(c) = 0$ and either $c_o < c(\boldsymbol{\xi})$ or $c_o > c(\boldsymbol{\xi})$ almost everywhere in D (Cakoni et al., 2010d). The set of transmission eigenvalues degenerates to an empty set, $\Lambda = \emptyset$, when *either* the background medium or the obstacle are dissipative, i.e. when either $\mathcal{I}(c_o) < 0$ and $\mathcal{I}(c) = 0$, or $\mathcal{I}(c_o) = 0$ and $\mathcal{I}(c) < 0$. If both $\mathcal{I}(c_o) < 0$ and $\mathcal{I}(c) < 0$, however, particular examples indicate the existence of (real-valued) excitation frequencies ω that give rise to (complex) transmission eigenvalues k^2 (Bellis and Guzina, 2010; Cakoni et al., 2010a).

Remark 10. The Dirichlet eigenvalues corresponding to region V_r, bounded by the closed observation surface(s) S_r in the case of near-field observations, can be considered as being artificially injected into the problem. At a given testing frequency, these eigenvalues are not necessarily detrimental to the linear sampling method since it is possible to adjust S_r, and thus V_r, such that the prescribed frequency of excitation does not correspond to an eigenvalue for V_r. In the context of multi-frequency obstacle reconstruction that is of interest in this study, there are two possible ways to avoid these extraneous eigenvalues. In the first approach which assumes band-limited illumination in the frequency domain, one finds by virtue of the Faber-Krahn inequality for the first Dirichlet eigenvalue of V_r (the latter is greater than $\pi k_{01}^2/|V_r|$, where k_{01} is the first zero of the spherical Bessel function j_0), that it is possible to reduce V_r so that none of its (Dirichlet) eigenvalues are triggered by the frequencies from the prescribed bandwitdh. Alternatively, one may modify the near-field testing configuration by considering an array

of receivers located on an *open* surface taken as a part of an analytic surface S_c enclosing both D and S_r. On invoking the regularity of a solution to the homogeneous Helmholtz equation and the principle of analytic continuation, one finds that if the radiating fields Ng given by (3.3.7) and $G(\cdot, z, k)$ coincide on S_r, they will also coincide on a closed surface $S_c \supset S_r$. By making an appeal to the uniqueness of the exterior Dirichlet problem outside S_c and the analytic continuation principle, one finally concludes that $Ng = G(\cdot, z, k)$ wherever both are defined, which in turn implies all the results established in Section 3.3.

In light of Remark 10, the eigenvalues of V_r will hereon be ignored, whereby Λ should be understood as a countable set containing the relevant eigenvalues of D.

To examine the possibility and effectiveness of multi-frequency obstacle reconstruction, the ensuing study focuses on a generic situation where the scattered field due to multiple incident wavefields, synthesized via v_∞ or v, is monitored over a *frequency band*, $\omega \in F_\omega := [\omega_1, \omega_2] \subset \mathbb{R}^+$, $\omega_2 < \infty$. For clarity of exposition, all frequency-dependent quantities referred to in the sequel will have ω added to their list of arguments whereby $v(\boldsymbol{\xi}, \boldsymbol{\zeta})$ is superseded by $v(\boldsymbol{\xi}, \boldsymbol{\zeta}, \omega)$, $g_{\boldsymbol{z}}(\boldsymbol{\zeta})$ by $g_{\boldsymbol{z}}(\boldsymbol{\zeta}, \omega)$, and so on. In this setting, the multi-frequency counterparts of (3.3.1) and (3.3.6) can be postulated as

$$
\begin{aligned}
(Fg_{\boldsymbol{z}})(\hat{\boldsymbol{\xi}}, \omega) &= G_\infty(\hat{\boldsymbol{\xi}}, z, \omega/c_{\mathrm{o}}), & \hat{\boldsymbol{\xi}} \in \Sigma, & \quad \omega \in F_\omega \\
(Ng_{\boldsymbol{z}})(\boldsymbol{\xi}, \omega) &= G(\boldsymbol{\xi}, z, \omega/c_{\mathrm{o}}), & \boldsymbol{\xi} \in S_r, & \quad \omega \in F_\omega
\end{aligned}
\tag{3.4.1}
$$

where $F : L^2(\Sigma) \times L^2(F_\omega) \to L^2(\Sigma) \times L^2(F_\omega)$ and $N : L^2(S_s) \times L^2(F_\omega) \to L^2(S_r) \times L^2(F_\omega)$ are bounded linear operators such that

$$
\begin{aligned}
(Fg)(\hat{\boldsymbol{\xi}}, \omega) &:= \int_\Sigma v_\infty(\hat{\boldsymbol{\xi}}, \boldsymbol{\delta}, \omega) \, g(\boldsymbol{\delta}, \omega) \, \mathrm{d}S_\delta, \\
(Ng)(\boldsymbol{\xi}, \omega) &:= \int_{S_s} v(\boldsymbol{\xi}, \boldsymbol{\zeta}, \omega) \, g(\boldsymbol{\zeta}, \omega) \, \mathrm{d}S_\zeta.
\end{aligned}
\tag{3.4.2}
$$

For a systematic treatment of such extended inverse scattering problem, the key issues to be addressed pertain to: i) the choice of a "cumulative" indicator function that reflects the extended data set, and ii) the situation where the chosen frequency band traverses at least one interior eigenvalue, i.e. when

$$
\Lambda \cap F_{k^2} \neq \emptyset, \qquad F_{k^2} := \left\{ k^2 : k = c_{\mathrm{o}}^{-1}\left(\omega_1 + \eta(\omega_2 - \omega_1)\right), \, \eta \in [0, 1] \right\}.
$$

3.4.1 "Serial" indicator function

Perhaps the most obvious extension of the monochromatic indicator function, $\Pi(\boldsymbol{z}) = 1 / \| g_{\boldsymbol{z}} \|_{L^2(\bullet)}$, can be written as

$$
\Pi_F^{(1)}(\boldsymbol{z}) := \frac{1}{\| g_{\boldsymbol{z}} \|_{L^2(\bullet) \times L^2(F_\omega)}} = \left(\int_{\omega_1}^{\omega_2} \| g_{\boldsymbol{z}}(\cdot, \omega) \|_{L^2(\bullet)}^2 \, \mathrm{d}\omega \right)^{-1/2}, \quad \begin{cases} \bullet = \Sigma & \text{(plane waves),} \\ \bullet = S_s & \text{(point sources).} \end{cases}
\tag{3.4.3}
$$

Assuming that $\Lambda \cap F_{k^2} = \emptyset$, one finds on the basis of the results highlighted in Section 3.3 that distribution (3.4.3), similar to its monochromatic companion, becomes vanishingly small for $\boldsymbol{z} \in \mathbb{R}^3 \setminus D$ which justifies its candidacy for a characteristic function of the support of the scatterer.

Relevance to inverse scattering in the time domain. An intriguing feature of (3.4.3) resides in its appeal, upon subtle modification, to the time-domain treatment of inverse scattering via linear sampling – a proposition that is currently in its early stages (Chen et al., 2010). To investigate this possibility, it is instructive to consider an auxiliary frequency function $\mathcal{W} \in C^1(\mathbb{R})$, compactly supported over interval $[-\omega_2, \omega_2]$, and to modify (3.4.3) by setting $\omega_1 = 0$ and weighting the integrand on the right-hand side by $2|\mathcal{W}|$. Such modified indicator function can be written as

$$\Pi_{F,\mathcal{W}}^{(1)}(\boldsymbol{z}) \;=\; \left(\int_0^{\omega_2} 2|\mathcal{W}(\omega)| \, \|g_{\boldsymbol{z}}(\cdot,\omega)\|_{L^2(\bullet)}^2 \, \mathrm{d}\omega \right)^{-1/2}. \tag{3.4.4}$$

To maintain physical relevance, it is further assumed that $\mathcal{W}(-\omega) = \overline{\mathcal{W}}(\omega)$, where overbar signifies complex conjugation. As a result, the restriction of $2|\mathcal{W}|$ to $F_\omega = [0, \omega_2]$ can be interpreted as the one-sided, compactly-supported Fourier amplitude spectrum of a given wavelet, e.g. the raised cosine function (Porat, 1996).

Here it is useful to note that the scattered field $v(\boldsymbol{\xi}, \boldsymbol{\zeta}, \omega)$ and fundamental solution $G(\boldsymbol{\xi}, \boldsymbol{z}, \omega/c_0)$, together with their far-field patterns $v_\infty(\hat{\boldsymbol{\xi}}, \boldsymbol{\delta}, \omega)$ and $G_\infty(\hat{\boldsymbol{\xi}}, \boldsymbol{z}, \omega/c_0)$ in (3.4.1) and (3.4.2) permit physical interpretation as the Fourier transforms of their respective time-domain companions, $\tilde{v}(\boldsymbol{\xi}, \boldsymbol{\zeta}, t)$, $\tilde{G}(\boldsymbol{\xi}, \boldsymbol{z}, t)$, $\tilde{v}_\infty(\hat{\boldsymbol{\xi}}, \boldsymbol{\delta}, t)$ and $\tilde{G}_\infty(\hat{\boldsymbol{\xi}}, \boldsymbol{z}, t)$. Owing to the fact that the latter four quantities, which all signify relevant solutions to the wave equation, are necessarily real-valued, it follows that

$$\begin{aligned} h(\cdot,\cdot,-\omega) &= \overline{h}(\cdot,\cdot,\omega), & h &\in \{v_\infty, v\}, \\ \Phi(\cdot,\cdot,-\omega/c_0) &= \overline{\Phi}(\cdot,\cdot,\omega/c_0), & \Phi &\in \{G_\infty, G\}. \end{aligned} \tag{3.4.5}$$

On the basis of (3.4.5), the consideration and solution of (3.4.1) can, for a given data set (v_∞ or v) specified over $F_\omega = [0, \omega_2]$, be formally extended to the frequency range $[-\omega_2, \omega_2]$ such that $g_{\boldsymbol{z}}(\cdot, -\omega) = \overline{g}_{\boldsymbol{z}}(\cdot, \omega)$.

In this setting, either of (3.4.1) can be conveniently modified by extending its frequency support to $[-\omega_2, \omega_2]$, and weighting its right-hand side by $\mathcal{W}$, namely

$$\begin{aligned} (F g_{\boldsymbol{z}}^{\mathcal{W}})(\hat{\boldsymbol{\xi}}, \omega) &= \mathcal{W}(\omega) \, G_\infty(\hat{\boldsymbol{\xi}}, \boldsymbol{z}, \omega/c_0), & \hat{\boldsymbol{\xi}} &\in \Sigma, & \omega &\in [-\omega_2, \omega_2], \\ (N g_{\boldsymbol{z}}^{\mathcal{W}})(\boldsymbol{\xi}, \omega) &= \mathcal{W}(\omega) \, G(\boldsymbol{\xi}, \boldsymbol{z}, \omega/c_0), & \boldsymbol{\xi} &\in S_r, & \omega &\in [-\omega_2, \omega_2]. \end{aligned} \tag{3.4.6}$$

In situations where $\Lambda \cap \mathbb{R} = \emptyset$ i.e. when there are no interior eigenvalues on the real axis, the modified indicator function (3.4.4) accordingly carries the physical meaning of

$$\Pi_{F,\mathcal{W}}^{(1)}(\boldsymbol{z}) \;=\; \frac{1}{2\,\|g_{\boldsymbol{z}}^{\mathcal{W}}\|_{L^2(\bullet) \times L^2(F_\omega)}} \;=\; \frac{1}{\|g_{\boldsymbol{z}}^{\mathcal{W}}\|_{L^2(\bullet) \times L^2([-\omega_2,\omega_2])}} \;=\; \frac{1}{\|g_{\boldsymbol{z}}^{\mathcal{W}}\|_{L^2(\bullet) \times L^2(\mathbb{R})}}, \tag{3.4.7}$$

owing to the compact support of $\mathcal{W}$ and injectivity of F and N (Colton et al., 2000; Cakoni et al., 2002).

With the above results in place, one may take the inverse Fourier transform of (3.4.6) with respect to ω to formally arrive at a *time-domain* variant of the linear sampling method, namely

$$\begin{aligned} (\tilde{F} \tilde{g}_{\boldsymbol{z}}^{\mathcal{W}})(\hat{\boldsymbol{\xi}}, t) &= \tilde{G}_\infty^{\mathcal{W}}(\hat{\boldsymbol{\xi}}, \boldsymbol{z}, t), & \hat{\boldsymbol{\xi}} &\in \Sigma, & t &\in \mathbb{R}, \\ (\tilde{N} \tilde{g}_{\boldsymbol{z}}^{\mathcal{W}})(\boldsymbol{\xi}, t) &= \tilde{G}^{\mathcal{W}}(\boldsymbol{\xi}, \boldsymbol{z}, t), & \boldsymbol{\xi} &\in S_r, & t &\in \mathbb{R}. \end{aligned} \tag{3.4.8}$$

Here $\tilde{g}_{\boldsymbol{z}}^{\mathcal{W}}$ denotes the inverse Fourier transform of $g_{\boldsymbol{z}}^{\mathcal{W}}$; $\tilde{G}^{\mathcal{W}}(\cdot, \boldsymbol{z}, t)$ and $\tilde{G}_\infty^{\mathcal{W}}(\cdot, \boldsymbol{z}, t)$ are respectively the radiating Green's function for the wave equation in $\mathbb{R}^3$ due to "wavelet" point source $\delta(\boldsymbol{\xi} - z)\tilde{\mathcal{W}}(t)$ and its

far-field pattern, while $\tilde{F} \colon L^2(\Sigma) \times L^2(\mathbb{R}) \to L^2(\Sigma) \times L^2(\mathbb{R})$ and $\tilde{N} \colon L^2(S_s) \times L^2(\mathbb{R}) \to L^2(S_r) \times L^2(\mathbb{R})$ are the linear operators given by

$$(\tilde{F}\tilde{g})(\hat{\boldsymbol{\xi}}, t) := \int_{\Sigma} \int_{-\infty}^{t} \tilde{v}_\infty(\hat{\boldsymbol{\xi}}, \boldsymbol{\delta}, t - \tau)\, \tilde{g}(\boldsymbol{\delta}, \tau)\, \mathrm{d}\tau\, \mathrm{d}S_\delta,$$

$$(\tilde{N}\tilde{g})(\boldsymbol{\xi}, t) := \int_{S_s} \int_{-\infty}^{t} \tilde{v}(\boldsymbol{\xi}, \boldsymbol{\zeta}, t - \tau)\, \tilde{g}(\boldsymbol{\zeta}, \tau)\, \mathrm{d}\tau\, \mathrm{d}S_\zeta,$$

(3.4.9)

where e.g. $\tilde{v}(\boldsymbol{\xi}, \boldsymbol{\zeta}, t)$ is the scattered field due to u generated by an impulsive point source $\delta(\boldsymbol{\xi} - \boldsymbol{\zeta})\delta(t)$. To justify the claim of the domain and the range of $\tilde{F}$ and $\tilde{N}$, it is noted by way of the Plancherel identity and the compact frequency support of $g_z^{\mathcal{W}}$, see (3.4.7), that

$$\begin{aligned}
\| \tilde{Q}\tilde{g}_z^{\mathcal{W}} \|_{L^2(\bullet) \times L^2(\mathbb{R})} &= 2\, \| Q g_z^{\mathcal{W}} \|_{L^2(\bullet) \times L^2(F_\omega)}, &\bullet \in \{\Sigma, S_r\}, \quad Q \in \{F, N\} \\
\| \tilde{g}_z^{\mathcal{W}} \|_{L^2(\bullet) \times L^2(\mathbb{R})} &= 2\, \| g_z^{\mathcal{W}} \|_{L^2(\bullet) \times L^2(F_\omega)}, &\bullet \in \{\Sigma, S_s\}
\end{aligned}$$

(3.4.10)

where the norms on the right-hand sides are implicit to postulated frequency-domain mapping, see (3.4.9). By virtue of (3.4.7) and the second of (3.4.10), it is clear that the (weighted) *multi-frequency* indicator function (3.4.4) can be interpreted as that stemming from either of the *time-domain* linear sampling equations (3.4.8), i.e. that

$$\Pi_{F,\mathcal{W}}^{(1)}(\boldsymbol{z}) = \frac{1}{\| \tilde{g}_z^{\mathcal{W}} \|_{L^2(\bullet) \times L^2(\mathbb{R})}}.$$

It is recalled, however, that the above analogy is established under a severe limitation that $\omega_1 = 0$, i.e. that the observations of the time-harmonic scattered field are available down to zero frequency which is in practice never the case. Nonetheless, the featured example may help shed light on the relationship between the time- and frequency-domain treatments and, in situations where the featured quantities do not vary significantly over the "bottom" frequency range $[-\omega_1, \omega_1]$, augmented by suitable interpolation to establish the actual link.

3.4.2 "Parallel" indicator function

Another possible choice of a cumulative indicator function can be written as an L^2-norm of the "monochromatic" indicator over the featured frequency band, i.e.

$$\Pi_F^{(2)}(\boldsymbol{z}) := \left\| \frac{1}{\| g_z \|_{L^2(\bullet)}} \right\|_{L^2(F_\omega)} = \left(\int_{\omega_1}^{\omega_2} \| g_z(\cdot, \omega) \|_{L^2(\bullet)}^{-2}\, \mathrm{d}\omega \right)^{1/2}, \quad \begin{cases} \bullet = \Sigma & \text{(plane waves),} \\ \bullet = S_s & \text{(point sources).} \end{cases}$$

(3.4.11)

The reasoning behind proposition (3.4.11) is that of "constructive interference" where, again assuming that $\Lambda \cap F_{k^2} = \emptyset$, distributions $1/\| g_z(\cdot, \omega) \|_{L^2(S_s)}$, $\omega \in F_\omega$ reinforce each other in exposing the support of the scatterer by jointly vanishing when $\boldsymbol{z} \in \mathbb{R}^3 \backslash D$.

To ensure the robustness of the multi-frequency reconstruction scheme, however, the critical issue with both (3.4.3) and (3.4.11) is their behavior and performance in situations when $\Lambda \cap F_{k^2} \neq \emptyset$ – a possibility that cannot be discarded beforehand for the logical value of the latter inequality is, for given F_{k^2}, dependent on the geometry and nature of a hidden scatterer. Given the fact that both $\Pi_F^{(1)}$ and $\Pi_F^{(2)}$ vanish when $\boldsymbol{z} \notin D$ and $\Lambda \cap F_{k^2} = \emptyset$, of particular concern here is the situation when $\boldsymbol{z} \in D$ and F_{k^2} contains at least one eigenvalue of the relevant interior problem. Indeed, if either candidate for a cumulative indicator function necessarily vanishes in this case, such behavior would preclude its utility as a characteristic function of the support of the obstacle in a generic scattering environment.

3.4.3 Behavior of the solution in a neighborhood of an eigenvalue

To expose the utility of (band-limited) cumulative indicator functions proposed in Sections 3.4.1 and 3.4.2, it is critical to understand the behavior an approximate solution, $g_{\boldsymbol{z}}^{\varepsilon}$, to the far-field equation (3.3.1) or its near-field counterpart (3.3.6) in the *neighborhood* of a "resonant" frequency ω_*, such that $\omega_*^2/c_{\mathrm{o}}^2 = k_*^2 \in \Lambda$. In the context of far-field scattering, the first result in this direction was provided in Cakoni et al. (2010b) where it was shown that for $k^2 = k_*^2 \in \Lambda$ and almost every $\boldsymbol{z} \in D$, Herglotz wave function $u_{g_{\boldsymbol{z},\delta}}^{\varepsilon}$ (where $\varepsilon = \varepsilon(\delta)$ and $g_{\boldsymbol{z},\delta}^{\varepsilon}$ is the Tikhonov-regularized solution of (3.3.16)) becomes unbounded, when $\delta \to 0$, in the $H^1(D)$-norm considering (3.2.2), and in the $L^2(D)$-norm considering (3.2.3). A similar result can be established for the unboundedness of the near-field potential $\mathcal{U}_{g_{\boldsymbol{z}}^{\varepsilon}}$ as $\varepsilon \to 0$, where $g_{\boldsymbol{z}}^{\varepsilon}$ satisfies (3.3.8). In the context of multi-frequency indicator functions (3.4.3) and (3.4.11), however, it is necessary to examine the *blow-up rate* of the relevant solution $g_{\boldsymbol{z},\varepsilon}$ in the neighborhood of an eigenvalue $k_*^2 \in \Lambda$. Specifically, one needs to know whether $\|g_{\boldsymbol{z}}(\cdot,\omega)\|_{L^2(\bullet)}$ is square-integrable with respect to ω over a given interval $[\omega_1, \omega_2]$, containing "resonant" frequency ω_* that corresponds to an eigenvalue of the germane interior problem.

Dirichlet obstacle. Starting with the case of a sound-soft obstacle, consider the interior Dirichlet problem of finding $u_{\boldsymbol{z}} \in H^1(D)$ that satisfies (3.3.10), and let $\theta := G(\cdot, \boldsymbol{z}, k)\,\chi$ where χ is a C^∞ cutoff function equaling unity in a neighborhood of ∂D and zero in a neighborhood of $\boldsymbol{z}$. In a weak form, (3.3.10) can be written for $\varphi := u_{\boldsymbol{z}} - \theta \in H_0^1(D)$ as

$$A\varphi - k^2 B\varphi = -\ell_{\boldsymbol{z},k}, \qquad (3.4.12)$$

see e.g. Cakoni and Colton (2006), Section 5.3, where $H_0^1(D)$ denotes the Hilbert space of all $u \in H^1(D)$ such that $u = 0$ on ∂D; invertible bounded operator $A : H_0^1(D) \to H_0^1(D)$ and compact bounded operator $B : H_0^1(D) \to H_0^1(D)$ are defined, with help of the Riesz representation theorem, as

$$(A\varphi, \psi)_{H^1(D)} = \int_D \boldsymbol{\nabla}\varphi \cdot \boldsymbol{\nabla}\overline{\psi}\,\mathrm{d}V, \qquad (B\varphi, \psi)_{H^1(D)} = \int_D \varphi\,\overline{\psi}\,\mathrm{d}V, \qquad \forall\psi \in H_0^1(D),$$

and

$$(\ell_{\boldsymbol{z},k}, \psi)_{H^1(D)} = \int_D \left(\boldsymbol{\nabla}\theta \cdot \boldsymbol{\nabla}\overline{\psi} - k^2\theta\,\overline{\psi}\right)\mathrm{d}V \qquad \forall\psi \in H_0^1(D). \qquad (3.4.13)$$

For further reference, it is noted by virtue of (3.4.13) and the analyticity of $G(\cdot, \boldsymbol{z}, k)$ with respect to k that $\ell_{\boldsymbol{z},k}$ is continuous in k over any compact region in the complex plane.

Theorem 1. *Let k_*^2 be an isolated Dirichlet eigenvalue for $-\Delta$ in D, and consider $\alpha > 0$ such that the ball $\mathcal{B}_{k_*^2,\alpha} := \{k^2 : |k^2 - k_*^2| < \alpha,\ k^2 \neq k_*^2\}$ does not contain any eigenvalues other than k_*^2. Next, let $g_{\boldsymbol{z}}^{\varepsilon}$ be an approximate solution of either the far-field or the near-field equation, specified respectively in Lemma 8 and Lemma 7. Then for sufficiently small $\varepsilon > 0$ and $\alpha > 0$, and almost every $\boldsymbol{z} \in D$ one has*

$$\|u_{g_{\boldsymbol{z}}^{\varepsilon}}\|_{H^1(D)} \geqslant \frac{C_1}{|k^2 - k_*^2|} \quad and \quad \|g_{\boldsymbol{z}}^{\varepsilon}\|_{L^2(\Sigma)} \geqslant \frac{C_2}{|k^2 - k_*^2|} \quad (far\text{-}field\ observations), \qquad (3.4.14)$$

and

$$\|\mathcal{U}_{g_{\boldsymbol{z}}^{\varepsilon}}\|_{H^1(D)} \geqslant \frac{C_1}{|k^2 - k_*^2|} \quad and \quad \|g_{\boldsymbol{z}}^{\varepsilon}\|_{L^2(S_s)} \geqslant \frac{C_2}{|k^2 - k_*^2|} \quad (near\text{-}field\ observations) \qquad (3.4.15)$$

for all $k^2 \in \mathcal{B}_{k_*^2,\alpha}$, where u_g and $\mathcal{U}_g$ are given respectively by (3.3.5) and (3.3.9), while C_1 and C_2 are positive constants depending on $\boldsymbol{z}$, k_* and α, but not on k and ε.

Proof. Consider the compact self-adjoint operator $T := A^{-1/2}BA^{-1/2} : H_0^1(D) \to H_0^1(D)$, and set $\xi := 1/k^2$ (note that $A^{1/2}$ is defined via spectral decomposition since A is self-adjoint and positive definite). Obviously, $\lambda_* := 1/k_*^2$ is an isolated eigenvalue for T. To facilitate the ensuing discussion, let E_{λ_*} denote the eigenspace of T corresponding to λ_*, and let $M_{\lambda_*} \supseteq E_{\lambda_*}$ denote the *generalized* eigenspace of T associated with λ_* that is spanned by the functions $w_* \in H_0^1(D)$ for which $(T - \lambda_* I)^p w_* = 0$, $p \geqslant 1$. In this setting it can be shown (see Kato (1995), p. 180), that the resolvent $R(\xi) := (T - \xi I)^{-1}$ of compact operator T admits the Laurent series expansion

$$R(\xi) \;=\; -\frac{P}{(\xi - \lambda_*)} - \sum_{p=1}^{\infty} \frac{Q^p}{(\xi - \lambda_*)^{p+1}} + \sum_{p=0}^{\infty} (\xi - \lambda_*)^p S^{p+1} \qquad (3.4.16)$$

in a neighborhood of λ_*, where $P : H_0^1(D) \to M_{\lambda_*}$ is the orthogonal projection onto the generalized eigenspace of T corresponding to λ_*, bounded operator $Q = (T - \lambda_* I)P$ is the so-called eigen-nilpotent projection satisfying $Q = PQ = QP$, and S is a bounded operator satisfying $(T - \lambda_* I)S = I - P$ such that $SP = PS = 0$. By virtue of the compactness of T, $Q^p = 0$ for $p \geqslant m_* \geqslant 1$ where (finite integer) $m_* = \dim M_{\lambda_*}$, which reduces the principal part of the Laurent series to a finite sum. Thus, without loss of generality one can choose an orthonormal basis in M_{λ_*}. One may also note that the range of Q^{m_*-1} is contained in the eigenspace E_{λ_*} of T since $(T - \lambda_* I)Q^{m_*-1} = Q^{m_*} = 0$. If k^2 is not a Dirichlet eigenvalue for D, (3.4.12) requires that $\varphi := u_z - \theta$ satisfies $k^2(T - \xi I)A^{1/2}\varphi = A^{-1/2}\ell_{z,k}$ whereby $k^2 A^{1/2}\varphi = R(\xi)A^{-1/2}\ell_{z,k}$ i.e.

$$k^2 A^{1/2}\varphi \;=\; -\frac{PA^{-1/2}\ell_{z,k}}{(\xi - \lambda_*)} - \sum_{p=1}^{m_*-1} \frac{Q^p A^{-1/2}\ell_{z,k}}{(\xi - \lambda_*)^{p+1}} + \sum_{p=0}^{\infty} (\xi - \lambda_*)^p S^{p+1} A^{-1/2}\ell_{z,k}.$$

Thus

$$\begin{aligned}
\|k^2 A^{1/2}\varphi\| \;=\;\; &\frac{1}{(\xi - \lambda_*)^{m_*}} \left\| Q^{m_*-1} A^{-1/2}\ell_{z,k} + \sum_{p=1}^{m_*-2} (\xi - \lambda_*)^{m_*-p-1} Q^p A^{-1/2}\ell_{z,k} \right. \\
&\left. + (\xi - \lambda_*)^{m_*-1} PA^{-1/2}\ell_{z,k} - \sum_{p=0}^{\infty} (\xi - \lambda_*)^{p+m_*} S^{p+1} A^{-1/2}\ell_{z,k} \right\| \qquad (3.4.17)
\end{aligned}$$

Substituting $\xi := 1/k^2$ ($k^2 \in \mathcal{B}_{k_*^2,\alpha}$) and $\lambda_* := 1/k_*^2$ in (3.4.17), it further follows from i) the reverse triangle inequality, ii) the facts that A, Q and S are bounded operators and iii) the fact that $\ell_{z,k}$ is uniformly bounded, that for α sufficiently small

$$\|k^2 A^{1/2}\varphi\|_{H^1(D)} \;\geqslant\; \frac{|k^2 k_*^2|^{m_*}}{|k^2 - k_*^2|^{m_*}} \|Q^{m_*-1} A^{-1/2}\ell_{z,k}\|_{H^1(D)} - C_p, \qquad (3.4.18)$$

where $C_p \geqslant 0$ depends on z and k_*, but not on k. With this result in place, it suffices to show that $Q^{m_*-1} A^{-1/2}\ell_{z,k_*} \neq 0$ for almost all $z \in D$. Indeed, if this is the case then by the continuity argument one finds that $\|Q^{m_*-1} A^{-1/2}\ell_{z,k}\| \geqslant \frac{1}{2}\|Q^{m_*-1} A^{-1/2}\ell_{z,k_*}\|$ for $k^2 \in \mathcal{B}_{k_*^2,\alpha}$ and sufficiently small $\alpha > 0$, whereby

$$\|k^2 A^{1/2}\varphi\|_{H^1(D)} \;\geqslant\; \frac{|k^2 k_*^2|^{m_*}}{2|k^2 - k_*^2|^{m_*}} \|Q^{m_*-1} A^{-1/2}\ell_{z,k_*}\|_{H^1(D)} - C_p, \qquad m_* \geqslant 1. \qquad (3.4.19)$$

Now assuming the contrary i.e. that $Q^{m_*-1}A^{-1/2}\ell_{\boldsymbol{z},k_*} = 0$, one finds that $A^{-1/2}\ell_{\boldsymbol{z},k_*}$ is orthogonal to at least one eigenvector, hereon denoted by u_*, in E_{λ_*}. Owing to the fact that operator $A^{-1/2}$ is self-adjoint, this implies

$$(\ell_{\boldsymbol{z},k_*}, A^{-1/2}u_*) = 0, \quad \text{where} \quad (I - k_*^2\, A^{-1/2}BA^{-1/2})u_* = 0,$$

$$\text{i.e.} \quad A^{-1/2}(A - k_*^2 B)A^{-1/2}u_* = 0.$$

By the bijectivity of $A^{-1/2}$, this result in turn requires that $\ell_{\boldsymbol{z},k_*}$ be orthogonal to an element in the kernel of $A - k_*^2 B$, i.e. that $\ell_{\boldsymbol{z},k_*}$ is orthogonal to an eigenfunction corresponding to Dirichlet eigenvalue k_*^2. Letting ϕ_* denote this Dirichlet eigenfunction, the use of (3.4.13) and the first Green's identity demonstrates that

$$0 \;=\; (\ell_{\boldsymbol{z},k_*}, \phi_*)_{H^1(D)} = \int_D \left(\boldsymbol{\nabla}\theta \cdot \boldsymbol{\nabla}\overline{\phi}_* - k_*^2\, \theta\, \overline{\phi}_*\right)\, \mathrm{d}V \;=\; \int_{\partial D} (\overline{\phi}_*(\boldsymbol{\xi}))_{,\boldsymbol{n}}\, G(\boldsymbol{\xi}, \boldsymbol{z}, k_*)\, \mathrm{d}S_\xi,$$

for $\boldsymbol{z} \in D$. By virtue of the the symmetry of G with respect to its first two arguments, one consequently finds that

$$w(\boldsymbol{z}) := \int_{\partial D} (\overline{\phi}_*(\boldsymbol{\xi}))_{,\boldsymbol{n}}\, G(\boldsymbol{z}, \boldsymbol{\xi}, k_*)\, \mathrm{d}S_\xi = 0,$$

Since $w(\boldsymbol{z}) = 0$ for $\boldsymbol{z} \in \mathcal{Z} \subset D$ such that $\mathcal{Z}$ has nonzero measure it follows, by virtue of unique continuation applied to $w(\boldsymbol{z})$ which solves the Helmholtz equation, that $w(\boldsymbol{z}) = 0$ in D and thus $w(\boldsymbol{z}) = 0$ on ∂D by the continuity of single-layer potentials. The latter result implies that $w = 0$ in $\mathbb{R}^3 \setminus \overline{D}$ as a radiating solution to the exterior Dirichlet problem with zero boundary data, which in turn requires that $\partial\phi_*/\partial\boldsymbol{n} = 0$ on ∂D since $w = 0$ everywhere. In light of the Holmgren's uniqueness theorem and the fact that $\phi_* = 0$ on ∂D, one concludes that $\phi_* = 0$ in D which contradicts the premise that ϕ_* is an eigenfunction.

Since C_p in (3.4.18) behaves as $O(1)$ with diminishing α, (3.4.19) implies that

$$\|A^{1/2}\varphi\|_{H^1(D)} \;\geqslant\; \frac{C}{|k^2 - k_*^2|}\|Q^{m_*-1}A^{-1/2}\ell_{\boldsymbol{z},k_*}\|_{H^1(D)}$$

for $k^2 \in \mathcal{B}_{k_*^2,\alpha}$ and sufficiently small α, where C is a positive constant independent of k such that $0 < C < \frac{1}{2}|k^2 k_*^2|^{m_*}\ \forall k^2 \in \mathcal{B}_{k_*^2,\alpha}$. Since i) $A^{-1/2}$ and Q are both bounded operators; ii) $\ell_{\boldsymbol{z},k_*}$ is finite; iii) χ vanishes in a neighborhood of $\boldsymbol{z}$; and iv) $Q^{m_*-1}A^{-1/2}\ell_{\boldsymbol{z},k_*} \neq 0$, $q \geqslant 0$ for almost all $\boldsymbol{z} \in D$, the above inequality implies that

$$\|u_{\boldsymbol{z}}\|_{H^1(D)} \geqslant \left|\|\varphi\|_{H^1(D)} - \|G(\cdot, \boldsymbol{z}, k)\chi(\cdot)\|_{H^1(D)}\right| \geqslant \frac{C'}{|k^2 - k_*^2|} - C'' \geqslant \frac{C'''}{|k^2 - k_*^2|}$$

for suitably chosen constant $C''' > 0$ dependent on $\boldsymbol{z}$, k_* and α, but not on k. Next, let $g_{\boldsymbol{z}}^\varepsilon$ be the approximate solution to either the far-field or the near-field equation provided, respectively, by Lemma 8 and Lemma 7. These lemmas stipulate that the Herglotz wave function $u_{g_{\boldsymbol{z}}^\varepsilon}$ given by (3.3.5) and the single-layer potential $\mathcal{U}_{g_{\boldsymbol{z}}^\varepsilon}$ given by (3.3.9) converge to $u_{\boldsymbol{z}}$ in the $H^1(D)$ norm as $\varepsilon \to 0$ uniformly for $k^2 \in \mathcal{B}_{k_*^2,\alpha}$. Thus, for sufficiently small $\varepsilon > 0$, $u_{g_{\boldsymbol{z}}^\varepsilon}$ and $\mathcal{U}_{g_{\boldsymbol{z}}^\varepsilon}$ inherit the behavior of $u_{\boldsymbol{z}}$ i.e

$$\|u_{g_{\boldsymbol{z}}^\varepsilon}\|_{H^1(D)} \geqslant \frac{C_1'}{|k^2 - k_*^2|} \qquad \text{and} \qquad \|\mathcal{U}_{g_{\boldsymbol{z}}^\varepsilon}\|_{H^1(D)} \geqslant \frac{C_2'}{|k^2 - k_*^2|}$$

where C_1' and C_2' are positive constants independent of k and ε. With this result in place, the claim of the theorem is established by way of estimates

$$\|g_{\boldsymbol{z}}^{\varepsilon}\|_{L^2(\Sigma)} \geqslant C_1'' \|u_{g_{\boldsymbol{z}}^{\varepsilon}}\|_{H^1(D)} \geqslant \frac{C_1}{|k^2 - k_*^2|} \quad \text{and} \quad \|g_{\boldsymbol{z}}^{\varepsilon}\|_{L^2(S_c)} \geqslant C_2'' \|\varphi_{g_{\boldsymbol{z}}^{\varepsilon}}\|_{H^1(D)} \geqslant \frac{C_2}{|k^2 - k_*^2|},$$

where $C_1 = C_1' C_1''$ and $C_2 = C_2' C_2''$ are positive constants dependent on $\boldsymbol{z}$, k_* and α, but not on k and ε. $\qquad\qquad\qquad\qquad\qquad\qquad\qquad\qquad\qquad\qquad\qquad\qquad\qquad\qquad\qquad\quad\square$

Penetrable obstacle. Next, consider the interior transmission problem of finding $u_{\boldsymbol{z}} \in L^2(D)$ and $w_{\boldsymbol{z}} \in L^2(D)$ solving (3.3.13) so that $v_{\boldsymbol{z}} = w_{\boldsymbol{z}} - u_{\boldsymbol{z}} \in H^2(D)$. Analogous to the treatment of the Dirichlet problem, let $\theta := G(\cdot, \boldsymbol{z}, k)\chi$ where χ is a C^∞ cut-off function equaling unity in a neighborhood of ∂D, and vanishing in a neighborhood of $\boldsymbol{z} \in D$. To facilitate the analysis, it is hereon assumed that $n(\boldsymbol{\xi})$ is real-valued such that $n > 1 + \delta_n$ in D for some constant $\delta_n > 0$ (the case of when $n < 1 - \delta_n$ can be handled in exactly the same way). The reason for this restriction resides in the fact that the analytical framework for dealing with the transmission eigenvalue problem corresponding to complex-valued n, which entails complex eigenvalues k^2, is not yet completely developed, see e.g. Bellis and Guzina (2010); Cakoni et al. (2010a).

Following Rynne and Sleeman (1991); Cakoni et al. (2007), one can show that (3.3.13) can be written as a fourth-order equation in terms of $v_{\boldsymbol{z}} \in H^2(D)$, namely

$$\left(\Delta + k^2\right) \frac{1}{n-1} \left(\Delta + k^2 n\right) v_{\boldsymbol{z}} = 0 \qquad \text{in} \quad D, \tag{3.4.20}$$

that is accompanied by the boundary conditions $v_{\boldsymbol{z}} = G(\cdot, \boldsymbol{z}, k)$ and $(v_{\boldsymbol{z}})_{,\boldsymbol{n}} = G_{,\boldsymbol{n}}(\cdot, \boldsymbol{z}, k)$ on ∂D. In what follows, let $H_0^2(D)$ denote the Hilbert space of all $u \in H^2(D)$ such that $u = 0$ and $u_{,\boldsymbol{n}} = 0$ on ∂D. In this setting, the variational form of (3.4.20) can be written in terms of $\upsilon := v_{\boldsymbol{z}} - \theta \in H_0^2(D)$ as

$$\int_D \frac{1}{n-1}(\Delta \upsilon + k^2 n\, \upsilon)(\Delta \overline{\psi} + k^2 \overline{\psi})\,\mathrm{d}V = -\int_D \frac{1}{n-1}(\Delta \theta + k^2 n\, \theta)(\Delta \overline{\psi} + k^2 \overline{\psi})\,\mathrm{d}V \quad \forall \psi \in H_0^2(D),$$

i.e.

$$A\upsilon - k^2 B_1 \upsilon + k^4 B_2 \upsilon = -\ell_{\boldsymbol{z},k}. \tag{3.4.21}$$

Here $A : H_0^2(D) \to H_0^2(D)$ is a bounded, positive definite self-adjoint operator given by

$$(A\varphi, \psi)_{H^2(D)} = \int_D \frac{1}{n-1}\Delta \varphi\, \Delta \overline{\psi}\,\mathrm{d}V,$$

(note that the $H^2(D)$ norm of a field with zero Cauchy data on ∂D is equivalent to the $L^2(D)$ norm of its Laplacian); $B_1 : H_0^2(D) \to H_0^2(D)$ and $B_2 : H_0^2(D) \to H_0^2(D)$ are compact bounded operators such that

$$(B_1\varphi, \psi)_{H^2(D)} = -\int_D \frac{1}{n-1}\left(\Delta \varphi\, \overline{\psi} + \varphi\, \Delta \overline{\psi}\right)\,\mathrm{d}V - \int_D \varphi\, \Delta \overline{\psi}\,\mathrm{d}V,$$

$$(B_2\varphi, \psi)_{H^2(D)} = \int_D \frac{n}{n-1}\varphi\, \overline{\psi}\,\mathrm{d}V,$$

and

$$(\ell_{\boldsymbol{z},k}, \psi)_{H^2(D)} = \int_D \frac{1}{n-1}(\Delta \theta + k^2 n\, \theta)(\Delta \overline{\psi} + k^2 \overline{\psi})\,\mathrm{d}V, \quad \forall \psi \in H_0^2(D).$$

Theorem 2. *Let k_*^2 be an isolated transmission eigenvalue, and consider $\alpha > 0$ such that the ball $\mathcal{B}_{k_*^2,\alpha} := \{k^2 : |k^2 - k_*^2| < \alpha, \ k^2 \neq k_*^2\}$ does not contain any eigenvalues other than k_*^2. Further, let $g_{\boldsymbol{z}}^\varepsilon$ be the approximate solution of either the far-field or the near-field equation, specified respectively in Lemma 9 and Lemma 10. Then for sufficiently small $\varepsilon > 0$ and $\alpha > 0$, and almost every $\boldsymbol{z} \in D$ one has*

$$\|u_{g_{\boldsymbol{z}}^\varepsilon}\|_{L^2(D)} \geqslant \frac{C_1}{|k^2 - k_*^2|} \quad \text{and} \quad \|g_{\boldsymbol{z}}^\varepsilon\|_{L^2(\Sigma)} \geqslant \frac{C_2}{|k^2 - k_*^2|} \quad \text{(far-field observations)}, \qquad (3.4.22)$$

and

$$\|\mathcal{U}_{g_{\boldsymbol{z}}^\varepsilon}\|_{L^2(D)} \geqslant \frac{C_1}{|k^2 - k_*^2|} \quad \text{and} \quad \|g_{\boldsymbol{z}}^\varepsilon\|_{L^2(S_s)} \geqslant \frac{C_2}{|k^2 - k_*^2|} \quad \text{(near-field observations)} \qquad (3.4.23)$$

for all $k^2 \in \mathcal{B}_{k_*^2,\alpha}$, where u_g and $\mathcal{U}_g$ are given respectively by (3.3.5) and (3.3.9), while C_1 and C_2 are positive constants depending on $\boldsymbol{z}$, k_* and α, but not on k and ε.

Proof. Let $v_B := k^2 B_2^{1/2} v$ (note that $B_2^{1/2}$ is defined via spectral decomposition for B_2 is positive semi-definite), and let $T \colon H_0^2(D) \times H_0^2(D) \to H_0^2(D) \times H_0^2(D)$ be a compact operator given by

$$T := \begin{pmatrix} A^{-1/2}B_1 A^{-1/2} & -A^{-1/2}B_2^{1/2}A^{-1/2} \\ A^{-1/2}B_2^{1/2}A^{-1/2} & 0 \end{pmatrix}. \qquad (3.4.24)$$

In light of the relationship

$$A^{1/2}\big(I - k^2 A^{-1/2}B_1 A^{-1/2} + k^4 A^{-1/2}B_2 A^{-1/2}\big) A^{1/2} v \; = \; -\ell_{\boldsymbol{z},k},$$

(3.4.24) permits (3.4.21) to be rewritten as

$$k^2\big(T - \xi I\big) A^{1/2}\varphi \; = \; A^{-1/2} l_{\boldsymbol{z},k}, \qquad \varphi = \begin{pmatrix} v \\ v_B \end{pmatrix}, \qquad l_{\boldsymbol{z},k} = \begin{pmatrix} \ell_{\boldsymbol{z},k} \\ 0 \end{pmatrix},$$

where $\xi := 1/k^2$. This transformation allows the resolvent of (3.4.24), namely $R(\xi) = (T - \xi I)^{-1}$, to be treated in the way analogous to that in Theorem 1. As a result, one finds that

$$\|A^{1/2}\varphi\|_{H^2(D)} \; \geqslant \; \frac{C}{|k^2 - k_*^2|}\|Q^{m_*-1}A^{-1/2}l_{\boldsymbol{z},k_*}\|_{H^2(D)}$$

for $k^2 \in \mathcal{B}_{k_*^2,\alpha}$, where $0 < C < 1$ is independent of k, and $Q^{m_*-1} \colon H_0^2(D) \times H_0^2(D) \to E_{\lambda_*}$ is the projection to the eigenspace of (3.4.24) corresponding to $\lambda_* := 1/k_*^2$. Now it remains to show that $Q^{m_*-1}A^{-1/2}l_{\boldsymbol{z},k_*} \neq 0$ for almost all $\boldsymbol{z} \in D$. Again, assuming the contrary i.e. that $Q^{m_*-1}A^{-1/2}l_{\boldsymbol{z},k_*} = 0$ over $\mathcal{Z} \subset D$ with non-zero measure for $k^2 \in \mathcal{B}_{k_*^2,\alpha}$, it follows as in Theorem 1 that $l_{\boldsymbol{z},k_*} \in H_0^2(D)$ is orthogonal to an element in the kernel of $A - k_*^2 B_1 + k_*^4 B_2$ which is a transmission eigenfunction corresponding to λ_*. On letting ϕ_* denote this eigenfunction, one has

$$0 \; = \; (l_{\boldsymbol{z},k_*}, \phi_*)_{H^2(D)} \; = \; \int_D \frac{1}{n-1}(\Delta\theta + k_*^2 n\,\theta)(\Delta\overline{\phi}_* + k_*^2\overline{\phi}_*) \; \mathrm{d}V. \qquad (3.4.25)$$

Integration of (3.4.25) by parts yields

$$\int_{\partial D} \frac{1}{n-1}(\Delta + k_*^2 n)\overline{\phi}_*(\boldsymbol{\xi})\, G_{,\boldsymbol{n}}(\boldsymbol{\xi}, \boldsymbol{z}, k_*) \; \mathrm{d}S_\xi - \int_{\partial D} \Big(\frac{1}{n-1}(\Delta + k_*^2 n)\overline{\phi}_*(\boldsymbol{\xi})\Big)_{,\boldsymbol{n}} G(\boldsymbol{\xi}, \boldsymbol{z}, k_*) \; \mathrm{d}S_\xi = 0,$$
$$(3.4.26)$$

by virtue of the definition of ϕ_* and the boundary conditions imposed on $\theta := G\chi$, where the two integrals are understood in the sense of $H^{\mp 1/2}$ resp. $H^{\mp 3/2}$ duality pairing. On setting

$$w := \frac{1}{n-1}(\Delta + k_*^2 n)\overline{\phi}_* \tag{3.4.27}$$

which satisfies the Helmholtz equation in D (recall that n is real-valued), one finds via the Green's representation theorem that

$$w(\boldsymbol{z}) = \int_{\partial D}\Big(w(\boldsymbol{\xi})\,G_{,\boldsymbol{n}}(\boldsymbol{z},\boldsymbol{\xi},k_*) - w_{,\boldsymbol{n}}(\boldsymbol{\xi})\,G(\boldsymbol{z},\boldsymbol{\xi},k_*)\Big)\,\mathrm{d}S_\xi \qquad \text{for } \boldsymbol{z}\in D. \tag{3.4.28}$$

On the basis of (3.4.26) which applies over $\mathcal{Z}\subset D$, (3.4.28), the symmetry of G with respect to its first two arguments, and the unique continuation principle, it follows that $w = 0$ in D. By virtue of (3.4.27), ϕ_* solves the Helmholtz equation in D with zero Cauchy data since $\phi_* \in H_0^2(D)$. As a result one finds, again exercising unique continuation, that $\phi_* = 0$ in D which contradicts the premise that ϕ_* is an eigenfunction. Proceeding with the proof as in the case of a Dirichlet obstacle and employing the fact that B_2 is bounded, one finds that for almost all $\boldsymbol{z}\in D$ and $|k_*^2 - k^2| < \alpha$

$$\|w_{\boldsymbol{z}} - u_{\boldsymbol{z}}\|_{H^2(D)} = \|v_{\boldsymbol{z}}\|_{H^2(D)} \geqslant \frac{C'}{|k^2 - k_*^2|},$$

for sufficiently small $\alpha > 0$ and some $C' > 0$ dependent on $\boldsymbol{z}$, k_* and α, but not on k. By making an appeal to the well-posedness of (3.3.14) as in Lemma 7, one finally obtains the estimate

$$\|u_{\boldsymbol{z}}\|_{L^2(D)} \geqslant C''\|v_{\boldsymbol{z}}\|_{H^2(D)} \geqslant \frac{C'''}{|k^2 - k_*^2|}$$

for suitably chosen $C'' > 0$ and $C''' > 0$ dependent on $\boldsymbol{z}$, k_* and α, but not on k. With this result in place, the convergence of $u_{g_{\boldsymbol{z}}^\varepsilon}$ (in the case of far-field observations) and $\mathcal{U}_{g_{\boldsymbol{z}}^\varepsilon}$ (in the case of near-field observations) to $u_{\boldsymbol{z}}$ in the $L^2(D)$-norm as $\varepsilon \to 0$, stipulated respectively in Lemma 9 and Lemma 10, completes the proof of (3.4.22) and (3.4.23) as in Theorem 1. $\qquad\square$

Remark 11. As a follow-up to the discussion in Section 3.3.2 it is noted that, in the case of far-field measurements, it is possible to extend the results of Theorem 1 and Theorem 2 to Tikhonov-regularized solution (3.3.16) of the far-field equation.

Remark 12. For penetrable obstacles, it is further feasible to remove the assumption that the mass density ρ is constant throughout the system and to consider a generalization of (3.2.3), where $\rho = \rho(\boldsymbol{\xi})$ inside the obstacle while maintaining $\rho = \rho_\mathrm{o} = \text{const.}$ in $\mathbb{R}^3\setminus\overline{D}$. For this configuration, the relevant scattering problem can be written as

$$\begin{aligned}
\Delta v + k^2 v &= 0 && \text{in} \quad \mathbb{R}^3\setminus\overline{D}, \\
\Delta w + k^2 n\, w &= 0 && \text{in} \quad D, \\
w - v = u, \quad \beta w_{,\boldsymbol{n}} - v_{,\boldsymbol{n}} &= u_{,\boldsymbol{n}} && \text{on} \quad \partial D, \\
\lim_{|\boldsymbol{\xi}|\to\infty}|\boldsymbol{\xi}|\left(\frac{\partial v}{\partial|\boldsymbol{\xi}|} - \mathrm{i}kv\right) &= 0,
\end{aligned} \tag{3.4.29}$$

where $\beta = \rho_{\mathrm{o}}/\rho$ and $\rho(\boldsymbol{\xi})$ is, similar to the hypothesis on $n(\boldsymbol{\xi})$, assumed to be "slowly" varying so that the term containing $\nabla \rho$ can be omitted from the field equation. By making reference to the existing studies of the affiliated interior transmission problem (Cakoni et al., 2002; Cakoni and Kirsch, 2010), the claims of Section 3.3.1 can be extended verbatim to this more general configuration. A commensurate extension of the results obtained in Section 3.4.3 is, however, fairly involved and entails additional assumptions on β and n employed by the analysis of the featured interior transmission problem.

Remark 13. From Theorem 1 and Theorem 2, it is clear that $\|g_{\boldsymbol{z}}^{\varepsilon}\|_{L^2(\bullet)}$, $\bullet = \Sigma, S_s$ behaves as $O(|\omega - \omega_*|^{-m})$, $m \geqslant 1$ when $\omega \to \omega_* = c_{\mathrm{o}} k_*$. As a result, the multi-frequency solution density $g_{\boldsymbol{z}}^{\varepsilon}$ featured in (3.4.3) and (3.4.11) does not belong to $L^2(\bullet) \times L^2(F_\omega)$ when the relevant interior problem over D is characterized by eigenvalues k_*^2 such that $\omega_* = c_{\mathrm{o}} k_* \in F_\omega$. In light of this result it is noted that "serial" indicator function (3.4.3), in contrast to its "parallel" companion (3.4.11), is not applicable to such configurations – a finding that is illustrated in the sequel.

3.5 Results

In what follows, an attempt at multi-frequency obstacle reconstruction via the linear sampling method is made for two sample configurations, namely that entailing far-field scattering by a unit ball in $\mathbb{R}^3$ – a problem investigated analytically, and an affiliated far-field problem for a square scatterer in $\mathbb{R}^2$ Cakoni et al. (2010c) which exposes the performance of the method in a generic computational setting. With regard to the latter example, it is noted that both the claim and the structure of the proof of Theorem 1 and Theorem 2 is independent of the dimensionality of the problem, and could be extended to scattering in $\mathbb{R}^2$ by invoking the two-dimensional counterparts of Lemmas 7-10 (see, e.g. Cakoni and Colton (2006)). For the brevity of exposition, however, the treatment of the two-dimensional case is in this study limited to a numerical example.

3.5.1 Analytical study: spherical scatterer in $\mathbb{R}^3$

To shed light on the foregoing developments, consider the scattering of plane waves by a *unit ball* D, centered at the origin so that $\partial D = \{\boldsymbol{\xi} \in \mathbb{R}^3 : |\boldsymbol{\xi}| = 1\}$. Assuming both the obstacle and the background to be non-dissipative, the remainder of this study focuses on the existence of real-valued eigenvalues characterizing the associated interior (Dirichlet or transmission) problem, and their effect on indicator functions (3.4.3) and (3.4.11), in the context of the *far-field* formulation (3.3.1) of the linear sampling method. For a unified analytical and computational treatment, the reference is hereon made to the generalized scattering problem (3.4.29) which permits the Dirichlet case (3.2.2) and penetrable case (3.2.3) to be recovered by setting respectively $\beta \to \infty$ and $\beta = 1$.

Far-field pattern. Assuming the incident field u to be in the form of a plane wave as in (3.2.1a), v and w solving (3.4.29) can be expanded over the set of spherical harmonics, $(Y_p^m)_{p \in \mathbb{N}_0, m \in \{-p, \dots, p\}}$, as

$$v(\boldsymbol{\xi}, \boldsymbol{\delta}) = \sum_{p=0}^{\infty} \sum_{m=-p}^{p} \lambda_p^m(\boldsymbol{\delta}) \, h_p(k|\boldsymbol{\xi}|) \, Y_p^m(\hat{\boldsymbol{\xi}}), \quad \boldsymbol{\xi} \in \mathbb{R}^3 \backslash D, \quad \boldsymbol{\delta} \in \Sigma,$$

$$w(\boldsymbol{\xi}, \boldsymbol{\delta}) = \sum_{p=0}^{\infty} \sum_{m=-p}^{p} \mu_p^m(\boldsymbol{\delta}) \, j_p(\gamma k|\boldsymbol{\xi}|) \, Y_p^m(\hat{\boldsymbol{\xi}}), \quad \boldsymbol{\xi} \in D, \quad \boldsymbol{\delta} \in \Sigma,$$

(3.5.1)

where $\mathbb{N}_0$ is the set of all non-negative integers; $\gamma = \sqrt{n} = c_\mathrm{o}/c$; λ_p^m and μ_p^m are, for fixed k and d, constants dependent only on their indexes, and j_p and h_p denote respectively the pth-order spherical Bessel and Hankel functions of the first kind. On employing the boundary conditions over the unit sphere ∂D and the orthonormality of spherical harmonics, the solution for the scattered field in $\mathbb{R}^3 \backslash D$ can be found as

$$v(\boldsymbol{\xi}, \boldsymbol{\delta}) = \sum_{p=0}^{\infty} \mathrm{i}^p (2p+1)\, \Theta_p(k)\, h_p(k|\boldsymbol{\xi}|)\, P_p(\hat{\boldsymbol{\xi}} \cdot \boldsymbol{\delta}), \qquad \Theta_p(k) = \frac{j_p'(k) - \alpha_p j_p(k)}{\alpha_p h_p(k) - h_p'(k)}, \qquad (3.5.2)$$

where P_p denotes the pth-order Legendre polynomial; f' is the derivative of f with respect to its argument, and

$$\alpha_p(k) \;=\; \beta \, \gamma \, \frac{j_p'(\gamma k)}{j_p(\gamma k)} \qquad\qquad (3.5.3)$$

signifies an effective admittance of surface ∂D at wavenumber k and pth spherical harmonic. Here it is noted that (3.5.2) is well behaved since the denominator $\alpha_p h_p - h_p'$ does not vanish when $k \in \mathbb{R}^+$ and $p \in \mathbb{N}_0$, see also Collino et al. (2003) for a similar argument in electromagnetism. Indeed, by assuming the contrary one finds via Nicholson's formula that

$$\alpha_p(k)|h_p(k)|^2 \;-\; h_p'(k)\overline{h_p}(k) \;=\; 0, \qquad\qquad (3.5.4)$$

which guarantees that $h_p(k) \neq 0$ for $k \in \mathbb{R}^+$. The imaginary part of (3.5.4) requires that the Wronskian $W(j_p(k), y_p(k)) = j_p(k)y_p'(k) - j_p'(k)y_p(k)$, involving spherical Bessel functions of the first and second kind, vanishes when $k \in \mathbb{R}^+$. But this cannot hold owing to the identity

$$W(j_p(k), y_p(k)) \;=\; \frac{1}{k^2}, \qquad\qquad (3.5.5)$$

see e.g. Colton and Kress (1992).

By way of (3.5.2) and Theorem 2.15 in Colton and Kress (1992), the scattered far-field pattern generated by the plane waves impinging on a unit ball centered at the origin can be computed as

$$v_\infty(\hat{\boldsymbol{\xi}}, \boldsymbol{\delta}) \;=\; \sum_{p=0}^{\infty} \frac{(2p+1)}{\mathrm{i}k}\, \Theta_p(k)\, P_p(\hat{\boldsymbol{\xi}} \cdot \boldsymbol{\delta}), \qquad\qquad (3.5.6)$$

which can be used to compute the far-field variation of a solution to both (3.2.2), by setting $\beta \to \infty$, and (3.2.3) by taking $\beta = 1$. In the former case, one in particular finds that

$$\Theta_p(k) = -\frac{j_p(k)}{h_p(k)}. \qquad\qquad (3.5.7)$$

Interior problem. As examined in Section 3.3.1, the solvability of integral equation (3.3.1) in the far-field formulation of the method hinges on the uniqueness of a solution to the corresponding interior problem. With reference to the "unifying" scattering problem (3.4.29), one can in particular show following the approach exercised earlier that the associated far-field operator $F : L^2(\Sigma) \to L^2(\Sigma)$, given by (3.3.2), is injective with dense range if and only if there does not exist a Herglotz wave function u_g

of form (3.3.5) with non-zero density $g \in L^2(\Sigma)$ such that pair (u_g, w) solves the homogeneous interior transmission problem

$$\begin{aligned}
\Delta u_g + k^2 u_g &= 0 && \text{in} \quad D, \\
\Delta w + k^2 n\, w &= 0 && \text{in} \quad D, \\
u_g = w, \quad (u_g)_{,\boldsymbol{n}} &= \beta\, w_{,\boldsymbol{n}} && \text{on} \quad \partial D.
\end{aligned} \tag{3.5.8}$$

On seeking the solution to (3.5.8) in terms of spherical harmonics

$$\begin{aligned}
u_g(\boldsymbol{\xi}) &= \sum_{p=0}^{\infty} \sum_{m=-p}^{p} u_p^m \, j_p(k|\boldsymbol{\xi}|)\, Y_p^m(\hat{\boldsymbol{\xi}}), && \boldsymbol{\xi} \in D, \\
w(\boldsymbol{\xi}) &= \sum_{p=0}^{\infty} \sum_{m=-p}^{p} w_p^m \, j_p(\gamma k|\boldsymbol{\xi}|)\, Y_p^m(\hat{\boldsymbol{\xi}}), && \boldsymbol{\xi} \in D,
\end{aligned} \tag{3.5.9}$$

and employing the Funk-Hecke formula

$$\int_{\Sigma} e^{-ik\boldsymbol{\xi}\cdot\boldsymbol{\delta}} Y_p^m(\boldsymbol{\delta})\, \mathrm{d}S_\delta = \frac{4\pi}{i^p} j_p(k|\boldsymbol{\xi}|)\, Y_p^m(\hat{\boldsymbol{\xi}}), \qquad \forall \boldsymbol{\xi} \in \mathbb{R}^3, \quad p \in \mathbb{N}_0, \quad m \in \{-p, \dots, p\},$$

one finds that u_g, as given by (3.5.9a), is indeed a Herglotz wave function in the sense of (3.3.5). With such result in place, it can next be shown by exercising the homogeneous boundary conditions over ∂D in terms of (3.5.9) that a non-trivial solution to (3.5.8) exists if and only if there are values $k \in \mathbb{R}$ such that

$$j'_{p_\star}(k) - \alpha_{p_\star}(k)\, j_{p_\star}(k) = 0, \qquad p_\star \in \mathbb{N}_0, \tag{3.5.10}$$

where $\alpha_{p_\star}$ is defined via (3.5.3). From (3.5.10), it is in particular useful to note that $\Theta_{p_\star}(k)=0$ in the context of the scattered-field solution (3.5.2). As a result, the set of transmission eigenvalues characterizing (3.5.8) can be written as

$$\Lambda = \left\{ k^2 \colon \Theta_{p_\star}(k)=0, \ p_\star \in \mathbb{N}_0 \right\}. \tag{3.5.11}$$

In the case of a Dirichlet obstacle ($\beta \to \infty$), (3.5.11) reduces to

$$\Lambda = \left\{ k^2 \colon j_{p_\star}(k)=0, \ p_\star \in \mathbb{N}_0 \right\}. \tag{3.5.12}$$

Indicator functions. With reference to (3.3.1) and spherical-harmonics expansion (3.5.6) of v_∞, the far-field pattern of the fundamental solution G can be computed as

$$G_\infty(\hat{\boldsymbol{\xi}}, \boldsymbol{z}, k) = \frac{1}{4\pi} e^{-ik\hat{\boldsymbol{\xi}}\cdot\boldsymbol{z}} = \sum_{p=0}^{\infty} \sum_{m=-p}^{p} i^{-p}\, j_p(k|\boldsymbol{z}|)\, \overline{Y_p^m}(\hat{\boldsymbol{z}})\, Y_p^m(\hat{\boldsymbol{\xi}}). \tag{3.5.13}$$

As a result the source density $g_{\boldsymbol{z}}$, solving (3.3.1) at a given sampling point $\boldsymbol{z} \in \mathbb{R}^3$, is sought in the form

$$g_{\boldsymbol{z}}(\boldsymbol{\delta}) = \sum_{p=0}^{\infty} \sum_{m=-p}^{p} g_p^m\, Y_p^m(\boldsymbol{\delta}), \qquad \boldsymbol{\delta} \in \Sigma \tag{3.5.14}$$

which, on substitution, yields

$$g_{\boldsymbol{z}}(\boldsymbol{\delta}) = \frac{k}{(4\pi)^2} \sum_{p=0}^{\infty} \frac{(2p+1)}{i^{p-1}\Theta_p(k)} j_p(k|\boldsymbol{z}|)\, P_p(\hat{\boldsymbol{z}}\cdot\boldsymbol{\delta}), \qquad \boldsymbol{\delta} \in \Sigma, \tag{3.5.15}$$

provided that the condition

$$\Theta_p(k) \neq 0, \qquad p \in \mathbb{N}_0$$

is met, i.e. that k^2 is not an eigenvalue of the interior problem (3.5.8). Unfortunately, series (3.5.15) does not belong to $L^2(\Sigma)$ for any $k \in \mathbb{R}^+$ owing to the fact that its norm is given by

$$\|g_{\boldsymbol z}\|_{L^2(\Sigma)}^2 = \frac{k^2}{(4\pi)^3} \sum_{p=0}^{\infty} \frac{(2p+1)}{|\Theta_p(k)|^2} \, j_p(k|{\boldsymbol z}|)^2, \qquad (3.5.16)$$

where the featured spherical (Bessel and Hankel) functions behave asymptotically such that

$$\frac{(2p+1)}{|\Theta_p(k)|^2} \, j_p(k|{\boldsymbol z}|)^2 = \frac{4}{k^2} \left(\frac{1+\beta}{1-\beta}\right)^2 \left(\frac{2|{\boldsymbol z}|}{e\,k}\right)^{2p} p^{2p+1} \left(1 + O(p^{-1})\right) \qquad \text{as} \quad p \to \infty, \qquad (3.5.17)$$

see e.g. Colton and Kress (1992). Indeed from (3.5.16) and (3.5.17), it is clear that

$$\|g_{\boldsymbol z}\|_{L^2(\Sigma)} = \infty, \qquad {\boldsymbol z} \in \mathbb{R}^3 \backslash \{0\}.$$

This result is not surprising since the far-field operator F is known to be compact with eigenvalues

$$\sigma_p = \frac{4\pi}{ik} \Theta_p(k), \qquad p \in \mathbb{N}_0, \qquad (3.5.18)$$

that have the asymptotic behavior

$$\sigma_p = \pi \left(\frac{1-\beta}{1+\beta}\right) \left(\frac{e\,k}{2}\right)^{2p} \frac{1}{p^{2p+1}} \left(1 + O(p^{-1})\right) \qquad \text{as} \quad p \to \infty, \qquad (3.5.19)$$

and thus accumulate at zero. The blow-off feature of $\|g_{\boldsymbol z}\|_{L^2(\Sigma)}$ in $\mathbb{R}^3 \backslash \{0\}$ can therefore be attributed to the smallest eigenvalues of the far-field operator. For practical purposes, however, this behavior can be regularized by truncating the spectrum of F "from below" at sufficiently small eigenvalues (Collino et al., 2003), i.e. by seeking a solution to the far-field equation (3.3.1) within a manifold

$$\text{span}\left(Y_p^m, \, p \in \{0, \dots, N_t\}, \, m \in \{-p, \dots, p\}\right), \qquad N_t < \infty.$$

With the above results in place, indicator functions (3.4.3) and (3.4.11), cumulative over $F_\omega = [\omega_1, \omega_2]$, can now be approximated by evaluating (3.5.16) up to truncation level N_t and employing piecewise-constant approximation of $g_{\boldsymbol z}(\cdot, \omega)$ over a discrete set of *sampling frequencies*

$$F_\omega^h = \left\{\omega_1^s, \omega_2^s, \dots \omega_{N_h}^s\right\} \subset F_\omega, \quad \omega_1^s = \omega_1, \quad \omega_{N_h}^s = \omega_2, \quad \omega_{m+1}^s - \omega_m^s = O(h) > 0, \quad m \in \{1, \dots N_h\}$$

where h is the chosen level of discretization. Accordingly, one finds that

$$\check{\Pi}_F^{(1)}({\boldsymbol z}) = (4\pi)^{3/2} \left(\sum_{k \in F_k^h} \sum_{p=0}^{N_t} \frac{(2p+1)k^2}{|\Theta_p(k)|^2} \, j_p(k|{\boldsymbol z}|)^2\right)^{-1/2} \qquad (3.5.20)$$

and

$$\check{\Pi}_F^{(2)}({\boldsymbol z}) = (4\pi)^{3/2} \left(\sum_{k \in F_k^h} \left(\sum_{p=0}^{N_t} \frac{(2p+1)k^2}{|\Theta_p(k)|^2} \, j_p(k|{\boldsymbol z}|)^2\right)^{-1}\right)^{1/2}, \qquad (3.5.21)$$

where $\check{\Pi}$ is a regularized approximation of Π, and $F_k^h = c_{\mathrm{o}}^{-1} F_\omega^h$. To facilitate the ensuing discussion, one may also introduce an auxiliary indicator function

$$\lambda_{N_t}(k) \;=\; \sum_{p=0}^{N_t} \frac{1}{j_p'(k) - \alpha_p(k) j_p(k)} \tag{3.5.22}$$

which, in light of (3.5.10), has the property that $\lambda_{N_t}(k) \to \infty$ as k approaches a transmission eigenvalue associated with $p_* \leqslant N_t$.

Examples. In what follows the featured obstacle configuration, $D = \{ \boldsymbol{x} \in \mathbb{R}^3 : |\boldsymbol{\xi}| < 1 \}$, is exercised numerically to highlight the existence of interior (Dirichlet or transmission) eigenvalues, and to assess their effect on the behavior of (3.5.20) and (3.5.21). As an illustration, the results are computed assuming frequency band $F_\omega = [10c_{\mathrm{o}}, 15c_{\mathrm{o}}]$ i.e. $F_k = [10, 15]$ and truncation level $N_t = 10$, chosen such that $|\sigma_p| < 10^{-3}$, $p > N_t$ for all configurations examined, see (3.5.18). For completeness, obstacle reconstruction is effected assuming both "fine" discretization of F_k, namely

$$F_k^{h_1} := \big\{ k \colon k = 10 + m\, h_1, \; h_1 = 10^{-3}, \; m \in \{0, 1, \ldots, 5 \cdot 10^3\} \big\}, \tag{3.5.23}$$

and four "coarse" discretizations

$$\begin{aligned}
F_k^{h_2} &= \big\{ 10, 11, 12, 13, 14, 15 \big\}, \\
F_k^{h_3} &= \big\{ 10, 11, 12, 13, 14.0662, 15 \big\}, \\
F_k^{h_4} &= \big\{ 10, 11.25, 12.5, 13.75, 15 \big\}, \\
F_k^{h_5} &= \big\{ 10, 11.25, 12.5664, 13.75, 15 \big\}.
\end{aligned}$$

Fig. 3.2a shows the variation of auxiliary indicator function (3.5.22) for a Dirichlet obstacle ($\beta \to \infty$), which clearly indicates the existence of Dirichlet eigenvalues within first N_t spherical harmonic modes of the truncated solution. The spatial distribution of $\check{\Pi}_F^{(1)}$ and $\check{\Pi}_F^{(2)}$ in the $z_3 = 0$ plane, as computed from (3.5.20) and (3.5.21) assuming $F_k^{h_1}$ as a discrete set of wavenumbers over which the far-field observations $v_\infty(\hat{\boldsymbol{\xi}}, \boldsymbol{\delta})$, $\hat{\boldsymbol{\xi}}, \boldsymbol{\delta} \in \Sigma$ are available, is plotted on a normalized scale $[0, 1]$ in Fig. 3.2b and 3.2c. The featured indicator distributions, spherically symmetric due to assumed geometry of the problem, show that the "serial" indicator (3.5.20) is strongly affected by traversing the Dirichlet eigenvalues owing to its particular structure which requires that $\check{\Pi}_F^{(1)} \to 0$ uniformly in $\mathbb{R}^3$ as $\Theta_p(k) \to 0$, $p \in \{0, \ldots, N_t\}$. From (3.5.21) and Fig. 3.2c, on the other hand, it is also apparent that the far-field observations v_∞ taken at "resonant" frequencies make only a *trivial* contribution to $\check{\Pi}_F^{(2)}$, and thus do not degrade the quality of multi-frequency obstacle reconstruction when executed in terms of the latter indicator function. The above conclusions are further substantiated by the results in Fig. 3.3 which plots $\lambda_{N_t}(k)$, $\check{\Pi}_F^{(1)}(\boldsymbol{z})$ and $\check{\Pi}_F^{(2)}(\boldsymbol{z})$ for a sample penetrable-obstacle configuration, characterized by $\beta = 1$ and $\gamma = 2$. In particular, it is noted that the spatial distribution of $\check{\Pi}_F^{(1)}$ plotted in Fig. 3.3b provides no visible clues as to the support of a hidden ball.

For completeness, the above Dirichlet and penetrable obstacle are each reconstructed anew using the far-field data from two "coarse" wavenumber sets. In particular, the Dirichlet obstacle is reconstructed in Figs. 3.4 and 3.5 from the data taken respectively over $F_k^{h_2}$ and $F_k^{h_3}$, designed such that $F_{k^2}^{h_2} \cap \Lambda = \emptyset$ and $F_{k^2}^{h_3} \cap \Lambda \neq \emptyset$, where Λ signifies the set of Dirichlet eigenvalues for a unit ball with sound speed c_{o}. As can

(a) λ_{N_t}

(b) $\breve{\Pi}_F^{(1)}$

(c) $\breve{\Pi}_F^{(2)}$
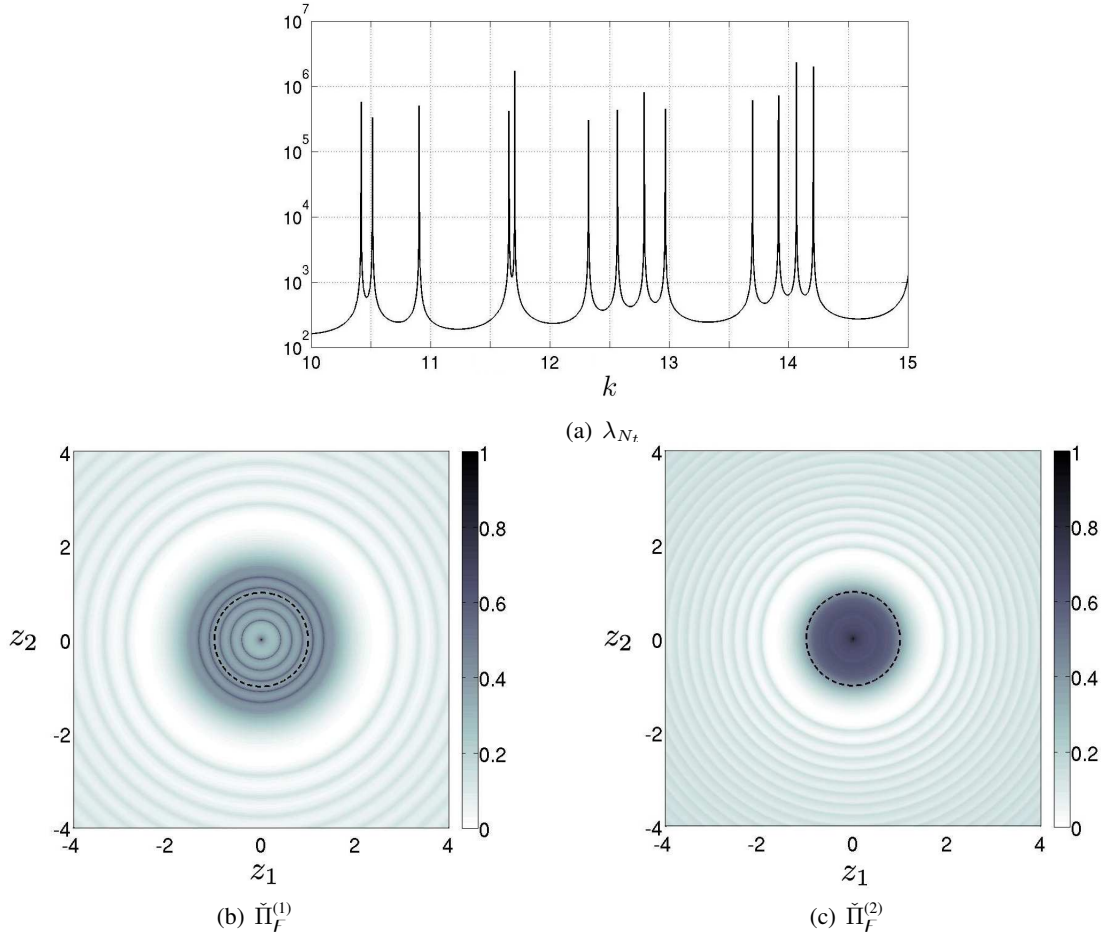
Figure 3.2: *Reconstruction of a Dirichlet obstacle $(\beta \to \infty)$ from the far-field data taken over a "fine" wavenumber set $F_k^{h_1}$.*

be seen from the display, both $\breve{\Pi}_F^{(1)}$ and $\breve{\Pi}_F^{(2)}$ (this time plotted versus $|z|$) appear to effectively reconstruct the obstacle on the basis of $F_k^{h_2}$ while, commensurate with the earlier result, only $\breve{\Pi}_F^{(1)}$ succeeds when using $F_k^{h_3}$ as the sampled set of wavenumbers. The same conclusion can be drawn from Figs. 3.6 and 3.7 which illustrate the reconstruction of a penetrable defect $(\beta = 1, \gamma = 2)$ on the basis of $F_k^{h_4}$ and $F_k^{h_5}$, chosen such that $F_{k^2}^{h_4} \cap \Lambda = \emptyset$ and $F_{k^2}^{h_5} \cap \Lambda \neq \emptyset$, where Λ denotes the germane (countable) set of transmission eigenvalues.

3.5.2 Numerical study: square obstacle in $\mathbb{R}^2$

In this section the "multitonal" indicator functions (3.4.3) and (3.4.11) are applied to the inverse scattering of planes waves by a unit square, $D = \{\boldsymbol{\xi} \in \mathbb{R}^2 : \boldsymbol{\xi} \in [-0.5, 0.5] \times [-0.5, 0.5]\}$, assuming penetrable obstacle as in (3.4.29) with $n = 4$ and $\beta = 1/4$. To this end, a discrete set of directions of plane-wave

(a) λ_{N_*}

(b) $\check{\Pi}_F^{(1)}$　　　　　　　　　　　　(c) $\check{\Pi}_F^{(2)}$
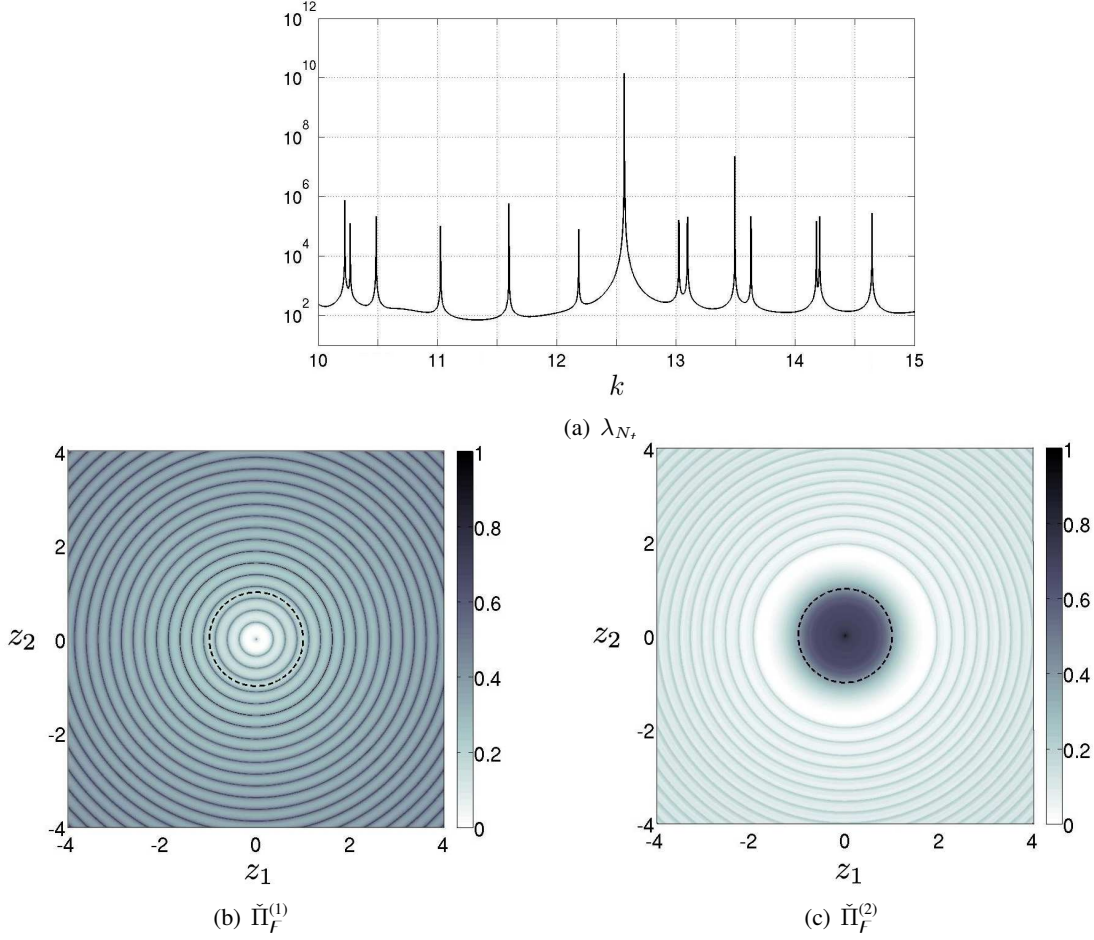
Figure 3.3: *Reconstruction of a penetrable obstacle $(\beta = 1, \gamma = 2)$ from the far-field data taken over a "fine" wavenumber set $F_k^{h_1}$.*

incidence and observation is assumed as

$$\Sigma^h := \big\{\hat{\boldsymbol{x}} = \big(\cos(2\pi mh), \sin(2\pi mh)\big),\ h = \frac{1}{M},\ m \in \{0, 1, \ldots, M-1\}\big\}, \quad M = 61.$$

By analogy to (3.5.23), a "fine" discretization of the example wavenumber band $[3, 8]$ is taken as

$$F_k^{h_6} := \big\{k : k = 3 + m\,h_6,\ h_6 = 5 \cdot 10^{-2},\ m \in \{0, 1, \ldots, 10^2\}\big\}.$$

Here it is noted that the featured interval $k^2 \in [9, 64] \subset \mathbb{R}$ contains, at least numerically, several transmission eigenvalues associated with the assumed scattering configuration in terms of D (see Cakoni et al. (2010c) for details).

For any fixed frequency $k \in F_k^{h_6}$ and sampling point $\boldsymbol{z} \in \mathbb{R}^2$, a discretized version of the *far-field* formulation (3.3.1) of the linear sampling method corresponding to $(\hat{\boldsymbol{x}}, \boldsymbol{\delta}) \in \Sigma^h$ is written in the form

$$F_h\, g_{\boldsymbol{z},h} = f_{\boldsymbol{z},h}, \tag{3.5.24}$$

where F_h is a discretized far-field operator, and $f_{\boldsymbol{z},h} = (G_\infty(\hat{\boldsymbol{x}}, \boldsymbol{z}, k))_{\hat{\boldsymbol{x}} \in \Sigma_h}$. To solve (3.5.24), the singular value decomposition of F_h is computed as $F_h = U\,S\,V^*$, where $U, V \in \mathbb{C}^{M \times M}$ are unitary
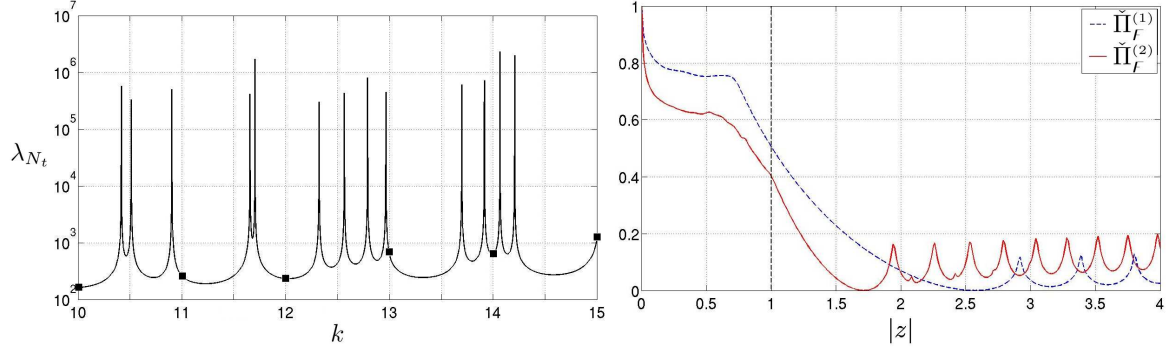
Figure 3.4: *Reconstruction of a Dirichlet obstacle $(\beta \rightarrow \infty)$ from the far-field data taken over a "coarse" wavenumber set $F_k^{h_2}$ (indicated by markers), taken such that $\Lambda \cap F_{k^2}^{h_2} = \emptyset$*
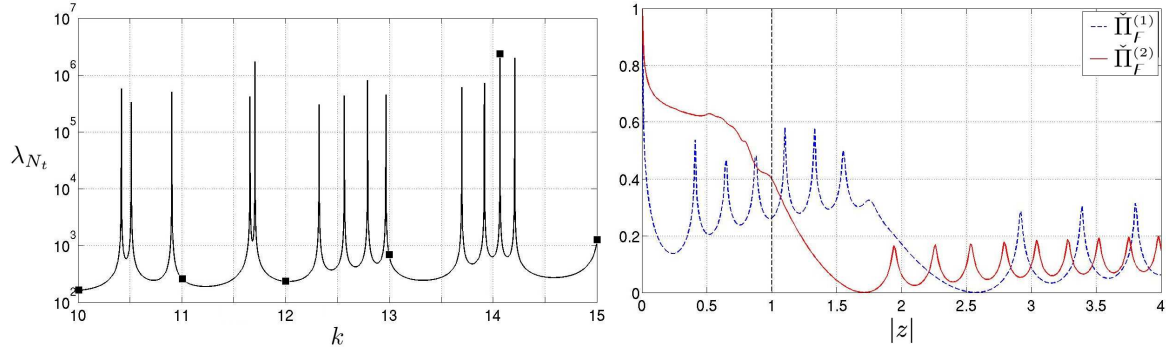
Figure 3.5: *Reconstruction of a Dirichlet obstacle $(\beta \rightarrow \infty)$ from the far-field data taken over a "coarse" wavenumber set $F_k^{h_3}$ (indicated by markers), chosen such that $\Lambda \cap F_{k^2}^{h_3} \neq \emptyset$*

matrices, V^* is the Hermitian transpose of V, and $S \in \mathbb{R}^{M \times M}$ a diagonal matrix such that $S_{jj} = \sigma_j$ is the jth singular value of F_h. With reference to (3.3.16), the norm of a Tikhonov-regularized solution $g_{\boldsymbol{z},h}^{\varepsilon}$ to (3.5.24), with regularization parameter ε, is accordingly computed as

$$\|g_{\boldsymbol{z},h}^{\varepsilon}\|_{L^2(\Sigma_h)}^2 = \sum_{j=1}^{M} \frac{\sigma_j^2}{(\sigma_j^2 + \varepsilon)^2} |(U^* f_{\boldsymbol{z},h})_j|^2. \tag{3.5.25}$$

Fig. 3.8 plots the normalized distribution of indicator functions (3.4.3) and (3.4.11), on a scale $[0, 1]$, computed by way of (3.5.25) with $\varepsilon = 10^{-4}$. Consistent with the earlier results, the two-dimensional reconstruction of a square scatterer via the "serial" indicator $\check{\Pi}_F^{(1)}$ is inferior to that obtained using its "parallel" companion $\check{\Pi}_F^{(2)}$, not only in tems of the contrast of an image, but also in terms of the reconstructed shape.
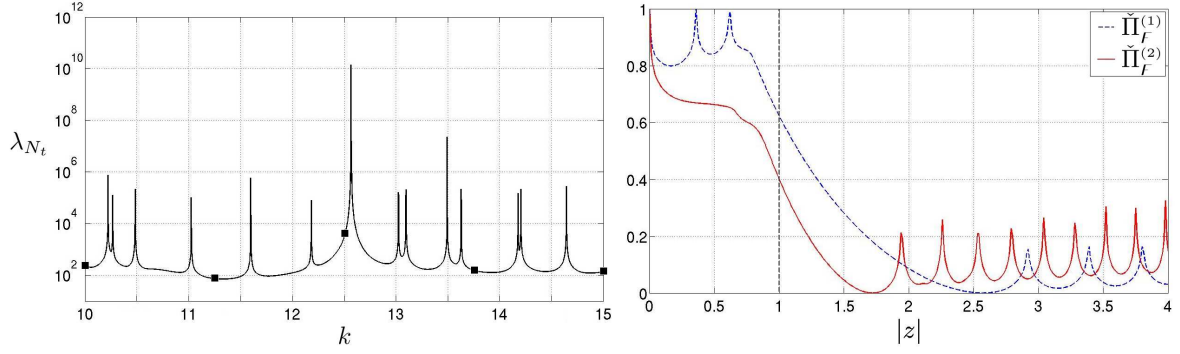
Figure 3.6: *Reconstruction of a penetrable obstacle* $(\beta = 1, \gamma = 2)$ *from the far-field data taken over a "coarse" wavenumber set* $F_k^{h_4}$ *(indicated by markers), taken such that* $\Lambda \cap F_{k^2}^{h_4} = \emptyset$.
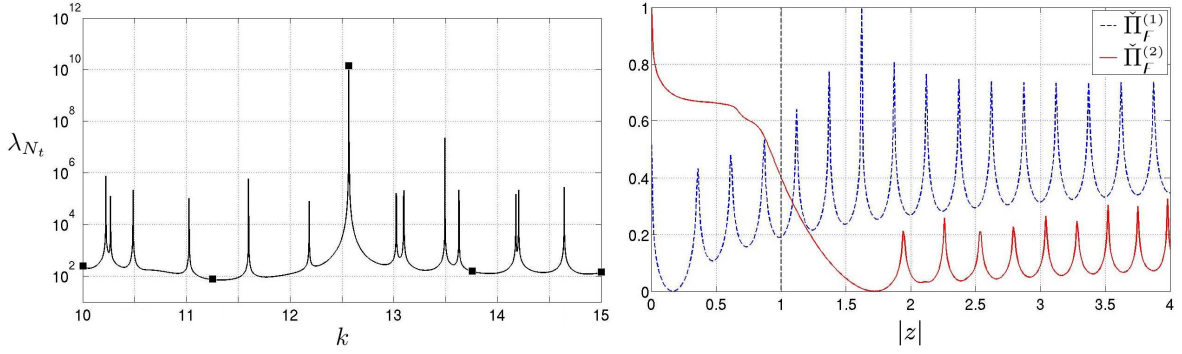
Figure 3.7: *Reconstruction of a penetrable obstacle* $(\beta = 1, \gamma = 2)$ *from the far-field data taken over a "coarse" wavenumber set* $F_k^{h_5}$ *(indicated by markers), selected such that* $\Lambda \cap F_{k^2}^{h_5} \neq \emptyset$.

(a) Normalized $\check{\Pi}_F^{(1)}$ (b) Normalized $\check{\Pi}_F^{(2)}$
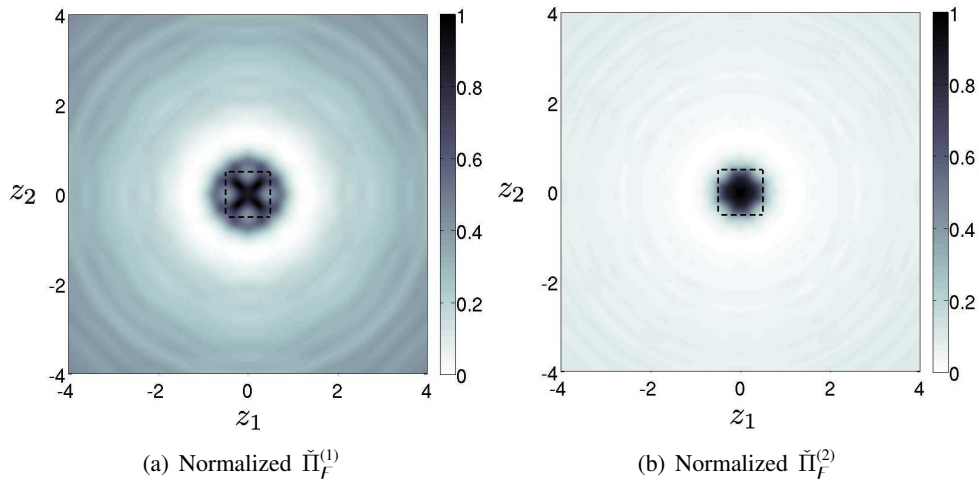
Figure 3.8: *Reconstruction of a penetrable obstacle from the far-field data taken over a "fine" wavenumber set* $F_k^{h_6}$.

3.6   Conclusions

In this study, multi-frequency reconstruction of sound-soft and penetrable obstacles is examined in the context of the linear sampling method entailing either far-field or near-field measurements. On establishing a suitable approximate solution to the linear sampling equation under the premise of continuous frequency sweep, two possible choices for a cumulative multi-frequency indicator function of the scatterer's support are proposed. The first alternative, termed the "serial" indicator, is taken as a natural extension of its customary monochromatic counterpart in the sense that its computation entails *space-frequency* (as opposed to space) L^2-norm of a solution to the linear sampling equation. Under certain assumptions which include experimental observations down to zero frequency and compact frequency support of the wavelet used to illuminate the obstacle, this indicator function is further related to its time-domain companion. As a second possibility, the so-called "parallel" indicator is proposed as an L^2-norm, in the frequency domain, of the monochromatic indicator function. On the basis of the perturbation analysis which demonstrates that the monochromatic solution of the linear sampling equation behaves as $O(|k^2 - k_*^2|^{-m})$, $m \geqslant 1$ in the neighborhood of an isolated eigenvalue, k_*^2, of the associated interior (Dirichlet or transmission) problem, it is found that the "serial" indicator is unable to distinguish the interior from the exterior of a scatterer in situations when the prescribed frequency band traverses at least one such eigenvalue. In contrast the "parallel" indicator is, due to its particular structure, shown to be insensitive to the presence of pertinent interior eigenvalues (which typically form a countable set – unknown beforehand), and thus to be robust in a generic scattering environment. A set of numerical results, including both "fine" and "coarse" frequency sampling, is included to illustrate the performance of the competing (multi-frequency) indicator functions, demonstrating behavior that is consistent with the theoretical results.

Chapter 4

On the well-posedness of the visco-elastic interior transmission problem

Contents

4.1   Introduction

In the context of penetrable scatterers (e.g. elastic inclusions within the framework of mechanical waves), the *linear sampling method* and the *factorization method* have exposed the need to study and understand a non-traditional boundary value problem, termed the *interior transmission problem* (ITP), where two bodies with common support are subjected to a prescribed jump in Cauchy data between their boundaries. Covered by no classical theory, this problem has been the subject of early investigations since late 1980's (Colton et al., 1989; Rynne and Sleeman, 1991). The critical step in studying the ITP involves determination of conditions (in terms of input parameters) under which the problem is well-posed in the sense of Hadamard. Invariably, this leads to the analysis of the interior transmission eigenvalues, i.e. frequencies for which the homogeneous ITP permits a non-trivial solution. In particular, the characterization of such eigenvalue set has become of key importance in recent studies (Päivärinta and Sylvester, 2008; Kirsch, 2009).

So far, two distinct methodologies have been pursued to investigate the well-posedness of the ITP, mainly within the context of Helmholtz and Maxwell equations. On the one hand, integral equation-type formulations have been developed in Colton et al. (1989); Rynne and Sleeman (1991) for scalar-wave problems, and later adapted to deal with electromagnetic waves (Haddar, 2004; Kirsch, 2007). On the other hand, starting from the seminal work in Hähner (2000), an alternative treatment of the ITP has been developed in Cakoni et al. (2002) that involves a customized variational formulation combined with the compact perturbation argument. This approach has since been successfully applied in a series of papers to a variety of acoustic and electromagnetic scattering problems, see e.g. Cakoni and Haddar (2001, 2007).

In the context of elastic waves, investigation of the ITP has been spurred by the introduction of the linear sampling method for far-field (Arens, 2001; Charalambopoulos et al., 2002) and near-field (Nintcheu Fata and Guzina, 2004; Baganas et al., 2006; Nintcheu Fata and Guzina, 2004; Guzina and Madyarov, 2007) inverse scattering problems, as well as the development of the factorization method for elastodynamics (Charalambopoulos et al., 2007). To date, the elastodynamic ITP has been investigated mainly within the framework established for the Helmholtz and Maxwell equations, notably via integral equation approach (Charalambopoulos et al., 2002) for homogeneous dissipative scatterers, and the variational treatment (Charalambopoulos, 2002) for heterogeneous, anisotropic, and elastic scatterers in a homogeneous elastic background. Recently, a method combining integral equation approach and compact perturbation argument has been proposed in Charalambopoulos and Anagnostopoulos (2008) for homogeneous-isotropic elasticity to obtain sufficient conditions for the well-posedness of the ITP.

To extend the validity of the linear sampling and factorization methods to a wider and more realistic class of inverse scattering problems, the focus of this study is the ITP for situations where both the obstacle and the background solid are piecewise-homogeneous, anisotropic, and either elastic or viscoelastic. This type of heterogeneity concerning the background solid has particular relevance to e.g. seismic imaging and non-destructive material testing where layered configurations are common, as created either via natural deposition or the manufacturing process. For generality, the obstacle is allowed to be multiply connected, having both penetrable components (inclusions) and impenetrable parts (cavities). In this setting, emphasis is made on the well-posedess of the visco-elastodynamic ITP, and in particular on the sufficient conditions under which the set of interior transmission eigenvalues is either countable or empty. For an in-depth study of the problem, a variational approach that generalizes upon the results in Cakoni et al. (2002) and Charalambopoulos (2002) is developed, including a treatment of the less-understood "viscoelastic-viscoelastic" case where both the obstacle and the background solid are

dissipative. The key result of the proposed developments are the sufficient conditions under which the ITP involving piecewise-homogeneous, anisotropic, and viscoelastic solids is well-posed provided that the excitation frequency does not belong to (at most) countable spectrum of transmission eigenvalues. These conditions aim to overcome some of the limitations of the earlier treatments in (visco-) elasto-dynamics in that: i) they pose a precise, previously unavailable provision for the well-posedness of the ITP in situations when the obstacle and the background solid are both heterogeneous, and ii) they are dimensionally consistent i.e. invariant under the choice of physical units.

4.2 Preliminaries

Consider a piecewise-homogeneous, "background" viscoelastic solid $\Omega \subset \mathbb{R}^3$ (not necessarily bounded and isotropic) composed of N homogeneous regular regions Ω_n. Assuming time-harmonic motion with implicit factor $e^{i\omega t}$ and making reference to the correspondence principle (Flügge, 1975), let $\rho > 0$ and $\mathcal{C}$ denote respectively the piecewise-constant mass density and (complex-valued) viscoelasticity tensor characterizing Ω. For clarity, all quantities appearing in this study are interpreted as *dimensionless* following the scaling scheme in Table 4.1 where d_0 is the characteristic length, K_0 is the reference elastic modulus, and ρ_0 is the reference mass density. Without loss of generality, ρ_0 can be taken such that $\inf\{\rho(\boldsymbol{\xi}) : \boldsymbol{\xi} \in \Omega\} = 1$, leaving the choice of K_0 at this point arbitrary.

Table 4.1: *Scaling scheme*

	Dimensionless quantity	Scale
Mass density	ρ	ρ_0
Viscoelasticity tensor, traction vector	$\mathcal{C}, \boldsymbol{t}$	K_0
Displacement and position vectors	$\boldsymbol{u}, \boldsymbol{\xi}$	d_0
Vibration frequency	ω	$d_0^{-1}\sqrt{K_0/\rho_0}$

Next, let Ω be perturbed by a bounded obstacle $\overline{D} \subset \Omega$ composed of M_* homogeneous viscoelastic inclusions D_*^m and M_o disconnected cavities D_o^j. In this setting one may write $\overline{D} = \overline{D_* \cup D_\mathrm{o}}$, where $\overline{D_*} = \bigcup_{m=1}^{M_*} \overline{D_*^m}$ and $\overline{D_\mathrm{o}} = \bigcup_{j=1}^{M_\mathrm{o}} \overline{D_\mathrm{o}^j}$. Here it is assumed that the cavities are separated from inclusions i.e. $\overline{D_*} \cap \overline{D_\mathrm{o}} = \emptyset$, and that $\Omega \backslash \overline{D_\mathrm{o}}$ is connected. Similar to the case of the background solid, the viscoelasticity tensor $\mathcal{C}_*$ and mass density $\rho_* > 0$ characterizing D_* are understood in a piecewise-constant sense. For the purpose of this study, the reference length d_0 appearing in Table 4.1 can be taken as $d_0 = |D|^{1/3}$, i.e. as the characteristic obstacle size.

To facilitate the ensuing discussion, consider next N_* subsets Θ_*^p of D_* where both $(\mathcal{C}, \rho)$ and $(\mathcal{C}_*, \rho_*)$ are constant, i.e.

$$\forall (n, m) \in \{1, \ldots, N\} \times \{1, \ldots, M_*\} \quad \overline{\Omega_n} \cap \overline{D_*^m} \neq \emptyset \;\Rightarrow\; \exists p \in \{1, \ldots, N_*\} \colon \overline{\Theta_*^p} = \overline{\Omega_n} \cap \overline{D_*^m}.$$

Since $D_* \subset \Omega$, one has $M_* \leqslant N_*$ and geometrically $\overline{D_*} = \bigcup_{p=1}^{N_*} \overline{\Theta_*^p}$. Likewise, one may identify the N_o subsets, Θ_o^q, of $\overline{D_\mathrm{o}}$ where $(\mathcal{C}, \rho)$ is constant

$$\forall (n, j) \in \{1, \ldots, N\} \times \{1, \ldots, M_\mathrm{o}\} \quad \overline{\Omega_n} \cap \overline{D_\mathrm{o}^j} \neq \emptyset \;\Rightarrow\; \exists q \in \{1, \ldots, N_\mathrm{o}\} \colon \overline{\Theta_\mathrm{o}^q} = \overline{\Omega_n} \cap \overline{D_\mathrm{o}^j},$$

see also Fig. 4.2. In each Θ_*^p, the mass density of the inclusion and the background medium will be denoted respectively by ρ_*^p and ρ^p; the background mass density in each Θ_o^q will be similarly denoted by ρ_o^q.
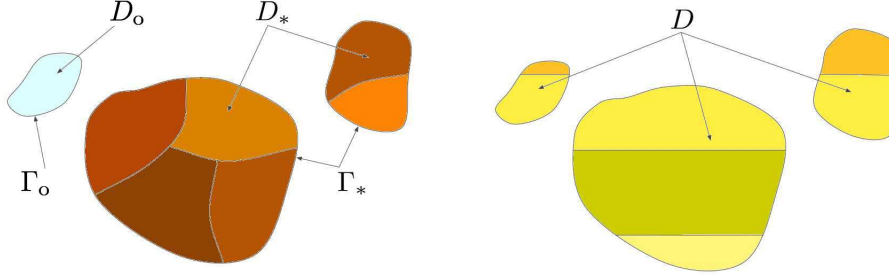
Figure 4.1: *ITP configuration: scatterer composed of inclusions D_* and cavities D_o (left) and scatterer support, D, occupied by the background material (right).*

In what follows it is assumed that $\mathcal{C}_*$ and $\mathcal{C}$, synthesizing respectively the anisotropic viscoelastic behavior of the obstacle and the background, have the following properties.

Definition 1. *Let $\Re[\cdot]$ and $\Im[\cdot]$ denote respectively the real and imaginary part of a complex-valued quantity. The fourth-order tensors $\mathcal{C}$ and $\mathcal{C}_*$ are bounded by piecewise-constant, real-valued, strictly positive functions $\mathsf{c}, \mathsf{c}_*, \mathsf{C}$ and C_* and non-negative functions $\mathsf{v}, \mathsf{v}_*, \mathsf{V}$ and V_* such that*

$$\begin{aligned}
\mathsf{c}|\boldsymbol{\varphi}|^2 &\leqslant \Re[\boldsymbol{\varphi}\!:\!\mathcal{C}\!:\!\bar{\boldsymbol{\varphi}}] \leqslant \mathsf{C}|\boldsymbol{\varphi}|^2 &&\text{in } \Omega, \\
\mathsf{c}_*|\boldsymbol{\varphi}|^2 &\leqslant \Re[\boldsymbol{\varphi}\!:\!\mathcal{C}_*\!:\!\bar{\boldsymbol{\varphi}}] \leqslant \mathsf{C}_*|\boldsymbol{\varphi}|^2 &&\text{in } D_*,
\end{aligned} \tag{4.2.1}$$

and

$$\begin{aligned}
\mathsf{v}|\boldsymbol{\varphi}|^2 &\leqslant \Im[\boldsymbol{\varphi}\!:\!\mathcal{C}\!:\!\bar{\boldsymbol{\varphi}}] \leqslant \mathsf{V}|\boldsymbol{\varphi}|^2 &&\text{in } \Omega, \\
\mathsf{v}_*|\boldsymbol{\varphi}|^2 &\leqslant \Im[\boldsymbol{\varphi}\!:\!\mathcal{C}_*\!:\!\bar{\boldsymbol{\varphi}}] \leqslant \mathsf{V}_*|\boldsymbol{\varphi}|^2 &&\text{in } D_*
\end{aligned} \tag{4.2.2}$$

for all complex-valued, second-order tensor fields $\boldsymbol{\varphi}$ in $\Omega \supset D_*$. For further reference, let $\mathsf{c}^p, \mathsf{c}_*^p, \mathsf{C}^p, \mathsf{C}_*^p, \mathsf{v}^p, \mathsf{v}_*^p, \mathsf{V}^p$ and V_*^p signify the respective (constant) values of $\mathsf{c}, \mathsf{c}_*, \mathsf{C}, \mathsf{C}_*, \mathsf{v}, \mathsf{v}_*, \mathsf{V}$ and V_* in each Θ_*^p, $p \in \{1, \ldots, N_*\}$, and let $\mathsf{c}_o^q, \mathsf{C}_o^q, \mathsf{v}_o^q$ and V_o^q denote the respective values of $\mathsf{c}, \mathsf{C}, \mathsf{v}$ and V in each Θ_o^q, $q \in \{1, \ldots, N_o\}$. With such definitions, $\mathsf{V}^p = \mathsf{v}^p \equiv 0$ and $\mathsf{V}^p \geqslant \mathsf{v}^p > 0$ respectively when $\mathcal{C}$ is elastic and viscoelastic (i.e. complex-valued) in Θ^p, with analogous restrictions applying to the bounds on $\mathcal{C}_*$ and $\mathcal{C}_o$. In this setting, (4.2.1) and (4.2.2) de facto require that both real and imaginary parts of a viscoelastic tensor be positive definite and bounded.

Comment. With reference to the result in Mataraezo (2001) which establishes the major symmetry of a (tensor) relaxation function by virtue of the Onsager's reciprocity principle (Shter, 1973) , it follows that $\mathcal{C}_*$ and $\mathcal{C}$ have the usual major and minor symmetries whereby

$$\begin{aligned}
\Re[\boldsymbol{\varphi}\!:\!\mathcal{C}\!:\!\bar{\boldsymbol{\varphi}}] = \boldsymbol{\varphi} : \Re[\mathcal{C}] : \bar{\boldsymbol{\varphi}}, &\qquad \Re[\boldsymbol{\varphi}\!:\!\mathcal{C}_*\!:\!\bar{\boldsymbol{\varphi}}] = \boldsymbol{\varphi} : \Re[\mathcal{C}_*] : \bar{\boldsymbol{\varphi}}, \\
\Im[\boldsymbol{\varphi}\!:\!\mathcal{C}\!:\!\bar{\boldsymbol{\varphi}}] = \boldsymbol{\varphi} : \Im[\mathcal{C}] : \bar{\boldsymbol{\varphi}}, &\qquad \Im[\boldsymbol{\varphi}\!:\!\mathcal{C}_*\!:\!\bar{\boldsymbol{\varphi}}] = \boldsymbol{\varphi} : \Im[\mathcal{C}_*] : \bar{\boldsymbol{\varphi}}.
\end{aligned} \tag{4.2.3}$$

One may also note that the imposition of the upper bounds, $\mathsf{C}, \mathsf{C}_*, \mathsf{V}$ and V_* in (4.2.1) and (4.2.2) is justified by the boundedness of the moduli comprising $\mathcal{C}$ and $\mathcal{C}_*$, whereas $\mathsf{c}, \mathsf{c}_*, \mathsf{v}$ and v_* ensure thermomechanical stability of the system (Mehrabadi et al., 1993; Findley et al., 1989). These upper and

lower bounds can be shown to signify the extreme eigenvalues of (the real and imaginary parts of) a fourth-order viscoelasticity tensor, defined with respect to a second-order eigentensor. Explicit treatment of such eigenvalue problems is difficult in a general anisotropic case, which may feature up to six distinct eigenvalues per real and imaginary part. In the isotropic case, however, tensors $\mathcal{C}$ and $\mathcal{C}_*$ can be synthesized in terms of the respective (complex) shear moduli μ and μ_*, and bulk moduli κ and κ_*. Under such restriction, $\mathcal{C}$ and $\mathcal{C}_*$ have only two distinct eigenvalues (Knowles, 1995), given respectively by $\{2\mu, 3\kappa\}$ and $\{2\mu_*, 3\kappa_*\}$. Depending on the sign of the real parts of the underlying Poisson's ratios ν and ν_* (Pritz, 2007), these moduli satisfy the relationships

$$\begin{aligned}
0 < \Re[\nu] < \tfrac{1}{2} &\quad \Rightarrow \quad & \mathsf{C} = 3\Re[\kappa] \; > 2\Re[\mu] = \mathsf{c}, \\
-1 < \Re[\nu] < 0 &\quad \Rightarrow \quad & \mathsf{C} = 2\Re[\mu] \; > 3\Re[\kappa] = \mathsf{c}, \\
0 < \Re[\nu_*] < \tfrac{1}{2} &\quad \Rightarrow \quad & \mathsf{C}_* = 3\Re[\kappa_*] \; > 2\Re[\mu_*] = \mathsf{c}_*, \\
-1 < \Re[\nu_*] < 0 &\quad \Rightarrow \quad & \mathsf{C}_* = 2\Re[\mu_*] \; > 3\Re[\kappa_*] = \mathsf{c}_*.
\end{aligned} \tag{4.2.4}$$
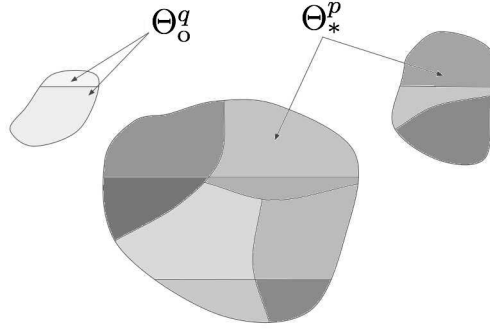
Figure 4.2: *Schematics of the "intersection" domains Θ_*^p and Θ_o^q wherein the scatterer and the background solid both maintain constant material properties (see also Fig. 4.1).*

For further reference it can be shown on the basis of (4.2.1), (4.2.2), the aforementioned eigen-representations of the viscoelasticity tensor, the triangle inequality, and the Cauchy-Schwarz inequality that

$$\begin{aligned}
\left| \int_{\Theta_*^p} \boldsymbol{\varphi} : \mathcal{C}_* : \bar{\boldsymbol{\psi}} \, \mathrm{d}V \right| &\leqslant (\mathsf{C}_* + \mathsf{V}_*) \, \|\boldsymbol{\varphi}\|_{L^2(\Theta_*^p)} \, \|\boldsymbol{\psi}\|_{L^2(\Theta_*^p)}, \\
\left| \int_{\Theta_*^p} \boldsymbol{\varphi} : \mathcal{C} : \bar{\boldsymbol{\psi}} \, \mathrm{d}V \right| &\leqslant (\mathsf{C} + \mathsf{V}) \, \|\boldsymbol{\varphi}\|_{L^2(\Theta_*^p)} \, \|\boldsymbol{\psi}\|_{L^2(\Theta_*^p)}, \\
\left| \int_{\Theta_o^q} \boldsymbol{\varphi} : \mathcal{C} : \bar{\boldsymbol{\psi}} \, \mathrm{d}V \right| &\leqslant (\mathsf{C} + \mathsf{V}) \, \|\boldsymbol{\varphi}\|_{L^2(\Theta_o^q)} \, \|\boldsymbol{\psi}\|_{L^2(\Theta_o^q)},
\end{aligned} \tag{4.2.5}$$

where $\boldsymbol{\varphi}$ and $\boldsymbol{\psi}$ are square-integrable, complex-valued, second-order tensor fields in Θ_*^p and Θ_o^q, $p \in \{1, \ldots, N_*\}$, $q \in \{1, \ldots, N_o\}$.

4.3 Interior transmission problem

Consider the time-harmonic scattering of viscoelastic waves at frequency ω where the so-called free field $\boldsymbol{u}$, namely the displacement field that would have existed in the obstacle-free domain Ω, is perturbed

(scattered) by a bounded obstacle $D = D_* \cup D_\mathrm{o} \subset \Omega$ described earlier. This boundary value problem can be conveniently written as

$$\boldsymbol{\nabla} \cdot [\boldsymbol{\mathcal{C}}_* : \boldsymbol{\nabla} \boldsymbol{w}] + \rho_* \omega^2 \boldsymbol{w} = \boldsymbol{0} \qquad\qquad \text{in } D_*, \qquad (4.3.1\text{a})$$

$$\boldsymbol{\nabla} \cdot [\boldsymbol{\mathcal{C}} : \boldsymbol{\nabla} \boldsymbol{v}] + \rho\, \omega^2 \boldsymbol{v} = \boldsymbol{0} \qquad\qquad \text{in } \Omega \backslash \overline{D}, \qquad (4.3.1\text{b})$$

$$\boldsymbol{w} = \boldsymbol{v} + \boldsymbol{u} \qquad\qquad\qquad\qquad \text{on } \partial D_*, \qquad (4.3.1\text{c})$$

$$\boldsymbol{t}_*[\boldsymbol{w}] = \boldsymbol{t}[\boldsymbol{v}] + \boldsymbol{t}[\boldsymbol{u}] \qquad\qquad\quad \text{on } \partial D_*, \qquad (4.3.1\text{d})$$

$$\boldsymbol{t}[\boldsymbol{v}] + \boldsymbol{t}[\boldsymbol{u}] = \boldsymbol{0} \qquad\qquad\qquad\quad \text{on } \partial D_\mathrm{o} \qquad (4.3.1\text{e})$$

where $\boldsymbol{w}$ is the (total) displacement field within piecewise-homogeneous inclusion D_*; $\boldsymbol{v}$ is the so-called scattered field signifying the *perturbation* of $\boldsymbol{u}$ in $\Omega \backslash \overline{D}$ due to the presence of the scatterer; $\boldsymbol{t}_*[\boldsymbol{\varphi}] = \boldsymbol{\mathcal{C}}_*\!: \boldsymbol{\nabla}\boldsymbol{\varphi} \cdot \boldsymbol{n}$ and $\boldsymbol{t}[\boldsymbol{\varphi}] = \boldsymbol{\mathcal{C}}\!: \boldsymbol{\nabla}\boldsymbol{\varphi} \cdot \boldsymbol{n}$ refer to the surface tractions on ∂D; $\boldsymbol{\nabla}$ implies differentiation "to the left" (Malvern, 1969), and $\boldsymbol{n}$ is the unit normal on the boundary of D oriented toward its exterior. Here (4.3.1a) is to be interpreted as a short-hand notation for the set of M_* governing equations applying over the respective homogeneous regions D_*^m ($m = 1, \ldots M_*$), supplemented by the continuity of displacements and tractions across ∂D_*^m where applicable. Analogous convention holds in terms of (4.3.1b) strictly applying over open homogeneous regions $\Omega_n \backslash \overline{D}$.

In what follows, it is assumed that the boundary of Ω (if any) is subject to Robin-type conditions whereby (4.3.1) are complemented by

$$\lambda(\boldsymbol{I}_2 - \boldsymbol{N}) \cdot \boldsymbol{v} + \boldsymbol{N} \cdot \boldsymbol{t}[\boldsymbol{v}] = \boldsymbol{0} \quad \text{on } \partial\Omega, \qquad (4.3.2)$$

where $\lambda > 0$ is a constant; $\boldsymbol{n}$, implicit in the definition of $\boldsymbol{t}[\boldsymbol{v}]$, is oriented outward from Ω; and $\boldsymbol{N}$ is a suitable second-order tensor that varies continuously along smooth pieces of $\partial\Omega$. Note that (4.3.2) include homogeneous Dirichlet ($\boldsymbol{N} \equiv \boldsymbol{0}$) and Neumann ($\boldsymbol{N} \equiv \boldsymbol{I}_2$) boundary conditions as special cases. In situations where Ω is unbounded (e.g. a half-space), (4.3.1) and (4.3.2) are completed by the generalized radiation condition (Madyarov and Guzina, 2006), namely

$$\lim_{R \to \infty} \int_{\Gamma_R} \left[\boldsymbol{t}[\boldsymbol{v}](\boldsymbol{\xi}) \cdot \boldsymbol{U}(\boldsymbol{\xi}, \boldsymbol{\zeta}) - \boldsymbol{v}(\boldsymbol{\xi}) \cdot \boldsymbol{T}(\boldsymbol{\xi}, \boldsymbol{\zeta}) \right] \mathrm{d}S_\xi \;=\; \boldsymbol{0}, \quad \forall \boldsymbol{\zeta} \in \Omega, \qquad (4.3.3)$$

where $\Gamma_R = S_R \cap \Omega$; S_R is a sphere of radius R centered at the origin; $\boldsymbol{U}$ denotes the displacement Green's tensor for the obstacle-free solid Ω, and $\boldsymbol{T}$ is the traction Green's tensor associated with $\boldsymbol{U}$.

Interior transmission problem.   With reference to the direct scattering framework (4.3.1)–(4.3.3), henceforth referred to as the transmission problem (TP), investigation of the associated *inverse scattering* problem in terms of the linear sampling and factorization methods (Colton and Kirsch, 1996; Charalambopoulos et al., 2002; Guzina and Madyarov, 2007; Kirsch and Grinberg, 2008; Charalambopoulos et al., 2007) leads to the analysis of the so-called interior transmission problem (ITP) (Cakoni and Colton, 2006). In the context of the present study, the ITP can be stated as the task of finding an elastodynamic field that solves the *counterpart* of (4.3.1) where the support of (4.3.1b), namely $\Omega \backslash \overline{D}$, is *replaced* by D. Previous studies have, however, shown that the analysis of an ITP is complicated by the *loss of ellipticity* relative to its "mother" TP that is well known to be elliptic. An in-depth study of this phenomenon can be found in Colton et al. (2007) who showed, making reference to acoustic waves, that the ITP is not elliptic at any frequency. Here it is also useful to recall that the TP (4.3.1)–(4.3.3) and the associated ITP can both be represented by a common set of boundary integral equations (written over

∂D), which leads to the well-known phenomenon of fictitious frequencies (Burton and Miller, 1971; Liu and Rizzo, 1993; Pyl et al., 2004) plaguing the boundary integral treatment of direct scattering problems.

For a comprehensive treatment of the problem, the ITP associated with (4.3.1)–(4.3.3) is next formulated in a general setting which i) allows for the presence of body forces, and ii) interprets the interfacial conditions over ∂D_* as a prescribed jump in Cauchy data between $\boldsymbol{u}$ and $\boldsymbol{u}_*$. Making reference to Fig. 4.1 and the basic concepts of functional analysis (McLean, 2000), such generalized ITP can be conveniently stated as a task of finding $(\boldsymbol{u}_*, \boldsymbol{u}, \boldsymbol{u}_\mathrm{o}) \in H^1(D_*) \times H^1(D_*) \times H^1(D_\mathrm{o})$ satisfying

$$\boldsymbol{\nabla}{\cdot}[\boldsymbol{\mathcal{C}}_*{:}\boldsymbol{\nabla}\boldsymbol{u}_*] + \rho_*\omega^2\boldsymbol{u}_* = \boldsymbol{f}_* \qquad \text{in } D_*, \tag{4.3.4a}$$

$$\boldsymbol{\nabla}{\cdot}[\boldsymbol{\mathcal{C}}{:}\boldsymbol{\nabla}\boldsymbol{u}] + \rho\omega^2\boldsymbol{u} = \boldsymbol{f} \qquad \text{in } D_*, \tag{4.3.4b}$$

$$\boldsymbol{\nabla}{\cdot}[\boldsymbol{\mathcal{C}}{:}\boldsymbol{\nabla}\boldsymbol{u}_\mathrm{o}] + \rho\omega^2\boldsymbol{u}_\mathrm{o} = \boldsymbol{f} \qquad \text{in } D_\mathrm{o}, \tag{4.3.4c}$$

$$\boldsymbol{u}_* = \boldsymbol{u} + \boldsymbol{g} \qquad \text{on } \partial D_*, \tag{4.3.4d}$$

$$\boldsymbol{t}_*[\boldsymbol{u}_*] = \boldsymbol{t}[\boldsymbol{u}] + \boldsymbol{h}_* \qquad \text{on } \partial D_*, \tag{4.3.4e}$$

$$\boldsymbol{t}[\boldsymbol{u}_\mathrm{o}] = \boldsymbol{h}_\mathrm{o} \qquad \text{on } \partial D_\mathrm{o}, \tag{4.3.4f}$$

where $H^k \equiv W^{k,2}$ denotes the usual Sobolev space; $(\boldsymbol{f}_*, \boldsymbol{f}) \in L^2(D_*) \times L^2(D)$; $\boldsymbol{g} \in H^{\frac{1}{2}}(\partial D_*)$; $(\boldsymbol{h}_*, \boldsymbol{h}_\mathrm{o}) \in H^{-\frac{1}{2}}(\partial D_*) \times H^{-\frac{1}{2}}(\partial D_\mathrm{o})$, and

$$\begin{aligned} \boldsymbol{t}_*[\boldsymbol{u}_*] &= \boldsymbol{\mathcal{C}}_*{:}\boldsymbol{\nabla}\boldsymbol{u}_*{\cdot}\boldsymbol{n} \in H^{-\frac{1}{2}}(\partial D_*), \\ \boldsymbol{t}[\boldsymbol{u}] &= \boldsymbol{\mathcal{C}}{:}\boldsymbol{\nabla}\boldsymbol{u}{\cdot}\boldsymbol{n} \in H^{-\frac{1}{2}}(\partial D_*), \\ \boldsymbol{t}[\boldsymbol{u}_\mathrm{o}] &= \boldsymbol{\mathcal{C}}{:}\boldsymbol{\nabla}\boldsymbol{u}_\mathrm{o}{\cdot}\boldsymbol{n} \in H^{-\frac{1}{2}}(\partial D_\mathrm{o}). \end{aligned} \tag{4.3.5}$$

For completeness, it is noted that (4.3.4a)–(4.3.4c) and (4.3.4d)–(4.3.5) are interpreted respectively in the sense of distributions and the trace operator while $\boldsymbol{f}_*$ and $\boldsymbol{f}$, signifying the negatives of body forces, are placed on the right-hand side to facilitate the discussion.

Definition 2. *Values of ω for which the homogeneous ITP, defined by setting $(\boldsymbol{f}_*, \boldsymbol{f}, \boldsymbol{g}, \boldsymbol{h}_*, \boldsymbol{h}_o) = (\boldsymbol{0}, \boldsymbol{0}, \boldsymbol{0}, \boldsymbol{0}, \boldsymbol{0})$ in (4.3.4), has a non-trivial solution are called* transmission eigenvalues.

Modified interior transmission problem. To deal with anticipated non-ellipticity of the featured ITP, it is next useful to consider the compact perturbation of (4.3.4) as

$$\boldsymbol{\nabla}{\cdot}[\boldsymbol{\mathcal{C}}_*{:}\boldsymbol{\nabla}\boldsymbol{u}_*] - \rho_*\boldsymbol{u}_* = \boldsymbol{f}_* \qquad \text{in } D_* \tag{4.3.6a}$$

$$\boldsymbol{\nabla}{\cdot}[\boldsymbol{\mathcal{C}}{:}\boldsymbol{\nabla}\boldsymbol{u}] - \rho\boldsymbol{u} = \boldsymbol{f} \qquad \text{in } D_* \tag{4.3.6b}$$

$$\boldsymbol{\nabla}{\cdot}[\boldsymbol{\mathcal{C}}{:}\boldsymbol{\nabla}\boldsymbol{u}_\mathrm{o}] - \rho\boldsymbol{u}_\mathrm{o} = \boldsymbol{f} \qquad \text{in } D_\mathrm{o} \tag{4.3.6c}$$

$$\boldsymbol{u}_* = \boldsymbol{u} + \boldsymbol{g} \qquad \text{on } \partial D_* \tag{4.3.6d}$$

$$\boldsymbol{t}_*[\boldsymbol{u}_*] = \boldsymbol{t}[\boldsymbol{u}] + \boldsymbol{h}_* \qquad \text{on } \partial D_* \tag{4.3.6e}$$

$$\boldsymbol{t}[\boldsymbol{u}_\mathrm{o}] = \boldsymbol{h}_\mathrm{o} \qquad \text{on } \partial D_\mathrm{o}, \tag{4.3.6f}$$

see also Cakoni et al. (2002) in the context of the acoustic waves. To demonstrate the compact nature of such perturbation, one may introduce the auxiliary space

$$\begin{aligned} \Xi(D) := \big\{ (\boldsymbol{u}_*, \boldsymbol{u}, \boldsymbol{u}_\mathrm{o}) &\in H^1(D_*) \times H^1(D_*) \times H^1(D_\mathrm{o}) : \\ &\boldsymbol{\nabla}{\cdot}[\boldsymbol{\mathcal{C}}_*{:}\boldsymbol{\nabla}\boldsymbol{u}_*] \in L^2(D_*),\ \boldsymbol{\nabla}{\cdot}[\boldsymbol{\mathcal{C}}{:}\boldsymbol{\nabla}\boldsymbol{u}] \in L^2(D_*),\ \boldsymbol{\nabla}{\cdot}[\boldsymbol{\mathcal{C}}{:}\boldsymbol{\nabla}\boldsymbol{u}_\mathrm{o}] \in L^2(D_\mathrm{o}) \big\}, \end{aligned} \tag{4.3.7}$$

and a differential-trace operator $\mathcal{M}$ representing (4.3.6) from $\Xi(D)$ into $L^2(D_*) \times L^2(D_*) \times L^2(D_o) \times H^{\frac{1}{2}}(\partial D_*) \times H^{-\frac{1}{2}}(\partial D_*) \times H^{-\frac{1}{2}}(\partial D_o)$ such that

$$\mathcal{M}(\boldsymbol{u}_*, \boldsymbol{u}, \boldsymbol{u}_o) := \big(\boldsymbol{\nabla}\cdot[\mathcal{C}_*\!:\!\boldsymbol{\nabla}\boldsymbol{u}_*]-\rho_*\boldsymbol{u}_*, \ \boldsymbol{\nabla}\cdot[\mathcal{C}\!:\!\boldsymbol{\nabla}\boldsymbol{u}]-\rho\,\boldsymbol{u}, \ \boldsymbol{\nabla}\cdot[\mathcal{C}\!:\!\boldsymbol{\nabla}\boldsymbol{u}_o]-\rho\,\boldsymbol{u}_o,$$
$$(\boldsymbol{u}_*-\boldsymbol{u})_{|\partial D_*}, \ (\boldsymbol{t}_*[\boldsymbol{u}_*]-\boldsymbol{t}[\boldsymbol{u}])_{|\partial D_*}, \ \boldsymbol{t}[\boldsymbol{u}_o]_{|\partial D_o}\big) \quad (4.3.8)$$

where $\boldsymbol{t}$ and $\boldsymbol{t}_*$ are defined as in (4.3.5). On the basis of (4.3.6) and (4.3.8), interior transmission problem (4.3.4) can be identified with operator $\mathcal{O} \equiv \mathcal{M} + (1+\omega^2)\mathcal{P}$ from $\Xi(D)$ into $L^2(D_*) \times L^2(D_*) \times L^2(D_o) \times H^{\frac{1}{2}}(\partial D_*) \times H^{-\frac{1}{2}}(\partial D_*) \times H^{-\frac{1}{2}}(\partial D_o)$, where the featured perturbation operator

$$\mathcal{P}(\boldsymbol{u}_*, \boldsymbol{u}, \boldsymbol{u}_o) := \big(\rho_*\boldsymbol{u}_*, \ \rho\,\boldsymbol{u}, \ \rho\,\boldsymbol{u}_o, \ \boldsymbol{0}, \ \boldsymbol{0}, \ \boldsymbol{0}\big) \quad (4.3.9)$$

is clearly compact by virtue of compact embedding of $H^1(D_*)$ into $L^2(D_*)$ and $H^1(D_o)$ into $L^2(D_o)$.

Definition 3. *Triplet $(\boldsymbol{u}_*, \boldsymbol{u}, \boldsymbol{u}_o) \in H^1(D_*) \times H^1(D_*) \times H^1(D_o)$ solving (4.3.6a)–(4.3.6c) in the sense of distributions and (4.3.6d)–(4.3.6f) in the sense of the trace operator is called a* strong solution *of the modified ITP.*

4.3.1 Weak formulation of the modified ITP

The next step is to examine the ellipticity of the modified ITP (4.3.6) through a variational formulation, following the methodology originally introduced in Hähner (2000) and later deployed in Cakoni et al. (2002); Charalambopoulos (2002). To this end, recall the definition of the "background" viscoelasticity tensor and consider the space of symmetric second-order tensor fields

$$W(D_*) := \big\{ \boldsymbol{\Phi} \in L^2(D_*): \ \boldsymbol{\Phi} = \boldsymbol{\Phi}^{\mathrm{T}}, \ \boldsymbol{\nabla}\cdot\boldsymbol{\Phi} \in L^2(D_*) \text{ and } \boldsymbol{\nabla}\times[\mathcal{C}^{-1}\!:\!\boldsymbol{\Phi}] = \boldsymbol{0} \big\}, \quad (4.3.10)$$

equipped with the inner product

$$(\boldsymbol{\Phi}_1, \boldsymbol{\Phi}_2)_{W(D_*)} := (\boldsymbol{\Phi}_1, \boldsymbol{\Phi}_2)_{L^2(D_*)} + (\boldsymbol{\nabla}\cdot\boldsymbol{\Phi}_1, \boldsymbol{\nabla}\cdot\boldsymbol{\Phi}_2)_{L^2(D_*)}, \quad (4.3.11)$$

and implied norm

$$\|\boldsymbol{\Phi}\|^2_{W(D_*)} := \|\boldsymbol{\Phi}\|^2_{L^2(D_*)} + \|\boldsymbol{\nabla}\cdot\boldsymbol{\Phi}\|^2_{L^2(D_*)}. \quad (4.3.12)$$

For clarity it is noted that the curl operator in (4.3.10), defined as that "to the left" (Malvern, 1969), is to be interpreted in the weak sense. With reference to (4.3.6) and (4.3.10), let further $\mathbb{E} := H^1(D_*) \times W(D_*) \times H^1(D_o)$ and define the sesquilinear form $\mathcal{A} : \mathbb{E} \times \mathbb{E} \to \mathbb{C}$ as

$$\mathcal{A}(U, V) := \int_{D_*} \big[\boldsymbol{\nabla}\boldsymbol{u}_* : \mathcal{C}_*\!:\!\boldsymbol{\nabla}\bar{\boldsymbol{\varphi}}_* + \rho_*\boldsymbol{u}_*\cdot\bar{\boldsymbol{\varphi}}_*\big]\,\mathrm{d}V + \int_{D_*}\Big[\frac{1}{\rho}(\boldsymbol{\nabla}\cdot\mathcal{U})\cdot(\boldsymbol{\nabla}\cdot\bar{\boldsymbol{\Phi}}) + \mathcal{U}\!:\!\mathcal{C}^{-1}\!:\!\bar{\boldsymbol{\Phi}}\Big]\,\mathrm{d}V$$
$$+ \int_{D_o} \big[\boldsymbol{\nabla}\boldsymbol{u}_o : \mathcal{C}\!:\!\boldsymbol{\nabla}\bar{\boldsymbol{\varphi}} + \rho\,\boldsymbol{u}_o\cdot\bar{\boldsymbol{\varphi}}\big]\,\mathrm{d}V - \int_{\partial D_*} \big[\boldsymbol{u}_*\cdot\bar{\boldsymbol{\Phi}}\cdot\boldsymbol{n} + (\mathcal{U}\cdot\boldsymbol{n})\cdot\bar{\boldsymbol{\varphi}}_*\big]\,\mathrm{d}S,$$
$$(4.3.13)$$

together with the antilinear form $\mathcal{L} : \mathbb{E} \to \mathbb{C}$

$$\mathcal{L}(V) := \int_{D_*} \frac{1}{\rho}\boldsymbol{f}\cdot(\boldsymbol{\nabla}\cdot\bar{\boldsymbol{\Phi}})\,\mathrm{d}V - \int_{D_o} \boldsymbol{f}\cdot\bar{\boldsymbol{\varphi}}\,\mathrm{d}V - \int_{D_*} \boldsymbol{f}_*\cdot\bar{\boldsymbol{\varphi}}_*\,\mathrm{d}V$$
$$+ \int_{\partial D_*} \big[\boldsymbol{h}_*\cdot\bar{\boldsymbol{\varphi}}_* - \boldsymbol{g}\cdot\bar{\boldsymbol{\Phi}}\cdot\boldsymbol{n}\big]\,\mathrm{d}S + \int_{\partial D_o} \boldsymbol{h}_o\cdot\bar{\boldsymbol{\varphi}}\,\mathrm{d}S,$$
$$(4.3.14)$$

where $\mathbb{C}$ denotes the complex plane, $U = (\boldsymbol{u}_*, \boldsymbol{\mathcal{U}}, \boldsymbol{u}_{\mathrm{o}}) \in \mathbb{E}$, and $V = (\boldsymbol{\varphi}_*, \boldsymbol{\Phi}, \boldsymbol{\varphi}) \in \mathbb{E}$.

With such definitions, one may recast (4.3.6) in a variational setting as a task of finding $U = (\boldsymbol{u}_*, \boldsymbol{\mathcal{U}}, \boldsymbol{u}_{\mathrm{o}}) \in \mathbb{E}$ such that

$$\mathcal{A}(U, V) \;=\; \mathcal{L}(V) \qquad \forall V = (\boldsymbol{\varphi}_*, \boldsymbol{\Phi}, \boldsymbol{\varphi}) \in \mathbb{E}. \tag{4.3.15}$$

Theorem 3. *If problem (4.3.6) has unique strong solution $(\boldsymbol{u}_*, \boldsymbol{u}, \boldsymbol{u}_o) \in H^1(D_*) \times H^1(D_*) \times H^1(D_o)$, then the variational problem (4.3.15) has unique weak solution $U = (\boldsymbol{u}_*, \boldsymbol{\mathcal{C}} : \boldsymbol{\nabla}\boldsymbol{u}, \boldsymbol{u}_o) \in \mathbb{E}$. Equally, if problem (4.3.15) has unique weak solution $U = (\boldsymbol{u}_*, \boldsymbol{\mathcal{U}}, \boldsymbol{u}_o) \in \mathbb{E}$, then modified ITP (4.3.6) has unique strong solution $(\boldsymbol{u}_*, \boldsymbol{u}, \boldsymbol{u}_o) \in H^1(D_*) \times H^1(D_*) \times H^1(D_o)$ such that $(\boldsymbol{\nabla}\boldsymbol{u} + \boldsymbol{\nabla}^\mathsf{T}\boldsymbol{u})/2 = \boldsymbol{\mathcal{C}}^{-1} : \boldsymbol{\mathcal{U}}$.*

Proof. The proof of this theorem has two parts. The first part establishes that $(\boldsymbol{u}_*, \boldsymbol{u}, \boldsymbol{u}_{\mathrm{o}})$ solves (4.3.6) if and only if $(\boldsymbol{u}_*, \boldsymbol{\mathcal{U}}, \boldsymbol{u}_{\mathrm{o}})$ solves (4.3.15), while the second part demonstrates the equivalence between the existence of *unique* solutions.

Parity between the existence of solutions.

- Suppose that $(\boldsymbol{u}_*, \boldsymbol{u}, \boldsymbol{u}_{\mathrm{o}})$ solves (4.3.6), and define $\boldsymbol{\mathcal{U}} = \boldsymbol{\mathcal{C}} : \boldsymbol{\nabla}\boldsymbol{u}$ whereby $\boldsymbol{\mathcal{U}} \in W(D_*)$. By taking the $L^2(D_*)$ scalar product of (4.3.6a) with $\boldsymbol{\varphi}_* \in H^1(D_*)$ and applying the divergence theorem, one finds that

$$\int_{D_*} \left[\boldsymbol{\nabla}\boldsymbol{u}_* : \boldsymbol{\mathcal{C}}_* : \boldsymbol{\nabla}\bar{\boldsymbol{\varphi}}_* + \rho_* \boldsymbol{u}_* \cdot \bar{\boldsymbol{\varphi}}_* \right] \mathrm{d}V - \int_{\partial D_*} (\boldsymbol{\mathcal{U}} \cdot \boldsymbol{n}) \cdot \bar{\boldsymbol{\varphi}}_* \, \mathrm{d}S =$$
$$\int_{\partial D_*} \boldsymbol{h}_* \cdot \bar{\boldsymbol{\varphi}}_* \, \mathrm{d}S - \int_{D_*} \boldsymbol{f}_* \cdot \bar{\boldsymbol{\varphi}}_* \, \mathrm{d}V, \quad (4.3.16)$$

by virtue of the boundary condition (4.3.6e). Similarly, application of the divergence theorem to the $L^2(D_{\mathrm{o}})$-scalar product of (4.3.6c) with $\boldsymbol{\varphi} \in H^1(D_{\mathrm{o}})$ yields

$$\int_{D_{\mathrm{o}}} \left[\boldsymbol{\nabla}\boldsymbol{u}_{\mathrm{o}} : \boldsymbol{\mathcal{C}} : \boldsymbol{\nabla}\bar{\boldsymbol{\varphi}} + \rho \, \boldsymbol{u}_{\mathrm{o}} \cdot \bar{\boldsymbol{\varphi}} \right] \mathrm{d}V = \int_{\partial D_{\mathrm{o}}} \boldsymbol{h}_{\mathrm{o}} \cdot \bar{\boldsymbol{\varphi}} \, \mathrm{d}S - \int_{D_{\mathrm{o}}} \boldsymbol{f} \cdot \bar{\boldsymbol{\varphi}} \, \mathrm{d}V. \tag{4.3.17}$$

Finally, by taking the $L^2(D_*)$-scalar product of (4.3.6b) with $\rho^{-1}\boldsymbol{\nabla}\cdot\boldsymbol{\Phi}$ for some $\boldsymbol{\Phi} \in W(D_*)$ and making use of (4.3.6d), one obtains

$$\int_{D_*} \left[\frac{1}{\rho}(\boldsymbol{\nabla}\cdot\boldsymbol{\mathcal{U}}) \cdot (\boldsymbol{\nabla}\cdot\bar{\boldsymbol{\Phi}}) + \boldsymbol{\mathcal{U}} : \boldsymbol{\mathcal{C}}^{-1} : \bar{\boldsymbol{\Phi}} \right] \mathrm{d}V - \int_{\partial D_*} \boldsymbol{u}_* \cdot \bar{\boldsymbol{\Phi}} \cdot \boldsymbol{n} \, \mathrm{d}S$$
$$= \int_{D_*} \frac{1}{\rho} \boldsymbol{f} \cdot (\boldsymbol{\nabla}\cdot\bar{\boldsymbol{\Phi}}) \, \mathrm{d}V - \int_{\partial D_*} \boldsymbol{g} \cdot \bar{\boldsymbol{\Phi}} \cdot \boldsymbol{n} \, \mathrm{d}S. \tag{4.3.18}$$

The weak statement (4.3.15) is now recovered by summing (4.3.16)–(4.3.18), which demonstrates that $U = (\boldsymbol{u}_*, \boldsymbol{\mathcal{U}}, \boldsymbol{u}_{\mathrm{o}}) \in \mathbb{E}$ is indeed a solution of the variational problem.

- Conversely, let $U = (\boldsymbol{u}_*, \boldsymbol{\mathcal{U}}, \boldsymbol{u}_{\mathrm{o}}) \in \mathbb{E}$ be a weak solution to (4.3.15). Since the hypothesis $\boldsymbol{\nabla} \times [\boldsymbol{\mathcal{C}}^{-1} : \boldsymbol{\mathcal{U}}] = \boldsymbol{0}$ guarantees that $\boldsymbol{\mathcal{C}}^{-1} : \boldsymbol{\mathcal{U}}$ meets the strain compatibility conditions (Malvern, 1969), there exists a function $\boldsymbol{u} \in H^1(D_*)$ such that $(\boldsymbol{\nabla}\boldsymbol{u} + \boldsymbol{\nabla}^\mathsf{T}\boldsymbol{u})/2 = \boldsymbol{\mathcal{C}}^{-1} : \boldsymbol{\mathcal{U}}$ in the sense of a

distribution, defined up to a rigid-body motion. By virtue of the fact that U solves the variational problem (4.3.15) for all $(\boldsymbol{\varphi}_*, \boldsymbol{\Phi}, \boldsymbol{\varphi}) \in \mathbb{E}$, it follows by setting the triplet of weighting fields respectively to $(\boldsymbol{\varphi}_*, \mathbf{0}, \mathbf{0})$, $(\mathbf{0}, \mathbf{0}, \boldsymbol{\varphi})$, and $(\mathbf{0}, \boldsymbol{\Phi}, \mathbf{0})$ that $(\boldsymbol{u}_*, \boldsymbol{u}, \boldsymbol{u}_\mathrm{o})$ must be such that (4.3.16), (4.3.17) and (4.3.18) are satisfied independently.

By way of the divergence theorem, (4.3.16) yields

$$\int_{D_*} (\boldsymbol{\nabla}\cdot[\boldsymbol{\mathcal{C}}_*\!:\!\boldsymbol{\nabla}\boldsymbol{u}_*] - \rho_*\boldsymbol{u}_* - \boldsymbol{f}_*) \cdot \bar{\boldsymbol{\varphi}}_* \,\mathrm{d}V$$
$$+ \int_{\partial D_*} (\boldsymbol{h}_* + (\boldsymbol{\mathcal{C}}\!:\!\boldsymbol{\nabla}\boldsymbol{u})\cdot\boldsymbol{n} - (\boldsymbol{\mathcal{C}}_*\!:\!\boldsymbol{\nabla}\boldsymbol{u}_*)\cdot\boldsymbol{n}) \cdot \bar{\boldsymbol{\varphi}}_* \,\mathrm{d}S = 0, \qquad \forall\,\boldsymbol{\varphi}_* \in H^1(D_*)$$

whereby $(\boldsymbol{u}_*, \boldsymbol{u})$ satisfies

$$\begin{aligned} \boldsymbol{\nabla}\cdot[\boldsymbol{\mathcal{C}}_*\!:\!\boldsymbol{\nabla}\boldsymbol{u}_*] - \rho_*\boldsymbol{u}_* &= \boldsymbol{f}_* \quad \text{in } D_*, \\ \boldsymbol{t}_*[\boldsymbol{u}_*] &= \boldsymbol{t}[\boldsymbol{u}] + \boldsymbol{h}_* \qquad \text{on } \partial D_*. \end{aligned} \tag{4.3.19}$$

Similarly, equality (4.3.17) leads to

$$\int_{D_\mathrm{o}} (\boldsymbol{\nabla}\cdot[\boldsymbol{\mathcal{C}}\!:\!\boldsymbol{\nabla}\boldsymbol{u}_\mathrm{o}] - \rho\boldsymbol{u}_\mathrm{o} - \boldsymbol{f}) \cdot \bar{\boldsymbol{\varphi}} \,\mathrm{d}V \; + \int_{\partial D_\mathrm{o}} (\boldsymbol{h}_\mathrm{o} - \boldsymbol{\mathcal{C}}\!:\!\boldsymbol{\nabla}\boldsymbol{u}_\mathrm{o}\cdot\boldsymbol{n}) \cdot \bar{\boldsymbol{\varphi}} \,\mathrm{d}S = 0, \quad \forall\boldsymbol{\varphi}\in H^1(D_\mathrm{o})$$

which requires $(\boldsymbol{u}, \boldsymbol{u}_\mathrm{o})$ to satisfy

$$\begin{aligned} \boldsymbol{\nabla}\cdot[\boldsymbol{\mathcal{C}}\!:\!\boldsymbol{\nabla}\boldsymbol{u}_\mathrm{o}] - \rho\boldsymbol{u}_\mathrm{o} &= \boldsymbol{f} \quad \text{in } D_\mathrm{o}, \\ \boldsymbol{t}[\boldsymbol{u}_\mathrm{o}] &= \boldsymbol{h}_\mathrm{o} \qquad \text{on } \partial D_\mathrm{o}. \end{aligned} \tag{4.3.20}$$

On substituting $\boldsymbol{\mathcal{U}} = \boldsymbol{\mathcal{C}}\!:\!\boldsymbol{\nabla}\boldsymbol{u}$ in (4.3.18), on the other hand, it follows that for all $\boldsymbol{\Phi} \in W(D_*)$

$$\int_{D_*} \left(\frac{1}{\rho}\boldsymbol{\nabla}\cdot[\boldsymbol{\mathcal{C}}\!:\!\boldsymbol{\nabla}\boldsymbol{u}] - \boldsymbol{u} - \frac{1}{\rho}\boldsymbol{f}\right) \cdot (\boldsymbol{\nabla}\cdot\bar{\boldsymbol{\Phi}}) \,\mathrm{d}V \; + \int_{\partial D_*} (\boldsymbol{g} + \boldsymbol{u} - \boldsymbol{u}_*) \cdot \bar{\boldsymbol{\Phi}}\cdot\boldsymbol{n} \,\mathrm{d}S = 0. \tag{4.3.21}$$

To deal with (4.3.21), it is convenient to introduce the "zero-mean and zero-first-order-moment" space of vector fields

$$L_0^2(D_*) = \left\{ \boldsymbol{\varphi} \in L^2(D_*) : \int_{D_*} \boldsymbol{\varphi} \,\mathrm{d}V = \boldsymbol{0}, \; \int_{D_*} \boldsymbol{\xi}\times\boldsymbol{\varphi} \,\mathrm{d}V = \boldsymbol{0} \right\},$$

and to consider solution $\boldsymbol{\chi} \in H^1(D_*)$ of the elastostatic problem

$$\begin{aligned} \boldsymbol{\nabla}\cdot[\boldsymbol{\mathcal{C}}\!:\!\boldsymbol{\nabla}\boldsymbol{\chi}] &= \boldsymbol{\Lambda} \quad \text{in } D_*, \qquad \boldsymbol{\Lambda} \in L_0^2(D_*), \\ \boldsymbol{\mathcal{C}}\!:\!\boldsymbol{\nabla}\boldsymbol{\chi}\cdot\boldsymbol{n} &= \boldsymbol{0} \quad \text{on } \partial D_*. \end{aligned}$$

By taking $\boldsymbol{\Phi} = \boldsymbol{\mathcal{C}}:\boldsymbol{\nabla}\boldsymbol{\chi}$ in (4.3.21) whereby $\boldsymbol{\Phi} \in W(D_*)$, $\boldsymbol{\nabla}\cdot\boldsymbol{\Phi} = \boldsymbol{\Lambda}$ in D_*, and $\boldsymbol{\Phi}\cdot\boldsymbol{n} = \boldsymbol{0}$ on ∂D_*, one finds that

$$\int_{D_*} \left(\frac{1}{\rho}\boldsymbol{\nabla}\cdot[\boldsymbol{\mathcal{C}}\!:\!\boldsymbol{\nabla}\boldsymbol{u}] - \boldsymbol{u} - \frac{1}{\rho}\boldsymbol{f}\right) \cdot \bar{\boldsymbol{\Lambda}} \,\mathrm{d}V = 0 \qquad \forall\boldsymbol{\Lambda}\in L_0^2(D_*),$$

and consequently, using identity $(\boldsymbol{\omega} \times \boldsymbol{\xi}) \cdot \bar{\boldsymbol{\Lambda}} = \boldsymbol{\omega} \cdot (\boldsymbol{\xi} \times \bar{\boldsymbol{\Lambda}})$, that

$$\frac{1}{\rho} \boldsymbol{\nabla} \cdot [\boldsymbol{\mathcal{C}} : \boldsymbol{\nabla} \boldsymbol{u}] - \boldsymbol{u} - \frac{1}{\rho} \boldsymbol{f} \; = \; \mathbf{c} + \boldsymbol{\omega} \times \boldsymbol{\xi} \qquad \text{in } D_*, \tag{4.3.22}$$

which specifies $\boldsymbol{u}$ up to a rigid-body motion given by the translation vector $\mathbf{c}$ and (infinitesimal) rotation vector $\boldsymbol{\omega}$.

Consider next solution $\boldsymbol{\chi} \in H^1(D_*)$ to the problem

$$\begin{aligned} \boldsymbol{\nabla} \cdot [\boldsymbol{\mathcal{C}} : \boldsymbol{\nabla} \boldsymbol{\chi}] &= \mathbf{0} \quad \text{in } D_* \\ \boldsymbol{\mathcal{C}} : \boldsymbol{\nabla} \boldsymbol{\chi} \cdot \boldsymbol{n} &= \boldsymbol{\Lambda} \quad \text{on } \partial D_*, \qquad \boldsymbol{\Lambda} \in L_0^2(\partial D_*). \end{aligned} \tag{4.3.23}$$

Again taking $\boldsymbol{\Phi} = \boldsymbol{\mathcal{C}} : \boldsymbol{\nabla} \boldsymbol{\chi}$ in (4.3.21), which this time implies $\boldsymbol{\Phi} \in W(D_*)$, $\boldsymbol{\nabla} \cdot \boldsymbol{\Phi} = \mathbf{0}$ in D_* and $\boldsymbol{\Phi} \cdot \boldsymbol{n} = \boldsymbol{\Lambda}$ on ∂D_*, leads to

$$\int_{\partial D_*} (\boldsymbol{g} + \boldsymbol{u} - \boldsymbol{u}_*) \cdot \bar{\boldsymbol{\Lambda}} \, \mathrm{d}S = 0 \qquad \forall \boldsymbol{\Lambda} \in L_0^2(\partial D_*), \tag{4.3.24}$$

so that

$$\boldsymbol{g} + \boldsymbol{u} - \boldsymbol{u}_* \; = \; \mathbf{c}' + \boldsymbol{\omega}' \times \boldsymbol{\xi} \qquad \text{on } \partial D_*, \tag{4.3.25}$$

where $\mathbf{c}'$ and $\boldsymbol{\omega}'$ are vector constants.

On substituting (4.3.22) and (4.3.25) into (4.3.21), one finds by virtue of the divergence theorem and identity $\boldsymbol{\omega} \times \boldsymbol{\xi} = \boldsymbol{\Omega} \cdot \boldsymbol{\xi}$ where $\boldsymbol{\Omega} \equiv \boldsymbol{\omega} \times \boldsymbol{I}$ that

$$\int_{\partial D_*} \left[(\mathbf{c} + \mathbf{c}') + (\boldsymbol{\omega} + \boldsymbol{\omega}') \times \boldsymbol{\xi} \right] \cdot \bar{\boldsymbol{\Phi}} \cdot \boldsymbol{n} \, \mathrm{d}S \; + \; \int_{D_*} \boldsymbol{\Omega} : \boldsymbol{\Phi} \, \mathrm{d}V \; = \; 0 \qquad \forall \boldsymbol{\Phi} \in W(D_*). \tag{4.3.26}$$

Since the second integral vanishes due to the symmetry of $\boldsymbol{\Phi}$ and antisymmetry of $\boldsymbol{\Omega}$, (4.3.26) requires that $\mathbf{c}' = -\mathbf{c}$ and $\boldsymbol{\omega} = -\boldsymbol{\omega}'$. From (4.3.19), (4.3.20), (4.3.22) and (4.3.25), it now immediately follows that $(\boldsymbol{u}_*, \boldsymbol{u} + \mathbf{c} + \boldsymbol{\omega} \times \boldsymbol{\xi})$ is a solution to (4.3.6).

Parity between the existence of unique solutions.

- Assume that problem (4.3.6) has a unique strong solution, and let $U^1 = (\boldsymbol{u}_*^1, \boldsymbol{\mathcal{U}}^1, \boldsymbol{u}_\mathrm{o}^1)$ and $U^2 = (\boldsymbol{u}_*^2, \boldsymbol{\mathcal{U}}^2, \boldsymbol{u}_\mathrm{o}^2)$ denote two weak solutions to (4.3.15). By the equivalence between solutions to the two problems, one has that $(\boldsymbol{u}_*^1, \boldsymbol{u}^1, \boldsymbol{u}_\mathrm{o}^1)$ and $(\boldsymbol{u}_*^2, \boldsymbol{u}^2, \boldsymbol{u}_\mathrm{o}^2)$, with $(\boldsymbol{\nabla} \boldsymbol{u}^1 + \boldsymbol{\nabla}^\mathsf{T} \boldsymbol{u}^1)/2 = \boldsymbol{\mathcal{C}}^{-1} : \boldsymbol{\mathcal{U}}^1$ and $(\boldsymbol{\nabla} \boldsymbol{u}^2 + \boldsymbol{\nabla}^\mathsf{T} \boldsymbol{u}^2)/2 = \boldsymbol{\mathcal{C}}^{-1} : \boldsymbol{\mathcal{U}}^2$, are consequently solutions to (4.3.6). Since the latter two triplets must coincide by premise, it follows that that $\boldsymbol{u}_*^1 = \boldsymbol{u}_*^2$, $\boldsymbol{\mathcal{U}}^1 = \boldsymbol{\mathcal{U}}^2$ and $\boldsymbol{u}_\mathrm{o}^1 = \boldsymbol{u}_\mathrm{o}^2$, i.e. that the solution to the variational problem (4.3.15) is likewise unique.

- Conversely, assume that (4.3.15) has a unique weak solution, and let $(\boldsymbol{u}_*^1, \boldsymbol{u}^1, \boldsymbol{u}_\mathrm{o}^1)$ and $(\boldsymbol{u}_*^2, \boldsymbol{u}^2, \boldsymbol{u}_\mathrm{o}^2)$ denote two strong solutions to (4.3.6). Since $(\boldsymbol{u}_*^1, \boldsymbol{\mathcal{C}} : \boldsymbol{\nabla} \boldsymbol{u}^1, \boldsymbol{u}_\mathrm{o}^1)$ and $(\boldsymbol{u}_*^2, \boldsymbol{\mathcal{C}} : \boldsymbol{\nabla} \boldsymbol{u}^2, \boldsymbol{u}_\mathrm{o}^2)$ are consequently solutions to (4.3.15), one must have $\boldsymbol{u}_*^1 = \boldsymbol{u}_*^2$, $\boldsymbol{\nabla} \boldsymbol{u}^1 + \boldsymbol{\nabla}^\mathsf{T} \boldsymbol{u}^1 = \boldsymbol{\nabla} \boldsymbol{u}^2 + \boldsymbol{\nabla}^\mathsf{T} \boldsymbol{u}^2$ and $\boldsymbol{u}_\mathrm{o}^1 = \boldsymbol{u}_\mathrm{o}^2$ by premise. The proof is completed by noting that $\boldsymbol{u}^1$ and $\boldsymbol{u}^2$ are equal up to a rigid body motion, which must vanish thanks to the boundary condition (4.3.6d).

$\square$

4.4   Existence and uniqueness of a solution to the modified ITP

Having reduced the study of the modified ITP (4.3.6) to that of its variational statement (4.3.15), the question arises as to the conditions under which the latter problem is well-posed. For clarity of exposition, the focus is made on the *sufficient* conditions that compare the *elastic* parameters of the inclusion, comprising $\Re[\mathcal{C}_*]$, to those of the background in terms of $\Re[\mathcal{C}]$. In general, it is possible that the consideration of material dissipation (synthesized via $\Im[\mathcal{C}_*]$ and $\Im[\mathcal{C}]$) may relax the "elasticity" conditions under which (4.3.6) and (4.3.15) are elliptic, and thus help establish the sufficient *and* necessary conditions. The latter subject is, however, beyond the scope of this study. With such restraint, the following lemma helps establish the sufficient "elasticity" conditions.

Lemma 11. *With reference to Definition 1 specifying the bounds on the viscoelastic tensors $\mathcal{C}$ and $\mathcal{C}_*$, the sesquilinear form $\mathcal{A}$ is elliptic if the inequalities $\rho^p < \rho_*^p$ and $\mathsf{C}^p < \mathsf{c}_*^p$ hold in each "intersection" domain Θ_*^p, $p \in \{1, \ldots, N_*\}$.*

Proof. For $U = (\boldsymbol{u}_*, \mathcal{U}, \boldsymbol{u}_{\mathrm{o}}) \in \mathbb{E}$, one finds from (4.3.13) that

$$
\begin{aligned}
\mathcal{A}(U, U) = &\int_{D_*} [\boldsymbol{\nabla}\boldsymbol{u}_* : \mathcal{C}_* : \boldsymbol{\nabla}\bar{\boldsymbol{u}}_* + \rho_* \boldsymbol{u}_* \cdot \bar{\boldsymbol{u}}_*] \, \mathrm{d}V + \int_{D_*} \left[\frac{1}{\rho}(\boldsymbol{\nabla}\cdot\mathcal{U})\cdot(\boldsymbol{\nabla}\cdot\bar{\mathcal{U}}) + \mathcal{U} : \mathcal{C}^{-1} : \bar{\mathcal{U}}\right] \mathrm{d}V \\
&+ \int_{D_{\mathrm{o}}} [\boldsymbol{\nabla}\boldsymbol{u}_{\mathrm{o}} : \mathcal{C} : \boldsymbol{\nabla}\bar{\boldsymbol{u}}_{\mathrm{o}} + \rho\, \boldsymbol{u}_{\mathrm{o}} \cdot \bar{\boldsymbol{u}}_{\mathrm{o}}] \, \mathrm{d}V - \int_{\partial D_*} [\boldsymbol{u}_* \cdot \bar{\mathcal{U}} \cdot \boldsymbol{n} + (\mathcal{U}\cdot\boldsymbol{n})\cdot\bar{\boldsymbol{u}}_*] \, \mathrm{d}S.
\end{aligned}
\tag{4.4.1}
$$

On employing the divergence theorem, the triangle inequality, the Cauchy-Schwarz inequality, and definition of the "intersection" domains Θ_*^p, one finds

$$
\left|\int_{\partial D_*} \boldsymbol{\varphi}_* \cdot \bar{\boldsymbol{\Phi}} \cdot \boldsymbol{n} \, \mathrm{d}S\right| \leqslant \sum_{p=1}^{N_*} \left[\|\boldsymbol{\varphi}_*\|_{L^2(\Theta_*^p)}\|\boldsymbol{\nabla}\cdot\boldsymbol{\Phi}\|_{L^2(\Theta_*^p)} + \|\boldsymbol{\nabla}\boldsymbol{\varphi}_*\|_{L^2(\Theta_*^p)}\|\boldsymbol{\Phi}\|_{L^2(\Theta_*^p)}\right].
\tag{4.4.2}
$$

By virtue of the fact that $|\mathcal{A}(U,U)| \geqslant \Re[\mathcal{A}(U,U)]$, (4.4.2), and bounds (4.2.1) on (the real parts of) the viscoelasticity tensors $\mathcal{C}_*$ and $\mathcal{C}$ in each Θ_*^p, it can be further shown that

$$
\begin{aligned}
|\mathcal{A}(U,U)| \geqslant &\sum_{p=1}^{N_*} \left[\mathsf{c}_*^p\|\boldsymbol{\nabla}\boldsymbol{u}_*\|_{L^2(\Theta_*^p)}^2 + \rho_*^p\|\boldsymbol{u}_*\|_{L^2(\Theta_*^p)}^2 + \frac{1}{\rho^p}\|\boldsymbol{\nabla}\cdot\mathcal{U}\|_{L^2(\Theta_*^p)}^2 + \frac{1}{\mathsf{C}^p}\|\mathcal{U}\|_{L^2(\Theta_*^p)}^2\right] \\
&- 2\sum_{p=1}^{N_*} \left[\|\boldsymbol{u}_*\|_{L^2(\Theta_*^p)}\|\boldsymbol{\nabla}\cdot\mathcal{U}\|_{L^2(\Theta_*^p)} + \|\boldsymbol{\nabla}\boldsymbol{u}_*\|_{L^2(\Theta_*^p)}\|\mathcal{U}\|_{L^2(\Theta_*^p)}\right] \\
&+ \sum_{q=1}^{N_{\mathrm{o}}} \left[\mathsf{c}_{\mathrm{o}}^q\|\boldsymbol{\nabla}\boldsymbol{u}_{\mathrm{o}}\|_{L^2(\Theta_{\mathrm{o}}^q)}^2 + \rho_{\mathrm{o}}^q\|\boldsymbol{u}_{\mathrm{o}}\|_{L^2(\Theta_{\mathrm{o}}^q)}^2\right].
\end{aligned}
\tag{4.4.3}
$$

Since for every $(x, y) \in \mathbb{R}^2$, $\alpha > 0$, and $\beta > 0$ one has

$$
\alpha x^2 + \frac{1}{\beta}y^2 - 2xy = \frac{\alpha + \beta}{2}\left(x - \frac{2}{\alpha + \beta}y\right)^2 + (\alpha - \beta)\left(\frac{1}{2}x^2 + \frac{1/\beta}{\alpha + \beta}y^2\right),
\tag{4.4.4}
$$

inequality (4.4.3) can be rewritten as

$$
\begin{aligned}
|\mathcal{A}(U,U)| \geqslant \sum_{p=1}^{N_*} \Bigg[&\frac{\mathsf{c}_*^p + \mathsf{C}^p}{2} \left(\|\boldsymbol{\nabla}\boldsymbol{u}_*\|_{L^2(\Theta_*^p)} - \frac{2}{\mathsf{c}_*^p + \mathsf{C}^p} \|\boldsymbol{\mathcal{U}}\|_{L^2(\Theta_*^p)} \right)^2 \\
&+ (\mathsf{c}_*^p - \mathsf{C}^p) \left(\frac{1}{2}\|\boldsymbol{\nabla}\boldsymbol{u}_*\|_{L^2(\Theta_*^p)}^2 + \frac{1/\mathsf{C}^p}{\mathsf{c}_*^p + \mathsf{C}^p} \|\boldsymbol{\mathcal{U}}\|_{L^2(\Theta_*^p)}^2 \right) \\
&+ \frac{\rho_*^p + \rho^p}{2} \left(\|\boldsymbol{u}_*\|_{L^2(\Theta_*^p)} - \frac{2}{\rho_*^p + \rho^p} \|\boldsymbol{\nabla}\cdot\boldsymbol{\mathcal{U}}\|_{L^2(\Theta_*^p)} \right)^2 \\
&+ (\rho_*^p - \rho^p) \left(\frac{1}{2}\|\boldsymbol{u}_*\|_{L^2(\Theta_*^p)}^2 + \frac{1/\rho^p}{\rho_*^p + \rho^p} \|\boldsymbol{\nabla}\cdot\boldsymbol{\mathcal{U}}\|_{L^2(\Theta_*^p)}^2 \right) \Bigg] \\
&+ \sum_{q=1}^{N_\mathrm{o}} \left[\mathsf{c}_\mathrm{o}^q \|\boldsymbol{\nabla}\boldsymbol{u}_\mathrm{o}\|_{L^2(\Theta_\mathrm{o}^q)}^2 + \rho_\mathrm{o}^q \|\boldsymbol{u}_\mathrm{o}\|_{L^2(\Theta_\mathrm{o}^q)}^2 \right].
\end{aligned}
\tag{4.4.5}
$$

On introducing the lower-bound parameter

$$
\gamma = \min_{\substack{p=1,\ldots,N_* \\ q=1,\ldots,N_\mathrm{o}}} \left(\frac{\mathsf{c}_*^p - \mathsf{C}^p}{2}, \frac{\mathsf{c}_*^p - \mathsf{C}^p}{\mathsf{C}^p(\mathsf{c}_*^p + \mathsf{C}^p)}, \frac{\rho_*^p - \rho^p}{2}, \frac{\rho_*^p - \rho^p}{\rho^p(\rho_*^p + \rho^p)}, \mathsf{c}_\mathrm{o}^q, \rho_\mathrm{o}^q \right),
\tag{4.4.6}
$$

one finds that $\gamma > 0$ since $\rho^p < \rho_*^p$ and $\mathsf{C}^p < \mathsf{c}_*^p$ in each Θ_*^p by premise. On the basis of this result one finds, by dropping the "squared-difference" terms in (4.4.5), that

$$
|\mathcal{A}(U,U)| \geqslant \gamma \left[\sum_{p=1}^{N_*} \left(\|\boldsymbol{u}_*\|_{H^1(\Theta_*^p)}^2 + \|\boldsymbol{\mathcal{U}}\|_{W(\Theta_*^p)}^2 \right) + \sum_{q=1}^{N_\mathrm{o}} \|\boldsymbol{u}_\mathrm{o}\|_{H^1(\Theta_\mathrm{o}^q)}^2 \right].
\tag{4.4.7}
$$

Recalling that $U = (\boldsymbol{u}_*, \boldsymbol{\mathcal{U}}, \boldsymbol{u}_\mathrm{o}) \in \mathbb{E}$, the sesquilinear form $\mathcal{A}$ is consequently elliptic with

$$
|\mathcal{A}(U,U)| \geqslant \gamma \left(\|\boldsymbol{u}_*\|_{H^1(D_*)}^2 + \|\boldsymbol{\mathcal{U}}\|_{W(D_*)}^2 + \|\boldsymbol{u}_\mathrm{o}\|_{H^1(D_\mathrm{o})}^2 \right),
\tag{4.4.8}
$$

which completes the proof. $\qquad\square$

One is now in position to investigate the variational formulation of the modified ITP.

Theorem 4. *Under the assumptions of Lemma 11, variational problem (4.3.15) has a unique weak solution $U = (\boldsymbol{u}_*, \boldsymbol{\mathcal{U}}, \boldsymbol{u}_o) \in \mathbb{E}$ with an a priori estimate*

$$
\begin{aligned}
\|\boldsymbol{u}_*\|_{H^1(D_*)} &+ \|\boldsymbol{\mathcal{U}}\|_{W(D_*)} + \|\boldsymbol{u}_o\|_{H^1(D_o)} \leqslant \\
&\frac{3\,C}{\gamma} \left(\|\boldsymbol{f}_*\|_{L^2(D)} + \|\boldsymbol{f}\|_{L^2(D_*)} + \|\boldsymbol{g}\|_{H^{\frac{1}{2}}(\partial D_*)} + \|\boldsymbol{h}_*\|_{H^{-\frac{1}{2}}(\partial D_*)} + \|\boldsymbol{h}_o\|_{H^{-\frac{1}{2}}(\partial D_o)} \right),
\end{aligned}
\tag{4.4.9}
$$

where $\gamma > 0$ is given by (4.4.6), and $C > 0$ is a constant independent of $\boldsymbol{f}_*$, $\boldsymbol{f}$, $\boldsymbol{g}$, $\boldsymbol{h}_*$ and $\boldsymbol{h}_o$.

Proof. The norm of the antilinear operator $\mathcal{L}$ in (4.3.14) can be shown, by exercising the triangle inequality, the Cauchy-Schwarz inequality, the divergence theorem (applied to $\bar{\boldsymbol{\Phi}}$) and the trace theorem, to be continuous i.e. bounded with constant $C > 0$ independent of $\boldsymbol{f}_*$, $\boldsymbol{f}$, $\boldsymbol{g}$, $\boldsymbol{h}_*$ and $\boldsymbol{h}_\mathrm{o}$ such that

$$
\begin{aligned}
\|\mathcal{L}\|_{\mathbb{E}^\star} \leqslant C\Big(&\|\boldsymbol{f}_*\|_{L^2(D)} + \|\boldsymbol{f}\|_{L^2(D_*)} \\
&+ \|\boldsymbol{g}\|_{H^{\frac{1}{2}}(\partial D_*)} + \|\boldsymbol{h}_*\|_{H^{-\frac{1}{2}}(\partial D_*)} + \|\boldsymbol{h}_\mathrm{o}\|_{H^{-\frac{1}{2}}(\partial D_\mathrm{o})} \Big),
\end{aligned}
\tag{4.4.10}
$$

where $\mathbb{E}^{\star}$ denotes the dual of $\mathbb{E}$.

To establish the boundedness of the sesquilinear form $\mathcal{A}(U, V)$, on the other hand, one may introduce the notation

$$
\begin{aligned}
||U||_{\mathbb{E}}^2 &:= \|\boldsymbol{u}_*\|_{H^1(D_*)}^2 + \|\boldsymbol{\mathcal{U}}\|_{W(D_*)}^2 + \|\boldsymbol{u}_{\mathrm{o}}\|_{H^1(D_{\mathrm{o}})}^2, \\
||V||_{\mathbb{E}}^2 &:= \|\boldsymbol{\varphi}_*\|_{H^1(D_*)}^2 + \|\boldsymbol{\Phi}\|_{W(D_*)}^2 + \|\boldsymbol{\varphi}\|_{H^1(D_{\mathrm{o}})}^2,
\end{aligned}
\tag{4.4.11}
$$

for $U, V \in \mathbb{E}$ defined as in (4.3.15). In this setting, it follows from (4.3.15), the triangle inequality, (4.2.5), the Cauchy-Schwarz inequality, (4.4.2), (4.4.11), and bounds such as $||\boldsymbol{\nabla}\boldsymbol{u}_*||_{L^2(D_*)} \leqslant ||U||_{\mathbb{E}}$ that there is a constant $C' > 0$ such that

$$
|\mathcal{A}(U, V)| \leqslant C' \, ||U||_{\mathbb{E}} \, ||V||_{\mathbb{E}}.
\tag{4.4.12}
$$

Using the notation introduced in (4.4.11), (4.4.8) can also be rewritten more compactly as

$$
|\mathcal{A}(U, U)| \geqslant \gamma \, ||U||_{\mathbb{E}}^2.
\tag{4.4.13}
$$

With the boundedness (4.4.12) and coercivity (4.4.13) of $\mathcal{A}$ now verified, the existence of a unique solution to the variational problem (4.3.15) follows directly from the Lax-Milgram theorem (McLean, 2000) which ensures that $||U||_{\mathbb{E}} \leqslant \gamma^{-1}||\mathcal{L}||_{\mathbb{E}^{\star}}$. In this setting, a priori estimate (4.4.9) is derived as a consequence of (4.4.10), (4.4.11a), and upper bounds such as $\|\boldsymbol{u}_*\|_{H^1(D_*)} \leqslant ||U||_{\mathbb{E}}$. $\qquad\square$

Theorem 5. *Under the hypotheses of Lemma 11, modified ITP (4.3.6) has a unique strong solution* $(\boldsymbol{u}_*, \boldsymbol{u}, \boldsymbol{u}_o) \in H^1(D_*) \times H^1(D_*) \times H^1(D_o)$ *with an a priori estimate*

$$
\begin{aligned}
\|\boldsymbol{u}_*\|_{H^1(D_*)} &+ \|\boldsymbol{u}\|_{H^1(D_*)} + \|\boldsymbol{u}_o\|_{H^1(D_o)} \leqslant \\
&c \left(\|\boldsymbol{f}_*\|_{L^2(D)} + \|\boldsymbol{f}\|_{L^2(D_*)} + \|\boldsymbol{g}\|_{H^{\frac{1}{2}}(\partial D_*)} + \|\boldsymbol{h}_*\|_{H^{-\frac{1}{2}}(\partial D_*)} + \|\boldsymbol{h}_o\|_{H^{-\frac{1}{2}}(\partial D_o)} \right),
\end{aligned}
\tag{4.4.14}
$$

where $c > 0$ is a constant independent of $\boldsymbol{f}_*$, $\boldsymbol{f}$, $\boldsymbol{g}$, $\boldsymbol{h}_*$ and $\boldsymbol{h}_o$.

Proof. The first part of the claim, namely the existence and uniqueness of a strong solution to (4.3.6) follow directly from Theorems 3 and 4, while inequality (4.4.14) can be obtained on the basis of (4.3.6) and (4.4.9). In particular, from the relationship $\boldsymbol{\mathcal{U}} = \boldsymbol{\mathcal{C}} : \boldsymbol{\nabla}\boldsymbol{u}$ and the fact that $\boldsymbol{u}$ satisfies (4.3.6b), it follows via triangle inequality that

$$
\|\boldsymbol{u}\|_{L^2(D_*)} \leqslant \alpha \left(\|\boldsymbol{\mathcal{U}}\|_{W(D_*)} + \|\boldsymbol{f}\|_{L^2(D_*)} \right),
\tag{4.4.15}
$$

for some constant $\alpha > 0$. By virtue of the bounds on the viscoelasticity tensor $\boldsymbol{\mathcal{C}}$ in (4.2.1) and (4.2.2), on the other hand, one finds

$$
\|\boldsymbol{\nabla}\boldsymbol{u}\|_{L^2(D_*)} = \|\boldsymbol{\mathcal{C}}^{-1} : \boldsymbol{\mathcal{U}}\|_{L^2(D_*)} \leqslant \beta \, \|\boldsymbol{\mathcal{U}}\|_{W(D_*)},
\tag{4.4.16}
$$

for some $\beta > 0$. On combining (4.4.15) and (4.4.16) to obtain the $H^1(D_*)$ norm of $\boldsymbol{u}$, estimate (4.4.14) follows directly as a consequence of (4.4.9) with

$$
c \leqslant \left(2 + \sqrt{\alpha^2(1+\gamma)^2 + \beta^2} \right) \frac{C}{\gamma}.
$$

$\qquad\square$

4.5 Well-posedness of the ITP

Having established the conditions under which the modified problem (4.3.6) is uniquely solvable, one is now in position to study the existence and uniqueness of a solution to the (original) ITP (4.3.4).

Theorem 6. *Under the hypothesis that $\rho^p < \rho_*^p$ and $\mathsf{C}^p < \mathsf{c}_*^p$ in each "intersection" domain Θ_*^p, $p \in \{1, \ldots, N_*\}$ as in Lemma 11, the set of transmission eigenvalues $\omega \in \mathbb{C}$ for which the interior transmission problem (4.3.4) does not have a unique solution is either empty or forms a discrete set with infinity as the only possible accumulation point.*

Proof. With reference to the space $\Xi(D)$ introduced in (4.3.7), it is recalled that the modified ITP (4.3.6) is represented by the differential-trace operator $\mathcal{M}$ as in (4.3.8), while the original problem (4.3.4) is identified with operator $\mathcal{O} = \mathcal{M} + (1+\omega^2)\mathcal{P}$, where $\mathcal{P}$ is the compact perturbation given by (4.3.9). In Theorem 5 it is shown that $\mathcal{M}^{-1}$ exists, and furthermore that it is bounded i.e. continuous under the assumptions of Lemma 11. Theorem 6 claims that the operator $\mathcal{M} + (1+\omega^2)\mathcal{P}$ is invertible for all $\omega \in \mathbb{C}\backslash S$, where S is either an empty set or a discrete set of points in the complex plane $\mathbb{C}$. Since $\mathcal{M}^{-1}$ is continuous, this claim can be established by showing the analogous result for the operator

$$\mathcal{I} + (1+\omega^2)\,\mathcal{M}^{-1}\mathcal{P},$$

where $\mathcal{I}$ is the identity operator from $\Xi(D)$ into $\Xi(D)$. As shown in Section 4.3, operator $\mathcal{P}$ is compact owing to the compact embedding of $H^1(D)$ into $L^2(D)$, and so is $\mathcal{M}^{-1}\mathcal{P}$ by virtue of the continuity of $\mathcal{M}^{-1}$ (McLean, 2000). For this situation, the Fredholm alternative applies (Yosida, 1980) whereby

$$\left(\mathcal{I} + (1+\omega^2)\mathcal{M}^{-1}\mathcal{P}\right)^{-1}$$

exists and is bounded except for, at most, a *discrete* set of transmission eigenvalues $\omega \in S \subset \mathbb{C}$ (see also Definition 2). Finally, since the countable spectrum of (compact) operator $\mathcal{M}^{-1}\mathcal{P}$ can only accumulate at zero (Wloka, 1992), S is further characterized by infinity as the only possible accumulation point. $\qquad\square$

4.5.1 Relaxed solvability criterion

With reference to Theorem 6, it is noted that the eigenvalues of ITP (4.3.4) may form a countable set even in situations that violate the aforestated restriction: $\rho^p < \rho_*^p$ and $\mathsf{C}^p < \mathsf{c}_*^p$ in each Θ_*^p, $p \in \{1, \ldots, N_*\}$. Indeed, the latter condition can be relaxed in a way similar to that proposed in Charalambopoulos (2002), albeit without introducing additional complexities. To this end, recall (4.3.4) and let w denote the "combined" elastodynamic field in $D = D_* \cup D_\mathrm{o}$ so that u and u_o are the *restrictions* of w on D_* and D_o, respectively. Given $(f_*, f) \in L^2(D_*) \times L^2(D)$, $g \in H^{\frac{1}{2}}(\partial D_*)$, and $(h_*, h_\mathrm{o}) \in H^{-\frac{1}{2}}(\partial D_*) \times H^{-\frac{1}{2}}(\partial D_\mathrm{o})$, the focus is then made on finding $(u_*, w) \in H^1(D_*) \times H^1(D)$ that satisfies

$$\begin{aligned}
\boldsymbol{\nabla}\cdot[\mathcal{C}_*\!:\!\boldsymbol{\nabla}u_*] + \rho_*\omega^2 u_* &= f_* &&\text{in } D_*, \\
\boldsymbol{\nabla}\cdot[\mathcal{C}\!:\!\boldsymbol{\nabla}w] + \rho\omega^2 w &= f &&\text{in } D, \\
u_* &= w + g &&\text{on } \partial D_*, \\
t_*[u_*] &= t[w] + h_* &&\text{on } \partial D_*, \\
t[w] &= h_\mathrm{o} &&\text{on } \partial D_\mathrm{o},
\end{aligned} \qquad (4.5.1)$$

which is simply a restatement of (4.3.4). Following the developments in Section 4.3, the modified i.e. "regularized" counterpart of ITP (4.5.1) can be written as

$$\nabla \cdot [\mathcal{C}_* : \nabla \boldsymbol{u}_*] - \rho_* \boldsymbol{u}_* = \boldsymbol{f}_* \qquad \text{in } D_*, \tag{4.5.2a}$$

$$\nabla \cdot [\mathcal{C} : \nabla \boldsymbol{w}] - \rho \boldsymbol{w} = \boldsymbol{f} \qquad \text{in } D, \tag{4.5.2b}$$

$$\boldsymbol{u}_* = \boldsymbol{w} + \boldsymbol{g} \qquad \text{on } \partial D_*, \tag{4.5.2c}$$

$$\boldsymbol{t}_*[\boldsymbol{u}_*] = \boldsymbol{t}[\boldsymbol{w}] + \boldsymbol{h}_* \qquad \text{on } \partial D_*, \tag{4.5.2d}$$

$$\boldsymbol{t}[\boldsymbol{w}] = \boldsymbol{h}_{\mathrm{o}} \qquad \text{on } \partial D_{\mathrm{o}}, \tag{4.5.2e}$$

where $(\boldsymbol{u}_*, \boldsymbol{w}) \in H^1(D_*) \times H^1(D)$. In this setting, the conditions under which the transmission eigenvalues of (4.3.4) i.e. (4.5.1) form a countable set (see Theorem 6) can be extended through the following theorem.

Theorem 7. *Under the hypothesis that $\rho^p > \rho_*^p$ and $\mathsf{c}^p > \mathsf{C}_*^p$ in each "intersection" domain Θ_*^p, $p \in \{1, \ldots, N_*\}$, the set of transmission eigenvalues $\omega \in \mathbb{C}$ for which the interior transmission problem (4.5.1) i.e. (4.3.4) does not have a unique solution is either empty or forms a discrete set with infinity as the only possible accumulation point.*

Proof. The proof of the theorem follows directly from the foregoing developments provided that the variational formulation is slightly modified. To this end, define the space of second-order tensors

$$W_*(D_*) := \left\{ \boldsymbol{\Phi}_* \in L^2(D_*) : \boldsymbol{\Phi}_* = \boldsymbol{\Phi}_*^{\mathrm{T}}, \ \nabla \cdot \boldsymbol{\Phi}_* \in L^2(D_*) \text{ and } \nabla \times [\mathcal{C}_*^{-1} : \boldsymbol{\Phi}_*] = 0 \right\}, \tag{4.5.3}$$

equipped with the norm

$$\|\boldsymbol{\Phi}_*\|_{W_*(D_*)}^2 := \|\boldsymbol{\Phi}_*\|_{L^2(D_*)}^2 + \|\nabla \cdot \boldsymbol{\Phi}_*\|_{L^2(D_*)}^2. \tag{4.5.4}$$

Note that the only difference between (4.3.10) and (4.5.3) is that $\mathcal{C}$ has been replaced by $\mathcal{C}_*$. Next, let $\mathbb{E}_* = W_*(D_*) \times H^1(D)$ and define the sesquilinear form $\mathcal{A}_* : \mathbb{E}_* \times \mathbb{E}_* \to \mathbb{C}$ as

$$\mathcal{A}_*(U, V) := \int_{D_*} \left[\frac{1}{\rho_*} (\nabla \cdot \mathcal{U}_*) \cdot (\nabla \cdot \bar{\boldsymbol{\Phi}}_*) + \mathcal{U}_* : \mathcal{C}_*^{-1} : \bar{\boldsymbol{\Phi}}_* \right] \mathrm{d}V$$

$$+ \int_D \left[\nabla \boldsymbol{w} : \mathcal{C} : \nabla \bar{\boldsymbol{\varphi}} + \rho \, \boldsymbol{w} \cdot \bar{\boldsymbol{\varphi}} \right] \mathrm{d}V - \int_{\partial D_*} \left[(\mathcal{U}_* \cdot \boldsymbol{n}) \cdot \bar{\boldsymbol{\varphi}} + \boldsymbol{w} \cdot \bar{\boldsymbol{\Phi}}_* \cdot \boldsymbol{n} \right] \mathrm{d}S, \tag{4.5.5}$$

together with the antilinear form $\mathcal{L}_* : \mathbb{E}_* \to \mathbb{C}$

$$\mathcal{L}_*(V) := \int_{D_*} \frac{1}{\rho_*} \boldsymbol{f}_* \cdot (\nabla \cdot \bar{\boldsymbol{\Phi}}_*) \, \mathrm{d}V - \int_D \boldsymbol{f} \cdot \bar{\boldsymbol{\varphi}} \, \mathrm{d}V$$

$$+ \int_{\partial D_*} \left[\boldsymbol{g} \cdot \bar{\boldsymbol{\Phi}}_* \cdot \boldsymbol{n} - \boldsymbol{h}_* \cdot \bar{\boldsymbol{\varphi}} \right] \mathrm{d}S + \int_{\partial D_{\mathrm{o}}} \boldsymbol{h}_{\mathrm{o}} \cdot \bar{\boldsymbol{\varphi}} \, \mathrm{d}S, \tag{4.5.6}$$

where $U = (\mathcal{U}_*, \boldsymbol{w}) \in \mathbb{E}_*$ and $V = (\boldsymbol{\Phi}_*, \boldsymbol{\varphi}) \in \mathbb{E}_*$.

   With reference to the developments in Section (4.3), it can be next shown that $(\boldsymbol{u}_*, \boldsymbol{w}) \in H^1(D_*) \times H^1(D)$ uniquely solves ITP (4.5.2) *if and only if* $(\mathcal{U}_*, \boldsymbol{w}) \in \mathbb{E}_*$, such that $(\nabla \boldsymbol{u}_* + \nabla^{\mathrm{T}} \boldsymbol{u}_*)/2 = \mathcal{C}^{-1} : \mathcal{U}_*$, uniquely solves the variational problem

$$\mathcal{A}_*(U, V) = \mathcal{L}_*(V) \qquad \forall V = (\boldsymbol{\Phi}_*, \boldsymbol{\varphi}) \in \mathbb{E}_*. \tag{4.5.7}$$

With such equivalence, one may again make use of the fact that $|\mathcal{A}(U, U)| \geqslant \Re\left[\mathcal{A}(U, U)\right]$, (4.4.2), and bounds in (4.2.1) on the real parts of the viscoelasticity tensors $\mathcal{C}_*$ and $\mathcal{C}$ in each Θ_*^p, to show that

$$
\begin{aligned}
|\mathcal{A}_*(U, U)| \geqslant \sum_{p=1}^{N_*} & \left[\frac{1}{\rho_*^p}\|\boldsymbol{\nabla}\cdot\boldsymbol{\mathcal{U}}_*\|_{L^2(\Theta_*^p)}^2 + \frac{1}{\mathsf{C}_*^p}\|\boldsymbol{\mathcal{U}}_*\|_{L^2(\Theta_*^p)}^2 + \mathsf{c}^p\|\boldsymbol{\nabla}\boldsymbol{w}\|_{L^2(\Theta_*^p)}^2 + \rho^p\|\boldsymbol{w}\|_{L^2(\Theta_*^p)}^2\right] \\
& - 2\sum_{p=1}^{N_*} \left[\|\boldsymbol{w}\|_{L^2(\Theta_*^p)}\|\boldsymbol{\nabla}\cdot\boldsymbol{\mathcal{U}}_*\|_{L^2(\Theta_*^p)} + \|\boldsymbol{\nabla}\boldsymbol{w}\|_{L^2(\Theta_*^p)}\|\boldsymbol{\mathcal{U}}_*\|_{L^2(\Theta_*^p)}\right] \\
& + \sum_{q=1}^{N_\mathrm{o}} \left[\mathsf{c}_\mathrm{o}^q\|\boldsymbol{\nabla}\boldsymbol{w}\|_{L^2(\Theta_\mathrm{o}^q)}^2 + \rho_\mathrm{o}^q\|\boldsymbol{w}\|_{L^2(\Theta_\mathrm{o}^q)}^2\right].
\end{aligned}
\tag{4.5.8}
$$

On introducing the auxiliary parameter

$$
\gamma_* = \min_{\substack{p=1,\ldots,N_* \\ q=1,\ldots,N_\mathrm{o}}} \left(\frac{\mathsf{c}^p - \mathsf{C}_*^p}{2}, \frac{\mathsf{c}^p - \mathsf{C}_*^p}{\mathsf{C}_*^p(\mathsf{c}^p + \mathsf{C}_*^p)}, \frac{\rho^p - \rho_*^p}{2}, \frac{\rho^p - \rho_*^p}{\rho_*^p(\rho^p + \rho_*^p)}, \mathsf{c}_\mathrm{o}^q, \rho_\mathrm{o}^q\right),
\tag{4.5.9}
$$

which is strictly positive ($\gamma_* > 0$) when $\rho^p > \rho_*^p$ and $\mathsf{c}^p > \mathsf{C}_*^p$ in each Θ_*^p, one finds by virtue of (4.4.4) that

$$
|\mathcal{A}_*(U, U)| \geqslant \gamma_* \left[\sum_{p=1}^{N_*} \left(\|\boldsymbol{\mathcal{U}}_*\|_{W_*(\Theta_*^p)}^2 + \|\boldsymbol{w}\|_{H^1(\Theta_*^p)}^2\right) + \sum_{q=1}^{N_\mathrm{o}} \|\boldsymbol{w}\|_{H^1(\Theta_\mathrm{o}^q)}^2\right].
\tag{4.5.10}
$$

As a result, the sesquilinear form $\mathcal{A}_*$ is coercive with

$$
|\mathcal{A}_*(U, U)| \geqslant \gamma_*\|U\|_{\mathbb{E}_*}^2, \qquad \|U\|_{\mathbb{E}_*}^2 := \|\boldsymbol{\mathcal{U}}_*\|_{W_*(D_*)}^2 + \|\boldsymbol{w}\|_{H^1(D)}^2.
\tag{4.5.11}
$$

With the continuity i.e. boundedness of both antilinear form $\mathcal{L}_*$ and sesquilinear form $\mathcal{A}_*$ being direct consequences of the triangle inequality and the Cauchy-Schwarz inequality, the hypotheses of Lax-Milgram theorem are thus verified. This in turn guarantees a unique solution to the variational problem (4.5.7) with an a priori estimate

$$
\begin{aligned}
\|\boldsymbol{\mathcal{U}}_*\|_{W_*(D_*)} + \|\boldsymbol{w}\|_{H^1(D)} \leqslant \frac{2\,C_*}{\gamma_*}\Big(&\|\boldsymbol{f}_*\|_{L^2(D)} + \|\boldsymbol{f}\|_{L^2(D_*)} \\
& + \|\boldsymbol{g}\|_{H^{\frac{1}{2}}(\partial D_*)} + \|\boldsymbol{h}_*\|_{H^{-\frac{1}{2}}(\partial D_*)} + \|\boldsymbol{h}_\mathrm{o}\|_{H^{-\frac{1}{2}}(\partial D_\mathrm{o})}\Big),
\end{aligned}
\tag{4.5.12}
$$

where constant $C_* > 0$ is independent of $\boldsymbol{f}_*$, $\boldsymbol{f}$, $\boldsymbol{g}$, $\boldsymbol{h}_*$ and $\boldsymbol{h}_\mathrm{o}$, cf. (4.4.9). Following the argument presented in Section 4.4, one consequently finds that the strong solution $(\boldsymbol{u}_*, \boldsymbol{w}) \in H^1(D_*) \times H^1(D)$ solving modified ITP (4.5.2) i.e. (4.3.6) is likewise unique with an estimate

$$
\begin{aligned}
\|\boldsymbol{u}_*\|_{H^1(D_*)} + \|\boldsymbol{w}\|_{H^1(D)} \leqslant c_*\Big(&\|\boldsymbol{f}_*\|_{L^2(D)} + \|\boldsymbol{f}\|_{L^2(D_*)} \\
& + \|\boldsymbol{g}\|_{H^{\frac{1}{2}}(\partial D_*)} + \|\boldsymbol{h}_*\|_{H^{-\frac{1}{2}}(\partial D_*)} + \|\boldsymbol{h}_\mathrm{o}\|_{H^{-\frac{1}{2}}(\partial D_\mathrm{o})}\Big),
\end{aligned}
\tag{4.5.13}
$$

such that constant $c_* > 0$ is independent of $\boldsymbol{f}_*$, $\boldsymbol{f}$, $\boldsymbol{g}$, $\boldsymbol{h}_*$ and $\boldsymbol{h}_\mathrm{o}$, cf. (4.4.14). The proof of Theorem 7 can be brought to a close by introducing the auxiliary space

$$
\Xi_*(D) := \left\{(\boldsymbol{u}_*, \boldsymbol{w}) \in H^1(D_*) \times H^1(D) : \boldsymbol{\nabla}\cdot[\mathcal{C}_* : \boldsymbol{\nabla}\boldsymbol{u}_*] \in L^2(D_*),\, \boldsymbol{\nabla}\cdot[\mathcal{C} : \boldsymbol{\nabla}\boldsymbol{w}] \in L^2(D)\right\}
$$

and a *bijective* differential-trace operator $\mathcal{M}_*$, representing (4.5.2), from $\Xi_*(D)$ onto $L^2(D_*) \times L^2(D) \times H^{\frac{1}{2}}(\partial D_*) \times H^{-\frac{1}{2}}(\partial D_*) \times H^{-\frac{1}{2}}(\partial D_o)$ such that

$$\mathcal{M}_*(\boldsymbol{u}_*, \boldsymbol{w}) := \Big(\boldsymbol{\nabla} \cdot [\mathcal{C}_* : \boldsymbol{\nabla} \boldsymbol{u}_*] - \rho_* \boldsymbol{u}_*, \ \boldsymbol{\nabla} \cdot [\mathcal{C} : \boldsymbol{\nabla} \boldsymbol{w}] - \rho \boldsymbol{w},$$
$$(\boldsymbol{u}_* - \boldsymbol{w})_{|\partial D_*}, \ (\boldsymbol{t}_*[\boldsymbol{u}_*] - \boldsymbol{t}[\boldsymbol{w}])_{|\partial D_*}, \ \boldsymbol{t}[\boldsymbol{w}]_{|\partial D_o} \Big). \quad (4.5.14)$$

On defining the perturbation operator $\mathcal{P}_*$ from $\Xi_*(D)$ into $L^2(D_*) \times L^2(D) \times H^{\frac{1}{2}}(\partial D_*) \times H^{-\frac{1}{2}}(\partial D_*) \times H^{-\frac{1}{2}}(\partial D_o)$, namely

$$\mathcal{P}_*(\boldsymbol{u}_*, \boldsymbol{w}) := (\rho_* \boldsymbol{u}_*, \ \rho \, \boldsymbol{w}, \ \boldsymbol{0}, \ \boldsymbol{0}, \boldsymbol{0}) \quad (4.5.15)$$

that is compact by virtue of compact embedding of $H^1(D_*)$ into $L^2(D_*)$ and $H^1(D)$ into $L^2(D)$, one can finally apply the Fredholm alternative to the compound operator $\mathcal{I} + (1 + \omega^2)\,\mathcal{M}_*^{-1}\mathcal{P}_*$ whereby

$$\big(\mathcal{I} \ + \ (1 + \omega^2)\,\mathcal{M}_*^{-1}\mathcal{P}_* \big)^{-1}$$

exists and is bounded except for at most a countable set of values $\omega \in S_* \subset \mathbb{C}$. Again, S_* is characterized by infinity as the only possible accumulation point, since the countable spectrum of $\mathcal{M}_*^{-1}\mathcal{P}_*$ can only accumulate at zero.

$\square$

Remark.   With reference to Theorems 6 and 7, it will be assumed throughout the remainder of this study that either

$$\rho^p < \rho_*^p \quad \text{and} \quad \mathsf{C}^p < \mathsf{c}_*^p, \qquad \forall p \in \{1, \ldots, N_*\}, \quad (4.5.16)$$

or

$$\rho^p > \rho_*^p \quad \text{and} \quad \mathsf{c}^p > \mathsf{C}_*^p, \qquad \forall p \in \{1, \ldots, N_*\}. \quad (4.5.17)$$

As shown via the foregoing theorems, the compliance with either (4.5.16) or (4.5.17) represents a *sufficient condition* for the ellipticity of the modified ITP (4.3.6) and thus for the unique solvability of ITP (4.3.4) provided that ω does not belong to a countable spectrum of transmission eigenvalues.

4.6   Can the set of transmission eigenvalues be empty?

In light of the foregoing results which establish sufficient conditions for the countability of the transmission eigenvalue set via the analysis of *elastic* parameters $\Re[\mathcal{C}]$ and $\Re[\mathcal{C}_*]$, it is next of interest to examine whether the material attenuation, manifest via $\Im[\mathcal{C}]$ and $\Im[\mathcal{C}_*]$, can bring about the uniqueness of a solution to the interior transmission problem (4.3.4) for all $\omega \in \mathbb{C}$. To this end, it is useful to introduce two auxiliary measures of the "viscosity" of the system

$$\begin{aligned}
\mathscr{V}_{\min}[\mathcal{C}, D] &:= \quad \inf\{\Im[\boldsymbol{\xi} : \mathcal{C} : \bar{\boldsymbol{\xi}}] : \boldsymbol{\xi} \in D\} \geqslant 0, \\
\mathscr{V}_{\max}[\mathcal{C}, D] &:= \quad \sup\{\Im[\boldsymbol{\xi} : \mathcal{C} : \bar{\boldsymbol{\xi}}] : \boldsymbol{\xi} \in D\} \geqslant 0,
\end{aligned}$$

where $\boldsymbol{\xi}$ is a complex-valued, second-order tensor field in D such that $|\boldsymbol{\xi}|^2 = 1$. On the basis of Definition 1, it is clear that $\mathscr{V}_{\max}[\mathcal{C}, D]$ takes zero value only if $\Im[\mathcal{C}]$ (and thus V) vanishes identically in D.

Theorem 8. *Let $D'_o \subseteq D_o$ and $D'_* \subseteq D_*$ denote the "viscoelastic" regions, preserving respectively the topology of D_o and D_*, that each have a support of non-zero measure. If either*

$$\mathcal{V}_{min}[\mathcal{C}, D'_o] > 0 \quad and \quad \mathcal{V}_{min}[\mathcal{C}, D'_*] > 0 \quad and \quad \mathcal{V}_{max}[\mathcal{C}_*, D_*] = 0 \tag{4.6.1}$$

or

$$\mathcal{V}_{min}[\mathcal{C}, D'_o] > 0 \quad and \quad \mathcal{V}_{max}[\mathcal{C}, D_*] = 0 \quad and \quad \mathcal{V}_{min}[\mathcal{C}_*, D'_*] > 0 \tag{4.6.2}$$

the interior transmission problem (4.3.4) has at most one solution. In other words, the multiplicity of solutions to ITP (4.3.4) is precluded if there is a region $D'_o \subseteq D_o$ where $\mathcal{C}$ is viscoelastic and a region $D'_* \subseteq D_*$ where <u>either</u> $\mathcal{C}$ or $\mathcal{C}_*$ is viscoelastic.

Proof. Let $(\boldsymbol{u}_*, \boldsymbol{u}, \boldsymbol{u}_o)$ be the algebraic difference between two solutions to the interior transmission problem (4.3.4). The displacement field $\boldsymbol{u}_o$, being solution to the homogeneous Neumann problem over D_o, vanishes identically owing to the premise that $\mathcal{V}_{min}[\mathcal{C}, D'_o] > 0$ where D'_o preserves the topology of D_o. From the homogeneous counterparts of (4.3.4a) and (4.3.4b), on the other hand, one finds by employing the divergence theorem together with boundary conditions $\boldsymbol{u} = \boldsymbol{u}_*$ and $\boldsymbol{t}[\boldsymbol{u}] = \boldsymbol{t}_*[\boldsymbol{u}_*]$ over ∂D_* that

$$\int_{D_*} \left[\boldsymbol{\nabla}\boldsymbol{u} : \mathcal{C} : \boldsymbol{\nabla}\bar{\boldsymbol{u}} - \rho\,\omega^2 \boldsymbol{u} \cdot \bar{\boldsymbol{u}} \right] \, \mathrm{d}V = \int_{\partial D_*} \boldsymbol{t}[\boldsymbol{u}] \cdot \bar{\boldsymbol{u}} \, \mathrm{d}S =$$
$$= \int_{\partial D_*} \boldsymbol{t}_*[\boldsymbol{u}_*] \cdot \bar{\boldsymbol{u}}_* \, \mathrm{d}S = \int_{D_*} \left[\boldsymbol{\nabla}\boldsymbol{u}_* : \mathcal{C}_* : \boldsymbol{\nabla}\bar{\boldsymbol{u}}_* - \rho_*\omega^2 \boldsymbol{u}_* \cdot \bar{\boldsymbol{u}}_* \right] \, \mathrm{d}V. \tag{4.6.3}$$

The triviality of $\boldsymbol{u}$ and $\boldsymbol{u}_*$ can now be established by taking the imaginary part of (4.6.3) which reads

$$\int_{D_*} \boldsymbol{\nabla}\boldsymbol{u} : \Im[\mathcal{C}] : \boldsymbol{\nabla}\bar{\boldsymbol{u}} \, \mathrm{d}V = \int_{D_*} \boldsymbol{\nabla}\boldsymbol{u}_* : \Im[\mathcal{C}_*] : \boldsymbol{\nabla}\bar{\boldsymbol{u}}_* \, \mathrm{d}V. \tag{4.6.4}$$

Assuming (4.6.1) which requires the right-hand side of (4.6.4) to vanish, one finds by virtue of (4.2.2) that

$$0 \leq \int_{D'_*} \boldsymbol{\nabla}\boldsymbol{u} : \Im[\mathcal{C}] : \boldsymbol{\nabla}\bar{\boldsymbol{u}} \, \mathrm{d}V \leq \int_{D_*} \boldsymbol{\nabla}\boldsymbol{u} : \Im[\mathcal{C}] : \boldsymbol{\nabla}\bar{\boldsymbol{u}} \, \mathrm{d}V = 0,$$

which via Korn's inequality (Nečas and Hlaváček, 1981; Marsden and Hughes, 1994) yields $\boldsymbol{\nabla}\boldsymbol{u} = \boldsymbol{0}$ in D'_*. On recalling the field equation (4.3.4b) with $\boldsymbol{f} = \boldsymbol{0}$, it follows that $\boldsymbol{u} = \boldsymbol{0}$ in D'_* as well. By way of the Holmgren's uniqueness theorem for piecewise-homogeneous bodies (Guzina and Madyarov, 2007) and hypothesis that D'_* preserves the topology of D_*, the trivial Cauchy data $\boldsymbol{u} = \boldsymbol{t}[\boldsymbol{u}] = \boldsymbol{0}$ on $\partial D'_*$ can now be uniquely extended to demonstrate that $\boldsymbol{u} = \boldsymbol{0}$ in D_* and consequently that $\boldsymbol{u} = \boldsymbol{t}[\boldsymbol{u}] = \boldsymbol{0}$ on ∂D_*. On the basis of the interfacial conditions (4.3.4d) and (4.3.4e) with $\boldsymbol{g} = \boldsymbol{0}$ and $\boldsymbol{h}_* = \boldsymbol{0}$, one further has $\boldsymbol{u}_* = \boldsymbol{t}_*[\boldsymbol{u}_*] = \boldsymbol{0}$ on ∂D_*, so that finally $\boldsymbol{u}_* = \boldsymbol{0}$ in D_* by virtue of the Holmgren's uniqueness theorem. The companion claim, namely that the solution difference $(\boldsymbol{u}_*, \boldsymbol{u}, \boldsymbol{u}_o)$ vanishes identically when (4.6.2) is met, can be established in an analogous fashion. $\qquad\square$

One is now in position to demonstrate, under suitable restriction on $\mathcal{C}$, $\mathcal{C}_*$, ρ and ρ_*, the existence of a unique strong solution to the interior transmission problem (4.3.4) $\forall\omega \in \mathbb{C}$.

Theorem 9. *Assuming that either (4.5.16) or (4.5.17) hold in terms of $\rho, \rho_*, \Re[\mathcal{C}]$ and $\Re[\mathcal{C}_*]$, and that either (4.6.1) or (4.6.2) hold in terms of $\Im[\mathcal{C}]$ and $\Im[\mathcal{C}_*]$, ITP (4.3.4) has a unique strong solution $(\boldsymbol{u}_*, \boldsymbol{u}, \boldsymbol{u}_o) \in H^1(D_*) \times H^1(D_*) \times H^1(D_o)$ with an a priori estimate*

$$\|\boldsymbol{u}_*\|_{H^1(D_*)} + \|\boldsymbol{u}\|_{H^1(D_*)} + \|\boldsymbol{u}_o\|_{H^1(D_o)} \leqslant c \Big(\|\boldsymbol{f}_*\|_{L^2(D)} + \|\boldsymbol{f}\|_{L^2(D_*)}$$

$$+ \|\boldsymbol{g}\|_{H^{\frac{1}{2}}(\partial D_*)} + \|\boldsymbol{h}_*\|_{H^{-\frac{1}{2}}(\partial D_*)} + \|\boldsymbol{h}_o\|_{H^{-\frac{1}{2}}(\partial D_o)} \Big) \quad (4.6.5)$$

where constant $c > 0$ is independent of $\boldsymbol{f}_*, \boldsymbol{f}, \boldsymbol{g}, \boldsymbol{h}_*$ and $\boldsymbol{h}_o$.

Proof. The above claim is a direct consequence of Theorems 6, 7, and 8. To illustrate the proof, assume that (4.5.16) and either (4.6.1) or (4.6.2) are met, and recall the definition of operators $\mathcal{M}$ and $\mathcal{P}$ given respectively by (4.3.8) and (4.3.9). By Theorem 6, operator $\mathcal{O} = \mathcal{M} + (1+\omega^2)\mathcal{P}$ identified with ITP (4.3.4) is surjective, whereas Theorem 8 assures that $\mathcal{O}$ is injective. As a consequence, $\mathcal{O}$ is bijective with bounded inverse (Cakoni and Colton, 2006). Thus there exists a unique solution to the interior transmission problem (4.3.4), for all $\omega \in \mathbb{C}$, verifying the a priori estimate (4.6.5). The proof when (4.5.17) holds in lieu of (4.5.16) can be established in an analogous fashion on the basis of Theorems 7 and 8, recalling that $\boldsymbol{u} \equiv \boldsymbol{w}_{|D_*}$ and $\boldsymbol{u}_o \equiv \boldsymbol{w}_{|D_o}$ in terms of the "combined" field $\boldsymbol{w}$ such that $(\boldsymbol{u}_*, \boldsymbol{w}) \in H^1(D_*) \times H^1(D)$ solves (4.5.1). □

Remark. Implicit in the foregoing analysis is the fact that the solution, $\boldsymbol{u}_o$, to the homogeneous ITP over D_o is *uncoupled* from $\boldsymbol{u}$ and $\boldsymbol{u}_*$ in that it solves the interior Neumann problem

$$\boldsymbol{\nabla} \cdot [\mathcal{C} : \boldsymbol{\nabla} \boldsymbol{u}_o] + \rho\omega^2 \boldsymbol{u}_o = \boldsymbol{0} \quad \text{in } D_o,$$

$$\boldsymbol{t}[\boldsymbol{u}_o] = \boldsymbol{0} \qquad\qquad \text{on } \partial D_o.$$

As a result, $\boldsymbol{u}_o$ will by itself introduce discrete eigenvalues into the problem (Kupradze, 1965) as soon as the restriction $\mathcal{C}_{|D_o}$ is elastic i.e. real-valued. This is reflected in Theorem 8 which precludes such possibility by requiring that $\mathscr{V}_{\min}[\mathcal{C}, D_o'] > 0$ where $D_o' \subseteq D_o$ has a support of non-zero measure and preserves the topology of D_o. To provide a focus in the study, this assumption will be retained hereon.

With the above premise, consider next the "elastic-elastic" case

$$\mathscr{V}_{\min}[\mathcal{C}, D_o'] > 0 \qquad \text{and} \qquad \mathscr{V}_{\max}[\mathcal{C}, D_*] = 0 \qquad \text{and} \qquad \mathscr{V}_{\max}[\mathcal{C}_*, D_*] = 0,$$

where both $\mathcal{C}$ and $\mathcal{C}_*$ are real-valued everywhere in D_*. In this situation, both sides of (4.6.4) vanish which precludes the foregoing analysis from emptying the (countable) set of transmission eigenvalues. This is consistent with the well-known behavior of the interior Dirichlet and Neumann problems in elastodynamics Kupradze (1965) which are known to have discrete eigenvalues.

If the same procedure as in Theorem 8 is applied to the "viscoelastic-viscoelastic" case, on the other hand, where both $\mathcal{C}$ and $\mathcal{C}_*$ are (at least intermittently) complex-valued such that

$$\mathscr{V}_{\min}[\mathcal{C}, D_o'] > 0 \qquad \text{and} \qquad \mathscr{V}_{\min}[\mathcal{C}, D_*'] > 0 \qquad \text{and} \qquad \mathscr{V}_{\min}[\mathcal{C}_*, D_*''] > 0, \qquad (4.6.6)$$

where $D_*' \cap D_c \neq \emptyset$, $D_*'' \cap D_c \neq \emptyset$, and $D_c \subset D_*$ is *connected*, one finds that both sides of (4.6.4) are non-trivial over D_c, which again fails to eliminate the transmission eigenvalues. Note that the featured assumption on D_*' and D_*'' physically means that there is at least one connected piece, $D_c \subset D_*$, where

both $\mathcal{C}$ and $\mathcal{C}_*$ are at least partially viscoelastic. This of course encompasses the case where $\mathcal{C}$ and $\mathcal{C}_*$ are complex-valued throughout. To better understand such counter-intuitive result whereby the introduction of "additional" material dissipation relative to that in Theorem 8 may lead to the loss of injectivity, it is useful to re-examine the problem within an energetic framework.

4.6.1 Energy balance

To establish the energetic analogue of (4.6.3) and (4.6.4), involved in the proof of Theorem 8, consider the case of steady-state viscoelastic vibrations as in Carcione and Cavallini (1993). With reference to the implicit time-harmonic factor $e^{i\omega t}$, one may recall the expressions for the *velocity* fields, $\boldsymbol{v} = i\omega\boldsymbol{u}$ and $\boldsymbol{v}_* = i\omega\boldsymbol{u}_*$, over D_* which allows one to interpret

$$
\begin{aligned}
\Im[\boldsymbol{\nabla u}:\mathcal{C}:\boldsymbol{\nabla\bar{u}}] &= \frac{1}{\pi}\int_0^T \Re[\mathcal{C}:\boldsymbol{\nabla u}\,e^{i\omega t}]:\Re[\boldsymbol{\nabla v}e^{i\omega t}]\,\mathrm{d}t \equiv \frac{1}{\pi}\,\mathcal{E}^{\mathrm{D}}, \\
\Im[\boldsymbol{\nabla u}_*:\mathcal{C}_*:\boldsymbol{\nabla\bar{u}}_*] &= \frac{1}{\pi}\int_0^T \Re[\mathcal{C}_*:\boldsymbol{\nabla u}_*\,e^{i\omega t}]:\Re[\boldsymbol{\nabla v}_*e^{i\omega t}]\,\mathrm{d}t \equiv \frac{1}{\pi}\,\mathcal{E}_*^{\mathrm{D}},
\end{aligned}
\tag{4.6.7}
$$

in terms of the dissipated energy densities, $\mathcal{E}^{\mathrm{D}}$ and $\mathcal{E}_*^{\mathrm{D}}$ in D_*, calculated per period of vibrations $T = 2\pi/\omega$. Similarly, one finds that

$$
\begin{aligned}
\Im[\boldsymbol{t}[\boldsymbol{u}]\cdot\boldsymbol{\bar{u}}] &= \frac{1}{\pi}\int_0^T \Re[\boldsymbol{t}[\boldsymbol{u}]e^{i\omega t}]\cdot\Re[\boldsymbol{v}e^{i\omega t}]\,\mathrm{d}t \equiv \frac{1}{\pi}\,\mathcal{F}^{\mathrm{D}}, \\
\Im[\boldsymbol{t}_*[\boldsymbol{u}_*]\cdot\boldsymbol{\bar{u}}_*] &= \int_0^T \Re[\boldsymbol{t}_*[\boldsymbol{u}_*]e^{i\omega t}]\cdot\Re[\boldsymbol{v}_*e^{i\omega t}]\,\mathrm{d}t \equiv \frac{1}{\pi}\,\mathcal{F}_*^{\mathrm{D}},
\end{aligned}
\tag{4.6.8}
$$

carry the meaning of energy influx densities, $\mathcal{F}^{\mathrm{D}}$ and $\mathcal{F}_*^{\mathrm{D}}$ over ∂D_*, reckoned per period of vibrations. On the basis of (4.6.7) and (4.6.8), the imaginary part of (4.6.3) can be written as

$$
\int_{D_*}\mathcal{E}^{\mathrm{D}}\,\mathrm{d}V = \int_{\partial D_*}\mathcal{F}^{\mathrm{D}}\,\mathrm{d}S = \int_{D_*}\mathcal{E}_*^{\mathrm{D}}\,\mathrm{d}V = \int_{\partial D_*}\mathcal{F}_*^{\mathrm{D}}\,\mathrm{d}S,
\tag{4.6.9}
$$

which states that any solution to the homogeneous ITP must be such that the dissipated energies over D_*, and corresponding energy influxes over ∂D_*, are the same for both bodies. In this setting it is clear that when either body is purely elastic over D_* as specified by (4.6.1) and (4.6.2), the equality of dissipated energies (4.6.9) requires the displacement field in the viscoelastic companion to vanish by virtue of the positive definiteness (4.2.2) of the imaginary part of the viscoelastic tensor. From the vanishing Cauchy data on ∂D_*, one consequently finds by virtue of the Holmgren's uniqueness theorem (Guzina and Madyarov, 2007) that the solution in the elastic body must vanish as well. When both bodies are viscoelastic as in (4.6.6), on the other hand, one finds from (4.6.9) that

$$
\int_{D_c}\mathcal{E}^{\mathrm{D}}\,\mathrm{d}V = \int_{\partial D_c}\mathcal{F}^{\mathrm{D}}\,\mathrm{d}S = \int_{D_c}\mathcal{E}_*^{\mathrm{D}}\,\mathrm{d}V = \int_{\partial D_c}\mathcal{F}_*^{\mathrm{D}}\,\mathrm{d}S > 0,
\tag{4.6.10}
$$

where D_c is a connected piece of D_*, and the foregoing approach provides no means to preclude the existence of non-trivial solutions to the homogeneous ITP. In particular, (4.6.10) demonstrates the homogeneous ITP is *not mechanically isolated* from its surroundings in the sense that it permits positive energy influx into both bodies over $\partial D_c \subset \partial D_*$ even though the jump between the respective Cauchy data, specified via $\boldsymbol{g}$ and $\boldsymbol{h}_*$, vanishes.

4.7 Results and discussion

Comparison with existing results. In Section 4.5, it is shown that ITP (4.3.4) is well-posed when ω does not belong to (at most) countable set of transmission eigenvalues, *provided* that either (4.5.16) or (4.5.17) holds. These sufficient conditions, formulated in terms of the material-parameter distributions $(\mathcal{C}, \rho)$ and $(\mathcal{C}_*, \rho_*)$, state that

$$\text{either} \qquad \rho^p < \rho_*^p, \ \ \mathsf{C}^p < \mathsf{c}_*^p \qquad \text{or} \qquad \rho^p > \rho_*^p, \ \ \mathsf{c}^p > \mathsf{C}_*^p \qquad \forall p \in \{1, \dots, N_*\}, \qquad (4.7.1)$$

where C and c signify respectively the maximum and minimum eigenvalues of the real part of a fourth-order viscoelasticity tensor $\mathcal{C}$ as examined earlier.

To the authors' knowledge, the first (and only existing) study of an elastodynamic ITP involving heterogeneous bodies can be found in Charalambopoulos (2002), who assumed that: i) the obstacle and the background are both non-dissipative i.e. elastic; ii) the background is homogeneous with unit mass density, and iii) the obstacle is in the form of a single connected inclusion with bounded but otherwise arbitrary distribution of elastic properties. Within the framework of the present investigation, these hypotheses can be summarized as

$$\Im[\mathcal{C}] = \Im[\mathcal{C}_*] = \mathbf{0}, \qquad \mathcal{C} = \text{const.}, \qquad \rho = 1, \qquad \mathcal{C}_* < \infty, \qquad D \equiv D_*. \qquad (4.7.2)$$

With such assumptions, (Charalambopoulos, 2002) employed the variational formulation analogous to that in this study (following Hähner (2000); Cakoni et al. (2002)) and obtained sufficient conditions for the countability of the transmission eigenvalue spectrum as

$$\text{either} \qquad \rho_*^{\min} \geqslant \mathsf{c}_*^{\min} > \frac{\mathsf{C}^2}{\mathsf{c}} \qquad \text{or} \qquad \rho_*^{\max} < \frac{\mathsf{c}}{\mathsf{C}^2}, \ \ \mathsf{C}_*^{\max} < \frac{\mathsf{c}}{\mathsf{C}^2}, \qquad (4.7.3)$$

where

$$\begin{aligned} \rho_*^{\min} &= \inf\{\rho_* : \boldsymbol{\xi} \in D\}, \qquad \rho_*^{\max} = \sup\{\rho_* : \boldsymbol{\xi} \in D\}, \\ \mathsf{c}_*^{\min} &= \inf\{\mathsf{c}_* : \boldsymbol{\xi} \in D\}, \qquad \mathsf{C}_*^{\max} = \sup\{\mathsf{C}_* : \boldsymbol{\xi} \in D\}. \end{aligned} \qquad (4.7.4)$$

Despite the fact that all quantities in (4.7.3) are dimensionless, conditions (4.7.3) are unfortunately non-informative as either set of inequalities could be, for a given ITP, *both* met and violated depending on the choice of the reference modulus K_0 in Table 4.1 used to normalize $\mathcal{C}$ and $\mathcal{C}_*$ (note that ρ_0 must equal the mass density of the background solid to have $\rho = 1$). As a point of reference, sufficient conditions (4.7.1) obtained in this study can be degenerated by virtue of (4.7.2) and (4.7.4) to conform with the hypotheses made in Charalambopoulos (2002) as

$$\text{either} \qquad \rho_*^{\min} > 1, \ \ \mathsf{c}_*^{\min} > \mathsf{C} \qquad \text{or} \qquad \rho_*^{\max} < 1, \ \ \mathsf{C}_*^{\max} < \mathsf{c}. \qquad (4.7.5)$$

This counterpart of (4.7.3), that is invariant under the choice of ρ_0 and K_0, can be qualitatively described as a requirement that the inclusion be either "denser and stiffer" or "lighter and softer" than the background solid throughout – a condition which guarantees that ITP (4.3.4), subject to hypotheses (4.7.2), is characterized by a countable spectrum of transmission eigenvalues.

In the context of dissipative solids, (Charalambopoulos et al., 2002) considered the ITP for a homogeneous viscoelastic obstacle in a homogeneous elastic background. For the particular case where the prescribed jump in Cauchy data, manifest via $\boldsymbol{g}$ and $\boldsymbol{h}_*$ in the present study, is given by the traces of the elastodynamic fundamental solution, they established the existence and uniqueness of a solution to the

featured ITP via a volume integral approach. Most recently, Charalambopoulos and Anagnostopoulos (2008) investigated the ITP in isotropic elasticity for the canonical case where both the inclusion and the background solid are homogeneous. By making recourse to the integral equation approach, ellipticity of the elastostatic ITP, and the compact perturbation argument, they arrived at sufficient conditions for the countability of the transmission eigenvalue spectrum as

$$\text{either} \quad \mu_* > \mu, \ \kappa_* > \kappa \quad \text{or} \quad \mu_* < \mu, \ \kappa_* < \kappa. \tag{4.7.6}$$

For completeness, sufficient conditions (4.7.1) can be degenerated by virtue of (4.2.4) to the homogeneous-isotropic-elastic case as

$$\begin{aligned} 0 < \nu < \tfrac{1}{2} \quad &\Rightarrow \quad \text{either} \quad \rho_* > \rho, \ 2\mu_* > 3\kappa \quad \text{or} \quad \rho_* < \rho, \ 3\kappa_* < 2\mu, \\ -1 < \nu_* < 0 \quad &\Rightarrow \quad \text{either} \quad \rho_* > \rho, \ 3\kappa_* > 2\mu \quad \text{or} \quad \rho_* < \rho, \ 2\mu_* < 3\kappa. \end{aligned} \tag{4.7.7}$$

Clearly, inequalities (4.7.7) are more restrictive than those in (4.7.6), most notably in that they entail a relationship between the mass densities of the inclusion and the background. The principal reason for such distinction lies in the fact that Charalambopoulos and Anagnostopoulos (2008) centered their analysis around the *elastostatic* ITP, deployed as an elliptic (and compact) perturbation of the featured (elastodynamic) ITP. Unfortunately, the weak formulation of the modified ITP employed in this study does not permit elastostatic analysis as it would formally require setting ρ and ρ_* in (4.3.6) and thus in (4.3.13) and (4.3.14) to zero, which both introduces unbounded terms and destroys the required H^1-structure of the quadratic form $\mathcal{A}(U, U)$. Despite this apparent limitation formulas (4.7.1) provide, for the first time, an objective set of sufficient conditions that ensure the well-posedness of the visco-elastodynamic ITP in a fairly general situation (where both the obstacle and the background solid can be heterogeneous, anisotropic, and dissipative) provided that the excitation frequency does not belong to (at most) countable spectrum of transmission eigenvalues.

4.7.1 Analytical examples

Assuming that either (4.5.16) or (4.5.17) holds, it is shown in Section 4.5 that the set of transmission eigenvalues characterizing ITP (4.3.4) is at most discrete. Except for the "elastic-viscoelastic" case examined in Theorem 8, however, it is not known whether this set is nonempty. For the ITP in acoustics, it was demonstrated in Colton and Kirsch (1996) that the transmission eigenvalues indeed exist for certain problem configurations. For completeness, this possibility is examined in the context of (visco-) elastic waves via two analytical examples.

Longitudinal waves in rods. Consider the interior transmission problem involving longitudinal waves in two thin prismatic rods having unit length and equal cross-sectional areas. In this setting, let $(E, E_*) \in \mathbb{C}^2$ and $(\rho, \rho_*) \in \mathbb{R}^2$ denote respectively the constant Young's moduli and mass densities of the two rods. One seeks a non-trivial displacement solution, (u, u_*), of the homogeneous ITP associated with

frequency $\omega > 0$ so that

$$
\begin{aligned}
& E_* \frac{d^2 u_*}{dx^2} + \rho_* \omega^2 u_* = 0 && \text{in } [0, 1], \\
& E \frac{d^2 u}{dx^2} + \rho\, \omega^2 u = 0 && \text{in } [0, 1], \\
& u_*(0) = u(0), \qquad u_*(1) = u(1), \\
& E_* \frac{du_*}{dx}(0) = E \frac{du}{dx}(0), \qquad E_* \frac{du_*}{dx}(1) = E \frac{du}{dx}(1).
\end{aligned}
\tag{4.7.8}
$$

Clearly, the solution to (4.7.8) entails four unknown constants, computable from the algebraic system of equations whose determinant vanishes when ω is a transmission eigenvalue. To examine this possibility, one may adopt the inverse of the featured determinant, termed F_r, as an indicator function. On the basis of (4.7.8), on finds that

$$
F_r = \left| \det \begin{pmatrix}
1 & 1 & -1 & -1 \\
e^{\mathrm{i}\frac{\omega}{c}} & e^{-\mathrm{i}\frac{\omega}{c}} & -e^{\mathrm{i}\frac{\omega}{c_*}} & -e^{-\mathrm{i}\frac{\omega}{c_*}} \\
\frac{E}{c} & -\frac{E}{c} & -\frac{E_*}{c_*} & \frac{E_*}{c_*} \\
\frac{E}{c} e^{\mathrm{i}\frac{\omega}{c}} & -\frac{E}{c} e^{-\mathrm{i}\frac{\omega}{c}} & -\frac{E_*}{c_*} e^{\mathrm{i}\frac{\omega}{c_*}} & \frac{E_*}{c_*} e^{-\mathrm{i}\frac{\omega}{c_*}}
\end{pmatrix} \right|^{-1},
\tag{4.7.9}
$$

where $c = \sqrt{E/\rho}$ and $c_* = \sqrt{E_*/\rho_*}$ denote the phase velocities in the two rods. The left panel in Fig. 4.7.1 plots F_r versus ω for the "elastic-elastic" case assuming $E_* = 2E \in \mathbb{R}$ and $\rho_* = 2\rho$, noting that the featured set of material parameters conforms with the one-dimensional variant of (4.5.16) which guarantees that the set of transmission eigenvalues is at most countable. From the display, one can clearly see the indication of transmission eigenvalues, spread uniformly along the frequency range of interest. As a complement to this result, the right panel in Fig. 4.7.1 plots F_r versus ω for the "elastic-viscoelastic" case which assumes $E_* = (2 + 0.1\mathrm{i})E \in \mathbb{C}$ and $\rho_* = 2\rho$. Consistent with the claim of Theorem 8, the latter result indicates absence of transmission eigenvalues when E is real and E_* is complex-valued (note that the local maximum at $\omega = 0$, present in both diagrams, takes significantly smaller value than the truncated "dynamic" maxima in the left panel).

(a) "Elastic-elastic" case, $(E, E_*) \in \mathbb{R}^2$ (b) "Elastic-viscoelastic" case, $(E, E_*) \in \mathbb{R} \times \mathbb{C}$
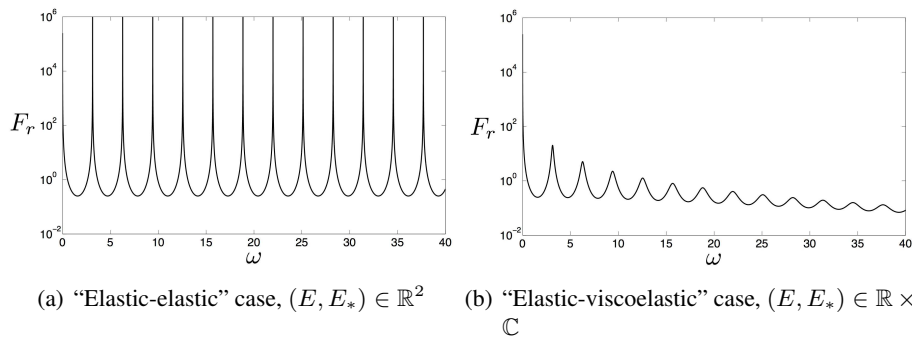
Figure 4.3: *Eigenvalue indicator F_r versus vibration frequency ω*

Oscillations of spheres. The second example deals with the ITP for two homogeneous and isotropic spheres of unit radius, characterized by the respective shear moduli $(\mu, \mu_*) \in \mathbb{C}^2$, Poisson's ratios $(\nu, \nu_*) \in \mathbb{R}^2$, and mass densities $(\rho, \rho_*) \in \mathbb{R}^2$. Once again, the transmission eigenvalues are associated with non-trivial solutions to the homogeneous ITP for which the two spheres share the Cauchy data on the boundary. Assuming that the two spheres are subjected respectively to constant radial pressures p and p_*, the induced (radial) boundary displacements u and u_* can be computed following Bonnet and Guzina (2004) as

$$u_* = \frac{p_*}{4\mu_*} \frac{Q_* \cos(Q_*) - \sin(Q_*)}{Q_* \cos(Q_*) - (1 - \alpha_*^2 Q_*^2) \sin(Q_*)},$$
$$u = \frac{p}{4\mu} \frac{Q \cos(Q) - \sin(Q)}{Q \cos(Q) - (1 - \alpha^2 Q^2) \sin(Q)},$$

(4.7.10)

where

$$\alpha^2 = \frac{1 - \nu}{2 - 4\nu}, \qquad \alpha_*^2 = \frac{1 - \nu_*}{2 - 4\nu_*}, \qquad Q^2 = \frac{\rho \, \omega^2}{4\mu\alpha^2}, \qquad Q_*^2 = \frac{\rho_* \omega^2}{4\mu_* \alpha_*^2}. \tag{4.7.11}$$

To develop an eigenvalue indicator function in the spirit of the previous example, one may assume that equality $p = p_*$ holds on the boundary, and define

$$F_s = \frac{|u \, u_*|}{\left| \frac{u}{p} - \frac{u_*}{p_*} \right|}, \tag{4.7.12}$$

as a quantity which becomes unbounded when ω is a transmission eigenvalue. As an illustration, the left panel in Fig. 4.7.1 plots F_s versus ω for the "elastic-elastic" case assuming $\mu_* = 2\mu \in \mathbb{R}$, $\nu_* = \nu = 1/8$ and $\rho_* = 2\rho$, while the right panel describes the corresponding "elastic-viscoelastic" situation where $\mu_* = (2 + 0.1i)\mu \in \mathbb{C}$. Similar to the previous example, the numerical results indicate the existence of transmission eigenvalues when both spheres are elastic, as well as their suppression when one of the two spheres is dissipative.

(a) "Elastic-elastic" case, $(\mu, \mu_*) \in \mathbb{R}^2$ (b) "Elastic-viscoelastic" case, $(\mu, \mu_*) \in \mathbb{R} \times \mathbb{C}$
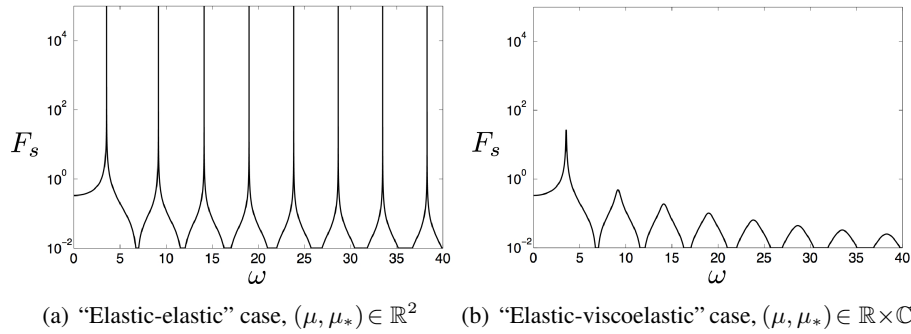
Figure 4.4: *Eigenvalue indicator F_s versus vibration frequency ω*

Viscoelastic-viscoelastic case. In the above examples, the focus was made on "conventional" ITP configurations where neither or either of the two bodies is dissipative. In light of the results in Section 4.6 where the analysis used to demonstrate the absence of transmission eigenvalues in the "elastic-viscoelastic" case failed to yield the same result for "viscoelastic-viscoelastic" (VV) configurations, it is

of interest to examine the latter class of problems via the example of oscillating spheres. To ascertain whether transmission eigenvalues could indeed exist in the VV case, the spheres problem is approached from an alternative point of view, namely by fixing the vibration frequency at $\omega = \omega_o \in \mathbb{R}$, and then seeking admissible sets of viscoelastic parameters for which ω_o is a transmission eigenvalue. To this end, one may introduce an auxiliary set of material parameters $(\beta, \gamma) \in \mathbb{C}^2$ and $(\beta_*, \gamma_*) \in \mathbb{C}^2$ as

$$\beta = \mu\alpha^2, \qquad \gamma = \frac{\alpha^2}{\mu}, \qquad \beta_* = \mu_*\alpha_*^2, \qquad \gamma_* = \frac{\alpha_*^2}{\mu_*}. \tag{4.7.13}$$

From (4.7.11) and (4.7.13), one finds

$$Q^2 = \frac{\rho\omega^2}{4\beta}, \qquad Q_*^2 = \frac{\rho_*\omega^2}{4\beta_*},$$

which allows the boundary displacements in (4.7.10) to be rewritten as

$$u_* = \frac{p_*}{4}\left(\frac{\gamma_*}{\beta_*}\right)^{\frac{1}{2}} \frac{Q_* \cos(Q_*) - \sin(Q_*)}{Q_* \cos(Q_*) - [1 - (\beta_*\gamma_*)^{\frac{1}{2}} Q_*^2]\sin(Q_*)},$$

$$u = \frac{p}{4}\left(\frac{\gamma}{\beta}\right)^{\frac{1}{2}} \frac{Q \cos(Q) - \sin(Q)}{Q \cos(Q) - [1 - (\beta\gamma)^{\frac{1}{2}} Q^2]\sin(Q)}. \tag{4.7.14}$$

Given $\omega_o \in \mathbb{R}$, $(\rho, \rho_*) \in \mathbb{R}^2$, and $(\beta, \beta_*, \gamma_*) \in (\mathbb{C}\backslash\mathbb{R})^3$, one is now in position to seek $\gamma \in \mathbb{C}\backslash\mathbb{R}$ such that $u = u_*$ and $p = p_*$. On the basis of (4.7.14), the explicit solution is given by

$$\gamma = \frac{\beta\Lambda^2(Q\cos(Q) - \sin(Q))^2}{[Q\cos(Q) - (1 + \Lambda\beta Q^2)\sin(Q)]^2}, \tag{4.7.15}$$

where

$$\Lambda = \left(\frac{\gamma_*}{\beta_*}\right)^{\frac{1}{2}} \frac{Q_* \cos(Q_*) - \sin(Q_*)}{Q_* \cos(Q_*) - [1 - (\beta_*\gamma_*)^{\frac{1}{2}} Q_*^2]\sin(Q_*)}. \tag{4.7.16}$$

In this setting, any relevant solution in terms of γ must also satisfy the conditions of physical admissibility in terms of the shear and bulk moduli

$$\mu = \left(\frac{\beta}{\gamma}\right)^{\frac{1}{2}}, \qquad \kappa = 4\beta - \frac{4}{3}\left(\frac{\beta}{\gamma}\right)^{\frac{1}{2}},$$

which are subject to the ellipticity and thermomechanical stability requirements

$$\Re[\mu] > 0, \qquad \Im[\mu] \geqslant 0, \qquad \Re[\kappa] > 0, \qquad \Im[\kappa] \geqslant 0. \tag{4.7.17}$$

Despite the multitude of inequality constraints in (4.7.17), it is indeed possible to find an admissible solution (4.7.15) in terms of γ given ω_o, (ρ, ρ_*) and $(\beta, \beta_*, \gamma_*)$ as shown in Table 4.2. For completeness, this result is accompanied by the variation of the eigenvalue indicator function (4.7.12) in Fig. 4.5, where F_s is plotted versus frequency for each of the three VV configurations highlighted in Table 4.2. From the display, it is seen that the three diagrams of F_s exhibit apparent "blow-off" behavior respectively at $\omega = 2, 10$ and 25 as expected. In unison, Table 4.2 and Fig. 4.5 provide a clear indication that the transmission eigenvalues may appear even in situations when both the obstacle and the background solid are viscoelastc i.e. dissipative - a finding that may be especially relevant in the application of inverse scattering theories to real-life problems (e.g. seismic imaging) were many materials are known to exhibit dissipative constitutive behavior.

Table 4.2: *Oscillating spheres problem - VV configuration: numerical values of material parameters for which $\omega = \omega_o$ is a transmission eigenvalue.*

ω_{o}	ρ	ρ_*	μ	μ_*	κ	κ_*	Config.
2	3	1.5	$8.833 + 1.214i$	$3.139 + 0.314i$	$12.22 + 0.781i$	$11.82 + 0.782i$	1
10	3	1.5	$4.157 + 1.684i$	$3.139 + 0.314i$	$26.46 + 0.155i$	$11.82 + 0.782i$	2
25	6	3.4	$173.6 + 4.320i$	$1.414 + 0.071i$	$368.5 + 52.24i$	$14.11 + 1.106i$	3
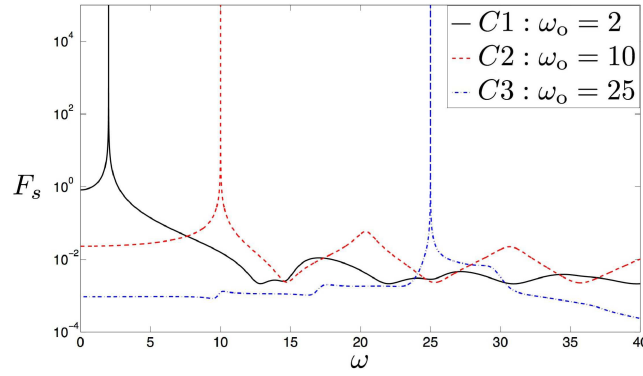
Figure 4.5: *Oscillating spheres problem - VV configuration: numerical manifestation of the transmission eigenvalues exposed in Table 4.2*

.

4.8 Conclusions

In this study the analysis of the interior transmission problem (ITP), that plays a critical role in a number of inverse scattering theories, is extended to enable the treatment of problems in piecewise-homogeneous, anisotropic, elastic and viscoelastic solids involving multiply-connected penetrable and impenetrable obstacles. Making recourse to a particular variational formulation, the Lax-Milgram theorem, and the compact perturbation argument, a set of sufficient conditions is established in terms of the elasticity and density parameters of the obstacle and the background solid that ensure the ellipticity of the ITP provided that the excitation frequency does not belong to (at most) countable set of transmission eigenvalues. It is further shown that this set is empty in situations when either the obstacle or the background solid are dissipative i.e. viscoelastic. When *both* the obstacle and the background are either elastic or viscoelastic, on the other hand, the same type of analysis fails to produce any further restrictions on the (countable) set of transmission eigenvalues. Given the counter-intuitive nature of such finding for the "viscoelastic-viscoelastic" (VV) case, the problem is further investigated via an energetic argument which shows that the homogeneous ITP involving VV configurations is not mechanically isolated from its surroundings in that it permits a non-zero energy influx into the system even though the prescribed excitation (given by the jump in Cauchy data between the two bodies) vanishes. A set of numerical results, computed for configurations that meet the sufficient "solvability" conditions, is included to illustrate the problem. Consistent with the underpinning analysis, the results indicate that the set of transmission values is indeed empty in the "elastic-viscoelastic" case, and countable for the "elastic-elastic" and VV configurations.

Chapter 5

On a spectral theory for the elastic interior transmission problem

Contents

143

5.1   Introduction

The interior transmission problem (ITP), which appears in inverse scattering theory for inhomogeneous medium, is a boundary value problem formulated as a pair of equations defined in a bounded domain and coupled through the Cauchy data on the boundary. Solving the *homogeneous* ITP, for a fixed frequency value, can be seen as the task of finding an incident wave field that has no scattered counterpart. In the context of inverse scattering methods, that aim at reconstructing the support of the scatterer, such frequency, which is an eigenvalue of the problem, should be avoided. The ITP which suffers from a lack of self-adjointness and of ellipticity, is not covered by any classical theory and a survey of the particular issues raised by its study can be found in Colton et al. (2007). Earlier studies have focused on the question of its well-posedness, and mainly two approaches have been employed: integral equation methods (Colton et al., 1989; Rynne and Sleeman, 1991; Kirsch, 2007; Charalambopoulos et al., 2002) and variational formulations (Hähner, 2000; Cakoni et al., 2002; Charalambopoulos, 2002; Bellis and Guzina, 2010). Previous studies have shown in particular, by recourse to the analytic Fredholm theory that the set of frequency eigenvalues of the ITP, namely transmission eigenvalues, is at most countable with infinity as the only possible accumulation point.

Initiated by Päivärinta and Sylvester (2008) where the question of existence of transmission eigenvalues has been addressed for the first time, the interest for the study of the spectrum associated with the ITP has grown recently (Charalambopoulos and Anagnostopoulos, 2008; Cakoni and Haddar, 2009; Kirsch, 2009; Cakoni et al., 2010d,e; Cakoni and Kirsch, 2010; Cakoni and Gintides, 2010). Moreover, transmission eigenvalues can be used to obtain qualitative informations on the material properties of the scatterers (Cakoni et al., 2007, 2008, 2009) which can provide a significant improvement of non-iterative inverse scattering techniques, such as the linear sampling method, that have solely been used for topological identification until now.

This chapter is dedicated to the study of the interior transmission eigenvalue problem in the elasticity case, using the tools developed in the references given previously. It aims at giving a systematic treatment of the ITP in elasticity, where conditions on material parameters, namely elastic tensors and mass densities, that ensure solvability of the problem and existence of transmission eigenvalues are established. Moreover, the question of the relation between elastic parameters and lower bounds of transmission eigenvalues is addressed. The introduction of the problem in Section 5.2 is followed by a reference analytical example for which the existence of eigenvalues can be proved. Sections 5.3 and 5.4 then provide a comprehensive study of the eigenvalue problem for different material configurations.

5.2   Preliminaries

Consider the time-harmonic vibrations of a bounded domain $D \subset \mathbb{R}^3$, with smooth boundary ∂D, at frequency ω. For clarity, all quantities in this study are interpreted as *dimensionless* by making reference to the characteristic length d_0, reference elastic modulus μ_0, and reference mass density ρ_0. Next, let $(\mathcal{C}, \rho) \in L^\infty(D)$ and $(\mathcal{C}_*, \rho_*) \in L^\infty(D)$ denote two sets of bounded material-parameter distributions over D, where $\mathcal{C}(\xi)$ and $\mathcal{C}_*(\xi)$ are real-valued, symmetric, fourth-order elastic tensor fields, while $\rho(\xi)$ and $\rho_*(\xi)$ are mass density distributions such that

$$\begin{aligned} \mathsf{c}|\varphi|^2 \leqslant \varphi\!:\!\mathcal{C}(\xi)\!:\!\bar\varphi \leqslant \mathsf{C}|\varphi|^2, \\ \mathsf{c}_*|\varphi|^2 \leqslant \varphi\!:\!\mathcal{C}_*(\xi)\!:\!\bar\varphi \leqslant \mathsf{C}_*|\varphi|^2, \end{aligned} \qquad \xi \in D, \tag{5.2.1}$$

and

$$\begin{aligned} \mathsf{p} &\leqslant \rho(\boldsymbol{\xi}) \leqslant \mathsf{P}, \\ \mathsf{p}_* &\leqslant \rho_*(\boldsymbol{\xi}) \leqslant \mathsf{P}_*, \end{aligned} \qquad \boldsymbol{\xi} \in D. \tag{5.2.2}$$

Here φ is a complex-valued, second-order tensor, while $\mathsf{c}, \mathsf{c}_*, \mathsf{p}, \mathsf{p}_*$ and $\mathsf{C}, \mathsf{C}_*, \mathsf{P}, \mathsf{P}_*$ are strictly positive constants, signifying respectively the *infima* and *suprema* of the associated scalar quantities. With reference to (5.2.1), it is further noted that $\mathsf{c}, \mathsf{C}, \mathsf{c}_*$ and C_* represent the bounds on the extreme eigenvalues of $\boldsymbol{\mathcal{C}}$ and $\boldsymbol{\mathcal{C}}_*$, computed with respect to double contraction with a second-order tensor. In the most general anisotropic case $\boldsymbol{\mathcal{C}}$ and $\boldsymbol{\mathcal{C}}_*$, which are endowed with major symmetry (Bellis and Guzina, 2010), may each have up to six distinct eigenvalues.

Hereon, it is assumed that the two distributions of material properties are "*non-intersecting*" in the sense that either

$$\mathsf{c}_* \geqslant 1 \geqslant \mathsf{C} \qquad \text{or} \qquad \mathsf{c} \geqslant 1 \geqslant \mathsf{C}_* \qquad \text{or} \qquad \boldsymbol{\mathcal{C}} = \boldsymbol{\mathcal{C}}_* \text{ in } D, \tag{5.2.3}$$

and either

$$\mathsf{p}_* \geqslant 1 \geqslant \mathsf{P} \qquad \text{or} \qquad \mathsf{p} \geqslant 1 \geqslant \mathsf{P}_* \qquad \text{or} \qquad \rho = \rho_* \text{ in } D, \tag{5.2.4}$$

with the unity as a point of demarcation achieved via suitable choice of the normalization constants μ_0 and ρ_0. Note that the strict equalities in (5.2.3) and (5.2.4) are, when applicable, assumed to hold almost everywhere in D, with the additional constraint

$$\left(\mathsf{c}_* = \mathsf{C} \vee \mathsf{c} = \mathsf{C}_* \vee \boldsymbol{\mathcal{C}} = \boldsymbol{\mathcal{C}}_* \text{ in } D \right) \wedge \left(\mathsf{p}_* = \mathsf{P} \vee \mathsf{p} = \mathsf{P}_* \vee \rho = \rho_* \text{ in } D \right) = \perp, \tag{5.2.5}$$

imposed on (5.2.3) and (5.2.4) to facilitate the variational analysis of the ensuing eigenvalue problem.

5.2.1 Interior transmission eigenvalue problem

With the above definitions the interior transmission eigenvalue problem (ITEP), that arises in a variety of inverse scattering problems (Colton and Kress, 1992), can be stated as a task of finding the non-trivial pair $(\boldsymbol{u}, \boldsymbol{u}_*) \in H^1(D) \times H^1(D)$ that solves the homogeneous interior transmission problem

$$\begin{aligned} \boldsymbol{\nabla} \cdot [\boldsymbol{\mathcal{C}} : \boldsymbol{\nabla} \boldsymbol{u}] + \rho \omega^2 \boldsymbol{u} &= \boldsymbol{0} & \text{in } D, \\ \boldsymbol{\nabla} \cdot [\boldsymbol{\mathcal{C}}_* : \boldsymbol{\nabla} \boldsymbol{u}_*] + \rho_* \omega^2 \boldsymbol{u}_* &= \boldsymbol{0} & \text{in } D, \\ \boldsymbol{u} - \boldsymbol{u}_* &= \boldsymbol{0} & \text{on } \partial D, \\ \boldsymbol{n} \cdot \boldsymbol{\mathcal{C}} : \boldsymbol{\nabla} \boldsymbol{u} - \boldsymbol{n} \cdot \boldsymbol{\mathcal{C}}_* : \boldsymbol{\nabla} \boldsymbol{u}_* &= \boldsymbol{0} & \text{on } \partial D, \end{aligned} \tag{5.2.6}$$

where $H^1 := W^{1,2}$ denotes the usual Sobolev space, and $\boldsymbol{n}$ is the unit normal on ∂D oriented toward the exterior of D.

Definition 4. *Values of ω^2 for which homogeneous problem (5.2.6) permits non-trivial solution $(\boldsymbol{u}, \boldsymbol{u}_*) \in H^1(D) \times H^1(D)$ are called the transmission eigenvalues corresponding to transmission eigenfunctions $(\boldsymbol{u}, \boldsymbol{u}_*)$.*

The ITEP plays a central role in the development of qualitative techniques for obstacle reconstruction such as the linear sampling method (Colton et al., 2000; Cakoni and Colton, 2006) and the factorization method (Kirsch and Grinberg, 2008), that commonly revolve around the behavior of the so-called *measurements operator* which maps a set of incident wave patterns onto the set of scattered wavefields. To

provide specificity for the discussion, let $(\mathcal{C}_*, \rho_*)$ and $(\mathcal{C}, \rho)$ hereon denote respectively the material properties of a hidden obstacle $D \subset \Omega$ and the background domain Ω (e.g. $\mathbb{R}^3$ or a half-space). With such premise, it can be shown that the scattering operator characterizing D is injective with dense range provided that there does not exist a non-trivial solution $(\boldsymbol{u}, \boldsymbol{u}_*)$ to homogeneous boundary value problem (5.2.6), where $\boldsymbol{u}$ is in the form of a single-layer potential over Ω whose source density is distributed over the source surface. Thus, if ω^2 is a transmission eigenvalue of (5.2.6), the scattering operator fails to be one-to-one and the linear sampling and factorization methods can no longer be applied.

The difficulties plaguing the study of the above-described ITEP stem from the structure of the boundary conditions prescribed over ∂D whereby (5.2.6) is neither self-adjoint, nor elliptic at any frequency (see Colton et al. (2007) in the context of the scalar Helmholtz equation). These impediments are reflected in the fact that the existing studies of the ITEP for elastic bodies (Charalambopoulos, 2002; Charalambopoulos and Anagnostopoulos, 2008; Bellis and Guzina, 2010) are each formulated under fairly restrictive conditions in terms of the "contrast" between $(\mathcal{C}_*, \rho_*)$ and $(\mathcal{C}, \rho)$. To shed further light on the problem, this investigation aims to generalize upon the recent developments for the Helmholtz equation and Maxwell equations (Päivärinta and Sylvester, 2008; Kirsch, 2009; Cakoni and Haddar, 2009; Cakoni and Kirsch, 2010; Cakoni et al., 2010e; Hitrik et al., 2010) toward: a) studying the solvability of (5.2.6) in situations when the contrast between $(\mathcal{C}_*, \rho_*)$ and $(\mathcal{C}, \rho)$ transcends the restrictions imposed by earlier studies, and b) establishing, for the first time, the *existence* of transmission eigenvalues in elasticity. To this end, the task of investigating the ITEP for elastic bodies is recast as that of characterizing the kernel of a differential-trace operator $\mathbb{J} - f(\omega)\mathbb{K}$ that synthesizes the left-hand side of (5.2.6), constructed such that i) $\mathbb{J}$ and $\mathbb{K}$ are both self-adjoint, and ii) $\mathbb{K}$ is compact. Such decomposition in turn permits the analysis to proceed by focusing on the so-called "material ellipticity conditions" under which operator $\mathbb{J}$ is invertible.

5.2.2   Analytical example

To help lay the foundation for the ensuing analysis, consider first the canonical case where D is a ball of radius R, while pairs $(\mathcal{C}, \rho)$ and $(\mathcal{C}_*, \rho_*)$ each correspond to a *homogeneous isotropic* solid. By virtue of its simplicity, this example allows one to explicitly demonstrate the existence of a countable set of transmission eigenvalues associated with radially-symmetric eigenfunctions.

In the isotropic case, the fourth-order elastic tensors $\mathcal{C}$ and $\mathcal{C}_*$ can be synthesized in terms of the respective Lamé parameters (λ, μ) and (λ_*, μ_*). Under such restriction $\mathcal{C}$ and $\mathcal{C}_*$ have only two distinct eigenvalues (Knowles, 1995), given respectively by $\{2\mu, 3\lambda + 2\mu\}$ and $\{2\mu_*, 3\lambda_* + 2\mu_*\}$, and their strong ellipticity is ensured by the well-known inequalities

$$\mu > 0, \qquad \mu_* > 0$$
$$3\lambda + 2\mu > 0, \qquad 3\lambda_* + 2\mu_* > 0. \tag{5.2.7}$$

For completeness, it is noted that λ and λ_* are sign-indefinite by virtue of the fact that $\text{sign}(\lambda) = \text{sign}(\nu)$ and $\text{sign}(\lambda_*) = \text{sign}(\nu_*)$, where $\nu \in (-1, \frac{1}{2})$ and $\nu_* \in (-1, \frac{1}{2})$ are the Poisson's ratios affiliated respectively with $\mathcal{C}$ and $\mathcal{C}_*$. In what follows, it is for simplicity assumed that $\nu \geqslant 0$ and $\nu_* \geqslant 0$. With such hypothesis, one has

$$\lambda = \frac{\mathsf{C} - \mathsf{c}}{3} \geqslant 0, \qquad \mu = \frac{\mathsf{c}}{2} > 0, \qquad \lambda_* = \frac{\mathsf{C}_* - \mathsf{c}_*}{3} \geqslant 0, \qquad \mu_* = \frac{\mathsf{c}_*}{2} > 0. \tag{5.2.8}$$

When the solution to the interior transmission problem is sought in the form of radially-symmetric vector fields $\boldsymbol{u}(\boldsymbol{\xi}) = u(r)\boldsymbol{e}_r$ and $\boldsymbol{u}_*(\boldsymbol{\xi}) = u_*(r)\boldsymbol{e}_r$ such that $r = |\boldsymbol{\xi}|$ and $\boldsymbol{e}_r = \boldsymbol{\xi}/r$, the field equations (5.2.6a) and (5.2.6b) can next be reduced as

$$
\begin{aligned}
u''(r) + \frac{2}{r}u'(r) + \left(\frac{\omega^2}{c^2} - \frac{2}{r^2}\right)u(r) = 0, \qquad r \in [0, R] \\
u_*''(r) + \frac{2}{r}u_*'(r) + \left(\frac{\omega^2}{c_*^2} - \frac{2}{r^2}\right)u_*(r) = 0, \qquad r \in [0, R]
\end{aligned}
\tag{5.2.9}
$$

where $c = \sqrt{(\lambda+2\mu)/\rho}$; $c_* = \sqrt{(\lambda_*+2\mu_*)/\rho_*}$, while f' and f'' denote respectively first and second derivative of $f(r)$ with respect to its argument. As a result, the solution to (5.2.6) can be written in terms of the spherical Bessel functions of the first order $j_1\left(\frac{\omega}{c}r\right)$ and $j_1\left(\frac{\omega}{c_*}r\right)$, which exposes the existence of a non-trivial solution when ω^2 is a transmission eigenvalue satisfying the characteristic equation

$$
F(\omega) := \left| \begin{matrix} j_1\left(\frac{\omega}{c}R\right) & j_1\left(\frac{\omega}{c_*}R\right) \\ \omega\sqrt{\rho(\lambda+2\mu)}j_1'\left(\frac{\omega}{c}R\right) + \frac{2\lambda}{R}j_1\left(\frac{\omega}{c}R\right) & \omega\sqrt{\rho_*(\lambda_*+2\mu_*)}j_1'\left(\frac{\omega}{c_*}R\right) + \frac{2\lambda_*}{R}j_1\left(\frac{\omega}{c_*}R\right) \end{matrix} \right| = 0.
\tag{5.2.10}
$$

Previous studies of the ITEP for elastic solids (Charalambopoulos, 2002; Charalambopoulos and Anagnostopoulos, 2008; Bellis and Guzina, 2010) have consistently shown that the transmission eigenvalues, when they exist, can only accumulate at infinity. Accordingly, it is natural to investigate the asymptotic behavior of $F(\omega)$ as $\omega \to \infty$. To this end, one may employ the relationships

$$
\begin{aligned}
j_1(t) \underset{t \to \infty}{=} -\frac{\cos(t)}{t} + O\left(\frac{1}{t^2}\right), \\
j_1'(t) \underset{t \to \infty}{=} \frac{\sin(t)}{t} + O\left(\frac{1}{t^2}\right),
\end{aligned}
\tag{5.2.11}
$$

to find

$$
F(\omega) \underset{\omega \to \infty}{=} \frac{c\,c_*}{\omega R^2}\left[\sqrt{\rho(\lambda+2\mu)}\sin\left(\frac{\omega}{c}R\right)\cos\left(\frac{\omega}{c_*}R\right) - \right.
$$
$$
\left. \sqrt{\rho_*(\lambda_*+2\mu_*)}\cos\left(\frac{\omega}{c}R\right)\sin\left(\frac{\omega}{c_*}R\right) \right] + O\left(\frac{1}{\omega^2}\right). \tag{5.2.12}
$$

Assuming non-zero material contrast between $(\mathcal{C}, \rho)$ and $(\mathcal{C}_*, \rho_*)$, one finds that the leading terms in (5.2.12) are nearly-periodic functions of frequency as $\omega \to \infty$, and so is F (Katznelson, 1976). Thus, expansion (5.2.12) demonstrates that F has infinitely many zeros, i.e. that the set of transmission eigenvalues stemming from (5.2.10) is indeed countable. In concluding the example, it is noted that (5.2.9)–(5.2.12) represent an elastic-solid analogue of the well known spherically-symmetric study of the scalar Helmholtz equation, see e.g. Cakoni and Kirsch (2010); Colton et al. (2007).

5.3 Configurations with material similitude

In what follows, let $\mathcal{D}_\rho := (\rho_* - \rho)^{-1}$ and $\mathcal{D}_{\mathcal{C}} := (\mathcal{C}_*^{-1} - \mathcal{C}^{-1})^{-1}$ quantify respectively the contrasts in mass density and elasticity between the two materials. With such notation, this section is devoted to

investigating the ITEP for elastic solids in situations where either $\mathcal{D}_\rho$ or $\mathcal{D}_{\mathcal{C}}$ vanishes identically in D. Following the approach suggested in Rynne and Sleeman (1991); Haddar (2004); Cakoni and Haddar (2007); Cakoni et al. (2009), the problem at hand can be conveniently formulated as a system of fourth-order differential equations that is amenable to eigen-analysis in terms of variational methods.

For clarity of the ensuing developments, it is important to recall the underpinning analytical framework introduced in Cakoni and Haddar (2009). To this end, let $\mathbb{J}$ a bounded, positive definite, self-adjoint linear operator on separable Hilbert space W, and let $\mathbb{K}$ be a non-negative, self-adjoint, compact bounded linear operator on W. With such hypotheses, it can be shown that there exists an increasing sequence of positive real numbers λ_n and associated sequence of elements $\boldsymbol{w}_n \in W$ such that $\mathbb{J}\boldsymbol{w}_n = \lambda_n\mathbb{K}\boldsymbol{w}_n$. Next, letting $\tau \mapsto \mathbb{J}_\tau$ be a continuous mapping from $(0, +\infty)$ to the set of self-adjoint, positive definite, bounded linear operators on W, consider the eigenvalue problem of finding $\boldsymbol{w} \in W$ such that

$$\mathbb{J}_\tau \boldsymbol{w} \, - \, \lambda_n(\tau)\mathbb{K}\boldsymbol{w} \, = \, \boldsymbol{0}. \tag{5.3.1}$$

The following theorem, established in Cakoni and Haddar (2009), is a fundamental tool toward demonstrating the existence of transmission eigenvalues.

Theorem 10. *Let $\tau \mapsto \mathbb{J}_\tau$ be a continuous mapping from $(0, +\infty)$ to the set of self-adjoint, positive definite, bounded linear operators on W, and let $\mathbb{K}$ be a non-negative, self-adjoint, compact bounded linear operator on W. Assume the existence of two positive constants $\tau_0 > 0$ and $\tau_1 > 0$ such that*

   1. *$\mathbb{J}_{\tau_0} - \tau_0\mathbb{K}$ is positive on W, and*

   2. *$\mathbb{J}_{\tau_1} - \tau_1\mathbb{K}$ is non-positive on an m-dimensional subspace of W.*

Then each of the equations $\lambda_n(\tau) = \tau$, $n = 1, 2 \ldots, m$ has at least one solution for $\tau \in [\tau_0, \tau_1]$ where $\lambda_n(\tau)$ is the nth eigenvalue (counting multiplicity) of $\mathbb{J}_\tau$ with respect to $\mathbb{K}$, i.e. $\ker(\mathbb{J}_\tau - \lambda_n(\tau)\mathbb{K}) \neq \{\boldsymbol{0}\}$.

5.3.1 Equal elastic tensors

In this section, it postulated that $\mathcal{D}_{\mathcal{C}}$ vanishes (i.e. $\mathcal{C} = \mathcal{C}_*$) while $\mathcal{D}_\rho \neq 0$ almost everywhere in D according to (5.2.5). On introducing the Sobolev space of vector fields with zero Cauchy data on ∂D, namely

$$H_0^2(D) = \left\{ \boldsymbol{\varphi} \in H^2(D) \colon \; \boldsymbol{\varphi} = \boldsymbol{0} \text{ and } \boldsymbol{n} \cdot \mathcal{C} : \boldsymbol{\nabla}\boldsymbol{\varphi} = \boldsymbol{0} \text{ on } \partial D \right\}, \tag{5.3.2}$$

and assuming that pair $(\boldsymbol{u}, \boldsymbol{u}_*) \in L^2(D) \times L^2(D)$ solves the interior transmission problem

$$\begin{aligned}
\boldsymbol{\nabla} \cdot [\mathcal{C} : \boldsymbol{\nabla}\boldsymbol{u}] + \rho\,\omega^2\boldsymbol{u} &= \boldsymbol{0} && \text{in } D, \\
\boldsymbol{\nabla} \cdot [\mathcal{C} : \boldsymbol{\nabla}\boldsymbol{u}_*] + \rho_*\omega^2\boldsymbol{u}_* &= \boldsymbol{0} && \text{in } D, \\
\boldsymbol{u} - \boldsymbol{u}_* &= \boldsymbol{0} && \text{on } \partial D, \\
\boldsymbol{n} \cdot \mathcal{C} : \boldsymbol{\nabla}(\boldsymbol{u} - \boldsymbol{u}_*) &= \boldsymbol{0} && \text{on } \partial D,
\end{aligned} \tag{5.3.3}$$

one finds that the solution difference $\boldsymbol{v} := \boldsymbol{u} - \boldsymbol{u}_* \in H_0^2$ solves the fourth-order equation

$$\left(\boldsymbol{\nabla} \cdot [\mathcal{C} : \boldsymbol{\nabla}] + \rho\,\omega^2 \right) \mathcal{D}_\rho \left(\boldsymbol{\nabla} \cdot [\mathcal{C} : \boldsymbol{\nabla}] + \rho_*\omega^2 \right) \boldsymbol{v} \, = \, \boldsymbol{0} \qquad \text{in } D, \tag{5.3.4}$$

when $\rho_* \neq \rho$ and $\omega > 0$.

The variational formulation of (5.3.4) consists in finding $\boldsymbol{v} \in H_0^2(D)$ such that

$$\int_D \mathcal{D}_\rho \left(\boldsymbol{\nabla}\cdot[\boldsymbol{\mathcal{C}}:\boldsymbol{\nabla}\boldsymbol{v}] + \rho_*\omega^2\boldsymbol{v} \right) \cdot \left(\boldsymbol{\nabla}\cdot[\boldsymbol{\mathcal{C}}:\boldsymbol{\nabla}\bar{\boldsymbol{\varphi}}] + \rho\,\omega^2\bar{\boldsymbol{\varphi}} \right) \, \mathrm{d}V \;=\; 0 \qquad \forall\boldsymbol{\varphi} \in H_0^2(D). \tag{5.3.5}$$

To facilitate the treatment of the variational problem at hand, let $\tau := \omega^2$, and define the auxiliary bounded sesquilinear forms on $H_0^2(D) \times H_0^2(D)$ as

$$\mathcal{A}_\tau(\boldsymbol{\varphi},\boldsymbol{\psi}) \;:=\; \big\langle \mathcal{D}_\rho \left(\boldsymbol{\nabla}\cdot[\boldsymbol{\mathcal{C}}:\boldsymbol{\nabla}\boldsymbol{\varphi}] + \rho\,\tau\boldsymbol{\varphi} \right), \left(\boldsymbol{\nabla}\cdot[\boldsymbol{\mathcal{C}}:\boldsymbol{\nabla}\boldsymbol{\psi}] + \rho\,\tau\boldsymbol{\psi} \right) \big\rangle_{L^2(D)} \;+\; \tau^2 \big\langle \rho\,\boldsymbol{\varphi}, \boldsymbol{\psi} \big\rangle_{L^2(D)},$$

$$\mathcal{A}_\tau^*(\boldsymbol{\varphi},\boldsymbol{\psi}) \;:=\; -\,\big\langle \mathcal{D}_\rho \left(\boldsymbol{\nabla}\cdot[\boldsymbol{\mathcal{C}}:\boldsymbol{\nabla}\boldsymbol{\varphi}] + \rho_*\tau\boldsymbol{\varphi} \right), \left(\boldsymbol{\nabla}\cdot[\boldsymbol{\mathcal{C}}:\boldsymbol{\nabla}\boldsymbol{\psi}] + \rho_*\tau\boldsymbol{\psi} \right) \big\rangle_{L^2(D)} \;+\; \tau^2 \big\langle \rho_*\boldsymbol{\varphi}, \boldsymbol{\psi} \big\rangle_{L^2(D)},$$

$$\mathcal{B}(\boldsymbol{\varphi},\boldsymbol{\psi}) \;\;:=\; \big\langle \boldsymbol{\mathcal{C}}:\boldsymbol{\nabla}\boldsymbol{\varphi}, \boldsymbol{\nabla}\boldsymbol{\psi} \big\rangle_{L^2(D)},$$
$$\tag{5.3.6}$$

for all $(\boldsymbol{\varphi},\boldsymbol{\psi}) \in H_0^2(D) \times H_0^2(D)$, where the inner product between two nth-order tensors is understood in the sense of n-tuple contraction. On exercising (5.3.6) and the divergence theorem, (5.3.5) can be equivalently formulated as a task of finding $\boldsymbol{v} \in H_0^2(D)$ that satisfies either

$$\mathcal{A}_\tau(\boldsymbol{v},\boldsymbol{\varphi}) \;-\; \tau\,\mathcal{B}(\boldsymbol{v},\boldsymbol{\varphi}) \;=\; 0 \qquad \forall\boldsymbol{\varphi} \in H_0^2(D), \tag{5.3.7}$$

or

$$\mathcal{A}_\tau^*(\boldsymbol{v},\boldsymbol{\varphi}) \;-\; \tau\,\mathcal{B}(\boldsymbol{v},\boldsymbol{\varphi}) \;=\; 0 \qquad \forall\boldsymbol{\varphi} \in H_0^2(D). \tag{5.3.8}$$

Note that the boundedness of the featured operators is a consequence of tensor $\boldsymbol{\mathcal{C}}$ being positive definite and bounded. To expose the sufficient conditions for the ellipticity of $\mathcal{A}_\tau$ and $\mathcal{A}_\tau^*$, the latter can be conveniently recast as

$$\begin{aligned}
\mathcal{A}_\tau(\boldsymbol{\varphi},\boldsymbol{\psi}) \;=\;& \big\langle \rho\mathcal{D}_\rho \left(\boldsymbol{\nabla}\cdot[\boldsymbol{\mathcal{C}}:\boldsymbol{\nabla}\boldsymbol{\varphi}] + \tau\boldsymbol{\varphi} \right), \left(\boldsymbol{\nabla}\cdot[\boldsymbol{\mathcal{C}}:\boldsymbol{\nabla}\boldsymbol{\psi}] + \tau\boldsymbol{\psi} \right) \big\rangle_{L^2(D)} \\
& +\; \big\langle (1-\rho)\mathcal{D}_\rho \boldsymbol{\nabla}\cdot[\boldsymbol{\mathcal{C}}:\boldsymbol{\nabla}\boldsymbol{\varphi}], \boldsymbol{\nabla}\cdot[\boldsymbol{\mathcal{C}}:\boldsymbol{\nabla}\boldsymbol{\psi}] \big\rangle_{L^2(D)} \;+\; \tau^2\big\langle \rho\mathcal{D}_\rho(\rho_*-1)\boldsymbol{\varphi}, \boldsymbol{\psi} \big\rangle_{L^2(D)}, \\
\mathcal{A}_\tau^*(\boldsymbol{\varphi},\boldsymbol{\psi}) \;=\;& -\,\big\langle \rho_*\mathcal{D}_\rho \left(\boldsymbol{\nabla}\cdot[\boldsymbol{\mathcal{C}}:\boldsymbol{\nabla}\boldsymbol{\varphi}] + \tau\boldsymbol{\varphi} \right), \left(\boldsymbol{\nabla}\cdot[\boldsymbol{\mathcal{C}}:\boldsymbol{\nabla}\boldsymbol{\psi}] + \tau\boldsymbol{\psi} \right) \big\rangle_{L^2(D)} \\
& -\; \big\langle (1-\rho_*)\mathcal{D}_\rho \boldsymbol{\nabla}\cdot[\boldsymbol{\mathcal{C}}:\boldsymbol{\nabla}\boldsymbol{\varphi}], \boldsymbol{\nabla}\cdot[\boldsymbol{\mathcal{C}}:\boldsymbol{\nabla}\boldsymbol{\psi}] \big\rangle_{L^2(D)} \;-\; \tau^2\big\langle \rho_*\mathcal{D}_\rho(\rho-1)\boldsymbol{\varphi}, \boldsymbol{\psi} \big\rangle_{L^2(D)}.
\end{aligned}$$
$$\tag{5.3.9}$$

Lemma 12. *Assuming $\boldsymbol{\mathcal{C}} = \boldsymbol{\mathcal{C}}_*$ and restrictions on the contrast in mass densities as in (5.2.4) and (5.2.5), either $\mathcal{A}_\tau$ or $\mathcal{A}_\tau^*$ is a coercive sesquilinear form on $H_0^2(D) \times H_0^2(D)$.*

Proof. For brevity, the ensuing analysis focuses on the case when $\mathsf{p}_* \geqslant 1 \geqslant \mathsf{P}$ and $\mathcal{D}_\rho \neq 0$; the companion claim (when $\mathsf{p} \geqslant 1 \geqslant \mathsf{P}_*$ and $\mathcal{D}_\rho \neq 0$) can be established by interchanging the roles of ρ and ρ_*. With such restriction, the stated hypotheses of the Lemma imply the existence of real-valued constants α, α_* and γ such that

$$\begin{aligned}
1 - \rho &\geqslant \alpha \geqslant 0 \\
\rho_* - 1 &\geqslant \alpha_* \geqslant 0 \qquad \text{in } D, \\
\mathcal{D}_\rho &\geqslant \gamma > 0
\end{aligned} \tag{5.3.10}$$

where α and α_* cannot vanish simultaneously.

When $\boldsymbol{\varphi} \in H_0^2(D)$, one finds by virtue of (5.3.9a), (5.3.10), the Cauchy-Schwarz inequality, and triangle inequality that

$$\mathcal{A}_\tau(\boldsymbol{\varphi},\boldsymbol{\varphi}) \;\geqslant\; \mathsf{p}\,\gamma \left\{ \left(1 + \frac{\alpha}{\mathsf{p}} \right) x^2 + (1+\alpha_*)\,y^2 - 2xy \right\}, \tag{5.3.11}$$

where $x := \|\boldsymbol{\nabla} \cdot [\boldsymbol{\mathcal{C}} : \boldsymbol{\nabla}\boldsymbol{\varphi}]\|_{L^2(D)}$ and $y := \tau \|\boldsymbol{\varphi}\|_{L^2(D)}$. In this setting, several combinations in terms of α and α_* must be considered separately to provide a valid lower bound for $\mathcal{A}_\tau$. In particular, it can be shown that

$$\mathcal{A}_\tau(\boldsymbol{\varphi}, \boldsymbol{\varphi}) \;\geqslant\; \mathsf{p}\gamma \left\{ \frac{\alpha}{\mathsf{p}} x^2 + \alpha_* y^2 + (x - y)^2 \right\} \qquad \text{when} \qquad \begin{matrix} \alpha > 0, \\ \alpha_* > 0, \end{matrix} \tag{5.3.12}$$

$$\mathcal{A}_\tau(\boldsymbol{\varphi}, \boldsymbol{\varphi}) \;\geqslant\; \mathsf{p}\gamma \left\{ \left(1 - \frac{1}{\delta_*}\right) x^2 + (1 + \alpha_* - \delta_*)\, y^2 + \delta_* \left(y - \frac{x}{\delta_*}\right)^2 \right\} \qquad \text{when} \qquad \begin{matrix} \alpha = 0, \\ \alpha_* > 0, \end{matrix} \tag{5.3.13}$$

assuming $\delta_* \in (1, 1+\alpha_*)$, and

$$\mathcal{A}_\tau(\boldsymbol{\varphi}, \boldsymbol{\varphi}) \;\geqslant\; \mathsf{p}\gamma \left\{ \left(1 + \frac{\alpha}{\mathsf{p}} - \delta\right) x^2 + \left(1 - \frac{1}{\delta}\right) y^2 + \delta \left(x - \frac{y}{\delta}\right)^2 \right\} \qquad \text{when} \qquad \begin{matrix} \alpha > 0, \\ \alpha_* = 0, \end{matrix} \tag{5.3.14}$$

where $\delta \in (1, 1+\alpha/\mathsf{p})$.

From the lower bound in (5.2.1) on elastic tensor $\boldsymbol{\mathcal{C}}$, on the other hand, there exists a constant $\beta > 0$ such that

$$\|\boldsymbol{\nabla} \cdot [\boldsymbol{\mathcal{C}} : \boldsymbol{\nabla}\boldsymbol{\varphi}]\|^2_{L^2(D)} \;+\; \|\boldsymbol{\varphi}\|^2_{L^2(D)} \;\geqslant\; \beta \|\boldsymbol{\varphi}\|^2_{H^2(D)}, \tag{5.3.15}$$

see, e.g., Marsden and Hughes (1994). On dropping the squared-difference terms on the right-hand sides of (5.3.12), (5.3.13) and (5.3.14), one finally concludes from (5.3.15) that there exists a constant $C_\tau > 0$ (dependent on τ) such that

$$\mathcal{A}_\tau(\boldsymbol{\varphi}, \boldsymbol{\varphi}) \;\geqslant\; C_\tau \|\boldsymbol{\varphi}\|^2_{H^2(D)},$$

which concludes the proof.

$\square$

On employing the Riesz representation theorem and identifying $H_0^2(D)$ with its dual, one can introduce bounded linear operators $\mathbb{A}_\tau, \mathbb{A}_\tau^*, \mathbb{B} : H_0^2(D) \to H_0^2(D)$ such that for all $(\boldsymbol{\varphi}, \boldsymbol{\psi}) \in H_0^2(D) \times H_0^2(D)$

$$\langle \mathbb{A}_\tau \boldsymbol{\varphi}, \boldsymbol{\psi} \rangle_{H_0^2(D)} = \mathcal{A}_\tau(\boldsymbol{\varphi}, \boldsymbol{\psi}), \qquad \langle \mathbb{A}_\tau^* \boldsymbol{\varphi}, \boldsymbol{\psi} \rangle_{H_0^2(D)} = \mathcal{A}_\tau^*(\boldsymbol{\varphi}, \boldsymbol{\psi}), \qquad \langle \mathbb{B}\boldsymbol{\varphi}, \boldsymbol{\psi} \rangle_{H_0^2(D)} = \mathcal{B}(\boldsymbol{\varphi}, \boldsymbol{\psi}). \tag{5.3.16}$$

As a result, (5.3.7) and (5.3.8) can be rewritten respectively as

$$\langle (\mathbb{A}_\tau - \tau\mathbb{B})\boldsymbol{v}, \boldsymbol{\varphi} \rangle_{H_0^2(D)} \;=\; 0 \qquad \forall \boldsymbol{\varphi} \in H_0^2(D) \tag{5.3.17}$$

and

$$\langle (\mathbb{A}_\tau^* - \tau\mathbb{B})\boldsymbol{v}, \boldsymbol{\varphi} \rangle_{H_0^2(D)} \;=\; 0 \qquad \forall \boldsymbol{\varphi} \in H_0^2(D). \tag{5.3.18}$$

Thus if ω^2 is a transmission eigenvalue associated with (5.3.3) then, recalling that $\tau = \omega^2$, one has that either

$$\ker(\mathbb{A}_\tau - \tau\mathbb{B}) \neq \{\mathbf{0}\} \qquad \text{or} \qquad \ker(\mathbb{A}_\tau^* - \tau\mathbb{B}) \neq \{\mathbf{0}\}.$$

Lemma 13. *Assuming $\boldsymbol{\mathcal{C}} = \boldsymbol{\mathcal{C}}_*$, linear operator $\mathbb{A}_\tau : H_0^2(D) \to H_0^2(D)$ (resp. $\mathbb{A}_\tau^* : H_0^2(D) \to H_0^2(D)$) is positive definite, self-adjoint, and depends continuously on $\tau > 0$ when $\mathsf{p}_* \geqslant 1 \geqslant \mathsf{P}$ (resp. $\mathsf{p} \geqslant 1 \geqslant \mathsf{P}_*$) and $\mathcal{D}_\rho \neq 0$ hold almost everywhere in D. Further, $\mathbb{B} : H_0^2(D) \to H_0^2(D)$ is a self-adjoint and positive compact linear operator.*

Proof. Since ρ, ρ_* and $\mathcal{C}$ are by premise real-valued and $\mathcal{C}$ possesses the major symmetry, the sesquilinear forms $\mathcal{A}_\tau$, $\mathcal{A}_\tau^*$ and $\mathcal{B}$ are Hermitian which requires that operators $\mathbb{A}_\tau$, $\mathbb{A}_\tau^*$ and $\mathbb{B}$ be self-adjoint. The positive definite character of $\mathbb{A}_\tau$ and $\mathbb{A}_\tau^*$ is a direct consequence of (5.3.16) and Lemma 12, while their continuous dependence on $\tau > 0$ arises from the premise that $\mathcal{A}_\tau$ and $\mathcal{A}_\tau^*$ depend continuously on $\tau > 0$.

To establish the claim that $\mathbb{B}$ is compact, consider a bounded sequence $\boldsymbol{\varphi}_n \in H_0^2(D)$, such that there exists a subsequence $\tilde{\boldsymbol{\varphi}}_n$ that weakly converges with respect to the $H_0^2(D)$-norm to $\boldsymbol{\varphi}_{\mathrm{o}} \in H_0^2(D)$. Since $\tilde{\boldsymbol{\varphi}}_n \in H_0^2(D)$, it follows that $\boldsymbol{\nabla}\tilde{\boldsymbol{\varphi}}_n \in H^1(D)$. By virtue of the compact embedding of $H^1(D)$ in $L^2(D)$, one accordingly finds that $\boldsymbol{\nabla}\tilde{\boldsymbol{\varphi}}_n$ converges strongly to $\boldsymbol{\nabla}\boldsymbol{\varphi}_{\mathrm{o}}$ with respect to the $L^2(D)$-norm. Finally using the definition of $\mathbb{B}$ in (5.3.16), the Cauchy-Schwarz inequality, and the boundedness of elastic tensor $\mathcal{C}$, one finds that

$$\|\mathbb{B}(\tilde{\boldsymbol{\varphi}}_n - \boldsymbol{\varphi}_{\mathrm{o}})\|_{H_0^2(D)} \leqslant \mathsf{C}\,\|\boldsymbol{\nabla}(\tilde{\boldsymbol{\varphi}}_n - \boldsymbol{\varphi}_{\mathrm{o}})\|_{L^2(D)}, \tag{5.3.19}$$

which implies that $\mathbb{B}$ is compact since $\mathbb{B}\tilde{\boldsymbol{\varphi}}_n$ strongly converges to $\mathbb{B}\tilde{\boldsymbol{\varphi}}_{\mathrm{o}}$ with respect to the $H_0^2(D)$-norm. With this result in place, the proof of the lemma can now be completed by noting that $\mathbb{B}$ is positive owing to the positive definiteness of $\mathcal{C}$ stipulated in (5.2.1). $\qquad\square$

The ensuing theorem establishes a lower bound for the transmission eigenvalues. To this end consider the negative Laplace operator $-\Delta$ for which, as shown by classical eigenvalue theory (Henrot, 2006), there exist an increasing sequence of real-valued, positive Dirichlet eigenvalues $\lambda_n(D)$ and a sequence of corresponding first-order eigentensors $\boldsymbol{\varphi}_n$ satisfying

$$\begin{aligned} -\Delta\boldsymbol{\varphi}_n &= \lambda_n(D)\boldsymbol{\varphi}_n && \text{in } D, \\ \boldsymbol{\varphi}_n &= \mathbf{0} && \text{on } \partial D. \end{aligned} \tag{5.3.20}$$

In this setting $\lambda_1(D) > 0$ denotes the first, i.e. the smallest Dirichlet eigenvalue of the negative Laplace operator.

Theorem 11. *If either $\mathsf{p}_* \geqslant 1 \geqslant \mathsf{P}$ or $\mathsf{p} \geqslant 1 \geqslant \mathsf{P}_*$ while $\mathcal{D}_{\mathcal{C}} = \mathbf{0}$ and $\mathcal{D}_\rho \neq 0$ hold almost everywhere in D, the set of transmission eigenvalues affiliated with (5.2.6) is discrete, with infinity being the only possible accumulation point. Moreover, every feasible transmission eigenvalue ω^2 is such that*

$$\omega^2 \;>\; \lambda_1(D)\,\frac{\mathsf{c}}{\max(\mathsf{P}, \mathsf{P}_*)}.$$

Proof. When $\mathsf{p}_* \geqslant 1 \geqslant \mathsf{P}$ (resp. $\mathsf{p} \geqslant 1 \geqslant \mathsf{P}_*$) and $\mathcal{D}_\rho \neq 0$ holds almost everywhere in D, linear operator $\mathbb{A}_\tau$ (resp. $\mathbb{A}_\tau^*$) is invertible due to Lemma 13 and, since $\mathbb{B}$ is a compact operator, so is $\mathbb{A}_\tau^{-1}\mathbb{B}$ (resp. $\mathbb{A}_\tau^{*-1}\mathbb{B}$). On denoting by $\mathbb{I}$ the identity operator on $H_0^2(D)$, the Fredholm alternative applies (Yosida, 1980) whereby $\mathbb{I} - \tau\mathbb{A}_\tau^{-1}\mathbb{B}$ (resp. $\mathbb{I} - \tau\mathbb{A}_\tau^{*-1}\mathbb{B}$) is invertible except for, at most, a discrete set of values $\tau \in \mathbb{C}$ that can only accumulate at infinity.

Assuming for the time being that $\mathsf{p} \geqslant 1 \geqslant \mathsf{P}_*$ i.e. $\mathcal{D}_\rho < 0$, let $\boldsymbol{v} \in H_0^2(D)$ such that $\boldsymbol{v} \in \ker(\mathbb{A}_\tau - \tau\mathbb{B})$. Then $\langle(\mathbb{A}_\tau - \tau\mathbb{B})\boldsymbol{v}, \boldsymbol{v}\rangle_{H_0^2(D)} = 0$ yields

$$-\int_D \mathcal{D}_\rho\,|\boldsymbol{\nabla}\cdot[\mathcal{C}:\boldsymbol{\nabla}\boldsymbol{v}] + \rho\,\tau\boldsymbol{v}|^2 \,\mathrm{d}V \;+\; \tau\int_D \left(\boldsymbol{\nabla}\boldsymbol{v}:\mathcal{C}:\boldsymbol{\nabla}\bar{\boldsymbol{v}} - \rho\,\tau|\boldsymbol{v}|^2\right) \,\mathrm{d}V \;=\; 0. \tag{5.3.21}$$

Whenever the second integral is non-negative, one must clearly have $\boldsymbol{\nabla}\cdot[\mathcal{C}:\boldsymbol{\nabla}\boldsymbol{v}] + \rho\,\tau\boldsymbol{v} = \mathbf{0}$ in D. Since $\boldsymbol{v} = \mathbf{0}$ and $\mathcal{C}:\boldsymbol{\nabla}\boldsymbol{v}:\boldsymbol{n} = \mathbf{0}$ on ∂D for $\boldsymbol{v} \in H_0^2(D)$, it follows that $\boldsymbol{v}$ must also vanish in D by virtue of

the Holmgren's uniqueness theorem (see Guzina and Madyarov (2007) for a discussion in the context of elasticity). Due to (5.2.1) and Courant-Fischer min-max formulae (Henrot, 2006), on the other hand, the Rayleigh quotient of elastic tensor $\mathcal{C}$ is found to be bounded from below as

$$\inf_{\boldsymbol{v}\in H_0^2(D)} \frac{\displaystyle\int_D \boldsymbol{\nabla v}\!:\!\mathcal{C}\!:\!\boldsymbol{\nabla\bar v}\,\mathrm{d}V}{\displaystyle\int_D |\boldsymbol{v}|^2\,\mathrm{d}V} \;\geqslant\; \mathsf{c}\inf_{\boldsymbol{v}\in H_0^1(D)} \frac{\displaystyle\int_D |\boldsymbol{\nabla v}|^2\,\mathrm{d}V}{\displaystyle\int_D |\boldsymbol{v}|^2\,\mathrm{d}V} \;\geqslant\; \mathsf{c}\lambda_1(D), \tag{5.3.22}$$

so that

$$\int_D \left(\boldsymbol{\nabla v}\!:\!\mathcal{C}\!:\!\boldsymbol{\nabla\bar v} - \rho\,\tau|\boldsymbol{v}|^2\right)\,\mathrm{d}V \;\geqslant\; \|\boldsymbol{v}\|_{L^2(D)}^2\left(\mathsf{c}\lambda_1(D) - \tau\mathsf{P}\right). \tag{5.3.23}$$

As a result, the last integral in (5.3.21) is necessarily non-negative whenever $\omega^2 = \tau \leqslant \lambda_1(D)\mathsf{c}/\mathsf{P}$, whereby no eigenvalues can exist within interval $(0, \lambda_1(D)\mathsf{c}/\mathsf{P}]$.

Alternatively when $\mathsf{p}_* \geqslant 1 \geqslant \mathsf{P}$ i.e. $\mathcal{D}_\rho > 0$, let $\boldsymbol{v} \in \ker(\mathbb{A}_\tau^* - \tau\mathbb{B})$. In this case, the inferred equality

$$\int_D \mathcal{D}_\rho|\boldsymbol{\nabla}\!\cdot\![\mathcal{C}\!:\!\boldsymbol{\nabla v}] + \rho_*\omega^2\boldsymbol{v}|^2\,\mathrm{d}V \;+\; \tau\int_D \left(\boldsymbol{\nabla v}\!:\!\mathcal{C}\!:\!\boldsymbol{\nabla\bar v} - \rho_*\tau|\boldsymbol{v}|^2\right)\,\mathrm{d}V \;=\; 0 \tag{5.3.24}$$

and inequality

$$\int_D \left(\boldsymbol{\nabla v}:\mathcal{C}:\boldsymbol{\nabla\bar v} - \rho_*\tau|\boldsymbol{v}|^2\right)\,\mathrm{d}V \;\geqslant\; \|\boldsymbol{v}\|_{L^2(D)}^2\left(\mathsf{c}\lambda_1(D) - \tau\mathsf{P}_*\right) \tag{5.3.25}$$

require that $\boldsymbol{v} = \boldsymbol{0}$ in D whenever $\tau \leqslant \lambda_1(D)\mathsf{c}/\mathsf{P}_*$, i.e. that no transmission eigenvalues can exist within interval $(0, \lambda_1(D)\mathsf{c}/\mathsf{P}_*]$. The combination of the above two cases concludes the proof.

$\qquad\square$

Theorem 12. *If either* $\mathsf{p} \geqslant 1 \geqslant \mathsf{P}_*$ *or* $\mathsf{p}_* \geqslant 1 \geqslant \mathsf{P}$ *while* $\mathcal{D}_{\mathcal{C}} = 0$ *and* $\mathcal{D}_\rho \neq 0$ *hold almost everywhere in* D, *there exists a countable set of transmission eigenvalues affiliated with (5.2.6).*

Proof. The proof of the theorem relies on the existence of a countable set of transmission eigenvalues for the spherically-symmetric case of homogeneous isotropic elastic bodies examined in Section 5.2.2. Suppose that $\mathsf{p}_* \geqslant 1 \geqslant \mathsf{P}$ and that $\mathcal{D}_\rho \neq 0$ holds almost everywhere in D. Then by virtue of Lemma 13, operators $\mathbb{A}_\tau$ and $\mathbb{B}$ satisfy the hypotheses of Theorem 10 with $W := H_0^2(D)$. In this case, inequalities (5.3.12)–(5.3.14) of Lemma 12 further ensure the existence of a real-valued constant $\beta' > 0$ such that

$$\langle\mathbb{A}_\tau\boldsymbol{v}, \boldsymbol{v}\rangle_{H_0^2(D)} \;\geqslant\; \beta'\,\|\boldsymbol{\nabla}\!\cdot\![\mathcal{C}\!:\!\boldsymbol{\nabla v}]\|_{L^2(D)}^2, \tag{5.3.26}$$

for all $\boldsymbol{v} \in H_0^2(D)$. Moreover since $\boldsymbol{n}\!\cdot\!\mathcal{C}\!:\!\boldsymbol{\nabla v} = \boldsymbol{0}$ on ∂D, one finds from (5.2.1), the major symmetry of $\mathcal{C}$, and application of the Poincaré inequality as in Henrot (2006) that

$$\langle\mathcal{C}\!:\!\boldsymbol{\nabla v}, \boldsymbol{\nabla v}\rangle_{L^2(D)} \;\leqslant\; \frac{1}{\mathsf{c}}\langle\mathcal{C}\!:\!\boldsymbol{\nabla v}, \mathcal{C}\!:\!\boldsymbol{\nabla v}\rangle_{L^2(D)} \;\leqslant\; \frac{1}{\mathsf{c}\lambda_1(D)}\|\boldsymbol{\nabla}\!\cdot\![\mathcal{C}\!:\!\boldsymbol{\nabla v}]\|_{L^2(D)}^2, \tag{5.3.27}$$

whereby

$$\langle(\mathbb{A}_\tau - \tau\mathbb{B})\boldsymbol{v}, \boldsymbol{v}\rangle_{H_0^2(D)} \;\geqslant\; \left(\beta' - \frac{\tau}{\mathsf{c}\lambda_1(D)}\right)\|\boldsymbol{\nabla}\!\cdot\![\mathcal{C}\!:\!\boldsymbol{\nabla v}]\|_{L^2(D)}^2. \tag{5.3.28}$$

Accordingly when $0 < \tau_0 < \mathsf{c}\lambda_1(D)\beta'$, operator $\mathbb{A}_{\tau_0} - \tau_0\mathbb{B}$ is positive on $H_0^2(D)$ and thus meets Assumption 1 of Theorem 10.

Next, from the results in Section 5.2.2 it follows that interior transmission problem (5.3.3), formulated for a ball $B_r \subset D$ of radius r with *constant* material parameters $\hat{\mathcal{C}} = \hat{\mathcal{C}}_*$, $\hat{\rho} := \mathsf{P}$ and $\hat{\rho}_* := \mathsf{p}_*$, is affiliated with a countable set of transmission eigenvalues. To help establish the claim of the theorem, let $\hat{\tau}$ be one such eigenvalue and let $\hat{\boldsymbol{v}} \in H_0^2(B_r)$ be the corresponding eigenfunction. In particular, $\hat{\boldsymbol{v}}$ satisfies (5.3.17) with $\tau = \hat{\tau}$, $H_0^2(D)$ replaced by $H_0^2(B_r)$, and with featured operators corresponding to the assumed (constant) material parameters. Accordingly, by taking $\varphi = \hat{\boldsymbol{v}}$ and integrating (5.3.17) by parts, one finds

$$\mathsf{p}_*\mathsf{P}\,\hat{\tau}^2\|\hat{\boldsymbol{v}}\|_{L^2(B_r)}^2 \;=\; -\|\boldsymbol{\nabla}\!\cdot\![\hat{\mathcal{C}}\!\cdot\!\boldsymbol{\nabla}\hat{\boldsymbol{v}}]\|_{L^2(B_r)}^2 \;+\; (\mathsf{p}_*+\mathsf{P})\,\hat{\tau}\int_{B_r}\boldsymbol{\nabla}\hat{\boldsymbol{v}}\!:\!\hat{\mathcal{C}}\!:\!\boldsymbol{\nabla}\bar{\hat{\boldsymbol{v}}}\;\mathrm{d}V. \tag{5.3.29}$$

Moreover, if $\hat{\boldsymbol{v}}_0 \in H_0^2(D)$ denotes the extension of $\hat{\boldsymbol{v}}$ by zero to the whole of D one has

$$\left\langle (\mathbb{A}_{\hat{\tau}} - \hat{\tau}\mathbb{B})\hat{\boldsymbol{v}}_0, \hat{\boldsymbol{v}}_0 \right\rangle_{H_0^2(D)} \;\leqslant\; \left(\frac{1+\mathsf{P}-\mathsf{p}}{\mathsf{p}_*-\mathsf{P}}\right)\|\boldsymbol{\nabla}\!\cdot\![\mathcal{C}\!:\!\boldsymbol{\nabla}\hat{\boldsymbol{v}}]\|_{L^2(B_r)}^2 - \left(\frac{\mathsf{p}_*+\mathsf{P}}{\mathsf{p}_*-\mathsf{P}}\right)\hat{\tau}\int_{B_r}\boldsymbol{\nabla}\hat{\boldsymbol{v}}:\mathcal{C}:\boldsymbol{\nabla}\bar{\hat{\boldsymbol{v}}}\;\mathrm{d}V$$
$$+ \left(\frac{\mathsf{P}\mathsf{P}_*}{\mathsf{p}_*-\mathsf{P}}\right)\hat{\tau}^2\|\hat{\boldsymbol{v}}\|_{L^2(B_r)}^2, \tag{5.3.30}$$

where $\mathbb{A}_{\hat{\tau}}$ and $\mathbb{B}$ are given by (5.3.16) assuming $\tau = \hat{\tau}$ and the original set of material parameters in terms of distributions $(\mathcal{C}, \rho)$ and $(\mathcal{C}_*, \rho_*)$ over D. A substitution of (5.3.29) into (5.3.30) yields

$$\left\langle (\mathbb{A}_{\hat{\tau}} - \hat{\tau}\mathbb{B})\hat{\boldsymbol{v}}_0, \hat{\boldsymbol{v}}_0 \right\rangle_{H_0^2(D)} \;\leqslant\; \frac{1}{\mathsf{p}_*-\mathsf{P}}\left\{(1+\mathsf{P}-\mathsf{p})\|\boldsymbol{\nabla}\!\cdot\![\mathcal{C}\!:\!\boldsymbol{\nabla}\hat{\boldsymbol{v}}]\|_{L^2(B_r)}^2 - \frac{\mathsf{P}_*}{\mathsf{p}_*}\|\boldsymbol{\nabla}\!\cdot\![\hat{\mathcal{C}}\!:\!\boldsymbol{\nabla}\hat{\boldsymbol{v}}]\|_{L^2(B_r)}^2\right\}$$
$$+ \left(\frac{\mathsf{p}_*+\mathsf{P}}{\mathsf{p}_*-\mathsf{P}}\right)\hat{\tau}\int_{B_r}\boldsymbol{\nabla}\hat{\boldsymbol{v}}:\left[\frac{\mathsf{P}_*}{\mathsf{p}_*}\hat{\mathcal{C}} - \mathcal{C}\right]:\boldsymbol{\nabla}\bar{\hat{\boldsymbol{v}}}\;\mathrm{d}V. \tag{5.3.31}$$

On choosing the maximum eigenvalue, $\hat{\mathsf{C}}$, of elastic tensor $\hat{\mathcal{C}}$ such that

$$\hat{\mathsf{C}} \;<\; \frac{\mathsf{p}_*}{\mathsf{P}_*}\mathsf{c}, \tag{5.3.32}$$

inequality (5.3.31) demonstrates that for sufficiently large $\hat{\tau} = \tau_1$, operator $\mathbb{A}_{\tau_1} - \tau_1\mathbb{B}$ is non-positive on the subspace of $H_0^2(D)$ spanned by $\hat{\boldsymbol{v}}_0$ – a result which constitutes Assumption 2 of Theorem 10. As a consequence, one concludes from Theorem 10 that there is at least one transmission eigenvalue within interval $[\tau_0, \tau_1]$ located on the positive real axis, where $0 < \tau_0 < \mathsf{c}\lambda_1(D)\beta'$ as examined earlier.

Next, consider $\varepsilon > 0$ such that D contains $m \geqslant 1$ disjoint balls $B_\varepsilon^1, B_\varepsilon^2, \ldots B_\varepsilon^m$ of radius εr, whence $\overline{B_\varepsilon^i} \subset D$ for $i = 1, \ldots, m$ and $\overline{B_\varepsilon^i} \cap \overline{B_\varepsilon^j} = \emptyset$ for $i \neq j$. By the scaling argument, $\hat{\tau}_\epsilon = \hat{\tau}/\varepsilon^2$ is a transmission eigenvalue for each of these balls associated with the interior transmission problem formulated assuming mass densities $\hat{\rho} = \mathsf{P}$ and $\hat{\rho}_* = \mathsf{p}_*$, and homogeneous isotropic elastic tensor $\hat{\mathcal{C}}$ verifying (5.3.32). Thus, if $\hat{\boldsymbol{v}}^i \in H_0^2(B_\varepsilon^i)$ is an eigenfunction corresponding to $\hat{\tau}_\epsilon$ for all $i = 1, \ldots, m$ whose extension by zero to the whole of D is denoted by $\hat{\boldsymbol{v}}_0^i \in H_0^2(D)$, vectors $\{\hat{\boldsymbol{v}}_0^1, \hat{\boldsymbol{v}}_0^2, \ldots, \hat{\boldsymbol{v}}_0^m\}$ are linearly independent and orthogonal in $H_0^2(D)$ since they have disjoint supports. With reference to (5.3.31) and (5.3.32), on the other hand, operator $\mathbb{A}_{\hat{\tau}_{\varepsilon 1}} - \tau_{\varepsilon 1}\mathbb{B}$ is non-positive on the m-dimensional subspace of $H_0^2(D)$ spanned by $\{\hat{\boldsymbol{v}}_0^1, \hat{\boldsymbol{v}}_0^2, \ldots, \hat{\boldsymbol{v}}_0^m\}$ for sufficiently large $\tau_{\varepsilon 1} = \tau_1/\varepsilon^2$. By virtue of Theorem 10, there exist at least m transmission eigenvalues within interval $[\tau_0, \tau_{\varepsilon 1}]$, counting their multiplicity. By letting $\varepsilon \to 0$ and

$m \to \infty$, one concludes that the set of transmission eigenvalues characterizing (5.3.3) is countable with infinity being the only possible point of accumulation.

The case when $\mathsf{p} \geqslant 1 \geqslant \mathsf{P}_*$ and $\mathcal{D}_\rho \neq 0$ almost everywhere in D can be treated by the same argument due to the symmetry in ρ and ρ_* of the formulation employed.

$\square$

The above analysis allows one to establish *implicit bounds* on ρ, ρ_* and $\mathcal{C} = \mathcal{C}_*$ in terms of the first transmission eigenvalue (see Corollary 2.6 in Cakoni et al. (2010e) for detailed proof). To this end, denote by B_r the largest ball of radius r such that $B_r \subset D$, and by B_R the smallest ball of radius R such that $D \subset B_R$. Further, let $\hat{\mathcal{C}}$ be a constant elastic tensor satisfying (5.3.32), and let $\omega_1^{\mathrm{ball}}(r, \hat{\mathcal{C}}, \mathsf{P}, \mathsf{p}_*)$ and $\omega_1^{\mathrm{ball}}(R, \hat{\mathcal{C}}, \mathsf{p}, \mathsf{P}_*)$ denote respectively the first transmission eigenvalue of (5.3.3) for ball B_r with material parameters $\hat{\mathcal{C}}_* = \hat{\mathcal{C}}$, $\hat{\rho} := \mathsf{P}$ and $\hat{\rho}_* := \mathsf{p}_*$, and ball B_R with material parameters $\hat{\mathcal{C}}_* = \hat{\mathcal{C}}$, $\hat{\rho} := \mathsf{p}$ and $\hat{\rho}_* := \mathsf{P}_*$.

Corollary 1. *Assume that $\mathcal{C} = \mathcal{C}_*$, and let ρ and ρ_* satisfy $\mathsf{p} \geqslant 1 \geqslant \mathsf{P}_*$. Then the first transmission eigenvalue ω_1 affiliated with (5.3.3) is such that*

$$\max\left(\omega_1^{ball}(R, \hat{\mathcal{C}}, \mathsf{p}, \mathsf{P}_*), \sqrt{\mathsf{c}\,\frac{\lambda_1(D)}{\mathsf{P}}} \right) \;\leqslant\; \omega_1 \;\leqslant\; \omega_1^{ball}(r, \hat{\mathcal{C}}, \mathsf{P}, \mathsf{p}_*). \tag{5.3.33}$$

where c is defined in (5.2.1), $\hat{\mathcal{C}}$ satisfies (5.3.32), and $\lambda_1(D)$ is the first Dirichlet eigenvalue for $-\Delta$ in D. For completeness, it is noted that the analogous bounds when $\mathsf{p}_* \geqslant 1 \geqslant \mathsf{P}$ can be obtained from (5.3.33) by reversing the roles of ρ and ρ_* due to symmetry of the problem.

5.3.2 Equal mass densities

This section deals with the case when $\mathcal{D}_\rho$ vanishes (i.e. $\rho = \rho_*$), while $\mathcal{D}_{\mathcal{C}} \neq 0$ almost everywhere in D following (5.2.5). With such premise, consider the pair $(\boldsymbol{u}, \boldsymbol{u}_*) \in H^1(D) \times H^1(D)$ satisfying

$$
\begin{aligned}
\boldsymbol{\nabla} \cdot [\mathcal{C} : \boldsymbol{\nabla u}] + \rho\,\omega^2 \boldsymbol{u} &= \boldsymbol{0} && \text{in } D, \\
\boldsymbol{\nabla} \cdot [\mathcal{C}_* : \boldsymbol{\nabla u}_*] + \rho\,\omega^2 \boldsymbol{u}_* &= \boldsymbol{0} && \text{in } D, \\
\boldsymbol{u} - \boldsymbol{u}_* &= \boldsymbol{0} && \text{on } \partial D, \\
\boldsymbol{n} \cdot \mathcal{C} : \boldsymbol{\nabla u} - \boldsymbol{n} \cdot \mathcal{C}_* : \boldsymbol{\nabla u}_* &= \boldsymbol{0} && \text{on } \partial D,
\end{aligned}
\tag{5.3.34}
$$

and introduce the Sobolev spaces of symmetric second-order tensor fields

$$
\begin{aligned}
\mathcal{V}(D) &:= \left\{ \boldsymbol{\Phi} \in L^2(D) :\ \boldsymbol{\Phi} = \boldsymbol{\Phi}^{\mathrm{T}},\ \boldsymbol{\nabla} \cdot \boldsymbol{\Phi} \in L^2(D) \right\}, \\
\mathcal{V}_0(D) &:= \left\{ \boldsymbol{\Phi} \in \mathcal{V}(D) :\ \boldsymbol{n} \cdot \boldsymbol{\Phi} = \boldsymbol{0}\ \text{ on } \partial D \right\},
\end{aligned}
\tag{5.3.35}
$$

and

$$
\begin{aligned}
\mathcal{W}(D) &= \left\{ \boldsymbol{\Phi} \in \mathcal{V}(D) :\ \boldsymbol{\Phi} = \boldsymbol{\Phi}^{\mathrm{T}},\ \boldsymbol{\nabla} \cdot \boldsymbol{\Phi} \in H^1(D) \right\}, \\
\mathcal{W}_0(D) &= \left\{ \boldsymbol{\Phi} \in \mathcal{V}_0(D) :\ \boldsymbol{\nabla} \cdot \boldsymbol{\Phi} \in H_0^1(D) \right\},
\end{aligned}
\tag{5.3.36}
$$

equipped with the inner product $\left\langle \boldsymbol{\Phi}, \boldsymbol{\Psi} \right\rangle_{\mathcal{W}(D)} = \left\langle \boldsymbol{\Phi}, \boldsymbol{\Psi} \right\rangle_{L^2(D)} + \left\langle \boldsymbol{\nabla} \cdot \boldsymbol{\Phi}, \boldsymbol{\nabla} \cdot \boldsymbol{\Psi} \right\rangle_{H^1(D)}$.

To facilitate the ensuing developments, one may recall that any vector field $\boldsymbol{\varphi} \in H^1(D)$ and second-order tensor field $\boldsymbol{\Phi} \in \mathcal{V}(D)$ satisfy the relationship

$$\int_D (\boldsymbol{\nabla} \cdot \boldsymbol{\Phi}) \cdot \boldsymbol{\varphi}\, \mathrm{d}V \;=\; \int_{\partial D} \boldsymbol{n} \cdot \boldsymbol{\Phi} \cdot \boldsymbol{\varphi}\, \mathrm{d}S \;-\; \int_D \boldsymbol{\Phi} : \boldsymbol{\nabla \varphi}\, \mathrm{d}V, \tag{5.3.37}$$

and note that $\boldsymbol{\Phi} \in \mathcal{W}_0(D)$ verifies $\boldsymbol{n} \cdot \boldsymbol{\Phi} = \boldsymbol{0}$ and $\nabla \cdot \boldsymbol{\Phi} = \boldsymbol{0}$ on ∂D. In this setting, one may take the gradient of the field equations in (5.3.34) and reformulate the problem in terms of $\boldsymbol{\mathcal{U}} := \boldsymbol{\mathcal{C}} : \nabla \boldsymbol{u} \in \mathcal{W}(D)$ and $\boldsymbol{\mathcal{U}}_* := \boldsymbol{\mathcal{C}}_* : \nabla \boldsymbol{u}_* \in \mathcal{W}(D)$ as

$$
\begin{aligned}
\nabla\nabla \cdot \boldsymbol{\mathcal{U}} + \rho \omega^2 \boldsymbol{\mathcal{C}}^{-1} : \boldsymbol{\mathcal{U}} &= \boldsymbol{0} && \text{in } D, \\
\nabla\nabla \cdot \boldsymbol{\mathcal{U}}_* + \rho \omega^2 \boldsymbol{\mathcal{C}}_*^{-1} : \boldsymbol{\mathcal{U}}_* &= \boldsymbol{0} && \text{in } D, \\
\nabla \cdot (\boldsymbol{\mathcal{U}} - \boldsymbol{\mathcal{U}}_*) &= \boldsymbol{0} && \text{on } \partial D, \\
\boldsymbol{n} \cdot (\boldsymbol{\mathcal{U}} - \boldsymbol{\mathcal{U}}_*) &= \boldsymbol{0} && \text{on } \partial D.
\end{aligned}
\tag{5.3.38}
$$

Following the developments in Section 5.3.1, one finds that the featured solution difference $\boldsymbol{\mathcal{V}} := \boldsymbol{\mathcal{U}} - \boldsymbol{\mathcal{U}}_*$ satisfies $\boldsymbol{\mathcal{V}} \in \mathcal{W}_0(D)$ and meets the fourth-order differential equation

$$
\left(\nabla\nabla \cdot + \rho \omega^2 \boldsymbol{\mathcal{C}}^{-1} : \right) \boldsymbol{\mathcal{D_C}} : \left(\nabla\nabla \cdot + \rho \omega^2 \boldsymbol{\mathcal{C}}_*^{-1} : \right) \boldsymbol{\mathcal{V}} = \boldsymbol{0} \quad \text{in } D,
\tag{5.3.39}
$$

when $\boldsymbol{\mathcal{D_C}} \neq \boldsymbol{0}$, $\rho > 0$ and $\omega > 0$. By virtue of (5.3.37), the variational formulation of (5.3.39) can be posed as the task of finding $\boldsymbol{\mathcal{V}} \in \mathcal{W}_0(D)$ such that

$$
\int_D \left(\nabla\nabla \cdot \boldsymbol{\mathcal{V}} + \rho \omega^2 \boldsymbol{\mathcal{C}}_*^{-1} : \boldsymbol{\mathcal{V}} \right) : \boldsymbol{\mathcal{D_C}} : \left(\nabla\nabla \cdot \bar{\boldsymbol{\Phi}} + \rho \omega^2 \boldsymbol{\mathcal{C}}^{-1} : \bar{\boldsymbol{\Phi}} \right) \, dV = 0 \quad \forall \boldsymbol{\Phi} \in \mathcal{W}_0(D).
\tag{5.3.40}
$$

To aid the treatment of the featured variational problem, one may introduce the auxiliary sesquilinear forms on $\mathcal{W}_0(D) \times \mathcal{W}_0(D)$ as

$$
\begin{aligned}
\mathcal{F}_\tau(\boldsymbol{\Phi}, \boldsymbol{\Psi}) &= \big\langle \boldsymbol{\mathcal{D_C}} : \left(\nabla\nabla \cdot \boldsymbol{\Phi} + \rho \tau \boldsymbol{\mathcal{C}}^{-1} : \boldsymbol{\Phi} \right), \left(\nabla\nabla \cdot \boldsymbol{\Psi} + \rho \tau \boldsymbol{\mathcal{C}}^{-1} : \boldsymbol{\Psi} \right) \big\rangle_{L^2(D)} + \tau^2 \big\langle \rho^2 \boldsymbol{\mathcal{C}}^{-1} : \boldsymbol{\Phi}, \boldsymbol{\Psi} \big\rangle_{L^2(D)}, \\
\mathcal{F}_\tau^*(\boldsymbol{\Phi}, \boldsymbol{\Psi}) &= - \big\langle \boldsymbol{\mathcal{D_C}} : \left(\nabla\nabla \cdot \boldsymbol{\Phi} + \rho \tau \boldsymbol{\mathcal{C}}_*^{-1} : \boldsymbol{\Phi} \right), \left(\nabla\nabla \cdot \boldsymbol{\Psi} + \rho \tau \boldsymbol{\mathcal{C}}_*^{-1} : \boldsymbol{\Psi} \right) \big\rangle_{L^2(D)} + \tau^2 \big\langle \rho^2 \boldsymbol{\mathcal{C}}_*^{-1} : \boldsymbol{\Phi}, \boldsymbol{\Psi} \big\rangle_{L^2(D)}, \\
\mathcal{G}(\boldsymbol{\Phi}, \boldsymbol{\Psi}) &= \big\langle \rho \nabla \cdot \boldsymbol{\Phi}, \nabla \cdot \boldsymbol{\Psi} \big\rangle_{L^2(D)},
\end{aligned}
\tag{5.3.41}
$$

where again the inner product between two nth-order tensors is understood in the sense of n-tuple contraction. With such definitions, (5.3.40) can be restated as either

$$
\mathcal{F}_\tau(\boldsymbol{\mathcal{V}}, \boldsymbol{\Phi}) - \tau \mathcal{G}(\boldsymbol{\mathcal{V}}, \boldsymbol{\Phi}) = 0 \qquad \forall \boldsymbol{\Phi} \in \mathcal{W}_0(D),
\tag{5.3.42}
$$

or

$$
\mathcal{F}_\tau^*(\boldsymbol{\mathcal{V}}, \boldsymbol{\Phi}) - \tau \mathcal{G}(\boldsymbol{\mathcal{V}}, \boldsymbol{\Phi}) = 0 \qquad \forall \boldsymbol{\Phi} \in \mathcal{W}_0(D).
\tag{5.3.43}
$$

By virtue of the symmetry of elastic tensors $\boldsymbol{\mathcal{C}}$ and $\boldsymbol{\mathcal{C}}_*$, $\mathcal{F}_\tau$ and $\mathcal{F}_\tau^*$ can be conveniently rewritten as

$$
\begin{aligned}
\mathcal{F}_\tau(\boldsymbol{\Phi}, \boldsymbol{\Psi}) &= \big\langle \boldsymbol{\mathcal{C}}^{-1} : \boldsymbol{\mathcal{D_C}} : \left(\nabla\nabla \cdot \boldsymbol{\Phi} + \rho \tau \boldsymbol{\Phi} \right), \left(\nabla\nabla \cdot \boldsymbol{\Psi} + \rho \tau \boldsymbol{\Psi} \right) \big\rangle_{L^2(D)} \\
&\quad + \big\langle (\boldsymbol{\mathcal{I}}^{\mathrm{sym}} - \boldsymbol{\mathcal{C}}^{-1}) : \boldsymbol{\mathcal{D_C}} : \nabla\nabla \cdot \boldsymbol{\Phi}, \nabla\nabla \cdot \boldsymbol{\Psi} \big\rangle_{L^2(D)} + \tau^2 \big\langle \rho^2 (\boldsymbol{\mathcal{C}}_*^{-1} - \boldsymbol{\mathcal{I}}^{\mathrm{sym}}) : \boldsymbol{\mathcal{C}}^{-1} : \boldsymbol{\mathcal{D_C}} : \boldsymbol{\Phi}, \boldsymbol{\Psi} \big\rangle_{L^2(D)}, \\
\mathcal{F}_\tau^*(\boldsymbol{\Phi}, \boldsymbol{\Psi}) &= - \big\langle \boldsymbol{\mathcal{C}}_*^{-1} : \boldsymbol{\mathcal{D_C}} : \left(\nabla\nabla \cdot \boldsymbol{\Phi} + \rho \tau \boldsymbol{\Phi} \right), \left(\nabla\nabla \cdot \boldsymbol{\Psi} + \rho \tau \boldsymbol{\Psi} \right) \big\rangle_{L^2(D)} \\
&\quad - \big\langle (\boldsymbol{\mathcal{I}}^{\mathrm{sym}} - \boldsymbol{\mathcal{C}}_*^{-1}) : \boldsymbol{\mathcal{D_C}} : \nabla\nabla \cdot \boldsymbol{\Phi}, \nabla\nabla \cdot \boldsymbol{\Psi} \big\rangle_{L^2(D)} - \tau^2 \big\langle \rho^2 (\boldsymbol{\mathcal{C}}^{-1} - \boldsymbol{\mathcal{I}}^{\mathrm{sym}}) : \boldsymbol{\mathcal{C}}_*^{-1} : \boldsymbol{\mathcal{D_C}} : \boldsymbol{\Phi}, \boldsymbol{\Psi} \big\rangle_{L^2(D)},
\end{aligned}
\tag{5.3.44}
$$

to help expose the conditions for their ellipticity, where $\boldsymbol{\mathcal{I}}^{\mathrm{sym}}$ is the symmetric fourth-order identity tensor.

Remark 14. *When $\mathcal{D}_{\mathcal{C}} \neq \mathbf{0}$ and $\mathcal{D}_\rho = 0$ almost everywhere in D, condition $\mathsf{c} \geqslant 1 \geqslant \mathsf{C}_*$ implies the existence of real-valued constants $\alpha \geqslant 0$, $\alpha_* \geqslant 0$ and $\gamma > 0$ such that*

$$\boldsymbol{\varphi} : (\boldsymbol{\mathcal{I}}^{sym} - \boldsymbol{\mathcal{C}}^{-1}) : \bar{\boldsymbol{\varphi}} \;\geqslant\; \alpha |\boldsymbol{\varphi}|^2$$
$$\boldsymbol{\varphi} : (\boldsymbol{\mathcal{C}}_*^{-1} - \boldsymbol{\mathcal{I}}^{sym}) : \bar{\boldsymbol{\varphi}} \;\geqslant\; \alpha_* |\boldsymbol{\varphi}|^2 \tag{5.3.45}$$
$$\boldsymbol{\varphi} : \boldsymbol{\mathcal{D}}_{\mathcal{C}} : \bar{\boldsymbol{\varphi}} \;\geqslant\; \gamma |\boldsymbol{\varphi}|^2;$$

similarly, condition $\mathsf{c}_* \geqslant 1 \geqslant \mathsf{C}$ ensures that there are constants $\alpha' \geqslant 0$, $\alpha'_* \geqslant 0$ and $\gamma' > 0$ verifying

$$\boldsymbol{\varphi} : (\boldsymbol{\mathcal{I}}^{sym} - \boldsymbol{\mathcal{C}}_*^{-1}) : \bar{\boldsymbol{\varphi}} \;\geqslant\; \alpha'_* |\boldsymbol{\varphi}|^2$$
$$\boldsymbol{\varphi} : (\boldsymbol{\mathcal{C}}^{-1} - \boldsymbol{\mathcal{I}}^{sym}) : \bar{\boldsymbol{\varphi}} \;\geqslant\; \alpha' |\boldsymbol{\varphi}|^2 \tag{5.3.46}$$
$$- \boldsymbol{\varphi} : \boldsymbol{\mathcal{D}}_{\mathcal{C}} : \bar{\boldsymbol{\varphi}} \;\geqslant\; \gamma' |\boldsymbol{\varphi}|^2.$$

for all complex-valued second-order tensors $\boldsymbol{\varphi}$.

Lemma 14. *Assuming $\rho = \rho_*$ and restrictions on the contrast in elastic tensors given by (5.2.3) and (5.2.5), either $\mathcal{F}_\tau$ or $\mathcal{F}_\tau^*$ is a coercive sesquilinear form on $\mathcal{W}_0(D) \times \mathcal{W}_0(D)$.*

Proof. Owing to the fact that the roles of $\mathcal{C}$ and $\mathcal{C}_*$ are interchangeable, the ensuing analysis considers the coercivity of $\mathcal{F}_\tau$ as an example.

Assume that $\mathsf{c} \geqslant 1 \geqslant \mathsf{C}_*$. On the basis of (5.2.1) and Remark 14, one accordingly has

$$\mathcal{F}_\tau(\boldsymbol{\Phi}, \boldsymbol{\Phi}) \;\geqslant\; \frac{\gamma}{\mathsf{C}} \left\{ (1 + \alpha \mathsf{C}) \, x^2 + (1 + \alpha_*) \, y^2 - 2xy \right\} \tag{5.3.47}$$

for all $\boldsymbol{\Phi} \in \mathcal{W}_0(D)$, where $x = \|\boldsymbol{\nabla}\boldsymbol{\nabla}\!\cdot\!\boldsymbol{\Phi}\|_{L^2(D)}$ and $y = \tau \|\rho \boldsymbol{\Phi}\|_{L^2(D)}$. Depending on the sign of α and α_*, one further has

$$\mathcal{F}_\tau(\boldsymbol{\Phi}, \boldsymbol{\Phi}) \;\geqslant\; \frac{\gamma}{\mathsf{C}} \left\{ \alpha \mathsf{C} x^2 + \alpha_* y^2 + (x - y)^2 \right\}, \qquad \text{when} \qquad \begin{array}{l} \alpha > 0, \\ \alpha_* > 0, \end{array} \tag{5.3.48}$$

$$\mathcal{F}_\tau(\boldsymbol{\Phi}, \boldsymbol{\Phi}) \;\geqslant\; \frac{\gamma}{\mathsf{C}} \left\{ \left(1 - \frac{1}{\delta_*}\right) x^2 + (1 + \alpha_* - \delta_*) \, y^2 + \delta_* \left(y - \frac{x}{\delta_*}\right)^2 \right\}, \qquad \text{when} \qquad \begin{array}{l} \alpha = 0, \\ \alpha_* > 0, \end{array} \tag{5.3.49}$$

assuming $\delta_* \in (1, 1 + \alpha_*)$, and

$$\mathcal{F}_\tau(\boldsymbol{\Phi}, \boldsymbol{\Phi}) \;\geqslant\; \frac{\gamma}{\mathsf{C}} \left\{ (1 + \alpha \mathsf{C} - \delta) \, x^2 + \left(1 - \frac{1}{\delta}\right) y^2 + \delta \left(x - \frac{y}{\delta}\right)^2 \right\}, \qquad \text{when} \qquad \begin{array}{l} \alpha > 0, \\ \alpha_* = 0, \end{array} \tag{5.3.50}$$

where $\delta \in (1, 1 + \alpha \mathsf{C})$. Moreover since $\boldsymbol{\nabla}\!\cdot\!\boldsymbol{\Phi} \in H_0^1(D)$ the Poincaré inequality holds, i.e. there exists a constant $C_P > 0$, dependent only on D, such that

$$\|\boldsymbol{\nabla}\!\cdot\!\boldsymbol{\Phi}\|_{L^2(D)} \;\leqslant\; C_P \|\boldsymbol{\nabla}\boldsymbol{\nabla}\!\cdot\!\boldsymbol{\Phi}\|_{L^2(D)}. \tag{5.3.51}$$

On dropping the squared-difference terms in (5.3.48)–(5.3.50) and recalling (5.2.2) which guarantees that ρ is bounded, one concludes that there is a constant $C_\tau' > 0$ such that

$$\mathcal{F}_\tau(\boldsymbol{\Phi}, \boldsymbol{\Phi}) \;\geqslant\; C_\tau' \, \|\boldsymbol{\Phi}\|_{\mathcal{W}(D)}^2,$$

which concludes the proof.

$\square$

With reference to (5.3.41), the Riesz representation theorem ensures the existence of bounded linear operators $\mathbb{F}_\tau, \mathbb{F}_\tau^*, \mathbb{G} : \mathcal{W}_0(D) \to \mathcal{W}_0(D)$ such that for all $(\boldsymbol{\Phi}, \boldsymbol{\Psi}) \in \mathcal{W}_0(D) \times \mathcal{W}_0(D)$

$$\langle \mathbb{F}_\tau \boldsymbol{\Phi}, \boldsymbol{\Psi} \rangle_{\mathcal{W}_0(D)} = \mathcal{F}_\tau(\boldsymbol{\Phi}, \boldsymbol{\Psi}) \quad ; \quad \langle \mathbb{F}_\tau^* \boldsymbol{\Phi}, \boldsymbol{\Psi} \rangle_{\mathcal{W}_0(D)} = \mathcal{F}_\tau^*(\boldsymbol{\Phi}, \boldsymbol{\Psi}) \quad ; \quad \langle \mathbb{G} \boldsymbol{\Phi}, \boldsymbol{\Psi} \rangle_{\mathcal{W}_0(D)} = \mathcal{G}(\boldsymbol{\Phi}, \boldsymbol{\Psi}),$$
$$(5.3.52)$$

which permits (5.3.42) and (5.3.43) to be rewritten respectively as

$$\langle (\mathbb{F}_\tau - \tau\mathbb{G})\boldsymbol{\mathcal{V}}, \boldsymbol{\Phi} \rangle_{\mathcal{W}_0(D)} = 0 \qquad \forall \boldsymbol{\Phi} \in \mathcal{W}_0(D), \tag{5.3.53}$$

and

$$\langle (\mathbb{F}_\tau^* - \tau\mathbb{G})\boldsymbol{\mathcal{V}}, \boldsymbol{\Phi} \rangle_{\mathcal{W}_0(D)} = 0 \qquad \forall \boldsymbol{\Phi} \in \mathcal{W}_0(D). \tag{5.3.54}$$

Here it is again noted, analogous to the observation made in Section 5.3.1, that $\tau = \omega^2$ is a transmission eigenvalue associated (5.3.34) if either $\ker(\mathbb{F}_\tau - \tau\mathbb{G}) \neq \{\mathbf{0}\}$ or $\ker(\mathbb{F}_\tau^* - \tau\mathbb{G}) \neq \{\mathbf{0}\}$.

Lemma 15. *Assuming $\rho = \rho_*$, linear operator $\mathbb{F}_\tau : \mathcal{W}_0(D) \to \mathcal{W}_0(D)$ (resp. $\mathbb{F}_\tau^* : \mathcal{W}_0(D) \to \mathcal{W}_0(D)$) is positive definite, self-adjoint and depends continuously on $\tau > 0$ when $\mathsf{c} \geqslant 1 \geqslant \mathsf{C}_*$ (resp. $\mathsf{c}_* \geqslant 1 \geqslant \mathsf{C}$) and $\mathcal{D}_{\mathcal{C}} \neq \mathbf{0}$ holds almost everywhere in D. Further, linear operator $\mathbb{G} : \mathcal{W}_0(D) \to \mathcal{W}_0(D)$ is self-adjoint, positive, and compact.*

Proof. Linear operators $\mathbb{F}_\tau$, $\mathbb{F}_\tau^*$ and $\mathbb{G}$ are self-adjoint since ρ, $\mathcal{C}$ and $\mathcal{C}_*$ are real-valued functions; the positivity of either $\mathbb{F}_\tau$ or $\mathbb{F}_\tau^*$ is a direct consequence of Lemma 14, while the positivity of $\mathbb{G}$ is implied by the fact that ρ is positive according to (5.2.2).

Next, let $\boldsymbol{\Phi}_n$ denote a bounded sequence in $\mathcal{W}_0(D)$ whose subsequence, $\tilde{\boldsymbol{\Phi}}_n$, converges weakly with respect to the $\mathcal{W}_0(D)$-norm to $\boldsymbol{\Phi}_{\mathrm{o}} \in \mathcal{W}_0(D)$. Since $\tilde{\boldsymbol{\Phi}}_n \in \mathcal{W}_0(D)$, one has by (5.3.36) that $\boldsymbol{\nabla} \cdot \tilde{\boldsymbol{\Phi}}_n \in H^1(D)$ which is compactly embedded in $L^2(D)$, whereby $\boldsymbol{\nabla} \cdot \tilde{\boldsymbol{\Phi}}_n$ converges strongly to $\boldsymbol{\nabla} \cdot \boldsymbol{\Phi}_{\mathrm{o}}$ in $L^2(D)$. Accordingly, one has

$$\|\mathbb{G}(\tilde{\boldsymbol{\Phi}}_n - \boldsymbol{\Phi}_{\mathrm{o}})\|_{\mathcal{W}_0(D)} \leqslant \mathsf{P}\|\boldsymbol{\nabla} \cdot (\tilde{\boldsymbol{\Phi}}_n - \boldsymbol{\Phi}_{\mathrm{o}})\|_{L^2(D)}, \tag{5.3.55}$$

which ensures the strong convergence of $\mathbb{G}\tilde{\boldsymbol{\Phi}}_n$ in the $\mathcal{W}_0(D)$-norm sense to $\mathbb{G}\boldsymbol{\Phi}_{\mathrm{o}}$, and thus the compactness of $\mathbb{G}$. $\qquad\square$

Following the path established in Section 5.3.1, the ensuing theorem provides a lower bound for possible transmission eigenvalues when $\rho = \rho_*$. To this end consider the linear operator $-\boldsymbol{\nabla}\boldsymbol{\nabla}\cdot$, which is known to possess an increasing sequence of positive eigenvalues $\tilde{\lambda}_n(D)$ and associated (second-order) eigentensors $\boldsymbol{\Phi}_n$ (Ahusborde et al., 2007; Azaïez et al., 2006) such that

$$\begin{aligned} -\boldsymbol{\nabla}\boldsymbol{\nabla}\cdot\boldsymbol{\Phi}_n &= \tilde{\lambda}_n(D)\boldsymbol{\Phi}_n \qquad \text{in } D, \\ \boldsymbol{\nabla}\cdot\boldsymbol{\Phi}_n &= \mathbf{0} \qquad \text{on } \partial D. \end{aligned} \tag{5.3.56}$$

Alternatively, (5.3.56) can be written in terms of the sequence of first-order tensors $\boldsymbol{\varphi}_n := \boldsymbol{\nabla}\cdot\boldsymbol{\Phi}_n$ as

$$\begin{aligned} -\Delta\boldsymbol{\varphi}_n &= \tilde{\lambda}_n(D)\boldsymbol{\varphi}_n \qquad \text{in } D, \\ \boldsymbol{\varphi}_n &= \mathbf{0} \qquad \text{on } \partial D, \end{aligned} \tag{5.3.57}$$

where $(\tilde{\lambda}_n(D), \boldsymbol{\varphi}_n)$ are the solutions of the Laplace eigenvalue problem over D assuming Dirichlet boundary conditions. Thus if $\lambda_1(D)$ denotes the first Dirichlet eigenvalue of the negative Laplace operator, one has that $\tilde{\lambda}_1(D) \geqslant \lambda_1(D)$.

Theorem 13. *If either* $\mathsf{c} \geqslant 1 \geqslant \mathsf{C}_*$ *or* $\mathsf{c}_* \geqslant 1 \geqslant \mathsf{C}$ *while* $\mathcal{D}_{\mathcal{C}} \neq \mathbf{0}$ *and* $\mathcal{D}_\rho = 0$ *hold almost everywhere in* D, *the set of transmission eigenvalues associated with* (5.2.6) *is discrete, with infinity being the only possible accumulation point. Further, every feasible transmission eigenvalue* ω^2 *is such that*

$$\omega^2 \;>\; \lambda_1(D)\,\frac{\min(\mathsf{c},\mathsf{c}_*)}{\mathsf{P}}.$$

Proof. Under the premises of the theorem, either $\mathbb{F}_\tau$ or $\mathbb{F}_\tau^*$ is invertible owing to Lemma 15 and, since $\mathbb{G}$ is a compact operator, so is $\mathbb{F}_\tau^{-1}\mathbb{G}$ or $\mathbb{F}_\tau^{*-1}\mathbb{G}$. The Fredholm alternative then ensures that $\mathbb{I} - \tau\mathbb{F}_\tau^{*-1}\mathbb{G}$ or $\mathbb{I} - \tau\mathbb{F}_\tau^{-1}\mathbb{G}$ is invertible except for, at most, a discrete set of values $\tau \in \mathbb{C}$ that can only accumulate at infinity.

Next, assume that $\mathsf{c}_* \geqslant 1 \geqslant \mathsf{C}$ whereby $-\boldsymbol{\xi} : \mathcal{D}_{\mathcal{C}} : \bar{\boldsymbol{\xi}} \geqslant \gamma_* |\boldsymbol{\xi}|^2$ for some $\gamma_* > 0$ due to (5.3.46), and let $\mathcal{V} \in \mathcal{W}_0(D)$ such that $\mathcal{V} \in \ker(\mathbb{F}_\tau - \tau\mathbb{G})$. Then $\langle (\mathbb{F}_\tau - \tau\mathbb{G})\mathcal{V}, \mathcal{V} \rangle_{\mathcal{W}_0(D)} = 0$ implies

$$- \int_D \left(\boldsymbol{\nabla}\boldsymbol{\nabla}\cdot\mathcal{V} + \tau\rho\,\mathcal{C}^{-1} : \mathcal{V} \right) : \mathcal{D}_{\mathcal{C}} : \left(\boldsymbol{\nabla}\boldsymbol{\nabla}\cdot\bar{\mathcal{V}} + \tau\rho\,\mathcal{C}^{-1} : \bar{\mathcal{V}} \right) \, \mathrm{d}V$$
$$+ \int_D \left(\tau\rho\,(\boldsymbol{\nabla}\cdot\mathcal{V})\cdot(\boldsymbol{\nabla}\cdot\bar{\mathcal{V}}) - \tau^2\rho^2\,\mathcal{V} : \mathcal{C}^{-1} : \bar{\mathcal{V}} \right) \, \mathrm{d}V = 0. \tag{5.3.58}$$

Whenever the second integral is non-negative, one finds that $\boldsymbol{\nabla}\boldsymbol{\nabla}\cdot\mathcal{V} + \rho\,\tau\,\mathcal{C}^{-1} : \mathcal{V} = \mathbf{0}$ in D. However, since $\boldsymbol{n} \cdot \mathcal{V} = \mathbf{0}$ and $\boldsymbol{\nabla}\cdot\mathcal{V} = \mathbf{0}$ on ∂D, one must also have $\mathcal{V} = \mathbf{0}$ in D due to Holmgren's uniqueness theorem. From an application of the Courant-Fischer min-max formulae (Henrot, 2006), on the other hand, one has

$$\inf_{\mathcal{V} \in \mathcal{W}_0(D)} \frac{\displaystyle\int_D (\boldsymbol{\nabla}\cdot\mathcal{V})\cdot(\boldsymbol{\nabla}\cdot\bar{\mathcal{V}}) \, \mathrm{d}V}{\displaystyle\int_D |\mathcal{V}|^2 \, \mathrm{d}V} \;\geqslant\; \inf_{\substack{\mathcal{V} \in \mathcal{W}(D) \\ \boldsymbol{\nabla}\cdot\mathcal{V} = \mathbf{0} \text{ on } \partial D}} \frac{\displaystyle\int_D (\boldsymbol{\nabla}\cdot\mathcal{V})\cdot(\boldsymbol{\nabla}\cdot\bar{\mathcal{V}}) \, \mathrm{d}V}{\displaystyle\int_D |\mathcal{V}|^2 \, \mathrm{d}V} \;\geqslant\; \lambda_1(D) \tag{5.3.59}$$

and, owing to the bounds on $\mathcal{C}$ and ρ as in (5.2.1),

$$\int_D \left(\rho\,(\boldsymbol{\nabla}\cdot\mathcal{V})\cdot(\boldsymbol{\nabla}\cdot\bar{\mathcal{V}}) - \tau\rho^2\mathcal{V} : \mathcal{C}^{-1} : \bar{\mathcal{V}} \right) \, \mathrm{d}V \;\geqslant\; \mathsf{p}\,\|\mathcal{V}\|_{L^2(D)}^2 \left(\lambda_1(D) - \tau\mathsf{P}\mathsf{c}^{-1} \right), \tag{5.3.60}$$

whereby $\tau \leqslant \lambda_1(D)\mathsf{c}/\mathsf{P}$ clearly cannot be a transmission eigenvalue.

Similarly if $\mathsf{c} \geqslant 1 \geqslant \mathsf{C}_*$ (so that $\boldsymbol{\xi} : \mathcal{D}_{\mathcal{C}} : \bar{\boldsymbol{\xi}} \geqslant \gamma|\boldsymbol{\xi}|^2$ for some $\gamma > 0$, see (5.3.45)) and $\mathcal{V} \in \ker(\mathbb{F}_\tau^* - \tau\mathbb{G})$, then the inequality

$$\int_D \left(\boldsymbol{\nabla}\boldsymbol{\nabla}\cdot\mathcal{V} + \tau\rho\,\mathcal{C}_*^{-1} : \mathcal{V} \right) : \mathcal{D}_{\mathcal{C}} : \left(\boldsymbol{\nabla}\boldsymbol{\nabla}\cdot\bar{\mathcal{V}} + \tau\rho\,\mathcal{C}_*^{-1} : \bar{\mathcal{V}} \right) \, \mathrm{d}V$$
$$+ \int_D \left(\tau\rho\,(\boldsymbol{\nabla}\cdot\mathcal{V})\cdot(\boldsymbol{\nabla}\cdot\bar{\mathcal{V}}) - \tau^2\rho^2\,\mathcal{V} : \mathcal{C}_*^{-1} : \bar{\mathcal{V}} \right) \, \mathrm{d}V = 0, \tag{5.3.61}$$

implies that $\mathcal{V} = \mathbf{0}$ in D, i.e. that $\tau = \omega^2$ cannot be a transmission eigenvalue as long as

$$\int_D \left(\rho\,(\boldsymbol{\nabla}\cdot\mathcal{V})\cdot(\boldsymbol{\nabla}\cdot\bar{\mathcal{V}}) - \tau\rho^2\mathcal{V} : \mathcal{C}_*^{-1} : \bar{\mathcal{V}} \right) \, \mathrm{d}V \;\geqslant\; \mathsf{p}\,\|\mathcal{V}\|_{L^2(D)}^2 \left(\lambda_1(D) - \tau\mathsf{P}\mathsf{c}_*^{-1} \right) \geqslant 0, \tag{5.3.62}$$

i.e. when $\tau \leqslant \lambda_1(D)\mathsf{c}_*/\mathsf{P}$.

$\square$

Theorem 14. *If either* $c \geqslant 1 \geqslant C_*$ *or* $c_* \geqslant 1 \geqslant C$ *while* $\mathcal{D}_{\mathcal{C}} \neq \mathbf{0}$ *and* $\mathcal{D}_\rho = 0$ *hold almost everywhere in D, there exists a countable set of transmission eigenvalues affiliated with* (5.2.6).

Proof. The proof in this case follows the ideas developed in the context of Theorem 12. Suppose that $c \geqslant 1 \geqslant C_*$ and that $\mathcal{D}_{\mathcal{C}} \neq \mathbf{0}$ holds almost everywhere in D, so that operators $\mathbb{F}_\tau$ and $\mathbb{G}$ satisfy the hypotheses of Theorem 10 with $W \equiv \mathcal{W}_0(D)$.

With reference to the proof of Lemma 14 and inequalities (5.3.48)–(5.3.50), there exists a constant $\beta'' > 0$ such that for all $\mathcal{V} \in \mathcal{W}_0(D)$

$$\langle \mathbb{F}_\tau \mathcal{V}, \mathcal{V} \rangle_{\mathcal{W}_0(D)} \geqslant \beta'' \|\boldsymbol{\nabla}\boldsymbol{\nabla}\cdot\mathcal{V}\|^2_{L^2(D)}, \qquad (5.3.63)$$

which together with Poincaré inequality (5.3.51) ensures that

$$\langle (\mathbb{F}_\tau - \tau\mathbb{G})\mathcal{V}, \mathcal{V} \rangle_{\mathcal{W}_0(D)} \geqslant (\beta'' - \tau\mathsf{P}C_P) \|\boldsymbol{\nabla}\cdot\mathcal{V}\|^2_{L^2(D)}. \qquad (5.3.64)$$

From (5.3.64), one concludes that $\mathbb{F}_{\tau_0} - \tau_0\mathbb{G}$ is positive on $\mathcal{W}_0(D)$ for $0 < \tau_0 < \beta''/(\mathsf{P}C_P)$, which meets Assumption 1 of Theorem 10.

Next, consider the interior transmission problem (5.3.34) for a ball $B_r \subset D$ of radius r with constant mass densities $\hat{\rho} = \hat{\rho}_* = \text{const.}$ and homogeneous isotropic elastic tensors $\hat{\mathcal{C}}$ and $\hat{\mathcal{C}}_*$ given by their eigenvalues

$$\begin{aligned} \hat{\mathsf{C}} &= \mathsf{C}, & \hat{\mathsf{C}}_* &= \mathsf{C}_*, \\ \hat{\mathsf{c}} &= \mathsf{c}, & \hat{\mathsf{c}}_* &= \mathsf{c}_*. \end{aligned} \qquad (5.3.65)$$

From the analytical solution in Section 5.2.2, it is known that there exists an infinite set of transmission eigenvalues for this problem. To help establish the claim of the theorem, let $\hat{\tau}$ be one such eigenvalue and let $\hat{\mathcal{V}} \in \mathcal{W}_0(B_r)$ be the corresponding eigenfunction. Accordingly, $\hat{\mathcal{V}}$ satisfies (5.3.53) with $\tau = \hat{\tau}$, D superseded by B_r, and with the featured operators taken as those corresponding to assumed (constant) material parameters. Accordingly by taking $\boldsymbol{\Phi} = \hat{\mathcal{V}}$, recalling that $\mathsf{c}_*^{-1} > \mathsf{C}^{-1}$, and integrating (5.3.53) by parts, one finds that

$$\mathsf{C}^{-1}\mathsf{C}_*^{-1}\hat{\rho}^2\hat{\tau}^2\|\hat{\mathcal{V}}\|^2_{L^2(B_r)} \leqslant -\left(1 + \mathsf{C}^{-1} - \mathsf{c}^{-1}\right)\|\boldsymbol{\nabla}\boldsymbol{\nabla}\cdot\hat{\mathcal{V}}\|^2_{L^2(B_r)} + \left(\mathsf{c}_*^{-1} + \mathsf{C}^{-1}\right)\hat{\rho}\hat{\tau}\|\boldsymbol{\nabla}\cdot\hat{\mathcal{V}}\|^2_{L^2(B_r)}. \qquad (5.3.66)$$

If $\hat{\mathcal{V}}_0 \in \mathcal{W}_0(D)$ is the extension of $\hat{\mathcal{V}}$ by zero to the whole D, then

$$\begin{aligned} \langle (\mathbb{F}_{\hat{\tau}} - \hat{\tau}\mathbb{G})\hat{\mathcal{V}}_0, \hat{\mathcal{V}}_0 \rangle_{\mathcal{W}_0(D)} \leqslant{}& \left(\frac{1 + \mathsf{c}^{-1} - \mathsf{C}^{-1}}{\mathsf{C}_*^{-1} - \mathsf{c}^{-1}}\right)\|\boldsymbol{\nabla}\boldsymbol{\nabla}\cdot\hat{\mathcal{V}}\|^2_{L^2(B_r)} - \left(\frac{\mathsf{C}_*^{-1} + \mathsf{c}^{-1}}{\mathsf{C}_*^{-1} - \mathsf{c}^{-1}}\right)\mathsf{p}\hat{\tau}\|\boldsymbol{\nabla}\cdot\hat{\mathcal{V}}\|^2_{L^2(B_r)} \\ &+ \left(\frac{\mathsf{c}^{-1}\mathsf{c}_*^{-1}}{\mathsf{C}_*^{-1} - \mathsf{c}^{-1}}\right)\mathsf{P}^2\hat{\tau}^2\|\hat{\mathcal{V}}\|^2_{L^2(B_r)}, \end{aligned} \qquad (5.3.67)$$

where $\mathbb{F}_{\hat{\tau}}$ and $\mathbb{G}$ are given by (5.3.52) assuming $\tau = \hat{\tau}$ and the original set of material parameters in terms of distributions $(\mathcal{C}, \rho)$ and $(\mathcal{C}_*, \rho_*)$ over D. A substitution of (5.3.66) into (5.3.67) yields

$$\begin{aligned} \langle (\mathbb{F}_{\hat{\tau}} - \hat{\tau}\mathbb{G})\hat{\mathcal{V}}_0, \hat{\mathcal{V}}_0 \rangle_{\mathcal{W}_0(D)} \leqslant{}& \left\{\left(\frac{1 + \mathsf{c}^{-1} - \mathsf{C}^{-1}}{\mathsf{C}_*^{-1} - \mathsf{c}^{-1}}\right) - \frac{\mathsf{c}^{-1}\mathsf{c}_*^{-1}}{\mathsf{C}^{-1}\mathsf{C}_*^{-1}}\left(\frac{1 + \mathsf{C}^{-1} - \mathsf{c}^{-1}}{\mathsf{C}_*^{-1} - \mathsf{c}^{-1}}\right)\frac{\mathsf{P}^2}{\hat{\rho}^2}\right\}\|\boldsymbol{\nabla}\boldsymbol{\nabla}\cdot\hat{\mathcal{V}}\|^2_{L^2(B_r)} \\ &+ \left\{\frac{\mathsf{c}^{-1}\mathsf{c}_*^{-1}}{\mathsf{C}^{-1}\mathsf{C}_*^{-1}}\left(\frac{\mathsf{c}_*^{-1} + \mathsf{C}^{-1}}{\mathsf{C}_*^{-1} - \mathsf{c}^{-1}}\right)\frac{\mathsf{P}^2}{\hat{\rho}} - \left(\frac{\mathsf{C}_*^{-1} + \mathsf{c}^{-1}}{\mathsf{C}_*^{-1} - \mathsf{c}^{-1}}\right)\mathsf{p}\right\}\hat{\tau}^2\|\hat{\mathcal{V}}\|^2_{L^2(B_r)}. \end{aligned} \qquad (5.3.68)$$

Recalling further that $C_*^{-1} > c^{-1}$ and choosing the constant mass density $\hat{\rho} > 0$ such that

$$\hat{\rho} > \frac{c^{-1}c_*^{-1}}{C^{-1}C_*^{-1}} \left(\frac{c_*^{-1} + C^{-1}}{C_*^{-1} + c^{-1}} \right) \frac{P^2}{p}, \tag{5.3.69}$$

one finds from (5.3.68) that for sufficiently large $\hat{\tau} = \tau_1$, operator $\mathbb{F}_{\tau_1} - \tau_1\mathbb{G}$ is non-positive on the subspace of $\mathcal{W}_0(D)$ spanned by $\hat{\boldsymbol{\mathcal{V}}}_0$ – a result which meets Assumption 2 of Theorem 10. As a result, one finds from the latter theorem that there is at least one transmission eigenvalue of B_r within interval $[\tau_0, \tau_1]$, where $\tau_0 < \beta''/(PC_P)$. The reminder of the proof mimics that in Theorem 12 and is omitted for brevity.

<div align="right">□</div>

Note again that the above analysis allows one to establish implicit estimates on the extreme eigenvalues of $\mathcal{C}$ and $\mathcal{C}_*$ in terms of the first transmission eigenvalue, ω_1, of (5.3.34) in a way analogous to that in Corollary 1.

5.4 Configurations without material similitude

For a comprehensive treatment of the subject, this section assumes that the mass density and elasticity contrasts between the two solids, $\Delta_\rho := \rho_* - \rho$ and $\boldsymbol{\Delta_\mathcal{C}} := \mathcal{C}_* - \mathcal{C}$, are *both* non-zero almost everywhere in D. The difficulty in the treatment of such class of configurations stems from the imposed "dual" boundary condition in (5.2.6). In particular, if one attempts to apply the methods of analysis established in Section 5.3, the fact that $\Delta_\rho \neq 0$ and $\boldsymbol{\Delta_\mathcal{C}} \neq \mathbf{0}$ simultaneously makes it impossible to deploy the featured functional spaces which postulate homogeneous boundary conditions over ∂D. To deal with the impediment, the ensuing analysis pursues an alternate route by generalizing upon the developments in Bellis and Guzina (2010) and Cakoni and Kirsch (2010).

To help establish the necessary framework, one may recast the interior transmission problem (5.2.6) in a variational setting as either of

$$\begin{aligned}
\int_D \left(\boldsymbol{\nabla u} : \mathcal{C} : \boldsymbol{\nabla}\bar{\boldsymbol{\varphi}} - \rho\,\omega^2 \boldsymbol{u} \cdot \bar{\boldsymbol{\varphi}} \right) \mathrm{d}V &= 0 \\
\int_D \left(\boldsymbol{\nabla u_*} : \mathcal{C}_* : \boldsymbol{\nabla}\bar{\boldsymbol{\varphi}} - \rho_*\omega^2 \boldsymbol{u_*} \cdot \bar{\boldsymbol{\varphi}} \right) \mathrm{d}V &= 0
\end{aligned} \qquad \forall \boldsymbol{\varphi} \in H_0^1(D), \tag{5.4.1}$$

and

$$\int_D \left(\boldsymbol{\nabla u} : \mathcal{C} : \boldsymbol{\nabla}\bar{\boldsymbol{\varphi}} - \rho\,\omega^2 \boldsymbol{u} \cdot \bar{\boldsymbol{\varphi}} \right) \mathrm{d}V = \int_D \left(\boldsymbol{\nabla u_*} : \mathcal{C}_* : \boldsymbol{\nabla}\bar{\boldsymbol{\varphi}} - \rho_*\omega^2 \boldsymbol{u_*} \cdot \bar{\boldsymbol{\varphi}} \right) \mathrm{d}V \qquad \forall \boldsymbol{\varphi} \in H^1(D), \tag{5.4.2}$$

where $H_0^1(D)$ denotes the Hilbert space of all $\boldsymbol{\varphi} \in H^1(D)$ such that $\boldsymbol{\varphi} = \mathbf{0}$ on ∂D. As a result, if $\boldsymbol{v} := \boldsymbol{u} - \boldsymbol{u_*}$ then clearly $\boldsymbol{v} \in H_0^1(D)$ and from (5.4.2) it follows that

$$\int_D \left(\boldsymbol{\nabla u} : \boldsymbol{\Delta_\mathcal{C}} : \boldsymbol{\nabla}\bar{\boldsymbol{\varphi}} - \Delta_\rho\omega^2 \boldsymbol{u} \cdot \bar{\boldsymbol{\varphi}} \right) \mathrm{d}V = \int_D \left(\boldsymbol{\nabla v} : \mathcal{C}_* : \boldsymbol{\nabla}\bar{\boldsymbol{\varphi}} - \rho_*\omega^2 \boldsymbol{v} \cdot \bar{\boldsymbol{\varphi}} \right) \mathrm{d}V \qquad \forall \boldsymbol{\varphi} \in H^1(D), \tag{5.4.3}$$

or alternatively

$$\int_D \left(\boldsymbol{\nabla u_*} : \boldsymbol{\Delta_\mathcal{C}} : \boldsymbol{\nabla}\bar{\boldsymbol{\varphi}} - \Delta_\rho\omega^2 \boldsymbol{u_*} \cdot \bar{\boldsymbol{\varphi}} \right) \mathrm{d}V = \int_D \left(\boldsymbol{\nabla v} : \mathcal{C} : \boldsymbol{\nabla}\bar{\boldsymbol{\varphi}} - \rho\,\omega^2 \boldsymbol{v} \cdot \bar{\boldsymbol{\varphi}} \right) \mathrm{d}V \qquad \forall \boldsymbol{\varphi} \in H^1(D). \tag{5.4.4}$$

5.4.1 Elasticity and mass density contrasts of opposite sign

To examine the issues of discreteness and existence of the transmission eigenvalues characterizing (5.2.6) that have, for this class of material configurations, eluded earlier studies (Bellis and Guzina, 2010), set $\tau = \omega^2$ and let $\mathcal{M}_\tau$ and $\mathcal{M}_\tau^*$ be the bilinear forms on $H^1(D) \times H^1(D)$ defined by

$$\begin{aligned}
\mathcal{M}_\tau(\boldsymbol{\varphi}, \boldsymbol{\psi}) &:= \langle \boldsymbol{\Delta}_{\boldsymbol{\mathcal{C}}} : \boldsymbol{\nabla}\boldsymbol{\varphi}, \boldsymbol{\nabla}\boldsymbol{\psi} \rangle_{L^2(D)} - \tau \langle \Delta_\rho \boldsymbol{\varphi}, \boldsymbol{\psi} \rangle_{L^2(D)}, \\
\mathcal{M}_\tau^*(\boldsymbol{\varphi}, \boldsymbol{\psi}) &:= \langle \boldsymbol{\Delta}_{\boldsymbol{\mathcal{C}}} : \boldsymbol{\nabla}\boldsymbol{\varphi}, \boldsymbol{\nabla}\boldsymbol{\psi} \rangle_{L^2(D)} - \tau \langle \Delta_\rho \boldsymbol{\varphi}, \boldsymbol{\psi} \rangle_{L^2(D)}.
\end{aligned} \tag{5.4.5}$$

Next, for given $\boldsymbol{v} \in H_0^1(D)$, let $\mathcal{N}_{\tau,\boldsymbol{v}}$ and $\mathcal{N}_{\tau,\boldsymbol{v}}^*$ be the linear forms on $H^1(D)$ such that

$$\begin{aligned}
\mathcal{N}_{\tau,\boldsymbol{v}}(\boldsymbol{\psi}) &:= \langle \boldsymbol{\mathcal{C}}_* : \boldsymbol{\nabla}\boldsymbol{v}, \boldsymbol{\nabla}\boldsymbol{\psi} \rangle_{L^2(D)} - \tau \langle \rho_* \boldsymbol{v}, \boldsymbol{\psi} \rangle_{L^2(D)}, \\
\mathcal{N}_{\tau,\boldsymbol{v}}^*(\boldsymbol{\psi}) &:= \langle \boldsymbol{\mathcal{C}} : \boldsymbol{\nabla}\boldsymbol{v}, \boldsymbol{\nabla}\boldsymbol{\psi} \rangle_{L^2(D)} - \tau \langle \rho \, \boldsymbol{v}, \boldsymbol{\psi} \rangle_{L^2(D)},
\end{aligned} \tag{5.4.6}$$

for all $(\boldsymbol{\varphi}, \boldsymbol{\psi}) \in H^1(D) \times H^1(D)$. With such definitions, variational problems (5.4.3) and (5.4.4) consist respectively in finding $\boldsymbol{u} \in H^1(D)$ such that

$$\mathcal{M}_\tau(\boldsymbol{u}, \boldsymbol{\varphi}) = \mathcal{N}_{\tau,\boldsymbol{v}}(\boldsymbol{\varphi}) \quad \forall \boldsymbol{\varphi} \in H^1(D), \tag{5.4.7}$$

and solving for $\boldsymbol{u}_* \in H^1(D)$ that satisfies

$$\mathcal{M}_\tau^*(\boldsymbol{u}_*, \boldsymbol{\varphi}) = \mathcal{N}_{\tau,\boldsymbol{v}}^*(\boldsymbol{\varphi}) \quad \forall \boldsymbol{\varphi} \in H^1(D). \tag{5.4.8}$$

Lemma 16. *For every $\boldsymbol{v} \in H_0^1(D)$ and $\tau \in \mathbb{C}$ such that $\Re(\tau) > -\delta$ for some $\delta > 0$, there exists unique $\boldsymbol{u} \in H^1(D)$ satisfying (5.4.3) (resp. $\boldsymbol{u}_* \in H^1(D)$ satisfying (5.4.4)) when $\mathsf{P}_* < \mathsf{p}$ and $\mathsf{c}_* > \mathsf{C}$ (resp. $\mathsf{p}_* > \mathsf{P}$ and $\mathsf{C}_* < \mathsf{c}$). Further, the linear operator $\mathbb{M}_\tau : H_0^1(D) \to H^1(D)$ constructed such that $\mathbb{M}_\tau \boldsymbol{v} = \boldsymbol{u}$ is solution of (5.4.3) (resp. $\mathbb{M}_\tau^* : H_0^1(D) \to H^1(D)$ constructed such that $\mathbb{M}_\tau^* \boldsymbol{v} = \boldsymbol{u}_*$ is solution of (5.4.4)) is bounded and depends analytically on $\tau \in \{z \in \mathbb{C} : \Re(z) > -\delta\}$.*

Proof. The proof is essentially the same in the two cases, and is shown here assuming $\mathsf{P}_* < \mathsf{p}$ and $\mathsf{c}_* > \mathsf{C}$. Assuming $\boldsymbol{v} \in H_0^1(D)$ and setting $\boldsymbol{\varphi}$ in (5.4.7) to be a constant vector, one finds that

$$\int_D \Delta_\rho \boldsymbol{u} \cdot \bar{\boldsymbol{\varphi}} \, \mathrm{d}V = \int_D \rho_* \boldsymbol{v} \cdot \bar{\boldsymbol{\varphi}} \, \mathrm{d}V.$$

As a result, the solution $\boldsymbol{u} \in H^1(D)$ of (5.4.7) when $\tau = 0$ is unique up to a constant vector which can be chosen such that the above equality holds for three linearly independent constant vectors $\boldsymbol{\varphi}$. In light of this result, the solution for $\tau \in \mathbb{C}$ can be conveniently sought as $\boldsymbol{u} = \tilde{\boldsymbol{u}} + \mathbf{k}$, where $\mathbf{k}$ is a constant vector and $\tilde{\boldsymbol{u}} \in \tilde{H}^1(D)$ belongs to the space of "zero-weighted-mean" functions

$$\tilde{H}^1(D) := \left\{ \boldsymbol{\psi} \in H^1(D) : \int_D \Delta_\rho \boldsymbol{\psi} \, \mathrm{d}V = \boldsymbol{0} \right\},$$

equipped with the usual $H^1(D)$ norm. On selecting $\mathbf{k}$ independent of τ as

$$\mathbf{k} = \frac{\displaystyle\int_D \rho_* \boldsymbol{v} \, \mathrm{d}V}{\displaystyle\int_D \Delta_\rho \, \mathrm{d}V},$$

one finds from (5.4.5)-(5.4.7) that $\tilde{\boldsymbol{u}}$ satisfies the same equation as $\boldsymbol{u}$. By the standard arguments for $\boldsymbol{\psi} \in \tilde{H}^1(D)$, it also follows that $\|\boldsymbol{\nabla}\boldsymbol{\psi}\|^2_{L^2(D)}$ is an equivalent norm in $\tilde{H}^1(D)$ since

$$\frac{\mu}{\mu+1}\|\boldsymbol{\psi}\|^2_{H^1(D)} \leq \|\boldsymbol{\nabla}\boldsymbol{\psi}\|^2_{L^2(D)} \leq \|\boldsymbol{\psi}\|^2_{H^1(D)}, \qquad (5.4.9)$$

where $\mu > 0$ is the unique minimizer

$$\mu = \inf_{\boldsymbol{\psi} \in \tilde{H}^1(D)} \frac{\|\boldsymbol{\nabla}\boldsymbol{\psi}\|^2_{L^2(D)}}{\|\boldsymbol{\psi}\|^2_{L^2(D)}}.$$

When $\mathsf{c}_* > \mathsf{C}$ and $\mathsf{P}_* < \mathsf{p}$, it follows from (5.4.5a) and (5.4.9) that for sufficiently small $\delta > 0$ one has

$$\Re\left(\mathcal{M}_\tau(\boldsymbol{\varphi}, \boldsymbol{\varphi})\right) \geqslant (\mathsf{c}_* - \mathsf{C})\|\boldsymbol{\nabla}\boldsymbol{\varphi}\|^2_{L^2(D)} - \delta\left(\mathsf{P} - \mathsf{p}_*\right)\|\boldsymbol{\varphi}\|^2_{L^2(D)} \geqslant C''\|\boldsymbol{\varphi}\|^2_{H^1(D)}, \qquad (5.4.10)$$

for all $\boldsymbol{\varphi} \in \tilde{H}^1(D)$ and some positive constant C'' independent of $\tau \in \{z \in \mathbb{C} : \Re(z) > -\delta\}$, whereby $\mathcal{M}_\tau$ is coercive in $\tilde{H}^1(D)$. Since $\mathcal{M}_\tau$ and $\mathcal{N}_{\tau,\boldsymbol{v}}$ are also continuous, application of the Lax-Milgram theorem ensures the existence of a unique $\tilde{\boldsymbol{u}}$ that solves (5.4.7) and depends continuously on $\boldsymbol{v}$. Furthermore $\boldsymbol{u} = \tilde{\boldsymbol{u}} + \mathbf{k}$ also satisfies (5.4.7) by the definition of $\mathbf{k}$. As a result, one concludes that bounded linear operator $\mathbb{M}_\tau$, which maps $\boldsymbol{v}$ to a unique solution $\boldsymbol{u}$ of (5.4.7), is well defined and depends analytically on $\tau \in \{z \in \mathbb{C} : \Re(z) > -\delta\}$. $\qquad\square$

On recalling (5.4.1) and making reference to the relationships $\boldsymbol{u} = \mathbb{M}_\tau \boldsymbol{v}$ and $\boldsymbol{u}_* = \mathbb{M}_\tau^* \boldsymbol{v}$ where $\boldsymbol{v} \in H^1_0(D)$, one can define the respective linear forms on $H^1_0(D)$ as

$$\mathcal{L}_\tau(\boldsymbol{\varphi}) := \left\langle \boldsymbol{\mathcal{C}} : \boldsymbol{\nabla}\boldsymbol{u}, \boldsymbol{\nabla}\boldsymbol{\varphi} \right\rangle_{L^2(D)} - \tau\left\langle \rho\boldsymbol{u}, \boldsymbol{\varphi} \right\rangle_{L^2(D)}, \qquad (5.4.11)$$

and

$$\mathcal{L}_\tau^*(\boldsymbol{\varphi}) := \left\langle \boldsymbol{\mathcal{C}}_* : \boldsymbol{\nabla}\boldsymbol{u}_*, \boldsymbol{\nabla}\boldsymbol{\varphi} \right\rangle_{L^2(D)} - \tau\left\langle \rho_*\boldsymbol{u}_*, \boldsymbol{\varphi} \right\rangle_{L^2(D)}, \qquad (5.4.12)$$

such that, in light of Lemma 16 and the Riesz representation theorem, there exists a bounded linear operator $\mathbb{L}_\tau$ (resp. $\mathbb{L}_\tau^*$) from $H^1_0(D)$ into $H^1_0(D)$ such that for all $\boldsymbol{\varphi} \in H^1_0(D)$ one has $\left\langle \mathbb{L}_\tau \boldsymbol{v}, \boldsymbol{\varphi} \right\rangle_{H^1_0(D)} = \mathcal{L}_\tau(\boldsymbol{\varphi})$ (resp. $\left\langle \mathbb{L}_\tau^* \boldsymbol{v}, \boldsymbol{\varphi} \right\rangle_{H^1_0(D)} = \mathcal{L}_\tau^*(\boldsymbol{\varphi})$). Thus if $\mathsf{P}_* < \mathsf{p}$ and $\mathsf{c}_* > \mathsf{C}$ (resp. $\mathsf{p}_* > \mathsf{P}$ and $\mathsf{C}_* < \mathsf{c}$) and $\tau = \omega^2$ is a transmission eigenvalue of (5.2.6) associated with eigenfunction pair $(\boldsymbol{u}, \boldsymbol{u}_*) \in H^1(D) \times H^1(D)$, then $\boldsymbol{v} = \boldsymbol{u} - \boldsymbol{u}_* \in H^1_0(D)$ verifies $\boldsymbol{v} \neq \boldsymbol{0}$ and $\boldsymbol{v} \in \ker(\mathbb{L}_\tau)$ (resp. $\boldsymbol{v} \in \ker(\mathbb{L}_\tau^*)$). Conversely, if $\boldsymbol{v} \in \ker(\mathbb{L}_\tau)\backslash\{\boldsymbol{0}\}$ (resp. $\boldsymbol{v} \in \ker(\mathbb{L}_\tau^*)\backslash\{\boldsymbol{0}\}$), then $\boldsymbol{u} = \mathbb{M}_\tau \boldsymbol{v}$ and $\boldsymbol{u}_* = \boldsymbol{u} - \boldsymbol{v}$ solve (5.4.1a) and (5.4.2) as a consequence of (5.4.3) (resp. $\boldsymbol{u}_* = \mathbb{M}_\tau^* \boldsymbol{v}$ and $\boldsymbol{u} = \boldsymbol{v} + \mathbb{M}_\tau^* \boldsymbol{v}$ satisfy (5.4.1b) and (5.4.2) owing to (5.4.4)). Thus, $(\boldsymbol{u}, \boldsymbol{u}_*)$ defines a set of transmission eigenfunctions in $H^1(D) \times H^1(D)$ in each case. Note that, owing to Lemma 16, $\mathbb{L}_\tau$ (resp. $\mathbb{L}_\tau^*$) depends analytically on $\tau \in \{z \in \mathbb{C} : \Re(z) > -\delta\}$

Lemma 17. *Linear operator $\mathbb{L}_0 : H^1_0(D) \to H^1_0(D)$ (resp. $\mathbb{L}_0^*$) is coercive if $\mathsf{P}_* < \mathsf{p}$ and $\mathsf{c}_* > \mathsf{C}$ (resp. $\mathsf{p}_* > \mathsf{P}$ and $\mathsf{C}_* < \mathsf{c}$).*

Proof. Again, the proof is shown only for the case where $\mathsf{P}_* < \mathsf{p}$ and $\mathsf{c}_* > \mathsf{C}$. With reference to (5.4.11), one finds by setting $\tau = 0$ that

$$\left\langle \mathbb{L}_0 \boldsymbol{v}, \boldsymbol{v} \right\rangle_{H^1_0(D)} = \int_D \boldsymbol{\nabla}\boldsymbol{u} : \boldsymbol{\mathcal{C}} : \boldsymbol{\nabla}\bar{\boldsymbol{v}} \, \mathrm{d}V, \qquad (5.4.13)$$

where $v \in H_0^1(D)$ and $u = \mathbb{M}_0 v$ also satisfies (5.4.3) due to Lemma 16. On substituting $u = v + u_*$ in (5.4.3) and (5.4.13), one further has

$$\langle \mathbb{L}_0 v, v \rangle_{H_0^1(D)} = \int_D \left(\boldsymbol{\nabla} v : \boldsymbol{\mathcal{C}} : \boldsymbol{\nabla} \bar{v} + \boldsymbol{\nabla} u_* : \boldsymbol{\Delta}_{\boldsymbol{\mathcal{C}}} : \boldsymbol{\nabla} \bar{u}_* \right) \, \mathrm{d}V \tag{5.4.14}$$

and, due to the bounds in (5.2.1) on elastic tensors,

$$\langle \mathbb{L}_0 v, v \rangle_{H_0^1(D)} \geqslant \mathsf{c} \|\boldsymbol{\nabla} v\|_{L^2(D)}^2 + (\mathsf{c}_* - \mathsf{C}) \|\boldsymbol{\nabla} u_*\|_{L^2(D)}^2 . \tag{5.4.15}$$

Finally, since $v \in H_0^1(D)$ one finally concludes from the Poincaré inequality that there exists a constant $C > 0$ such that

$$\langle \mathbb{L}_0 v, v \rangle_{H_0^1(D)} \geqslant C \|v\|_{H_0^1(D)}^2 , \tag{5.4.16}$$

whereby $\mathbb{L}_0$ is coercive on $H_0^1(D)$.

$\square$

Lemma 18. *Linear operator $\mathbb{L}_\tau$ (resp. $\mathbb{L}_\tau^*$) from $H_0^1(D)$ into $H_0^1(D)$ is self-adjoint and has the property that $\mathbb{L}_\tau - \mathbb{L}_0$ (resp. $\mathbb{L}_\tau^* - \mathbb{L}_0^*$) is compact on $H_0^1(D)$, if $\mathsf{P}_* < \mathsf{p}$ and $\mathsf{c}_* > \mathsf{C}$ (resp. $\mathsf{p}_* > \mathsf{P}$ and $\mathsf{C}_* < \mathsf{c}$).*

Proof. Suppose that $\mathsf{P}_* < \mathsf{p}$ and $\mathsf{c}_* > \mathsf{C}$, and let $(v, v') \in H_0^1(D) \times H_0^1(D)$. Due to Lemma 16, $u = \mathbb{M}_\tau v$ and $u' = \mathbb{M}_\tau v'$ each satisfy (5.4.3). With reference to (5.4.11), one has

$$\begin{aligned}
\langle \mathbb{L}_\tau v, v' \rangle_{H_0^1(D)} &= \int_D \left(\boldsymbol{\nabla} u : \boldsymbol{\mathcal{C}} : \boldsymbol{\nabla} \bar{v}' - \rho \tau u \cdot \bar{v}' \right) \, \mathrm{d}V \\
&= - \int_D \left(\boldsymbol{\nabla} u : \boldsymbol{\Delta}_{\boldsymbol{\mathcal{C}}} : \boldsymbol{\nabla} \bar{v}' - \Delta_\rho \tau u \cdot \bar{v}' \right) \, \mathrm{d}V \\
&\quad + \int_D \left(\boldsymbol{\nabla} u : \boldsymbol{\mathcal{C}}_* : \boldsymbol{\nabla} \bar{v}' - \rho_* \tau u \cdot \bar{v}' \right) \, \mathrm{d}V,
\end{aligned} \tag{5.4.17}$$

which by applying (5.4.3) twice, yields

$$\begin{aligned}
\langle \mathbb{L}_\tau v, v' \rangle_{H_0^1(D)} &= - \int_D \left(\boldsymbol{\nabla} v : \boldsymbol{\mathcal{C}}_* : \boldsymbol{\nabla} \bar{v}' - \rho_* \tau v \cdot \bar{v}' \right) \, \mathrm{d}V \\
&\quad + \int_D \left(\boldsymbol{\nabla} u' : \boldsymbol{\Delta}_{\boldsymbol{\mathcal{C}}} : \boldsymbol{\nabla} \bar{u} - \Delta_\rho \tau u' \cdot \bar{u} \right) \, \mathrm{d}V.
\end{aligned} \tag{5.4.18}$$

As a result, $\langle \mathbb{L}_\tau v, v' \rangle_{H_0^1(D)} = \overline{\langle \mathbb{L}_\tau v', v \rangle}_{H_0^1(D)}$ i.e. $\mathbb{L}_\tau$ is self-adjoint.

To establish the compactness of $\mathbb{L}_\tau - \mathbb{L}_0$, consider a bounded sequence v_n in $H_0^1(D)$ for which there exists a subsequence $\tilde{v}_n$ that weakly converges with respect to the $H_0^1(D)$-norm to $v \in H_0^1(D)$. Since $H_0^1(D)$ is compactly embedded in $L^2(D)$, $\tilde{v}_n$ converges strongly to v with respect to the $L^2(D)$-norm and, due to Lemma 16, sequences $\tilde{u}_n := \mathbb{M}_\tau \tilde{v}_n$ and $\tilde{u}_n^0 := \mathbb{M}_0 \tilde{v}_n$ converge strongly in $L^2(D)$ to u and u^0, respectively. On the basis of (5.4.11), the Cauchy-Schwarz inequality, and the bounds on $\boldsymbol{\mathcal{C}}$ and ρ as in (5.2.1), on the other hand, one has

$$\|(\mathbb{L}_\tau - \mathbb{L}_0)(\tilde{v}_n - v)\|_{H_0^1(D)} \leqslant \mathsf{C} \left\{ \|\boldsymbol{\nabla}(\tilde{u}_n - u)\|_{L^2(D)} + \|\boldsymbol{\nabla}(\tilde{u}_n^0 - u^0)\|_{L^2(D)} \right\} + \mathsf{P} \tau \|\tilde{u}_n - u\|_{L^2(D)}, \tag{5.4.19}$$

which guarantees that $(\mathbb{L}_\tau - \mathbb{L}_0) \tilde{v}_n$ converges strongly to $(\mathbb{L}_\tau - \mathbb{L}_0) v$ with respect to the $H_0^1(D)$-norm, i.e. that $\mathbb{L}_\tau - \mathbb{L}_0$ is compact.

$\square$

Theorem 15. *If either* $\mathsf{P}_* < \mathsf{p}$ *and* $\mathsf{c}_* > \mathsf{C}$ *or* $\mathsf{p}_* > \mathsf{P}$ *and* $\mathsf{C}_* < \mathsf{c}$, *the set of transmission eigenvalues associated with* (5.2.6) *is discrete, with infinity being the only possible accumulation point. Further, every feasible transmission eigenvalue* ω^2 *is such that*

$$\omega^2 \;\geqslant\; \lambda_1(D)\,\frac{\min(\mathsf{c},\mathsf{c}_*)}{\max(\mathsf{P},\mathsf{P}_*)}.$$

Proof. The discreteness of the set of transmission eigenvalues is a direct consequence of Lemmas 16, 17 and 18. Indeed, under the hypothesis that $\mathsf{P}_* < \mathsf{p}$ and $\mathsf{c}_* > \mathsf{C}$ (resp. $\mathsf{p}_* > \mathsf{P}$ and $\mathsf{C}_* < \mathsf{c}$), one has that $\mathbb{L}_0$ (resp. $\mathbb{L}_0^*$) is invertible and that $\mathbb{L}_\tau - \mathbb{L}_0$ (resp. $\mathbb{L}_\tau^* - \mathbb{L}_0^*$) is compact, while $\mathbb{L}_\tau$ (resp. $\mathbb{L}_\tau^*$) depends analytically on τ in a neighborhood of the real axis. On employing the decomposition $\mathbb{L}_\tau = \mathbb{L}_0 + (\mathbb{L}_\tau - \mathbb{L}_0)$ (resp. $\mathbb{L}_\tau^* = \mathbb{L}_0^* + (\mathbb{L}_\tau^* - \mathbb{L}_0^*)$), it follows from the analytic Fredholm theory (Colton and Kress, 1992) that compact operator $\mathbb{I} + \mathbb{L}_0^{-1}(\mathbb{L}_\tau - \mathbb{L}_0)$ (resp. $\mathbb{I} + \mathbb{L}_0^{*-1}(\mathbb{L}_\tau^* - \mathbb{L}_0^*)$) is invertible except for a discrete set of values $\tau \in \mathbb{C}$ that can only accumulate at infinity.

To establish the remainder of the claim, assume first $\mathsf{P}_* < \mathsf{p}$ and $\mathsf{c}_* > \mathsf{C}$, and let $\boldsymbol{v} \in H_0^1(D)$ such that $\boldsymbol{v} \in \ker(\mathbb{L}_\tau)$. On recalling that $\boldsymbol{u} = \mathbb{M}_\tau \boldsymbol{v}$ and $\boldsymbol{u}_* = \boldsymbol{u} - \boldsymbol{v}$, one finds from (5.4.1a) and (5.4.3) that

$$\int_D (\boldsymbol{\nabla}\boldsymbol{u}_* : \boldsymbol{\Delta_C} : \boldsymbol{\nabla}\bar{\boldsymbol{u}}_* - \Delta_\rho \tau\, \boldsymbol{u}_* \cdot \bar{\boldsymbol{u}}_*)\; \mathrm{d}V \;+\; \int_D (\boldsymbol{\nabla}\boldsymbol{v} : \boldsymbol{\mathcal{C}} : \boldsymbol{\nabla}\bar{\boldsymbol{v}} - \rho\,\tau\, \boldsymbol{v} \cdot \bar{\boldsymbol{v}})\; \mathrm{d}V \;=\; 0. \qquad (5.4.20)$$

But

$$\int_D (\boldsymbol{\nabla}\boldsymbol{u}_* : \boldsymbol{\Delta_C} : \boldsymbol{\nabla}\bar{\boldsymbol{u}}_* - \Delta_\rho \tau\, \boldsymbol{u}_* \cdot \bar{\boldsymbol{u}}_*)\; \mathrm{d}V \;\geqslant\; (\mathsf{c}_* - \mathsf{C})\|\boldsymbol{\nabla}\boldsymbol{u}_*\|_{L^2(D)}^2 + (\mathsf{p} - \mathsf{P}_*)\tau\|\boldsymbol{u}_*\|_{L^2(D)}^2 \;\geqslant\; 0, \qquad (5.4.21)$$

and since $\boldsymbol{v} \in H_0^1(D)$ one has

$$\int_D (\boldsymbol{\nabla}\boldsymbol{v} : \boldsymbol{\mathcal{C}} : \boldsymbol{\nabla}\bar{\boldsymbol{v}} - \rho\,\tau\, \boldsymbol{v} \cdot \bar{\boldsymbol{v}})\; \mathrm{d}V \;\geqslant\; \|\boldsymbol{v}\|_{L^2(D)}^2\, (\lambda_1(D)\mathsf{c} - \tau\mathsf{P})\,, \qquad (5.4.22)$$

due to (5.2.1) and Courant-Fischer min-max formulae. As a result, one finds from (5.4.20)–(5.4.22) assuming $\tau < \lambda_1(D)\mathsf{c}/\mathsf{P}$ that $\|\boldsymbol{v}\|_{L^2(D)} = \|\boldsymbol{u}_*\|_{L^2(D)} = 0$ and consequently that $\boldsymbol{u} = \boldsymbol{u}_* = \boldsymbol{0}$, whereby such τ cannot be a transmission eigenvalue.

Next, assume $\mathsf{p}_* > \mathsf{P}$ and $\mathsf{C}_* < \mathsf{c}$, and let $\boldsymbol{v} \in H_0^1(D)$ such that $\boldsymbol{v} \in \ker(\mathbb{L}_\tau^*)$. By invoking the relationships $\boldsymbol{u}_* = \mathbb{M}_\tau^* \boldsymbol{v}$ and $\boldsymbol{u} = \boldsymbol{u}_* + \boldsymbol{v}$ together with (5.4.1b) and (5.4.4), one finds that

$$- \int_D (\boldsymbol{\nabla}\boldsymbol{u} : \boldsymbol{\Delta_C} : \boldsymbol{\nabla}\bar{\boldsymbol{u}} - \Delta_\rho \tau \boldsymbol{u} \cdot \bar{\boldsymbol{u}})\; \mathrm{d}V \;+\; \int_D (\boldsymbol{\nabla}\boldsymbol{v} : \boldsymbol{\mathcal{C}}_* : \boldsymbol{\nabla}\bar{\boldsymbol{v}} - \rho_*\tau \boldsymbol{v} \cdot \bar{\boldsymbol{v}})\; \mathrm{d}V = 0, \qquad (5.4.23)$$

which leads to the conclusion that $\|\boldsymbol{v}\|_{L^2(D)} = \|\boldsymbol{u}\|_{L^2(D)} = 0$ whenever $\tau < \lambda_1(D)\mathsf{c}_*/\mathsf{P}_*$. $\qquad \square$

The last step of the analysis is to demonstrate the *existence* of a countable set of (real-valued) transmission eigenvalues associated with (5.2.6) assuming that Δ_ρ and $\boldsymbol{\Delta_C}$ are both non-zero almost everywhere in D. In what follows, this is accomplished by employing the methodology proposed in Cakoni and Kirsch (2010) for scalar problems and making an *additional restriction* that the medium represented by $(\boldsymbol{\mathcal{C}}, \rho)$ is homogeneous and isotropic, i.e. that

$$\rho = \mathsf{p} \qquad \text{and} \qquad \begin{cases} \boldsymbol{\mathcal{C}} = \frac{1}{3}(\mathsf{c}-\mathsf{C})\,\boldsymbol{I} \otimes \boldsymbol{I} + \mathsf{C}\,\boldsymbol{\mathcal{I}}^{\mathrm{sym}} & \text{for} \quad \nu \in (-1, 0], \\ \boldsymbol{\mathcal{C}} = \frac{1}{3}(\mathsf{C}-\mathsf{c})\,\boldsymbol{I} \otimes \boldsymbol{I} + \mathsf{c}\,\boldsymbol{\mathcal{I}}^{\mathrm{sym}} & \text{for} \quad \nu \in [0, \frac{1}{2}), \end{cases} \qquad (5.4.24)$$

where $\otimes$ signifies the (outer) tensor product, $\boldsymbol{I}$ and $\boldsymbol{\mathcal{I}}^{\text{sym}}$ are the symmetric second- and fourth-order identity tensors respectively. In this setting one may first invoke the result of Lemma 17 and note, assuming $\mathsf{P}_* < \mathsf{p}$ and $\mathsf{c}_* > \mathsf{C}$, that the kernel of $\mathbb{L}_\tau$ coincides with that of $\mathbb{I} + (\mathbb{L}_0)^{-1/2}\mathbb{C}_\tau(\mathbb{L}_0)^{-1/2}$, $\mathbb{C}_\tau := (\mathbb{L}_\tau - \mathbb{L}_0)$ owing to the fact that operator $\mathbb{L}_0 : H_0^1(D) \to H_0^1(D)$ is positive definite (recall that $\mathbb{C}_\tau$ is compact by virtue of Lemma 18). As a result, the multiplicity of any given transmission eigenvalue is finite for τ is a transmission eigenvalue of (5.2.6) if and only if 1 is an eigenvalue of the compact self-adjoint operator $-(\mathbb{L}_0)^{-1/2}\mathbb{C}_\tau(\mathbb{L}_0)^{-1/2}$. Here it is noted that operator $\mathbb{T}_\tau := (\mathbb{L}_0)^{-1/2}\mathbb{C}_\tau(\mathbb{L}_0)^{-1/2}$, being compact and self-adjoint, is characterized by an infinite sequence of eigenvalues $\mu_j(\tau)$ accumulating at $+\infty$. Owing to the Courant-Fischer min-max principle, one can further deduce that $\mu_j(\tau)$ are continuous in τ. For completeness, it is worth mentioning that the analogous result can be established for $\mathbb{L}_\tau^*$ in situations when $\mathsf{p}_* > \mathsf{P}$ and $\mathsf{C}_* < \mathsf{c}$.

Making use of the above discussion, the proof of the existence of transmission eigenvalues is based on the following theorem established in Päivärinta and Sylvester (2008), which plays a similar role as Theorem 10 in Section 5.3.

Theorem 16. *Assume that $\mathsf{P}_* < \mathsf{p}$ and $\mathsf{c}_* > \mathsf{C}$ (resp. $\mathsf{p}_* > \mathsf{P}$ and $\mathsf{C}_* < \mathsf{c}$), and let $\tau \to \mathbb{L}_\tau$ (resp. $\tau \to \mathbb{L}_\tau^*$) be a continuous mapping from $[0, +\infty)$ to the set of linear self-adjoint operators $H_0^1(D) \to H_0^1(D)$ with property that $\mathbb{L}_0$ (resp. $\mathbb{L}_0^*$) is coercive and $\mathbb{L}_\tau - \mathbb{L}_0$ (resp. $\mathbb{L}_\tau^* - \mathbb{L}_0^*$) is compact. Provided that there are two nonnegative constants $\tau_0 \geqslant 0$ and $\tau_1 > \tau_0$ such that*

1. *$\mathbb{L}_{\tau_0}$ (resp. $\mathbb{L}_{\tau_0}^*$) is positive on $H_0^1(D)$,*

2. *$\mathbb{L}_{\tau_1}$ (resp. $\mathbb{L}_{\tau_1}^*$) is non-positive on an m-dimensional subspace of $H_0^1(D)$,*

operator $\mathbb{L}_\tau$ (resp. $\mathbb{L}_\tau^*$) possesses m transmission eigenvalues (counting multiplicity) within interval $[\tau_0, \tau_1]$, i.e. m values of τ for which $\ker(\mathbb{L}_\tau) \neq \{\mathbf{0}\}$ (resp. $\ker(\mathbb{L}_\tau^*) \neq \{\mathbf{0}\}$).

With the above result in place, the next theorem establishes the existence of an infinite set of transmission eigenvalues.

Theorem 17. *Assume that the medium represented by $(\mathcal{C}, \rho)$ is homogeneous and isotropic as in (5.4.24), and let either $\mathsf{P}_* < \mathsf{p}$ and $\mathsf{c}_* > \mathsf{C}$, or $\mathsf{p}_* > \mathsf{p}$ and $\mathsf{C}_* < \mathsf{c}$. Then there exists an infinite sequence of transmission eigenvalues $\tau_j = \omega_j^2$ associated with (5.2.6) with $+\infty$ as their only accumulation point.*

Proof. The proof is essentially the same in the two cases, and is shown here for $\mathsf{P}_* < \mathsf{p}$ and $\mathsf{c}_* > \mathsf{C}$. Without loss of generality, it is also assumed that the Poisson's ratio ν affiliated with the homogeneous background solid, see (5.4.24), is non-negative. First recall that, by virtue of Lemma 17, the first assumption of Theorem 16 is satisfied for $\tau_0 = 0$. From Theorem 15, self-adjoint operator $\mathbb{L}_{\tau_0}$ (see Lemma 18) is thus positive on $H_0^1(D)$ for all sufficiently small $\tau_0 \geqslant 0$. Next, from (5.4.17) and the fact that $\boldsymbol{u} = \boldsymbol{v} + \boldsymbol{u}_*$ one finds

$$
\begin{aligned}
\left\langle \mathbb{L}_\tau \boldsymbol{v}, \boldsymbol{v} \right\rangle_{H_0^1(D)} &= \int_D \left(\boldsymbol{\nabla} \boldsymbol{u} : \boldsymbol{\mathcal{C}} : \boldsymbol{\nabla} \bar{\boldsymbol{v}} - \rho\tau \boldsymbol{u} \cdot \bar{\boldsymbol{v}} \right) \, \mathrm{d}V \\
&= \int_D \left(\boldsymbol{\nabla} \boldsymbol{u}_* : \boldsymbol{\mathcal{C}} : \boldsymbol{\nabla} \bar{\boldsymbol{v}} - \rho\tau \boldsymbol{u}_* \cdot \bar{\boldsymbol{v}} + \boldsymbol{\nabla} \boldsymbol{v} : \boldsymbol{\mathcal{C}} : \boldsymbol{\nabla} \bar{\boldsymbol{v}} - \rho\tau \boldsymbol{v} \cdot \bar{\boldsymbol{v}} \right) \, \mathrm{d}V
\end{aligned}
\tag{5.4.25}
$$

which, combined with (5.4.4) when $\boldsymbol{\varphi} = \boldsymbol{u}_*$, yields

$$
\left\langle \mathbb{L}_\tau \boldsymbol{v}, \boldsymbol{v} \right\rangle_{H_0^1(D)} = \int_D \left(\boldsymbol{\nabla} \boldsymbol{u}_* : \boldsymbol{\Delta}_{\boldsymbol{\mathcal{C}}} : \boldsymbol{\nabla} \bar{\boldsymbol{u}}_* - \tau \Delta_\rho |\boldsymbol{u}_*|^2 + \boldsymbol{\nabla} \boldsymbol{v} : \boldsymbol{\mathcal{C}} : \boldsymbol{\nabla} \bar{\boldsymbol{v}} - \rho\tau |\boldsymbol{v}|^2 \right) \, \mathrm{d}V
\tag{5.4.26}
$$

due to major symmetry of the elastic tensor. To facilitate the application of (5.4.26), let $B_r \subset D$ be an arbitrary ball of radius r included in D, and let $\hat{\tau}$ be a transmission eigenvalue corresponding to ball B_r, see Section 5.2.2, affiliated with two sets of *constant* material properties $(\hat{\boldsymbol{\mathcal{C}}}, \hat{\rho}) := (\boldsymbol{\mathcal{C}}, \rho)$ and $(\hat{\boldsymbol{\mathcal{C}}}_*, \hat{\rho}_*) := (\mathsf{c}_* \boldsymbol{\mathcal{I}}^{\mathrm{sym}}, \mathsf{P}_*)$, where $\boldsymbol{\mathcal{C}}$ and ρ are given by (5.4.24). Recalling an earlier assumption that $\nu \geqslant 0$, such configuration in particular implies that

$$\boldsymbol{\Delta}_{\hat{\boldsymbol{\mathcal{C}}}} = \hat{\boldsymbol{\mathcal{C}}}_* - \hat{\boldsymbol{\mathcal{C}}} = \frac{1}{3}\big[(\mathsf{c}_* - \mathsf{C}) - (\mathsf{c}_* - \mathsf{c})\big] \boldsymbol{I} \otimes \boldsymbol{I} + (\mathsf{c}_* - \mathsf{c}) \boldsymbol{\mathcal{I}}^{\mathrm{sym}} \tag{5.4.27}$$

which is, in of itself, an isotropic elastic tensor whose maximum and minimum eigenvalue are given respectively by $\mathsf{c}_* - \mathsf{c} > 0$ and $\mathsf{c}_* - \mathsf{C} > 0$ (compare with the expression for $\boldsymbol{\mathcal{C}}$ in (5.4.24) for negative Poisson's ratio). Hereon, the nontrivial solutions corresponding to $\hat{\tau}$ are denoted by $\hat{\boldsymbol{u}}$ and $\hat{\boldsymbol{u}}_*$, and their difference by $\hat{\boldsymbol{v}} = \hat{\boldsymbol{u}} - \hat{\boldsymbol{u}}_*$ which is clearly in $H_0^1(B_r)$. If $\hat{\mathbb{L}}_\tau$ is the corresponding operator constructed from $\hat{\boldsymbol{v}}$ and $\hat{\boldsymbol{u}}$ by the same procedure as in Lemma 16, one has

$$0 = \big\langle \hat{\mathbb{L}}_{\hat{\tau}} \hat{\boldsymbol{v}}, \hat{\boldsymbol{v}} \big\rangle_{H_0^1(B_r)} = \int_{B_r} \big(\boldsymbol{\nabla}\hat{\boldsymbol{u}}_* : \boldsymbol{\Delta}_{\hat{\boldsymbol{\mathcal{C}}}} : \boldsymbol{\nabla}\bar{\hat{\boldsymbol{u}}}_* - \hat{\tau}\Delta_{\hat{\rho}}|\hat{\boldsymbol{u}}_*|^2 + \boldsymbol{\nabla}\hat{\boldsymbol{v}} : \boldsymbol{\mathcal{C}} : \boldsymbol{\nabla}\bar{\hat{\boldsymbol{v}}} - \rho\hat{\tau}|\hat{\boldsymbol{v}}|^2 \big) \, \mathrm{d}V.$$
$$\tag{5.4.28}$$

Next, letting $\tilde{\boldsymbol{v}} \in H_0^1(D)$ be the extension by zero of $\hat{\boldsymbol{v}} \in H_0^1(B_r)$ to the whole of D, and taking the corresponding unique solution of (5.4.3) as $\tilde{\boldsymbol{u}} := \mathbb{M}_{\hat{\tau}}\tilde{\boldsymbol{v}}$ and $\tilde{\boldsymbol{u}}_* := \tilde{\boldsymbol{u}} - \tilde{\boldsymbol{v}}$, sequential application of (5.4.4) to pairs $(\tilde{\boldsymbol{u}}_*, \tilde{\boldsymbol{v}})$ and $(\hat{\boldsymbol{u}}_*, \hat{\boldsymbol{v}})$ yields

$$\int_D \big(\boldsymbol{\nabla}\tilde{\boldsymbol{u}}_* : \boldsymbol{\Delta}_{\boldsymbol{\mathcal{C}}} : \boldsymbol{\nabla}\bar{\boldsymbol{\varphi}} - \hat{\tau}\Delta_\rho \tilde{\boldsymbol{u}}_* \cdot \bar{\boldsymbol{\varphi}} \big) \, \mathrm{d}V = \int_D \big(\boldsymbol{\nabla}\tilde{\boldsymbol{v}} : \boldsymbol{\mathcal{C}} : \boldsymbol{\nabla}\bar{\boldsymbol{\varphi}} - \rho\hat{\tau}\tilde{\boldsymbol{v}} \cdot \bar{\boldsymbol{\varphi}} \big) \, \mathrm{d}V$$

$$= \int_{B_r} \big(\boldsymbol{\nabla}\hat{\boldsymbol{v}} : \boldsymbol{\mathcal{C}} : \boldsymbol{\nabla}\bar{\boldsymbol{\varphi}} - \rho\hat{\tau}\hat{\boldsymbol{v}} \cdot \bar{\boldsymbol{\varphi}} \big) \, \mathrm{d}V = \int_{B_r} \big(\boldsymbol{\nabla}\hat{\boldsymbol{u}}_* : \boldsymbol{\Delta}_{\hat{\boldsymbol{\mathcal{C}}}} : \boldsymbol{\nabla}\bar{\boldsymbol{\varphi}} - \hat{\tau}\Delta_{\hat{\rho}}\hat{\boldsymbol{u}}_* \cdot \bar{\boldsymbol{\varphi}} \big) \, \mathrm{d}V \tag{5.4.29}$$

for all $\boldsymbol{\varphi} \in H^1(D)$. Since $\boldsymbol{\Delta}_{\hat{\boldsymbol{\mathcal{C}}}}$ is positive definite, see (5.4.27) while $\Delta_{\hat{\rho}} < 0$, the last integral in (5.4.29) is positive for $\boldsymbol{\varphi} = \tilde{\boldsymbol{u}}_*$. With the latter restriction on the trial function, one accordingly finds from (5.4.27) and (5.4.29) via the Cauchy-Schwarz inequality that

$$\int_D \big(\boldsymbol{\nabla}\tilde{\boldsymbol{u}}_* : \boldsymbol{\Delta}_{\boldsymbol{\mathcal{C}}} : \boldsymbol{\nabla}\bar{\tilde{\boldsymbol{u}}}_* - \hat{\tau}\Delta_\rho|\tilde{\boldsymbol{u}}_*|^2 \big) \, \mathrm{d}V = \int_{B_r} \big(\boldsymbol{\nabla}\hat{\boldsymbol{u}}_* : \boldsymbol{\Delta}_{\hat{\boldsymbol{\mathcal{C}}}} : \boldsymbol{\nabla}\bar{\tilde{\boldsymbol{u}}}_* - \hat{\tau}\Delta_{\hat{\rho}}\hat{\boldsymbol{u}}_* \cdot \bar{\tilde{\boldsymbol{u}}}_* \big) \, \mathrm{d}V$$

$$\leqslant \left[\int_{B_r} \big(\boldsymbol{\nabla}\hat{\boldsymbol{u}}_* : \boldsymbol{\Delta}_{\hat{\boldsymbol{\mathcal{C}}}} : \boldsymbol{\nabla}\bar{\hat{\boldsymbol{u}}}_* - \hat{\tau}\Delta_\rho|\hat{\boldsymbol{u}}_*|^2 \big) \, \mathrm{d}V \right]^{1/2} \left[\int_{B_r} \big(\boldsymbol{\nabla}\tilde{\boldsymbol{u}}_* : \boldsymbol{\Delta}_{\hat{\boldsymbol{\mathcal{C}}}} : \boldsymbol{\nabla}\bar{\tilde{\boldsymbol{u}}}_* - \hat{\tau}\Delta_{\hat{\rho}}|\tilde{\boldsymbol{u}}_*|^2 \big) \, \mathrm{d}V \right]^{1/2} \tag{5.4.30}$$

$$\leqslant \left[\int_{B_r} \big(\boldsymbol{\nabla}\hat{\boldsymbol{u}}_* : \boldsymbol{\Delta}_{\hat{\boldsymbol{\mathcal{C}}}} : \boldsymbol{\nabla}\bar{\hat{\boldsymbol{u}}}_* - \hat{\tau}\Delta_{\hat{\rho}}|\hat{\boldsymbol{u}}_*|^2 \big) \, \mathrm{d}V \right]^{1/2} \left[\int_D \big(\boldsymbol{\nabla}\tilde{\boldsymbol{u}}_* : \boldsymbol{\Delta}_{\boldsymbol{\mathcal{C}}} : \boldsymbol{\nabla}\bar{\tilde{\boldsymbol{u}}}_* - \hat{\tau}\Delta_\rho|\tilde{\boldsymbol{u}}_*|^2 \big) \, \mathrm{d}V \right]^{1/2}$$

since $\boldsymbol{\xi} : \boldsymbol{\Delta}_{\hat{\boldsymbol{\mathcal{C}}}} : \bar{\boldsymbol{\xi}} = \boldsymbol{\xi} : (\hat{\boldsymbol{\mathcal{C}}}_* - \hat{\boldsymbol{\mathcal{C}}}) : \bar{\boldsymbol{\xi}} \leqslant \boldsymbol{\xi} : (\boldsymbol{\mathcal{C}}_* - \boldsymbol{\mathcal{C}}) : \bar{\boldsymbol{\xi}} = \boldsymbol{\xi} : \boldsymbol{\Delta}_{\boldsymbol{\mathcal{C}}} : \bar{\boldsymbol{\xi}}$ and $-\Delta_{\hat{\rho}} = \rho - \mathsf{P}_* \leqslant \rho - \rho_* = -\Delta_\rho$. As a result, one has

$$\int_D \big(\boldsymbol{\nabla}\tilde{\boldsymbol{u}}_* : \boldsymbol{\Delta}_{\boldsymbol{\mathcal{C}}} : \boldsymbol{\nabla}\bar{\tilde{\boldsymbol{u}}}_* - \hat{\tau}\Delta_\rho|\tilde{\boldsymbol{u}}_*|^2 \big) \, \mathrm{d}V \leqslant \int_{B_r} \big(\boldsymbol{\nabla}\hat{\boldsymbol{u}}_* : \boldsymbol{\Delta}_{\hat{\boldsymbol{\mathcal{C}}}} : \boldsymbol{\nabla}\bar{\hat{\boldsymbol{u}}}_* - \hat{\tau}\Delta_{\hat{\rho}}|\hat{\boldsymbol{u}}_*|^2 \big) \, \mathrm{d}V.$$

A substitution of this result into (5.4.26) with $\tau = \hat{\tau}$ and $\boldsymbol{v} = \tilde{\boldsymbol{v}}$, followed by the use of (5.4.28), yields

$$\big\langle \mathbb{L}_{\hat{\tau}}\tilde{\boldsymbol{v}}, \tilde{\boldsymbol{v}} \big\rangle_{H_0^1(D)} = \int_D \big(\boldsymbol{\nabla}\tilde{\boldsymbol{u}}_* : \boldsymbol{\Delta}_{\boldsymbol{\mathcal{C}}} : \boldsymbol{\nabla}\bar{\tilde{\boldsymbol{u}}}_* - \hat{\tau}\Delta_\rho|\tilde{\boldsymbol{u}}_*|^2 + \boldsymbol{\nabla}\tilde{\boldsymbol{v}} : \boldsymbol{\mathcal{C}} : \boldsymbol{\nabla}\bar{\tilde{\boldsymbol{v}}} - \rho\hat{\tau}|\tilde{\boldsymbol{v}}|^2 \big) \, \mathrm{d}V$$

$$\leqslant \int_{B_r} \big(\boldsymbol{\nabla}\hat{\boldsymbol{u}}_* : \boldsymbol{\Delta}_{\hat{\boldsymbol{\mathcal{C}}}} : \boldsymbol{\nabla}\bar{\tilde{\boldsymbol{u}}}_* - \hat{\tau}\Delta_{\hat{\rho}}|\hat{\boldsymbol{u}}_*|^2 + \boldsymbol{\nabla}\hat{\boldsymbol{v}} : \boldsymbol{\mathcal{C}} : \boldsymbol{\nabla}\bar{\hat{\boldsymbol{v}}} - \rho\hat{\tau}|\hat{\boldsymbol{v}}|^2 \big) \, \mathrm{d}V = 0.$$

By making reference to Theorem 16, one concludes that there exists at least one transmission eigenvalue within interval $(0, \hat{\tau}]$. Finally, by arguing in exactly the same way as in the last part of the proof of Theorem 12, it is possible to demonstrate that in fact there exists a countable set of transmission eigenvalues affiliated with (5.2.6). $\qquad\square$

Remark 15. *As a consequence of the proof of Theorem, 17 one obtains an upper bound for the first transmission eigenvalue ω_1. More specifically, consider $B_r \subset D$ as the largest ball contained in D. If $\mathsf{P}_* < \mathsf{p}$ and $\mathsf{c}_* > \mathsf{C}$, then the first eigenvalue associated with (5.2.6) is not larger than the first transmission eigenvalue corresponding to B_r endowed with a pair of constant material properties $(\hat{\mathcal{C}}, \hat{\rho}) := (\mathcal{C}, \rho)$ and $(\hat{\mathcal{C}}_*, \hat{\rho}_*) := (\mathsf{c}_* \mathcal{I}^{sym}, \mathsf{P}_*)$, where $\mathcal{C}$ and ρ are given by (5.4.24). Conversely if $\mathsf{p}_* > \mathsf{p}$ and $\mathsf{C}_* < \mathsf{c}$, then the first eigenvalue affiliated with (5.2.6) is not larger than the first transmission eigenvalue corresponding to B_r endowed with $(\hat{\mathcal{C}}, \hat{\rho}) := (\mathcal{C}, \rho)$ and $(\hat{\mathcal{C}}_*, \hat{\rho}_*) := (\mathsf{C}_* \mathcal{I}^{sym}, \mathsf{p}_*)$.*

5.4.2 Elasticity and mass density contrasts of the same sign

The methodology proposed in Hähner (2000); Cakoni et al. (2002), together with its extensions to the elasticity case (Charalambopoulos, 2002; Bellis and Guzina, 2010), allow one to deal with situations where (5.2.6) involves contrasts in material parameters that are of the same sign, namely when either $\mathsf{p}_* > \mathsf{P}$ and $\mathsf{c}_* > \mathsf{C}$, or $\mathsf{p} > \mathsf{P}_*$ and $\mathsf{c} > \mathsf{C}_*$. To facilitate the discussion, one may introduce the space of first-order tensors

$$\mathscr{H}(D) := \{(\boldsymbol{\varphi}, \boldsymbol{\varphi}_*) \in H^1(D) \times H^1(D) : \boldsymbol{\nabla}\cdot[\mathcal{C}:\boldsymbol{\nabla}\boldsymbol{\varphi}] \in L^2(D), \ \boldsymbol{\nabla}\cdot[\mathcal{C}_*:\boldsymbol{\nabla}\boldsymbol{\varphi}_*] \in L^2(D)\}, \quad (5.4.31)$$

together with the pair of (linear) differential-trace operators $\mathbb{P}, \mathbb{Q} : \mathscr{H}(D) \to L^2(D) \times L^2(D) \times H^{\frac{1}{2}}(\partial D) \times H^{-\frac{1}{2}}(\partial D)$ defined by

$$\mathbb{P}(\boldsymbol{\varphi}, \boldsymbol{\varphi}_*) := \left(\boldsymbol{\nabla}\cdot[\mathcal{C}:\boldsymbol{\nabla}\boldsymbol{\varphi}] - \rho\boldsymbol{\varphi}, \ \boldsymbol{\nabla}\cdot[\mathcal{C}_*:\boldsymbol{\nabla}\boldsymbol{\varphi}_*] - \rho_*\boldsymbol{\varphi}_*, \ (\boldsymbol{\varphi} - \boldsymbol{\varphi}_*)_{|\partial D}, \ \boldsymbol{n}\cdot(\mathcal{C}:\boldsymbol{\nabla}\boldsymbol{\varphi} - \mathcal{C}_*:\boldsymbol{\nabla}\boldsymbol{\varphi}_*)_{|\partial D}\right),$$
$$\mathbb{Q}(\boldsymbol{\varphi}, \boldsymbol{\varphi}_*) := (\rho\boldsymbol{\varphi}, \ \rho_*\boldsymbol{\varphi}_*, \ \boldsymbol{0}, \ \boldsymbol{0}).$$
$$(5.4.32)$$

for all $(\boldsymbol{\varphi}, \boldsymbol{\varphi}_*) \in \mathscr{H}(D)$. On the basis of (5.4.31) and (5.4.32), the interior transmission problem (5.2.6) can be recast as a task of finding $(\boldsymbol{u}, \boldsymbol{u}_*) \in \mathscr{H}(D)$ such that

$$\mathbb{P}(\boldsymbol{u}, \boldsymbol{u}_*) + (1+\tau)\mathbb{Q}(\boldsymbol{u}, \boldsymbol{u}_*) = \boldsymbol{0}. \quad (5.4.33)$$

Next, it is useful to define the auxiliary spaces of symmetric second-order tensors

$$\begin{aligned}
\mathscr{W}(D) &:= \{\boldsymbol{\Phi} \in L^2(D) : \boldsymbol{\Phi} = \boldsymbol{\Phi}^{\mathrm{T}}, \ \boldsymbol{\nabla}\cdot\boldsymbol{\Phi} \in L^2(D), \ \boldsymbol{\nabla}\times[\mathcal{C}^{-1}:\boldsymbol{\Phi}] = \boldsymbol{0}\}, \\
\mathscr{W}_*(D) &:= \{\boldsymbol{\Phi}_* \in L^2(D) : \boldsymbol{\Phi}_* = \boldsymbol{\Phi}_*^{\mathrm{T}}, \boldsymbol{\nabla}\cdot\boldsymbol{\Phi}_* \in L^2(D), \ \boldsymbol{\nabla}\times[\mathcal{C}_*^{-1}:\boldsymbol{\Phi}_*] = \boldsymbol{0}\},
\end{aligned} \quad (5.4.34)$$

and introduce a bounded bilinear form, $\mathcal{R}$, on $\mathscr{K}(D) := \mathscr{W}(D) \times H^1(D)$ so that

$$\begin{aligned}
\mathcal{R}\big((\boldsymbol{\Phi}, \boldsymbol{\varphi}_*), (\boldsymbol{\Psi}, \boldsymbol{\psi}_*)\big) &:= \big\langle \rho^{-1}\boldsymbol{\nabla}\cdot\boldsymbol{\Phi}, \boldsymbol{\nabla}\cdot\boldsymbol{\Psi}\big\rangle_{L^2(D)} + \big\langle \mathcal{C}^{-1}:\boldsymbol{\Phi}, \boldsymbol{\Psi}\big\rangle_{L^2(D)} + \big\langle \mathcal{C}_*:\boldsymbol{\nabla}\boldsymbol{\varphi}_*, \boldsymbol{\nabla}\boldsymbol{\psi}_*\big\rangle_{L^2(D)} \\
&\quad + \big\langle \rho_*\boldsymbol{\varphi}_*, \boldsymbol{\psi}_*\big\rangle_{L^2(D)} - \big\langle \boldsymbol{\varphi}_*, \boldsymbol{\Psi}\cdot\boldsymbol{n}\big\rangle_{L^2(\partial D)} - \big\langle \boldsymbol{\Phi}\cdot\boldsymbol{n}, \boldsymbol{\psi}_*\big\rangle_{L^2(\partial D)},
\end{aligned}$$
$$(5.4.35)$$

for all $(\boldsymbol{\Phi}, \boldsymbol{\varphi}_*)$ and $(\boldsymbol{\Psi}, \boldsymbol{\psi}_*)$ in $\mathscr{K}(D)$, together with its companion on $\mathscr{K}_*(D) := H^1(D) \times \mathscr{W}_*(D)$, given by

$$\mathcal{R}_*\big((\boldsymbol{\varphi}, \boldsymbol{\Phi}_*), (\boldsymbol{\psi}, \boldsymbol{\Psi}_*)\big) := \big\langle \rho_*^{-1} \boldsymbol{\nabla} \cdot \boldsymbol{\Phi}_*, \boldsymbol{\nabla} \cdot \boldsymbol{\Psi}_* \big\rangle_{L^2(D)} + \big\langle \mathcal{C}_*^{-1} : \boldsymbol{\Phi}_*, \boldsymbol{\Psi}_* \big\rangle_{L^2(D)} + \big\langle \mathcal{C} : \boldsymbol{\nabla} \boldsymbol{\varphi}, \boldsymbol{\nabla} \boldsymbol{\psi} \big\rangle_{L^2(D)}$$
$$+ \big\langle \rho \boldsymbol{\varphi}, \boldsymbol{\psi} \big\rangle_{L^2(D)} - \big\langle \boldsymbol{\varphi}, \boldsymbol{\Psi}_* \cdot \boldsymbol{n} \big\rangle_{L^2(\partial D)} - \big\langle \boldsymbol{\Phi}_* \cdot \boldsymbol{n}, \boldsymbol{\psi} \big\rangle_{L^2(\partial D)},$$
$$(5.4.36)$$

for all $(\boldsymbol{\varphi}, \boldsymbol{\Phi}_*)$ and $(\boldsymbol{\psi}, \boldsymbol{\Psi}_*)$ in $\mathscr{K}_*(D)$. With reference to (5.4.35) and (5.4.36), the Riesz representation theorem guarantees the existence of a linear operator $\mathbb{R} : \mathscr{K}(D) \to \mathscr{K}(D)$ such that

$$\big\langle \mathbb{R}(\boldsymbol{\Phi}, \boldsymbol{\varphi}_*), (\boldsymbol{\Psi}, \boldsymbol{\psi}_*) \big\rangle_{\mathscr{K}(D)} = \mathcal{R}\big((\boldsymbol{\Phi}, \boldsymbol{\varphi}_*), (\boldsymbol{\Psi}, \boldsymbol{\psi}_*)\big), \tag{5.4.37}$$

for all $(\boldsymbol{\Phi}, \boldsymbol{\varphi}_*)$ and $(\boldsymbol{\Psi}, \boldsymbol{\psi}_*)$ in $\mathscr{K}(D)$, and linear operator $\mathbb{R}_* : \mathscr{K}_*(D) \to \mathscr{K}_*(D)$ satisfying

$$\big\langle \mathbb{R}_*(\boldsymbol{\varphi}, \boldsymbol{\Phi}_*), (\boldsymbol{\psi}, \boldsymbol{\Psi}_*) \big\rangle_{\mathscr{K}_*(D)} = \mathcal{R}_*\big((\boldsymbol{\varphi}, \boldsymbol{\Phi}_*), (\boldsymbol{\psi}, \boldsymbol{\Psi}_*)\big), \tag{5.4.38}$$

for all $(\boldsymbol{\varphi}, \boldsymbol{\Phi}_*)$ and $(\boldsymbol{\psi}, \boldsymbol{\Psi}_*)$ in $\mathscr{K}_*(D)$.

With the above notation in place, one is in position to state the key results from Bellis and Guzina (2010) that are essential for the treatment of the problem at hand.

Lemma 19. *Operator $\mathbb{P}$ is bijective if and only if operators $\mathbb{R}$ and $\mathbb{R}_*$ are bijective.*

Lemma 20. *Operator $\mathbb{R} : \mathscr{K}(D) \to \mathscr{K}(D)$ (resp. $\mathbb{R}_* : \mathscr{K}_*(D) \to \mathscr{K}_*(D)$) is self-adjoint and positive definite if $\mathsf{P} < \mathsf{p}_*$ and $\mathsf{C} < \mathsf{c}_*$ (resp. $\mathsf{P}_* < \mathsf{p}$ and $\mathsf{C}_* < \mathsf{c}$). Further, linear operator $\mathbb{Q} : \mathscr{H}(D) \to L^2(D) \times L^2(D) \times H^{\frac{1}{2}}(\partial D) \times H^{-\frac{1}{2}}(\partial D)$ is self-adjoint, positive and compact.*

To establish a lower bound for the transmission eigenvalues of (5.2.6) under the featured restriction on material contrasts, one may introduce the Sobolev space of weighted zero-mean functions as

$$\tilde{H}^1(D) := \left\{ \boldsymbol{\varphi} \in H^1(D) : \int_D \Delta_\rho \boldsymbol{\varphi} \, \mathrm{d}V = \boldsymbol{0} \right\}. \tag{5.4.39}$$

For further reference, it is also recalled that the negative Laplace operator, $-\Delta$, admits an increasing sequence of positive Neumann eigenvalues $\mu_n(D)$ and associated (first-order) eigentensors $\boldsymbol{\psi}_n$ (Henrot, 2006) satisfying

$$\begin{aligned} -\Delta \boldsymbol{\psi}_n &= \mu_n(D) \boldsymbol{\psi}_n && \text{in } D, \\ \boldsymbol{\nabla} \boldsymbol{\psi}_n \cdot \boldsymbol{n} &= \boldsymbol{0} && \text{on } \partial D. \end{aligned} \tag{5.4.40}$$

Due to the fact that the first eigenvalue in (5.4.40) is $\mu_1 = 0$, μ_2 denotes the smallest non-zero Neumann eigenvalue of the negative Laplace operator.

Theorem 18. *If either $\mathsf{P} < \mathsf{p}_*$ and $\mathsf{C} < \mathsf{c}_*$ or $\mathsf{P}_* < \mathsf{p}$ and $\mathsf{C}_* < \mathsf{c}$, the set of transmission eigenvalues associated with (5.2.6) is discrete, with infinity being the only possible accumulation point. Moreover, every feasible transmission eigenvalue ω^2 is such that*

$$\omega^2 \geqslant \min\left[\lambda_1(D) \min(\mathsf{c}, \mathsf{c}_*) \left(\frac{1}{\min(\mathsf{P}, \mathsf{P}_*)} - \frac{1}{\max(\mathsf{p}, \mathsf{p}_*)} \right), \ \mu_2(D) \frac{\max(\mathsf{c}, \mathsf{c}_*) - \min(\mathsf{C}, \mathsf{C}_*)}{\max(\mathsf{P}, \mathsf{P}_*) - \min(\mathsf{p}, \mathsf{p}_*)} \right].$$
$$(5.4.41)$$

Proof. The first part of the theorem is a direct consequence of Lemmas 19 and 20. Under the hypothesis that either $\mathbb{R}$ or $\mathbb{R}_*$ is positive definite (which is ensured by the featured restriction on material contrasts), the use of the Lax-Milgram theorem demonstrates that $\mathbb{P}$ is invertible (Bellis and Guzina, 2010). In light of the "operator" formulation (5.4.33) of the interior transmission problem (5.2.6), on the other hand, the Fredholm alternative applied to compact operator $\mathbb{I} + (1 + \tau)\mathbb{P}^{-1}\mathbb{Q}$ (where $\mathbb{I}$ is the relevant identity operator) affirms the claim regarding the nature of the set of transmission eigenvalues.

To establish the lower bound (5.4.41) on the transmission eigenvalues, assume first that $\mathsf{P}_* < \mathsf{p}$ and $\mathsf{C}_* < \mathsf{c}$. The combination of (5.4.1b) and (5.4.4) then yields

$$\int_D (\boldsymbol{\nabla u} : \boldsymbol{\Delta_\mathcal{C}} : \boldsymbol{\nabla \bar u} - \Delta_\rho \tau \boldsymbol{u} \cdot \boldsymbol{\bar u}) \ \mathrm{d}V \ = \ \int_D (\boldsymbol{\nabla v} : \boldsymbol{\mathcal{C}_*} : \boldsymbol{\nabla \bar v} - \rho_* \tau \boldsymbol{v} \cdot \boldsymbol{\bar v}) \ \mathrm{d}V, \qquad (5.4.42)$$

see also (5.4.23). If $\boldsymbol{u}$ is next decomposed as $\boldsymbol{u} = \tilde{\boldsymbol{u}} + \boldsymbol{c}$ where $\tilde{\boldsymbol{u}} \in \tilde{H}^1(D)$ and $\boldsymbol{c}$ is a complex-valued vector constant, then taking $\boldsymbol{\varphi} = \mathbf{1}$ in (5.4.3) shows that

$$\boldsymbol{c} \ = \ \frac{\displaystyle\int_D \rho_* \boldsymbol{v} \ \mathrm{d}V}{\displaystyle\int_D \Delta_\rho \ \mathrm{d}V}, \qquad (5.4.43)$$

which reduces (5.4.42) to

$$\int_D (\boldsymbol{\nabla \tilde u} : \boldsymbol{\Delta_\mathcal{C}} : \boldsymbol{\nabla \bar{\tilde u}} - \Delta_\rho \tau \tilde{\boldsymbol{u}} \cdot \bar{\tilde{\boldsymbol{u}}}) \ \mathrm{d}V \ = \ \int_D (\boldsymbol{\nabla v} : \boldsymbol{\mathcal{C}_*} : \boldsymbol{\nabla \bar v} - \rho_* \tau \boldsymbol{v} \cdot \boldsymbol{\bar v}) \ \mathrm{d}V \ + \ \tau |\boldsymbol{c}|^2 \int_D \Delta_\rho \ \mathrm{d}V. \qquad (5.4.44)$$

Here the application of relationship $\boldsymbol{u} = \tilde{\boldsymbol{u}} + \boldsymbol{c}$ and Courant-Fischer min-max formulae (Henrot, 2006) yield

$$\inf_{\tilde{\boldsymbol{u}} \in \tilde{H}^1(D)} \frac{\displaystyle\int_D |\boldsymbol{\nabla \tilde u}|^2 \ \mathrm{d}V}{\displaystyle\int_D |\tilde{\boldsymbol{u}}|^2 \ \mathrm{d}V} \ \geqslant \ \inf_{\substack{\boldsymbol{u} \in H^1(D) \\ \int_D \boldsymbol{u} \, \mathrm{d}V = \mathbf{0}}} \frac{\displaystyle\int_D |\boldsymbol{\nabla u}|^2 \ \mathrm{d}V}{\displaystyle\int_D |\boldsymbol{u}|^2 \ \mathrm{d}V} \ \geqslant \ \mu_2(D), \qquad (5.4.45)$$

while (5.2.1) requires that $\sup_D \Delta_\rho = \mathsf{P}_* - \mathsf{p} < 0$ and $\sup_D \sup_{\boldsymbol{\xi}} \boldsymbol{\xi} : \boldsymbol{\Delta_\mathcal{C}} : \bar{\boldsymbol{\xi}} = (\mathsf{C}_* - \mathsf{c})|\boldsymbol{\xi}|^2 \leqslant 0$ for all complex-valued vectors $\boldsymbol{\xi}$. As a result, the left-hand side of (5.4.44) can be shown to be bounded from above as

$$\int_D (\boldsymbol{\nabla \tilde u} : \boldsymbol{\Delta_\mathcal{C}} : \boldsymbol{\nabla \bar{\tilde u}} - \Delta_\rho \tau \tilde{\boldsymbol{u}} \cdot \bar{\tilde{\boldsymbol{u}}}) \ \mathrm{d}V \ \leqslant \ \left((\mathsf{C}_* - \mathsf{c})\mu_2(D) - \tau(\mathsf{p}_* - \mathsf{P})\right) \|\tilde{\boldsymbol{u}}\|^2_{L^2(D)}. \qquad (5.4.46)$$

On recalling that $\boldsymbol{v} \in H^1_0(D)$, a similar treatment of the right-hand side yields

$$\int_D (\boldsymbol{\nabla v} : \boldsymbol{\mathcal{C}_*} : \boldsymbol{\nabla \bar v} - \rho_* \tau \boldsymbol{v} \cdot \boldsymbol{\bar v}) \ \mathrm{d}V \ + \ \tau |\boldsymbol{c}|^2 \int_D \Delta_\rho \ \mathrm{d}V \ \geqslant \ \left(\mathsf{c}_* \lambda_1(D) + \tau \frac{\mathsf{p}\mathsf{P}_*}{\mathsf{P}_* - \mathsf{p}}\right) \|\boldsymbol{v}\|^2_{L^2(D)}. \quad (5.4.47)$$

Thus, if $\tau = \omega^2$ satisfies

$$\tau \ < \ \mu_2(D) \frac{\mathsf{c} - \mathsf{C}_*}{\mathsf{P} - \mathsf{p}_*} \qquad \text{and} \qquad \tau \ < \ \mathsf{c}_* \lambda_1(D) \left(\frac{1}{\mathsf{P}_*} - \frac{1}{\mathsf{p}}\right), \qquad (5.4.48)$$

inequalities (5.4.46) and (5.4.47) together with (5.4.44) require that $\tilde{\boldsymbol{u}} = \boldsymbol{v} = \mathbf{0}$ and consequently $\boldsymbol{u} = \boldsymbol{u}_* = \mathbf{0}$, whereby such τ cannot be a transmission eigenvalue.

Alternatively when $P < p_*$ and $C < c_*$, the use of (5.4.1a) and (5.4.3) demonstrates that

$$-\int_D \left(\boldsymbol{\nabla}\boldsymbol{u}_* : \boldsymbol{\Delta}_{\mathcal{C}} : \boldsymbol{\nabla}\bar{\boldsymbol{u}}_* - \Delta_\rho \tau \boldsymbol{u}_* \cdot \bar{\boldsymbol{u}}_*\right) \, \mathrm{d}V \;=\; \int_D \left(\boldsymbol{\nabla}\boldsymbol{v} : \mathcal{C} : \boldsymbol{\nabla}\bar{\boldsymbol{v}} - \rho\tau\boldsymbol{v}\cdot\bar{\boldsymbol{v}}\right) \, \mathrm{d}V, \qquad (5.4.49)$$

see also (5.4.20). In this setting $\boldsymbol{u}_*$ can be decomposed in $\boldsymbol{u}_* = \tilde{\boldsymbol{u}}_* + \boldsymbol{c}_*$, where $\tilde{\boldsymbol{u}}_* \in \tilde{H}^1(D)$ and $\boldsymbol{c}_*$ is a complex-valued vector constant. Then (5.4.4) provides the value of the constant as

$$\boldsymbol{c}_* \;=\; \frac{\displaystyle\int_D \rho\boldsymbol{v} \, \mathrm{d}V}{\displaystyle\int_D \Delta_\rho \, \mathrm{d}V}, \qquad (5.4.50)$$

which permits (5.4.49) to be rewritten as

$$-\int_D \left(\boldsymbol{\nabla}\tilde{\boldsymbol{u}}_* : \boldsymbol{\Delta}_{\mathcal{C}} : \boldsymbol{\nabla}\bar{\tilde{\boldsymbol{u}}}_* - \Delta_\rho\tau\tilde{\boldsymbol{u}}_*\cdot\bar{\tilde{\boldsymbol{u}}}_*\right) \, \mathrm{d}V \;=\; \int_D \left(\boldsymbol{\nabla}\boldsymbol{v} : \mathcal{C} : \boldsymbol{\nabla}\bar{\boldsymbol{v}} - \rho\tau\boldsymbol{v}\cdot\bar{\boldsymbol{v}}\right) \, \mathrm{d}V \;-\; \tau|\boldsymbol{c}_*|^2\int_D \Delta_\rho \, \mathrm{d}V.$$
$$(5.4.51)$$

Since in this case $\inf_D \Delta_\rho = p_* - P > 0$ and $\inf_D \inf_{\boldsymbol{\xi}} \boldsymbol{\xi} : \boldsymbol{\Delta}_{\mathcal{C}} : \bar{\boldsymbol{\xi}} = (c_* - C)|\boldsymbol{\xi}|^2 \geqslant 0$ for all complex-valued vectors $\boldsymbol{\xi}$, one can show that the left and the right-hand side of (5.4.51) are bounded respectively as

$$-\int_D \left(\boldsymbol{\nabla}\tilde{\boldsymbol{u}}_* : \boldsymbol{\Delta}_{\mathcal{C}} : \boldsymbol{\nabla}\bar{\tilde{\boldsymbol{u}}}_* - \Delta_\rho\tau\tilde{\boldsymbol{u}}_*\cdot\bar{\tilde{\boldsymbol{u}}}_*\right) \, \mathrm{d}V \;\leqslant\; \left(-\mu_2(D)(c_* - C) + \tau(P_* - p)\right)\|\tilde{\boldsymbol{u}}_*\|^2_{L^2(D)}, \quad (5.4.52)$$

and

$$\int_D \left(\boldsymbol{\nabla}\boldsymbol{v} : \mathcal{C} : \boldsymbol{\nabla}\bar{\boldsymbol{v}} - \rho\tau\boldsymbol{v}\cdot\bar{\boldsymbol{v}}\right) \, \mathrm{d}V - \tau|\boldsymbol{c}_*|^2\int_D \Delta_\rho \, \mathrm{d}V \;\geqslant\; \left(c\lambda_1(D) - \tau\frac{p_* P}{p_* - P}\right)\|\boldsymbol{v}\|^2_{L^2(D)}. \quad (5.4.53)$$

As a result, when τ is such that

$$\tau \;<\; \mu_2(D)\frac{c_* - C}{P_* - p} \qquad \text{and} \qquad \tau \;<\; c\lambda_1(D)\left(\frac{1}{P} - \frac{1}{p_*}\right), \qquad (5.4.54)$$

substitution of (5.4.52) and (5.4.53) into (5.4.51) guarantees that $\tilde{\boldsymbol{u}}_* = \boldsymbol{v} = \boldsymbol{0}$ and consequently $\boldsymbol{u}_* = \boldsymbol{u} = \boldsymbol{0}$, whereby such τ cannot be a transmission eigenvalue. Finally, the combination of conditions (5.4.48) and (5.4.54) recovers (5.4.41) and thus completes the proof. $\qquad\square$

To establish the existence of the transmission eigenvalues in situations where the elasticity and mass density contrasts of the same sign, it is possible to adapt the methodology developed in Section 5.4.1. To this end, it is again assumed that the background medium is *homogeneous and isotropic*, whereby $\mathcal{C}$ and ρ are given by (5.4.24). For brevity, the ensuing discussion assumes that $P < p_*$ and $C < c_*$, noting that the case when $P_* < p$ and $C_* < c$ can be handled in exactly the same way. To avoid repetition, the focus is made on the differences between the current treatment and that in Section 5.4.1.

The main difficulty in dealing with the problem at hand resides in solving (5.4.3), i.e. finding $\boldsymbol{u} \in H^1(D)$ such that

$$\mathcal{M}_\tau(\boldsymbol{u}, \boldsymbol{\varphi}) \;=\; \mathcal{N}_{\tau,\boldsymbol{v}}(\boldsymbol{\varphi}) \quad \forall\boldsymbol{\varphi} \in H^1(D),$$

for given $\boldsymbol{v} \in H^1_0(D)$, due to general lack of coercivity of the bilinear form $\mathcal{M}_\tau(\boldsymbol{\varphi}, \boldsymbol{\psi})$ given by (5.4.5). To deal with the impediment, let $B_r \subset D$ be a ball of radius r contained in D, and let $\hat{\tau}$ be the

first transmission eigenvalue corresponding to B_r endowed with two sets of constant material properties $(\hat{\mathcal{C}}, \hat{\rho}) := (\frac{1}{2}\mathcal{C}, \rho)$ and $(\hat{\mathcal{C}}_*, \hat{\rho}_*) := (\frac{1}{2}c_*\mathcal{I}^{\mathrm{sym}}, \mathsf{P}_*)$, where $\mathcal{C}$ and ρ are given by (5.4.24). In this setting, it is further required that

$$(\mathsf{P}_* - \mathsf{p}) \; < \; \frac{\mu}{2\hat{\tau}}(\mathsf{c}_* - \mathsf{C}), \tag{5.4.55}$$

where μ is the unique minimizer defined via (5.4.9). With reference to the analytical framework developed in Lemma 16, for $\varphi \in \tilde{H}^1(D)$ and $\tau \in \{z \in \mathbb{C}\colon \Re(z) \leqslant \hat{\tau}\}$ one now has

$$\begin{aligned}
\Re\left(\mathcal{M}_\tau(\varphi, \varphi)\right) \;&=\; \Re\left(\langle \boldsymbol{\Delta}_{\mathcal{C}} : \boldsymbol{\nabla}\varphi, \boldsymbol{\nabla}\varphi \rangle_{L^2(D)} \;-\; \tau\langle \Delta_\rho\varphi, \varphi \rangle_{L^2(D)}\right) \\
&\geqslant\; (\mathsf{c}_* - \mathsf{C})\|\boldsymbol{\nabla}\varphi\|^2_{L^2(D)} \;-\; \hat{\tau}\,(\mathsf{P}_* - \mathsf{p})\|\varphi\|^2_{L^2(D)} \\
&\geqslant\; (\mathsf{c}_* - \mathsf{C})\|\boldsymbol{\nabla}\varphi\|^2_{L^2(D)} \;-\; \frac{\hat{\tau}}{\mu}\,(\mathsf{P}_* - \mathsf{p})\|\boldsymbol{\nabla}\varphi\|^2_{L^2(D)} \\
&\geqslant\; \left[(\mathsf{c}_* - \mathsf{C}) - \frac{\hat{\tau}}{\mu}\,(\mathsf{P}_* - \mathsf{p})\right]\|\boldsymbol{\nabla}\varphi\|^2_{L^2(D)} \;\geqslant\; \frac{(\mathsf{c}_* - \mathsf{C})}{2}\frac{\mu}{\mu + 1}\|\varphi\|^2_{H^1(D)},
\end{aligned}$$

which ensures the coercivity of $\mathcal{M}_\tau$ in $\tilde{H}^1(D)$ under the featured set of of restrictions. Following the proof of Lemma 16, one can consequently construct a linear operator $\mathbb{M}_\tau\colon H_0^1(D) \to H^1(D)$ such that $\mathbb{M}_\tau \boldsymbol{v} = \boldsymbol{u}$. This construction leads to the definition of operator $\mathbb{L}_\tau\colon H_0^1(D) \to H_0^1(D)$ as

$$\langle \mathbb{L}_\tau \boldsymbol{v}, \varphi \rangle_{H_0^1(D)} \;=\; \int_D (\boldsymbol{\nabla}\boldsymbol{u} : \mathcal{C} : \boldsymbol{\nabla}\bar{\varphi} - \rho\tau\boldsymbol{u}\cdot\bar{\varphi}) \; \mathrm{d}V,$$

where $\boldsymbol{u} = \mathbb{M}_\tau\boldsymbol{v}$. By mimicking the proofs of Lemma 17 and Lemma 18, one can next show that $\mathbb{L}_0$ is coercive, that $\mathbb{L}_\tau$ is self-adjoint, and that $\mathbb{L}_\tau - \mathbb{L}_0$ is compact. On recalling the first transmission eigenvalue $\hat{\tau}$ for ball $B_r \subset D$ described earlier and denoting the corresponding nonzero solutions as $\hat{\boldsymbol{u}}$ and $\hat{\boldsymbol{u}}^*$ so that $\hat{\boldsymbol{v}} = \hat{\boldsymbol{u}} - \hat{\boldsymbol{u}}^* \in H_0^1(B_r)$, it follows that (5.4.28) also holds for $\hat{\mathbb{L}}_{\hat{\tau}}$ in the present case. Further, if $\tilde{\boldsymbol{v}} \in H_0^1(D)$ is the extension by zero of $\hat{\boldsymbol{v}} \in H_0^1(B_r)$ to the whole of D, one finds by taking $\tilde{\boldsymbol{u}} := \mathbb{M}_{\hat{\tau}}\tilde{\boldsymbol{v}}$ and $\tilde{\boldsymbol{u}}_* := \tilde{\boldsymbol{u}} - \tilde{\boldsymbol{v}}$, and performing similar calculations as in (5.4.29) and (5.4.30) that

$$\begin{aligned}
\int_D \left(\boldsymbol{\nabla}\tilde{\boldsymbol{u}}_* : \boldsymbol{\Delta}_{\mathcal{C}} : \boldsymbol{\nabla}\bar{\tilde{\boldsymbol{u}}}_* - \hat{\tau}\Delta_\rho|\tilde{\boldsymbol{u}}_*|^2\right) \; \mathrm{d}V \;&\leqslant\; \int_D \left(\boldsymbol{\nabla}\tilde{\boldsymbol{u}}_* : \boldsymbol{\Delta}_{\mathcal{C}} : \boldsymbol{\nabla}\bar{\tilde{\boldsymbol{u}}}_*\right) \; \mathrm{d}V \\
= \int_D \left(\boldsymbol{\nabla}\tilde{\boldsymbol{v}} : \mathcal{C} : \boldsymbol{\nabla}\bar{\tilde{\boldsymbol{u}}}_*\right) \; \mathrm{d}V \;=\; \int_{B_r}\left(\boldsymbol{\nabla}\hat{\boldsymbol{v}} : \mathcal{C} : \boldsymbol{\nabla}\bar{\tilde{\boldsymbol{u}}}_*\right) \; \mathrm{d}V \;&=\; \int_{B_r}\left(\boldsymbol{\nabla}\hat{\boldsymbol{u}}_* : \boldsymbol{\Delta}_{\hat{\mathcal{C}}} : \boldsymbol{\nabla}\bar{\tilde{\boldsymbol{u}}}_*\right) \; \mathrm{d}V \\
\leqslant \left[\int_{B_r}\left(\boldsymbol{\nabla}\hat{\boldsymbol{u}}_* : \boldsymbol{\Delta}_{\hat{\mathcal{C}}} : \boldsymbol{\nabla}\bar{\hat{\boldsymbol{u}}}_*\right) \; \mathrm{d}V\right]^{1/2} &\left[\int_{B_r}\left(\boldsymbol{\nabla}\tilde{\boldsymbol{u}}_* : 2\boldsymbol{\Delta}_{\hat{\mathcal{C}}} : \boldsymbol{\nabla}\bar{\tilde{\boldsymbol{u}}}_* - \boldsymbol{\nabla}\tilde{\boldsymbol{u}}_* : \boldsymbol{\Delta}_{\hat{\mathcal{C}}} : \boldsymbol{\nabla}\bar{\tilde{\boldsymbol{u}}}_*\right) \; \mathrm{d}V\right]^{1/2} \\
\leqslant \left[\int_{B_r}\left(\boldsymbol{\nabla}\hat{\boldsymbol{u}}_* : \boldsymbol{\Delta}_{\hat{\mathcal{C}}} : \boldsymbol{\nabla}\bar{\hat{\boldsymbol{u}}}_*\right) \; \mathrm{d}V\right]^{1/2} &\left[\int_D\left(\boldsymbol{\nabla}\tilde{\boldsymbol{u}}_* : \boldsymbol{\Delta}_{\mathcal{C}} : \boldsymbol{\nabla}\bar{\tilde{\boldsymbol{u}}}_* - (\mathsf{c}_* - \mathsf{C})|\boldsymbol{\nabla}\tilde{\boldsymbol{u}}_*|^2\right) \; \mathrm{d}V\right]^{1/2} \\
\leqslant \left[\int_{B_r}\left(\boldsymbol{\nabla}\hat{\boldsymbol{u}}_* : \boldsymbol{\Delta}_{\hat{\mathcal{C}}} : \boldsymbol{\nabla}\bar{\hat{\boldsymbol{u}}}_*\right) \; \mathrm{d}V\right]^{1/2} &\left[\int_D\left(\boldsymbol{\nabla}\tilde{\boldsymbol{u}}_* : \boldsymbol{\Delta}_{\mathcal{C}} : \boldsymbol{\nabla}\bar{\tilde{\boldsymbol{u}}}_* - \hat{\tau}\Delta_\rho|\tilde{\boldsymbol{u}}_*|^2\right) \; \mathrm{d}V\right]^{1/2},
\end{aligned}$$

due to (5.4.55) and relationships $\boldsymbol{\xi} : 2\boldsymbol{\Delta}_{\hat{\mathcal{C}}} : \bar{\boldsymbol{\xi}} = \boldsymbol{\xi} : 2(\hat{\mathcal{C}}_* - \hat{\mathcal{C}}) : \bar{\boldsymbol{\xi}} \leqslant \boldsymbol{\xi} : (\mathcal{C}_* - \mathcal{C}) : \bar{\boldsymbol{\xi}} = \boldsymbol{\xi} : \boldsymbol{\Delta}_{\mathcal{C}} : \bar{\boldsymbol{\xi}}$ and $\mathsf{P}_* - \mathsf{p} \geqslant \rho_* - \mathsf{p} = \Delta_\rho$. As a result,

$$\int_D \left(\boldsymbol{\nabla}\tilde{\boldsymbol{u}}_* : \boldsymbol{\Delta}_{\mathcal{C}} : \boldsymbol{\nabla}\bar{\tilde{\boldsymbol{u}}}_* - \hat{\tau}\Delta_\rho|\tilde{\boldsymbol{u}}_*|^2\right) \; \mathrm{d}V \;\leqslant\; \int_{B_r}\left(\boldsymbol{\nabla}\hat{\boldsymbol{u}}_* : \boldsymbol{\Delta}_{\hat{\mathcal{C}}} : \boldsymbol{\nabla}\bar{\hat{\boldsymbol{u}}}_*\right) \; \mathrm{d}V.$$

On substituting this result into (5.4.26) when $\tau = \hat{\tau}$ and $\boldsymbol{v} = \tilde{\boldsymbol{v}}$, it follows by virtue of (5.4.28) that

$$
\begin{aligned}
\langle \mathbb{L}_{\hat{\tau}} \tilde{\boldsymbol{v}}, \tilde{\boldsymbol{v}} \rangle_{H_0^1(D)} &= \int_D \left(\boldsymbol{\nabla} \tilde{\boldsymbol{u}}_* : \boldsymbol{\Delta}_{\boldsymbol{\mathcal{C}}} : \boldsymbol{\nabla} \bar{\tilde{\boldsymbol{u}}}_* - \hat{\tau} \, \Delta_\rho |\tilde{\boldsymbol{u}}_*|^2 + \boldsymbol{\nabla} \tilde{\boldsymbol{v}} : \boldsymbol{\mathcal{C}} : \boldsymbol{\nabla} \bar{\tilde{\boldsymbol{v}}} - \rho \, \hat{\tau} |\tilde{\boldsymbol{v}}|^2 \right) \, \mathrm{d}V \\
&\leqslant \int_{B_r} \left(\boldsymbol{\nabla} \hat{\boldsymbol{u}}_* : \boldsymbol{\Delta}_{\hat{\boldsymbol{\mathcal{C}}}} : \boldsymbol{\nabla} \bar{\hat{\boldsymbol{u}}}_* + \boldsymbol{\nabla} \hat{\boldsymbol{v}} : \boldsymbol{\mathcal{C}} : \boldsymbol{\nabla} \bar{\hat{\boldsymbol{v}}} - \rho \, \hat{\tau} |\hat{\boldsymbol{v}}|^2 \right) \, \mathrm{d}V,
\end{aligned}
$$

which implies, via Theorem 16, that there exists at least one transmission eigenvalue within interval $(0, \hat{\tau}]$. The above analysis proves the following result abut the existence of transmission eigenvalues for the case where the elasticity and mass density contrasts are of the same sign.

Theorem 19. *Assume that the medium represented by* $(\boldsymbol{\mathcal{C}}, \rho)$ *is homogeneous and isotropic as in (5.4.24). If either*

1. $\mathsf{p} < \mathsf{p}_*$ *and* $\mathsf{C} < \mathsf{c}_*$ *such that*
$$
(\mathsf{P}_* - \mathsf{p}) \; < \; \frac{\mu}{2\hat{\tau}} (\mathsf{c}_* - \mathsf{C})
$$
where $\hat{\tau}$ *is the first transmission eigenvalue corresponding to ball* $B_r \subset D$ *endowed with constant material properties* $(\hat{\boldsymbol{\mathcal{C}}}, \hat{\rho}) := (\frac{1}{2}\boldsymbol{\mathcal{C}}, \rho)$ *and* $(\hat{\boldsymbol{\mathcal{C}}}_*, \hat{\rho}_*) := (\frac{1}{2}\mathsf{c}_* \boldsymbol{\mathcal{I}}^{sym}, \mathsf{P}_*)$, *or*

2. $\mathsf{P}_* < \mathsf{p}$ *and* $\mathsf{C}_* < \mathsf{c}$ *such that*
$$
(\mathsf{p} - \mathsf{p}_*) \; < \; \frac{\mu}{2\hat{\tau}} (\mathsf{c} - \mathsf{C}_*)
$$
where $\hat{\tau}$ *the first transmission eigenvalue corresponding to* $B_r \subset D$ *endowed with constant material properties* $(\hat{\boldsymbol{\mathcal{C}}}, \hat{\rho}) := (\frac{1}{2}\boldsymbol{\mathcal{C}}, \rho)$ *and* $(\hat{\boldsymbol{\mathcal{C}}}_*, \hat{\rho}_*) := (\frac{1}{2}\mathsf{C}_* \boldsymbol{\mathcal{I}}^{sym}, \mathsf{p}_*)$,

there exists at least one transmission eigenvalue associated with (5.2.6) within interval $(0, \hat{\tau}]$.

Remark 16. *The foregoing developments, catering for the case where the elasticity and mass density contrasts are of the same sign, unfortunately can not be carried further along the lines of the proof of Theorem 12 to establish the existence of infinitely many eigenvalues since the linear operator* $\mathbb{L}_\tau$ *has the required properties only for* $\tau \leqslant \hat{\tau}$, *where* $\hat{\tau}$ *is bounded by (5.4.55). However, if the mass density contrast is sufficiently small so that (5.4.55) is met for* $r > 0$ *such that* $m > 1$ *balls of radius* r *can be fitted in* D *(see the proof of Theorem 12), one can show that there are* $m > 1$ *transmission eigenvalues within interval* $(0, \hat{\tau}]$ *counting multiplicity.*

5.5 Conclusions

In this study, the existence and structure of the transmission eigenvalues for heterogeneous and anisotropic elastic bodies is considered for a wide class of mass density and elasticity contrasts between the two solids featured by the interior transmission problem. When no external excitation is present, the latter boundary value problem entails two body-force-free equations of (anisotropic, inhomogeneous) linear elasticity in a bounded domain $D \subset \mathbb{R}^3$, with shared Cauchy data over ∂D. In the context of the inverse scattering theory, these two equations model respectively penetrable obstacle D and background medium occupying region D. The resulting eigenvalue problem turns out to be nonlinear and may, at best, be transformed into a linear eigenvalue problem for a non-self-adjoint compact operator. For generality, the interior transmission eigenvalue problem is investigated for a wide class of material contrasts between the obstacle and the background, namely those with material similitude in terms of equal elastic

tensors or equal mass densities, and configurations without material similitude where the mass density and elasticity contrast are each sign-definite throughout D. For configurations involving either equal elastic tensor distributions or equal mass density distributions over D it is shown, via a suitable variational formulation of the interior transmission problem for heterogeneous anisotropic solids, that the latter is necessarily characterized by a countable set of (positive) transmission eigenvalues that accumulate only at infinity. For configurations without material similitude, on the other hand, a further distinction is made between the situations where the elasticity and mass density contrasts of the same sign, and those where the two are of the opposite sign. In the latter case the discreteness of transmission eigenvalues is again established for a general case involving anisotropic heterogeneous solids, while the existence of a countable set of transmission eigenvalues is proven under an additional restriction that either the background or the obstacle is homogeneous and isotropic. In situations where the elasticity and mass density contrasts share the sign over D, an earlier result on the discreteness of the transmission eigen-spectrum (Bellis and Guzina, 2010) is complemented by the proof of its nonemptiness, requiring again that either the background or the obstacle be homogeneous and isotropic. Necessitated by the breadth of material configurations studied, the above claims are established through the development of a suite of variational techniques, each customized to meet the needs of a particular class of eigenvalue problems. As a secondary result, the lower and upper bounds on the first transmission eigenvalue are obtained in terms of the elasticity and mass density contrasts between the obstacle and the background. Given the fact that the transmission eigenvalues are computable from the observations of the scattered field, such estimates may have significant potential toward estimating the nature (e.g. compliance) of penetrable scatterers in elasticity, see Cakoni et al. (2010b) for a discussion in the context of scalar problems.

Part III

A Glimpse at a Relationship between TSM and LSM

Chapter 6

Analytical comparative study in acoustic inverse scattering

Contents

6.1   Introduction

Previous developments in this dissertation have addressed theoretical or practical issues related to the topological sensitivity and the linear sampling methods. Their respective presentations in Parts I and II have shown that these techniques rely on different concepts but in spite which these methods have been successfully developed for various physical models and employed as two non-iterative techniques to obtain qualitative topological or geometrical informations on hidden scattering obstacles. On the one hand, the topological sensitivity method consists in a heuristic interpretation of an indicator function itself derived from a mathematically rigorous asymptotic analysis. On the other hand, the linear sampling method, which relies on the use of the solution to an integral equation of the first kind, is supported by key theoretical results that ensure the validity of the reconstruction of the unknown scatterers.

The purpose of the following study is i) to provide a simple but instructive analytical framework within which the two methods can effectively be compared, and ii) to give tangible elements of comprehension of their respective performances. The object of the study is the imaging of a penetrable obstacle embedded in an acoustic medium from a knowledge of the time harmonic incident waves and the corresponding scattered fields, using the two methods of interest. Within the framework of the analytical resolution of the direct acoustic scattering problem in a simple case, a parallel is drawn between the two methods in order to evaluate and compare their capabilities to tackle with the topological identification of the scatterer using full or partial observations of the scattered fields. Specificities and limitations of both techniques are also highlighted in this common setting. The effect of noisy data on the efficiency of the methods has been finally emphasized.

6.2   Preliminaries

6.2.1   Forward problem

The direct scattering of acoustic waves by penetrable homogeneous body is a well known subject (see e.g. Kittappa and Kleinman, 1975; Ramm, 1986) which is addressed in this section. Consider the *lossless* scattering of acoustic waves by a penetrable bounded obstacle B in the infinite medium $\mathbb{R}^3$ which is assumed to be homogeneous and isotropic with mass density ρ and elastic bulk modulus κ. These parameters are respectively denoted ρ_* and κ_* inside the homogeneous obstacle, defining the material coefficients $\beta = \rho/\rho_*$ and $\eta = \kappa/\kappa_*$. Moreover, if c and c_* denote the sound speed in the background medium and the obstacle respectively, then the relative index of refraction $\gamma = c/c_*$ is such that $\beta\gamma^2 = \eta$. Given a set Σ of unit directions, the domain is illuminated by incident time harmonic acoustic plane waves $u(\boldsymbol{\xi}, \boldsymbol{\delta}) = e^{ik\boldsymbol{\xi}\cdot\boldsymbol{\delta}}$ propagating in directions $\boldsymbol{\delta} \in \Sigma$ at frequency $\omega = ck$, with $|\boldsymbol{\delta}| = 1$ and the factor $e^{-i\omega t}$ being omitted henceforth for brevity. The presence of the obstacle gives rise to the acoustic scattered fields v such that the total acoustic fields, u_B in $\mathbb{R}^3$ can be decomposed as

$$u_B(\boldsymbol{\xi}, \boldsymbol{\delta}) = u(\boldsymbol{\xi}, \boldsymbol{\delta}) + v(\boldsymbol{\xi}, \boldsymbol{\delta}) \quad (\boldsymbol{\xi} \in \mathbb{R}^3 \backslash B, \boldsymbol{\delta} \in \Sigma). \tag{6.2.1}$$

The forward scattering problem entails solving the following set of Helmholtz equations and boundary conditions

$$
\begin{aligned}
\Delta v(\boldsymbol{\xi},\boldsymbol{\delta}) + k^2 v(\boldsymbol{\xi},\boldsymbol{\delta}) &= 0 & (\boldsymbol{\xi} \in \mathbb{R}^3 \backslash \overline{B}, \boldsymbol{\delta} \in \Sigma) \\
\Delta w(\boldsymbol{\xi},\boldsymbol{\delta}) + \gamma^2 k^2 w(\boldsymbol{\xi},\boldsymbol{\delta}) &= 0 & (\boldsymbol{\xi} \in B, \boldsymbol{\delta} \in \Sigma) \\
v(\boldsymbol{\xi},\boldsymbol{\delta}) + u(\boldsymbol{\xi},\boldsymbol{\delta}) &= w(\boldsymbol{\xi},\boldsymbol{\delta}) & (\boldsymbol{\xi} \in \partial B, \boldsymbol{\delta} \in \Sigma) \\
v_{,\boldsymbol{n}}(\boldsymbol{\xi},\boldsymbol{\delta}) + u_{,\boldsymbol{n}}(\boldsymbol{\xi},\boldsymbol{\delta}) &= \beta w_{,\boldsymbol{n}}(\boldsymbol{\xi},\boldsymbol{\delta}) & (\boldsymbol{\xi} \in \partial B, \boldsymbol{\delta} \in \Sigma) \\
\lim_{|\boldsymbol{\xi}| \to \infty} |\boldsymbol{\xi}| \left(\frac{\partial v(\boldsymbol{\xi},\boldsymbol{\delta})}{\partial |\boldsymbol{\xi}|} - ikv(\boldsymbol{\xi},\boldsymbol{\delta}) \right) &= 0 & (\boldsymbol{\delta} \in \Sigma),
\end{aligned}
\tag{6.2.2}
$$

where $f_{,\boldsymbol{n}}(\boldsymbol{\xi}) = \boldsymbol{\nabla} f(\boldsymbol{\xi}) \cdot \boldsymbol{n}(\boldsymbol{\xi})$ denotes the derivative with respect to the unit outward normal $\boldsymbol{n}$ to ∂B, the last equation defining the Sommerfeld radiation condition.

The problem (6.2.2) is formulated for any penetrable obstacle B, but for further developments it is interesting to characterize its solutions for some limit behaviors of the scatterer. With reference to the acoustic impedance of the background medium and the obstacle, respectively Z and Z_*, it is noticeable that, introducing the governing ratio $\sqrt{\beta\eta} = Z/Z_*$, one has (Kinsler et al., 1982; Dassios and Kleiman, 2000)

- If $Z/Z_* \gg 1$, the transmission problem (6.2.2) reduces to an exterior Dirichlet problem for which the acoustic pressure field in B vanishes while its velocity potential is non zero. The pressure release on the boundary ∂B characterizes a so-called *sound-soft* obstacle.

- Conversely, if $Z/Z_* \ll 1$ then (6.2.2) turns out to be an exterior Neumann problem whose solution has a maximum pressure amplitude in B with a vanishing velocity potential. The vanishing velocity field on ∂B is characteristic of a *sound-hard* obstacle.

6.2.2   Inverse problem

The aim of the inverse problem is to reconstruct the geometrical support of the obstacle from the measurements u^{obs}, over an observation surface S^{obs}, of the scattered fields v produced by incident plane waves in the set Σ of unit directions (Colton, 1984; Colton and Kress, 1992). In what follows it is assumed that the material obstacle characteristics, synthesized via β and η, are be known beforehand. In this setting, two non iterative techniques will be investigated analytically and numerically in simple cases in order to demonstrate and compare their efficiencies and accuracies.

Topological sensitivity method

To deal with the topological sensitivity method, let us introduce a cost functional

$$
\mathbb{J}(B_{\text{t}}, \beta, \eta) = \int_\Sigma \int_{S^{\text{obs}}} \varphi(u_{\text{t}}, \boldsymbol{\xi}, \boldsymbol{\delta}) \, \mathrm{d}S_\xi \, \mathrm{d}S_\delta,
\tag{6.2.3}
$$

where B_{t} is a trial obstacle in the background medium $\mathbb{R}^3$ and u_{t} the corresponding scattered acoustic field. The cost functional evaluates the difference between trial and true topologies and is expressed by mean of a misfist function φ. Its aim is to measure a gap between u_{t} and u^{obs} and in the following it is considered in the form of the commonly employed least-squares misfit function

$$
\varphi(u_{\text{t}}, \boldsymbol{\xi}, \boldsymbol{\delta}) = \frac{1}{2} |u_{\text{t}}(\boldsymbol{\xi}, \boldsymbol{\delta}) - u^{\text{obs}}(\boldsymbol{\xi}, \boldsymbol{\delta})|^2 \quad (\boldsymbol{\xi} \in S^{\text{obs}}, \boldsymbol{\delta} \in \Sigma).
\tag{6.2.4}
$$

Let $B_\varepsilon(\boldsymbol{z}) = \boldsymbol{z} + \varepsilon \mathcal{B}$ be the trial obstacle considered and characterized by its center $\boldsymbol{z}$, the unit bounded set $\mathcal{B} \subset \mathbb{R}^3$ containing the origin, the radius $\varepsilon > 0$ and material properties ρ_* and κ_* of the unknown obstacle. Following Sokolowski and Zochowski (1999) and Guzina and Bonnet (2006) one seeks for the asymptotic behavior of $\mathbb{J}(B_\varepsilon(\boldsymbol{z}), \beta, \eta)$ as $\varepsilon \to 0$ through the expansion

$$\mathbb{J}(B_\varepsilon(\boldsymbol{z}), \beta, \eta) \underset{\varepsilon \to 0}{=} \mathbb{J}(\emptyset, \beta, \eta) + \eta(\varepsilon)|\mathcal{B}|\mathbb{T}(\boldsymbol{z}, \beta, \eta) + o(\eta(\varepsilon)), \tag{6.2.5}$$

where $\mathbb{J}(\emptyset, \beta, \eta)$ denotes the cost functional evaluated without obstacle, $|\mathcal{B}|$ is the volume of the unit set $\mathcal{B}$ and the function $\eta(\varepsilon)$ vanishes in the limit $\varepsilon \to 0$. The topological derivative $\mathbb{T}(\boldsymbol{z}, \beta, \eta)$ arising in (6.2.5) remains only a function of the point $\boldsymbol{z}$ and constitutes a local indicator of obstacle location. Negative values are associated with local decreasings of the cost functional which means that infinitesimal obstacle added at these locations fit the measurements. Thus one seeks for sampling points $\boldsymbol{z}$ where the topological derivative attains maximum negative values, i.e. for a given positive real α, the obstacle can be reconstituted by the domain

$$B_{\text{TSM}}(\alpha) = \left\{ \boldsymbol{z} \in \mathbb{R}^3, \mathbb{T}(\boldsymbol{z}, \beta, \eta) \leqslant \alpha \min_{\boldsymbol{\xi} \in \mathbb{R}^3} \mathbb{T}(\boldsymbol{\xi}, \beta, \eta) < 0 \right\}. \tag{6.2.6}$$

Closed form of the topological derivative can be expressed by mean of an *adjoint field* $\hat{u}$ (see Bonnet and Guzina, 2004; Bonnet, 2006) which is solution of the set of equations

$$\begin{aligned} \Delta \hat{u}(\boldsymbol{\xi}, \boldsymbol{\delta}) + k^2 \hat{u}(\boldsymbol{\xi}, \boldsymbol{\delta}) &= 0 & (\boldsymbol{\xi} \in \mathbb{R}^3, \boldsymbol{\delta} \in \Sigma) \\ [\![\hat{u}_{,\boldsymbol{n}}]\!](\boldsymbol{\xi}, \boldsymbol{\delta}) &= \frac{\partial \varphi}{\partial u}(u, \boldsymbol{\xi}, \boldsymbol{\delta}) = -\overline{v}(\boldsymbol{\xi}, \boldsymbol{\delta}) & (\boldsymbol{\xi} \in S^{\text{obs}}, \boldsymbol{\delta} \in \Sigma) \\ \lim_{|\boldsymbol{\xi}| \to \infty} |\boldsymbol{\xi}| \left(\frac{\partial \hat{u}(\boldsymbol{\xi}, \boldsymbol{\delta})}{\partial |\boldsymbol{\xi}|} - ik\hat{u}(\boldsymbol{\xi}, \boldsymbol{\delta}) \right) &= 0 & (\boldsymbol{\delta} \in \Sigma), \end{aligned} \tag{6.2.7}$$

where the condition (6.2.7b) is associated with the first-order term of Taylor's expansion (6.2.5), assumed that the total field is known exactly, i.e. $u^{\text{obs}} \equiv v$ given by (6.2.1), and that, $\Re[\cdot]$ and $\Im[\cdot]$ denoting real and imaginary part of a quantity, one has

$$\frac{\partial \varphi}{\partial u} \equiv \frac{\partial \varphi}{\partial \Re[u]} - i \frac{\partial \varphi}{\partial \Im[u]}. \tag{6.2.8}$$

In the case of an infinitesimal *spherical* obstacle and following the developments presented in Guzina and Bonnet (2006), the topological sensitivity of the cost function is characterized by

$$\begin{aligned} \eta(\varepsilon) &= \varepsilon^3 \\ |\mathcal{B}| &= \frac{4\pi}{3} \\ \mathbb{T}(\boldsymbol{z}, \beta, \eta) &= \int_\Sigma \Re \left[(1 - \beta) \boldsymbol{\nabla} \hat{u} \cdot \boldsymbol{\mathcal{A}} \cdot \boldsymbol{\nabla} u - (1 - \eta) k^2 \hat{u} \, u \right] (\boldsymbol{z}, \boldsymbol{\delta}) \, \mathrm{d}S_\delta \\ \boldsymbol{\mathcal{A}} &= \frac{3}{2 + \beta} \boldsymbol{I}, \end{aligned} \tag{6.2.9}$$

where $\boldsymbol{I}$ is the second order identity tensor.

The topological sensitivity (6.2.9) of the cost functional (6.2.3) allows to tackle with geometrical identification of the obstacle with non iterative computations in a *obstacle-free* domain $\mathbb{R}^3$ in which both the

definition of the misfit function and the measurements are synthesized in the formulation of the adjoint field $\hat{u}$.

Linear sampling method

The linear sampling method (Cakoni and Colton, 2006) had been originally proposed in inverse acoustic scattering theory in far field formulations (Colton and Kirsch, 1996), and later extended to obstacle identification based on near-field observations (Colton et al., 2000; Nintcheu Fata and Guzina, 2004). In the present study the method conjugates these two approaches. Assuming that $u^{\text{obs}} \equiv v$, for a given sampling point $\boldsymbol{z} \in B$, one seeks the function $g_{\boldsymbol{z}} \in L^2(\Sigma)$ solution of the linear integral equation

$$[\mathcal{S}g_{\boldsymbol{z}}](\boldsymbol{\xi}) = \int_{\Sigma} v(\boldsymbol{\xi}, \boldsymbol{\delta})g_{\boldsymbol{z}}(\boldsymbol{\delta}) \, \mathrm{d}S_{\delta} = G(\boldsymbol{\xi}, \boldsymbol{z}) \quad (\forall \boldsymbol{\xi} \in S^{\text{obs}}), \tag{6.2.10}$$

where $\mathcal{S}$ denotes the so-called scattering operator and $G(\boldsymbol{\xi}, \boldsymbol{z}) = \frac{e^{ik|\boldsymbol{\xi}-\boldsymbol{z}|}}{4\pi|\boldsymbol{\xi}-\boldsymbol{z}|}$ is the full-space fundamental solution. Let us underline that the operator $\mathcal{S}$ is compact from $L^2(\Sigma)$ into $L^2(S^{\text{obs}})$, so the equation (6.2.10) is *ill-posed* (Kress, 1999). Nevertheless, the resolution of the integral equation (6.2.10) is based on the result (Colton and Kress, 1992) that $\mathcal{S}$ is injective with dense range if and only if there does not exist a pair of solutions u_g and w to the so-called homogeneous *interior transmission problem*

$$\begin{aligned}
\Delta u_g(\boldsymbol{\xi}) + k^2 u_g(\boldsymbol{\xi}) &= 0 && (\boldsymbol{\xi} \in B) \\
\Delta w(\boldsymbol{\xi}) + \gamma^2 k^2 w(\boldsymbol{\xi}) &= 0 && (\boldsymbol{\xi} \in B) \\
u_g(\boldsymbol{\xi}) &= w(\boldsymbol{\xi}) && (\boldsymbol{\xi} \in \partial B) \\
u_{g,\boldsymbol{n}}(\boldsymbol{\xi}) &= \beta w_{,\boldsymbol{n}}(\boldsymbol{\xi}) && (\boldsymbol{\xi} \in \partial B),
\end{aligned} \tag{6.2.11}$$

with a non zero density function $g \in L^2(\Sigma)$ such that

$$u_g(\boldsymbol{\xi}) = \int_{\Sigma} u(\boldsymbol{\xi}, \boldsymbol{\delta})g(\boldsymbol{\delta}) \, \mathrm{d}S_{\delta}. \tag{6.2.12}$$

The values k for which the problem (6.2.11) has a non-trivial solution are called *transmission eigenvalues*. For these values precisely the linear sampling method breaks down, so their study has become of great importance recently (Kirsch, 2009; Päivärinta and Sylvester, 2008). When k is not a transmission eigenvalue, it can be shown (Cakoni and Colton, 2006) that for every $\varepsilon > 0$, there exists a nearby solution $g_{\boldsymbol{z}}^{\varepsilon} \in L^2(\Sigma)$ such that

$$\|\mathcal{S}g_{\boldsymbol{z}}^{\varepsilon}(\cdot) - G(\cdot, \boldsymbol{z})\|_{L^2(S^{\text{obs}})} < \varepsilon. \tag{6.2.13}$$

The linear sampling method is supported by the key property that $\|g_{\boldsymbol{z}}^{\varepsilon}\|_{L^2(\Sigma)}$ becomes unbounded as $\boldsymbol{z} \to \partial B$. The description of the behavior of $g_{\boldsymbol{z}}^{\varepsilon}$ in the exterior domain $\boldsymbol{z} \in \mathbb{R}^3 \backslash \overline{B}$ requires a more involved analysis and its study can be found for acoustics and electromagnetism in Colton et al. (2000); Cakoni and Colton (2006) and for elasticity in Nintcheu Fata and Guzina (2004); Guzina and Madyarov (2007), and formally

$$\|g_{\boldsymbol{z}_e}^{\varepsilon}\|_{L^2(\Sigma)} \gg \|g_{\boldsymbol{z}_i}^{\varepsilon}\|_{L^2(\Sigma)} \quad (\forall \boldsymbol{z}_e \in \mathbb{R}^3 \backslash B, \forall \boldsymbol{z}_i \in B). \tag{6.2.14}$$

Then, according to a threshold value $0 \leqslant \alpha < 1$, we can assume that the unknown obstacle can be reconstituted as the domain

$$B_{\mathrm{LSM}}(\alpha) = \mathbb{R}^3 \backslash \left\{ \boldsymbol{z} \in \mathbb{R}^3, \frac{1}{\|g_{\boldsymbol{z}}^{\varepsilon}\|_{L^2(\Sigma)}} \ll \frac{1}{1-\alpha} \right\}. \tag{6.2.15}$$

Thus, in the linear sampling method, the indicator of obstacle location is constituted by the function $g_{\boldsymbol{z}}$ or its approximation $g_{\boldsymbol{z}}^{\varepsilon}$.

6.3 Analytical formulation for a spherical scatterer

In the following, the obstacle B is considered as a unit sphere. The observation surface S^{obs} is defined as a concentric sphere of radius R and the set of incident directions is taken as $\Sigma = \{\boldsymbol{\delta} \in \mathbb{R}^3, |\boldsymbol{\delta}| = 1\}$. An analytical solution to this acoustic inverse scattering problem can then be derived.

6.3.1 Scattered field

The topological sensitivity and linear sampling methods rely both on the knowledge of the field scattered by the obstacle and monitored on the observation surface. In the case of this study, equations (6.2.2) will be solved for an incident field u in direction $\boldsymbol{\delta} \in \Sigma$. The acoustic fields v and w respectively solutions of an *exterior* problem in $\mathbb{R}^3 \backslash B$ and an *interior* problem in B can be expanded over the set of spherical harmonics $(Y_n^m)_{n \in \mathbb{N}, -n \leqslant m \leqslant +n}$ (Nédélec, 2001) as

$$v(\boldsymbol{\xi}, \boldsymbol{\delta}) = \sum_{n=0}^{+\infty} \sum_{m=-n}^{+n} \lambda_n^m(\boldsymbol{\delta}) h_n(k|\boldsymbol{\xi}|) Y_n^m(\hat{\boldsymbol{\xi}}) \quad (\boldsymbol{\xi} \in \mathbb{R}^3 \backslash B, \boldsymbol{\delta} \in \Sigma),$$

$$w(\boldsymbol{\xi}, \boldsymbol{\delta}) = \sum_{n=0}^{+\infty} \sum_{m=-n}^{+n} \mu_n^m(\boldsymbol{\delta}) j_n(\gamma k|\boldsymbol{\xi}|) Y_n^m(\hat{\boldsymbol{\xi}}) \quad (\boldsymbol{\xi} \in B, \boldsymbol{\delta} \in \Sigma),$$

$$\tag{6.3.1}$$

where $\hat{\boldsymbol{\xi}} = \frac{\boldsymbol{\xi}}{|\boldsymbol{\xi}|}$, while j_n and h_n denote respectively the n-order spherical Bessel and Hankel functions of the *first kind*. On employing the boundary conditions over ∂B and the orthonormality of spherical harmonics (6.B.2), the scattered field v is expressed as

$$v(\boldsymbol{\xi}, \boldsymbol{\delta}) = \sum_{n=0}^{+\infty} \sum_{m=-n}^{+n} \left[\frac{\int_S \left(\frac{1}{k} u_{,\boldsymbol{n}}(\boldsymbol{\zeta}, \boldsymbol{\delta}) - \alpha_n u(\boldsymbol{\zeta}, \boldsymbol{\delta}) \right) \overline{Y_n^m}(\boldsymbol{\zeta}) \, \mathrm{d}S_{\zeta}}{-h_n'(k) + \alpha_n h_n(k)} \right] h_n(k|\boldsymbol{\xi}|) Y_n^m(\hat{\boldsymbol{\xi}}) \quad (\boldsymbol{\xi} \in \mathbb{R}^3 \backslash B, \boldsymbol{\delta} \in \Sigma),$$

$$\tag{6.3.2}$$

where $S = \{\boldsymbol{\zeta} \in \mathbb{R}^3, |\boldsymbol{\zeta}| = 1\}$ and defining an effective admittance of the surface ∂B for the n-order spherical harmonic (Morse and Ingard, 1986)

$$\alpha_n = \sqrt{\beta\eta} \frac{j_n'\left(k\sqrt{\eta/\beta}\right)}{j_n\left(k\sqrt{\eta/\beta}\right)}. \tag{6.3.3}$$

Written in terms of u, it is noticeable that the equation (6.3.2) can be used for arbitrary incident field. In the case of an incident plane wave in direction $\boldsymbol{\delta} \in \Sigma$, using the expansion (6.B.3) and the spherical harmonics addition theorem (6.B.4), relation (6.3.2) reduces to

$$v(\boldsymbol{\xi}, \boldsymbol{\delta}) = \sum_{n=0}^{+\infty} i^n (2n+1) \Lambda_n(\beta, \eta) h_n(k|\boldsymbol{\xi}|) P_n(\hat{\boldsymbol{\xi}} \cdot \boldsymbol{\delta}) \text{ with } \Lambda_n(\beta, \eta) = \frac{j_n'(k) - \alpha_n j_n(k)}{-h_n'(k) + \alpha_n h_n(k)}, \quad (6.3.4)$$

where P_n denotes the n-order Legendre polynomial, and j_n', h_n' the respective derivative of Bessel and Hankel functions with respect to their arguments. Note that if only one incident plane wave is considered to reconstruct the obstacle, i.e. $\Sigma = \{\boldsymbol{\delta}\}$ and if the system of spherical coordinates $\boldsymbol{\xi} = (\rho, \theta, \phi)$ is chosen such as $\hat{\boldsymbol{\xi}} \cdot \boldsymbol{\delta} = \cos\theta$ then the axisymmetry of the scattered field is explicit in (6.3.4).
From expression (6.3.4) one can recover some limiting behaviors:

- For a fixed η, the *sound-soft* obstacle corresponds to $\beta \to \infty$, and thus $\alpha_n \to \infty$ entails

$$\Lambda_n(\beta, \eta) = -\frac{j_n(k)}{h_n(k)}, \quad (6.3.5)$$

  which corresponds to the case treated in Colton and Kress (1992).

- Conversely, the *sound-hard* obstacle $\beta \to 0$ at fixed η, is such that $\alpha_n \to 0$ so

$$\Lambda_n(\beta, \eta) = -\frac{j_n'(k)}{h_n'(k)} \quad (6.3.6)$$

  as previously shown in e.g. Nédélec (2001).

- Finally, if the obstacle has the same compressibility modulus and mass density that the background medium ($\beta = \eta = 1$, i.e. no obstacle) then $\alpha_n = j_n'(k)/j_n(k)$ which implies $\Lambda_n = 0$ and $v = 0$ as expected.

6.3.2   Analytical topological sensitivity method

Analytical expression

The topological derivative (6.2.9) can now be given in the case of the scattered field (6.3.4). To find the adjoint field $\hat{u}$, the problem (6.2.7) can be reformulated as

$$\begin{aligned}
\Delta \hat{u}(\boldsymbol{\xi}, \boldsymbol{\delta}) + k^2 \hat{u}(\boldsymbol{\xi}, \boldsymbol{\delta}) &= F(\boldsymbol{\xi}, \boldsymbol{\delta}) && (\boldsymbol{\xi} \in \mathbb{R}^3, \boldsymbol{\delta} \in \Sigma) \\
F(\boldsymbol{\xi}, \boldsymbol{\delta}) &= -\overline{v}(\boldsymbol{\xi}, \boldsymbol{\delta}) \chi_{S^{\text{obs}}}(\boldsymbol{\xi}) && (\boldsymbol{\xi} \in \mathbb{R}^3, \boldsymbol{\delta} \in \Sigma) \\
\lim_{|\boldsymbol{\xi}| \to \infty} |\boldsymbol{\xi}| \left(\frac{\partial \hat{u}(\boldsymbol{\xi}, \boldsymbol{\delta})}{\partial |\boldsymbol{\xi}|} - ik\hat{u}(\boldsymbol{\xi}, \boldsymbol{\delta}) \right) &= 0 && (\boldsymbol{\delta} \in \Sigma),
\end{aligned} \quad (6.3.7)$$

where $\chi_{S^{\text{obs}}}$ denotes the characteristic function of the subset S^{obs}. Then using the Green's function, the adjoint field is given by the single layer potential

$$\hat{u}(\boldsymbol{\xi}, \boldsymbol{\delta}) = \int_{\mathbb{R}^3} F(\boldsymbol{\zeta}, \boldsymbol{\delta}) G(\boldsymbol{\xi}, \boldsymbol{\zeta}) \, dV_{\zeta} \quad (\boldsymbol{\xi} \in \mathbb{R}^3, \boldsymbol{\delta} \in \Sigma). \quad (6.3.8)$$

With the assumption that S^{obs} is a sphere of radius R, the equation (6.3.8) reduces to

$$\hat{u}(\boldsymbol{\xi}, \boldsymbol{\delta}) = -R^2 \int_S \overline{v}(R\hat{\boldsymbol{\zeta}}, \boldsymbol{\delta}) G(\boldsymbol{\xi}, R\hat{\boldsymbol{\zeta}}) \, dS_{\hat{\zeta}} \quad (\boldsymbol{\xi} \in \mathbb{R}^3, \boldsymbol{\delta} \in \Sigma). \quad (6.3.9)$$

The Green's function will then admit two different expansions (6.B.10) depending on whether $|\boldsymbol{\xi}| < R$ or $|\boldsymbol{\xi}| > R$. In the situation considered of seeking the obstacle inside of the observation surface, i.e. $\boldsymbol{\xi} \in \overset{\circ}{S}{}^{\mathrm{obs}}$ (interior of S^{obs}), the adjoint field is expressed by

$$\hat{u}(\boldsymbol{\xi}, \boldsymbol{\delta}) = -kR^2 \sum_{n=0}^{+\infty} (-1)^n i^{n+1} (2n+1) \overline{\Lambda_n}(\beta, \eta) |h_n(kR)|^2 j_n(k|\boldsymbol{\xi}|) P_n(\hat{\boldsymbol{\xi}} \cdot \boldsymbol{\delta}) \quad (|\boldsymbol{\xi}| \leqslant R, \boldsymbol{\delta} \in \Sigma).$$

(6.3.10)

One may note, that according to (6.B.10), expression (6.3.10) should be modified in the *exterior* domain $|\boldsymbol{\xi}| > R$, and will then verify the radiation condition (6.3.7c).

Finally, for a given sampling point $\boldsymbol{z} \in \overset{\circ}{S}{}^{\mathrm{obs}}$, using relation (6.3.10), Jacobi-Anger expansion (6.B.3) and properties (6.B.2), (6.B.6), and (6.B.8), with summation over the set Σ of incident directions, the topological derivative is given by the relation

$$\mathbb{T}(\boldsymbol{z}, \beta, \eta) = -4\pi kR^2 \sum_{n=0}^{+\infty} \Re \left\{ i(2n+1) \overline{\Lambda_n}(\beta, \eta) |h_n(kR)|^2 \cdot \right.$$
$$\left. \left[\left(n(n+1) \frac{3(1-\beta)}{2+\beta} - (1-\eta)k^2 \right) j_n(k|\boldsymbol{z}|)^2 + \frac{3k^2(1-\beta)}{2+\beta} j_n'(k|\boldsymbol{z}|)^2 \right] \right\}.$$

(6.3.11)

Truncation

The relation (6.3.11) involves infinite summation over index n which has to be truncated for computational purposes. On employing the results from Appendix 6.C, the leading terms in formula (6.3.11) for topological sensitivity can be written as

- $kR^2 i(2n+1)\overline{\Lambda_n}(\beta, \eta)|h_n(kR)|^2 \underset{n \to \infty}{=} \dfrac{1-\beta}{1+\beta} \left(\dfrac{1}{R} \right)^{2n} \left(1 + O\left(\dfrac{1}{n} \right) \right)$

- $\left(n(n+1)\dfrac{3(1-\beta)}{2+\beta} - (1-\eta)k^2 \right) j_n(k|\boldsymbol{z}|)^2 \underset{n \to \infty}{=} \dfrac{3(1-\beta)}{8(2+\beta)} \left(\dfrac{ek|\boldsymbol{z}|}{2} \right)^{2n} \dfrac{1}{n^{2n}} \left(1 + O\left(\dfrac{1}{n} \right) \right)$

- $\dfrac{3k^2(1-\beta)}{2+\beta} j_n'(k|\boldsymbol{z}|)^2 \underset{n \to \infty}{=} \dfrac{3(1-\beta)}{8(2+\beta)} |\boldsymbol{z}|^{2n-2} \left(\dfrac{ek}{2} \right)^{2n} \dfrac{1}{n^{2n}} \left(1 + O\left(\dfrac{1}{n} \right) \right).$

(6.3.12)

Accordingly, on writing $\mathbb{T}(\boldsymbol{z}, \beta, \eta) = \sum_{n=0}^{+\infty} \mathbb{T}_n(\boldsymbol{z}, \beta, \eta)$ one has

$$\mathbb{T}_n(\boldsymbol{z}, \beta, \eta) \underset{n \to \infty}{=} O\left(\frac{1}{n^{2n}} \right).$$

(6.3.13)

Thus, the sum in (6.3.11) can be evaluated by retaining the terms up to a prescribed order n_{o}. However it should be noted that the asymptotic behavior of the Bessel and Hankel function in (6.C.2) and their derivatives in (6.C.6) is such that the featured truncation errors are inversely proportional to the order of these functions. Consequently, as observed in Figure 6.1, increasing the wave number must increase the truncation order n_{o} in (6.3.11).
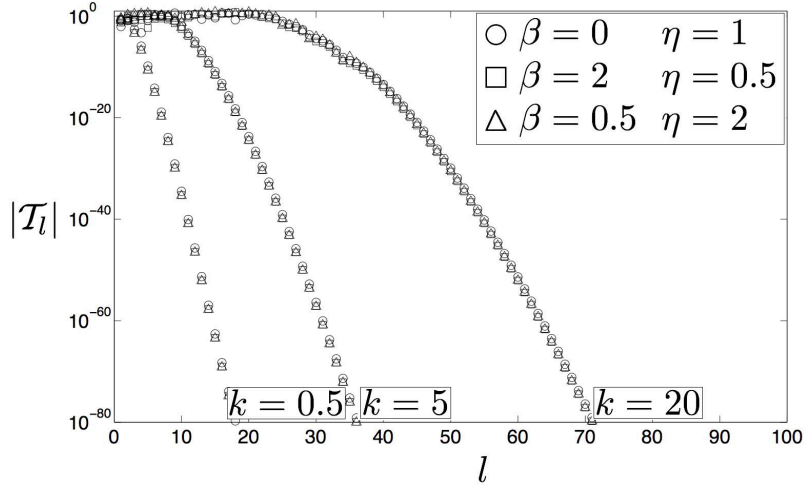
Figure 6.1: *Leading terms in topological derivative depending on frequency and material parameters*

Material sensitivity

The topological sensitivity method is based on an asymptotic expansion corresponding to the nucleation of an infinitesimal obstacle, whose properties have been bound to match the ones of the scattering obstacle in the previous developments for better understanding of the method. The behavior of the indicator (6.2.9) provided relies then strongly on the *a-priori* choice of the material properties of the nucleating obstacle. Thus, while a shape identification technique will rely on their correct match with the material parameters β^{true}, η^{true} of an unknown obstacle, which supposes a full prior information about its nature, the material sensitivity of the topological derivative can also be seen as a potential tool for material identification (Guzina and Chikichev, 2007). From an other point of view, following a study initiated in Malcolm and Guzina (2008) in the time domain, the focus can be made on the quality of the identification in the case where the assumed parameters β, η are incorrect. The idea being that if the signs of the two coefficients $(1 - \beta)$ and $(1 - \eta)$ of the two summands in (6.2.9) are correct relatively to $(1 - \beta^{\text{true}})$ and $(1 - \eta^{\text{true}})$ respectively, then the identification of the obstacle through pronounced *negative* values of the topological derivative is correct. On the contrary, if both signs are incorrect the contrast is inverted and the obstacle tends to be identified by the maximum *positive* values of the indicator. The investigation of this hypothesis in the sequel, for a given set of true parameters β^{true}, η^{true}, is based on the computation of an *a-priori* topological derivative $\mathbb{T}_{\text{ap}}$ derived from (6.3.11) as a function of *a-priori* parameters β and η as

$$\mathbb{T}_{\text{ap}}(\boldsymbol{z}, \beta, \eta) = -4\pi k R^2 \sum_{n=0}^{+\infty} \Re\left\{ i(2n+1)\overline{\Lambda_n}(\beta^{\text{true}}, \eta^{\text{true})} |h_n(kR)|^2 \cdot \right.$$

$$\left. \left[\left(n(n+1)\frac{3(1-\beta)}{2+\beta} - (1-\eta)k^2 \right) j_n(k|\boldsymbol{z}|)^2 + \frac{3k^2(1-\beta)}{2+\beta} j_n'(k|\boldsymbol{z}|)^2 \right] \right\}.$$

(6.3.14)

In the equation (6.3.14), the coefficients Λ_n still depend on the true parameters as they are associated to the field (6.3.4) scattered by the true obstacle and introduced in the topological derivative through the adjoint field (6.3.10).

For a given set of N sampling points $\boldsymbol{z}_1, \ldots, \boldsymbol{z}_N$, the sign correspondence with the topological derivative $\mathbb{T}(\boldsymbol{z}, \beta^{\text{true}}, \eta^{\text{true}})$ (6.3.11) is measured by computing the indicator $\mathcal{I}(\beta, \eta)$ defined by

$$\mathcal{I}(\beta, \eta) = \frac{1}{N} \sum_{j=1}^{N} \text{sign}\left(\frac{\mathbb{T}_{\text{ap}}(\boldsymbol{z}_j, \beta, \eta)}{\mathbb{T}(\boldsymbol{z}_j, \beta^{\text{true}}, \eta^{\text{true}})} \right), \tag{6.3.15}$$

where $\text{sign}(\alpha) = 1$ if $\alpha > 0$, and -1 if $\alpha < 0$. Thus $-1 \leqslant \mathcal{I}(\beta, \eta) \leqslant 1$, and the extremum values 1 and -1 correspond respectively to a total match or inversion of the signs of the two topological derivatives. Moreover small values of this indicator are associated with numerous differences of the signs of the two topological derivatives. Owing to the coefficients in (6.3.11), the coordinates are defined as

$$\begin{aligned} x &= \frac{(1 - \beta)}{(2 + \beta)} \frac{(2 + \beta^{\text{true}})}{(1 - \beta^{\text{true}})}, \\ y &= \frac{(1 - \eta)}{(1 - \eta^{\text{true}})}, \end{aligned} \tag{6.3.16}$$

and the Figure 6.2 is then plotted for a maximum range of $-4 \leqslant x \leqslant 4$ and $-4 \leqslant y \leqslant 4$ possibly restricted by admissible values of the material parameters β, η relatively to given β^{true} and η^{true}, and for a fixed wave number $k = 5$.

The Figure 6.2(a) corresponds to the case investigated in Malcolm and Guzina (2008), and clearly highlights the idea described previously that if $x \geqslant 0$ and $y \geqslant 0$ then $\mathcal{I}(\beta, \eta) \simeq 1$, i.e. the signs of the *a-priori* topological derivatives match the signs of the true ones, and if $x \leqslant 0$ and $y \leqslant 0$ then $\mathcal{I}(\beta, \eta) \simeq -1$, i.e. the signs of the topological derivatives are opposite. The intermediate cases where $xy \leqslant 0$ can be discussed with further reference to the Figure 6.2(b). In the domain considered it can be seen that the sign differences are greater than in the previous case as the values of the indicator $\mathcal{I}(\beta, \eta)$ are smaller. Furthermore the Figure 6.2(c) highlights that those differences can also be observed if $xy \geqslant 0$, which suggests a moderation of the statement proposed in Malcolm and Guzina (2008). Finally the Figure 6.2(d) corresponds to a situation where the hypothesis is valid almost essentially for the cases $x = y$.

In the light of the previous analysis, it can be claimed that the heuristic of the topological sensitivity method (obstacle revealed by maximum *negative* values of $\mathbb{T}$) can be strictly followed with incorrect *a-priori* material parameters which lead to coefficients $(1 - \beta)/(2 + \beta)$ and $(1 - \eta)$ of (i) correct signs and (ii) same proportional errors relatively to $(1 - \beta^{\text{true}})/(2 + \beta^{\text{true}})$ and $(1 - \eta^{\text{true}})$ respectively. Owing to the interpretation of the parameters β as the ratio of the mass densities, and η as the ratio of elastic moduli, the previous statements involve that the identification is correct if the infinitesimal obstacle used in the asymptotic expansion (6.2.5) matches qualitatively the material behavior of the obstacle sought. Furthermore, if (iii) both signs are opposite, providing (ii), then the infinitesimal obstacle presents a complete opposite mechanical behavior than the unknown obstacle, so the positive values of $\mathbb{T}$ become relevant since they correspond to the *less likely* possible matching location of these two obstacles. Finally, the relaxation of the statement (ii) should involve a careful interpretation of the topological derivative.

This material sensitivity, particularly significant in the time harmonic domain, can be moderated by multi-modal illumination of the obstacle or time domain formulation of the topological sensitivity method (see Bonnet (2006) and Malcolm and Guzina (2008)).
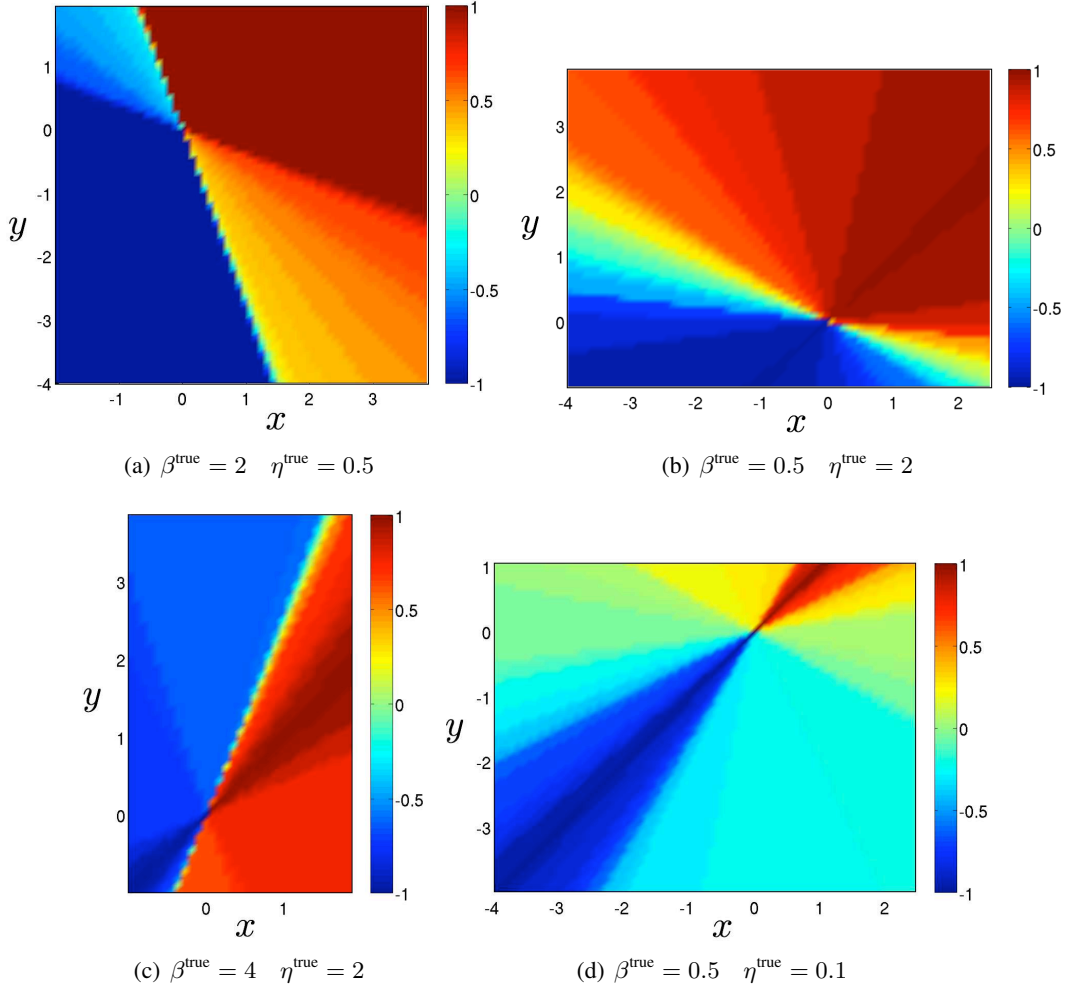
(a) $\beta^{\text{true}} = 2 \quad \eta^{\text{true}} = 0.5$

(b) $\beta^{\text{true}} = 0.5 \quad \eta^{\text{true}} = 2$

(c) $\beta^{\text{true}} = 4 \quad \eta^{\text{true}} = 2$

(d) $\beta^{\text{true}} = 0.5 \quad \eta^{\text{true}} = 0.1$

Figure 6.2: *Index $\mathcal{I}(\beta, \eta)$ function of $x = \frac{(1-\beta)}{(2+\beta)} \frac{(2+\beta^{true})}{(1-\beta^{true})}$ and $y = \frac{(1-\eta)}{(1-\eta^{true})}$*

Numerical results

Numerical results are presented in this section for the computation of the topological derivative (6.3.11), i.e. assuming that the nature of the obstacle is known. The set of incident direction is defined as $\Sigma = \{\boldsymbol{\delta} \in \mathbb{R}^3, |\boldsymbol{\delta}| = 1\}$, then since the observation surface is a sphere concentric to the spherical unit obstacle considered, the inversion is based on a unique observation, and the topological derivative is axisymmetric. Thus, the indicator $\mathbb{T}$ is plotted along a radius for different frequencies.

According to the previous considerations, the topological derivative relies strongly on the material properties of the obstacle considered, so rigorous and systematic interpretation of the behavior of the indicator is intricate. For better understanding let us differentiate the two different components in $\mathbb{T}$, namely the velocity term $\mathbb{T}_\text{v}$ and the pressure term $\mathbb{T}_\text{p}$, such that, according to (6.2.9) and (6.3.11), one has

$$\mathbb{T}(\boldsymbol{z}, \beta, \eta) = \frac{3(1-\beta)}{(2+\beta)} \mathbb{T}_\text{v}(\boldsymbol{z}, \beta, \eta) + (1-\eta)\mathbb{T}_\text{p}(\boldsymbol{z}, \beta, \eta). \tag{6.3.17}$$

One may note that the weighting of the terms $\mathbb{T}_v$ and $\mathbb{T}_p$ in (6.3.17) is governed respectively by the ratio of the mass densities β and the ratio of elastic moduli η, which is consistent with classical governing equations of acoustics (Morse and Ingard, 1986).

Figure 6.3 depicts the radial variation of the two components (6.3.17) of the topological derivative for several combinations of frequency and material parameters, chosen such that the ratio of the acoustic impedance described in section 6.2.1 is $\sqrt{\beta\eta} = 10^3$ for the case 6.3(a), and $\sqrt{\beta\eta} = 10^{-3}$ for 6.3(b). On the Figure 6.3(a) corresponding to the case of a *sound-soft* obstacle, one can observe that for $|z| > 0$, $\mathbb{T}_v$ attains its maximum negative value *inside* the obstacle ($|z| < 1$), while $\mathbb{T}_p$ has its minimum located *outside* of B ($|z| > 1$). Moreover, as the frequency increases, both minima move to the boundary of the obstacle. This is consistent with the qualitative description of the direct scattering by sound-soft obstacle in section 6.2.1, for which one can expect that an inversion technique based on the *velocity* field should able to image the *interior* of the obstacle (non zero velocity potential in B), while the use of the *pressure* field should emphasize its *boundary* (vanishing pressure on ∂B and in B). On the contrary, these behaviors are inverted for the scattering by a *sound-hard* obstacle, which match again the patterns observed in Figure 6.3(b).

The construction of the topological derivative $\mathbb{T}$ via the coefficients of the two summands in (6.3.17) involves complex interactions between velocity and pressure components. Nevertheless, as observed on Figure 6.4, as frequency increases, the method provides a reliable identification of the boundary ∂B of the obstacle. Moreover, it is noticeable on Figures 6.3 and 6.4, that whatever are the behaviors inside the obstacle, the indicators are relatively smooth and tend asymptotically to zero for $|z| > 1$, which contributes to increase the contrast between the obstacle and the background medium.

6.3.3   Analytical linear sampling method

Singular value decomposition of operator $\mathcal{S}$

The operator $\mathcal{S}$ from $L^2(\Sigma)$ into $L^2(S^{\mathrm{obs}})$ defined by (6.2.10) is compact (Kress, 1999). Moreover, $(Y_n^m)_{n\in\mathbb{N},-n\leqslant m\leqslant+n}$ constitutes a basis of $L^2(\Sigma)$, and $(h_n Y_n^m)_{n\in\mathbb{N},-n\leqslant m\leqslant+n}$ constitutes a basis for *outgoing* Helmholtz solutions in $\mathbb{R}^3$ (see Nédélec (2001)), so, restricted to S^{obs} it is a basis of restrictions to $L^2(S^{\mathrm{obs}})$ of such solutions.
From equations (6.3.4), (6.B.2) and (6.B.4) we can deduce that

$$[\mathcal{S}Y_n^m](\boldsymbol{\xi}) = 4\pi i^n \Lambda_n(\beta,\eta) h_n(kR) Y_n^m(\hat{\boldsymbol{\xi}}) \quad (\forall\boldsymbol{\xi} \in S^{\mathrm{obs}}, \forall n \in \mathbb{N}, \forall m \in \{-n,\dots,+n\}). \quad (6.3.18)$$

Thus the set $(\sigma_n)_{n\in\mathbb{N}}$ of singular values of $\mathcal{S}$ can be identified as

$$\sigma_n = 4\pi i^n \Lambda_n(\beta,\eta) \quad (\forall n \in \mathbb{N}). \quad (6.3.19)$$

On the basis of the results from Appendix 6.C, it can be seen that these singular values have the following asymptotic behavior which is independent of η

$$\sigma_n \underset{n\to\infty}{=} \pi i^{n+1} k \left(\frac{1-\beta}{1+\beta}\right) \left(\frac{ek}{2}\right)^{2n} \frac{1}{n^{2n+1}} \left(1 + O\left(\frac{1}{n}\right)\right). \quad (6.3.20)$$

We notice finally (see Figure 6.5) that the asymptotic behavior depends essentially on frequency rather than on material parameters. This dependence has to be considered in a regularization method.
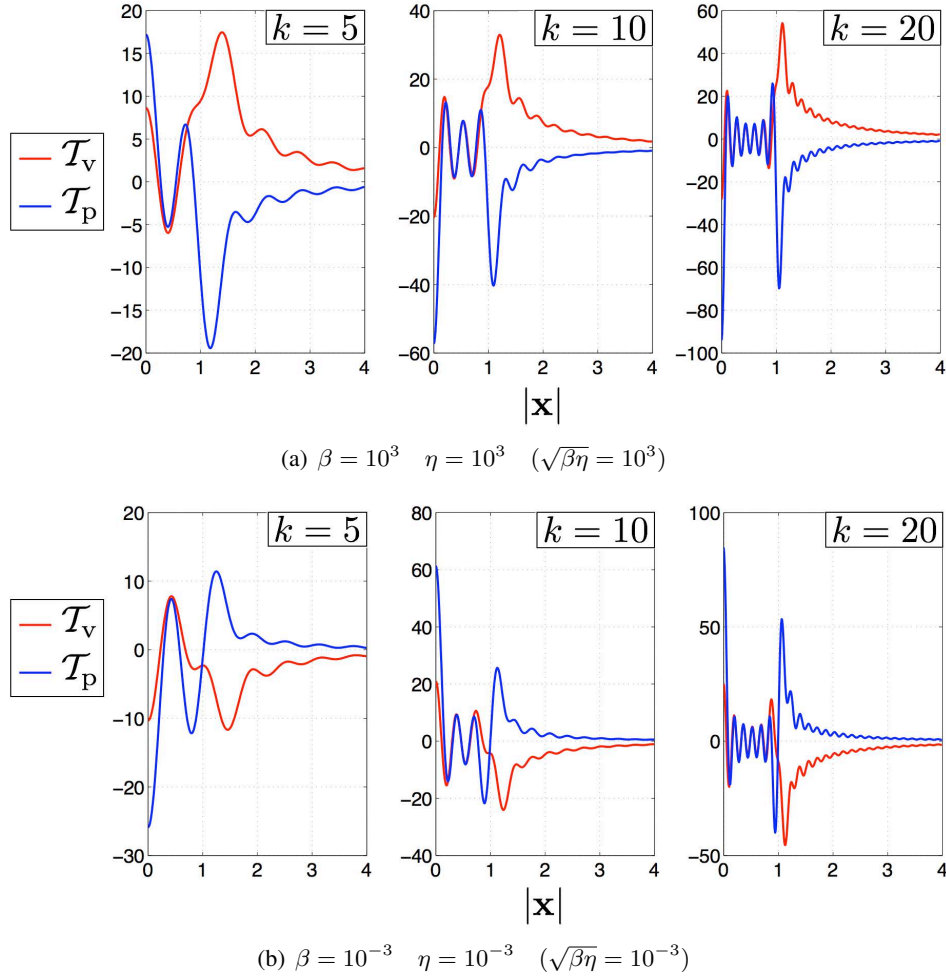
(a) $\beta = 10^3 \quad \eta = 10^3 \quad (\sqrt{\beta\eta} = 10^3)$

(b) $\beta = 10^{-3} \quad \eta = 10^{-3} \quad (\sqrt{\beta\eta} = 10^{-3})$

Figure 6.3: *Topological derivative components depending on frequency and material parameters*

Interior transmission problem

The integral equation (6.2.10) has a unique solution provided that k is not a *transmission eigenvalue* (see paragraph 6.2.2). This paragraph is then dedicated to the question of the existence of such eigenvalues, thus one seeks for a non trivial solutions u_g and w to the problem (6.2.11), where in the case of incident plane waves, the function u_g takes the form of a Herglotz wave function, i.e. a function of the form

$$u_g(\boldsymbol{\xi}) = \int_{\Sigma} e^{ik\boldsymbol{\xi}\cdot\boldsymbol{\delta}} g(\boldsymbol{\delta}) \, \mathrm{d}S_{\delta}, \tag{6.3.21}$$

where $g \in L^2(\Sigma)$. In the same fashion as (6.3.1), these solutions can be expanded in a series of spherical harmonics as
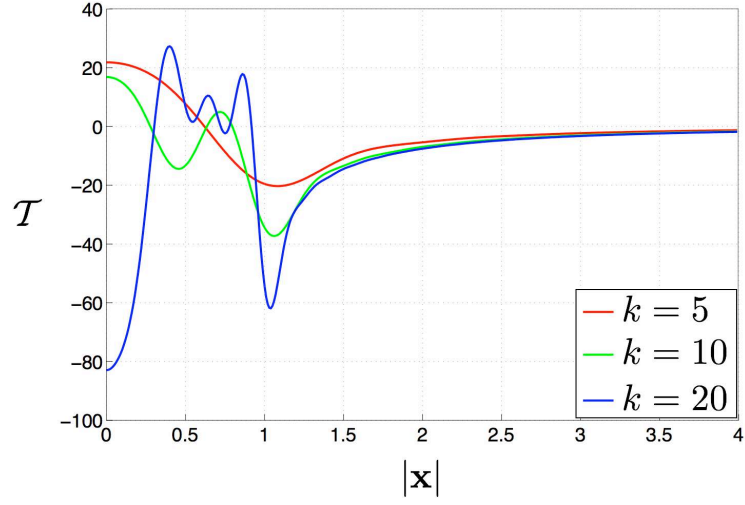
(a) $\beta = 2 \quad \eta = 0.5$
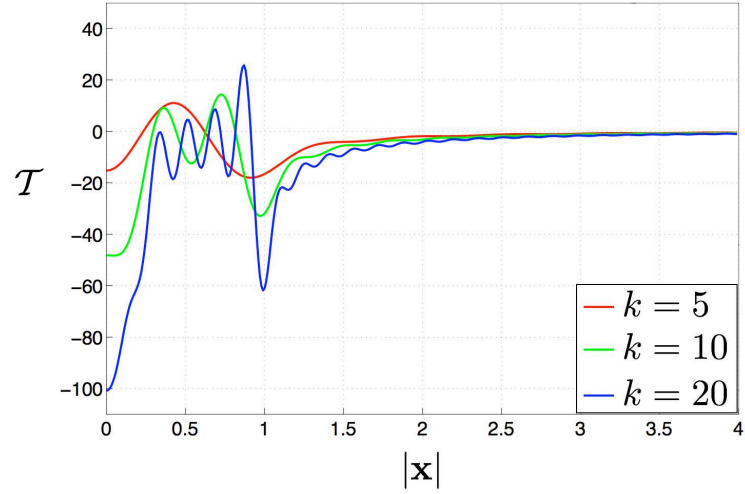
(b) $\beta = 1 \quad \eta = 0.1$

Figure 6.4: *Topological derivative depending on frequency and material parameters*

$$u_g(\boldsymbol{\xi}) = \sum_{n=0}^{+\infty} \sum_{m=-n}^{+n} u_n^m j_n(k|\boldsymbol{\xi}|) Y_n^m(\hat{\boldsymbol{\xi}}) \quad (\boldsymbol{\xi} \in B),$$

$$w(\boldsymbol{\xi}) = \sum_{n=0}^{+\infty} \sum_{m=-n}^{+n} w_n^m j_n(\gamma k|\boldsymbol{\xi}|) Y_n^m(\hat{\boldsymbol{\xi}}) \quad (\boldsymbol{\xi} \in B). \tag{6.3.22}$$

Thanks to Funk-Hecke formula (6.B.5), one clearly has that u_g is a Herglotz wave function as a series of such functions. Then owing to boundary conditions (6.2.11c) and (6.2.11d) one obtains that there exists a non trivial pair of solutions u_g and w if and only if there exists $n_{\rm o} \in \mathbb{N}$ and $k \in \mathbb{R}$, $k > 0$ such that
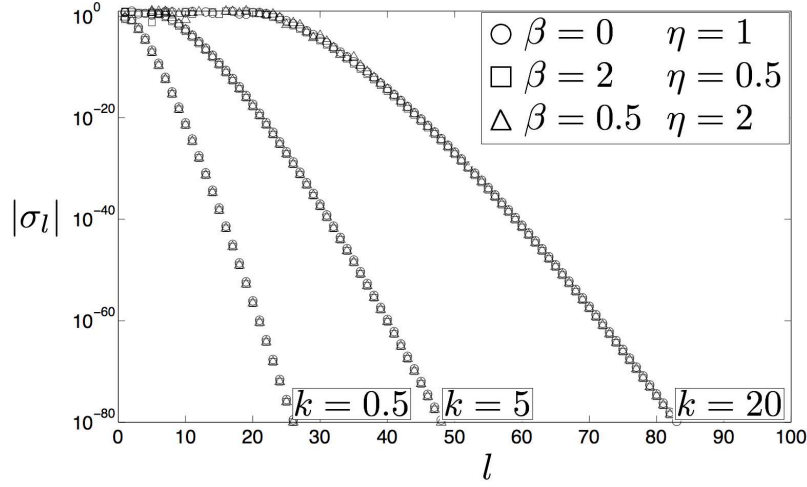
Figure 6.5: *Behavior of singular values depending on frequency and material parameters*

$$\alpha_{n_o} j_{n_o}(k) = j'_{n_o}(k), \tag{6.3.23}$$

where the term α_{n_o} is defined in (6.3.3). In particular, it is noticeable that (6.3.23) implies that the coefficient $\Lambda_{n_o}(\beta, \eta)$ in (6.3.4) is null.

Since the focus is made on the existence of transmission eigenvalues in the problem considered, one can restrict the study to non trivial solutions (6.3.22) depending only on $|\boldsymbol{\xi}|$, i.e. $u_g(\boldsymbol{\xi}) = u_o j_o(k|\boldsymbol{\xi}|)$ and $w(\boldsymbol{\xi}) = w_o j_o(\gamma k|\boldsymbol{\xi}|)$, which characterize values k solutions of (6.3.23) with $n_o = 0$. In the case considered of the scattering by a penetrable obstacle, this result is consistent with the result in the more restrictive study Colton et al. (2007), since $j_o(t) = \sin t / t$. The Figure 6.6 represents the function $J_o(k) = \alpha_o j_o(k) - j'_o(k)$ for different values of the material parameters and characterizes the existence of transmission eigenvalues k for which $J_o(k) = 0$. This example illustrates that such values do exist, and it is actually possible to show that they constitute an infinite countable set.

Analytical expression

By virtue of the spherical-harmonics expansion (6.3.2) of the scattered field, the indicator function $g_{\boldsymbol{z}}$ featured in the linear sampling equation (6.2.10) can now be computed analytically provided that k is not a transmission eigenvalue. For a given sampling point $\boldsymbol{z} \in \overset{\circ}{S^{\text{obs}}}$, then $g_{\boldsymbol{z}} \in L^2(\Sigma)$ can be expanded onto the set of spherical harmonics as

$$g_{\boldsymbol{z}}(\boldsymbol{\delta}) = \sum_{n=0}^{+\infty} \sum_{m=-n}^{+n} [g_{\boldsymbol{z}}]_n^m Y_n^m(\boldsymbol{\delta}) \quad (\forall \boldsymbol{\delta} \in \Sigma). \tag{6.3.24}$$

owing to the definition of the set Σ of plane wave unit incidence directions for which $|\boldsymbol{\delta}| = 1$. Thus, with relations (6.3.4), (6.B.2), and spherical harmonics orthonormality (6.B.10), equation (6.3.24) reads

$$g_{\boldsymbol{z}}(\boldsymbol{\delta}) = \frac{k}{(4\pi)^2} \sum_{n=0}^{+\infty} \frac{(2n+1)}{i^{l-1} \Lambda_n(\beta, \eta)} j_n(k|\boldsymbol{z}|) P_n(\hat{\boldsymbol{z}} \cdot \boldsymbol{\delta}) \quad (\forall \boldsymbol{\delta} \in \Sigma). \tag{6.3.25}$$

(a) $\beta = 0.5 \quad \eta = 0.1$

(b) $\beta = 4 \quad \eta = 2$
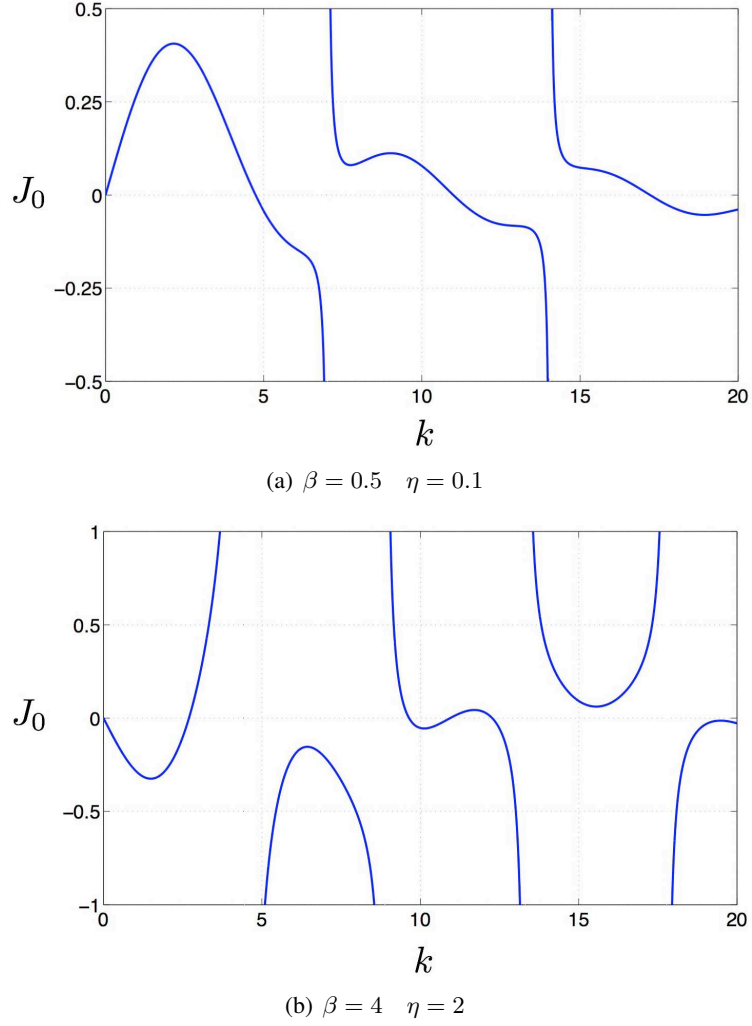
Figure 6.6: *Transmission eigenvalues depending on material parameters*

since $\Lambda_n(\beta, \eta) \neq 0$ for all $n \in \mathbb{N}$ if k is not a transmission eigenvalue.

Regularized solution

The previous section establishes the existence of the solution (6.3.25) to the linear sampling equation (6.2.10). Unfortunately, this solution does not belong in $L^2(\Sigma)$ as shown in the sequel. From the addition theorem (6.B.4) and spherical harmonics orthonormality condition (6.B.2) and finally (6.B.6), the $L^2(\Sigma)$-norm of the indicator function can be written as

$$\|g_{\boldsymbol{z}}\|_{L^2(\Sigma)}^2 = \frac{k^2}{(4\pi)^3} \sum_{n=0}^{+\infty} (2n+1) \left(\frac{j_n(k|\boldsymbol{z}|)}{|\Lambda_n(\beta, \eta)|} \right)^2. \tag{6.3.26}$$

Next, by means of the results in Appendix 6.C, one finds that

$$(2n+1)\left(\frac{j_n(k|\boldsymbol{z}|)}{|\Lambda_n(\beta,\eta)|}\right)^2 \underset{n\to\infty}{=} \frac{4}{k^2}\left(\frac{1+\beta}{1-\beta}\right)^2\left(\frac{2|\boldsymbol{z}|}{ek}\right)^{2n}n^{2n+1}\left(1+O\left(\frac{1}{n}\right)\right). \qquad (6.3.27)$$

From which it clearly follows that

$$\|g_{\boldsymbol{z}}\|_{L^2(\Sigma)} = +\infty. \qquad (6.3.28)$$

This result is not surprising since the countable spectrum of singular values (6.3.19) of operator $\mathcal{S}$ has a single point of accumulation at zero. The blow-off feature of the $L^2(\Sigma)$-norm of $g_{\boldsymbol{z}}$ can therefore be attributed to the smallest singular values. Then following the idea proposed in Collino et al. (2003) for electromagnetism, this solution can be regularized by truncation of the spectrum for sufficiently small eigenvalues.

Numerical results

On the Figure 6.7, one has represented the norm (6.3.26) of the indicator function provided by the linear sampling method for a truncation of singular values (6.3.19) smallest than 10^{-5}. Unlike the topological sensitivity method, there is no need of any *prior* information on the material behavior of the unknown obstacle, and the term Λ_n appearing in (6.3.26) comes from the exact knowledge of the scattered field (6.3.4). As highlighted by the Figure 6.7, these material properties have a little influence on the indicator function which behaves as expected in paragraph 6.2.2.

Nevertheless, as observed previously in Collino et al. (2003) in electromagnetism, it appears that for any sampling point $\boldsymbol{z}$ far from the obstacle boundary ∂B one has $\|g_{\boldsymbol{z}}\|^2_{L^2(\Sigma)} \gg 1$, while $\|g_{\boldsymbol{z}}\|^2_{L^2(\Sigma)}$ is relatively small for $|\boldsymbol{z}| \ll 1$. Moreover the transition region seems frequency dependent, so that for low frequency ($k = 5$), the interface ∂B is not identified with sufficient accuracy, whereas high frequency ($k = 20$) gives reasonable reconstruction of the obstacle.

6.4 Effect of noisy data

One of the key parameters affecting the quality of the identification with techniques such as the topological sensitivity method or the linear sampling method is the use of noisy data. This issue is discussed in this section to highlight the contrasting behaviors of the two methods. Thus, let ν denote a noise distribution over the observation surface defining a noisy measurement $\tilde{v}$ of the scattered field v such that

$$\tilde{v}(\boldsymbol{\xi},\boldsymbol{\delta}) = v(\boldsymbol{\xi},\boldsymbol{\delta}) + \nu(\boldsymbol{\xi}) \quad (\boldsymbol{\xi} \in S^{\text{obs}}, \boldsymbol{\delta} \in \Sigma). \qquad (6.4.1)$$

6.4.1 Topological sensitivity method

Let $\tilde{\mathbb{T}}$ denote the noisy topological derivative resulting from the noisy data (6.4.1), which is characterized by a noisy misfit function $\tilde{\varphi}$. Using the adjoint field formulation (6.2.7) and (6.2.9), the topological derivative can be expressed without loss of generality by
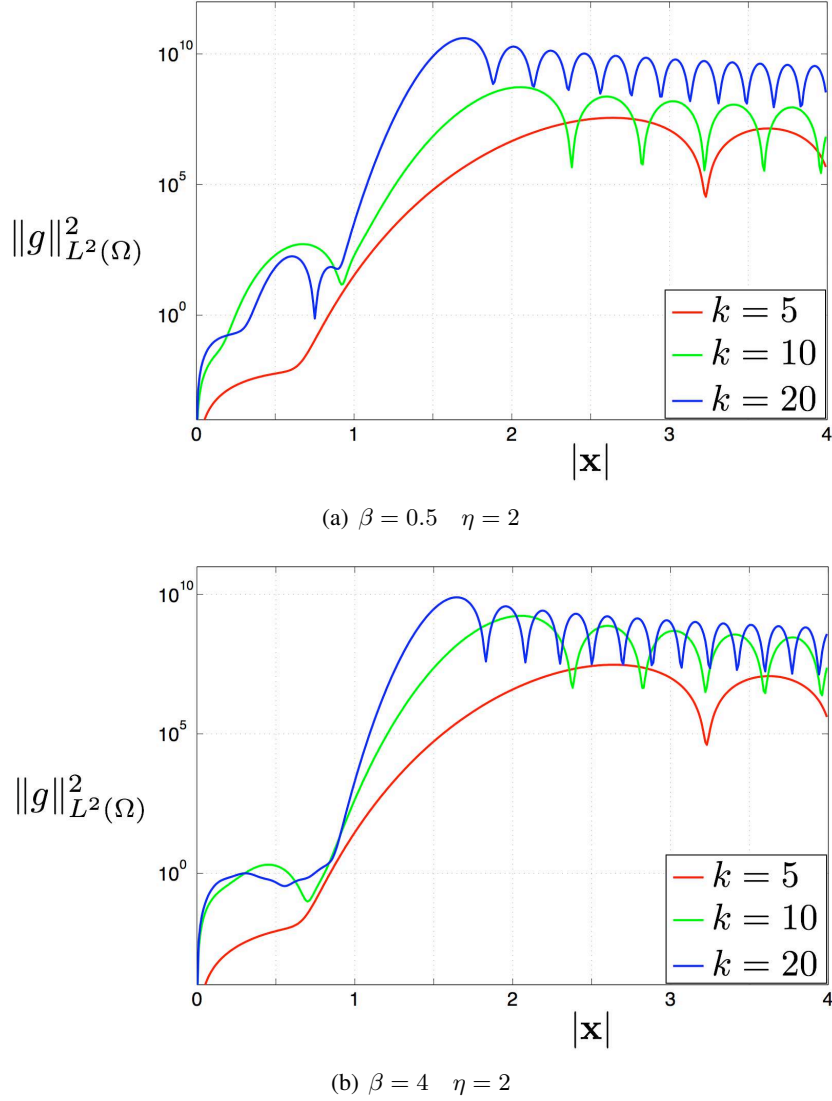
(a) $\beta = 0.5$ $\eta = 2$

(b) $\beta = 4$ $\eta = 2$

Figure 6.7: *Indicator from the linear sampling method depending on frequency and material parameters*

$$\mathbb{T}(\boldsymbol{z}, \beta, \eta) = \int_{\Sigma} \int_{S^{\text{obs}}} \Re \left\{ \frac{\partial \varphi}{\partial u}(u, \boldsymbol{\zeta}, \boldsymbol{\delta}) \left[(1 - \beta) \boldsymbol{\nabla}_{\boldsymbol{z}} G(\boldsymbol{z}, \boldsymbol{\zeta}) \cdot \boldsymbol{\mathcal{A}} \cdot \boldsymbol{\nabla} u(\boldsymbol{z}, \boldsymbol{\delta}) \right. \right.$$
$$\left. \left. - (1 - \eta) k^2 G(\boldsymbol{z}, \boldsymbol{\zeta}) u(\boldsymbol{z}, \boldsymbol{\delta}) \right] \right\} (\boldsymbol{z}, \boldsymbol{\delta}) \, \mathrm{d}S_\zeta \, \mathrm{d}S_\delta. \qquad (6.4.2)$$

where $\boldsymbol{\nabla}_{\boldsymbol{z}}$ involves partial derivative with respect to $\boldsymbol{z}$. Since the noisy counterpart of the topological derivative is obtained by replacing φ by $\tilde{\varphi}$ in the previous relation, the perturbation $\mathbb{T}_\nu$ induced by the noisy measurement can by defined as

$$|\mathbb{T}_\nu|(\boldsymbol{z},\beta,\eta) = |\tilde{\mathbb{T}} - \mathbb{T}|(\boldsymbol{z},\beta,\eta) = \left| \int_\Sigma \int_{S^{\mathrm{obs}}} \Re \left\{ \left(\frac{\partial \tilde{\varphi}}{\partial u} - \frac{\partial \varphi}{\partial u} \right) (u,\boldsymbol{\zeta},\boldsymbol{\delta}) \cdot \right. \right.$$
$$\left. \left. \left[(1-\beta) \boldsymbol{\nabla}_{\boldsymbol{z}} G(\boldsymbol{z},\boldsymbol{\zeta}) \cdot \boldsymbol{\mathcal{A}} \cdot \boldsymbol{\nabla} u(\boldsymbol{z},\boldsymbol{\delta}) - (1-\eta) k^2 G(\boldsymbol{z},\boldsymbol{\zeta}) u(\boldsymbol{z},\boldsymbol{\delta}) \right] \right\} (\boldsymbol{z},\boldsymbol{\delta}) \, \mathrm{d}S_\zeta \, \mathrm{d}S_\delta \right|. \tag{6.4.3}$$

An upper bound for the perturbation can be then deduced as

$$|\mathbb{T}_\nu|(\boldsymbol{z},\beta,\eta) \leqslant C(\boldsymbol{z},\beta,\eta) \left\| \frac{\partial \tilde{\varphi}}{\partial u} - \frac{\partial \varphi}{\partial u} \right\|_{L^2(S\mathrm{obs}\times\Sigma)}, \tag{6.4.4}$$

where the function C of the point $\boldsymbol{z}$ is defined with an intermediate constant c depending only on the material parameters through

$$C(\boldsymbol{z},\beta,\eta) = c(\beta,\eta) \left(\|\boldsymbol{\nabla}_{\boldsymbol{z}} G(\boldsymbol{z},\cdot)\|_{L^2(S^{\mathrm{obs}})} \|\boldsymbol{\nabla} u(\boldsymbol{z},\cdot)\|_{L^2(\Sigma)} + \|G(\boldsymbol{z},\cdot)\|_{L^2(S^{\mathrm{obs}})} \|u(\boldsymbol{z},\cdot)\|_{L^2(\Sigma)} \right), \tag{6.4.5}$$

and

$$\left\| \frac{\partial \tilde{\varphi}}{\partial u} - \frac{\partial \varphi}{\partial u} \right\|^2_{L^2(S\mathrm{obs}\times\Sigma)} = \int_\Sigma \int_{S^{\mathrm{obs}}} \left| \frac{\partial \tilde{\varphi}}{\partial u} - \frac{\partial \varphi}{\partial u} \right|^2 (\boldsymbol{\zeta},\boldsymbol{\delta}) \, \mathrm{d}S_\zeta \, \mathrm{d}S_\delta. \tag{6.4.6}$$

The right-hand side of the inequality (6.4.4) is related to the global amount of noise in the measurements, and in the case of the least-squares misfit function considered herein, it reduces to

$$\left\| \frac{\partial \tilde{\varphi}}{\partial u} - \frac{\partial \varphi}{\partial u} \right\|_{L^2(S\mathrm{obs}\times\Sigma)} = \|\tilde{v} - v\|_{L^2(S\mathrm{obs}\times\Sigma)} = |\Sigma|^{\frac{1}{2}} \cdot \|\nu\|_{L^2(S\mathrm{obs})}. \tag{6.4.7}$$

Since $\boldsymbol{z} \notin S^{\mathrm{obs}}$ and $\boldsymbol{z} \notin \Sigma$, the function C defined in (6.4.5) is clearly bounded, which implies the boundedness of the perturbation of the topological derivative. Thus, the robustness of the topological sensitivity method is highlighted in the inequality (6.4.4) and is essentially a consequence of the regularity of the Green's function and the incident field. Moreover, if the use of a least-squares misfit function involves that the perturbation of the topological derivative depends linearly on the noise, a misfit function of higher order can provide even more regularization against such perturbation.

6.4.2 Linear sampling method

Owing to the description of the linear sampling method (6.2.10), let $\tilde{\mathcal{S}}$ denote a noisy scattered operator, and let $\tilde{g}_{\boldsymbol{z}} \in L^2(\Sigma)$ be a solution of the integral equation

$$[\tilde{\mathcal{S}} \tilde{g}_{\boldsymbol{z}}](\boldsymbol{\xi}) = \int_\Sigma \tilde{v}(\boldsymbol{\xi},\boldsymbol{\delta}) \tilde{g}_{\boldsymbol{z}}(\boldsymbol{\delta}) \, \mathrm{d}S_\delta = G(\boldsymbol{\xi},\boldsymbol{z}) \quad (\forall \boldsymbol{\xi} \in S^{\mathrm{obs}}). \tag{6.4.8}$$

This operator can then be decomposed as $\tilde{\mathcal{S}} = \mathcal{S} + \mathcal{S}_\nu$, where $\mathcal{S}_\nu$ is the perturbation induced by the noise and which corresponds to the same decomposition of the solution $\tilde{g}_{\boldsymbol{z}}$ such that $\tilde{g}_{\boldsymbol{z}} = g_{\boldsymbol{z}} + g_{\boldsymbol{z},\nu}$. Equations (6.2.10) and (6.4.8) provide then

$$[(\mathcal{S} + \mathcal{S}_\nu)(g_{\boldsymbol{z}} + g_{\boldsymbol{z},\nu})](\boldsymbol{\xi}) = [\mathcal{S}g_{\boldsymbol{z}}](\boldsymbol{\xi}) \quad (\forall \boldsymbol{\xi} \in S^{\mathrm{obs}}). \tag{6.4.9}$$

Using a classical operator norm (see e.g. McLean (2000)) on $\mathcal{L}[L^2(\Sigma), L^2(S^{\mathrm{obs}})]$ denoted by $\|\cdot\|_{\mathrm{op}}$, it can be deduced that

$$\frac{\|g_{\boldsymbol{z},\nu}\|_{L^2(\Sigma)}}{\|g_{\boldsymbol{z}} + g_{\boldsymbol{z},\nu}\|_{L^2(\Sigma)}} \leqslant \|\mathcal{S}^{-1}\|_{\mathrm{op}}\|\mathcal{S}_\nu\|_{\mathrm{op}}, \tag{6.4.10}$$

which can be recast in

$$\frac{\|g_{\boldsymbol{z},\nu}\|_{L^2(\Sigma)}}{\|g_{\boldsymbol{z}} + g_{\boldsymbol{z},\nu}\|_{L^2(\Sigma)}} \leqslant \mathrm{Cond}(\mathcal{S})\frac{\|\mathcal{S}_\nu\|_{\mathrm{op}}}{\|\mathcal{S}\|_{\mathrm{op}}}, \tag{6.4.11}$$

where $\mathrm{Cond}(\mathcal{S}) = \|\mathcal{S}\|_{\mathrm{op}}\|\mathcal{S}^{-1}\|_{\mathrm{op}}$ stands for the condition number of the operator $\mathcal{S}$.
Since the operator $\mathcal{S}$ is compact, its singular values accumulate at zero and then $\|\mathcal{S}^{-1}\|_{\mathrm{op}} \gg 1$. This implies that $\mathcal{S}$ is ill-conditionned, and from the inequalities (6.4.10) and (6.4.11) it can be seen that the relative error on the indicator provided by the method results from a large amplification of the perturbation on the scattered operator. Thus the use of the linear sampling method requires an efficient regularization of this operator such as Tikhonov regularization widely employed in applications (Cakoni and Colton, 2006).

6.5   Conclusion

In this study, the acoustic inverse scattering by a penetrable obstacle is investigated by way of non iterative techniques that are the topological sensitivity and the linear sampling methods. To provide a common framework for the assessment and the comparison of the two methods, the forward problem of scattering by a sphere is solved analytically in a general setting which emphasizes the influence of the combined material properties of the background medium and the obstacle. On one hand, the topological sensitivity method, associated with the heuristic interpretation of an infinitesimal perturbation of a cost functional, is implemented via an adjoint field formulation which allows the use of generic measurements of the scattered fields. The closed form of the indicator function obtained permits a numerical investigation of its critical dependence on the material parameters involved in the problem, as well as its behavior as a function of the frequency of the excitation. On the other hand the analytical implementation of the linear sampling method, which is supported by key theoretical results, emphasizes the crucial role of the interior transmission problem characterizing frequency values at which the method is ineffective. Apart from this discrete countable set of particular values, the focus is made on the influence of the frequency on the accuracy of the indicator. These methods are then implemented in formulations which take into account partial and discrete monitoring of the scattered fields. In this specific setting, numerically fast computations are of particular interest with the use of separation between variables of observation and sampling points. Finally, special attention is given to characterize and compare the effects of the use of noisy data on the two methods that are formulated in a general setting.

6.A Partial and discrete observations

This section is concerned with the identification of the obstacle B within the framework of the foregoing discussion in situations where n^{obs} discrete observation points, located on a part of a non-concentric sphere $\mathcal{O} = \{\boldsymbol{\zeta}_p, p \in \{1, \ldots, n^{\text{obs}}\}\}$, are used to monitor the scattered field. The set of sampling points is denoted $\mathcal{D}$. Special attention is given to reducing numerical cost by a method of separation of variables.
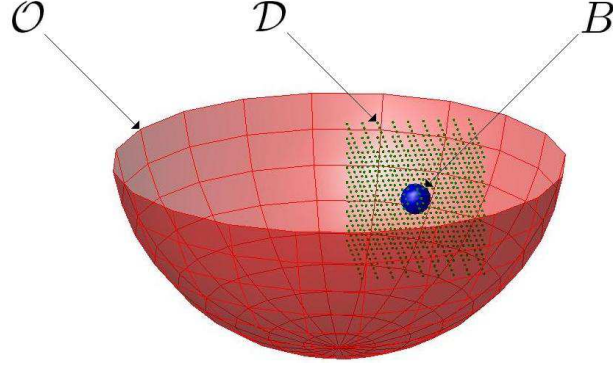
Figure 6.8: *Limited observation in obstacle identification*

6.A.1 Topological sensitivity method

Semi-analytical expression

With reference to the integral formulation (6.3.8), if the set of observation points is discrete a corresponding discrete adjoint field û is defined by

$$\hat{u}(\boldsymbol{\xi}, \boldsymbol{\delta}) = - \sum_{\boldsymbol{\zeta} \in \mathcal{O}} \overline{v}(\boldsymbol{\zeta}, \boldsymbol{\delta}) G(\boldsymbol{\xi}, \boldsymbol{\zeta}) \quad (\boldsymbol{\xi} \in \mathcal{D}, \boldsymbol{\delta} \in \Sigma), \tag{6.A.1}$$

where the scattered field is given by (6.3.4). Owing to the results of the previous section, the choice of the sets $\mathcal{O}$ and $\mathcal{D}$ to ensure the condition $\forall (\boldsymbol{\zeta}, \boldsymbol{\xi}) \in \mathcal{O} \times \mathcal{D}, |\boldsymbol{\zeta}| > |\boldsymbol{\xi}|$ can be made without loss of generality. Then using the Green's function expansion (6.B.10), the adjoint field can be expressed by

$$\hat{u}(\boldsymbol{\xi}, \boldsymbol{\delta}) = \frac{k}{4\pi} \sum_{\boldsymbol{\zeta} \in \mathcal{O}} \sum_{n=0}^{+\infty} \sum_{n'=0}^{+\infty} (-i)^{n+1} (2n+1)(2n'+1) \overline{\Lambda_n}(\beta, \eta) \overline{h_n}(k|\boldsymbol{\zeta}|) h_{n'}(k|\boldsymbol{\zeta}|) j_{n'}(k|\boldsymbol{\xi}|) P_n(\hat{\boldsymbol{\zeta}} \cdot \boldsymbol{\delta}) P_{n'}(\hat{\boldsymbol{\zeta}} \cdot \hat{\boldsymbol{\xi}}).$$
$$\tag{6.A.2}$$

Once again, for a given sampling point $\boldsymbol{z} \in \mathcal{D}$, using equations (6.A.2) and (6.B.3), property (6.B.2) and summation over $\boldsymbol{\delta} \in \Sigma$, a discrete topological sensitivity can be deduced as

$$
\mathsf{T}(\boldsymbol{z}, \beta, \eta) = - k \sum_{\boldsymbol{\zeta} \in \mathcal{O}} \sum_{n=0}^{+\infty} \sum_{n'=0}^{+\infty} \Re \Bigg\{ i(2n+1)(2n'+1)\overline{\Lambda_n}(\beta, \eta)\overline{h_n}(k|\boldsymbol{\zeta}|)h_{n'}(k|\boldsymbol{\zeta}|) \cdot
$$
$$
\left[j_n(k|\boldsymbol{z}|)j_{n'}(k|\boldsymbol{z}|) \left(\frac{3(1-\beta)}{2+\beta} \boldsymbol{\nabla} P_n(\hat{\boldsymbol{\zeta}} \cdot \hat{\boldsymbol{z}}) \cdot \boldsymbol{\nabla} P_{n'}(\hat{\boldsymbol{\zeta}} \cdot \hat{\boldsymbol{z}}) - (1-\eta)k^2 P_n(\hat{\boldsymbol{\zeta}} \cdot \hat{\boldsymbol{z}})P_{n'}(\hat{\boldsymbol{\zeta}} \cdot \hat{\boldsymbol{z}}) \right) \right.
$$
$$
\left. + \frac{3k^2(1-\beta)}{2+\beta} j_n'(k|\boldsymbol{z}|)j_{n'}'(k|\boldsymbol{z}|) P_n(\hat{\boldsymbol{\zeta}} \cdot \hat{\boldsymbol{z}})P_{n'}(\hat{\boldsymbol{\zeta}} \cdot \hat{\boldsymbol{z}}) \right] \Bigg\}.
$$

$$(6.A.3)$$

Using the addition theorem (6.B.4), the previous relation can written as

$$
\mathsf{T}(\boldsymbol{z}, \beta, \eta) = - (4\pi)^2 k \sum_{\boldsymbol{\zeta} \in \mathcal{O}} \sum_{n=0}^{+\infty} \sum_{m=-n}^{+n} \sum_{n'=0}^{+\infty} \sum_{m'=-n'}^{+n'} \Re \Bigg\{ i\overline{\Lambda_n}(\beta, \eta)\overline{h_n}(k|\boldsymbol{\zeta}|)h_{n'}(k|\boldsymbol{\zeta}|)Y_n^m(\hat{\boldsymbol{\zeta}})\overline{Y_{n'}^{m'}}(\hat{\boldsymbol{\zeta}}) \cdot
$$
$$
\left[j_n(k|\boldsymbol{z}|)j_{n'}(k|\boldsymbol{z}|) \left(\frac{3(1-\beta)}{2+\beta} \boldsymbol{\nabla} \overline{Y_n^m}(\hat{\boldsymbol{z}}) \cdot \boldsymbol{\nabla} Y_{n'}^{m'}(\hat{\boldsymbol{z}}) - (1-\eta)k^2 \overline{Y_n^m}(\hat{\boldsymbol{z}})Y_{n'}^{m'}(\hat{\boldsymbol{z}}) \right) \right.
$$
$$
\left. + \frac{3k^2(1-\beta)}{2+\beta} j_n'(k|\boldsymbol{z}|)j_{n'}'(k|\boldsymbol{z}|) \overline{Y_n^m}(\hat{\boldsymbol{z}})Y_{n'}^{m'}(\hat{\boldsymbol{z}}) \right] \Bigg\}.
$$

$$(6.A.4)$$

where the angular derivatives of the spherical harmonics are given by (6.B.11). One can check that the relation (6.A.4) can be transformed into (6.3.11) in the case of an observation on a complete sphere and using properties (6.B.2), (6.B.6) and (6.B.8).

Numerical implementation

The separation of variables achieved in the Green's function expansion (6.B.10) can be used to reduce the numerical computation cost. This is in fact, the idea of the fast multipole method (Nishimura, 2002). The topological sensitivity (6.A.4) is of the form

$$
\mathsf{T}(\boldsymbol{z}, \beta, \eta) = \sum_{\boldsymbol{\zeta} \in \mathcal{O}} \sum_{n=0}^{+\infty} \sum_{m=-n}^{+n} \sum_{n'=0}^{+\infty} \sum_{m'=-n'}^{+n'} \Re \left\{ \mathsf{a}(n, m, \boldsymbol{\zeta})\mathsf{b}(n, m, \boldsymbol{z})\mathsf{c}(n', m', \boldsymbol{\zeta})\mathsf{d}(n', m', \boldsymbol{z}) \right\}, \quad (6.A.5)
$$

where, owing to previous section and Appendix 6.C, the sums over n and n' can be truncated at n_{o} and n_{o}' respectively. Nevertheless, in practice the truncation orders are set to be equal $n_{\mathrm{o}} = n_{\mathrm{o}}'$. For the sake of brevity let us introduce the function of integer $\mathbb{M} : m \mapsto \mathbb{M}(m) = \max\{n \in \mathbb{N}, \mathrm{floor}(n^2/m) = 0\}$. Since $\mathcal{O} = \{\boldsymbol{\zeta}_p, p \in \{1, \dots, n^{\mathrm{obs}}\}\}$, the following quantities are computed

- $\mathsf{A}(n_{\mathrm{o}}, \mathcal{O}) \in \mathcal{M}_{n^{\mathrm{obs}}, (n_{\mathrm{o}}+1)^2}(\mathbb{C})$ whose entry indexed by (p, q) is defined by

$\mathsf{A}(n_{\mathrm{o}}, \mathcal{O})_{pq} = \mathsf{a}(n, m, \boldsymbol{\zeta}_p)$ with $n = \mathbb{M}(q)$ and $m = q - (n^2 + n + 1)$

- $\mathsf{B}(n_{\mathrm{o}}, \boldsymbol{z}) \in \mathcal{M}_{(n_{\mathrm{o}}+1)^2, 1}(\mathbb{C})$ whose entry p is given by

$\mathsf{B}(n_{\mathrm{o}}, \boldsymbol{z})_p = \mathsf{b}(n, m, \boldsymbol{z})$ with $n = \mathbb{M}(p)$ and $m = p - (n^2 + n + 1)$

- $\mathsf{C}(n_{\mathrm{o}}, \mathcal{O}) \in \mathcal{M}_{(n_{\mathrm{o}}+1)^2, n^{\mathrm{obs}}}(\mathbb{C})$ whose entry (p, q) is

$\mathsf{C}(n_{\mathrm{o}}, \mathcal{O})_{pq} = \mathsf{c}(n', m', \boldsymbol{\zeta}_q)$ with $n' = \mathbb{M}(p)$ and $m' = p - (n'^2 + n' + 1)$

- $\mathsf{D}(n_{\mathrm{o}}, \boldsymbol{z}) \in \mathcal{M}_{1, (n_{\mathrm{o}}+1)^2}(\mathbb{C})$ with

$\mathsf{D}(n_{\mathrm{o}}, \boldsymbol{z})_p = \mathsf{d}(n', m', \boldsymbol{z})$ with $n' = \mathbb{M}(p)$ and $m' = p - (n'^2 + n' + 1)$.

$$(6.A.6)$$

Then, for each $\boldsymbol{z} \in \mathcal{D}$, the topological sensitivity (6.A.3) can be computed as

$$\mathsf{T}(\boldsymbol{z}, \beta, \eta) = \Re \left\{ \mathsf{D}(n_{\mathrm{o}}, \boldsymbol{z}) \mathsf{C}(n_{\mathrm{o}}, \mathcal{O}) \mathsf{A}(n_{\mathrm{o}}, \mathcal{O}) \mathsf{B}(n_{\mathrm{o}}, \boldsymbol{z}) \right\}, \tag{6.A.7}$$

where the product $\mathsf{C}(n_{\mathrm{o}}, \mathcal{O}) \mathsf{A}(n_{\mathrm{o}}, \mathcal{O})$ is computed only once.

6.A.2 Linear sampling method

Semi-analytical expression

In the case of discrete and limited observations described earlier, for a given sampling point $\boldsymbol{z} \in \mathcal{D}$ and provided that k is not a transmission eigenvalue, one seeks for the function $\mathsf{g}_{\boldsymbol{z}} \in L^2(\Sigma)$ as a solution of the linear integral equation

$$[\mathcal{S}\mathsf{g}_{\boldsymbol{z}}](\boldsymbol{\zeta}) = G(\boldsymbol{\zeta}, \boldsymbol{z}) \quad (\forall \boldsymbol{\zeta} \in \mathcal{O}). \tag{6.A.8}$$

The use of (6.3.4) and the expansion of $\mathsf{g}_{\boldsymbol{z}}$ onto the set of spherical harmonics (see (6.3.24)) leads to

$$[\mathcal{S}\mathsf{g}_{\boldsymbol{z}}](\boldsymbol{\zeta}) = 4\pi \sum_{n=0}^{+\infty} \sum_{m=-n}^{+n} i^n \Lambda_n(\beta, \eta) h_n(k|\boldsymbol{\zeta}|) [\mathsf{g}_{\boldsymbol{z}}]_n^m Y_n^m(\hat{\boldsymbol{\zeta}}) \quad (\forall \boldsymbol{\zeta} \in \mathcal{O}). \tag{6.A.9}$$

Thus, with reference to the Green's function expansion (6.B.10), equation (6.A.8) can be solved numerically. Moreover, with reference to the previous section, this *ill-posed* problem can be regularized via truncation of the n-indexed summations.

Numerical implementation

One seeks the coefficients $\left([\mathsf{g}_{\boldsymbol{z}}]_n^m\right)_{n \leqslant n_{\mathrm{o}}, -n \leqslant m \leqslant +n}$, solution of the discrete problem for all $\boldsymbol{\zeta} \in \mathcal{O}$

$$\sum_{n=0}^{n_{\mathrm{o}}} \sum_{m=-n}^{+n} i^n \Lambda_n(\beta, \eta) h_n(k|\boldsymbol{\zeta}|) [\mathsf{g}_{\boldsymbol{z}}]_n^m Y_n^m(\hat{\boldsymbol{\zeta}}) = \frac{ik}{4\pi} \sum_{n'=0}^{n'_{\mathrm{o}}} \sum_{m'=-n'}^{+n'} h_{n'}(k|\boldsymbol{\zeta}|) j_{n'}(k|\boldsymbol{z}|) \overline{Y_{n'}^{m'}}(\hat{\boldsymbol{z}}) Y_{n'}^{m'}(\hat{\boldsymbol{\zeta}}),$$

$$(6.A.10)$$

where $\mathcal{O} = \{\boldsymbol{\zeta}_p, p \in \{1, \dots, n^{\mathrm{obs}}\}\}$ and $\Lambda_n(\beta, \eta) \neq 0$ for all $n \in \mathbb{N}$ (see paragraph 6.3.3) if k is not a transmission eigenvalue. For numerical purposes, the truncation orders are set to be equal $n_{\mathrm{o}} = n_{\mathrm{o}}'$, then the following quantities are computed

- $\mathsf{S}(n_{\mathrm{o}}, \mathcal{O}) \in \mathcal{M}_{n^{\mathrm{obs}}, (n_{\mathrm{o}}+1)^2}(\mathbb{C})$ whose entry (p, q) is defined by

$$\mathsf{S}(n_{\mathrm{o}}, \mathcal{O})_{pq} = i^n \Lambda_n(\beta, \eta) h_n(k|\boldsymbol{\zeta}_p|) Y_n^m(\hat{\boldsymbol{\zeta}}_p) \text{ with } n = \mathbb{M}(q) \text{ and } m = q - (n^2 + n + 1)$$

- $\mathbf{g}_{\boldsymbol{z}} \in \mathcal{M}_{(n_{\mathrm{o}}+1)^2, 1}(\mathbb{C})$ which defines the unknowns at point x

$$[\mathbf{g}_{\boldsymbol{z}}]_p = [\mathbf{g}_{\boldsymbol{z}}]_n^m \text{ with } n = \mathbb{M}(p) \text{ and } m = p - (n^2 + n + 1)$$

- $\mathsf{E}(n_{\mathrm{o}}, \mathcal{O}) \in \mathcal{M}_{n^{\mathrm{obs}}, (n_{\mathrm{o}}+1)^2}(\mathbb{C})$ whose entry (p, q) is defined by

    (6.A.11)

$$\mathsf{E}(n_{\mathrm{o}}, \mathcal{O})_{pq} = \frac{ik}{4\pi} h_n(k|\boldsymbol{\zeta}_p|) Y_n^m(\hat{\boldsymbol{\zeta}}_p) \text{ with } n = \mathbb{M}(q) \text{ and } m = q - (n^2 + n + 1)$$

- $\mathsf{F}(n_{\mathrm{o}}, \boldsymbol{z}) \in \mathcal{M}_{(n_{\mathrm{o}}+1)^2, 1}(\mathbb{C})$ depending on point x with

$$\mathsf{F}(n_{\mathrm{o}}, \boldsymbol{z})_p = j_n(k|\boldsymbol{z}|) \overline{Y_n^m}(\hat{\boldsymbol{z}}) \text{ with } n = \mathbb{M}(p) \text{ and } m = p - (n^2 + n + 1).$$

Then, for each $\boldsymbol{z} \in \mathcal{D}$, one seeks for the solution $\mathbf{g}_{\boldsymbol{z}}$ of the equation

$$\mathsf{S}(n_{\mathrm{o}}, \mathcal{O}) \mathbf{g}_{\boldsymbol{z}} = \mathsf{E}(n_{\mathrm{o}}, \mathcal{O}) \mathsf{F}(n_{\mathrm{o}}, \boldsymbol{z}), \tag{6.A.12}$$

where the terms $\mathsf{S}(n_{\mathrm{o}}, \mathcal{O})$ and $\mathsf{E}(n_{\mathrm{o}}, \mathcal{O})$ are computed only once.

The resolution of the previous equation faces the problem that in general $n^{\mathrm{obs}} \neq (n_{\mathrm{o}}+1)^2$, so the systems (6.A.12) can be either an over or under-determined problem. Furthermore, the operator $\mathsf{S}(n_{\mathrm{o}}, \mathcal{O})$ inherits the compactness of $\mathcal{S}$. To deal with these issues, the solution $\mathbf{g}_{\boldsymbol{z}}$ is computed using a Moore-Penrose pseudoinverse based on the singular values decomposition of the operator. Then the $L^2(\Sigma)$-norm of the indicator function is given by

$$\|g_{\boldsymbol{z}}\|_{L^2(\Sigma)}^2 = \sum_{p=1}^{(n_{\mathrm{o}}+1)^2} |[\mathbf{g}_{\boldsymbol{z}}]_p|^2. \tag{6.A.13}$$

6.B Spherical harmonics and their properties

Noting $S = \{\boldsymbol{\zeta} \in \mathbb{R}^3, |\boldsymbol{\zeta}| = 1\}$ and Δ_S the angular part of the Laplacian (i.e. the Laplace-Beltrami operator), then the set of spherical harmonics $(Y_n^m)_{n \in \mathbb{N}, -n \leqslant m \leqslant +n}$ verifying

$$\Delta_S Y_n^m(\boldsymbol{\zeta}) + n(n+1) Y_n^m(\boldsymbol{\zeta}) = 0 \quad (\forall \boldsymbol{\zeta} \in S, \forall n \in \mathbb{N}, \forall m \in \{-n, \dots, n\}), \tag{6.B.1}$$

constitutes an orthonormal basis of $L^2(S)$, so

$$\int_S Y_n^m(\boldsymbol{\zeta}) \overline{Y_{n'}^{m'}}(\boldsymbol{\zeta}) \, \mathrm{d}S_\zeta = \delta_{nn'} \delta_{mm'} \quad (\forall (n, n') \in \mathbb{N}^2, \forall (m, m') \in \{-n, \dots, +n\} \times \{-n', \dots, +n'\}). \tag{6.B.2}$$

The Jacobi-Anger expansion (Abramowitz and Stegun, 1965) for plane wave in direction $\boldsymbol{\delta} \in \Sigma$ is expressed by

$$e^{ik\boldsymbol{\zeta}\cdot\boldsymbol{\delta}} = \sum_{n=0}^{+\infty}(2n+1)i^n j_n(k|\boldsymbol{\zeta}|)P_n(\hat{\boldsymbol{\zeta}}\cdot\boldsymbol{\delta}) \quad (\forall\boldsymbol{\zeta}\in\mathbb{R}^3, \boldsymbol{\delta}\in\Sigma), \tag{6.B.3}$$

where P_n denotes the n-order Legendre polynomial. The spherical harmonics verify also the addition theorem

$$P_n(\boldsymbol{\xi}\cdot\boldsymbol{\zeta}) = \frac{4\pi}{2n+1}\sum_{m=-n}^{+n}Y_n^m(\boldsymbol{\xi})\overline{Y_n^m}(\boldsymbol{\zeta}) \quad (\forall(\boldsymbol{\xi},\boldsymbol{\zeta})\in S^2), \tag{6.B.4}$$

so that from (6.B.3), (6.B.4) and (6.B.2) one can obtain the Funk-Hecke formula

$$\int_S e^{ik\boldsymbol{\zeta}\cdot\boldsymbol{\delta}}Y_n^m(\boldsymbol{\delta})\,\mathrm{d}S_\delta = 4\pi i^n j_n(k|\boldsymbol{\zeta}|)Y_n^m(\hat{\boldsymbol{\zeta}}) \quad (\forall\boldsymbol{\zeta}\in\mathbb{R}^3, \forall n\in\mathbb{N}, \forall m\in\{-n,\ldots,n\}). \tag{6.B.5}$$

Moreover $\forall n\in\mathbb{N}\ P_n(1) = 1$ so

$$\sum_{m=-n}^{+n}Y_n^m(\boldsymbol{\zeta})\overline{Y_n^m}(\boldsymbol{\zeta}) = \frac{2n+1}{4\pi} \quad (\forall\boldsymbol{\zeta}\in S). \tag{6.B.6}$$

Using the fact that

$$\boldsymbol{\nabla}Y_n^m(\boldsymbol{\zeta})\cdot\boldsymbol{\nabla}\overline{Y_n^m}(\boldsymbol{\zeta}) = \frac{1}{2}\left[\Delta_S(Y_n^m(\boldsymbol{\zeta})\overline{Y_n^m}(\boldsymbol{\zeta})) - \Delta_S Y_n^m(\boldsymbol{\zeta})\overline{Y_n^m}(\boldsymbol{\zeta}) - Y_n^m(\boldsymbol{\zeta})\Delta_S\overline{Y_n^m}(\boldsymbol{\zeta})\right], \tag{6.B.7}$$

then, with relations (6.B.1) and (6.B.6), one obtains

$$\sum_{m=-n}^{+n}\boldsymbol{\nabla}Y_n^m(\boldsymbol{\zeta})\cdot\boldsymbol{\nabla}\overline{Y_n^m}(\boldsymbol{\zeta}) = \frac{n(n+1)(2n+1)}{4\pi} \quad (\forall\boldsymbol{\zeta}\in S). \tag{6.B.8}$$

To expand the Green's function onto the set of spherical harmonics, let us introduce the Gegenbauer theorem (Abramowitz and Stegun, 1965)

$$\frac{e^{ik|\boldsymbol{\xi}-\boldsymbol{\zeta}|}}{|\boldsymbol{\xi}-\boldsymbol{\zeta}|} = ik\sum_{n=0}^{+\infty}(2n+1)h_n(k|\boldsymbol{\zeta}|)j_n(k|\boldsymbol{\xi}|)P_n(\hat{\boldsymbol{\xi}}\cdot\hat{\boldsymbol{\zeta}}) \quad \text{if } |\boldsymbol{\zeta}|>|\boldsymbol{\xi}|, \tag{6.B.9}$$

then with the addition theorem (6.B.4), the Green's function is given by

$$G(\boldsymbol{\xi},\boldsymbol{\zeta}) = ik\sum_{n=0}^{+\infty}\sum_{m=-n}^{+n}h_n(k|\boldsymbol{\zeta}|)j_n(k|\boldsymbol{\xi}|)Y_n^m(\hat{\boldsymbol{\xi}})\overline{Y_n^m}(\hat{\boldsymbol{\zeta}}) \quad \text{if } |\boldsymbol{\zeta}|>|\boldsymbol{\xi}|. \tag{6.B.10}$$

Finally, for a point $\boldsymbol{\zeta} = (\rho,\theta,\phi)$ in spherical coordinates, the derivative of spherical harmonics w.r.t. angles θ and ϕ are given by relations

$$\begin{cases} \dfrac{\partial Y_{\mathrm{o}}^0(\hat{\zeta})}{\partial \theta} = 0 \\[2mm] \dfrac{\partial Y_n^m(\hat{\zeta})}{\partial \theta} = \sqrt{\dfrac{(2n+1)(n+m+1)(n-m+1)}{(2n+3)}} \dfrac{Y_{n+1}^m(\hat{\zeta})}{\sin\theta} - \dfrac{n+1}{\tan\theta} Y_n^m(\hat{\zeta}) \\[2mm] \dfrac{\partial Y_n^m(\hat{\zeta})}{\partial \phi} = im Y_n^m(\hat{\zeta}). \end{cases} \qquad (6.\text{B}.11)$$

6.C   Asymptotic behavior of special functions and their derivatives

6.C.1   Spherical Bessel and Hankel functions of the first kind

The asymptotic behaviors of the spherical Bessel and Hankel functions of the first kind with respect to the order n are given by (Colton and Kress, 1992)

$$\begin{aligned} j_n(t) &\underset{n\to\infty}{=} t^n \frac{2^n n!}{(2n+1)!} \left(1 + O\left(\frac{1}{n}\right) \right), \\ h_n(t) &\underset{n\to\infty}{=} \frac{1}{it^n} \frac{(2n-1)!}{2^{n-1}(n-1)!} \left(1 + O\left(\frac{1}{n}\right) \right), \end{aligned} \qquad (6.\text{C}.1)$$

owing to Stirling formulae $n! \underset{n\to\infty}{\sim} \left(\frac{n}{e}\right)^n \sqrt{2\pi n}$, it can be deduced that

$$\begin{aligned} j_n(t) &\underset{n\to\infty}{=} \frac{1}{2n\sqrt{2}} \left(\frac{et}{2n}\right)^n \left(1 + O\left(\frac{1}{n}\right) \right), \\ h_n(t) &\underset{n\to\infty}{=} \frac{\sqrt{2}}{it} \left(\frac{2n}{et}\right)^n \left(1 + O\left(\frac{1}{n}\right) \right). \end{aligned} \qquad (6.\text{C}.2)$$

With respect to the argument t, one also has the following asymptotic behavior at 0

$$j_n(t) \underset{t\to 0}{=} \frac{2^n n!}{(2n+1)!} t^n \left(1 + O(t) \right), \qquad (6.\text{C}.3)$$

and at infinity

$$j_n(t) \underset{t\to\infty}{=} \frac{1}{t} \cos\left[t - \frac{n+1}{2}\pi \right] \left(1 + O\left(\frac{1}{t}\right) \right). \qquad (6.\text{C}.4)$$

6.C.2   Derivatives of spherical Bessel and Hankel functions

The derivatives of j_n and h_n w.r.t. their arguments are given by the recursion formula (Abramowitz and Stegun, 1965)

$$\text{For } f_n = j_n \text{ or } h_n \text{ then } f_n'(t) = \frac{n f_{n-1}(t) - (n+1) f_{n+1}(t)}{2n+1}, \qquad (6.\text{C}.5)$$

then their asymptotic behavior w.r.t. the order n can be deduced from (6.C.2) as

$$j_n'(t) \underset{n\to\infty}{=} \frac{1}{2t\sqrt{2}} \left(\frac{et}{2n}\right)^n \left(1 + O\left(\frac{1}{n}\right)\right),$$

$$h_n'(t) \underset{n\to\infty}{=} \frac{-n\sqrt{2}}{it^2} \left(\frac{2n}{et}\right)^n \left(1 + O\left(\frac{1}{n}\right)\right),$$

(6.C.6)

as well as w.r.t. the argument t one has at 0

$$j_n'(t) \underset{t\to 0}{=} \frac{2^n n!}{(2n+1)!} n t^{n-1} \left(1 + O(t)\right),$$

(6.C.7)

and at infinity

$$j_n'(t) \underset{t\to\infty}{=} \frac{1}{t} \cos\left[t - \frac{n}{2}\pi\right] \left(1 + O\left(\frac{1}{t}\right)\right).$$

(6.C.8)

6.C.3 Legendre polynomials

From Bateman (1953) the following result is due to Stieltjes

$$(\sin\theta)^{\frac{1}{2}} |P_n(\cos\theta)| < \left(\frac{2}{\pi n}\right)^{\frac{1}{2}} \quad (\forall\theta \in [0; \pi]).$$

(6.C.9)

Then, owing to Szegö (1939), the Laplace relation for the asymptotic behavior of Legendre polynomials precises this property with

$$P_n(\cos\theta) \underset{n\to\infty}{=} \left(\frac{2}{\pi n \sin\theta}\right)^{\frac{1}{2}} \cos\left[\left(n + \frac{1}{2}\right)\theta - \frac{\pi}{4}\right] \left(1 + O\left(\frac{1}{n}\right)\right) \quad (\forall\theta \in]0; \pi[).$$

(6.C.10)

6.C.4 Derivatives of Legendre polynomials

The Legendre polynomials derivatives can be expressed by means of the recurrence relation

$$\begin{cases} P_0'(x) = 0 \\ P_n'(x) = \dfrac{n(n+1)}{(2n+1)} \dfrac{P_{n-1}(x) - P_{n+1}(x)}{1 - x^2} & \text{if } n \neq 0. \end{cases}$$

(6.C.11)

Then, the asymptotic behavior is deduced from (6.C.10) as

$$P_n'(\cos\theta) \underset{n\to\infty}{=} \left(\frac{2n}{\pi \sin\theta}\right)^{\frac{1}{2}} \frac{\sin\left[\left(n + \frac{1}{2}\right)\theta - \frac{\pi}{4}\right]}{\sin\theta} \left(1 + O\left(\frac{1}{n}\right)\right) \quad (\forall\theta \in]0; \pi[).$$

(6.C.12)

Conclusion

Contents

Conclusions

The focus of the research described in this dissertation is the theory of inverse scattering in solid mechanics which aims at *detecting* and *identifying* scattering obstacles in an elastic background medium through the use of elastic or acoustic illuminating waves. Over the past decade, the limitations of customary treatments of the latter class of problems, that employ either weak scatterer approximation or non-linear optimization techniques, have spurred the development of the so-called sampling methods for obstacle reconstruction. These methods have in common a paradigm change in their approach to inverse scattering, in that they seek only a qualitative information about hidden scatterers within a computationally efficient and robust framework that makes use of the full-waveform measurements of the scattered field. The qualitative information that is recoverable by these methods can be ordered by the level of "complexity" as i) information on the presence of obstacles, ii) geometrical information on their location and shape, and iii) information on the material characteristics of a hidden obstacle. In this context, the present study is concerned with the advancement of two such sampling methods, namely the topological sensitivity approach and the linear sampling method that jointly carry a potential of detecting, reconstructing, and characterizing obstacles in an elastic solid with moderate computational effort.

Even though the question of possible theoretical links between the two methods is addressed via a simple but instructive analytical case in Chapter 6, the TS and LSM techniques rely, to a large extent, on fundamentally different concepts. In particular, the topological sensitivity method is based on the heuristic interpretation of the perturbation of a given cost functional generated by the introduction of an infinitesimal flaw, whereas the linear sampling method relies on the resolution of a linear integral equation of the first kind featuring a fundamental singular solution to the wave (Navier or Helmholtz) equation. The developments proposed in this study aim to i) address the unresolved theoretical issues of the LSM, ii) extend the range of application of both the TS and LSM techniques and iii) demonstrate their usefulness for practical applications.

By building up on earlier TS studies, the topological sensitivity method is implemented within a classical FEM computational platform in Chapter 1 to assess its ability to deal with time-domain inverse scattering problems, and constitutes a first comprehensive study of this kind. Chapter 2 introduces a novel extension of the method to deal with three-dimensional time-domain crack identification with an empha-

205

sis on on the ability of the TS approach to furnish a comprehensive "point-by-point" information on both crack presence and its local orientation (i.e. the normal on a crack surface). The study demonstrates that in contrast to the relatively involved, but mathematically rigorous, analysis required to arrive at the correct formulation of the topological gradient field, the subsequent numerical implementation is rather simple. This feature, together with a remarkable robustness of the TS method in situations involving noisy data, highlight the promise of this tool in the context of real-life engineering applications.

A comprehensive study of the linear sampling method in the context of acoustic inverse scattering, together with a novel perturbation study that for the first time provides clues towards its performance in a multi-frequency setting, is given in Chapter 3. For completeness, the multi-frequency developments are illustrated through both analytical and numerical examples. Chapter 4 is concerned with the study of the interior transmission problem for (visco-) elastic bodies, a non-traditional boundary-value problem whose issue of well-posedness is critical for the applicability and performance of the LSM. Finally, the characterization of the set of frequencies, for which the homogeneous interior transmission problem does not have a unique solution, which is a lynchpin toward extension of the linear sampling method toward multi-frequency inverse scattering and material characterization of a hidden scatterer, is addressed in Chapter 5 in a comprehensive study of the corresponding eigenvalue problem.

As mentioned earlier, Chapter 6 represents the first step toward exposing the commonalities between the TS and LSM techniques that makes use of an instructive analytical study.

Possible directions for future work

In what follows, suggestions are given for future work and developments on inverse scattering in solid mechanics in the context of the topological sensitivity approach and the linear sampling method.

Topological sensitivity method

Error in constitutive relation. To a large extent, previous topological sensitivity studies have focused on the mathematical developments of the small-defect asymptotics and on the use of the topological gradient as a flaw indicator function, rather than on the structure of the featured cost functional. In solid mechanics, energy-like cost functionals which measure the error in the constitutive relationship, are of particular relevance, as their use to quantify local perturbations of properties of a reference body spread out from the seminal work by Ladevèze and Leguillon (1983). The topological sensitivity of energy-like functionals has been only recently established by Ben Abda et al. (2009) for Stokes flow problems and by Bonnet (2010b) in elastodynamics. These studies may soon inspire others, on both theoretical and numerical aspects, contributing to a wider use of the topological sensitivity method within the solid mechanics community.

Configurations with heterogeneous media. Most of the work on the topological sensitivity has been concerned with the nucleation of an infinitesimal flaw in a homogeneous linear elastic solid. The literature addressing TS for heterogeneous background media is scarce, notably Carpio and Rapún (2008) for the Helmholtz equation and Guzina and Yuan (2009) that deals with heterogeneous viscoelastic bodies with piecewise-analytic distribution of the material parameters. Further extension to configurations with randomly distributed physical properties, is a challenging problem that has numerous applications. In this respect one can refer to Krée and Soize (1986) for an introduction to stochastic mechanics and Fouque et al. (2007) for an overview of wave propagation and time reversal method in random media.

Use of dimensional analysis toward the asymptotic perturbation studies. The use of dimensional analysis toward the development of the topological sensitivity approach may lead to significant simplification of the formulation and may represent a completely new avenue toward extending the TS studies for more general configurations. The work by Guzina and Yuan (2009) in the context of heterogeneous solids is, to the authors' knowledge, the first attempt to use dimensional analysis for a topological perturbation study.

Quantitative approach by higher-order expansions. The first-order asymptotic expansion of a given cost functional, in terms of the linear size of the infinitesimal domain perturbation, leads to the formulation of the corresponding topological gradient which is used for a *qualitative* geometrical identification of unknown scattering objects. High-order developments, that have been addressed in Rocha de Faria et al. (2009); Bonnet (2009, 2010a) for 2D potential problems and in Bonnet (2008) in connection with the Helmholtz equation in 3D, were motivated by their potential for *quantitative* identification of the size of the scatterer(s) by minimization of higher-order terms. Such studies can be extended to a broader class of problems, including elastodynamic inverse scattering and crack identification.

Interface crack identification. The exploitation of the topological sensitivity approach, developed in this Ph.D. project, for the identification of cracks in homogeneous solids or interface cracks in bimaterial bodies, constitutes another promising perspective as this problem arises in a number of applications dealing in particular with composite materials. A numerical implementation of the method to perform, an extensive campaign of simulations is needed to assess its effectiveness. However, given in particular the availability in closed-form of the corresponding polarization tensors, the simplicity of the method may contribute to its generalization in an engineering context for non-destructive material testing.

Mathematical justification. The topological sensitivity method relies on the formulation of a topological gradient stemming from a mathematically rigorous asymptotic perturbation of a cost functional for an infinitesimal defect. The use of this method in inverse scattering problems is, however, based on a heuristic interpretation of this gradient to define an indicator function for finite defects. A deeper analysis of the method is needed to provide both a better understanding of this indicator and a firmer mathematical justification of its use in applications, so far supported by numerical experiments.

Linear sampling method

Formulation using reciprocity gap. The linear sampling method makes a recourse to the solution of a linear integral equation of the first kind, where the left-hand side of the equation (i.e. the kernel) is constructed from the experimental data, while the right-hand side depends on a singular solution to the featured wave equation in the reference (defect-free) domain. For applications that deal with full- or half-space configurations, this solution is usually the relevant Green's solution. However, for situations where the background medium is bounded, such fundamental solution is not known analytically and its numerical computation can suffer from prohibitive approximations (see e.g. Madyarov, 2006). To circumvent this drawback, the method can be combined with the reciprocity gap principle following the work by Colton and Haddar (2005) in acoustic inverse scattering. This strategy avoids the need to compute the fundamental solution and thus opens new perspectives for the use of the linear sampling method in inverse elastodynamic problems dealing with finite solids.

Qualitative material identification.   A comprehensive study of the interior transmission problem in the elasticity case presented in this dissertation represents a theoretical advancement in that it establishes a link between the lower bound on the (experimentally-observed) transmission eigenvalues and combined material properties of the scatterer and the background medium. In earlier studies by Cakoni et al. (2007, 2008, 2009), dealing with the Helmholtz equation, such relations are used to obtain qualitative information on the physical properties of a hidden scatterer. The question of such use of the LSM in elastodynamics is still open and may have a wide range of practical applications.

Inverse scattering in the time domain.   Most of qualitative inverse scattering methods have been initially formulated for time-harmonic problems. An obvious alley toward the extension of such works toward time-domain problems revolves around the use of the Fourier transform. Such extension however raises the issue of the so-called (interior) *transmission eigenfrequencies* that may pollute the observed spectrum of the scattered data and, depending on the sampling technique used, may render the method unusable. This in particular applies in the case of the linear sampling method, whose multi-frequency treatment is for the first time rigorously addressed in this thesis and cited reference work Guzina et al. (2010). For completeness, it is also noted that a time domain treatment of the LSM has been proposed in Chen et al. (2010). Notwithstanding the contribution of the latter work, however, a time domain scattering situation where the undesirable (interior) transmission eigenvalues intersect the Fourier spectrum of a prescribed transient signal as in Guzina et al. (2010) is still an open question.

Common challenges

Tests on real experimental data.   The topological sensitivity approach and the linear sampling method have each been the subject of a large number of studies that aim at establishing their theoretical foundation and exploring their range of applications, via numerical simulations that make use of synthetic measurements. At present, however, the supporting literature dealing with the experimental data is relatively scarce, and the only light in this direction was shed in Dominguez and Gibiat (2010) and Tacchino et al. (2002) in the context of the TS and the LSM, respectively. As a result, there is a significant need for additional experimental studies to build up examples using real scattering measurements which could be more effectively designed through the proposition of benchmark problems for qualitative inverse scattering methods.

Explore a* unified *inverse scattering theory.   Inverse scattering problems, that have been the subject of intense studies over the last twenty years, have witnessed the growth and the flourishing of qualitative methods that aim at providing a robust and computationally effective alternative to the customary linearization and non-linear optimization approaches. In light of the diversity of the sampling techniques developed so far, however, the question of the commonality (if any) of their theoretical platform, arises naturally. In *direct* scattering problems, the so-called *scattering operator* (see e.g. Lax and Phillips (1967)) plays a central role and inverse methods have early been conceived as strategies to extract the informations it contains (Colton and Kress, 1992; Kirsch, 1996). A brief review of the literature on the subject, with an emphasis on the methods covered by this dissertation, is given below to highlight the importance of the idea. It is believed that an in-depth review of the cited and related works may lead to significant progress towards a *unified* theory of qualitative methods for inverse scattering.

- Exploitation of the spectrum of the scattering operator: Colton and Kress (1995); Kirsch (1998); Mast et al. (1997).

- Linear sampling and factorization methods, seen as two comparable strategies (Arens and Lechleiter, 2009) to extract information from the scattering operator in a "simple" way (Cakoni and Colton, 2006).

- Parallels between the MUltiple SIgnal Classification (MUSIC) algorithm and linear sampling and factorization methods: Cheney (2001); Kirsch (2002).

- Use of the MUSIC algorithm to deal with inverse scattering problems: Ammari and Kang (2004).

- MUSIC algorithm and time reversal: Devaney (2000, 2005).

- Time reversal and imaging: Cassereau et al. (1990); Fink (1992); Prada et al. (1995); Borcea et al. (2002).

- Exploitation of the spectrum of the time reversal operator and DORT method (*Décomposition de l'Opérateur de Retournement Temporel*): Prada and Fink (1994); Prada et al. (1996, 1997).

- Time-domain topological sensitivity method and time reversal analogy: Dominguez et al. (2005).

- As the topological sensitivity method employing least-square misfit function leads to a topological gradient in the form of a single-layer potential over the observation domain and whose kernel is the scattered field, analogies naturally arise with the adjoint version of the linear sampling method proposed by Nintcheu Fata and Guzina (2007).

Figure A provides a synthetic diagram of these interconnections between the topological sensitivity method (TS) and the linear sampling method (LSM). Solid lines represent theoretically established links, while dashed lines stand for future research directions.
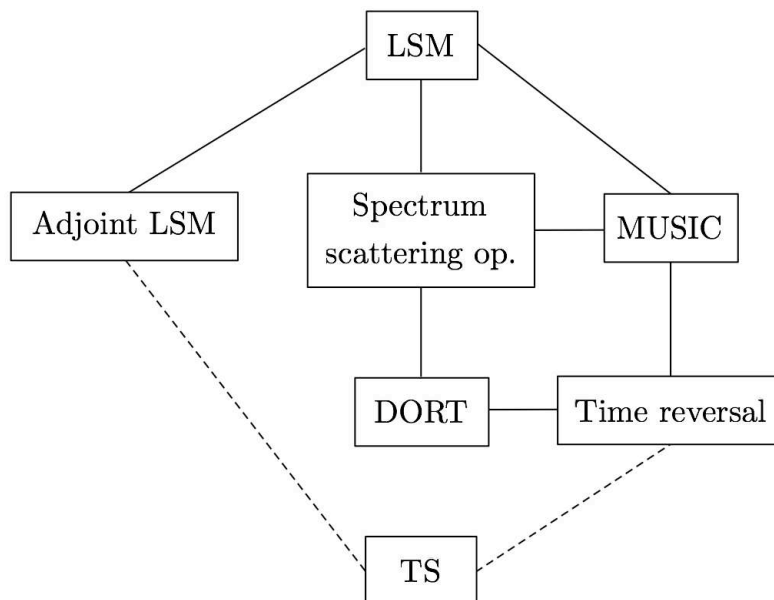
Figure A: *Towards a unified vision of inverse scattering methods.*

Bibliography

Abramowitz, M. and Stegun, I. A. (1965). *Handbook of mathematical functions, with formulas, graphs, and mathematical tables*. Dover.

Achenbach, J. D. (2003). *Reciprocity in elastodynamics*. Cambridge University Press.

Ahusborde, E., Azaïez, M., Deville, M., and Mund, E. (2007). Legendre spectral methods for the -**grad**(div) operator. *Comput. Methods Appl. Mech. Engrg.*, 196:4538–4547.

Aki, K. and Richards, P. G. (1980). *Quantitative Seismology: Theory and Methods*, volume 2. W.H. Freeman and Co., San Francisco.

Allaire, G., de Gournay, F., Jouve, F., and Toader, A.-M. (2005). Structural optimization using topological and shape sensitivity via a level-set method. *Control and Cybernetics*, 34:59–80.

Ammari, H., Guadarrama Bustos, L., Garapon, P., and Kang, H. (2009). Transient anomaly imaging by the acoustic radiation force. *Journal of Differential Equations*, 249:1579–1595.

Ammari, H. and Kang, H. (2004). *Reconstruction of small inhomogeneities from boundary measurements*. Lecture Notes in Mathematics 1846. Springer-Verlag.

Ammari, H. and Kang, H. (2006). Reconstruction of elastic inclusions of small volume via dynamic measurements. *Appl. Math. Opt.*, 54:223–235.

Ammari, H. and Kang, H. (2007). *Polarization and moment tensors with applications to inverse problems and effective medium theory*, volume 162. Springer-Verlag.

Ammari, H., Kang, H., Lee, H., and Park, W. K. (2010). Asymptotic imaging of perfectly conducting cracks. *SIAM J. Sci. Comput.*, 32:894–922.

Ammari, H., Kang, H., Nakamura, G., and Tanuma, K. (2002). Complete asymptotic expansions of solutions of the system of elastostatics in the presence of an inclusion of small diameter and detection of an inclusion. *J. Elast.*, 67:97–129.

Amstutz, S. and Dominguez, N. (2008). Topological sensitivity analysis in the context of ultrasonic non-destructive testing. *Engineering Analysis with Boundary Elements*, 32:936–947.

Amstutz, S., Horchani, I., and Masmoudi, M. (2005). Crack detection by the topological gradient method. *Control and Cybernetics*, 34:81–101.

Amstutz, S., Takahashi, T., and Vexler, B. (2008). Topological sensitivity analysis for time-dependent problems. *ESAIM: Control, Optimisation and Calculus of Variations*, 14:427–455.

Andrieux, S., Ben Abda, A., and Bui, H. D. (1999). Reciprocity principle and crack identification. *Inverse Problems*, 15:59–65.

Arens, T. (2001). Linear sampling methods for 2D inverse elastic wave scattering. *Inverse Problems*, 17:1445–

1464.

Arens, T. and Lechleiter, A. (2009). The linear sampling method revisited. *J. Integral Equations Appl.*, 21:179–202.

Azaïez, M., Gruber, R., Deville, M., and Mund, E. (2006). On a stable spectral method for the grad(div) eigenvalue problem. *Journal of Scientific Computing*, 27:41–50.

Baganas, K., Guzina, B. B., Charalambopoulos, A., and Manolis, G. D. (2006). A linear sampling method for the inverse transmission problem in near-field elastodynamics. *Inverse Problems*, 22:1835–1853.

Bateman, H. (1953). *Higher transcendental functions*, volume II. McGraw-Hill.

Bellis, C. and Bonnet, M. (2009). Crack identification by 3D time-domain elastic or acoustic topological sensitivity. *Comptes Rendus Mécanique*, 337:124–130.

Bellis, C. and Bonnet, M. (2010). A FEM-based topological sensitivity approach for fast qualitative identification of buried cavities from elastodynamic overdetermined boundary data. *Int. J. Solids Struct.*, 47:1221–1242.

Bellis, C. and Guzina, B. B. (2010). On the existence and uniqueness of a solution to the interior transmission problem for piecewise-homogeneous solids. *Journal of Elasticity*, 101:29–57.

Ben Abda, A., Ben Ameur, H., and Jaoua, M. (1999). Identification of 2D cracks by elastic boundary measurements. *Inverse Problems*, 15:67–77.

Ben Abda, A., Hassine, M., Jaoua, M., and Masmoudi, M. (2009). Topological sensitivity analysis for the location of small cavities in stokes flow. *SIAM J. Contr. Opt.*, 48:2871–2900.

Bleistein, N. (1984). *Mathematical methods for wave phenomena*. Academic Press, New York.

Bonnet, M. (1995). BIE and material differentiation applied to the formulation of obstacle inverse problems. *Engng. Anal. with Bound. Elem.*, 15:121–136.

Bonnet, M. (1999). *Boundary integral equations methods for solids and fluids*. Wiley.

Bonnet, M. (2006). Topological sensitivity for 3D elastodynamic and acoustic inverse scattering in the time domain. *Comp. Meth. Appl. Mech. Engng.*, 195:5239–5254.

Bonnet, M. (2008). Inverse acoustic scattering by small-obstacle expansion of misfit function. *Inverse Problems*, 24:035022.

Bonnet, M. (2009). Higher-order topological sensitivity for 2-D potential problems. Application to fast identification of inclusions. *Int. J. Solids Struct.*, 46:2275–2292.

Bonnet, M. (2010a). Fast identification of cracks using higher-order topological sensitivity for 2-D potential problems. *Engineering Analysis with Boundary Elements*, In Press.

Bonnet, M. (2010b). Topological sensitivity of energy cost functional for wave-based defect identification. *Comptes Rendus Mécanique*, 338:377–389.

Bonnet, M. and Constantinescu, A. (2005). Inverse problems in elasticity. *Inverse Problems*, 21:R1–R50.

Bonnet, M. and Guzina, B. B. (2004). Sounding of finite solid bodies by way of topological derivative. *Int. J. Num. Meth. in Eng.*, 61:2344–2373.

Bonnet, M. and Guzina, B. B. (2009). Elastic-wave identification of penetrable obstacles using shape-material sensitivity framework. *J. Comp. Phys.*, 228:294–311.

Borcea, L., Papanicolaou, G. C., Tsogka, C., and Berrymann, J. G. (2002). Imaging and time reversal in random media. *Inverse Problems*, 18:1247–1279.

Bui, H. D. (2006). *Fracture mechanics: Inverse problems and solutions*. Springer.

Bui, H. D., Constantinescu, A., and Maigre, H. (2004). Numerical identification of linear cracks in 2D elastodynamics using instantaneous reciprocity gap. *Inverse Problems*, 20:993–1001.

Burton, A. J. and Miller, G. F. (1971). The application of the integral equation methods to the numerical solution of some exterior boundary-value problems. *Proc. Roy. Soc. Lond. A*, 323:201–210.

Cakoni, F., Çayören, M., and Colton, D. (2008). Transmission eigenvalues and the nondestructive testing of dielectrics. *Inverse Problems*, 24:065016.

Cakoni, F. and Colton, D. (2003a). Combined far field operators in electromagnetic inverse scattering theory. *Math. Meth. Appl. Sci.*, 26:413–429.

Cakoni, F. and Colton, D. (2003b). The linear sampling method for cracks. *Inverse Problems*, 19:279–295.

Cakoni, F. and Colton, D. (2003c). On the mathematical basis of the linear sampling method. *Georgian Math. J.*, 10:911–925.

Cakoni, F. and Colton, D. (2004). The determination of the surface impedance of a partially coated obstacle from far field data. *SIAM J. Appl. Math.*, 64:709–723.

Cakoni, F. and Colton, D. (2006). *Qualitative methods in inverse scattering theory*. Springer-Verlag, Berlin.

Cakoni, F., Colton, D., and Gintides, D. (2010a). The interior transmission eigenvalue problem. *under review*, pages 1–10.

Cakoni, F., Colton, D., and Haddar, H. (2002). The linear sampling method for anisotropic media. *J. Comput. Appl. Math.*, 146:285–299.

Cakoni, F., Colton, D., and Haddar, H. (2009). The computation of lower bounds for the norm of the index of refraction in an anisotropic media from far field data. *J. Integral Equations Appl.*, 21:203–227.

Cakoni, F., Colton, D., and Haddar, H. (2010b). On the determination of Dirichlet and transmission eigenvalues from far field data. *C. R. Acad. Sci. Paris, Ser. I*, 348:379–383.

Cakoni, F., Colton, D., and Monk, P. (2007). On the use of transmission eigenvalues to estimate the index of refraction from far field data. *Inverse Problems*, 23:507–522.

Cakoni, F., Colton, D., Monk, P., and Sun, J. (2010c). The inverse electromagnetic scattering problem for anisotropic media. *Inverse Problems*, 26:074004.

Cakoni, F. and Gintides, D. (2010). New results on transmission eigenvalues. *Inverse Problems and Imaging*, 4:39–48.

Cakoni, F., Gintides, D., and Haddar, H. (2010d). The existence of an infinite discrete set of transmission eigenvalues. *SIAM J. Math. Anal.*, 42:237–255.

Cakoni, F., Gintides, D., and Haddar, H. (2010e). The interior transmission problem for regions with cavities. *SIAM J. Math. Anal.*, 42:145–162.

Cakoni, F. and Haddar, H. (2001). The linear sampling method for anisotropic media: Part 2. Preprints 26, MSRI Berkeley, California.

Cakoni, F. and Haddar, H. (2007). A variational approach for the solution of the electromagnetic interior transmission problem for anisotropic media. *Inverse Problems and Imaging*, 1:443–456.

Cakoni, F. and Haddar, H. (2009). On the existence of transmission eigenvalues in an inhomogeneous medium. *Applicable Analysis*, 88:475–493.

Cakoni, F. and Kirsch, A. (2010). On the interior transmission eigenvalue problem. *Int. J. Comput. Sci. Math.*, 3:142–167.

Carcione, J. M. and Cavallini, F. (1993). Energy balance and fundamental relations in anisotropic-viscoelastic media. *Wave motion*, 18:11–20.

Carpio, A. and Rapún, M.-L. (2008). Solving inhomogeneous inverse problems by topological derivative methods. *Inverse Problems*, 24:045014.

Cassereau, D., Wu, F., and Fink, M. (1990). Limits of self-focusing using closed time-reversal cavities and mirrors - theory and experiment. *IEEE Ultrasonics Symposium*, 3:1613–1618.

Charalambopoulos, A. (2002). On the interior transmission problem in nondissipative, inhomogeneous, anisotropic elasticity. *J. Elasticity*, 67:149–170.

Charalambopoulos, A. and Anagnostopoulos, K. A. (2008). On the spectrum of the interior transmission problem in isotropic elasticity. *J. Elasticity*, 90:295–313.

Charalambopoulos, A., Gintides, D., and Kiriaki, K. (2002). The linear sampling method for the transmission problem in three-dimensional linear elasticity. *Inverse Problems*, 18:547–558.

Charalambopoulos, A., Kirsch, A., Anagnostopoulos, K. A., Gintides, D., and Kiriaki, K. (2007). The factorization method in inverse elastic scattering from penetrable bodies. *Inverse Problems*, 23:27–51.

Chen, Q., Haddar, H., Lechleiter, A., and Monk, P. (2010). A sampling method for inverse scattering in the time domain. *Inverse Problems*, 26:085001.

Chen, Y. Z., Hasebe, N., and Lee, K. Y. (2003). *Multiple crack problems in elasticity*. WIT Press.

Cheney, M. (2001). The linear sampling method and the MUSIC algorithm. *Inverse Problems*, 17:591–595.

Chikichev, I. and Guzina, B. B. (2008). Generalized topological derivative for the navier equation and inverse scattering in the time domain. *Comp. Meth. Appl. Mech. Engng.*, 197:4467–4484.

Collino, F., Fares, M. B., and Haddar, H. (2003). Numerical and analytical studies of the linear sampling method in electromagnetic inverse scattering problems. *Inverse problems*, 19:1279–1298.

Colton, D. (1984). The inverse scattering problem for time-harmonic acoustic waves. *SIAM review*, 26:323–350.

Colton, D., Coyle, J., and Monk, P. (2000). Recent developments in inverse acoustic scattering theory. *SIAM Review*, 42:369–414.

Colton, D. and Haddar, H. (2005). An application of the reciprocity gap functional to inverse scattering theory. *Inverse Problems*, 21:383–398.

Colton, D., Haddar, H., and Piana, M. (2003). The linear sampling method in inverse electromagnetic scattering theory. *Inverse Problems*, 19:S105–S137.

Colton, D. and Kirsch, A. (1996). A simple method for solving inverse scattering problems in the resonance region. *Inverse Problems*, 12:383–393.

Colton, D., Kirsch, A., and Päivärinta, L. (1989). Far-field patterns for acoustic waves in an inhomogeneous medium. *SIAM J. Math. Anal.*, 20:1472–1483.

Colton, D. and Kress, R. (1992). *Inverse acoustic and electromagnetic scattering theory*. Springer, Berlin.

Colton, D. and Kress, R. (1995). Eigenvalues of the far field operator and inverse scattering theory. *SIAM J. Math. Anal.*, 26:601–615.

Colton, D. and Kress, R. (2006). Using fundamental solutions in inverse scattering. *Inverse Problems*, 22:R49–

R66.

Colton, D. and Monk, P. (1998). Linear sampling method for the detection of leukemia using microwaves. *SIAM J. Appl. Math.*, 58:926–941.

Colton, D., Paivarinta, L., and Sylvester, J. (2007). The interior transmission problem. *Inverse Problems and Imaging*, 1:13–28.

Colton, D. and Sleeman, B. D. (2001). An approximation property of importance in inverse scattering theory. *Proc. Edinburgh Math. Soc.*, 44:449–454.

Dassios, G. and Kleiman, R. (2000). *Low frequency scattering*. Oxford Science Publications.

Devaney, A. J. (2000). Super-resolution processing of multi-static data using time reversal and music. *Northeastern University Preprint*.

Devaney, A. J. (2005). Time reversal imaging of obscured targets from multistatic data. *IEEE Trans. Antennas Propag.*, 53:1600–1610.

Dominguez, N. and Gibiat, V. (2010). Non-destructive imaging using the time domain topological energy method. *Ultrasonics*, 50:367–372.

Dominguez, N., Gibiat, V., and Esquerré, Y. (2005). Time domain topological gradient and time reversal analogy: an inverse method for ultrasonic target detection. *Wave Motion*, 42:31–52.

Dorn, O. and Lesselier, D. (2006). Level set methods for inverse scattering. *Inverse Problems*, 22:R67–R131.

Erhard, K. and Potthast, R. (2006). A numerical study of the probe method. *SIAM J. Sci. Comput.*, 28:1597–1612.

Eringen, A. C. and Suhubi, E. S. (1975). *Elastodynamics (vol II - linear theory)*. Academic Press.

Eschenauer, H. A., Kobelev, V. V., and Schumacher, A. (1994). Bubble method for topology and shape optimization of structures. *Structural Optimization*, 8:42–51.

Feijóo, G. R. (2004). A new method in inverse scattering based on the topological derivative. *Inverse Problems*, 20:1819–1840.

Findley, W. N., Lai, J. S., and Onaran, K. (1989). *Creep and Relaxation of Nonlinear Viscoelastic Materials*. Dover, New York.

Fink, M. (1992). Time reversal of ultrasonic fields - part I: Basic principles. *IEEE Trans. Ultrason., Ferroelec., Freq. Contr.*, 39:555–566.

Flügge, W. (1975). *Viscoelasticity*. Springer-Verlag.

Fouque, J.-P., Garnier, J., Papanicolaou, G., and Sølna, K. (2007). *Wave propagation and time reversal in randomly layered media*. Springer.

Gallego, R. and Rus, G. (2004). Identification of cracks and cavities using the topological sensitivity boundary integral equation. *Comp. Mech.*, 33:154–163.

Garreau, S., Guillaume, P., and Masmoudi, M. (2001). The topological asymptotic for PDE systems: the elasticity case. *SIAM J. Contr. Opt.*, 39:1756–1778.

Graff, K. F. (1991). *Wave motion in elastic solids*. Dover Publication.

Guzina, B. B. and Bonnet, M. (2004). Topological derivative for the inverse scattering of elastic waves. *Quart. J. Mech. Appl. Math.*, 57:161–179.

Guzina, B. B. and Bonnet, M. (2006). Small-inclusion asymptotic of misfit functionals for inverse problems in

acoustics. *Inverse Problems*, 22:1761–1785.

Guzina, B. B., Cakoni, F., and Bellis, C. (2010). On the multi-frequency obstacle reconstruction via the linear sampling method. *Inverse Problems*, to appear.

Guzina, B. B. and Chikichev, I. (2007). From imaging to material identification: a generalized concept of topological sensitivity. *J. Mech. Phys. Solids*, 55:245–279.

Guzina, B. B. and Madyarov, A. I. (2007). A linear sampling approach to inverse elastic scattering in piecewise-homogeneous domains. *Inverse Problems*, 23:1467–1493.

Guzina, B. B., Nintcheu Fata, S., and Bonnet, M. (2003). On the stress-wave imaging of cavities in a semi-infinite solid. *Int. J. Solids Struct.*, 40:1505–1523.

Guzina, B. B. and Yuan, H. (2009). On the small-defect perturbation and sampling of heterogeneous solids. *Acta Mechanica*, 205:51–75.

Hadamard, J. (1923). *Lectures on the Cauchy problem in linear partial differential equations*. Yale University Press, New Haven.

Haddar, H. (2004). The interior transmission problem for anisotropic maxwell's equations and its applications to the inverse problem. *Math. Meth. Appl. Sci.*, 27:2111–2129.

Haddar, H. and Monk, P. (2002). The linear sampling method for solving the electromagnetic inverse medium problem. *Inverse Problems*, 18:891–906.

Hähner, P. (2000). On the uniqueness of the shape of a penetrable, anisotropic obstacle. *J. Comput. Appl. Math.*, 116:167–180.

Haug, E. J., Choi, K. K., and Komkov, V. (1986). *Design Sensitivity Analysis of Structural Systems*. Academic Press.

Henrot, A. (2006). *Extremum problems for eigenvalues of elliptic operators*. Birkhäuser Verlag.

Hitrik, M., Ksupchyk, K., Ola, P., and Päivärinta, L. (2010). The transmission eigenvalues for operators with constant coeficients. *SIAM J. Math Analysis*, to appear.

Hughes, T. J. R. (1987). *The finite element method - linear static and dynamic finite element analysis*. Prentice Hall, Englewood Cliffs, New Jersey, USA.

Ikehata, M. (1998a). Reconstruction of obstacle from boundary measurements. *Wave motion*, 30:205–223.

Ikehata, M. (1998b). Reconstruction of the shape of the inclusion by boundary measurements. *Commun. in partial differential equations*, 23:1459–1474.

Ikehata, M. (2006). Inverse crack problem and probe method. *Cubo*, 8:29–40.

Jackowska-Strumillo, L., Sokolowski, J., and Zochowski, A. (2002). Topological optimization and inverse problems. *Computer Assisted Mechanics and Engineering Sciences*, 10(2):163–176.

Kassir, M. and Sih, G. C. (1975). *Three-dimensional crack problems: a new selection of cracks solutions in three-dimensional elasticity*. Noordhoof International Pub.

Kato, T. (1995). *Perturbation Theory for Linear Operators*. Springer, Berlin, Heidelberg.

Katznelson, Y. (1976). *An introduction to harmonic analysis*. Dover, New York.

Kinsler, L. E., Frey, A. R., Coppens, A. B., and Sanders, J. V. (1982). *Fundamentals of acoustics*. John Wiley and Sons.

Kirsch, A. (1996). *An introduction to the mathematical theory of inverse problems*. Springer.

Kirsch, A. (1998). Characterization of the shape of a scattering obstacle using the spectral data of the far field operator. *Inverse Problems*, 14:1489–1512.

Kirsch, A. (2002). The MUSIC-algorithm and the factorization method in inverse scattering theory for inhomogeneous media. *Inverse Problems*, 18:1025–1040.

Kirsch, A. (2007). An integral equation approach and the interior transmission problem for maxwell's equations. *Inverse Problems and Imaging*, 1:107–127.

Kirsch, A. (2009). On the existence of transmission eigenvalues. *Inverse Problems and Imaging*, 3:155–172.

Kirsch, A. and Grinberg, N. (2008). *The Factorization Method for Inverse Problems*. Oxford University Press, New York.

Kittappa, R. and Kleinman, R. E. (1975). Acoustic scattering by penetrable homogeneous objects. *J. Math. Phys.*, 16:421–432.

Knowles, J. K. (1995). On the representation of the elasticity tensor for isotropic media. *J. Elasticity*, 39:175–180.

Krée, P. and Soize, C. (1986). *Mathematics of random phenomena*. D. Reidel Publishing Company.

Kress, R. (1999). *Linear integral equations*. Springer.

Kupradze, V. D. (1965). *Potential methods in the theory of elasticity*. Israel Program for Scientific Translations.

Ladevèze, P. and Leguillon, D. (1983). Error estimate procedure in the finite element method and applications. *SIAM J. Numer. Anal.*, 20:485–509.

Lax, P. and Phillips, R. S. (1967). *Scattering theory*. Academic Press.

Lines, C. and Chandler-Wilde, S. (2005). A time domain point source method for inverse scattering by rough surfaces. *Computing*, 75:157–180.

Liu, Y. and Rizzo, F. J. (1993). Hypersingular boundary integral equations for radiation and scattering of elastic waves in three dimensions. *Comp. Meth. Appl. Mech. Eng.*, 107:131–144.

Luke, D. (2004). Multifrequency inverse obstacle scattering: the point source method and generalized filtered backprojection. *Math. Comput. Simul.*, 66:297–314.

Luke, D. and Potthast, R. (2006). The point source method for inverse scattering in the time domain. *Math. Meth. Appl. Sci.*, 29:1501–1521.

Madyarov, A. I. (2006). *Fast solutions for 3D elastic-wave imaging of solid bodies*. PhD thesis, University of Minnesota, USA.

Madyarov, A. I. and Guzina, B. B. (2006). A radiation condition for layered elastic media. *J. Elasticity*, 82:73–98.

Malcolm, A. and Guzina, B. (2008). On the topological sensitivity of transient acoustic fields. *Wave Motion*, 45:821–834.

Malvern, L. E. (1969). *Introduction to the Mechanics of a Continuous Medium*. Prentice-Hall, Englewood Cliffs.

Marsden, J. E. and Hughes, T. J. R. (1994). *Mathematical foundations of elasticity*. Dover.

Masmoudi, M., Pommier, J., and Samet, B. (2005). The topological asymptotic expansion for the maxwell equations and some applications. *Inverse Problems*, 21:547–564.

Mast, T. D., Nachman, A. I., and Waag, R. C. (1997). Focusing and imaging using eigenfunctions of the scattering operator. *J. Acoust. Soc. Am.*, 102:715–725.

Mataraezo, G. (2001). Irreversibility of time and symmetry property of relaxation function in linear viscoelasticity. *Mechanics Research Communications*, 28:373–380.

McLean, W. (2000). *Strongly elliptic systems and boundary integral equations*. Cambridge University Press.

Mehrabadi, M. M., Cowin, S. C., and Horgan, C. O. (1993). Strain energy density bounds for linear anisotropic elastic materials. *J. Elasticity*, 30:191–196.

Morse, P. M. and Ingard, K. U. (1986). *Theoretical acoustics*. Princeton University Press.

Mura, T. (1982). *Miromechanics of defects in solids*. Martinus Nijhoff.

Nédélec, J.-C. (2001). *Acoustic and electromagnetic equations. Integral representations for harmonic problems*. Springer.

Nečas, J. and Hlaváček, I. (1981). *Mathematical theory of elastic and elasto-plastic bodies: an introduction*. Elsevier.

Nintcheu Fata, S. and Guzina, B. B. (2004). A linear sampling method for near-field inverse problems in elastodynamics. *Inverse Problems*, 20:713–736.

Nintcheu Fata, S. and Guzina, B. B. (2007). Elastic scatterer reconstruction via the adjoint sampling method. *SIAM J. Appl. Math.*, 67:1330–1352.

Nintcheu Fata, S., Guzina, B. B., and Bonnet, M. (2003). Computational framework for the BIE solution to inverse scattering problems in elastodynamics. *Computational Mechanics*, 32:370–380.

Nishimura, N. (2002). Fast multipole accelerated boundary integral equation methods. *Appl Mech Rev*, 55:299–324.

Päivärinta, L. and Sylvester, J. (2008). Transmission eigenvalues. *SIAM J. Math. Anal.*, 40:738–753.

Petrovskii, I. G. (1967). *Partial Differential Equations*. Iliffe Books LTD, London.

Pike, R. and Sabatier, P. (2002). *Scattering: Scattering and Inverse Scattering in Pure and Applied Science*. Academic Press, San Diego.

Plessix, R. E., De Roeck, Y. H., and Chavent, G. (1999). Waveform inversion of reflection seismic data for kinematic parameters by local optimization. *SIAM J. Sci. Comput.*, 20:1033–1052.

Pockels, F. (1892). Uber die partielle differentialgleichung $\Delta u + k^2 u = 0$ and deren auftreten in die mathematischen physik. *Z. Math. Physik*, 37:100–105.

Porat, B. (1996). *A Course in Digitial Signal Processing*. J. Wiley and Sons.

Potthast, R. (1996). A fast new method to solve inverse scattering problems. *Inverse Problems*, 12:731–742.

Potthast, R. (2001). *Point Sources and Multipoles in Inverse Scattering Theory*. Chapman and Hal/ CRC, DNew York.

Potthast, R. (2006). A survey on sampling and probe methods for inverse problems. *Inverse Problems*, 22:R1–R47.

Prada, C. and Fink, M. (1994). Eigenmodes of the time reversal operator: A solution to selective focusing in multiple target media. *Wave motion*, 20:151–163.

Prada, C., Manneville, S., Spoliansky, D., and Fink, M. (1996). Decomposition of the time reversal operator: Application to detection and selective focusing on two scatterers. *J. Acoust. Soc. Am.*, 99:2067–2076.

Prada, C., Tanter, M., and Fink, M. (1997). Flaw detection in solid with the D.O.R.T. method. *IEEE Ultrason. Symp. Proc.*, 1:681–686.

Prada, C., Thomas, J. L., and Fink, M. (1995). The iterative time reversal process: Analysis of the convergence. *J. Acoust. Soc. Am.*, 97:62–71.

Pritz, T. (2007). The poisson's loss factor of solid viscoelastic materials. *Journal of Sound and Vibration*, 306:790–802.

Pyl, L., Clouteau, D., and Degrande, G. (2004). A weakly singular boundary integral equation in elastodynamics for heterogeneous domains mitigating fictitious eigenfrequencies. *Eng. Anal. Bound. Elem.*, 28:1493–1513.

Ramm, A. G. (1986). *Scattering by obstacle*. Springer.

Ramm, A. G. (1992). *Multidimensional inverse scattering problems*. Longman Scientific & Wiley, New York.

Ramm, A. G. (2005). *Inverse problems: Mathematical and analytical techniques with applications to engineering*. Springer, New-York.

Rekanos, I. T., Yioultsis, T. V., and Tsiboukis, T. D. (1999). Inverse scattering using the finite element method and a nonlinear optimization technique. *IEEE Transactions on microwave theory and techniques*, 47:336–344.

Rocha de Faria, J., Novotny, A. A., Feijóo, R. A., and E., T. (2009). First- and second-order topological sensitivity for inclusions. *Inverse Problems in Sciences and Engineering*, 17:665–679.

Rovati, M. and Taliercio, A. (2003). Stationarity of the strain energy density for some classes of anisotropic solids. *Int. J. Solids Struct.*, 40:3043–6075.

Rynne, B. P. and Sleeman, B. D. (1991). The interior transmission problem and inverse scattering from inhomogeneous media. *SIAM J. Math. Anal.*, 22:1755–1762.

Schumacher, A. (1995). *Topologieoptimierung von Bauteilstrukturen unter Verwendung von Lochpositionierungskriterien*. PhD thesis, University of Siegen, Germany.

Shter, I. M. (1973). Generalization of onsager's principle and its application. *Journal of Engineering Physics and Thermophysics*, 25:1319–1323.

Sokolowski, J. and Zochowski, A. (1999). On the topological derivative in shape optimization. *SIAM J. Control Optim.*, 37:1251–1272.

Stavroulakis, G. E. (2001). *Inverse and crack identification problems in engineering mechanics*. Springer.

Szegö, G. (1939). *Orthogonal polynomials*. American Mathematical Society.

Tacchino, A., Coyle, J., and Piana, M. (2002). Numerical validation of the linear sampling method. *Inverse Problems*, 18:511–527.

Wang, X. D. and Huang, G. L. (2004). Identification of embedded cracks using back-propagating elastic waves. *Inverse Problems*, 20:1393–1409.

Wheeler, L. T. and Sternberg, E. (1968). Some theorems in classical elastodynamics. *Arch. Rat. Mech. Anal.*, 31:51–90.

Willis, J. R. (1972). The penny-shaped crack on an interface. *Quart. J. Mech. and Applied Math.*, 25:367–385.

Wloka, J. (1992). *Partial differential equations*. Cambridge University Press.

Yosida, K. (1980). *Functional Analysis*. Springer-Verlag, Berlin.